THEORETICAL AND EXPERIMENTAL STUDIES ON THE RESISTANCE OF SWATH SHIPS

by

HO HWAN CHUN, BSc, MSc

This thesis is submitted for the degree of Doctor of Philosophy in the Department of Naval Architecture and Ocean Engineering, University of Glasgow.

March 1988

Great Britain

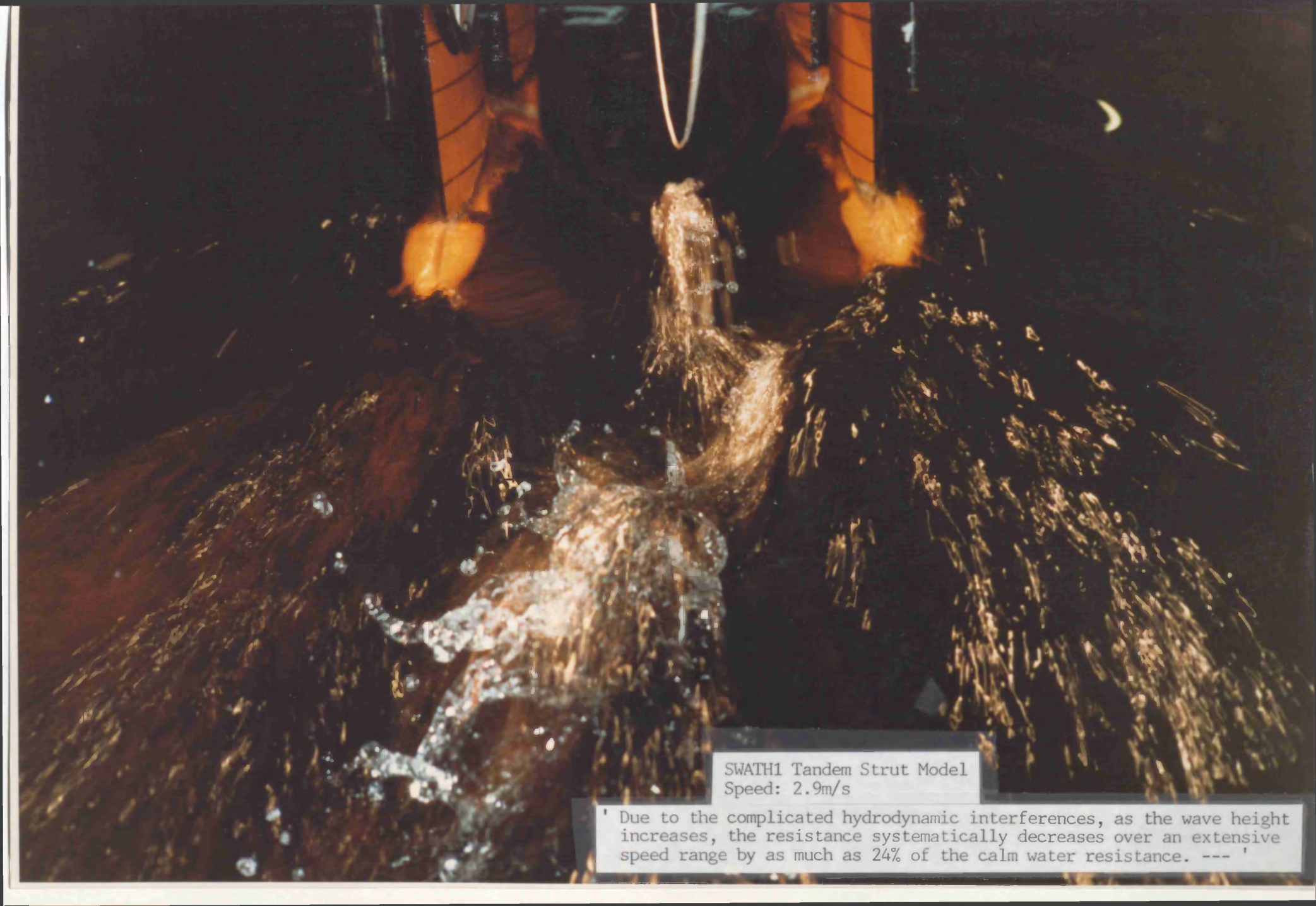

SWATH1 Tandem Strut Model
Speed: 2.9m/s

' Due to the complicated hydrodynamic interferences, as the wave height increases, the resistance systematically decreases over an extensive speed range by as much as 24% of the calm water resistance. --- '

DECLARATION

Except where reference is made to the work of others, this thesis is believed to be original

ACKNOWLEDGEMENTS

The author would like to extend his gratitude to all those people who have contributed to the research work presented in this thesis. The following are wholeheartedly acknowledged:

Professor D.Faulkner, Head of the Department, for his help in making this research possible, especially with regard to obtaining support for the author through the University Scholarship,

Dr. A.M.Ferguson, formerly the superintendent of the Hydrodynamics Laboratory, for his supervision, advice and encouragement throughout this research,

Dr. R.C.McGregor, the SWATH project supervisor, and Dr. A.Incecik, the superintendent of the Hydrodynamics Laboratory, for their guidance and helpful discussions,

The many researchers in the SWATH project group for their useful discussion and friendship, especially, J.R.MacGregor for his good friendship and useful discussion on the general design aspect of SWATH, and Mr.E.B.Djatmiko for his cooperation in some of the experimental work,

Mr.R.B.Christison, the chief technician, Messers.D.J.Sinclair, A.Khan, G.Dunning and D.Nicolson for their valued assistance in carrying out the experiments and Mr.J.M. Aitken for making the models,

The ship Hydromechanics Division of Gdansk Technical University, Poland, especially Mr.M Grygorowicz, for allowing the author to analyse valuable experimental data, especially relating their 'sledge bow concept which appears to promise a radical breakthrough in the further development of SWATH ships,

Mr.N.S. Miller, formerly senior lecturer in the Department, for his initial suggestion of the development of a rectangular hulled SWATH ship, and for his kind help, invaluable discussion, advice and encouragement throughout this research.

The author is very much indebted to the moral support and encouragement of his mother, father, brother and sisters throughout his life. Finally, this thesis is dedicated to his lovely wife, Jung Hee, pretty daughter, June Young, and second child to be born in April.

CONTENTS

ABSTRACT

Even though there are currently only 11 SWATH vessels at sea worldwide, there is increasing interest in SWATH ships due to their markedly superior seakeeping performance compared to monohulls. Today this growing interest is reflected by the reports on SWATH design which fill technical press.

This thesis is concerned with some hydrodynamic aspects of SWATH ships, mainly resistance performance in calm water and in waves and by implication, some motion aspects as well. The main objectives of the work presented in this thesis are 1) to develop an analytical tool which can give an improved prediction of SWATH ship resistance, 2) to compare the computational values of resistance with experimental results in order to verify the applicability of the tool and 3) on the basis of the computational and experimental analysis, to provide recommendations for the design of high performance SWATH ships with special reference to making feasible practical developments such as rectangular(with rounded corners) hulled SWATH ships.

Instead of the line source distribution commonly used for the submerged body of a SWATH ship, a plane source distribution is introduced in order to calculate wave-making resistance. This method is applicable to bodies with non-circular cross section. For this purpose, linearised wave theory and the linear superposition principle are effectively used due to the slenderness of the components of the SWATH ship. In addition, flat ship theory is applied to calculate the wave-making resistance of controllable fins which are essential to conventional SWATH ships in the light of pitch stability requirements.

Considering the total resistance of a SWATH ship in components of wave-making, frictional, appendage and additional drag(form effect, eddy, viscous pressure, wave-breaking and spray), two computer programs were written to predict the resistance of SWATH ships with and without fins. One deals with SWATH ships defined by mathematical formulae and the other is designed for SWATH ships defined in offset forms. The ITTC'57 frictional line is used to calculate the frictional resistance based on the Reynolds Number for the individual lengths of the components of a SWATH ship. Based on the difference between the calculated wave-making and measured residuary resistances, two curves of form resistance coefficient accounting

for the aforementioned additional drag are derived: one is intended for circular hulled SWATH ships and the other is applicable to non-circular hulled SWATH ships. These coefficients are compared with other published form effect correlations. Treating the resistance of controllable fins in profile, induced, hull-fin interference, tip and wave-making components, the drag of controllable fins is calculated. For this purpose, empirical formulae for foil sections and streamlined bodies are used for each component calculation. The experimental results of 9 SWATH models (three G.U models, two Polish models, one Chinese model and three NSRDC models) giving a total of 46 individual configurations are compared with the computational results. Also, the present predictions are compared with other published computational results.

In order to validate the developed theory, a large number of experiments with three SWATH models including a total of 24 configuration changes were conducted to measure the total calm water resistance at the Hydrodynamics Laboratory of Glasgow University. Two of the models are tandem strut configurations, one having circular cross section bodies, and the other having bodies of rectangular cross section with rounded corners. The third model is a single strut configuration with hulls of circular cross section. Mean sinkage and trim were measured to help improve the understanding of the speed-resistance characteristics of the SWATH models. This experimental data provides not only the validation of the theory developed but also empirical form correction factors. In addition, as part of research collaboration between the Dept of Naval Architecture and Ocean Engineering at Glasgow University and the Ship Hydromechanics Division of Gdansk Technical University(Poland), the calm water resistance test results of two Polish SWATH models(a total of 12 configuration changes) are included to provide a more useful database for theoretical investigations.

In order to investigate the hydrodynamic performances of the three SWATH models in waves, the experiments were conducted in regular head seas at the Laboratory. The constant velocity towing method was used due to its simplicity and accuracy compared to the constant thrust method. The measurements were taken of total resistance, motion responses(pitch, heave and surge), sinkage and trim in wave frequencies from 0.3 to 1.6 hz. Wave heights were varied to study the effect of wave steepness on the hydrodynamic performance of the models. Detailed comparisons between the single and tandem strut models and between the circular and rectangular

hulled SWATH models are made with regard to added resistance as well as motion responses. The resistance aug-ment due to the oncoming waves is derived by subtracting the still-water resistance from the total resistance in waves. The measured motion responses of the three models are compared with computational results from the computer program SWATHL which was developed at the Laboratory.

It is demonstrated that the present analytical tool gives excellent correlations with a wide range of SWATH configurations. Additionally, the effectiveness with which the computer program can be used in a resistance optimisation process is shown. This thesis also demonstrates that the hydrodynamic performance of SWATH vessels in waves is very much superior to that of equivalent monohulls. In contrast to conventional ships, there is little increase in the added resistance in waves of the SWATH models as speed increases. Further, in a range of speeds in the supercritical zone, a considerable degree of reduction in resistance occurs(as much as 24% of the calm water resistance) with the tandem strut models. For the same speed in waves, the powering requirement of the SWATH is around 60% less than that of the equivalent displacement Destroyer hull. Therefore, SWATH ships should be developed further at sea, emphasising the propulsion point of view and not only seakeeping benefits. It is also shown that a SWATH ship with hulls of rectangular cross section with rounded corners is superior to a circular hulled SWATH in terms of motion responses. resistance increase in waves, draft and construction cost. Therefore, a rectangular cross section hull is recommended for practical designs of SWATH ships up to moderately high speeds, without any serious penalty in resistance compared to the circular counterpart.

An analysis was carried of the 'sledge' bow concept introduced by the Polish experiments into their model designs. It is demonstrated that this technique can allow a SWATH ship to maintain level trim at high speeds without use of fins. This introduces the possibility of a radical breakthrough in SWATH design by removing the characteristic stabilising fins which cause substantial increase in weight and resistance and introduce control problems. With regard to this, further research on the 'sledge' concept is recommended.

NOMENCLATURE

GEOMETRY

$A(x)$ and A_m	Cross sectional area of body and its maximum, respectively
A_{wp}	Water plane area
AR	Effective aspect ratio
α	Angle between the tangential plane of body surface and x-axis
α_α	Angle of attack of fin
B_b	Breadth of body
2b	Spacing between the centreplanes of two demihulls
$B_1=4b/L_b$	Dimensionless spacing between two demihulls
c	Chord
C_f	Distance between the longitudinal centres of body and fin
C_s	Distance between the longitudinal centres of body and strut
C_{s1}	Distance between the longitudinal centres of body and 2nd strut
C_b	Block coefficient
C_p	Prismatic coefficient of body(hull)
$C_{w.p}$	Waterplane area coefficient of strut
D_b	Depth(height) of body(hull)
$D_s(h_s)$	Depth of strut
Di_b	Diameter of body
D1, D2	Depths(height) of the 2nd and 1st parallel sections for contoured body
ε	Perturbation parameter
F(x,y,z)	Boundary surface(free surface and body)
h(SDBC)	Submerged Depth to Body Centreline(SDBC)
h_f	Submerged depth to fin centreline
h_s , h_{s1}	Depth of strut and 2nd strut
$H_1=2h/Di_b$	Dimensionless submergence
l1, l2	Lengths of the 1st parallel section and transition section of contoured body

l_{be} , l_{br}	Entrance and run of body
l_{se} , l_{sr}	Entrance and run of strut
L_b	Length of body
Lc_f	Length of fin chord
L_s	Length of strut
$m(\xi,\eta,\zeta)$	Source strength
n	Unit normal vector
Pe	Perimeter
RC	Radius of rounded Corner of rectangular cross section body
S	Wetted area
S_{pl}	Plan form area
S_b	Sea bottom surface
S_f , S_{fo}	Free surface and undisturbed free surface(z=0 plane)
S_u , S_d	Vertical planes located far upstream and down stream
S_r , S_l	Vertical side planes at the far right and left side
S_{vw}	Surface of vertical plane
S_w , S_{wo}	Wetted surface of hull and its projected area on to y=0 plane
T	Draft
$t(x,z)$, $t_1(x,z)$	Half thickness distributions of strut and 2nd strut
T_f	Maximum thickness of fin
t_m	Maximum half thickness of strut
t_{mf}	Maximum Half thickness of fin
T_s	Maximum thickness of strut
x,y,z	Reference coordinate system
x',y', z'	Non-dimensionalised reference coordinate system
y=f(x,y,z)	Geometry form
$\zeta(x,y)$	Free surface elevation
∇	Displacement volume

FORCES

F	Force acting on body
R_o	Wave-making resistance of two demihull at infinate spacing
R_1	Wave-making resistance due to the presence of the other

	demihull
R_A	Aerodynamic drag
R_{AP}	Appendage resistance
R_{AW}	Added resistance due to waves
R_B	Wave-breaking resistance
R_E	Eddy-making resistance
R_F	Frictional resistance
R_{fm}	Form drag
R_{fs} , R_{fb} , R_{ff}	Frictional resistances of strut, body and fin, respectively
R_{HI}	Hull and fin interference resistance
R_I	Induced drag
R_S	Spray drag
R_T	Total resistance
R_{TI}	Tip drag
R_V	Viscous resistance
R_{VP}	Viscous pressure resistance
R_W	Wave-making resistance
R_{wb}, R_{ws}, R_{wsb}	Wave-making resistances of body, strut and interference between strut and body, respectively

NON - DIMENSIONAL COEFFICIENTS

C_A	Model ship correlation allowance
C_E	Eddy-making resistance coefficient
C_{fm}	Form drag coefficient
C_L	Lift coefficient
C_f	Frictional resistance coefficient
$C_{r.s}$,$C_{w.s}$, $C_{w.v}$, $C_{t.s}$, $C_{t.v}$	Residuary, wave and total resistance coefficient : s and v indicate that resistance is non-dimensionalised by $0.5\rho U^2S$ and $0.5\rho U^2\nabla^{2/3}$, respectively
$\sigma_{AW}=R_{AW}/\rho g\zeta_a^2\nabla^{1/3}$	Added Resistance Coefficient(A.R.C.)

VELOCITY

$Fn=U/\sqrt{gL}$	Froude number
$k_o=g/(U^2)$	Wave number
k_1, k_{1S} , k_{1f} , k_{1Sl}	Non-dimensional wave number
$Rn=UL/\nu$	Reynolds number
U	Steady velocity of model
u, v, w	Pertubation velocities in x, y, z directions, respectively
v	Velocity vector
ϕ	Perturbation potential ($u=-\partial\phi/\partial x$, $v=-\partial\phi/\partial y$, $w=-\partial\phi/\partial z$)
Φ	Total velocity potential(ϕ +Ux)

FLUID PROPERTIES

g=9.807	Acceleration due to gravity
ρ	Density of water
ν	Kinematic viscosity
p(x,y,z)	Fluid pressure given by Bernoulli's equation
p_o	Uniform pressure acting on a streamline

WAVE AND MOTION RESPONSES

$L_w(\lambda)$	Wave length
T_Z ,$T\theta$,$T\phi$	Natural periods of heave, pitch and roll, respectively
x_a	Surge amplitude
z_a	Heave amplitude
$X'=x_a/\zeta_a$	Dimensionless surge response
$Z'=z_a/\zeta_a$	Dimensionless heave response
ζ_a, ζ_w	Wave amplitude and height, respectively
θ_a	Pitch amplitude
$\Theta'=\theta_a g/\zeta_a\omega_e^2$	Dimensionless pitch response
ω	Wave frequency
ω_e	Encounter wave frequency
$\omega'=\omega\sqrt{L/g}$	Dimensionless wave frequency

MATHEMATICS

A_{bm} , B_{bm}	Coefficients of Chebyshev series for body
A_{sm} , B_{bm}	Coefficients of Chebyshev series for strut
A_{s1m} , B_{s1m}	Coefficients of Chebyshev series for 2nd strut
β	$k_1 \sec\theta$
β_s	$k_{1s} \sec\theta$
β_f	$k_{1f} \sec\theta$
$G(x,y,z; \xi,\eta,\zeta)$	Green's function
I , J	Real and Imaginary parts of integrand of wave-making resistance integrals, respectively,where subscript (in the text) s,b s 1 indicate the strut, body and second strut contributions
$j_m(\beta)$	Bessel function of the 1st kind with inte-ger order and argument (β)
$S_i(Y_i'')$	Spline function at i-th segment
$U_m(x)$, $V_m(x)$	Chebyshev cosine and sine series terms, respectively
T_{bmn}, W_{bmn}	Auxiliary wave resistance functions associated with body
T_{smn} ,W_{smn}	Auxiliary wave resistance functions associated with strut
T_{sbmn} , W_{sbmn}	Auxiliary wave resistance functions associated withbody-strut interference
T_{ss1mmn} , W_{ss1mn}	Auxiliary wave resistance functions associated with 1st and 2nd strut interference

LIST OF FIGURES

CHAPTER 1

CHAPTER 2

CHAPTER 3

CHAPTER 4

CHAPTER 5

LIST OF TABLES

CHAPTER 1

CHAPTER 4

CHAPTER 5

CHAPTER 1 INTRODUCTION

One of the challenges faced by the naval architect is to design hull forms which can achieve high speeds economically in smooth water and still exhibit good seakeeping qualities and minimum loss of speed in rough weather. Attempts to satisfy both criteria have encouraged the development of advanced vehicles such as Hydrofoil ships, Air Cushion Vehicles and Surface Effect Ships. These concept employ non-hydrostatic sources of lift at their operating speeds in order to reduce wave-making resistance. At the same time, extensive studies have been carried out to improve the capability and operability of conventional displacement ships[113]*. Other than further refinement and evolution of the typical monohull, alternative forms with the potential for improved performance may conveniently be classified in three categories(see Fig 1.1). The vertices of the triangle represent three distinct areas of development for displacement ships; semi-submerged ship, enlarged or slender ships, and variable draft ships. Each of these concepts has its own special particular advantages from the propulsion point of view.

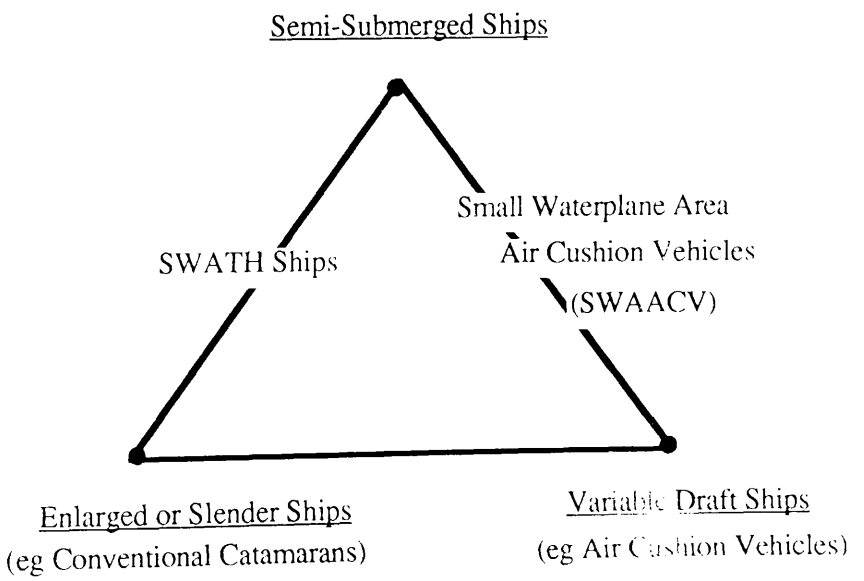

Fig.1.1 Extended Performance Displacement Ships Triangle

Semi-Submerged Ships : at comparatively high speeds, the semi-submerged ship

* References are listed on page 390

would become attractive owing to the reduced wave-making resistance.

Enlarged or Slender Ships : it is known that wave-making resistance is proportional to the square of the breadth of a ship. Thus, a vessel with a narrow beam(or increased length) is subject to less wave formulation and accordingly less wave-making resistance.

Variable Draft Ships : such a vessel may be designed to operate at optimal drafts for different speeds, in order to reduce propulsion power.

As well as these distinct concepts outlined, interest in hybrids which combine the virtues of two of the design philosophies is also growing. An outstanding example of this approach is the SWATH ship, which draws on the benefits of increased slenderness and submerged buoyancy.

The concept of the SWATH(Small Waterplane Area Twin/Triple Hull) ship has attracted considerable attention in the past two decades. Numerous advantages are claimed for the concept, including excellent motion characteristics at rest and underway, a high speed capability in waves, large deck area and greater design flexibility compared to its counterpart monohull. Today the interest in SWATH ships is rapidly growing and this is well reflected by the large number of publications on the subject in the technical press. The Royal Institution of Naval Architects(RINA) sponsored the first symposium(1985)[91] dedicated solely to SWATH and a second SWATH symposium is to be held in November 1988, sponsored by the same organisation. Also, one session of the International High-Performance Vehicle Conference sponsored by the Chinese Society of Naval Architecture and Ocean Engineering in Shanghai November 1988 will be dedicated to SWATH. The United States and Japan are the acknowledged leaders in the development and practical application of the SWATH concept. However, numerous leading shipbuilding countries worldwide including the U.K, Netherlands, Canada, China, West Germany, Italy, Poland and the Republic of Korea are currently involved with SWATH design and many are close to acquisition. There is therefore little doubt that the number of SWATH vessels(currently 11 at sea) will be significantly increased in a few years.

Although it is only in the last two decades or so that significant developments have been made in the design and construction of this type of vessel, the idea is not new. Tracing the origin of SWATH ships from the twin sources of multi-hulled ships and submerged hull ships, MacGregor[112] illustrates the development of this type of vessel from the ancient Polynesian(Pacific Islands) multi-hulls through the floating airport designs of Creed to the first modern SWATH ship(KAIMALINO). There is no doubt that the early European explorers were impressed by the seaworthyness and speed of the Pacific Multihulls compared to those of their own cumbersome ships.

The philosophy used in the design of the SWATH is that of placing as much as possible of the buoyancy well below the free surface. In this way there is less structure at the waterplane(Small Waterplane Area) subject to wave excitation. The main part of buoyancy for a SWATH is located in twin torpedo like hulls, placed well below the free surface, on each of which one or more surface piercing struts support an above superstructure. The strut(s) are so streamlined as not to create much wave-making resistance and provide a small waterplane area resulting in very large natural motion periods, in particular for angular responses(pitch and roll)[86]. Combined with the deeply submerged buoyancy, these increased natural periods lead to much reduced motion responses in operational sea states compared to equivalent monohull ships. However, at large wave lengths such as swell and in some following seas the motion response may be increased.

Due to the small size of the waterplane, the low hydrostatic restoring capability may allow a SWATH to be unstable, in particular, to permit a severe bow trim at high speeds. This is because the so called Munk moment, which is proportional to the heave added mass times the square of the ship speed, can far exceed the restoring pitch moment[87]. Hence, stabilising fins have been introduced to the design of SWATH ships to ensure dynamic pitch stability. These stabilising fins also provide much increased hydrodynamic damping which further significantly reduces motion responses in heave, pitch and roll, in particular, at resonant frequencies[72,88].

The seakeeping advantage of small waterplane area is provided at the expense of the major weakness of very low TPC(tonnes per centimetre immersion) so that SWATH ships can not compete with conventional monohull type of ships for missions

where a high payload is required. Also, the deep submergence of the hulls implies a deep draft, which can prohibit SWATHs of moderate size from use of many harbours. In order to improve the TPC, strut thickness can be increased at the cost of the resistance and non-circular cross sectional hulls such as rectangular with rounded corners can be introduced in order to reduce draught[90]. The increase of the strut thickness improves access into the hulls and increases the static stiffness without increasing beam[89]. The non-circular cross section hulls offer enhanced seakeeping performance due to large added mass and damping compared to the circular case, thus also contribute to reduce the resistance increase in waves[90].

Model experiments and full scale operations of existing SWATH ships[75,109,110] have demonstrated the advantages claimed for SWATH ships over similar sized conventional ships, and indicated that some of the disadvantages can be alleviated by relatively simple means. However, since the first SWATH 'KAIMALINO'[110] was launched in 1973, there have been very few further SWATH ships built. Table 1.1 lists the 11 existing SWATH ships in the universe at the time of writing.This is very much in contrast to the flood of SWATH designs currently appearing in the international technical journals.With regard to this, Warren(in discussing Ref.[111]) raised the question ' are there any grey areas left in the performance of the SWATH concept which would make a naval architect hesitate to use it more widely ?'.

One of the possible reasons for this hesitation may simply be the limited market for SWATH ships(high speed ferries, warships, oceanic research vessels, salvage support tugs and a number of offshore engineering roles etc). However, Allen and Holcomb[111] suggested that there are not more SWATH ships at sea because of the historical conservatism of the naval community. Also, it must be acknowledged that the image of the SWATH concept has been harmed by unrealistic design proposals from some of its advocates[112].

Apart from such possibilities, practical cause for hesitation on the part of ship owners and operators is not hard to find. Owing to the small number of existing SWATH ships, and the consequent lack of design data and construction experience

NAME	DATE	LOA (m)	BOA (m)	DISP (ton)	MAX speed(kts)	DRAFT (m)	STRUT (type)	HULL TYPE	MISSION	BUILT BY
KAIMALINO	1973	27.10	14.17	193/224	25/18	4.66	Twin	Simple, Circular	Workboat Demonstrator	U.S Coast Guard
MARINE ACE	1977	12.35	6.50	18.4/22.2	15.4	1.55	Twin/ Single	Simple, Elliptical	Experimental	Mitsui/Japan
MESA 80/ (SEAGULL)	1979	35.90	17.10	343	27.1	3.15	Single	Simple, Elliptical	Fast Passenger/ Ferry	Mitsui/Japan
OHTORI	1980	27.0	12.5	239	20.6	3.40	Single	--	Hydrographic/ Survey	Mitsubishi/ Japan
KOTOZAKI	1980	27.0	12.5	236	20.5	3.20	Single	Simple, Elliptical	Hydrographic/ Survey	Mitsui/Japan
SUAVE LINO	1981	19.2	9.10	53	18.0	2.13	Single	Simple, Circular	Fishing Boat/ Demonstrator	U.S Private
KAIYO	1984	61.55	28.0	3500	13.25	6.3	Single	Non-simple/ Elliptical	Diving Support	Mitsui/Japan
HALCYON	1985	18.29	9.14	432	18.0	2.13	Single	Simple/ Cylindrical	Demonstrator	RMI(U.S)
MARINE WAVE	1985	15.10	6.20	20	18.2	1.6	Single	Simple, Elliptical	Leisure/ Demonstrator	Mitsui/Japan
SUN MARINA	1987	15.05	6.4	--	---	1.6	Single	----	Leisure Cruiser	Mitsui/Japan
CHUBASCO								Contoured		U.S

Table 1.1 The Main Particulars of Existing SWATH Ships

together with a limited understanding of hydrodynamic performance, concern about the feasibility and cost of producing successful vessels of this type is understandable.

The large number of design variables associated with the SWATH geometry, such as shape of hulls and struts, individual dimensions and relative proportions, and the complex hydrodynamic interferences between the various components make the task of optimum design difficult. The greater freedom in the SWATH design arising from the many parameters implicit in the concept gives the designer more choice than his monohull counterpart.Consequently, the designer who does not have a full understanding of the hydrodynamic characteristics of the SWATH form will face more difficulty than the conventional ship naval architect. The scarcity of validated design techniques and tools ensures that growth in the necessary design skills is limited to very few centres of excellence. Outwith these establishments, real expertise is difficult to develop and so a well founded broad base of competitive interests which would allow for rapid practical development does not exist.

This thesis is concerned with the development and validation of practically useful theoretical tools for use in the design of SWATH ships. Specifically, this thesis deals with some hydrodynamic aspects of SWATH ships, mainly resistance in calm water and in waves and by implication, some motion aspects also. The main objectives of the work presented in this thesis are

1) to develop an analytical tool which can give an improved prediction of SWATH ship resistance,

2) to compare the computed results of resistance with experimental results in order to verify the applicability of the tool and

3) on the basis of the computational and experimental analysis, to provide recommendations for the design of high performance SWATH ships, particularly with regard to developing practical SWATH ship designs such as those with hulls of rectangular cross section with rounded corners.

The content of this thesis and its order of presentation is briefly summarised below

In Chapter 2, since a SWATH ship is a specific form of a catamaran, utilising the linearised wave theory and Green's theorem, the formula for wave-making resistance of a catamaran is derived based on momentum analysis. This is compared with that derived according to Lagally's theorem. Then, the derived general formulae are applied to SWATH ships having single and tandem struts on each demihull. For this purpose, a plane source distribution is introduced which is applicable to non-circular cross section bodies. This technique is compared with results using the line source distribution for three slender bodies of different cross section which have the same x-directional variation of cross section (dA(x)/dx), displacement and mean submerged depth. The results show that the present plane source approach gives different values for the different shapes of cross section while the line source distribution erroneously gives the same results for each section. Furthermore, for the same circular cross sectional body, the present approach gives values as much as 20-25% higher than the line source method depending on the submergence of the body. This phenomenon is due to the fact that the contribution to the wave-making of the part of the submerged body near to the free surface is taken into account by the present plane source distribution, but not by the line source distribution. In addition, flat ship theory is applied to calculate the wave-making resistance of stabilising fins which are characteristics of conventional SWATH ships in the light of pitch stability requirements. Based on the derived mathematical resistance formulae, general conclusions as to the effect on the wave-making resistance of parametric changes in breadth, length, bow shape, draft, and strut position on the demihull are drawn in an attempt to provide a useful understanding of, and general guidance on, the design of SWATH ships without resorting to the tedious numerical calculation of the formulae involved.

In Chapter 3, considering the total resistance of a SWATH ship in components of wave-making, frictional, appendage and additional drag(form effect, eddy, viscous pressure, wave-breaking and spray) , two computer programs(MSWATH and OSWATH) were written to estimate the total resistance of SWATH ships with and without fins. MSWATH is written for SWATH ships defined by mathematical formulae and OSWATH is designed for SWATH ships defined in offset forms. Based on the

wave-making resistance formulae derived in Chapter 2, the calculation procedures for the wave-making resistance for SWATH ships defined by mathematical formulae are shown in detail. Also, utilising the cubic spline curve fitting technique, the final wave-making resistance integrals, which will be integrated numerically by means of computer, are derived for SWATH ships defined in offset forms. Using the ITTC'57 frictional line, the frictional resistance is calculated based on the individual length of the components of a SWATH ship. The computational results are compared with the experimental results measured in the department using three SWATH models(SWATH1, SWATH2 and SWATH3). Also, these are compared with experimental results and computational results available in the open literature. Based on the difference between the calculated wave-making and measured residuary resistances, two curves of form resistance coefficient accounting for the aforementioned additional drag are derived: one is intended for circular hulled SWATH ships and the other is applicable to non-circular hulled SWATH ships. These coefficients are then compared with other published form effect correlations. Subdividing the resistance of controllable fins into profile, induced, hull-fin interference, tip and wave-making components, the resistance of controllable fins are calculated. For this purpose, empirical formulae for foil sections and streamlined bodies are used for each component calculation. In dealing with induced drag, the free surface effect is introduced. Then, the estimated total resistance including the form and fin resistances are compared with the experimental results for the SWATH1 model with a pair of fins and the SWATH-395 model with two pair of fins. This chapter includes the comparison of the two computer programs(MSWATH and OSWATH) together with some accounts of restrictions in their applications.

Chapter 4 is concerned with experimental work with three SWATH models(SWATH1, 2 and 3) including 24 individual configurations. The SWATH1 and SWATH2 models are tandem strut configurations and the former has circular cross section bodies and the latter has rectangular cross section(with rounded corners) bodies. The SWATH3 model is a single strut configuration with circular cross section bodies. All the experiments were conducted at the Hydrodynamics Laboratory of Glasgow

University. The constant velocity towing method was used due to its simplicity and accuracy compared to the constant thrust method. The measurements were the resistance, sinkage and trim in calm water and resistance increase, motion responses(heave, pitch and surge), sinkage and trim in regular head waves. Wave frequencies from 0.3 to 1.6 hz were investigated and wave heights were varied to study the effect of the wave steepness on the hydrodynamic performances of the SWATH models. Rigorous comparisons of calm water resistance between the single and tandem struts models and between the circular and rectangular hulled SWATH models are made. Also, detailed comparisons between them are made with regard to added resistance as well as motion responses. The added resistance due to the oncoming waves is derived by the still-water resistance from the total resistance in waves. The measured motion responses of the three models are all compared with the computational results from the computer program SWATHL[85] which was developed at the Laboratory.

As part of research collaboration between the Dept of Naval Architecture and Ocean Engineering of Glasgow University(G.U) and the Ship Hydromechanics Division of Gdansk Technical University(G.T.U), Poland, two series of model tests to measure the total resistance in calm water using two models. SWATH-386 and SWATH-395, were carried out at GTU and their analysis and comparison with computational results were conducted at G.U by the author and presented in Chapter 4. The test series included various changes in configurations of strut system, modifications of bow struts as well as of lower hulls and two spacings between the centrelines of the two demihulls which result in a total of 14 conditions. The experiments were aimed at obtaining an optimum strut system in terms of resistance and at finding a hull shape which could help prevent severe bow trim at high speeds and so permit stabilizing fins to be removed. The latter purpose was achieved by introducing a 'sledge bow' concept.

In Chapter 5, some parametric studies which were not covered in the experimental work are systematically performed. In order to investigate the resistance variations caused by altering parameters in SWATH design, a number of variables which are most

important in the design of SWATH ships with regard to resistance are covered: Spacing of the two demihulls, strut position on the demihull, number of struts(up to three) on the demihull, strut length and shape(simple and contoured), body shape(simple and contoured) and body cross section shape(circular, elliptical and rectangular with rounded corners), body breadth/depth ratio, radius of rounded corners for the rectangular cross section and draft etc. Also, the contribution of controllable fins to total resistance is investigated in detail. Additionally, in order to demonstrate the capability of the present analytical tool, it is employed to find 'optimum' configurations for a 2405 tonne SWATH ship at the two speeds of 8 knots(operating speed) and 14 knots(maximum speed). This work can be seen as illustrating the state-of-the-art in SWATH resistance studies as presented in this thesis. Finally, the resistance performance of the SWATH3 model is compared with those of equivalent monohulls(Destroyer DE-1006(C_b=0.49), Series-60(C_b=0.6 and C_b=0.7) in calm water and in regular waves. It is clearly demonstrated how well the SWATH ship can advance through waves compared with equivalent monohulls, in terms of speed reduction and of power increase.

Detailed findings and conclusions are drawn at the end of each chapter and finally, Chapter 6 concludes this thesis together with some recommendations for future study.

CHAPTER 2 FORMULATION OF WAVE-MAKING RESISTANCE

2.1 INTRODUCTION

Even though there are some problems such as viscosity-wave interaction, scale and form effects, Froude's method of extrapolation from model to full scale vessel is still in use today with some minor modifications. The total model resistance is divided into two independent parts, frictional resistance and residuary resistance, and these two parts are then extrapolated to full scale based on their own scale laws. The latter consists mainly of wave-making resistance but includes some form effects. Since the frictional resistance is simply calculated from an equivalent flat plate which has the same length and wetted area as the ship, it is of prime importance to determine the residuary resistance and in particular wave-making resistance.

Since Michell's pioneering work at the end of the 19th century[38] the problem of wave-making resistance has long been the subject of research by many naval architects and scientists in the field. To the author's knowledge, Havelock in 1936 considered for the first time the hydrodynamic interference of two bodies and derived the wave-making resistance of two bodies which travel abreast of each other, one behind the other and in a semi-eschelon position[28]. Srettensky[29] in 1936 formulated the wave-making resistance of a ship moving in an infinitely deep canal of a given width. Later in 1972, Chapman[1] utilised the Srettensky's formula in order to calculate the wave-making resistance of SWATH ships.

Following the two leading works, the wave-making resistance characteristics of catamaran or multi-hulled vessels have been studied by many investigators such as Lunde in 1951[30], Eggers in 1955[31], Lackenby and Slater in 1968[32], Everest in 1968[33], Lin in 1974[34], and Rich et al in 1985[35] etc. Their studies are all based on the linearised wave-making resistance theory and they, with the exception of Lin, treated only the effect of wave interference between two demihulls.

The resistance problem for a catamaran is far more complicated than that of a monohull since some interference effects between the two demihulls are to be expected. In general, these are regarded as a sum of two effects: wave interference and body(displacement) interference. Good accounts of these two interferences were given

by Pien[36], and the followings is a summary from that reference.

Wave interference arises from the superposition of two wave systems, each created by a demihull. The two wave systems sometimes reinforce and sometimes cancel each other and thus increase or decrease the wave-making resistance of a catamaran. Since the demihulls of a catamaran are close to one another, the flow around each hull is no longer symmetrical and a flow across the keel line will occur. Such a cross flow creates severe eddying and may result in an increase of the residuary resistance. This interference exists even in the absence of a free surface and thus is called a body or displacement interference. When a cross flow exists, each demihull acts as a thick foil with very low aspect ratio. Associated with the lift of such a foil there is an induced drag. A demihull operating in the curved flow created by the other demihull is similar to a single, cambered hull that is towed at angle of attack or yaw angle. Based on this idea and introducing an effective hull form, Pien developed a catamaran hull form design procedure.

All the aforementioned investigators treated the demihull of a catamaran as two separate but identical thin ships and the velocity potential of the problem was obtained from two sheet distributions of Havelock sources. In order to account for the asymmetric flow field around each hull, Lin[34] considered the distribution of doublets normal to the sheets which extended to infinitely in the downstream wake region. Using the so-called zero-Froude Number Green's function and assuming low draft-to-length ratio and small hull separation distance to length ratio approximations, general formulae for the force and moment expressed in terms of these singularity distribution densities were derived in an extended form of Lagally's theorem for thin lifting bodies making a uniform motion in the free surface. As an application of the derived formulae to SWATH ships, observing that the main body of a SWATH demihull has a round shape and its transverse dimension is wider than that of the strut, he assumed that the wake may be neglected in the initial investigation since a SWATH demihull is less likely to behave as a lifting surface compared to a conventional catamaran. Also he added that ' such an approach does not represent a serious compromise in accuracy since, as a consequency of linearisation, the effect of the wake may be superimposed on the results of the initial investigation as a later refinement, if necessary.'.

Based on the two sheets of distribution of Havelock sources on the centreplanes

of two demihulls, Chapman[1] introduced a line source distribution for the submerged body of a SWATH ship. Following this work, the wave-making resistance of SWATH ships have been investigated by such researchers as Lin[34], Salvesen et al in 1985[5] and Huang in 1987[6].

Although the line source distribution has been known to be, within the first order approximation, valid for any cross section slender body[37], it should be noted that a line source generates a body of revolution. Further,when this line source distribution is applied to a SWATH ship with non-circular cross sectional bodies associated with some strut combination, a wrong estimation of the wave-making resistance will be obtained. Fig.2.1-a shows typical cross sections of a SWATH ship which have a circular or elliptical cross section body. As shown in the figure, a point source generates an exact circle and hence, when this is applied to the non-circular hulled SWATH, the lower part of the strut, as cross-hatched in the figure, will be overlapped with the circular body which is generated by the line source. Accordingly, the virtual strut length for this problem is l_1, but the true strut length l is used to calculate the wave-making resistance which results in the cross-hatched part in the figure being considered twice and leads to a wrong estimation of the wave-making resistance. When a circular cross section hulled SWATH is considered, this problem will be automatically removed.

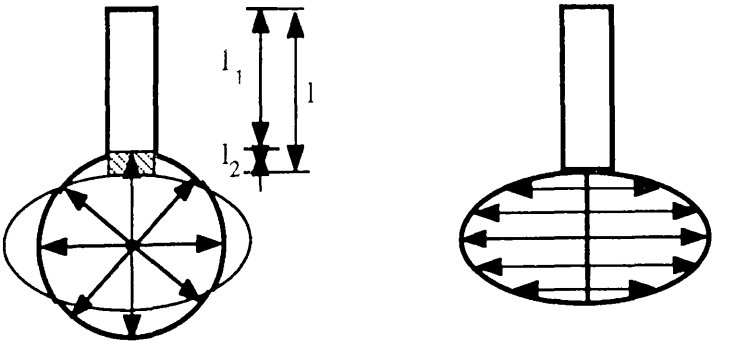

a) point source distribution b) a plane source distribution

Fig.2.1 typical Cross Section Hulls of a SWATH Ship Generated by a Point and Plane Source Distributions

Since interest in non-circular cross section hulled SWATH ships has increased due to some advantages over the circular hulls, it was felt necessary to develop

alternative theoretical tools to predict the wave-making resistance of non-circular SWATH ships rather than using the line source distribution technique. Therefore, using a plane source distribution on the centreplane of the body, as shown in Fig.2.1-b, the depth effect of the submerged body is considered and treated in detail in section 2.7.2.

As a SWATH ship is a specific form of a catamaran, this chapter begins with the formulation of exact boundary conditions for a ship moving along a deep vertical wall. Based on the systematic small perturbation parameter expansion, the first order(linearised) and second order boundary conditions are then derived. After obtaining the Green's function induced by a unit strength source which travels steadily along the deep vertical wall, the velocity potential which is induced by the source systems representing a given geometry is derived using Green's theorem in the fluid domain. After this,the wave resistance formula of a catamaran is derived based on momentum analysis and compared with that derived according to Lagally's theorem.

In section 2.7, using the linear superposition principle, it is shown how the derived general formulae are applied to SWATH ships having single and tandem struts on the demihull. Deriving a plane source approximation for the submerged body, the result is compared with the result using the line source distribution for three slender bodies which have the same x-directional variation of cross section, dA(x)/dx, displacement and mean submerged depth but different cross sections. The result shows that, as expected, the present plane source approach gives different values for the different shapes of cross section while the line source distribution gives the same results for each section. Furthermore, for the same circular cross sectional body the present approach gives values as much as 20-25% higher than the line source method depending on the submergence of the body. This phenomenon is due to the fact that the contribution to the wave-making of the part of the submerged body near to the free surface is taken into account by the present plane source distribution, but not by the line source distribution.

Since the contribution of stabilising fins to resistance seems to be substantial, the wave-making resistance formula of a fin is derived based on the flat ship approximation. For this purpose, it is assumed that the fin is attached to the submerged body at zero angle of attack.

Lastly, based on the derived mathematical resistance formulae, general

conclusions from them as to the effect of parametric changes in breadth, length, bow shape, draft and strut position on the demihull on the wave-making resistance are drawn in an attempt to provide a quick understanding of and general ideas on the design of SWATH ships in terms of resistance without resorting to the tedious numerical calculation of the formulae involved.

Throughout the work, linearised procedures have been used and only the wave interference is considered. It has been known that the existing linearised wave-making theory cannot always produce accurate results except in special cases such as very thin or slender ships.However, it has provided valuable guidance for the improvement of resistance performance as well as for the development of experimental work. Linearised wave-making theory shows good correlation with experimental results for SWATH models mostly due to the fact that they have very thin and slender demihulls which well satisfy the assumptions of the theory[34]. Also, it would appear that the aforementioned lifting effect is less important to SWATH configurations.

2.2 FORMULATIONS OF BOUNDARY CONDITIONS

In order to consider any analytical approach to the wave-making resistance of a ship, the boundary conditions should first be outlined. The problem for a twin hull, which advances abreast another at a small distance, can be approached in the way of a hull advancing along a vertical wall. In addition, as the slenderness of each component of a SWATH ship is much smaller than that of a conventional monohull ship, linearised boundary conditions obtained from the exact non-linear boundary conditions can be effectively used.

2.2.1 Assumptions, Co-ordinate System and Exact Boundary Conditions

As it is assumed that the fluid is inviscid and incompressible and that the fluid motion is steady and irrotational, the problem can be treated as a boundary value problem for potential flow. In addition, the flow has zero surface tension which means that the surface waves generated are mainly governed by the gravitational force. The cartesian reference co-ordinate system which is fixed in a moving body is used in such

a way that 0-xy plane coincides with the undisturbed free surface, the z-axis is directed in the opposite direction of gravity force and y-axis is directed to port, as shown in Figure 2.2

Assuming that a surface body advances through otherwise still deep water in the positive direction of the x-axis at a constant speed U and that the body is not free to move except in the forward direction, the velocity potential of the flow motion caused by the moving body can be expressed as:

$$\Phi = Ux + \phi\,(x,y,z) \tag{2.1}$$

where $\phi\,(x,y,z)$ is the disturbed velocity potential due to the existence of the body and Ux is due to the oncoming uniform flow. The continuity equation for potential flow leads to Laplace's equation:

$$\nabla^2\phi = \frac{\partial\phi^2}{\partial x^2} + \frac{\partial\phi^2}{\partial y^2} + \frac{\partial\phi^2}{\partial z^2} = 0 \tag{2.2}$$

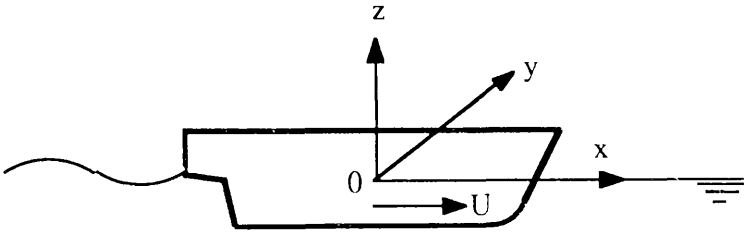

Figure 2.2 Reference co-ordinate system

Since this equation has many solutions due to its elliptic nature, some boundary conditions should be defined in the domain concerned in order to obtain the exact solution.

If the geometry of a body and the elevation of the disturbed free surface are expressed, respectively, as:

$$y = f(x,z) \tag{2.3}$$

$$z = \zeta\,(x,y) \tag{2.4}$$

exact boundary conditions to satisfy equation (2.2) will be as follows:

a. On the free surface $F = z - \zeta\,(x,y)$

1. Kinematic condition ; DF/Dt = 0

$$(U + \phi_x) \zeta_x + \phi_y \zeta_y - \phi_z = 0 \tag{2.5}$$

2. Dynamic condition

$$g\zeta + U\phi_x + \frac{1}{2} (\phi_x^2 + \phi_y^2 + \phi_z^2) = 0 \tag{2.6}$$

b. On the surface of the moving body F = y – f(x,z); DF/Dt = 0

$$(U + \phi_x) f_x - \phi_y + \phi_z f_z = 0 \tag{2.7}$$

c. Sea bottom condition

$$\lim \phi_z = 0 \tag{2.8}$$

d. Radiation condition : the function ϕ approaches the uniform stream potential on the far down stream side and there are no waves on the far upstream side. Symbolically:

$$\lim_{x \to \infty} \phi = 0 \quad \text{and} \quad \lim_{x \to -\infty} \phi = Ux \tag{2.9}$$

In addition, if a ship travels along a vertical wall located at y=b, there is no flow across the wall and hence, the wall boundary condition should be added:

e. Wall boundary condition

$$\phi_y = 0 \qquad \text{at } y=b \tag{2.10}$$

Since the aforementioned boundary conditions are highly non-linear and the elevation of the free surface ζ is not known a priori, it is very difficult and quite complicated to obtain the velocity potential which satisfies fully the non-linear boundary conditions. Furthermore, the fact that the wetted area of the moving body is instantaneously changing makes the problem mathematically intractable.

2.2.2 Various Approaches to Solving the Problem

Since Michell's pioneering work at the end of the 19th century[38], many of the most eminent scientists in the field have been trying to solve the problem in various

ways. In large, three general methods of approach to the problem can be seen from a huge number of published papers regarding the subject. Firstly, both the free surface and body boundary conditions are linearised. The linearisation means that all the quadratic terms appearing in the boundary conditions are assumed to be sufficiently small to be negligible compared to the first order terms. Secondly, the body boundary condition is described exactly while the free surface is linearised, which is called Neumann-Kelvin problem. Lastly, both the body and free surface boundary conditions are fully described in non-linear forms.

Since the panel source distribution method developed by Hess and Smith in 1962[39] turned out to be successful for flows without a free surface, this method have been extensively introduced for the calculation of the potential flow with the free surface. Recently, thanks to the advent of powerful computer hardware, the 3-D panel method including the locally or fully non-linear boundary conditions has been a challenge to computational hydrodynamicists. Instead of using the traditional Kelvin source, Gadd introduced simple Rankine sources that cover the hull and part of the undisturbed free surface[40,41]. Since then, quite considerable progress has been made and the state of the art can be seen from the two workshops held at DTNSRDC in 1979[42] and 1983[43]. Seo in 1985[44] and Xia in 1986[45] have attempted to solve the fully non-linear problem using Rankine sources distributed on the wetted surface of the body as well as on the exact free surface. The basic idea is that an iterative procedure is applied starting with an initial estimate of the wave elevation and of the velocity potential and then using the derived estimates for the next iteration until they satisfy the exact boundary conditions. Very recently, Ni in 1987[46] introduced a higher order panel method in which the panel is supposed to be a parabolic quadrilateral with a linearly varying source density. For these 3-D non-linear numerical procedures, the stability and convergence of the iterative processes has posed serious problems as well as being expensive in computation time.

On the other hand, the aforementioned 3-D non-linear panel method should be distinguished from higher order perturbation theory. Of course, in the higher order perturbation theory, non-linear terms appearing in the boundary conditions are included, but its approach to tackling the problem is different from the aforementioned 3-D direct approach by means of the computer. Instead of assuming the smallness of the perturbed velocity compared to the speed of the body so that the quadratic terms in

the boundary conditions can be eliminated, which is the so called linearised theory treated by Michell[38], Havelock[47] and many others, a systematic development of the solution of the problem by a power series of a small parameter was introduced by Peters and Stoker in 1957[48]. The first order term of the power series is known to be the same as the linearised solution. Using the small perturbation parameter, the problem can be solved systematically in a step by step fashion starting from the known lower order to as high an order as necessary and hence, the discrepancy between the theory and experiment can be expected to be eliminated. However, the solution becomes increasingly complicated as the order rises and the non-uniformity of the expansion near the bow and stern where the gradient of the geometry is not negligible has not been resolved[49].

Although linearised theory is faced with limited success in estimating the resistance of ships due to its assumptions, in particular, small beam to length ratio, several linearised theories such as thin ship, slender ship, flat ship and slow ship etc, have been extensively used for providing ship forms with low resistance as well as for quantitatively estimating the resistance of such specific types of ship. For a SWATH and catamaran type ships whose components have very small slendernesses and thinness compared to the monohull, a linearised theory can be effectively used. A fairly general approach to the linearisation can be based on the aforementioned systematic perturbation expansion scheme. Based on a small perturbation parameter, the linearised, first order and second order body and free surface boundary conditions are derived in the following section.

2.2.3 Linearisation Procedure Based on the Perturbation Expansion

The basic idea behind the perturbation expansion is as follows : The turbulent velocity potential (ϕ), which is induced by a uniformly moving body through the free surface or near the free surface, should be dependent on the body form factor. If ϕ is assumed to be a function of a body form, ie f_1, it can be also assumed that ϕ becomes small as f_1 becomes small and that ϕ disappears as f_1 approaches to zero. If f_1 is used as the perturbation parameter which is small, ϕ can be expressed as the following series.

$$\phi(x,y,z;\varepsilon) = \varepsilon\,\phi^{(1)}(x,y,z) + \varepsilon^2\phi^{(2)} + \varepsilon^3\phi^{(3)} + \cdots\cdots = \sum_{i=1}^{n} \varepsilon^i \phi^{(i)} \tag{2.11}$$

and the free surface elevation can be expressed as:

$$\zeta(x,y;\varepsilon) = \varepsilon\,\zeta(x,y)^{(1)} + \varepsilon^2\zeta^{(2)} + \varepsilon^3\zeta^{(3)} + \cdots\cdots = \sum_{i=1}^{n} \varepsilon^i \zeta^{(i)} \tag{2.12}$$

where $\phi^{(i)}$ and $\zeta^{(i)}$ are the i-th order velocity potential and free surface elevation, respectively.

There are various methods to express the ship form factor as the perturbation parameter; the thinness, slenderness, flatness, submergence and slow speed of the ship. Firstly, one can take $\varepsilon = B/L$. As this ratio approaches zero, the plane approaches zero thickness, which is the so called thin ship theory, so that the turbulent velocity may be neglected. Secondly, we can take $\varepsilon = T/L$ which is called flat ship theory and applies to forms such as high speed motor boats with nearly flat bottoms[50]. Thirdly, one can take both the beam-length ratio and draft-length ratio to be small which is known as slender body theory[51]. Next, for a submerged body, the submerged depth of the body is assumed so large that the turbulent effect on the free surface is small and ε is taken as the reciprocal of the submerged depth. Lastly, the ratio of the disturbance velocity to the forward speed U is small which is known as slow ship theory.

In the present study of SWATH ships whose struts and bodies are similar to the thin ship and the slender body, respectively, the thin ship approach is used based on the small perturbation parameter $\varepsilon=B/L$. Since the slender body approximation is a limited case of the the thin ship approximation[52], it can be derived from the known thin ship approximation by restricting the draft-length ratio to be small.

When the body geometry given by eq.(2.3) is expressed as:

$$y = \varepsilon\, f(x,z) \tag{2.13}$$

in a consistent manner, one can express the velocity potential given by eq.(2.11) in a Taylor series on the mean free surface z=0 as follows.

$$\phi(x,y,z;\varepsilon) = \varepsilon [\, \phi^{(1)}(x,y,0) + \phi_z^{(1)} z + \phi_{zz}^{(1)} \frac{z^2}{2!} + \cdots]$$

$$+ \varepsilon^2 [\, \phi^{(2)} + \phi_z^{(2)} z + \phi_{zz}^{(2)} \frac{z^2}{2!} + \cdots]$$

$$+ \varepsilon^3 [\, \phi^{(3)} + \phi_z^{(3)} z + \phi_{zz}^{(3)} \frac{z^2}{2!} + \cdots] + 0[\varepsilon^4] \tag{2.14}$$

Replacing z by the free surface elevation defined by equation (2.12) and rearranging the above equation in terms of the increasing power of ε, we obtain:

$$\phi(x,y,z;\varepsilon) = \varepsilon \phi^{(1)} + \varepsilon^2 [\, \phi^{(2)} + \zeta^{(1)} \phi_z^{(1)}]$$

$$+ \varepsilon^3 [\, \zeta^{(2)} \phi_z^{(1)} + \phi^{(3)} + \zeta^{(1)} \phi_z^{(2)} + \frac{1}{2} \zeta^{(1)^2} \phi_{zz}^{(1)}] + 0[\varepsilon^4] \tag{2.15}$$

Differentiating the above equation respect to x, y and z and substituting these derivatives into the kinematic free surface condition given by eq.(2.5), we obtain the first and second kinematical free surface conditions:

$$\varepsilon;\ U \zeta_x^{(1)} - \phi_z^{(1)} = 0 \qquad \text{on } z=0 \tag{2.16}$$

$$\varepsilon^2;\ U \zeta_x^{(2)} - \phi_z^{(2)} = - \phi_x^{(1)} \zeta_x^{(1)} - \phi_y^{(1)} \zeta_y^{(1)} + \phi_{zz}^{(1)} \zeta^{(1)} \qquad \text{on } z = 0 \tag{2.17}$$

In a similar way, from eq.(2.6), the first and second order dynamic free surface conditions are obtained:

$$\varepsilon;\ g\zeta^{(1)}(x,y) + U \phi_x^{(1)} = 0 \qquad \text{on } z=0 \tag{2.18}$$

$$\varepsilon^2;\ g\zeta^{(2)} + U\phi_x^{(2)} = - \frac{1}{2} [\, \phi_x^{(1)^2} + \phi_y^{(1)^2} + \phi_z^{(1)^2}] - U\zeta^{(1)} \phi_{xx}^{(1)} \quad \text{on } z = 0 \tag{2.19}$$

From eqs.(2.16) and (2.18) and eqs.(2.17) and (2.19), the combined first and second order free surface conditions are obtained as.

$$\varepsilon;\ \phi_{xx}^{(1)} + k_0 \phi_z^{(1)} = 0 \qquad \text{on } z = 0 \tag{2.20}$$

$$\varepsilon^2;\ \phi^{(2)}_{xx} + k_0\phi^{(2)}_z = -\frac{1}{U}\frac{\partial}{\partial x}\left[\ \phi^{(1)^2}_x + \phi^{(1)^2}_y + \phi^{(1)^2}_z\ \right]$$

$$+\frac{1}{U}\phi^{(1)}_x\frac{\partial}{\partial z}\left[\frac{U^2}{g}\phi^{(1)}_{xx} + \phi^{(1)}_z\right] \qquad \text{on } z = 0 \tag{2.21}$$

where $k_0 = g/U^2$ is the wave number.

The velocity potential given by eq.(2.11) can also be expanded into a Taylor series on the body centreplane y=0 and it is obtained in terms of increasing power of ε as:

$$\phi\ (x,y,z\ ;\ \varepsilon\ ) = \varepsilon\ \phi^{(1)}(x,0,z) + \varepsilon^2[\ \phi^{(2)} + f\ \phi^{(1)}_y\ ]$$

$$+\varepsilon^3\ [\ \phi^{(3)} + \phi^{(1)}_{yy}\frac{f^2}{2!} + f\ \phi^{(2)}_y\ ] + 0[\varepsilon^4] \tag{2.22}$$

Differentiating the above velocity potential with respect to x, y and z and substituting the derivative potentials into the body surface condition given by eq.(2.7), we obtain the first and second order body boundary conditions as :

$$\varepsilon\ ;\ \phi^{(1)}_y = U\ f_x(x,z) \qquad \text{on } y = 0 \tag{2.23}$$

$$\varepsilon^2;\ \phi^{(2)}_y = f_x\phi^{(1)}_x + f_z\phi^{(1)}_z - f\ \phi^{(1)}_{yy} \qquad \text{on } y = 0 \tag{2.24}$$

As given by eqs.(2.20) and (2.23), the free surface and body boundary conditions are both linearised as the first order terms of the power series which are the same as Michell's thin ship approximation. From the known first order solution the second order approximations given by eqs.(2.21) and (2.24) can be obtained and so on. Using these first and second order boundary conditions, the wave-making resistances for simple mathematical geometries were calculated and compared with each other[53].

2.3 GREEN'S FUNCTION

The turbulent velocity potential induced by a unit strength source, at the point $(\xi,0,\zeta)$, which travels through the still, open and deep water steadily at the constant speed U is written as[30] :

$$G_I(x,y,z) = \frac{1}{r_1} - \frac{1}{r_2} - \frac{k_0}{\pi}\int_{-\pi}^{\pi} \sec^2\theta \, d\theta \int_0^{\infty} \frac{e^{k[i\varpi + (z+\zeta)]}}{k - k_0\sec^2\theta + i\mu\sec\theta} \, dk$$

(2.25)

$$r_1^2 = (x-\xi)^2 + y^2 + (z+\zeta)^2$$

$$r_2^2 = (x-\xi)^2 + y^2 + (z-\zeta)^2$$

$$\varpi = (x-\xi)\cos\theta + y\sin\theta$$

where μ is the Rayleigh artificial viscosity proportional to the relative velocity which is introduced to fix the pole of the integration in the complex plane and it is allowed to go to zero after finishing the integration. Notwithstanding its simplicity and infallibility, some investigators consider this as a cheap trick[49] while Wehausen give more fundamental statements for this[54]. The above velocity potential, which is generally known as Kelvin or Havelock source potential, satisfies the linearised free surface boundary condition given by eq.(2.20), the bottom boundary condition given by eq.(2.8) and the radiation condition given by eq.(2.9).

Now, if a point source advances along a vertically infinite deep wall, the velocity potential which satisfies the wall boundary condition given by eq.(2.10) should be found. Since there is no flow across the wall, located at y=b, the reflecting(image) method can be used. The velocity potential for a moving unit strength source at the reflected point (ξ, 2b, ζ) is given by :

$$G_{II} = \frac{1}{r'_1} - \frac{1}{r'_2} - \frac{k_0}{\pi}\int_{-\pi}^{\pi} \sec^2\theta \, d\theta \int_0^{\infty} \frac{e^{k[i\varpi' + (z+\zeta)]}}{k - k_0\sec^2\theta + i\mu\sec\theta} \, dk \qquad (2.26)$$

where

$$r'^2_1 = (x - \xi)^2 + (y - 2b)^2 + (z + \zeta)^2$$

$$r'^2_2 = (x - \xi)^2 + (y - 2b)^2 + (z - \zeta)^2$$

$$\varpi' = (x - \xi) \cos\theta + (y - 2b) \sin\theta = \varpi - 2b \sin\theta$$

The summation of eqs.(2.25) and (2.26) leads to the velocity potential for a unit strength source moving along the wall located y=b :

$$G = G_I + G_{II}$$

$$= \frac{1}{r_1} - \frac{1}{r_2} + \frac{1}{r'_1} - \frac{1}{r'_2}$$

$$- \frac{k_0}{\pi} \int_{-\pi}^{\pi} \sec^2\theta \, d\theta \int_0^{\infty} dk \frac{e^{k (z + \zeta) + i k \varpi}}{k - k_0 \sec^2\theta + i \mu \sec\theta} (1 + e^{- i 2kb\sin\theta}) \qquad (2.27)$$

The above velocity potential satisfies all the boundary conditions including the wall boundary, but not the body surface condition, and will be used to obtain the velocity potential induced by the distributed sources representing a given body geometry. The equation includes the local non-oscillatory flows which disappear at a short distance from the ship as well as the regular oscillatory flows which travel far downstream. Since the wave making resistance is associated with the expenditure of energy in generating mostly the regularly travelling waves, the expression of eq.(2.27) at far downstream should be found first. The first four terms of the equation disappear at far downstream and the last integral term can be changed as :

$$N = - \frac{k_0}{\pi} \int_{-\pi}^{\pi} \sec^2\theta \, d\theta \int_0^{\infty} \frac{e^{k (z + \zeta) + i k \varpi}}{k - k_0 \sec^2\theta + i \mu \sec\theta} dk$$

$$= - \frac{k_0}{\pi} \int_0^{\pi/2} \sec^2\theta \, d\theta \int_0^{\infty} [\Psi_1(k,\theta) + \Psi_2(k,\theta) + \Psi_3(k,\theta) + \Psi_4(k,\theta)] e^{k (z + \zeta)} dk$$

$$\left.\begin{matrix}\Psi_1(k,\theta)\\ \Psi_2(k,\theta)\end{matrix}\right\} = \frac{e^{i\,k\,[\,(x-\xi)\cos\theta \pm (y-2b)\sin\theta\,]}}{k - k_0\sec^2\theta + i\,\mu\,\sec\theta}$$

$$\left.\begin{matrix}\Psi_3(k,\theta)\\ \Psi_4(k,\theta)\end{matrix}\right\} = \frac{e^{-i\,k\,[\,(x-\xi)\cos\theta \pm (y-2b)\sin\theta\,]}}{k - k_0\sec^2\theta - i\,\mu\,\sec\theta} \qquad (2.28)$$

The above integrations are performed in a complex plane as shown in Fig.2.3. The path of the integration varies with the sign of the power of the exponent and consists of two parts, namely, contour A and B. The detailed calculations are reported in Ref.[55] and the final result is taken as:

$$G \approx -8\,k_0 \int_0^{\pi/2} \sec^2\theta\, e^{k_0\sec^2\theta\,(z+\zeta)} \sin[\,k_0(x-\xi)\sec\theta\,]\cos(k_0 y\sec^2\theta\sin\theta)$$

$$[\,1+\cos(2k_0 b\sec^2\theta\sin\theta)\,]\,d\theta \quad \text{at far down stream} \qquad (2.29)$$

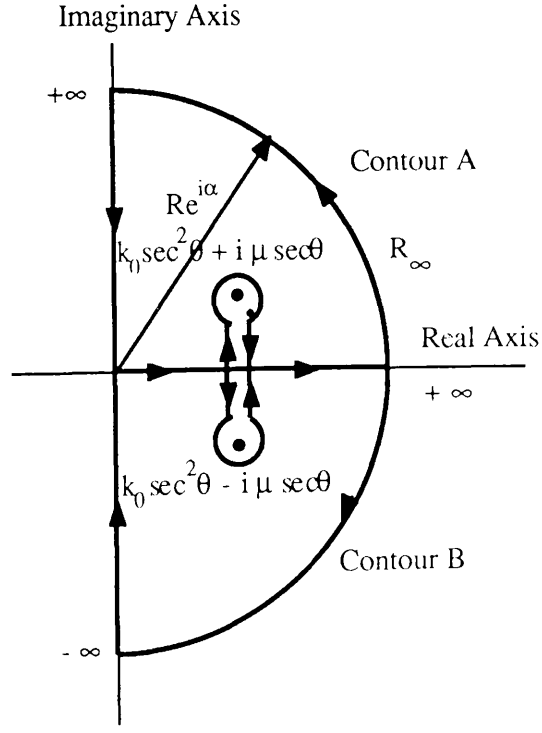

Fig 2.3 Integration Contour in the Complex Plane

2.4 DETERMINATION OF THE VELOCITY POTENTIAL BY GREEN'S THEOREM

To determine the velocity potential which is induced by the source system representing a given body geometry, Green's Theorem as given by[56].

$$\phi(p) = \frac{1}{4\pi} \iint_{\partial R} [\, \phi_n G(p\,;\,q) - \phi\, G_n \,]\, ds(q) \tag{2.30}$$

where p indicates a point (x,y,z) in the fluid domain and q is a source distributed point (ξ,η,ζ), is applied to the control volume surrounded by the control surfaces as shown in Fig.2.4. S_u and S_d denote vertical planes located far upstream and downstream of the body, respectively. S_b denotes the bottom surface corresponding to $z \to -\infty$, $S_{v.w}$ the vertical wall, S_r and S_l vertical side planes at the far right and left sides, respectively, S_f the free water surface and S_w the wetted surface of the body.

Considering the normal direction on each surface, eq.(2.30) becomes as

$$\begin{aligned}
\phi(x,y,z) = {} & \frac{1}{4\pi} \iint_{S_u} (\phi_\xi G - \phi\, G_\xi)\, d\eta\, d\zeta - \frac{1}{4\pi} \iint_{S_d} (\phi_\xi G - \phi G_\xi)\, d\eta\, d\zeta \\
& + \frac{1}{4\pi} \iint_{S_{v.w}} (\phi_\eta G - \phi\, G_\eta)\, d\xi\, d\zeta - \frac{1}{4\pi} \iint_{S_r} (\phi_\eta G - \phi\, G_\eta)\, d\xi\, d\zeta \\
& - \frac{1}{4\pi} \iint_{S_b} (\phi_\zeta G - \phi G_\eta)\, d\xi d\eta + \frac{1}{4\pi} \iint_{S_{fo}} (\phi_\zeta G - \phi G_\zeta)\, d\xi d\eta \\
& + \frac{1}{4\pi} \iint_{S_{wo}} (\phi_\eta G - \phi\, G_\eta)\, d\xi\, d\zeta + \frac{1}{4\pi} \iint_{S_l} (\phi_\eta G - \phi\, G_\eta)\, d\xi\, d\zeta
\end{aligned} \tag{2.31}$$

where the free surface (S_{fo}) and the body surface (S_{wo}) is assumed z=0 and y=0, respectively, and where the linearisation procedure has already been applied in section 2.2.3. Because of the wall boundary condition, bottom boundary condition and radiation conditions at far fields, the contributions from S_u, S_d, $S_{v.w}$, S_r, S_l and S_b to the velocity potential are all disappeared. The above equation is therefore reduced to the following;

$$\phi(x,y,z) = \phi_I(x,y,z) + \phi_{II}(x,y,z)$$

$$= \frac{1}{4\pi}\iint_{S_{fo}} (\phi_\zeta G - \phi G_\zeta)\, d\xi\, d\eta$$

$$+ \frac{1}{4\pi}\iint_{S_{wo}} (\phi_\eta G - \phi G_\eta)\, d\xi\, d\zeta \qquad (2.32)$$

where ϕ_I and ϕ_{II} denote the free surface and wetted surface contribution, respectively.

2.4.1 Free Surface Contribution

Using the linearised free surface condition given by eq.(2.20) and integrating ϕ_I partially with regard to ξ, the following equation will be obtained:

$$\phi_I = \frac{1}{4\pi k_0}\int_{L_0} (\phi_\xi^{(1)} G - \phi^{(1)} G_\xi)\, d\eta - \frac{1}{4\pi k_0}\int_{L} (\phi_\xi^{(1)} G - \phi^{(1)} G_\xi)\, d\eta \qquad (2.33)$$

where L_0 denotes the intersection between the body surface and the free surface and L the intersection between the free surface and the bounding vertical surfaces, S_u, S_r, S_d and $S_{v.w}$. From the radiation condition, it can be understood that the contributions from the surfaces, S_u, S_r, S_d, disappear. Again, if the image ship is considered, the line integration along the vertical wall will be cancelled out and the remaining part, the first integral part in the above equation, will be doubled. However, since a ship travelling along the vertical wall is considered here, the above equation will be kept and at the end, the resistance of two demihulls will be two times that of a single demihull.

In addition, the order of the first integral of eq.(2.33) is higher than the first order so that it can be assumed to be negligible. Even though it is included in the second order term, the line integral contribution becomes zero[53] so that it is possible to discard it without losing any legitimacy. As a result, as far as the first order approximation or linearised theory is concerned, the free surface contribution to the velocity potential is zero.

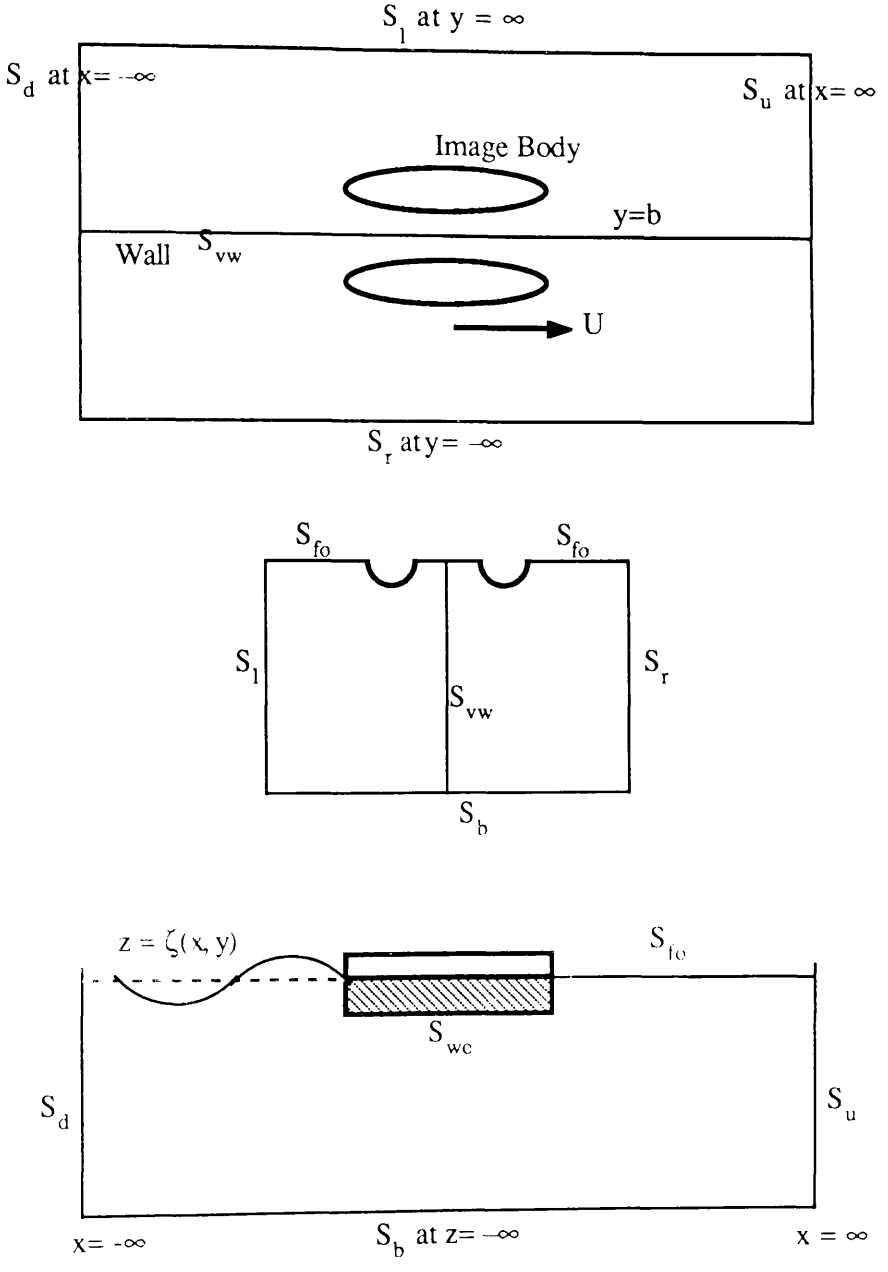

Fig 2.4 Control Surfaces

2.4.2 Body Contribution

Considering that the unit normal vector **n** changes its direction on opposing sides

of the body and using the linearised body boundary condition given by eq.(2.23), the body contribution part in eq(2.32) will be :

$$\phi_{II}=\frac{1}{4\pi}\iint_{S_{wo}}[\quad Uf_{\xi}(G^{+}+G^{-})-\phi\,(G_{\eta}^{+}-G_{\eta}^{-})\,]\,d\xi\,d\zeta \tag{2.34}$$

Using the Taylor expansions of ϕ, G and G_{η} on $\eta = 0$, and making use of the relationship $G^{+} + G^{-} = 2G(x,y,z\,;\,\xi,0,\zeta)$, the above expression will be of the following form:

$$\phi_{II}(x,y,z) = +\frac{U}{2\pi}\iint_{S_{wo}} f_{\xi}G(p\,;\,\xi,0,\zeta)\,d\xi\,d\zeta \tag{2.35}$$

where , as in the previous procedure, the higher order terms have already been discarded.

Consequently, to the first order approximation, the only contribution to the velocity potential is the projected body surface on the y = 0 plane and the form is from eq.(2.35) :

$$\phi\,(x,y,z) = +\frac{U}{2\pi}\iint_{S_{wo}} f_{\xi}G(p\,;\,\xi,0,\zeta)\,d\xi\,d\zeta \tag{2.36}$$

2.5 WAVE RESISTANCE ACCORDING TO MOMENTUM THEOREM

The wave resistance experienced by a moving body in a perfect fluid is given by the integration of x-directional components of the fluid dynamic pressure over the body's surface :

$$R_{w} = -\iint (p - p_{0})\,n_{x}\,ds \tag{2.37}$$

However, the fluid motion near the ship surface is so complicated that it is quite difficult to obtain the exact velocity potential very near the ship's surface. Michell[38] obtained his mathematical formula by way of a Fourier transform as the form :

$$R_{w} = -\iint_{S_{wo}} (p - p_{0})\frac{\partial f}{\partial x}\,dx\,dz \tag{2.38}$$

To avoid the difficulty in solving the potential flow very close to the ship surface,

many researchers including Havelock[58] and Lunde[30] have solved this problem by the energy method and momentum analysis. For these methods it is necessary only to know the fluid motion in the region far from the ship. It has been proved that these methods give results which coincide with each other.

From the known fact that the rate of change of momentum of the fluid bounded by the closed surfaces is the same as the force acting on the control surfaces, the wave resistance formula is written as [53]:

$$R_w = \frac{\rho}{2} \int_{-\infty}^{\infty} \int_{-\infty}^{0} [(\frac{\partial \phi}{\partial y})^2 + (\frac{\partial \phi}{\partial z})^2 - (\frac{\partial \phi}{\partial x})^2] \, dy \, dz + \frac{\rho U^2}{2g} \int_{-\infty}^{\infty} (\frac{\partial \phi}{\partial x})^2_{z=0} \, dy \tag{2.39}$$

In order to solve the above equation, eqs.(2.29) and (2.36) are used. Changing the integral limit of eq.(2.29) to (-π/2, π/2) and substituting the equation into eq.(2.36), the following expression will be obtained:

$$\phi(x,y,z) = \frac{-2k_0 U}{\pi} \int_{-\pi/2}^{\pi/2} d\theta \sec^2\theta \, [1 + \cos(2k_0 b \sec^2\theta \sin\theta)] \, e^{k_0 \sec^2\theta (z+\zeta)}$$

$$\iint \phi_\xi \sin[k_0(x-\xi) \sec\theta] \cos(k_0 y \sec^2\theta \sin\theta) \, d\xi \, d\zeta$$

$$= \frac{-2k_0 U}{\pi} \int_{-\pi/2}^{\pi/2} d\theta \sec^2\theta \, [1 + \cos(2k_0 b \sec^2\theta \sin\theta)] \, e^{k_0 \sec^2\theta z}$$

$$[I \sin(k_0 \varpi \sec^2\theta) - J \cos(k_0 \varpi \sec^2\theta)] \tag{2.40}$$

where

$$I = \iint f_\xi e^{k_0 \sec^2\theta \zeta} \cos(k_0 \xi \sec^2\theta) \, d\xi \, d\zeta$$

$$J = \iint f_\xi e^{k_0 \sec^2\theta \zeta} \sin(k_0 \xi \sec^2\theta) \, d\xi \, d\zeta$$

$$\varpi = x \cos\theta + y \sin\theta$$

Substituting eq.(2.40) into eq.(2.39) and using the Fourier double integral theorem, the ultimate wave resistance formula will become of the form:

$$R_w = \frac{4\rho g k_0}{\pi} \int_0^{\pi/2} d\theta \sec^3\theta \, [\, 1 + \cos(2k_0 b \sec^2\theta \sin\theta)] \, (I^2 + J^2)$$

$$I + i J = \iint_{S_{wo}} dx \, dz \, f_x(x,z) \, e^{k_0 \sec^2\theta \, (z + i \, x \cos\theta)}$$

(2.41)

This is the wave resistance experienced by the demihull moving along the vertical wall and hence, the wave resistance of a catamaram (twin body) will be twice this result. Dividing the above equation into two terms, the wave resistance experienced by a catamaran whose distance between the centreplanes of two demihulls is 2b is written as :

$$\begin{aligned} R_w &= R_0 + R_1 \\ &= \frac{8\rho g k_0}{\pi} \int_0^{\pi/2} d\theta \, (I^2 + J^2) \sec^3\theta \\ &\quad + \frac{8\rho g k_0}{\pi} \int_0^{\pi/2} d\theta \cos(2k_0 b \sec^2\theta \sin\theta) \sec^3\theta \, (I^2 + J^2) \end{aligned}$$

(2.42)

where R_0 is the wave resistance of two demihulls in infinite isolation and R_1 is the additional resistance due to the presence of the other demihull. The interference factor of the cosine term in the integral of the above equation varies from -1 to 1 mathematically. Consequently, the wave resistance of a catamaran is at the least zero and at the most four times the resistance of one demihull. Also, it should be noticed that if the two hulls of the catamaran merge together, ie b=0, the wave resistance is twice that of the catamaran whose spacing between the two demihulls is infinite, ie $b \rightarrow \infty$. This is explained due to the fact that the derived resistance formula is based on the linear superposition. Since the interference factor is a function of the speed and of the spacing distance of the two demihulls, it will be noticed that some advantages can be taken from a special combination of two demihulls at a particular speed.

2.6 WAVE RESISTANCE ACCORDING TO LAGALLY'S THEOREM

Lagally's Theorem has been used to calculate the forces upon any body which forms a closed body[59]. Hence, it should be applicable to a fully submerged body. However, since, to the first approximation wave theory , the contribution of the interfacing line between the free surface and the surface floating body to the velocity potential is zero, as stated in section 2.4.1, this theory can be applied to a floating body. The force acting on a source of strength m in a flow is given by:

$$\mathbf{F} = -4\pi\rho\, m\, \mathbf{v} \tag{2.43}$$

where $\mathbf{v}$ is the velocity vector of the source at the position. Thereby the total wave resistance experienced by the uniformly moving body, which is generated by a continuous distribution of sources over a finite part of the vertical plane y=0, through the still water will be the integral summation of the forces over the plane. Thus:

$$R_w = -4\pi\rho \iint m(\xi,0,-\zeta)\, u\, d\xi\, d\zeta \tag{2.44}$$

where u is the x-component of the fluid velocity at a source point $(\xi,0,-\zeta)$.

The velocity potential for a source system, distributed over the vertical plane y=0, moving along the vertical wall, which is located at y=b, will be from eqs.(2.1) and (2.27) :

$$\Phi = Ux + \iint \left(\frac{1}{r_1} - \frac{1}{r_2} + \frac{1}{r'_1} - \frac{1}{r'_2}\right) m\, d\xi\, d\zeta$$

$$-\frac{k_0}{\pi} \iint m\, d\xi\, d\zeta \int_{-\pi}^{\pi} \sec^2\theta\, d\theta \int_0^{\infty} dk \frac{e^{k(z+\zeta)+i\varpi}}{k - k_0\sec^2\theta + i\mu\sec\theta} \left(1 + e^{-i\,2kb\sin\theta}\right) \tag{2.45}$$

After differentiating the above equation with regard to x and substituting it into eq.(2.44), the contribution of the various terms to the wave making resistance is examined. The first term representing the uniform stream disappears since the total source strength is zero. The second term also disappears since the source and sinks cancel with their image system when the integration is carried out. Therefore, the only part contributing to the wave resistance is the x-derivative of the last term in eq.(2.45). Substituting its derivative into eq.(2.44), the following expression will be obtained:

$$R_w = i\,4\rho k_0 \iint m'\,d\xi'\,d\zeta' \iint m\,d\xi\,d\zeta \int_{-\pi}^{\pi} \sec\theta\,d\theta$$

$$\int_0^{\infty} \frac{e^{-k(\zeta'+\zeta)+ik(\xi'-\xi)\cos\theta}}{k - k_0\sec^2\theta + i\mu\sec\theta}\,(1 + e^{i\,2kb\sin\theta})\,k\,dk \qquad (2.46)$$

The integral part with regard to θ and k in the above equation can be changed to the following form:

$$N = \int_{-\pi}^{\pi} \sec\theta\,d\theta \int_0^{\infty} \frac{e^{-k(\zeta+\zeta')+ik[(\xi'-\xi)\cos\theta + 2b\sin\theta]}}{k - k_0\sec^2\theta + i\mu\sec\theta}\,k\,dk$$

$$= \int_0^{\pi/2} \sec\theta\,d\theta \int_0^{\infty} [\,\Psi_1(k,\theta) + \Psi_2(k,\theta) - \Psi_3(k,\theta) - \Psi_4(k,\theta)\,]\,dk \qquad (2.47)$$

where

$$\left.\begin{matrix}\Psi_1(k,\theta)\\ \Psi_2(k,\theta)\end{matrix}\right\} = \frac{e^{ik[(\xi'-\xi)\cos\theta \pm 2b\sin\theta]}}{k - k_0\sec^2\theta + i\mu\sec\theta}\,k$$

$$\left.\begin{matrix}\Psi_3(k,\theta)\\ \Psi_4(k,\theta)\end{matrix}\right\} = \frac{e^{-ik[(\xi'-\xi)\cos\theta \pm 2b\sin\theta]}}{k - k_0\sec^2\theta - i\mu\sec\theta}\,k$$

The integration of eq.(2.47) can be performed in the same way as in eq (2.28) and the final result for a twin hull ship will be :

$$R_w = 32\pi\rho k_0^2 \int_0^{\pi/2} d\theta\,(I^2 + J^2)\sec^3\theta\,[\,1 + \cos(2k_0 b\sec^2\theta\sin\theta)\,] \qquad (2.48)$$

$$I + iJ = \iint m\exp(ik_0 x\sec\theta + z\,k_0\sec^2\theta)\,dx\,dz \qquad (2.49)$$

As mentioned earlier, if a body is assumed to be a very thin and vertically infinite plate, the body can be generated by a source- sink distributions on the plane y = 0. This is known as the thin ship approximation and the strength is known as :

$$m(x,0,z) = -\frac{U}{2\pi}\frac{\partial f}{\partial x} \tag{2.50}$$

Therefore, eq.(2.49) will be :

$$I + i\,J = -\frac{U}{2\pi}\iint \frac{df}{dx}\exp(\,i\,k_0 x\,\sec\theta + z\,k_0\sec^2\theta\,)\,dx\,dz \tag{2.51}$$

Substituting the above equation into eq.(2.48), it is easily understood that the result is the same as eq.(2.42) which is derived by momentum analysis.

2.7 APPLICATION TO SWATH SHIPS

A typical demihull of a SWATH ship consists of an elongated, slender body with pointed ends and single or double streamlined thin strut(s) with usually uniform thickness vertically. In addition to the wave interference between two demihulls as in the catamaran ship and as given by the second part of eq.(2.42), it is, therefore, expected that other interference effects between the submerged body and the strut and further, between the forward and aft struts for a tandem strut SWATH will occur. These interference effects can be derived from eq.(2.49) based on the linear superposition principle.

For a single strut SWATH configuration, eq.(2.49) can be determined by:

$$I + i\,J = (\,I_B + I_S\,) + i\,(\,J_B + J_S\,) \tag{2.52}$$

Since this contribution to the resistance appears in the square form in eq.(2.48),

$$\begin{aligned} I^2 + J^2 &= (\,I_B + I_S\,)^2 + (\,J_B + J_S\,)^2 \\ &= I_B{}^2 + J_B{}^2 + I_S{}^2 + J_S{}^2 + 2\,(\,I_B\,I_S + J_B\,J_S\,) \end{aligned} \tag{2.53}$$

Similarly, for a tandem strut SWATH configuration,

$$\begin{aligned} I^2 + J^2 = {} & I_{SF}^2 + J_{SF}^2 + I_{SA}^2 + J_{SA}^2 + I_B^2 + J_B^2 \\ & + 2\,(\,I_{SF}\,I_B + J_{SF}\,J_B + I_{SA}\,I_B + J_{SA}\,J_B + I_{SF}\,I_{SA} + J_{SF}\,J_{SA}\,) \end{aligned} \tag{2.54}$$

where the indices S, SF, SA and B stand for strut, forward and aft struts, and body, respectively. From eqs.(2.53) and (2.54), it is found that the total wave resistance of the demihull of a SWATH ship consists of the resistances of the body and strut(s), plus

extra resistances. These extra resistances are interference resistances between strut(s) and body and between the struts due to the existence of the wave interference between the components of the SWATH ship.

In order to calculate eq.(2.49) for each component of a SWATH ship, the source strength m(x,0,z) should be determined by the boundary condition at the surface of each geometry. Since a typical strut is a wall sided, streamlined thin shape, the well known thin ship approximation given by eq.(2.50) can be applied to the strut and eq.(2.51) is rewritten:

$$I_S + i\,J_S = -\frac{U}{2\pi}\iint \frac{\partial f}{\partial x}\exp\left(i\,k_0 x\sec\theta + z\,k_0\sec^2\theta\right)dx\,dz \tag{2.55}$$

where f(x,z) is the geometry and for the wall sided strut, equals the half thickness, t(x).

2.7.1 Slender Body Approximation.

At the early stages of SWATH development, circular cross sections were mostly considered as the lower demihull and a slender body approximation has been adopted to generate this circular cross section hull.

Based on eq.(2.55), Chapman[1] simplified the equation using the concept of a line source distribution along the centreline of the body. The integral over z in the equation is replaced by the approximation as follows:

$$\int \frac{\partial f}{\partial x}\exp\left(z\,k_0\sec^2\theta\right)dz = \exp\left(k_0 h\sec^2\theta\right)\int \frac{\partial f}{\partial x}dz$$

$$= \exp\left(k_0 h\sec^2\theta\right)\frac{1}{2}\frac{dA(x)}{dx} \tag{2.56}$$

where h is the submerged depth of the body centreline from the undisturbed free surface(mean submerged depth). Hence, eq.(2.55) is reduced to the single integral form for the body,

$$I_B + i\,J_B = -\frac{U}{4\pi}\exp\left(k_0 h\sec^2\theta\right)\int \frac{dA}{dx}\exp\left(ik_0 x\sec\theta\right)dx \tag{2.57}$$

According to the above equation, the wave resistance of the body depends only on the mean submerged depth of the body and on the longitudinal distribution of displacement regardless of its shape in the cross section. Therefore, the line source

distribution is valid only for a circular cross sectional body since a point source generates the exact circle. As mentioned in the introduction,all computer programs developed so far are based on the above two approximations, eqs. (2.55) and (2.57).In particular, when this line source distribution is applied to non-circular SWATH ships, as mentioned in the introduction, a wrong estimation of the wave-making resistance for such SWATH ships will be obtained. Therefore, in order to predict the differences in the wave resistance of different cross sectional bodies such as circular, elliptical and rectangular cross sections with rounded corners etc, the line source distribution is not suitable.Since the designs of non-circular cross section hulled SWATH ships have increased due to some advantages over circular hulls, it was felt necessary to develop a theoretical tool to predict the differences in the resistance for the different cross section bodies. To achieve this objective a new approach utilizing a plane source distribution is derived from eq. (2.49).

2.7.2 Utilization of a Plane Source Distribution

Assuming that a uniform source strength of m(x,0,z) is distributed over the infinitesimally small surface $D_b dx$, and that the surface inclination of the body is negligible (usual for the slender and thin ship approximations), the total strength can be written as $4\pi m D_b dx$ at the section of x, where D_b is the maximum depth of the body . The boundary condition at the body surface is

$$\frac{\partial \phi}{\partial n} = - U \sin\alpha \tag{2.58}$$

where n denotes the outward normal to the body surface and α is the angle between the tangential plane of the body surface and x-axis. If the projection of n on a plane perpendicular to the x-axis is expressed as $n'=n\cos\alpha$, the above boundary condition becomes

$$\frac{\partial \phi}{\partial n'} = - U \tan\alpha \tag{2.59}$$

The outward flux through the surface, cdx where c is the mean contour of the body surface for an element of length of dx, is expressed as

$$\int_c \frac{\partial \phi}{\partial n'} dcdx = -U \int_c \tan\alpha dcdx \tag{2.60}$$

Using the relation of $dA(x)/dx=\int_c \tan\alpha dc$ and the fact that the total outward flux must be equal to the total flux from the sources in the plane, the source strength becomes

$$m = -\frac{U}{4\pi D_b} \frac{dA(x)}{dx} \tag{2.61}$$

If D_b is replaced by the half breadth of the body, the strength is the same as Maruo's slender body approximation[51]. Using the above equation, eq. (2.49) becomes for the body:

$$I_B + i J_B = -\frac{U}{4\pi D_b} \iint \frac{dA(x)}{dx} \exp (ik_0 x \sec\theta + z k_0 \sec^2\theta) dxdz \tag{2.62}$$

Now, comparing eqs (2.57) and (2.62), the difference is apparent. In order to demonstrate this, Fig 2.5 shows the wave resistance variations of three slender bodies ,which have the same x-directional variation of cross sectional areas, dA(x)/dx, displacements and mean submerged depths, versus Froude Number. According to the figure, the present approach gives different values for different shapes of cross section while the line source distribution gives the same results for each section. Furthermore, for the same circular cross sectional body the present theory gives values as much as 20-25% higher than the line source method depending on the submergence of the body. Above a body submergence of around three times the depth of the body, the two source distributions give nearly the same results as each other. This phenomenon is due to the fact that the contribution to the wave-making of the part of the submerged body near to the free surface is taken into account by the present plane source distribution, but not by the line source distribution. Again, this is demonstrated by the fact that the wave resistance of the horizontally elliptical body of revolution is less than that of the circular cross sectional body at the same mean draft despite its larger breadth. This proves that the present approach is successful, within the approximation, in predicting the differences in the wave resistance of different cross sectional bodies which the line source distribution can not.

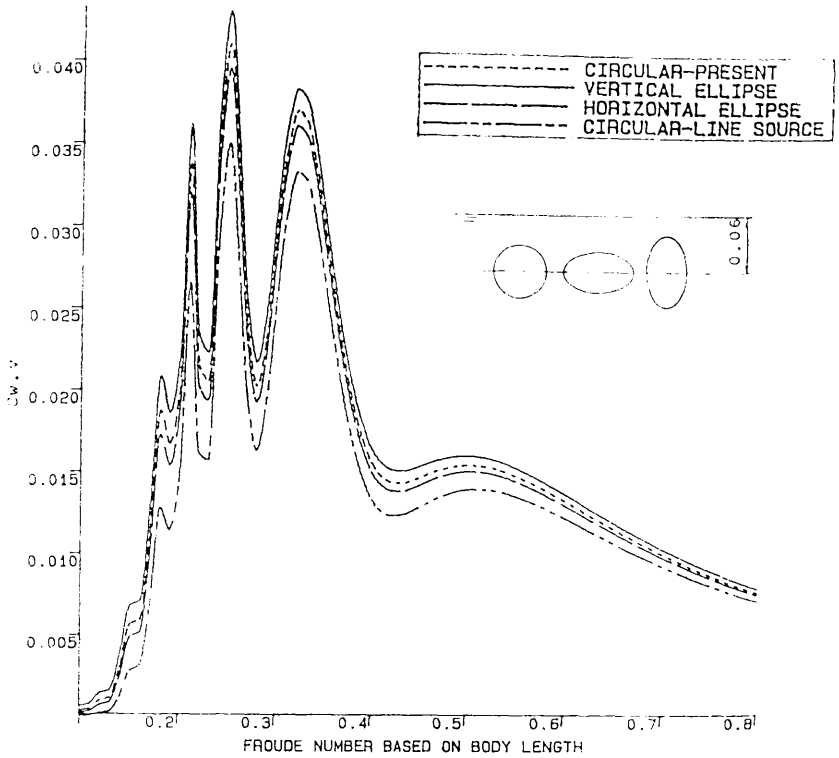

Fig.2.5 Wave Resistance Coefficient Variations of Three Submerged Bodies of VariousCross Sections at Fixed Submerged Depth to Body Centreline (Same Cross Sectional Area),L_b=1.5m, SDBC(h)=0.06m, C_p=0.921 Axis Dimension: Circular(0.0892,0.0892), Vertical(0.0792,0.1005). Horizontal(0.1005,0.0792)

2.7.3 Flat Ship Approximation

Due to its pitch instability at higher speeds, stabilising fins seem to be inevitable for the SWATH ship design and a pair of fins are fitted near either one end of the submerged bodies or in some cases both ends. Since an airfoil or a similarly shaped flat body has been used for the fin and placed well below the free surface, the contribution of the fin itself to the total wave-making resistance seems to be small. However, it is likely that these fins create interference wave systems with the components of the SWATH ship, in particular, with struts, and that the resistance increase caused by the interference wave system with the struts is not small.

If assuming that a fin has uniform thickness in the spanwise direction and that thickness-chord ratio is small, the problem can be approached based on the flat ship

approximation where draft length ratio(T/L) is assumed to be small. If the geometry of a fin is defined by:

$$z = f(x,y) \tag{2.63}$$

the body surface boundary condition as given by eq.(2.7) will be changed for the fin as:

$$(U + \phi_x)\, f_x + \phi_y\, f_y - \phi_z = 0 \tag{2.64}$$

Following the same procedure as in section 2.2 or simply discarding the quadratic terms in the above equation, the linearised fin surface boundary condition will be obtained as :

$$\phi_z = U\, f_x \tag{2.65}$$

and the source density to satisfy the above condition is:

$$m(x,y,0) = -\frac{U}{2\pi}\frac{\partial f}{\partial x} \tag{2.66}$$

Therefore, eq.(2.49) becomes :

$$I_F + i\, J_F = -\frac{U}{2\pi}\, Sp_f\, e^{-k_0 h_f \sec^2\theta} \int \frac{\partial z}{\partial x} \exp(\, i\, k_0 x \sec\theta\,)\, dx \tag{2.67}$$

where Sp_f is the span length of the fin and h_f is the submerged depth to the centre of the fin. The resistance of the fin can be calculated by substituting the above equation into eq.(2.48). Also, following the procedure as done in section 2.7, another extra interference between the fin and the components of the SWATH ship can be obtained.

2.8 GENERAL CONCLUSIONS FROM THE MATHEMATICAL RESISTANCE FORMULAE

Before proceeding to the numerical work on a specified SWATH ship using the previously derived formulae, it is desirable to draw some general information from them as to the effect of such parametric changes as breadth, length, bow shape, draft and strut position on the demihull, etc on the resistance. Such general information will provide a quick understanding of and a general idea on the design of SWATH ships in terms of resistance without resorting to lengthy numerical calculation of the formulae involved.

2.8.1 Effect of Breadth and Length on Wave Resistance.

The source density for a thin ship is given by eq.(2.50). Multiplying the source density, m, by a scalar value, s, and substituting it into eqs.(2.48) and (2.49), the resistance will be of the following form:

$$R_W' = s^2 R_w \qquad (2.68)$$

which means that the theoretical wave resistance based on the thin ship approximation varies with the square of the breadth. Therefore, it is concluded that the wave resistance severely decreases as the length of the ship increases for a fixed breadth or the breadth of the ship decreases for a fixed length. However, this is not true for all small changes in length in accordance with fixed breadth. If the length of a ship is designed to cancel the transverse bow and stern waves, small changes in length may cause their reinforcement and hence, increase the resistance. In general, the smaller the ratio B/L, the less the wave resistance. However, from a total resistance point of view, too narrow a slender body will result in a resistance penalty due to its increased skin frictional resistance.

2.8.2 Effect of Bow Shape on Wave Resistance

In order to examine the effect of a ship form(or specifically bow or stern shape) on the wave resistance, the analysis of the wave profile arising from the ship has been used[58,60,62]. In so far as an ideal fluid is concerned, the problem of the stern wave is the same as that of the bow wave and hence,the bow wave is considered in this section. Since the present study is not concerned with a detailed wave profile survey, the problem is made as simple as possible by assuming that the body is a wall sided shape, that is, it is not a function of depth but is a continuous function of length and has continuous derivatives of all orders with regard to x. From eqs.(2.18), (2.29) and (2.36), and making use of the above-mentioned assumption for the body, the wave elevation far downward of the body will be:

$$\zeta(x,y) = \frac{4}{U}\int_{-\pi/2}^{\pi/2} d\theta \int_{0}^{-L} d\xi\, m(\xi)\, [\, \cos(k_0\xi \sec\theta)\cos(k_0 x \sec\theta)\cos(k_0 y \sec^2\theta \sin\theta)$$

$$+ \sin(k_0\xi \sec\theta)\sin(k_0 x \sec\theta)\cos(k_0 y \sec^2\theta \sin\theta)\,]$$

$$[\, 1 + \cos(2k_0 b \sec^2\theta \sin\theta)\,] \sec\theta \qquad (2.69)$$

where $-U/2\pi\, f_\xi$ is replaced by $m(\xi)$ representing the source strength and L is the length of the body. Partial integrations of the above equation is performed as follows:

$$\int_{0}^{-L} m(\xi)\cos(k_0\xi \sec\theta)\sec\theta\, d\xi$$

$$= \frac{1}{k_0}\left[\frac{m'(0)}{k_0\sec^2\theta} - \frac{m'''(0)}{k_0^3\sec^3\theta} + ...\right]$$

$$-\frac{1}{k_0}\left[\, m(-L) - \frac{m''(-L)}{k_0^2\sec^2\theta} + \frac{m^{iv}(-L)}{k_0^4\sec^4\theta} ....\right]\sin(k_0 L \sec\theta)$$

$$+\frac{1}{k_0}\left[\frac{m'(-L)}{k_0\sec\theta} - \frac{m'''(-L)}{k_0^3\sec^3\theta} + ...\right]\cos(k_0 L \sec\theta)$$

$$= C(0,\theta) - S(-L,\theta)\sin(k_0 L \sec\theta) - C(-L,\theta)\cos(k_0 L \sec\theta) \qquad (2.70)$$

and

$$\int_{0}^{-L} m(\xi)\sin(k_0\xi \sec\theta)\sec\theta\, d\xi$$

$$= \frac{1}{k_0}\left[\, m(0) - \frac{m''(0)}{k_0^2\sec^2\theta} + ... \,\right]$$

$$-\frac{1}{k_0}\left[\, m(-L) - \frac{m''(-L)}{k_0^2\sec^2\theta} + \frac{m^{iv}(-L)}{k_0^4\sec^4\theta} ....\right]\cos(k_0 L \sec\theta)$$

$$+\frac{1}{k_0}\left[\frac{m'(-L)}{k_0\sec\theta}-\frac{m'''(-L)}{k_0^3\sec^3\theta}+....\right]\sin(k_0L\sec\theta)$$

$$=s(0,\theta)-S(-L,\theta)\cos(k_0L\sec\theta)-C(-L,\theta)\sin(k_0L\sec\theta) \qquad (2.71)$$

where

$$S(\xi,\theta)=\frac{1}{k_0}\left[m(\xi)-\frac{m''(\xi)}{k_0^2\sec^2\theta}+\frac{m^{iv}(\xi)}{k_0^4\sec^4\theta}+....\right]$$

$$C(\xi,\theta)=-\frac{1}{k_0}\left[\frac{m'(\xi)}{k_0\sec\theta}-\frac{m'''(\xi)}{k_0^3\sec^3\theta}+....\right] \qquad (2.72)$$

where $S(0,\theta)$ and $C(0,\theta)$ are evaluated at the bow and $S(-L,\theta)$ and $C(-L,\theta)$ are evaluated at the stern, respectively. Now, eq.(2.69) can be written in terms of S and C:

$$\zeta=\frac{4}{U}\int_{-\pi/2}^{\pi/2}S(0,\theta)\left[1+\cos(2k_0b\sec^2\theta\sin\theta)\right]\sin(k_0x\,\mathrm{secq})\cos(k_0y\sec^2\theta\sin\theta)\,d\theta$$

$$+\frac{4}{U}\int_{-\pi/2}^{\pi/2}C(0,\theta)\left[1+\cos(2k_0b\sec^2\theta\sin\theta)\right]\cos(k_0x\,\mathrm{secq})\cos(k_0y\sec^2\theta\sin\theta)\,d\theta$$

$$-\frac{4}{U}\int_{-\pi/2}^{\pi/2}S(-L,\theta)\left[1+\cos(2k_0b\sec^2\theta\sin\theta)\right]\sin[k_0(x+L)\sec\theta]\cos(k_0y\sec^2\theta\sin\theta)\,d\theta$$

$$-\frac{4}{U}\int_{-\pi/2}^{\pi/2}C(-L,\theta)\left[1+\cos(2k_0b\sec^2\theta\sin\theta)\right]\cos[k_0(x+L)\sec\theta]\cos(k_0y\sec^2\theta\sin\theta)\,d\theta \qquad (2.73)$$

Ignoring the interference between the bow and stern waves, the wave making resistance produced by the bow waves regarding terms of $S(0,\theta)$ and $C(0,\theta)$ in the integrand of the above equation can be written as[60] .

$$R_w=\text{Const.}\int_0^{\pi/2}\left[S(0,\theta)^2+C(0,\theta)^2\right]\left[\left(1+\cos(2k_0b\sec^2\theta\sin\theta)\right]\cos^3\theta\,d\theta\right. \qquad (2.74)$$

In general, the following conclusions can be drawn from this equation. For very low velocities ie k_0 very large, the dominant term in eq.(2.72) is the first term concerning $S(x,\theta)$. Therefore, for very slow speeds the smaller the source density the smaller the wave resistance. The source density at the bow is proportional to the angle of entrance except at the extreme bow. As a result, it is generally regarded that for very slow speeds the wave-making resistance increases as the entrance angle increases.

On the other hand, this is not true for higher speeds. As the speed increases, k_0 becomes smaller and other terms in S and C become important. For example, when k_0

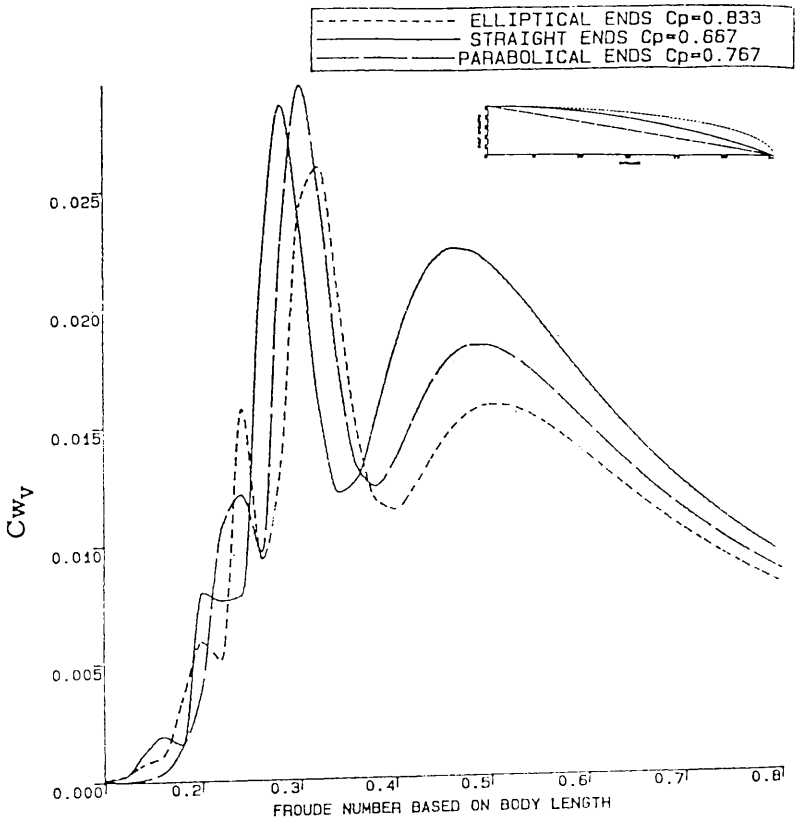

Fig.2.6 Wave Resistance Coefficient Variations of Submerged Bodies of Revolution with Three Different Ends vs Froude Number. SDBC(h)=0.06m, Di=0.0892, L_b=1.51m, Entrance =0.30m, Run = 0.45m.

is of the order of unity they become nearly the same order so that it is impossible to

discard them. Further, the sign of each term in S and C is changing alternatively so that it is likely to cancel out in some values of θ. If derivatives $m^k(0,\theta)$, k=1,3,4..., are assumed to be zero or small in magnitude, it is concluded that a ship of small resistance will have a large source density at the bow which means that the bow will have a blunt entrance.

Fig.2.6 illustrates the effect of three different ends shapes on the wave-making resistance where the lengths of the ends are all the same as each other. From the figure it is understood that the body with elliptical ends(the bluntest ends) is subject to the least resistance among the three candidates at medium to higher speeds which are of most interest for SWATH ships. The highest wave-making resistance is the body with straight end,viz, conical ends, over that speed range. Therefore, in order to have a small resistance for SWATH ships, components with larger entrance angles are recommended for higher speed, but should be smooth enough to prevent wave - breaking. When this blunt body is used for bow, a special care should be also paid to prevent the separation of flow which creates a large resistance increase compared to that in laminar flow.

2.8.3 Effect of Draught on Wave Resistance

One of the significant differences in SWATH design is a large draught compared to a conventional monohull ship. This is attributable to the fact that the main part of the buoyancy is submerged well below the free surface. As mentioned in Chapter 1, a large draft provides a promising future and potential for the development of this type of ship because of the significant improvement in the motion characteristics compared to the conventional ship. However, the large draught coupled with the twin hull concept produces penalties in resistance at low speeds due to the increased wetted area relative to the conventional ship. Therefore, from the point of view of resistance, SWATH ships can compete in higher speeds(wave-making) range compared to their counterparts.

According to eqs.(2.48) and (2.49), it can be seen that the wave-making resistance can be reduced as small as possible by the sources generating the ship being submerged deeper. This is due to the power of the exponential term regarding z in eq.(2.49). In general, the resisting force to a uniformly moving source due to the

wave-making decreases exponentially with its submergence below the free surface. For example, a deeply submerged submarine is not subject to the wave-making resistance and Fig.2.7, taken from Ref.[61], illustrates how the wave-

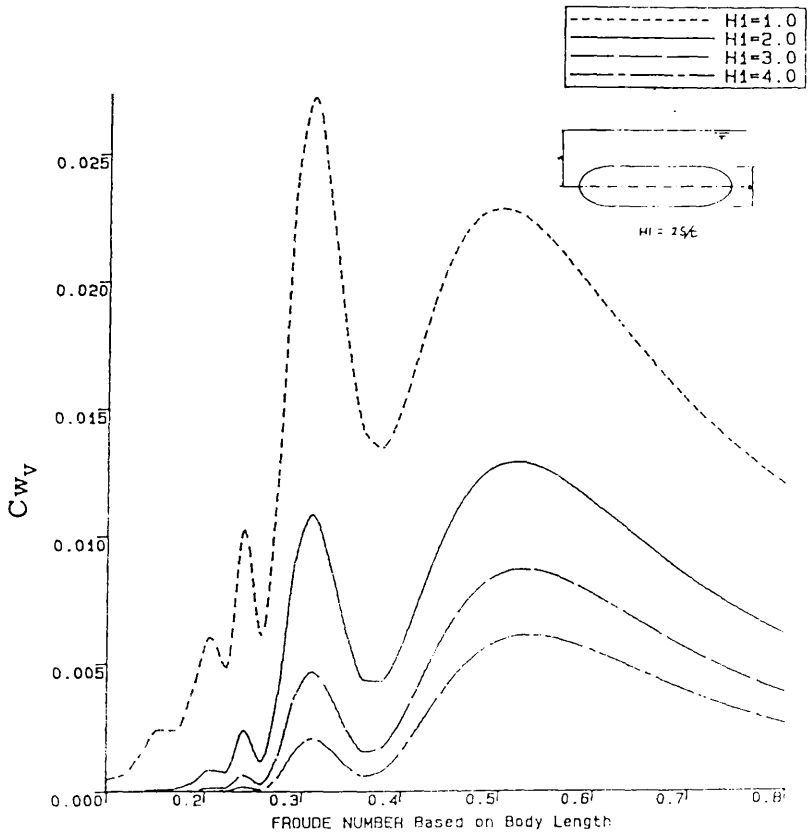

Fig.2.7 Wave Resistance Coefficient Variations of a Body of Revolution versus Speed with Four Different Submerged Depths.(L_b=1.5m, Di=0.1m,C_p=0.89,∇ =0.0105m^3)

making resistance of a body of revolution decreases with the submerged depth However, for a surface or near surface running vehicle, the wave-making can not be eliminated. From Shor's conclusion[62] for this problem, the part of the hull near the waterline can be designed for relatively low resistance at lower speeds and the part of the hull deep in the water for relatively low resistance at higher speeds. The interaction

terms between shallow and deep sources can be used to improve the behaviour at moderate speeds.

A SWATH ship has several components below the free surface which introduce complicated hydrodynamic interference effects between the structural components. Based on the the aforementioned facts, the greatest part of the displacement of the SWATH ship should be placed in the submerged body well away from the free surface and hence, creating less wave-making. In addition, it is desirable to make the strut thickness as small as possible since the wave-making resistance of the SWATH is mostly created by the surface piercing struts up to moderately high speeds. The interference effects between the body and strut(s) can be maximised by the proper distribution of the displacement to the body as well as to the strut(s) and by the well disposition of the strut(s) on the demihull.

It should be noted that a demihull consisting of the surface piercing strut and the submerged body which protrudes forward of the strut not only looks like a bulbous bow ship but also acts like a bulbous bow ship regarding wave interference effects.Namely, a strut set back of the submerged body gives rise to a favourable interference at moderate high speeds while it gives an unfavourable interference at higher speeds. However, the pattern for an overhanging strut forward of the submerged body is changed in such a way that the former favourable interference becomes unfavourable and that the unfavourable interference is much reduced at higher speeds[55]. Detailed parametric studies are givent in Chapters 4 and 5.

2.8.4 Effect of Spacing Distance on Wave Resistance

The effect of the spacing distance between two demihulls on the wave resistance is determined by the interference factor, $\cos(2k_0 b \sec^2\theta \sin\theta)$ where 2b is the distance between the centerlines of the two demihulls of a SWATH ship, in the integrand of eq.(2.48). The interference factor is a function of the speed and spacing distance of two demihulls and varies from -1 to 1, mathematically. Consequently, the wave resistance of twin hulls, which travel abreastly at a distance of 2b, is at the least zero and at the most four times the wave resistance of single hull.

If the ship speed is very high and the hull spacing is very small, that is, $k_0 b \to 0$,

the interference factor approaches unity so that the wave resistance becomes four times the wave resistance of a demihull. From this fact, it is unlikely that at the practical spacing distance of catamarans or SWATH ships, low wave resistance can be obtained at high speeds. On the other hand, if the ship speed is very low or hull spacing is very large, that is, $k_0 \rightarrow \infty$, the interference factor becomes zero and the wave interference effect becomes negligible. The wave resistance then becomes twice the wave resistance of a demihull. Therefore, between the extreme speeds and spacings it is likely that the interference factor will be negative, depending on the hull spacing and speed, thus obtaining low wave resistance.

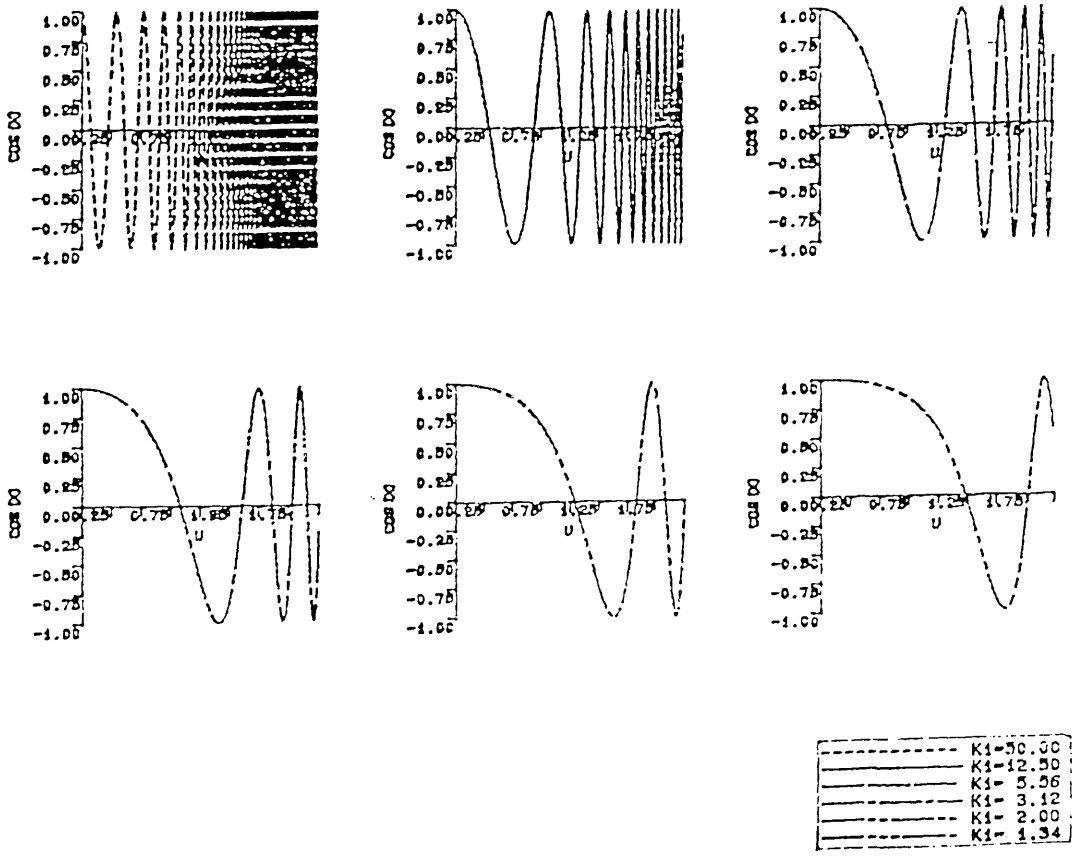

Fig. 2.8 Variations of the Interference Factor, $\cos(k_1 B_1 \cosh u \sinh u)$, as a Function of u at Six Different Speeds and at $B_1=0.2$

In an attempt to aid the understanding of the contribution of the interference factor

to the wave resistance integration, the variations of the interference factor are shown in Fig.2.8 as a function of the independent u for six different speeds at a non-dimensional spacing B_1=0.2. For this purpose, secθ in the integrand of eq.(2.48) is replaced by coshu to remove the singular point which will be explained in the next chapter and $k_1=L_bg/2U^2$ is the non-dimensional parameter. From the figure, it can be noticed that the interference factor slowly varies for the first small value of u and then rapidly varies, depending on the value of k_1. If the integration of eq.(2.48) is performed over the very rapidly varying regions, the value will cancel each other by anulling interference. The contributory part to the integration is mostly from the slowly varying regions, giving the negative or positive value depending on the parameters in the factor. As a result, by taking the appropriate speed for a given spacing or vice versa, the weighted interference factor in the integrand of eq.(2.48) can be phased in order to interfere favourably with each demihull and so reduce the wave-making resistance.

2.9 CONCLUSIONS

Using the linearised wave theory and Green's theorem, the velocity potential induced by sources systems(representing a given geometry) which travels steadily along the vertical wall is derived. The wave resistance formula of a catamaran(a SWATH is a specific form of a catamaran) is then obtained based on momentum analysis and, within the first order approximation, it is shown that the result is exactly the same as that derived according to Lagally's theorem

Using the linear superposition principle, it is shown how the derived formula is applied to SWATH ships having single or more strut(s) on the demihull. For this purpose, the plane source approximation for the submerged body is introduced and the result is compared with the result using the line source distribution technique(slender body approximation) for three slender bodies which have the same x-directional variation of cross section, dA(x)/dx, displacement and mean submerged depth but different cross sections. As a conclusion, the present plane source approach gives different values for the different shapes of cross section while the line source distribution gives the same results for each section. Furthermore, for the same circular

cross sectional body, the present approach gives values as much as 20-25% higher than the line source method depending on the submergence of the body. This phenomenon is due to the fact that the contribution to the wave-making of the part of the submerged body near to the free surface is taken into account by the present plane source distribution, but not by the line source distribution. However, above a body submergence of around three times the depth of the body, the two source distributions give nearly the same results as each other.

Assuming that controllable fins are attached to the submerged body at zero angle of attack, their wave-making resistance formula is derived based on the flat ship approximation. Lastly, based on the derived mathematical resistance formulae, general conclusions as to the effect of parametric changes in breadth, length, bow shape, draft and strut position on the demihull on the wave-making resistance are drawn in an attempt to provide a quick understanding of and general ideas on the design of SWATH ships without resorting to the tedious numerical calculation of the formulae involved. These numerical studies on such parameters will be treated in Chapter 5.

The derived wave-making resistance formulae in this chapter will be used to calculate the total resistance of SWATH ships in the following Chapter 3 and some detailed conclusions will be treated in that chapter.

CHAPTER 3 THE DEVELOPMENT OF TWO COMPUTER PROGRAMS TO ESTIMATE THE TOTAL RESISTANCE OF SWATH SHIPS IN CALM WATER (MSWATH AND OSWATH)

3.1 INTRODUCTION

A SWATH ship has several components below the free surface which cause complicated hydrodynamic interferences between them and accordingly, its hydrodynamic performance, in particular resistance, is very sensitive to changes in the composition or geometries of the components. With regard to this, compared to monohull ships, it is rather difficult to find an optimum SWATH ship configuration experimentally by varying the many parameters involved in the SWATH design because of time and cost. Therefore, at an early stage of the design process, the use of a reliable analytical tool to evaluate the performance of candidate SWATH ship forms is extremely important. This result can then be confirmed by means of experiments on the final ship form or can be provided as guidance for the further development of experimental work.

To the author's knowledge, there are four computational tools currently in use worldwide to estimate the total resistance of SWATH ships. Utilising a line source distribution along the longitudinal centreline of the submerged body and the plane source distribution over the centreplane of the surface piercing strut, Chapman initiated a solution to the wave-making resistance problem of semi-submerged ships[1] and wrote a computer program SWTHRP[2] to estimate the total resistance of SWATH ships defined by simple mathematical formulae. Based on the same theory as Chapman and using Chebyshev coefficients and the cubic spline(piecewise continuous polynomial) curve fitting method, Lin and Day developed a computer program to predict the total resistance of SWATH geometries defined by offsets[3].

Defining that a concept exploration model is a simplified form of a ship synthesis model which addresses the earliest phase of the ship selection process, SWATH CEM[4] was developed in which the resistance prediction was based on the SWTHRP developed by Chapman. Salveson et al developed a new computational method for the design of SWATH ships[5]. In dealing with the wave-making resistance they

introduced a correction term that accounts for the outflow between the strut and lower hull, but the general theory is the same as Chapman's. However, it is not clear that the line source distribution for the body can be used for the optimisation example of non-circular hulled SWATH ships.

Instead of using two sets of Chebyshev coefficients as employed by Lin and Day, but employing the first kind of Chebyshev polynomial(one set of Chebyshev coefficients) and recurrence formulae for Bessel functions of integrals involved in the wave resistance formulae, Huang[6] concluded that he had simplied the computational work involved in wave resistance formulae and saved computer time. As far as computer time is concerned, however, it seems that this is not always the case. The time for calculating the wave resistance formulae is entirely dependent upon the DO-looping times which are decided by the order of Chebyshev polynomial and this is related to the accuracy of prediction.

In order to estimate the total resistance experienced by a near-surface or surface running ship, it is usual to break down the total resistance into components with the assumption that each of them is caused by a different effect and that all the components are additive to give the total resistance. Although, in some cases, this is not strictly justifiable, it represents the only feasible approach to the problem in most cases. Fig.3.1 shows a schematic tree diagram of the resistance components[7].

In general, the total resistance of a surface running ship can be divided into the viscous resistance(R_V) and the wave-making resistance(R_W). The viscous resistance is the component of resistance associated with the expenditure of energy in generating vorticity,vortices and turbulence. The wave-making resistance is the component of resistance associated with the expenditure of energy in generating gravity waves by way of pressure differentials. The viscous resistance can be subdivided into the three components: frictional(R_F), viscous pressure(R_{VP}) and wave-breaking resistances(R_B). The frictional resistance is a tangential force so that it can be obtained by integrating tangential forces over the hull surface. The viscous pressure resistance is due to the pressure differentials arising from the existence of a boundary layer and the wake. The wave breaking resistance is due to the energy expended in generating turbulences arising from the breaking of waves. In practical terms, the frictional resistance is the

major part of the viscous resistance. Therefore, for simplicity, the frictional resistance is treated as that of an equivalent flat plane which has the same length and wetted area as the ship. In addition, the augumented resistance due to the 3-dimensional effect(form) of the body is treated as a component of viscous resistance(so called form resistance).

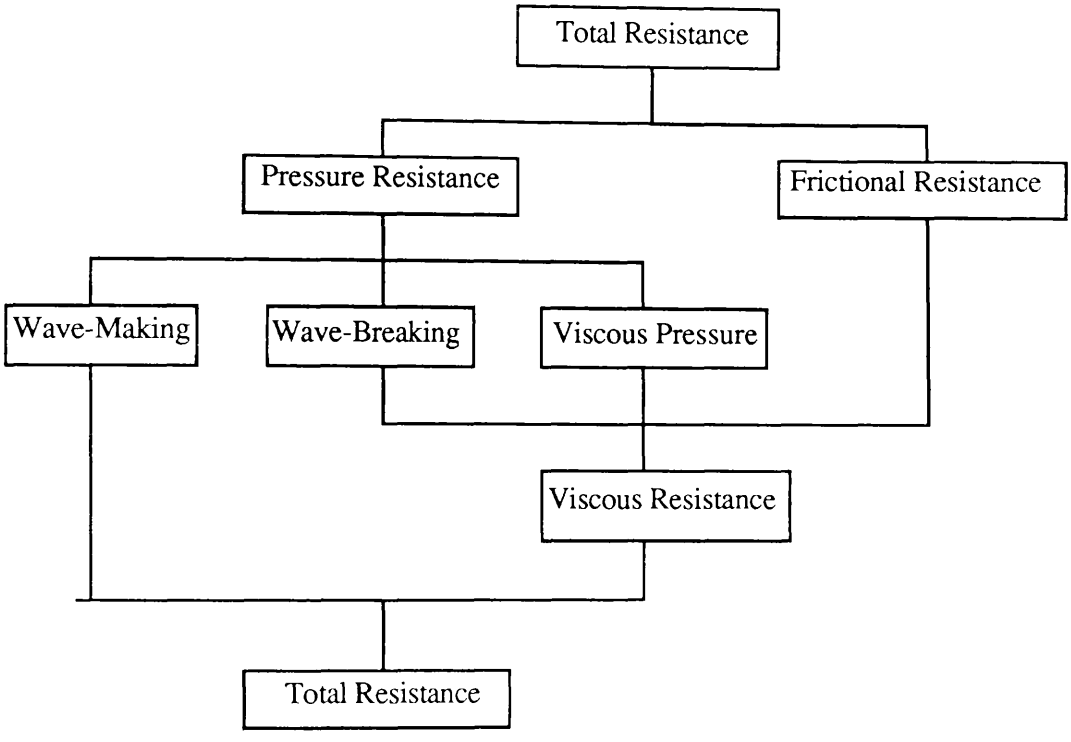

Fig.3.1 Schematic Tree Diagram of Total Resistance Component

In the aforementioned four programs(Huang considered only the wave-making resistance component) for calculating the total calm water resistance of SWATH ships, the authors treated the resistance components basically according to the above mentioned subdivision, but with slight differences from one another. In SWTHRP and SWATH CEM, the total resistance of a SWATH ship is divided into six components:

$$R_T = R_F + R_W + R_E + R_S + R_{AP} + R_A$$

where R_E is the eddy-making resistance, R_S is the spray resistance and R_A is the aerodynamic resistance. In dealing with the form effect, viscous pressure and wave breaking components, the eddy-making resistance was considered. Strut eddy-making

resistance was accounted for by multiplying the strut frictional resistance by an empirical factor and hull eddy-making resistance was taken as 10% of the hull frictional resistance. Unlike conventional monohulls, a SWATH ship has such streamlined surface piercing struts that beyond a certain speed,water starts to pile up and gradually forms a spray sheet over the surfaces of the struts which causes a considerable energy loss especially at higher speeds(so called spray drag). Spray drag calculations are based on the results of model tests, as described in Ref.[8]. The appendage resistance is calculated as 10% of the frictional resistance. The aerodynamic resistance is computed using the frontal area and an aerodynamic drag coefficient of 0.5.

Lin and Day calculated the total resistance of bare hulled SWATH ships(control surfaces is not included) as the sum of the wave-making, frictional and form resistance components. Here, the form resistance indicates the difference between the calculated wave-making resistance and experimentally measured residuary resistance. Based on experimental results on several SWATH models, they derived a form resistance coefficient curve.

In SWATHGEN, the total resistance is computed as the sum of the wave-making, frictional, form and appendage resistances. The form resistance is calculated as the sum of 17% of the strut frictional resistance and 10% of the body frictional resistance. After subdividing the resistance of controllable surfaces(fins and rudders) into profile, induced, tip, and body-controllable surfaces interference resistance, empirical formulae based on aerofoil sections and streamlined bodies were used for each component calculation.

For the present study, the total calm water resistance of a SWATH ship is divided into four components: wave-making, frictional, additional resistances(form effect, eddy, viscous pressure, wave-breaking and spray) and appendage resistance. Based on the wave-making resistance formulae derived in Chapter 2, the calculation procedures for the wave-making resistance for SWATH ships defined by mathematical formulae are shown in detail in section 3.2. Also, utilising the cubic spline curve fitting technique, the final wave-making resistance integrals, which will be integrated numerically by means of computer, are derived for SWATH ships defined in offset forms. In section 3.3, surfaces and volumes of SWATH ships defined by both mathematical formulae and offsets are calculated. Using the ITTC'57 frictional line, the

frictional resistance is calculated based on the individual length of the components of a SWATH ship.

Based on the approach described in sections 3.2 and 3.3, two computer programs (MSWATH and OSWATH) were written. MSWATH is designed for SWATH ships defined by mathematical formulae and OSWATH is written for offset inputs. In section 3.4, the computational results are compared with the experimental results measured in the department using three SWATH models(SWATH1, SWATH2 and SWATH3). Also these are compared with experimental results and computational results available in the open literatutre.

In section 3.5, based on the difference between the calculated wave-making and measured residuary resistances, two form resistance coefficient curves, which account for such additional resistances as form effect, eddy, viscous pressure, spray and wave-breaking and some non-linearities, are derived: one is for circular hulled SWATH ships and the other is for rectangular hulled SWATH ships. These coefficients are then compared with other form effect correlations published. Subdividing the resistance of controllable fins into profile, induced, hull-fin interference, tip and wave-making resistances, the resistance of controllable fins are calculated. For this purpose, empirical formulae for foil sections and streamlined bodies are used for each component calculation. In dealing with induced drag, the free surface effect is introduced. Then, the estimated total resistance including the form and fin resistances are compared with the experimental results for SWATH1 model with a pair of fins.

In section 3.6, a comparison is made of the two computer programs(MSWATH and OSWATH) together with some accounts of restrictions in their applications. Finally, based on the present study, a number of conclusions are drawn in section 3.7.

3.2 WAVE-MAKING RESISTANCE

As developed in Chapter 2, the wave-making resistance of the demihull of a SWATH ship is written as one half of eq.(2.48):

$$R_w = 16\pi\rho k_0^2 \int_0^{\pi/2} d\theta \, (I^2 + J^2) \sec^3\theta \, [1 + \cos(k_1 B_1 \sec^2\theta \sin\theta)] \qquad (3.1)$$

where

$$k_1 = \frac{gL_b}{2U^2} \quad \text{and} \quad B_1 = \frac{4b}{L_b} \tag{3.2}$$

which are the non-dimensional wave number and non-dimensional spacing between two demihull centerlines, respectively.

For the submerged body, from eq.(2.62),

$$I_B + i\,J_B = -\frac{U}{4\pi D_b}\iint \frac{dA(x)}{dx}\exp\left(i\,k_0 x\sec\theta + z\,k_0\sec^2\theta\right)dx\,dz \tag{3.3}$$

for the surface piercing strut, from eq.(2.55),

$$I_S + i\,J_S = -\frac{U}{2\pi}\iint \frac{dt}{dx}\exp\left(i\,k_0 x\sec\theta + z\,k_0\sec^2\theta\right)dx\,dz \tag{3.4}$$

and for the controllable fin, if any, from eq.(2.67),

$$I_F + i\,J_F = -\frac{U}{2\pi}\,Sp_f\,e^{-k_0 h_f \sec^2\theta}\int \frac{\partial z}{\partial x}\exp\left(i\,k_0 x\sec\theta\right)dx \tag{3.5}$$

In order to calculate the above equations numerically, such functions as the cross sectional area curve A(x) of the body, the strut half thickness t(x) and the fin geometry z(x,y) should be described analytically either by mathematical formulae or by curve fittings from given offset tables. First, SWATH ships defined by simple mathematical formulae will be treated and then, utilising a curve fitting technique, SWATH ships defined by offsets will be dealt with.

3.2.1 SWATH Ships Defined by Mathematical Forms

The submerged body of a SWATH ship can be a combination of conical, ellipsoidal and paraboloidal nose and tail sections which are joined together by a straight mid section of circular or elliptical cross section. Indeed, many worldwide SWATH models have been built by using these shapes and one of them, T-AGOS Baseline[9] was built with a ellipsoidal entrance and paraboloidal run of elliptical cross sections.

For the ellipsoidal entrance of a body with maximum cross sectional area, A_m ,

$$A(x) = A_m[\ 1 - (\frac{x-x_1}{l_{be}})^2\ ] \tag{3.6}$$

for the conical entrance,

$$A(x) = A_m(\ 1 - \frac{x-x_1}{l_{be}})^2 \tag{3.7}$$

and for the paraboloidal entrance,

$$A(x) = A_m[\ 1 - (\frac{x-x_1}{l_{be}})^2\ ]^2 \tag{3.8}$$

where l_{be} is the length of entrance and x_1 is the co-ordinate from the longitudinal centre of the body. Any other symbols used are shown in Fig.3.2.

And also, a wall sided strut with parabolic ends can be popularly used and the thickness distribution of a parabolic entrance with maximum half thickness t_m is given by:

$$t = t_m[\ 1 - (\frac{x-x_3}{l_{se}})^2\ ] \tag{3.9}$$

Lastly, for the controllable fin, a parabolic airfoil with maximum half thickness t_{mf} can be used:

$$z = t_{mf}[\ 1 - (x-C_f)^2] \tag{3.10}$$

where C_f is the distance between the longitudinal centres of the body and fin.

Using the mathematical formulae described above, the wave-making resistance of a SWATH ship, given by eq.(3.1), can be calculated from the contribution of each component given by eqs.(3.3) to (3.5).

3.2.1.1 Body contribution

From eq.(3.3),

$$I_B + iJ_B = -\frac{U}{4\pi D_b} \int_{-L_b/2}^{L_b/2} \int_{-h-D_b/2}^{-h+D_b/2} \frac{dA(x)}{dx} \exp(\ ik_0 x \sec\theta + z\, k_0 \sec^2\theta)\ dx\ dz \tag{3.11}$$

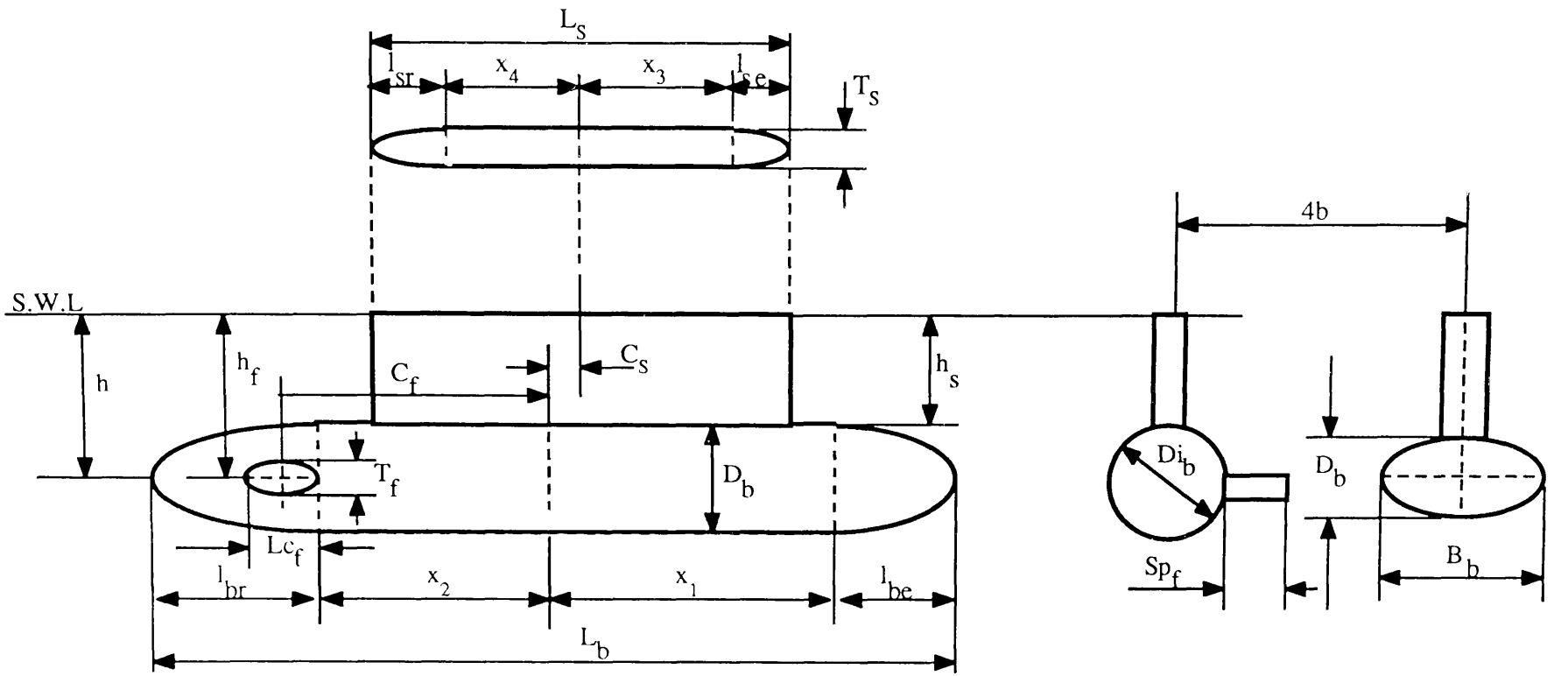

Fig.3.2 SWATH Ship Body, Strut and Fin Profiles together with Symbols

Introducing dimensionless co-ordinates such as $x'=2x/L_b$ and $z'=2z/D_b$, and $A'(x) = A(x)/A_m$, the above equation is written in the normalised(non-dimensionalised) form:

$$I_B + i\,J_B = -\frac{U}{8\pi} A_m \int_{-1}^{1} \frac{dA(x)}{dx} \exp(ik_1 \sec\theta\, x)\, dx \int_{-1-H_1}^{1-H_1} \exp(\frac{D_b}{L_b} k_1 \sec^2\theta\, z)\, dz \tag{3.12}$$

where, for simplicity, the superscript symbol ' is dropped out and $H_1=2h/D_b$ and k_1 is given in eq.(3.2).

The integration with regard to z in the above equation becomes.

$$E_b = \frac{1}{\frac{D_b}{L_b} k_1 \sec^2\theta} \{ \exp[\frac{D_b}{L_b} k_1 \sec^2\theta\, (1-H_1)] - \exp[\frac{D_b}{L_b} k_1 \sec^2\theta\, (1+H_1)] \} \tag{3.13}$$

and then, eq.(3.12) is written in the form:

$$I_B + i\,J_B = -\frac{U}{8\pi} A_m E_b \int_{-1}^{1} \frac{dA(x)}{dx} \exp(i\,\beta\, x)\, dx \tag{3.14}$$

where β is $k_1 \sec\theta$. For this calculation, one of eqs.(3.6) to (3.8) can be used. As an example, an ellipsoidal entrance given by eq.(3.6) is used here. Using the above mentioned non-dimensional co-ordinates, eq.(3.6) can be non-dimensionalised in the form:

$$A(x) = [\, 1 - (\frac{x-x_1}{l_{be}})^2 \,] \tag{3.15}$$

where l_{be} and x_1 are non-dimensionalised by $L_b/2$.

Substituting the x-derivative of the above equation into eq.(3.14), the x-integral term in the equation becomes:

$$-2 \frac{1}{l_{be}^2} \int_{x_1}^{1} (x - x_1) \exp(i\,\beta\, x)\, dx$$

$$= -\frac{2}{l_{be}^2}\left[\frac{\cos(\beta)}{\beta^2} + \frac{l_{be}\sin(\beta)}{\beta} - \frac{\cos(\beta x_1)}{\beta^2}\right]$$

$$+ 2\frac{i}{l_{be}^2}\left[\frac{\sin(\beta)}{\beta^2} - \frac{l_{be}\cos(\beta)}{\beta} - \frac{\sin(\beta x_1)}{\beta^2}\right] \qquad (3.16)$$

In the similar way, for an elliptical run,

$$-2\frac{1}{l_{br}^2}\int_{-1}^{x_2}(x - x_2)\exp(i\beta x)\,dx$$

$$= -2\frac{1}{l_{br}^2}\left[\frac{\cos(\beta)}{\beta^2} - \frac{l_{br}\sin(\beta)}{\beta} - \frac{\cos(\beta x_2)}{\beta^2}\right]$$

$$+ 2\frac{i}{l_{br}^2}\left[\frac{\sin(\beta)}{\beta^2} - \frac{l_{br}\cos(\beta)}{\beta} - \frac{\sin(\beta x_2)}{\beta^2}\right] \qquad (3.17)$$

Therefore, eq.(3.14) is written in the form:

$$I_B + i J_B = \frac{U}{8\pi} A_m E_b (Q_{e1} + i Q_{e2}) \qquad (3.18)$$

where

$$Q_{e1} = \frac{\cos(\beta)}{\beta^2}\left(\frac{1}{l_{be}^2} - \frac{1}{l_{br}^2}\right) + \frac{\sin(\beta)}{\beta}\left(\frac{1}{l_{be}} - \frac{1}{l_{br}}\right) - \frac{1}{\beta^2}\left[\frac{\cos(\beta x_1)}{l_{be}^2} - \frac{\cos(\beta x_2)}{l_{br}^2}\right]$$

$$Q_{e2} = \frac{\sin(\beta)}{\beta^2}\left(\frac{1}{l_{be}^2} + \frac{1}{l_{br}^2}\right) - \frac{\cos(\beta)}{\beta}\left(\frac{1}{l_{be}} + \frac{1}{l_{br}}\right) - \frac{1}{\beta^2}\left[\frac{\sin(\beta x_1)}{l_{be}^2} + \frac{\sin(\beta x_2)}{l_{br}^2}\right]$$

If the body has longitudinal symmetry, ie $x_1 = x_2$ and $l_{be} = l_{br}$, the real part Q_{e1} disappears and there remains only the imaginary part Q_{e2}. Then,

$$I_B^2 + J_B^2 = (I_B + i J_B)(I_B - i J_B)$$

$$= \frac{U^2}{64\pi^2} A_m^2 E_b^2 (Q_{e1}^2 + Q_{e2}^2) \tag{3.19}$$

Finally, the wave-making resistance of a body with ellipsoidal ends is written from eq.(3.1) in the form:

$$R_{wb} = 16\pi\rho k_0^2 \frac{U^2}{64\pi^2} A_m^2 \int_0^\infty E_b^2 (Q_{e1}^2 + Q_{e2}^2) \cosh^2 u [1 + \cos(k_1 B_1 \cosh u \sinh u)] \, du \tag{3.20}$$

where $\sec\theta$ in eq.(3.1) is replaced by $\cosh u$ in order to remove the singularity for numerical calculation.

Similarly, wave-making resistance formulae for bodies with conical ends, with paraboloidal ends and with elliptical entrance and paraboloidal run can be, without any difficulty, derived and only the results are written here.

For conical entrance and run,

$$I_B + i J_B = \frac{U}{8\pi} A_m E_b (Q_{c1} + i Q_{c2}) \tag{3.21}$$

$$R_{wb} = 16\pi\rho k_0^2 \frac{U^2}{64\pi^2} A_m^2 \int_0^\infty E_b^2 (Q_{c1}^2 + Q_{c2}^2) \cosh^2 u [1 + \cos(k_1 B_1 \cosh u \sinh u)] \, du \tag{3.22}$$

where

$$Q_{c1} = 2\frac{\sin(\beta)}{\beta} \left(\frac{1}{l_{be}} - \frac{1}{l_{br}} \right) - \frac{2}{\beta} \left[\frac{\sin(\beta x_1)}{l_{be}} - \frac{\sin(\beta x_2)}{l_{br}} \right]$$

$$Q_{c2} = -2\frac{\cos(\beta)}{\beta} \left(\frac{1}{l_{be}} + \frac{1}{l_{br}} \right) + \frac{2}{\beta} \left[\frac{\cos(\beta x_1)}{l_{be}} + \frac{\mathrm{coc}(\beta x_2)}{l_{br}} \right] \tag{3.23}$$

For paraboloidal entrance and run,

$$I_B + i\,J_B = \frac{U}{8\pi} A_m E_b \,(Q_{p1} + i\, Q_{p2}) \tag{3.24}$$

$$R_{wb} = 16\pi\rho k_0^2 \frac{U^2}{4\pi^2} A_m^2 \int_0^\infty E_b^2 \,(Q_{p1}^2 + Q_{p2}^2) \cosh^2 u[1+ \cos(k_1 B_1 \cosh u \sinh u)]\, du \tag{3.25}$$

where

$$Q_{p1} = \frac{\cos(\beta)}{\beta^2} \left(\frac{1}{l_{be}^2} - \frac{1}{l_{br}^2} \right) + \frac{\sin(\beta)}{\beta} \left(\frac{1}{l_{be}} - \frac{1}{l_{br}} \right) - \frac{1}{\beta^2} \left[\frac{\cos(\beta x_1)}{l_{be}^2} - \frac{\cos(\beta x_2)}{l_{br}^2} \right]$$

$$- \frac{3\cos(\beta)}{\beta^2} \left(\frac{1}{l_{be}^2} - \frac{1}{l_{br}^2} \right) + \frac{6\cos(\beta)}{\beta^4} \left(\frac{1}{l_{be}^4} - \frac{1}{l_{br}^4} \right) - \frac{\sin(\beta)}{\beta} \left(\frac{1}{l_{be}} - \frac{1}{l_{br}} \right)$$

$$+ \frac{6\sin(\beta)}{\beta^3} \left(\frac{1}{l_{be}^3} - \frac{1}{l_{br}^3} \right) - \frac{6}{\beta^4} \left[\frac{\cos(\beta x_1)}{l_{be}^4} - \frac{\cos(\beta x_2)}{l_{br}^4} \right]$$

$$Q_{p2} = \frac{\sin(\beta)}{\beta^2} \left(\frac{1}{l_{be}^2} + \frac{1}{l_{br}^2} \right) - \frac{\cos(\beta)}{\beta} \left(\frac{1}{l_{be}} + \frac{1}{l_{br}} \right) - \frac{1}{\beta^2} \left[\frac{\sin(\beta x_1)}{l_{be}^2} + \frac{\sin(\beta x_2)}{l_{br}^2} \right]$$

$$- \frac{3\sin(\beta)}{\beta^2} \left(\frac{1}{l_{be}^2} + \frac{1}{l_{br}^2} \right) + \frac{6\sin(\beta)}{\beta^4} \left(\frac{1}{l_{be}^4} + \frac{1}{l_{br}^4} \right) + \frac{\cos(\beta)}{\beta} \left(\frac{1}{l_{be}} + \frac{1}{l_{br}} \right)$$

$$- \frac{6\cos(\beta)}{\beta^3} \left(\frac{1}{l_{be}^3} + \frac{1}{l_{br}^3} \right) - \frac{6}{\beta^4} \left[\frac{\sin(\beta x_1)}{l_{be}^4} + \frac{\sin(\beta x_2)}{l_{br}^4} \right] \tag{3.26}$$

Lastly, for a body with ellipsoidal entrance and paraboloidal run,

$$I_B + i\,J_B = \frac{U}{8\pi} A_m E_b \left(Q_{ep1} + i\,Q_{ep2} \right) \tag{3.27}$$

$$R_{wb} = 16\pi\rho k_0^2 \frac{U^2}{16\pi^2} A_m^2 \int_0^\infty E_b^2 \left(Q_{ep1}^2 + Q_{cp2}^2 \right) \cosh^2 u \left[1 + \cos(k_1 B_1 \cosh u \sinh u) \right] du \tag{3.28}$$

where

$$Q_{ep1} = -\frac{2\cos(\beta)}{l_{br}^2\beta^2} - \frac{2\sin(\beta)}{l_{br}\beta} + \frac{2\cos(\beta x_2)}{l_{br}^2\beta^2}$$

$$+ 6\cos(\beta)\left(\frac{1}{l_{br}^2\beta^2} - \frac{2}{l_{br}^4\beta^4} \right) + 2\sin(\beta)\left(\frac{1}{l_{br}\beta} - \frac{6}{l_{br}^3\beta^3} \right) + \frac{12\cos(\beta x_2)}{l_{br}^4\beta^4}$$

$$+ \frac{1}{l_{bc}^2}\left[\frac{\cos(\beta)}{\beta^2} + \frac{l_{be}\sin(\beta)}{\beta} - \frac{\cos(\beta x_1)}{\beta^2} \right]$$

$$Q_{ep2} = \frac{2\sin(\beta)}{l_{br}^2\beta^2} - \frac{2\cos(\beta)}{l_{br}\beta} - \frac{2\sin(\beta x_2)}{l_{br}^2\beta^2}$$

$$- 6\sin(\beta)\left(\frac{1}{l_{br}^2\beta^2} - \frac{2}{l_{br}^4\beta^4} \right) - 2\cos(\beta)\left(\frac{1}{l_{br}\beta} - \frac{6}{l_{br}^3\beta^3} \right) + \frac{12\sin(\beta x_2)}{l_{br}^4\beta^4}$$

$$+ \frac{1}{l_{bc}^2}\left[\frac{\sin(\beta)}{\beta^2} - \frac{l_{be}\cos(\beta)}{\beta} - \frac{\sin(\beta x_1)}{\beta^2} \right] \tag{3.29}$$

3.2.1.2 Strut contribution

From eq.(3.4),

$$I_S + i\,J_S = -\frac{U}{2\pi}\int_{0}^{-h_s}\int_{-L_s/2}^{L_s/2}\frac{dt}{dx}\exp(\,i\,k_0 x\,\sec\theta + k_0 z\,\sec^2\theta\,)\,dx\,dz$$

$$= \frac{U}{2\pi}E_s\int_{-L_s/2}^{L_s/2}\frac{dt}{dx}\exp(\,i\,k_0 x\,\sec\theta\,)\,dx \qquad (3.30)$$

where

$$E_s = \frac{1}{k_0\sec^2\theta}\,[\,1-\exp(-h_s k_{1s}\sec^2\theta)\,] \qquad (3.31)$$

where

$$k_{1s}=\frac{g\,L_s}{2U^2} \quad \text{and} \quad h_s=\frac{2\,h_s}{L_s} \qquad (3.32)$$

Using $x'=2x/L_S$ and $t'=2t/T_S$, eq.(3.30) can be written in the normalised form:

$$I_S + i\,J_S = \frac{U}{4\pi}T_s\,E_s\int_{-1}^{1}\frac{dt}{dx}\exp(\,i\,\beta_s x)\,dx \qquad (3.33)$$

where β_S is $k_{1S}\sec\theta$ and, for convenience, the superscript symbol ' is dropped out. Also, a parabolical entrance given by eq.(3.9) is normalised in the form:

$$t = [\,1-(\frac{x-x_3}{l_{se}})^2] \qquad -1 \le x \le 1 \qquad (3.34)$$

Substituting the x-derivative of eq.(3.34) into eq.(3.33), the x-integral term of the equation will be as follows:

$$-\frac{2}{l_{se}^2}\int_{x_3}^{1}(x-x_3)\exp(i\beta_s x)\,dx$$

$$= -2\frac{1}{l_{se}^2}\left[\frac{\cos(\beta_s)-\cos(\beta_s x_3)}{\beta_s^2} + \frac{l_{se}\sin(\beta_s)}{\beta_s}\right]$$

$$+ 2\frac{i}{l_{se}^2}\left[\frac{\sin(\beta_s)-\sin(\beta_s x_3)}{\beta_s^2} + \frac{l_{se}\cos(\beta_s)}{\beta_s}\right] \qquad (3.35)$$

Considering the run contribution, eq.(3.33) will be:

$$I_S + i\,J_S = \frac{U}{4\pi} T_s E_s \left(Q_{s1} + i\,Q_{s2} \right) \qquad (3.36)$$

where

$$Q_{s1} = \frac{2\cos(\beta_s)}{\beta_s^2}\left(\frac{1}{l_{se}^2} - \frac{1}{l_{sr}^2}\right) - \frac{2\sin(\beta_s)}{\beta_s}\left(\frac{1}{l_{se}} - \frac{1}{l_{sr}}\right)$$

$$+ \frac{2}{\beta_s^2}\left(\frac{\cos(\beta_s x_3)}{l_{se}^2} - \frac{\cos(\beta_s x_4)}{l_{sr}^2}\right)$$

$$Q_{s2} = \frac{2\sin(\beta_s)}{\beta_s^2}\left(\frac{1}{l_{se}^2} + \frac{1}{l_{sr}^2}\right) - \frac{2\cos(\beta_s)}{\beta_s}\left(\frac{1}{l_{se}} + \frac{1}{l_{sr}}\right)$$

$$+ \frac{2}{\beta_s^2}\left(\frac{\sin(\beta_s x_3)}{l_{se}^2} + \frac{\sin(\beta_s x_4)}{l_{sr}^2}\right) \qquad (3.37)$$

and finally, the wave-making resistance of a strut with parabolic ends will be written from eq.(3.1) as follows:

$$R_{ws} = 16\pi\rho k_0^2 \frac{U^2 T_s^2}{16\pi^2} \int_0^\infty E_s^2 \left(Q_{s1}^2 + Q_{s2}^2\right) \cosh^2 u \left[1 + \cos(k_1 B_1 \cosh u \sinh u)\right] du \qquad (3.38)$$

3.1.1.3 Fin contribution

From eq.(3.5),

$$I_F + i J_F = -\frac{U}{2\pi} Sp_f \exp(-k_0 h_f \sec^2 q) \int_{-Lc_f/2+C_f}^{Lc_f+C_f} \frac{dz}{dx} \exp(i k_0 x \sec\theta)\, dx \qquad (3.39)$$

Introducing dimensionless co-ordinates $x'=2x/Lc_f$ and $z'=2z/T_f$ where T_f is the maximum thickness of fin, the above equation can be written in the normalised form:

$$I_F + i J_F = -\frac{U}{4\pi} Sp_f T_f \exp(-k_{1f} h_f \sec^2\theta) \int_{-1+C_f}^{1+C_f} \frac{dz}{dx} \exp(i \beta_f x)\, dx \qquad (3.40)$$

where the superscript symbol ' is dropped out, C_f and h_f are non-dimensionalised by $Lc_f/2$ and

$$k_{1f} = \frac{gLc_f}{2U^2} \qquad \beta_f = k_{1f}\sec\theta \qquad (3.41)$$

Also, non-dimensionalising eq.(3.10) and then substituting its x-derivative into eq.(3.40) gives:

$$I_F + i J_F = -\frac{U}{2\pi} Sp_f T_f \exp(-k_{1f} h_f \sec^2\theta)\,(Q_{f1} + i Q_{f2}) \qquad (3.42)$$

where

$$Q_{f1} = \frac{\cos(\beta_f(c_f+1)] - \cos(\beta_f(c_f-1)]}{\beta_f^2} + \frac{\sin[\beta_f(c_f+1)] + \sin[\beta_f(c_f-1)]}{\beta_f}$$

$$Q_{f2} = \frac{\sin(\beta_f(c_f+1)] - \sin(\beta_f(c_f-1)]}{\beta_f^2} - \frac{\cos[\beta_f(c_f+1)] + \cos[\beta_f(c_f-1)]}{\beta_f} \qquad (3.43)$$

Finally,

$$R_{wf} = 32\pi\rho k_0^2 \frac{U^2 T_f^2 Sp_f^2}{4\pi^2} \int_0^\infty E_f(u) \left(Q_{f1}^2 + Q_{f2}^2 \right) \cosh^2 u \, [1+\cos(k_1 B_1 \cosh u \sinh u)] \, du \tag{3.44}$$

where

$$E_f(u) = \exp(-2k_{1f} t_h \cosh^2 u) \tag{3.45}$$

3.2.1.4 Interferences contribution

So far, we have examined the contributions of body, strut and fin in isolation to the wave-making resistance. In addition, there are interference wave-making resistances between the components of a SWATH ship. As mentioned in section 2.7 of Chapter 2, based on the linear superposition principle, these interference components can be calculated from the formulae derived thus far. For instance, for a tandem strut (dissimilar to each other) SWATH ship with a pair of controllable fins, I^2+J^2 in the integrand of eq.(3.1) will be given by:

$$I^2 + J^2 = (I_B^2 + J_B^2) + (I_S^2 + J_S^2) + (I_{S1}^2 + J_{S1}^2) + (I_F^2 + J_F^2)$$

$$+ 2 [(I_S I_B + J_S J_B) + (I_{S1} I_B + J_{S1} J_B) + (I_S I_{S1} + J_S J_{S1}) + (I_F I_S + J_F J_S)$$

$$+ (I_F I_{S1} + J_F J_{S1}) + (I_F I_B + J_F J_B)] \tag{3.46}$$

where S_1 indicates the second strut for the tandem strut. If a SWATH has triple struts on the demihull, further interferences are to be expected and also, two pairs of fins, will create extra interferences.

For the dissimilar second or third strut,the dimensions of the second or third strut can be directly substituted into eqs.(3.36) and (3.37).

When the centre of the strut C_S is different from that of the body as shown in fig.3.2, the integration limit in eq.(3.33) should be changed to $(-1+C_S, 1+C_S)$:

$$I_S + i\,J_S = \frac{U}{4\pi} T_s E_s \int_{-1+C_s}^{1+C_s} \frac{dt}{dx} \exp(i\,\beta_s x)\,dx \tag{3.47}$$

The integration of the above equation with regard to x will lead to eq.(3.36), but Q_{S1} and Q_{S2} are changed to the followings:

$$Q_{s1} = -\frac{2}{\beta_s^2}\left(\frac{\cos[\beta_s(C_s+1)]}{l_{se}^2} - \frac{\cos[\beta_s(C_s-1)]}{l_{sr}^2}\right)$$

$$-\frac{2}{\beta_s}\left(\frac{\sin[\beta_s(C_s+1)]}{l_{se}} - \frac{\sin[\beta_s(C_s-1)]}{l_{sr}}\right)$$

$$+\frac{2}{\beta_s^2}\left(\frac{\cos(\beta_s x_3)}{l_{se}^2} - \frac{\cos(\beta_s x_4)}{l_{sr}^2}\right)$$

$$Q_{s2} = \frac{2}{\beta_s^2}\left(\frac{\sin[\beta_s(C_s+1)]}{l_{se}^2} + \frac{\sin[\beta_s(C_s-1)]}{l_{sr}^2}\right)$$

$$-\frac{2}{\beta_s}\left(\frac{\cos[\beta_s(C_s+1)]}{l_{se}} + \frac{\cos[\beta_s(C_s-1)]}{l_{sr}}\right)$$

$$+\frac{2}{\beta_s^2}\left(\frac{\sin(\beta_s x_3)}{l_{se}^2} - \frac{\sin(\beta_s x_4)}{l_{sr}^2}\right) \tag{3.48}$$

Using these results, the interference wave-making resistance between a strut and a body which have different centres from each other can be calculated.

For the second strut, from eq.(3.36),

$$I_{S1} + i\,J_{S1} = \frac{U}{4\pi} T_{s1} E_{s1} (Q_{s11} + i\,Q_{s12}) \tag{3.49}$$

where T_{S1} is the maximum thickness of the second strut and

$$E_{s1} = \frac{1}{k_0 \sec^2\theta}\left[\,1 - \exp(-h_{s1}k_{1s1}\sec^2\theta)\,\right]$$

$$h_{S1} = \frac{2h_{s1}}{L_{s1}} \quad \text{and} \quad k_{1S1} = \frac{g\,L_{s1}}{2U^2} \tag{3.50}$$

where h_{S1} is the depth of the second strut which is usually the same as h_S and L_{S1} is the second strut length. Q_{S11} and Q_{S12} can be obtained from eq.(3.48):

$$Q_{s11} = -\frac{2}{\beta_{s1}^2}\left(\frac{\cos[\beta_{s1}(C_{s1}+1)]}{l_{s1e}^2} - \frac{\cos[\beta_{s1}(C_{s1}-1)]}{l_{s1r}^2}\right)$$

$$-\frac{2}{\beta_{s1}}\left(\frac{\sin[\beta_{s1}(C_{s1}+1)]}{l_{s1e}} - \frac{\sin[\beta_{s1}(C_{s1}-1)]}{l_{s1r}}\right)$$

$$+\frac{2}{\beta_{s1}^2}\left(\frac{\cos(\beta_{s1}x_3)}{l_{s1e}^2} - \frac{\cos(\beta_{s1}x_4)}{l_{s1r}^2}\right)$$

$$Q_{s12} = \frac{2}{\beta_{s1}^2}\left(\frac{\sin[\beta_{s1}(C_{s1}+1)]}{l_{s1e}^2} + \frac{\sin[\beta_{s1}(C_{s1}-1)]}{l_{s1r}^2}\right)$$

$$-\frac{2}{\beta_{s1}}\left(\frac{\cos[\beta_{s1}(C_{s1}+1)]}{l_{s1e}} + \frac{\cos[\beta_{s1}(C_{s1}-1)]}{l_{s1r}}\right)$$

$$+\frac{2}{\beta_{s1}^2}\left(\frac{\sin(\beta_{s1}x_3)}{l_{s1e}^2} - \frac{\sin(\beta_{s1}x_4)}{l_{s1r}^2}\right) \tag{3.51}$$

where β_{S1} is $k_{1S}\sec\theta$. Therefore, using eqs.(3.47) and (3.49), the interference between the forward and aft struts can be calculated.

In the same way, I_{S2} and J_{S2} for the third strut and I_{F1} and J_{F1} for the second pair of fins can be derived and the additional interferences due to the presence of these items can also be calculated without any difficulty.

3.2.1.5 Contoured strut configuration

In order to achieve an optimum SWATH configuration with regard to resistance at certain speeds , contoured(locally bulged) hull or strut shapes have been recently considered. Using the mathematical formulae derived above, the distributions of strut thickness and of body cross sectional area can be longtitudinally varied.

As shown in Fig.3.3 which shows some of the more probable shapes, the local strut thickness can be linearly or parabolically reduced as desired. For the present study, the result derived for parabolical ends in section 3.2.1.2 can be directly utilised. The integration limits in eq.(3.35) is changed for each local segment and then, the imaginary and real parts are summed up to determine Q_{S1} and Q_{S2} given by eq.(3.37). Finally, the wave-making resistance of a contoured strut can be calculated from eq.(3.38)

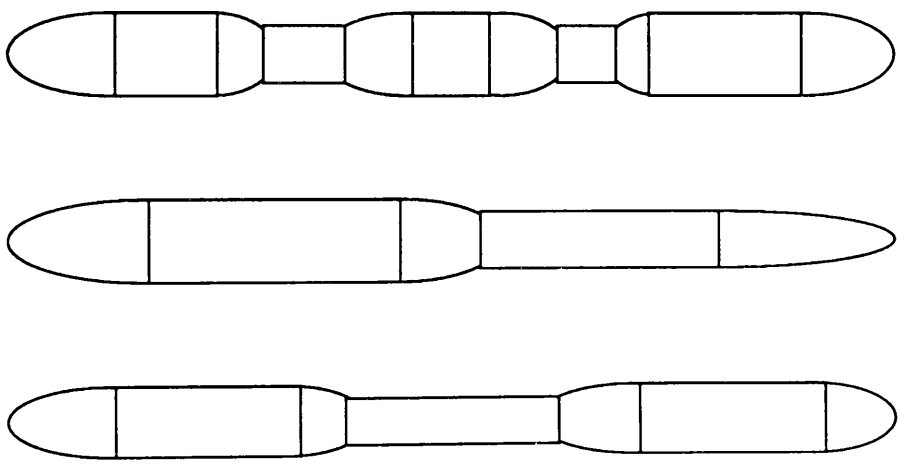

Fig.3.3 Most Probable Contoured Shapes for Strut(top view) and Body(side View)

Contoured hulls lead to non-uniform depth struts which cannot be expressed in simple mathematical formulae and thus the computation of the wave-making resistance is not as simple. By assuming that a strut with uniform depth stands on the maximum depth section of a contoured hull which means there are some discontinuities between strut and body, the wave-making resistance of a SWATH ship with contoured hulls can be relatively evaluated. Of course, the wave-making resistance of a contoured body itself can be calculated without any difficulty.

3.2.2 SWATH Ships Defined by Offsets

A series using some fundamental set of functions can generate a curved geometry. For instance, Chebyshev series has been used effectively and efficiently to represent a faired ship line from given offset tables.As mentioned in the introduction, utilising a special form of Chebyshev series(two set of Chebyshev coefficients) and the cubic spline (piecewise continuous polynomial) curve fitting method, Lin calculated the wave-making resistance of SWATH ships defined in offset form.

Defining

$$x = \sin\phi \qquad -1 \le x \le 1 \tag{3.52}$$

and using a fundamental set of Chebyshev series as follows:

$$U_m(x) = \cos(2m-1)\phi = \cos[(2m-1)\sin^{-1}x]$$

$$V_m(x) = \sin 2m\phi = \sin(2m\sin^{-1}x) \tag{3.53}$$

the half thickness t(x) of the strut and the cross sectional area A(x) of the body can then be expressed in the form of a finite sums of the series:

$$t(x) = \sum_{m=1}^{M} [\, A_{sm}U_m(x) + B_{sm}V_m(x) \,] \tag{3.54}$$

$$A(x) = \sum_{m=1}^{M} [\, A_{bm}U_m(x) + B_{bm}V_m(x) \,] \tag{3.55}$$

where A_{sm} and B_{sm} are the Chebyshev coefficients for the strut and A_{bm} and B_{bm} are the coefficients for the body. Using the property of the orthogonality of the series, these coefficients can be obtained from the following integrals:

$$A_{sm} = \frac{2}{\pi}\int_{-1}^{1} \frac{t(x)\,U_m(x)}{\sqrt{1-x^2}}\,dx = \frac{2}{\pi}\int_{\pi/2}^{\pi/2} t(\sin\phi)\cos(2m-1)\phi\,d\phi \tag{3.56}$$

$$B_{sm} = \frac{2}{\pi}\int_{-1}^{1} \frac{t(x)\, V_m(x)}{\sqrt{1-x^2}}dx = \frac{2}{\pi}\int_{-\pi/2}^{\pi/2} t(\sin\phi)\, \sin(2m\phi)\, d\phi \tag{3.57}$$

$$A_{bm} = \frac{2}{\pi}\int_{-1}^{1} \frac{A(x)\, U_m(x)}{\sqrt{1-x^2}}\, dx = \frac{2}{\pi}\int_{-\pi/2}^{\pi/2} A(\sin\phi)\, \cos(2m-1)\phi\, d\phi \tag{3.58}$$

$$B_{bm} = \frac{2}{\pi}\int_{-1}^{1} \frac{A(x)\, V_m(x)}{\sqrt{1-x^2}}\, dx = \frac{2}{\pi}\int_{-\pi/2}^{\pi/2} A(\sin\phi)\, \sin(2m\phi)\, d\phi \tag{3.59}$$

For the symmetrical fore and aft geometry, B_{sm} and B_{bm} disappear, thus necessitating the calculation of only one set of coefficients.

For two dissimilar struts(tandem) configuration, another series is introduced:

$$t_1(x) = \sum_{m=1}^{M} [\, A_{s1m} U_m(x) + B_{s1m} V_m(x) \,] \tag{3.60}$$

The maximum number of terms required in the series to represent a faired ship line varies with the shape of the specific lines and the degree of accuracy desired. Lin and Day[3] reported that for a typical ship line, twelve to fifteen terms are enough to graphically produce smooth curves with good accuracy and for the calculation of wave-making resistance integrals which will be derived later, a series of six terms seems to give satisfactory answers.

In order to calculate the integrals given by eqs.(3.56) to (3.59) from dicsrete offsets on the strut and hull, cubic splines[10] can be used to fit these discrete points. Given a set of n data points (X_i, Y_i), and provided that there be the continuity of the second derivatives $Y_i''(S_i)$ between the various segments of the spline, the following set of simultaneous linear algebraic equations of spline functions can be obtained:

$$S_1 - (1 + \frac{h_1}{h_2}) S_2 + \frac{h_1}{h_2} S_3 = 0$$

$$\frac{h_{i-1}}{2(h_{i-1}+h_i)} S_{i-1} + S_i + \frac{h_{i+1}}{2(h_{i-1}+h_{i+1})} S_{i+1} = \frac{3}{h_{i-1}+h_i}\left[\frac{Y_{i+1}-Y_i}{h_i} - \frac{Y_i-Y_{i-1}}{h_{i-1}}\right], \quad i=2,\text{-- } n-1$$

$$\frac{h_{n-1}}{h_{n-2}} S_{n-2} - \left(1 + \frac{h_{n-1}}{h_{n-2}}\right) S_{n-1} + S_n = 0 \tag{3.61}$$

The above equations can be written in a band matrix form which can be solved by linear decomposition to determine the unknown spline functions.

The integrands of eqs.(3.56) to (3.59) are very oscillatory, in particular, as m increases. One of the most effective methods of numerical integration for this kind of functions is Filon quadrature[11] for which the second derivatives obtained from solving the spline equations can be used directly. The Filon quadrature formulae which will be used to evaluate A_m(A_{sm} or A_{bm}) and B_m(B_{sm} or B_{bm}) can be written as follows:

$$A_m = \frac{2}{\pi} \sum_{i=1}^{N} \int_{\phi_i}^{\phi_i+1} f_i(\sin\phi)\, \cos k\phi \, d\phi$$

$$= \frac{2}{\pi} \sum_{i=1}^{N} \int_{\phi_i}^{\phi_{i+1}} \left[a\,(\sin\phi - \sin\phi_i)^3 + b\,(\sin\phi - \sin\phi_i)^2 - c\,(\sin\phi - \sin\phi_i) + d \right] \cos k\phi \, d\phi$$

$$= \frac{2}{\pi} \sum_{i=1}^{N} \left[\cos k\phi_i (A_1 a + B_1 b + C_1 c + D_1 d) - \sin k\phi_i (A_2 a + B_2 b + C_2 c + D_2 d) \right]$$

(3.62)

where $k = 2m-1$, and

$$B_m = \frac{2}{\pi} \sum_{i=1}^{N} \int_{\phi_i}^{\phi_i+1} f_i(\sin\phi)\, \sin k\phi \, d\phi$$

$$= \frac{2}{\pi} \sum_{i=1}^{N} \int_{\phi_i}^{\phi_{i+1}} \left[a\,(\sin\phi - \sin\phi_i)^3 + b\,(\sin\phi - \sin\phi_i)^2 - c\,(\sin\phi - \sin\phi_i) + d \right] \sin k\phi \, d\phi$$

$$= \frac{2}{\pi} \sum_{i=1}^{N} [\ \sin k\phi_i (\ A_1 a + B_1 b + C_1 c + D_1 d\ ) + \cos k\phi_i (\ A_2 a + B_2 b + C_2 c + D_2 d\ )\ ]$$

(3.63)

where k = 2m. The integrals given by eqs.(3.56) to (3.59) can be calculated using the above two schemes with the following substitutions:

$$h_i = \phi_{i+1} - \phi_i\ ,\ Y_i = f(\sin\phi_i)$$

$$a = \frac{S_{i+1} - S_i}{6h_i}\ ,\ b = \frac{S_i}{2}\ ,\ c = \frac{Y_{i+1} - Y_i}{h_i} - \frac{h_i (\ S_{i+1} + 2S_i)}{6}\ ,\ d = Y_i$$

and

$$A_1 = \frac{(3k^2 h_i^2 - 6)\cos kh_i}{k^4} + \frac{(k^2 h_i^3 - 6h_i)\sin kh_i}{k^3} + \frac{6}{k^4}\ ,$$

$$A_2 = \frac{3h_i^2 \sin kh_i}{k^2} - \frac{6\sin kh_i}{k^4} - \frac{h_i^3 \cos kh_i}{k} + \frac{6h_i \cos kh_i}{k^3}\ ,$$

$$B_1 = \frac{2h_i \cos kh_i}{k^2} - \frac{2\sin kh_i}{k^3} + \frac{h_i^2 \sin kh_i}{k}\ ,$$

$$B_2 = \frac{2h_i \sin kh_i}{k^2} + \frac{2\cos kh_i}{k^3} - \frac{h_i^2 \cos kh_i}{k} - \frac{2}{k^3}\ ,$$

$$C_1 = \frac{\cos kh_i}{k^2} + \frac{h_i \sin kh_i}{k} - \frac{1}{k^2}\ ,$$

$$C_2 = \frac{\sin kh_i}{k^2} - \frac{h_i \cos kh_i}{k}\ ,$$

$$D_1 = \frac{\sin kh_i}{k} \quad \text{and} \quad D_2 = \frac{-\cos kh_i}{k} + \frac{1}{k}\ .$$

where the above notations are used only for this purpose and have nothing to do with

the same notations, if any, appearing in other parts of the thesis. With the known Chebyshev coefficients for the strut and body, we can calculate the wave-making resistance given by eq.(3.1) using eqs.(3.3) and (3.4).

3.2.2.1 Body contribution

The partial integration of eq.(3.14) with regard to x gives the following:

$$I_B + iJ_B = -\frac{U}{8\pi} A_m E_b \{ [A(x) \exp(i \beta x)]_{-1}^{+1} - \int_{-1}^{1} A(x)\, i\beta \exp(i \beta x)\, dx \}$$

$$= \frac{U}{8\pi} A_m E_b \int_{-1}^{1} A(x)\, i\beta \exp(i \beta x)\, dx \qquad (3.64)$$

where it is assumed that A(1) and A(–1) disappear. The above equation can be written in the following form:

$$I_B = -\frac{U}{8\pi} A_m E_b \int_{-1}^{1} A(x)\, \beta \sin(\beta x)\, dx \qquad (3.65)$$

$$J_B = \frac{U}{8\pi} A_m E_b \int_{-1}^{1} A(x)\, \beta \cos(\beta x)\, dx \qquad (3.66)$$

In order to calculate eq.(3.1), the square terms of the above two equations are needed and using eq.(3.55), the following result can be obtained:

$$I_B^2 = \frac{U^2}{64\pi_2} A_m^2 E_b^2 \beta^2 \{ \sum_{m=1}^{M} \sum_{n=1}^{N} \int_{-1}^{1} [A_{bm} U_m(x) + B_{bm} V_m(x)] \sin(\beta x)\, dx$$

$$\int_{-1}^{1} [A_{bn} U_n(x) + B_{bn} V_n(x)] \sin(\beta x)\, dx \}$$

$$= \frac{U^2}{64\pi^2} A_m^2 E_b^2 \beta^2 \sum_{m=1}^{M} \sum_{n=1}^{N} \{$$

$$[\, A_{bm} A_{bn} \int_{-1}^{1} U_m(x) \sin(\beta x)\, dx \int_{-1}^{1} U_n(x) \sin(\beta x)\, dx$$

$$+ A_{bm} B_{bn} \int_{-1}^{1} U_m(x) \sin(\beta x)\, dx \int_{-1}^{1} V_n(x) \sin(\beta x)\, dx$$

$$+ B_{bm} A_{bn} \int_{-1}^{1} V_m(x) \sin(\beta x)\, dx \int_{-1}^{1} U_n(x) \sin(\beta x)\, dx$$

$$+ B_{bm} B_{bn} \int_{-1}^{1} V_m(x) \sin(\beta x)\, dx \int_{-1}^{1} V_n(x) \sin(\beta x)\, dx \,] \,\}$$

$$= \frac{U^2}{64\pi^2} A_m^2 E_b^2 \beta^2 \sum_{m=1}^{M} \sum_{n=1}^{N} [$$

$$B_{bm} B_{bn} \int_{-1}^{1} V_m(x) \sin(\beta x)\, dx \int_{-1}^{1} V_n(x) \sin(\beta x)\, dx \,] \tag{3.67}$$

where the remaining terms all disappear due to their odd functions in x. Similarly,

$$J_B^2 = \frac{U^2}{64\pi^2} A_m^2 E_b^2 \beta^2 \sum_{m=1}^{M} \sum_{n=1}^{N} [$$

$$A_{bm} A_{bn} \int_{-1}^{1} U_m(x) \cos(\beta x)\, dx \int_{-1}^{1} U_n(x) \cos(\beta x)\, dx \,] \tag{3.68}$$

Now, it will be shown that the above integrals can be expressed in terms of Bessel functions. Using $U_m(x) = \cos[(2m-1) \sin^{-1} x]$ given by eq.(3.53), it can be written:

$$\int_{-1}^{1} U_m(x) \cos(\beta x)\, dx = \int_{-1}^{1} \cos[(2m-1) \sin^{-1} x] \cos(\beta x)\, dx \tag{3.69}$$

The substitution of x=sinϕ given by eq.(3.52) into R.H.S of the above equation leads to:

$$\int_{-\pi/2}^{\pi/2} \cos[(2m-1)\phi \cos] \cos(\beta \sin\phi) \cos\phi \, d\phi \tag{3.70}$$

and the partial integration of eq.(3.70) will be written in the form:

$$\frac{2(2m-1)}{\beta} \int_{0}^{\pi/2} \sin[(2m-1)\phi] \sin(\beta \sin\phi) \, d\phi \tag{3.71}$$

Finally, this can be written as[12]:

$$\frac{\pi}{\beta} (2m-1) J_{2m-1}(\beta) \tag{3.72}$$

where $J_{2m-1}(\beta)$ is a Bessel function of the 1st kind with integer order and argument(β).

In the same way,

$$\int_{-1}^{1} U_n(x) \cos(\beta x) \, dx = \frac{\pi}{\beta} (2n-1) J_{2n-1}(\beta) \tag{3.73}$$

and also,

$$\int_{-1}^{1} V_m(x) \sin(\beta x) \, dx = \frac{\pi}{\beta} 2m J_{2m}(\beta) \tag{3.74}$$

$$\int_{-1}^{1} V_n(x) \sin(\beta x) \, dx = \frac{\pi}{\beta} 2n J_{2n}(\beta) \tag{3.75}$$

Substituting these Bessel functions into eqs.(3.67) and (3.68) and then, substituting these two equations into eq.(3.1), the body contribution to the wave-making resistance is written in the form:

$$R_{wb} = 16\pi\rho k_0^2 \frac{U^2}{64\pi^2} A_m^2 \pi^2 \int_{0}^{\pi/2} d\theta \, E_b^2 \sec^2\theta \, | \, 1 + \cos(B_1 k_1 \sec^2\theta \sin\theta) |$$

$$\{\sum_{m=1}^{M}\sum_{n=1}^{N}[\,(2m-1)(2n-1)\,A_{bm}A_{bn}J_{2m-1}(\beta)\,J_{2n-1}(\beta)\,]$$

$$+\sum_{m=1}^{M}\sum_{n=1}^{N}[\,2m\;2n\,B_{bm}B_{bn}J_{2m}(\beta)\,J_{2n}(\beta)\,]\,\} \tag{3.76}$$

As in section 3.2.1, in order to remove the singularity for numerical calculation, secθ in the above equation is replaced by coshu and then, finally, it can be written in the form:

$$R_{wb}=\frac{\pi\rho k_0^2U^2}{4}A_m^2\sum_{m=1}^{M}\sum_{n=1}^{N}(\,A_{bm}A_{bn}T_{bmn}+B_{bm}B_{bn}W_{bmn}\,) \tag{3.77}$$

where

$$T_{bmn}=(2m-1)(2n-1)\int_0^{\infty}E_b^2(u)\cosh^2u\,[1+\cos(\,B_1k_1\cosh u\sinh u)]J_{2m-1}(\beta)J_{2n-1}(\beta)\,du \tag{3.78}$$

$$w_{bmn}=2m\;2n\int_0^{\infty}E_b^2(u)\cosh^2u\,[1+\cos(\,B_1k_1\cosh u\sinh u)]J_{2m}(\beta)J_{2n}(\beta)\,du \tag{3.79}$$

$$E_b=\frac{1}{\frac{D_b}{L_b}k_1\cosh^2u}\{\exp[\,\frac{D_b}{L_b}k_1\cosh^2u\,(1-H_1)]-\exp[\,\frac{D_b}{L_b}k_1\cosh^2u\,(1+H_1)]\,\} \tag{3.80}$$

3.2.2.2 Strut contribution

Integrating eq.(3.33) by parts with regard to x leads to:

$$I_S+i\,J_S=\frac{U}{4\pi}T_sE_s\int_{-1}^{1}t(x)\,i\beta_s\exp(\,i\,\beta\,x)\,dx \tag{3.81}$$

which can be written in the form:

$$I_S = -\frac{U}{4\pi} T_s E_s \int_{-1}^{1} t(x)\ \beta_s \sin(\beta x)\, dx \tag{3.82}$$

$$J_S = \frac{U}{4\pi} T_s E_s \int_{-1}^{1} t(x)\ \beta_s \cos(\beta x)\, dx \tag{3.83}$$

Substituting eq.(3.54) into eq.(3.82) and then the square terms will be written in the form:

$$I_S^2 = \frac{U^2}{16\pi^2} T_s^2 E_s^2 \beta_s^2 \sum_{m=1}^{M} \sum_{n=1}^{N} [$$

$$A_{sm} A_{sn} \int_{-1}^{1} U_m(x) \sin(\beta_s x)\, dx \int_{-1}^{1} U_n(x) \sin(\beta_s x)\, dx$$

$$+ A_{sm} B_{sn} \int_{-1}^{1} U_m(x) \sin(\beta_s x)\, dx \int_{-1}^{1} V_n(x) \sin(\beta_s x)\, dx$$

$$+ B_{sn} A_{sm} \int_{-1}^{1} V_n(x) \sin(\beta_s x)\, dx \int_{-1}^{1} U_m(x) \sin(\beta_s x)\, dx$$

$$+ B_{sn} B_{sm} \int_{-1}^{1} V_n(x) \sin(\beta_s x)\, dx \int_{-1}^{1} V_m(x) \sin(\beta_s x)\, dx\ ]$$

$$= \frac{U^2}{16\pi^2} T_s^2 E_s^2 \beta_s^2 \sum_{m=1}^{M} \sum_{n=1}^{N} [\ (\frac{\pi}{\beta_s})^2 B_{sm} B_{sn}\ 2m\ 2n\ J_{2m}(\beta_s)\ J_{2n}(\beta_s)\ ] \tag{3.84}$$

where Bessel functions given by eqs.(374) and (3.75) are used and the remaining terms all disappear due to being odd functions in x. Similarly, from eq.(3.83), one can obtain:

$$J^2 = \frac{U^2}{16\pi^2} T_s^2 E_s^2 \beta_s^2 \sum_{m=1}^{M} \sum_{n=1}^{N} [\ (\frac{\pi}{\beta_s})^2 B_{sm} B_{sn}\ 2m\ 2n\ J_{2m}(\beta_s)\ J_{2n}(\beta_s)\ ] \tag{3.85}$$

Substituting eqs.(3.84) and (3.85) into eq.(3.1), finally the wave-making resistance of a strut can be obtained:

$$R_{ws} = \pi\rho U^2 k_0^2 T_s^2 \sum_{m=1}^{M}\sum_{n=1}^{N} (A_{sm}A_{sn}T_{smn} + B_{sm}B_{sn}W_{smn}) \tag{3.86}$$

where

$$T_{smn} = (2m-1)(2n-1) \int_0^{\infty} E_s^2(u) \cosh^2 u \, [1+\cos(B_1 k_1 \cosh u \sinh u)] J_{2m-1}(\beta_s) J_{2n-1}(\beta_s) \, du \tag{3.87}$$

$$w_{smn} = 2m\,2n \int_0^{\infty} E_s^2(u) \cosh^2 u \, [1+\cos(B_1 k_1 \cosh u \sinh u)] J_{2m}(\beta_s) J_{2n}(\beta_s) \, du \tag{3.88}$$

$$E_s(u) = \frac{1}{k_0 \cosh^2 u} [\, 1 - \exp(-h_s k_{1s} \cosh^2 u \,) \,] \tag{3.89}$$

3.2.2.3 Body and strut interference contribution

For this purpose, we have to consider a general case where the longitudinal centre of the strut is located at C_S from that of body as shown in Fig.3.1. Carrying out a partial integration of eq.(3.47) with regard to x, the real and imaginary parts can be separately written in the form:

$$I_S = \frac{UT_s}{4\pi} E_s \beta_s [\cos(\beta_s C_s) \int_{-1}^{1} t(x) \sin(\beta_s x) \, dx + \sin(\beta_s C_s) \int_{-1}^{1} t(x) \cos(\beta_s x) \, dx] \tag{3.90}$$

$$J_S = \frac{UT_s}{4\pi} E_s \beta_s [\sin(\beta_s C_s) \int_{-1}^{1} t(x) \sin(\beta_s x) \, dx - \cos(\beta_s C_s) \int_{-1}^{1} t(x) \cos(\beta_s x) \, dx] \tag{3.91}$$

Using the above two equations and eqs.(3.65) and (3.66), the interference component is calculated as follows:

$$2(I_S I_B + J_S J_B) = 2 \frac{U}{8\pi} A_m E_b \frac{UT_s}{4\pi} E_s \beta_s [$$

$$\int_{-1}^{1} A(x)\sin(\beta x)\,dx\Big[\cos(\beta_s C_s)\int_{-1}^{1} t(x)\sin(\beta_s x)\,dx + \sin(\beta_s C_s)\int_{-1}^{1} t(x)\cos(\beta_s x)\,dx\Big]$$

$$-\int_{-1}^{1} A(x)\cos(\beta x)\,dx\Big[\sin(\beta_s C_s)\int_{-1}^{1} t(x)\sin(\beta_s x)\,dx - \cos(\beta_s C_s)\int_{-1}^{1} t(x)\cos(\beta_s x)\,dx\Big]\Big\} \tag{3.92}$$

As in the previous sections, introducing the Chebyshev series for strut and body given by eqs.(3.54) and (3.55) into the above equations , it can be written in the simplified form:

$$2(I_S I_B + J_S J_B) = \frac{U^2}{16} A_m T_s E_b E_s \sum_{m=1}^{m}\sum_{n=1}^{n} \{$$

$$B_{bn}B_{sm}\cos(\beta_s C_s)\, 2n\, 2m\, J_{2n}(\beta)\, J_{2m}(\beta_s)$$

$$+ B_{bn}A_{sm}\sin(\beta_s C_s)\, 2n\, (2m-1)\, J_{2n}(\beta)\, J_{2m-1}(\beta_s)$$

$$- A_{bn}B_{sm}\sin(\beta_s C_s)\, (2n-1)\, 2m\, J_{2n-1}(\beta)\, J_{2m}(\beta_s)$$

$$+ A_{bn}A_{sm}\sin(\beta_s C_s)\, (2n-1)\, (2m-1)\, J_{2n-1}(\beta)\, J_{2m-1}(\beta_s)\ \} \tag{3.93}$$

Finally,

$$R_{wsb} = \pi\rho U^2 k_0 A_m T_s \sum_{m=1}^{M}\sum_{n=1}^{N} (A_{bn}A_{sm}T_{sbmn} - A_{bn}B_{sm}TW_{sbmn}$$

$$+ B_{bn}A_{sm}WT_{sbmn} + B_{bn}B_{sm}W_{sbmn}) \tag{3.94}$$

where

$$T_{sbmn} = (2m-1)(2n-1)\int_0^{\infty} E_s(u)\, E_b(u)\cosh^2 u\,[1+\cos(B_1 k_1 \cosh u \sinh u)]$$

$$J_{2n-1}(\beta)\, J_{2m-1}(\beta_s)\, du \tag{3.95}$$

$$TW_{sbmn} = 2m\,(2n-1) \int_0^{\infty} E_s(u)\, E_b(u) \cosh^2 u\, [1+\cos(B_1 k_1 \cosh u \sinh u)]$$

$$J_{2n-1}(\beta)\, J_{2m}(\beta_s)\, du \tag{3.96}$$

$$WT_{sbmn} = (2m-1)\, 2n \int_0^{\infty} E_s(u)\, E_b(u) \cosh^2 u\, [1+\cos(B_1 k_1 \cosh u \sinh u)]$$

$$J_{2n}(\beta)\, J_{2m-1}(\beta_s)\, du \tag{3.97}$$

$$W_{sbmn} = 2m\, 2n \int_0^{\infty} E_s(u)\, E_b(u) \cosh^2 u\, [1+\cos(B_1 k_1 \cosh u \sinh u)]$$

$$J_{2n}(\beta)\, J_{2m}(\beta_s)\, du \tag{3.98}$$

3.2.2.4 Fore and aft struts interference

For a tandem strut SWATH ship which has two different struts on a demihull, following the same procedure as in section 3.2.2.2, we can calculate the wave-making resistance of the second strut using the different series given by eq.(3.60). Also, in a similar way to the calculation of the interference between strut and body in the previous section, the interference between two struts on a demihull can be calculated. Using eqs.(3.90) and (3.91) and another two equivalent equations for the second strut, the interference factor between two struts can be written in the form:

$$2(I_S I_{S1} + J_S J_{S1}) = 2\,\frac{U^2}{16\pi^2}\, T_s T_{s1} E_s E_{s1} \beta_s \beta_{s1} \{$$

$$[\cos(\beta_s C_s) \int_{-1}^{1} t(x) \sin(\beta_s x)\, dx + \sin(\beta_s C_s) \int_{-1}^{1} t(x) \cos(\beta_s x)\, dx]$$

$$[\cos(\beta_{s1}C_{s1})\int_{-1}^{1} t_1(x)\sin(\beta_{s1}x)\,dx + \sin(\beta_{s1}C_{s1})\int_{-1}^{1} t_1(x)\cos(\beta_{s1}x)\,dx]$$

$$+ [\sin(\beta_s C_s)\int_{-1}^{1} t(x)\sin(\beta_s x)\,dx - \cos(\beta_s C_s)\int_{-1}^{1} t(x)\cos(\beta_s x)\,dx]$$

$$[\sin(\beta_{s1}C_{s1})\int_{-1}^{1} t_1(x)\sin(\beta_{s1}x)\,dx - \cos(\beta_{s1}C_{s1})\int_{-1}^{1} t_1(x)\cos(\beta_{s1}x)\,dx]\} \tag{3.99}$$

Introducing the Chebyshev series for the two struts given by eqs.(3.54) and (3.60) into the above equation, the final result can be written in the form:

$$R_{ws12} = 2\pi\rho U^2 k_0^2 T_s T_{s1}\sum_{m=1}^{M}\sum_{n=1}^{N}(A_{sn}A_{s1m}T_{ss1mn} + B_{sn}B_{s1m}W_{ss1mn}$$

$$+ B_{sn}A_{s1m}WT_{ss1mn} + A_{sn}B_{s1m}TW_{ss1mn}) \tag{3.100}$$

where

$$T_{ss1mn} = (2m-1)(2n-1)\int_0^{\infty} E_s(u)\,E_{s1}(u)\cosh^2 u\,[1+\cos(B_1 k_1 \cosh u \sinh u)]$$

$$J_{2n-1}(\beta)\,J_{2m-1}(\beta_{s1})\cos(\beta_s C_s - \beta_{s1}C_{s1})\,du \tag{3.101}$$

$$W_{ss1mn} = 2m\,2n\int_0^{\infty} E_s(u)\,E_{s1}(u)\cosh^2 u\,[1+\cos(B_1 k_1 \cosh u \sinh u)]$$

$$J_{2n}(\beta_s)\,J_{2m}(\beta_{s1})\cos(\beta_s C_s - \beta_{s1}C_{s1})\,du \tag{3.102}$$

$$WT_{ss1mn} = (2m-1)\,2n\int_0^{\infty} E_s(u)\,E_{s1}(u)\cosh^2 u\,[1+\cos(B_1 k_1 \cosh u \sinh u)]$$

$$J_{2n}(\beta)\,J_{2m-1}(\beta_{s1})\sin(\beta_s C_s - \beta_{s1}C_{s1})\,du \tag{3.103}$$

$$TW_{ss1\,mn} = 2m\,(2n-1) \int_0^{\infty} E_s(u)\, E_{s1}(u) \cosh^2 u\, [1+\cos(B_1 k_1 \cosh u \sinh u)]$$

$$J_{2n-1}(\beta)\, J_{2m}(\beta_{s1}) \sin(\beta_s C_s - \beta_{s1} C_{s1})\, du \qquad (3.104)$$

When two struts are identical to each other, eqs.(3.103) and (3.104) cancel each other so that the result can be calculated simply, without calculating eqs.(3.101) and (3.102), by multiplying the resistance of the strut given by eq.(3.86) by the factor $\cos[\beta_S(C_S - C_{S1})]$.

3.2.3 Numerical Integration Scheme for Wave Resistance Integrals

In order to develop an integration scheme, which can calculate the wave resistance integrals developed so far, effectively and economically with good accuracy, it is necessary to investigate the behaviour of the integrands. Fig.3.4 shows a typical integrand variation with the independent variable u which is given by eq.(3.25) for a body with paraboloidal ends. As seen in the figure, the integrand is oscillatory and varies rapidly or smoothly(sometimes with negative values as well) with ship form, speed and spacing between two demihulls. Also, as expected, the integrand dies out with the increase of the variable u as well as of the body submergence due to the prensence of the exponential term E_b in the integrand. As the body becomes closer to the free surface(H_1=1 means that the top of the body is touching the free surface), the oscillation becomes severe and the area below the curve, which will be the wave-making resistance of the body when multiplied by the constant in eq.(3.25), is increased. Since all the other intergands behave like this, thay can be integrated with good accuracy without any difficulty.

A Gaussian quadrature[13] which is suited to such high oscillatory functions is employed to the present purpose, as given by:

$$\int_A^B f(x)\, dx = \frac{B-A}{2} \sum_{i=1}^{N} w_i\, f\left[\frac{(B-A)\, t_i + (B+A)}{2}\right] \qquad (3.105)$$

where w_1 , w_2.... w_n are weighting coefficients and t_1 , t_2 .... t_n are the roots of the Legendre polynomial $P_n(t) = 0$. The value N changes depending on the density of oscillation up to 6.

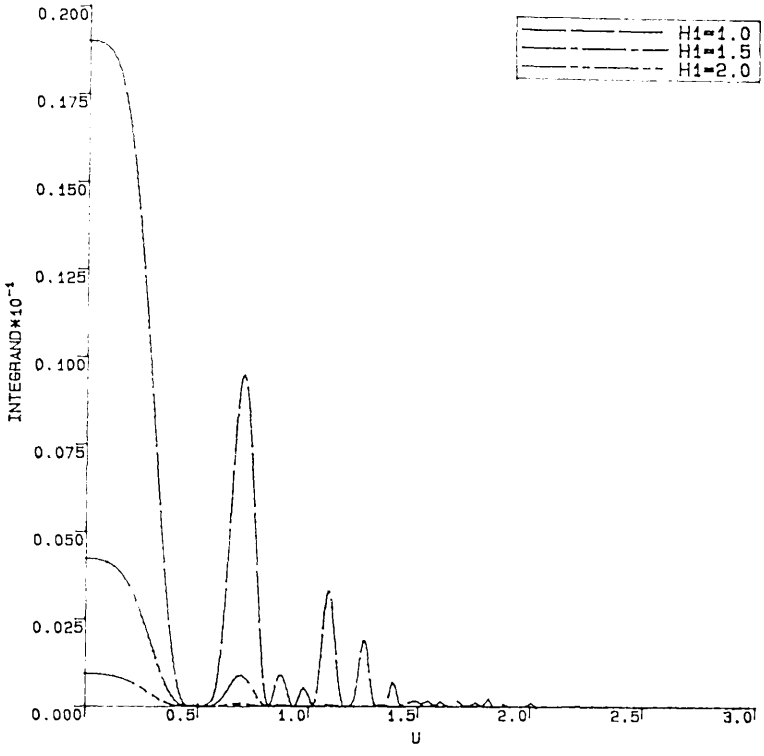

Fig.3.4 Typical Integrand with Variable U at three Submergence
k_{1S}=15.0, l_{be}=0.2, l_{sr}=0.3, B_1=0.4

As seen in Fig.3.4, the integrand is highly oscillatory in the first few values of u and then approaches zero quickly with increasing submergence of the body. Therefore, the integration range is divided into two regions, the initial and tail regions. The initial region ranges from zero to 1 in which 3-10 local intervals, depending on accuracy desired, can be made. For the each local interval, the quadrature given by eq.(3.105) is employed for the integration and is summed up to give the result in the initial region. It can be said, from experience, that 5 local intervals in the initial region are enough to give excellent answers for all the integrals.

Then, an interval 0.5, in which 2-3 local intervals can be made(3 is chosen for the present purpose), is added to the end of the initial region, 1.0, in order to carry out the

integration in the tail region with the introduction of the convergence factor given by:

$$\varepsilon \geq \frac{S_{n+1} - S_n}{S_n} \tag{3.106}$$

where S_n is the sum, including the sum in the initial region, up to n intervals. If the result fails to pass the above test, another 0.5 is added to the last value u and so on. The value of ε is also dependent upon on accuracy desired. However, $\varepsilon = 1.0\times10^{-7}$ is enough to give excellent answers. From experience, it can be said that for the submerged body, the integration converges in 2or 3 cycles(u=2.5) and for the surface piercing strut and interferences between strut and other parts, 5 or 6 cycles(u=4.0).

For SWATH ships defined by mathematical formulae, the calculation of the wave-making resistance for each component, as derived in section 3.2.1, is performed with the single integration of each integrand(ie, eq.(3.22) for the body). However, in the offset input case, the final equations, as given by eqs.(3.77), (3.86), (3.94) and (3.100), appear in double summation form with the single integral form of auxillary functions(T,W,TW,WT) which are equivalent to the final single integral form for SWATH ships defined by mathematical formulae. As a result, in principle, the computing time of these equations is (M×N) times longer than that of a mathematically represented SWATH ship. As mentioned in section 3.2.2, M and N are the order of Chebyshev series which is decided by the ship form and the accuracy desired. From experience, seven to ten give answers with good accuracy for the calculation of wave resistance integrals.

3.3 CALCULATION OF SKIN FRICTIONAL RESISTANCE

3.3.1 Calculation of Surfaces and Volumes

In order to calculate the frictional resistance accurately, it is essential to obtain the exact surface area of a ship. Also, the exact estimation of the displaced volume is important which is often used to non-dimensionalise the resistance in order to compare the resistances of ships with different displacements.

3.3.1.1 SWATH ships defined by mathematical formulae

For geometries defined by mathematical formulae given by eqs.(3.6) to (3.10), the surfaces and volumes can be all calculated analytically.

For an elliptical entrance given by eq.(3.6), the volume will be obtained as:

$$V = A_m \int_0^{l_{be}} [\, 1 - (\frac{x}{l_{be}})^2] \, dx = \frac{2}{3} A_m l_{be} \tag{3.107}$$

where A_m is $\pi(Di_b/2)^2$ for a circular cross section and $\pi(D_b/2)(B_b/2)$ for an elliptical cross section. Also, the wetted area will be obtained as:

$$S = Pe \int_0^{l_{be}} \sqrt{1 - (\frac{x}{l_{be}})^2} \, dx = Pe \frac{\pi l_{be}}{4} \tag{3.108}$$

where Pe(perimeter) is $2\pi(Di_b/2)$ for the circular cross section and for the elliptical cross section, is approximately given by[14]:

$$Pe = 2\pi \sqrt{\frac{1}{2}[\, (\frac{D_b}{2})^2 + (\frac{B_b}{2})^2]} \tag{3.109}$$

Parabolical and conical entrances can be analytically calculated in a similar manner.

The waterplane area of the strut entrance given by eq.(3.9) can be obtained as:

$$A_{wp} = 2\, t_m \int_0^{l_{se}} [\, 1 - (\frac{x}{l_{se}})^2] \, dx = \frac{2}{3} l_{se} 2\, t_m \tag{3.110}$$

Due to the shape of the strut-body intersection the strut will not have constant depth over its length. Dividing the strut into segments, the surface area and volume can be approximately calculated by taking the mean depth of each segment and summing up the value for each segment to give the total value for the strut. However, in order to use to the non-dimensionalised wave-making resistance, the surface area and volume which are generated by the source system should be, in a real sense, considered. Therefore, for the present study, it is assumed that the depth of strut is constant over its length. As a result, the volume of the strut can be calculated by multiplying the strut depth(from the waterline to the top of the submerged body) to the water plane area given by eq.(3.110). Also, the surface area of the strut can be obtained by:

$$S = h_s\, 2 \int_0^{l_{se}} \sqrt{1+ (\frac{\partial t}{\partial x})^2}\; dx$$

$$= 2h_s \frac{1}{k} [\, \frac{l_{se}\sqrt{l_{ce}^2+k^2}}{2} + \frac{k^2}{2} \ln(l_{se}+ \sqrt{l_{se}^2+k^2}) - \frac{k^2}{2} \ln(k) \,] \qquad (3.111)$$

where $k=(l_{se})^2/(2t)$. Finally, when the total surface is calculated, the cross section area between strut and body, which is taken equal to the waterplane of the strut, should be subtracted from the body surface area.

3.3.1.2 SWATH ships defined by offsets.

Using the Chebyshev series given by eq.(3.55), the volume of the body can be calculated analytically:

$$V_b = \int_{-L_b/2}^{L_b/2} \pi\, Di_b^2(x)\, dx = A_m \frac{L_b}{2} \int_{-1}^{1} \sum_{m=1}^{M} [\, A_{bm} U_m(x) + B_{bm} V_m(x) \,]\, dx$$

$$= A_m \frac{L_b}{2} \sum_{m=1}^{M} [\, A_{bm} \int_{-\pi/2}^{\pi/2} \cos(2m-1)\phi \cos\phi\, d\phi + B_{bm} \int_{-\pi/2}^{\pi/2} \sin 2m\phi \cos\phi\, d\phi \,]$$

$$= \frac{\pi}{4} A_m L_b A_{b1} \qquad (3.112)$$

It can be seen that the body volume is totally determined by one Chebyshev coefficient.

The computation of the surface area of a circular cross section body can be calculated by dividing the body into n segments of equal length which may be determined by the body shape. The surface of each part is then given by:

$$ds = 2\pi \frac{(r_i+r_{i+1})}{2} \sqrt{\delta x^2 + \delta r^2} \qquad (3.113)$$

where $\delta r = r_{i+1} - r_i$ is the increment of the radius of the part and the radius is assumed to increase(decrease) linearly over its length.The total surface area of the body can be obtained by summing up the values of n segments.

For an elliptical cross section body which has uniform ratio of B_b/D_b over its

length, the surface area can be calculated from the surface area of a circular cross section body, which has the same cross sectional area as that of the elliptical cross section body, by multiplying the ratio of the two perimeters(Pe_e/Pe_c) where Pe_e is the perimeter of the elliptical cross section body and Pe_c the perimeter of the equivalent circular cross section body. Also, for a rectangular cross section body with rounded corners, the wetted area can be calculated from the wetted area of an equivalent circular cross body by multiplying by the ratio of the two perimeters.

Using the Chebyshev series given by eq.(3.54), the waterplane area of a strut can also be calculated analytically:

$$A_{wp} = 2\int_{-L_s/2}^{L_s/2} t(x)\,dx = 2\,\frac{T_s}{2}\frac{L_s}{2}\int_{-1}^{1}\sum_{m=1}^{M}\left[\,A_{sm}U_m(x) + B_{sm}V_m(x)\,\right]dx$$

$$= \frac{\pi}{4} L_s T_s A_{s1} \tag{3.114}$$

The volume of the strut is then calculated by multiplying the waterplane area by the strut depth which is assumed to be constant over its length, as given by:

$$V_s = \frac{\pi}{4} L_s T_s A_{s1} h_s \tag{3.115}$$

As for the calculation of the body surface area, the wetted surface of a strut can be computed by dividing the strut into N segments of equal length. Assuming the half-thickness to change linearly over the length, the length of one wetted side of each segment can be obtained by:

$$dl = \sqrt{\delta x^2 + \delta t^2} \tag{3.116}$$

where δt is the increment of the half-thickness over the segment. Finally, the total wetted area of the strut can be calculated by:

$$S_s = 2h_s\sum_{i=1}^{N} dl_i \tag{3.117}$$

where the number N is also dependent upon the strut shape.

3.3.2 Calculation of Skin Friction Resistance

Since a SWATH ship has several components which are different in length from one another, the skin frictional coefficient for each component is first calculated using the ITTC'57 formulae[15] given by:

$$C_f = \frac{0.075}{(\log_{10}Rn - 2)^2} \tag{3.118}$$

where Reynolds number (Rn) is calculated based on the individual lengths of the strut(s), body and fin(s). Then, the skin frictional resistance for each component is calculated by multiplying the coefficient by the factor $0.5\,\rho U^2 S$, where S is the wetted area of each component. Finally, the total skin frictional resistance coefficient of a SWATH ship is obtained by dividing the sum of the skin frictional resistances of all components by the total wetted area:

$$C_f = \frac{(R_{fs}+R_{fb}+R_{ff})}{0.5\,\rho U^2 S} \tag{3.119}$$

The reason for the selection of the ITTC'57 skin frictional line is not only to keep consistency with most published SWATH resistance programs, but also, importantly, it is thought to be most suitable for slender bodies as mentioned in section 3.5.

A correlation, $C_A = 0.0005$, which accounts for the roughness allowance for full scale ship, has been used for most publised SWATH resistance data and programs used for resistance estimate[2]. However, it is reported[16] that the full scale trial data of SSP Kaimalino accords very well with the values extrapolated from the tank model tests with $C_A=0.0$. Therefore, due to the very limited sea trial data with SWATH ships at present, it is not easy to obtain the correct value. For the present study, $C_A = 0.0005$ is used.

3.4 Development of Two Computer Programs and Comparison with Experiments and Other Published Computational Results.

Based on the theory for the wave-making resistance developed in section 3.2 and

using the skin-frictional coefficient described in section 3.3, two computer programs, MSWATH and OSWATH, have been written. MSWATH is for SWATH ships defined by the mathematical formulae given by eqs.(3.6) to (3.10) and OSWATH is for SWATH ships defined by offset using the cubic spline curve fitting technique.

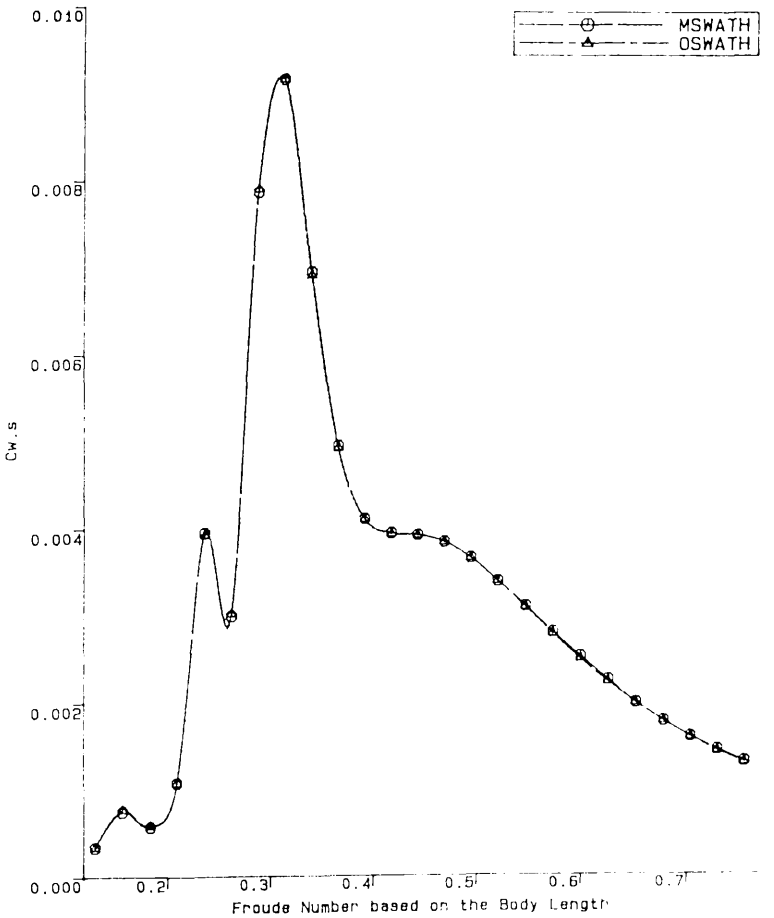

Fig. 3.5 Comparison of Wave Resistance Coefficients Calculated Using Two Computer Programs as a Function of Froude Number Body with Paraboloidal ends ; Lb=1.5M, Di=0.0892, Cp=0.876 Tandem Struts, each with parabolical waterline Ls1=Ls2=0.4, Bs1=Bs2=0.05, Cs1=0.4, Cs2=-0.4, SDBC=0.0896

In order to account for additional resistances such as form factor(3-D effect), eddying, viscous pressure, wave-breaking, spray resistances and some non-linearities, empirical formulae based on the great number of experiments on various SWATH

ships have been derived and built into both programs. Detailed accounts on these additional resistances are treated in the following section 3.5 and detailed descriptions on the two computer programs are given in section 3.6 together with some restrictions

In order to prove whether the curve fitting of geometries for OSWATH can be achieved successfully or not, the two computer programs were used to calculate the wave-making resistance of a tandem strut SWATH ship defined by simple mathematical formulae. The two struts on the demihull are identical to each other and have parabolic waterlines, as given by eq.(3.9). The body has circular cross sections with paraboloidal ends, as given by eq.(3.8). The offsets for OSWATH are generated from the mathematical formulae. Fig.3.5 shows that there is no difference in the predictions by the two computer programs despite the different mathematical modeling of the geometries, which means that the two programs can be used with confidence

3.4.1 Comparison with Experiments and Other Published Computational Results.

In order to validate the theory developed and to verify the applicability of the computer programs, a great number of experiments have been performed in the Hydrodynamics Laboratory of the Department using three SWATH models, SWATH1, SWATH2 and SWATH3. The SWATH1 and SWATH2 models are tandem strut configurations and the former has circular cross section bodies and the latter has rectangular cross section bodies with rounded corners. The SWATH3 model is a single strut configuration with circular cross section bodies. Detailed experimental procedures and discussions are reported in the following Chapter 4

Figs.4.15 to 4.24 show the comparisons between the estimated wave-making and measured residuary resistance coefficients of the SWATH1 model as well as demonstrating how each component of the model contributes to the total wave-making resistance. C1, C2 --- C11 in the figures indicate the series numberings of conditions tested as shown in Table 4.2. Fig.4.104 to 4.106 show the comparisons for the SWATH2 model and Figs.4.136 to 4.138 for the SWATH3 model. These figures also show the interference components such as between body and fore strut, between body and aft strut, between struts, and between two demihulls. The residuary resistance is obtained by subtracting the skin-frictional resistance from the measured total resistance.

The reason for the measured resistance having lower than the computed values at lower speeds might be due to the fact that no turbulence simulation devices were used in the model tests. As mentioned in the introduction,the difference between the two curves for wave-making resistance and residuary resistance is generally called form resistance which accounts for the additional resistances described in the following section. In general, it is known that the quantity of $(C_r - C_w)$ oscillates with speed about zero with a maximum amplitude of $\pm 1.0\times10^{-3}$. From these comparisons, it can be seen that the agreements between the calculated wave-making resistance and measured residuary resistance for all conditions of the SWATH models(including the rectangular hulled model) are excellent. At the highest speeds, the large increase in the measured resistance is caused by green water due to the severe bow trim.

Fig.3.6 shows the present calculations compared with two other computational results for SWATH4 NSRDC Model-5287. The Lin and Day calculation and experimental results are taken from Ref.[3]. The Huang calculation is redrawn based on his letter[17] to the author where he kindly gave corrected numerical values from Ref.[6]. As mentioned in the introduction, Lin and Day and Huang used the same line source distribution for the body. The present approach can be seen to give an improved prediction compared to the other two methods. This improvement can be seen more clearly from Fig.3.7 where calculated and residuary resistance coefficients are shown for a T-AGOS model which has elliptical cross section bodies. SWATHGEN and experimental results are taken from Ref.[5] The big difference between the two calculations seem to be mostly due to the non-circular hulled SWATH. As mentioned in Chapter 2, the line source distribution applied in SWATHGEN cannot predict the difference in the wave resistance for different cross sectional bodies. However, the bias of the peaks between the measurements and the two predictions can not be fully accounted for, but probably is due to modeling errors in the computations.

Fig.3.8 shows the comparison between the measurements and two calculations for the SWATH Passenger Vessel M8501. The Huang calculation and measurements are taken from Ref.[6]. The comparison between the measurements and two calculations of SWATH NSRDC Model-5276 demihull are shown in Fig.3.9 and in Fig 3.10 for the twin hull of the same model. The Lin and Day calculations and experiments for the both conditions are again taken from Ref.[3]. Fig 3.11 shows the results for the

SWATH3 NSRDC Model-5275E demihull whose simple strut was changed from the original 'coke-bottle' shape shown in Fig.3.13. Fig.3.12 shows the present predictions and measurements for the NSRDC Model-5276C at two different drafts[18]. For reference, profiles and strut sections for the NSRDC Model 5276 series are shown in Fig 3.13, taken from Ref.[18].

From the comparisons between the present predictions(wave-making resistance) and the large number of experimental results(residuary resistance) on various SWATH configurations carried out in the Department as well as in the other establishments worldwide and between the present predictions and the other published predictions for the same models, it can be said that the present method gives a satisfactory correlation with the experimental measurements and that the other theoretical methods give lower predicted values than the present method depending the submergence of the main body. It can be suggested that this is due to the utilisation of the present plane source distribution technique. In addition, it can be seen from Figs 4.15 to 4.24, 4.104 to 4.106 and 4.136 to 4.138 that the predicted resistance proportion of each component of the SWATH models is quite in agreement with the model tests. It is certain that the measured resistance variation caused by parametric changes(spacing between two demihulls, draft, strut positions on the demihull, single or tandem strut variation etc) can be read form the predicted component resistance changes(This is discussed in detail in Chapter 4). Therefore, the present computer programs can be effectively used to find an optimum SWATH shape and to find the best composition of each component as well as the displacement distributions on the component.

3.5 ADDITIONAL AND APPENDAGE RESISTANCES

3.5.1 Additional Resistances

Form resistance usually means the viscous component of the resistance due to the shape of a body which is the difference between the total viscous resistance and the viscous resistance of the equivalent flat plate of the same length.

Fig.3.14 shows the total resistance of a streamlined body of revolution[19], which is submerged at 5.5 times its breadth, together with the three basic frictional lines. Although it can be considered that the wave-making resistance of the body at such

submergence is negligible, waves can be created in the free surface at the high speeds tested. Using the theory developed, the wave-making resistance is calculated for the body and then subtracted from the total resistance measured, which(C_t–C_w as shown in the figure) can be regarded to be purely viscous resistance. Using Hoerner's formula[20, p.6-17], as given by:

$$C_f = \frac{C_v}{1+1.5(\frac{B}{L})^{3/2}+ 7(\frac{B}{L})^3} \qquad (3.120)$$

the skin frictional resistance is calculated and presented in the figure. From the figure, it can be seen that this curve coincides with ITTC'57 frictional line with some undulation. As just shown, empirical form factors for streamlined bodies or foil sections has been derived from series tests and can be obtained in the literature[20].

As the name itself says, form resistance considerably varies depending on the shapes of bodies[21]. This can be clearly understood from Fig.3.15[22] which shows the form resistance variations of a torpedo shaped body with L/D ratio as well as the length of parallel middle body. Therefore, it is not easy to estimate the form resistance of a body for which no experimental data is available. Furthermore, since a SWATH ship has several components which may interferre one another, it may be nearly impossible to derive a general formulae which can be applied to any SWATH ship with good accuracy. The best way to achieve this purpose is to accumulate as much experimental data as possible.This can best be achieved by cooperative work amongst the worldwide tanks. However,at the moment, experimental data on SWATH ships is very scarce and furthermore, many details are kept confidential so that it is extremely difficult to do this job. Also, SWATH ships are so sensitive to sinkage(rise) and trim which will affect the measured resistance and thus the scatter in measured resistances from different tanks will be significant compared to monohulls.

From the published literature, it can be seen that there are, in general, two approaches to estimate the form resistance of SWATH ships. One is that empirical form factors known for streamlined shapes and foil sections are seperately applied to the each component of a SWATH ship, as used in SWTHRP[2], SWATH CEM[4], and SWATHGEN[5]. In SWATHGEN, form factors of 0.17 and 0.10 for strut and body, respectively, are used which fall into the range of two dimensional airfoils and bodies

of revolution similar in proportion to typical SWATH struts and bodies. In both SWTHRP and SWATH CEM, the same form factor of 0.1 for bodies is used as in SWATHGEN , but a different approach is applied to struts. They consider the form resistance of a strut as the sum of eddy-making and spray resistances. The eddy-making resistance of a strut is accounted for by multyplying the strut frictional resistance by an empirical factor, as given by Hoerner[20,p6-6]:

$$1 + 2(\frac{T_m}{L_s}) + 60(\frac{T_m}{L_s})^4 \qquad (3.121)$$

The spray resistance calculations are based on the results of model tests, as described in Ref.[8].

The second is a more direct approach based on the experimental results of several SWATH ships. Defining form resistance as the difference between the measured residuary and calculated wave-making resistance of a bare SWATH ship, Lin and Day calculated such a difference for both NSRDC Model SWATH3 and SWATH4, as shown in Figs 3.6 and 3.9 to 3.12 and plotted as a function of strut speed-length ratio. A curve was then faired through the data, as shown in Fig.3.16, not allowing the form drag coefficient to go below 0.0005. If there are many experimental data on various SWATH configurations, this method is better and more accurate than the former. However, due to the present limited experimental data as mentioned above, there is some doubt about applying this curve to other SWATH configurations.

Based on the experimental results of the 16 configurations using the three SWATH models, as shown in Figs.4.15 to 4.24, 4.104 to 4.106 and 4.136 to 4.138, which were carried out in the Department, the difference between the residuary and calculated wave-making resistances for each configuration was derived. Despite the different configurations, as seen in these figures, the prime hump commonly occurs around Fn=0.5 which coincides with the prime hump of the bodies. This prime hump is decided by the longitudinal distribution of body displacement, in particular, the proportions of entrance and run. Also, it can be noticed that the largest difference between the measurements and predictions occurs around this Froude number and it can be assumed that the difference is constant with the increase of speed. The large increase in the measurements at higher speeds was due to green water in severe bow trim condition.

These differences are plotted as a function of Froude number instead of the strut speed-length ratio, as used in Lin and Day, and curves are then drawn through the data. Due to the scatter in the data, careful consideration was given before finally drawing two curves as shown in Fig.3.17(one is for circular hulled SWATH ships and the other for rectangular hulled SWATH ships). Firstly, as mentioned earlier, the lower measurements at lower speeds are due to the fact that no turbulance devices were used for the models and therefore the form resistance coefficient is not allowed to go below 0.0004 for circular hulled SWATH ships and 0.0006 for rectangular hulled SWATH ships at slow speeds. At higher speeds, the coefficient is kept at 0.0008 and 0.0012 for circular and rectangular hulled SWATH ships, respectively. Secondly, it can be seen that the form resistance coefficient decreases as the draft increases(compare SWATH1-C1 and C2, SWATH1-C4,C5 and C6, SWATH1-C7 and C8, SWATH1-C9 and C11). Therefore, the form resisistance coefficients are taken at the most probable draft range of 1.5 and 2.0 times the diameter of body. It is worthwile noting that the form resistance is almost constant with the spacing between two demihulls(compare SWATH1-C1,C4 and C7, SWATH1-C2,C5 and C7, SWATH1-C10 and C11).Also, as opposed to expectation, the form resistance of the single strut SWATH3 is slightly larger than that of the tandem strut SWATH1 at the same draft(compare SWATH3-C1 and SWATH1-C5, SWATH3-C2 and SWATH1-C6, SWATH3-C3 and SWATH1-C8), but the proposed coefficient curve can be used for both configurations without a serious compromise.

As mentioned earlier, these form resistance coefficients vary depending on the component shapes of SWATH ships, in particular, the proportions of body ends as shown in Fig.3.15. Therefore, these curves should be used to SWATH ships similarly shaped to SWATH1, 2 and 3, but when the components of a SWATH configuration do not depart greatly from these models, these curves can be used without a serious error. It should be noted that Lin and Day's coefficient as shown in Fig.3.16 is different from the present. There are two main reasons for this. Firstly, it seems that they calculated the coefficient based on the model captive condition, but the present coefficient is based on the model free condition. Secondly, it is certain that experimental results for the same model carried out in different tanks show a considerable scatter. In particular, SWATH ships are so sensitive to trim and sinkage(rise) that a scatter is to be expected.

Therefore, strictly speaking, a form resistance coefficient derived from one tank cannot be generalised for use in other tanks at present.

With experimental results on 14 configurations using two Polish models, SWATH-386[23] and SWATH 395, as also reported in section 4.6, and the other models including NSRDC SWATH3 andSWATH4 as shown in Figs. 3.6 and 3.9 to 3.12, TAGOS as shown in Fig.3.7 and one chinese model M8501 as shown in Fig.3.8, it can be noticed that the prime hump occurs around Fn=0.48-0.5 and the maximum difference between the wave making and residuary resistances is observed at this speed range and giving a constant difference above this speed. Therefore, the proposed coefficient based on the Froude number based on the body length can be validated. From the comparison of Figs.3.9 and 3.11, it isworthwhilenoting that the form resistance of the contoured strut Model 5276 is much higher than that of the simple strut Model-5275E and results in a larger total resistance throughout the speeds tested. Therefore, for a SWATH ship which has either contoured struts or hulls, a constant value of 0.0001 is recommended to be uniformly added to the value given in Fig.3.17.

The curves as shown in Fig.3.17 are stored in the form of discrete values in both OSWATH and MSWATH and the form resistance is calculated by the equation:

$$R_{fm} = C_{fm} \frac{1}{2} \rho U^2 S \tag{3.122}$$

where form resistance coefficient C_{fm} is calculated by means of linear interpolation.

Also, the approach proposed in SWTHRP and SWATH CEM are considered in both MSWATH and OSWATH for SWATH ships whose forms significantly depart from those of the three SWATH models of SWATH1, 2 and 3. The form resistance of a strut is regarded as the sum of the eddy making resistance and the spray resistance. The eddy making resistance of a strut is calculated by:

$$R_E = \frac{1}{2} \rho U^2 S \, C_E \tag{3.123}$$

where C_E is given by eq.(3.121). The spray resistance is calculated by [8].

$$R_{SP} = (0.003cT_m + 0.06\, T_m^2) \frac{1}{2} \rho U^2 \quad \text{when } x/c = 65\%$$

$$R_{SP}= (0.011cT_m+ 0.08\ T_m^2\ )\frac{1}{2}\rho U^2 \quad \text{when x/c =50\%}$$

$$R_{SP}= (0.009cT_m+ 0.13\ T_m^2\ )\frac{1}{2}\rho U^2 \quad \text{when x/c =35\%} \tag{3.124}$$

where x is the distance from the leading edge to the maximum thickness point and c is chord. Also, a form factor 0.1 is taken into account for body which means that the friction resistance of body(now can be called viscous resistance) is calculated by:

$$R_F= \frac{1}{2}\rho U^2 S\ C_f(1+0.1) \tag{3.125}$$

where S is the wetted area of body.

Using eqs.(3.123), (3.124) for x/c=50% and (3.125), the form resistance coefficient of SWATH1-C4 is calculated and drawn in Fig.3.18 as a function Froude number. Also, the figure shows the form resistance coefficient for the same model using form factors 0.17 for the strut and 0.10 for the body, as used in SWATHGEN. Compared to the present empirical form resistance coefficient as shown in Fig.3.17(for circular hull), the value used in SWTHRP and SWATH CEM is considerably large. This is due to the fact that the spray resistance, as given by eq.(3.124), is very large for the present tandem strut model. On the other hand, the form factors used in SWATHGEN gives reasonable values up to moderately high speeds, but at higher speeds the form factors becomes small for the present model.

3.5.2 Appendage(fins) Resistance Calculation

It has been known that in the case of high speed marine vehicles such as a SWATH, the contribution of appendage resistance to the total resistance is often greater than for displacement ships[24]. Practically, it is often impossible to make model sizes and test conditions such that the flow on model appendages is with fully developed turbulence which satisfies scaling requirements. Therefore, the prediction of ship performance from models where appendages significantly contribute the measured resistance will be in error if separate Reynolds scaling of the appendages is not included. The various scaling formulations which have been devised to over come this

problem are reviewed in the report of the high speed marine vehicle committee at 17th ITTC conference[24].

As in the bare hull resistance, it is necessary to break down the total resistance of an appendage into additive components, each of which is caused by a different effect. Basically, the resistance of an appendage may be assumed to consist of five components:

$$R_{APP} = R_P + R_I + R_{HAI} + R_{TI} + R_w \tag{3.126}$$

where R_P is the profile drag, R_I the induced drag, R_{HAI} the hull-appendage interference drag, R_{TI} the tip drag and R_W the wave-making drag due to the presence of free surface. The calculation can be carried out identically for all appendages such as aft fins, fore fins(called canard) and rudders, but fins only are considered in the programs MSWATH and OSWATH. It has often been proposed that an integrated part of the strut can be used as a rudder which makes a continuous streamline with the strut and forms part of the strut trailing edge profile. In this case, it is not necessary to calculate the wave-making resistance of the rudder separately, but this can be included in the strut resistance calculation. Then, the other components as given in the above equation can be calculated in the manner stated below.

In the program MSWATH, the wave-making resistance of fins as well as interference wave-making resistances associated with other components of SWATH ships are calculated based on the developed formulations in section 3.2.1. Fig.3.19 shows the total wave-making resistance coefficient of the SWATH model, which is used for Fig.3.5 but with a pair of fins, together with its components contribution to the total wave-making resistance. A fin with parabolic sections given by eq.(3.10) is attached to near the stern of the lower demihull(body) at the same submergence depth as the body centreline(SDBC=0.0892). The center of the fin is 0.5m away from the longitudinal centre of the body and its dimensions are span(Sp_f=0.1m), chord(Lc_f=0.094) and maximum thickness(T_f=0.014). From the figure, it can be seen that the wave-making contribution of the fin including the interferences with the other components is negligibly small. In practice, the draft of practical SWATH ships is deeper than that of the present model(1.5 times the diameter of body) so that the wave-making resistance contribution of controllable fins to the total resistace can be neglected without losing accuracy (However, for shallow running SWATH ships, this can not be

neglected).

For this reason, instead of the complicated formulae including interferences with other components stated in section 3.2.1, an approximation to wave making resistance of the foil is included in OSWATH, as given by[25]:

$$R_W = \frac{1}{2Fn^2} C_L^2 \exp\left(-\frac{2h_f}{cFn^2}\right) \frac{1}{2}\rho U^2 S_{pl} \tag{3.127}$$

This is an equivalent vortex line approximation to the wave effect of the foil and Froude number(Fn) should be calculated based on the chord. S_{pl} is the plan form area and the lift coefficient for the foil is given by[26]:

$$C_L = \frac{dC_L}{d\alpha_a} \alpha_a \tag{3.128}$$

where α_a is the angle of attack. For a symmetrical foil section and small angle of attack(up to around 6 degrees), the gradient term in the above equation(so called lift slope) becomes 2π. The substitution of the above approximate formulae into OSWATH is mainly from the reason of computational time. As mentioned in section 3.2.3, using the computer VAX 11/730 at the Hydrodynamics Laboratory, the computing time of OSWATH is approximately 40 times longer than that of MSWATH at one speed for a SWATH ship without fins. If fins are included, the difference will be greater than that.

All the other components in eq.(3.126) are considered by means of empirical or semi-empirical formulaefor the foil section as explained below.

The profile drag is composed of flat plate friction plus form drag(sometimes referred to as pressure drag). For fins, the following empirical formula is used[5]:

$$R_P = 2C_f\left[1 + 2\frac{T_m}{c} + 100\left(\frac{T_m}{c}\right)^4\right] S_{pl} \frac{1}{2}\rho U^2 \tag{3.129}$$

where c is the mean chord and T_m is the maximum thickness. The frictional coefficient is calculated based on the local Reynolds number[27].

The induced drag is calculated by the formula[20,p.7-3]:

$$R_I = C_L^2 \left(\frac{1+K}{\pi AR}\right) \frac{1}{2} \rho S_{pl} U^2 \tag{3.130}$$

where the AR is the effective aspect ratio and C_L the lift coefficient for the foil given by

eq.(3.128). The factor K accounts for the increase in induced drag due to nonelliptic spanwise loading of the foil. At higher speeds and in the vicinity of free surface, this factor can reasonably be approximated to, as given by[25, p.38]:

$$K = \frac{AR}{AR + 12(h_f/c)} \tag{3.131}$$

where h_f is the submerged depth to the fin centre.

For the interference drag of a lifting surface intersecting a flat plate,the hull-strut interference drag is calculated using the formula from Hoerner[20, p.8-10] :

$$R_{HAI} = [\, 0.75(\frac{t_m}{c}) - 0.0003(\frac{c}{t_m})^2] \frac{1}{2} \rho U^2 t_m^2 \tag{3.132}$$

The tip drag for each appendage can be estimated by the following formula,as given by Hoerner[20, p.6-4]:

$$R_{TI} = 0.075(\frac{t_m}{c})^2 \frac{1}{2} \rho U^2 c^2 \tag{3.133}$$

where it is assumed that the tips are blunt and the lift coefficient is zero

Using the computer program OSWATH which includes the form resistance coefficient given in Fig.3.17 and fin resistance formulae described above, the total resistance of the SWATH1 model with a pair of fins(NACA0015) is calculated and compared with the experimental results*(see Figs.5.15 to 5.19). For the calculation, the angle of attack of the fins is assumed to be 2 degrees. From these figures, it can be seen that the present estimations give excellent correlation with the five configurations tested. Fig.5.20 shows the component resistances of a fin(SWATH1-C4 demihull) in newtons. As expected, the profile drag(friction+pressure) is the highest of the components up to moderately high speeds and then, the induced drag becomes the highest. The smallest is the tip drag due to the blunt end of the foil section. The induced drag will be changed with the angle of attack. Also, Polish SWATH-395 model with two pair of fins(NACA0012) is compared with the present prediction as shown in Fig.4.184. Again, the angle of attack of the fins is assumed to 2 degrees and the agreement is excellent(discussed in detail Chapters 4 and 5)

* The results with a pair of fins are taken from Ref.[101]

3.6 COMPARISON AND RESTRICTIONS OF THE TWO COMPUTER PROGRAMS

MSWATH

The program MSWATH is designed for SWATH ships defined by mathematical formulae. Submerged bodies can be formed by a combination of conical, ellipsoidal or paraboloidal nose and tail sections which are joined together by a straight mid section of circular or elliptical cross section. A linear variation of displacement along the longitudinal direction can be made, allowing up to 5 different blocks of the body(so called contoured hull).

The strut can be formed by parabolic nose and tail sections joined together by a straight centre section. Again, a parabolic thickness variation along the longitudinal direction is allowed. The number of struts can be one, two or three on each demihull and they need not to be identical to each other.Up to two pair of controllable fins can be used in this program where the wave-making resistance of fins and the interferences associated with other components(bodies and struts) are exactly calculated based on the developed theory.

A SWATH geometry may be accurately defined by the above kind of mathematical shapes. Hence, this program can be useful for a Concept Exploration Model Study(CEMS) at the very early stage of the design process because the surface area can be calculated exactly, the parametric studies can be carried out easily and most importantly, computing time is very short compared to the offset input program OSWATH.

However, it cannot be expected that SWATH ships can always be expressed by simple mathematical formulae so that MSWATH has a limit of applications to many SWATH ships. In addition, for SWATH ships whose struts depths are not constant along the length because they have contoured bodies or their struts are extended over ends(entrance and run), the non-uniform strut depth parts cannot be expressed by simple mathematical formulae. Therefore, in this case, it is assumed that the strut(s) with uniform depth stand on the maximum depth section of a contoured body or parallel mid-section of non-contoured body which means there are some discontinuities between the strut(s) and body. As a result, the result will be in error.

OSWATH

The program OSWATH is written for SWATH ships defined in offset forms.Therefore, there is no geometry restrictions including contoured struts and bodies with any cross section. As in MSWATH, the depth of the strut is taken to be constant which is independent of the body shape.Instead, the non-uniform depth parts of the strut for a SWATH ship, which has either contoured bodies or its struts are extented over to the ends of the bodies, is considered to be part of the submerged bodies. This can be validated within the approximate theory which assumes that the wave-making resistance of the submerged body varies with the longitudinal variation of the cross section area, dA(x)/dx, with the depth correction. Therefore, the cross sectional area of the non-uniform depth part is added to the body cross sectional area at the same section. Fig.3.20 shows the comparison between the two different geometry modelling for a TAGOS model whose strut extends to over the entrance and run of the lower demihull , as used in Fig.3.7. When the strut local depth is taken as part of the submerged body, the predictions give lower values than those, when the local depth is not considered, at the higher speeds. This difference seems to be reasonable since the large difference(form resistance) can be accounted by the elliptical cross section bodies of the model. Since all the published programs assume that the strut depth is constant, this slight modification can be recommended.

One or two pair of fins can be used. Since it has been found that the wave-making resistance contribution of controllable fins to the total resistance is negligibly small at the draft range of practical SWATH ships, the wave-making resistance of the fins themselves, neglecting the wave-interferences with other SWATH components, is considered for the purpose of saving computing time. Nevertheless, there is little difference in the predictions using the two programs.

As mentioned in section 3.2.3, the wave-making resistance of each component of SWATH ships is calculated in the form of double summations with the single integral form of auxillary functions. Therefore, the computational time is very large compared to the program MSWATH in which the calculation is performed only through single integration.

Since the two computer programs have their own advantages and disadvantages and also, the two predictions give almost identical values for the same model, they can be used in a cooperative way. At the very early stage, MSWATH can be effectively used to find optimum or near optimum shapes by changing several parameters.Then, if the SWATH ship designer wishes to use a form which can not be expressed by simple mathematical formulae, OSWATH can be used to the final estimation of the resistance.

3.7 CONCLUSIONS

Based on the approach described in Chapter 2 and this Chapter, two computer programs have been written to estimate the total calm water resistance of SWATH ships (MSWATH and OSWATH). MSWATH is designed for SWATH ships defined by mathematical formulae and OSWATH is written for offset input. The computational results are compared with a great number of experimental results using three SWATH models including 21 configurations changes and two Polish SWATH models including 14 configurations(see section 4.6). Also, the present predictions are compared with other published experimental data as well as computational results. The present studies can be summarised as follows:

1) The calculated wave-making resistance based on the present approach utilising the plane source distribution for the submerged body gives satisfactory agreements with the measured residuary resistance on the various SWATH configurations. The other computational methods give lower predicted values than the present method(which is dependent upon the submergence of the main body). It is suggested that this improvement in accuracy of prediction is due to the utilisation of the plane source distribution technique. In particular, this is marked for the non-circular hulled SWATH ships.

2) Even though linear wave theory and the relatively simple centre plane source distribution technique are used, the agreement between the predictions and the measurements are excellent and better than can be expected for conventional monohulls.This seems to be due to the fact that SWATH ships have such thin and slender demihulls which well satisfy the assumptions of the theory compared to monohulls. Also, as mentioned in Chapter 2, lifting effect seems to be less important to

SWATH configurations. Therefore, the introduction of non-linear boundary conditions, or complicated panel source distribution techniques using either constant source strength distribution or higher order source distribution, as mentioned in Chapter 2, which have been directed to improve the predictions for monohulls, seems to be unnecessary for SWATH ships. Instead, research into the viscous flow including the boundary layer and wake region is most desirable so as to reduce the viscous resistance components which compose a large proportion of the total resistance of SWATH ships. Also, since a SWATH ship is so sensitive to trim and sinkage which might affect resistance, the prediction of resistance including trim and sinkage is desirable.

3) Based on the difference between the calculated wave-making resistance and measured residuary resistance with 16 SWATH configurations(including single and tandem strut SWATH configurations, and circular and rectangular hulled SWATH configurations), two form drag coefficients have been derived. It has been proved that these curves can be used to estimate the form drag for the practical range of SWATH ships.

4) Using known empirical formulae for foils and streamlined bodies and including free surface effects, the resistance caused by the controllable fins is estimated and compared with experimental results of 6 SWATH configurations. It has been shown that the agreement between the two curves is very good.

5) Despite the mathematical modelling difference, MSWATH and OSWATH give exactly the same results for the same SWATH ship. Hence, MSWATH can easily be used to carry out fast parametric hull form changes for SWATH ships defined by simple mathematical formulae and it can be effectively used for CEM study at the early stage of the design process. OSWATH can then be used to estimate the resistance of SWATH ships of interest which are defined in offset forms

6) Since it has been proved that the present computational tool gives very excellent correlation with the experimental results, it can be used with confidence for parametric and optimum studies of SWATH ships with regard to resistance. This is treated in Chapter 5.

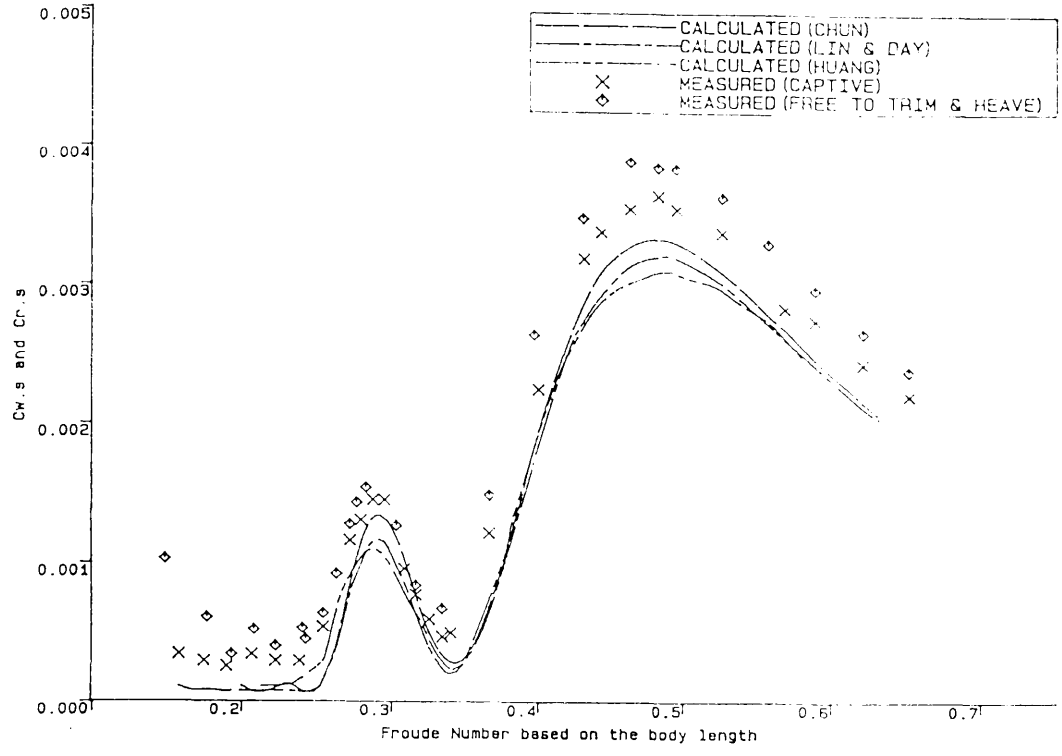

Fig.3.6 Comparison of Calculated and Measured (Residuary) Resistance Coefficients of SWATH4 NSRDC Model-5287

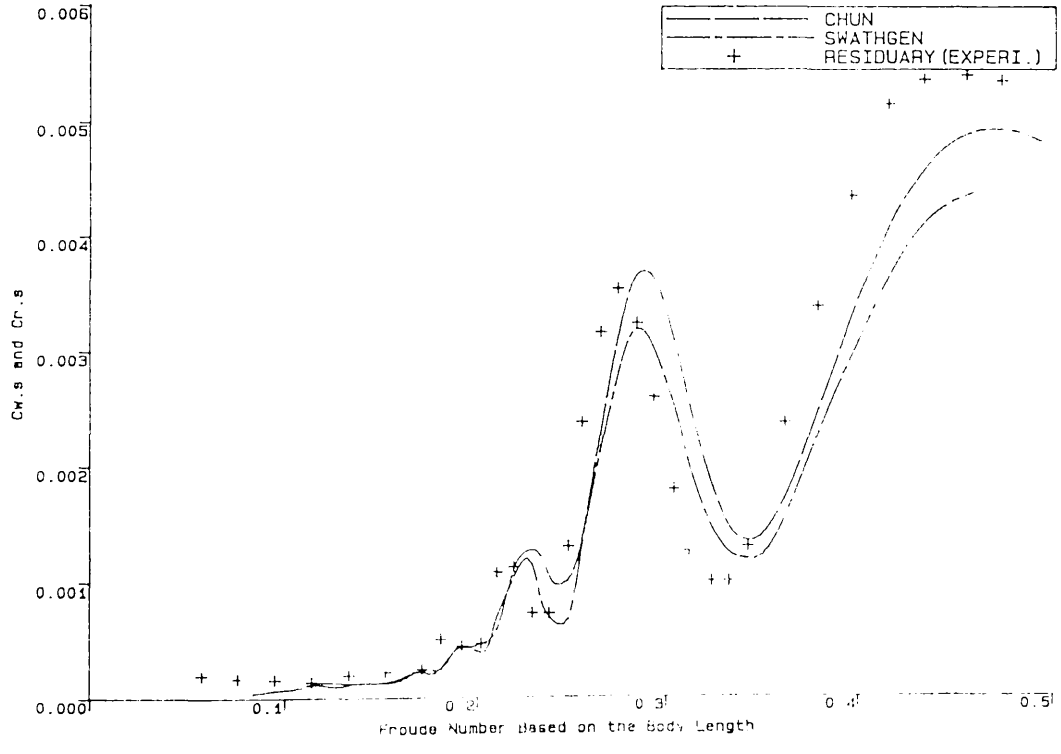

Fig.3.7 Comparison of Calculated and Measured (Residuary) Resistance Coefficients for TAGOS Model

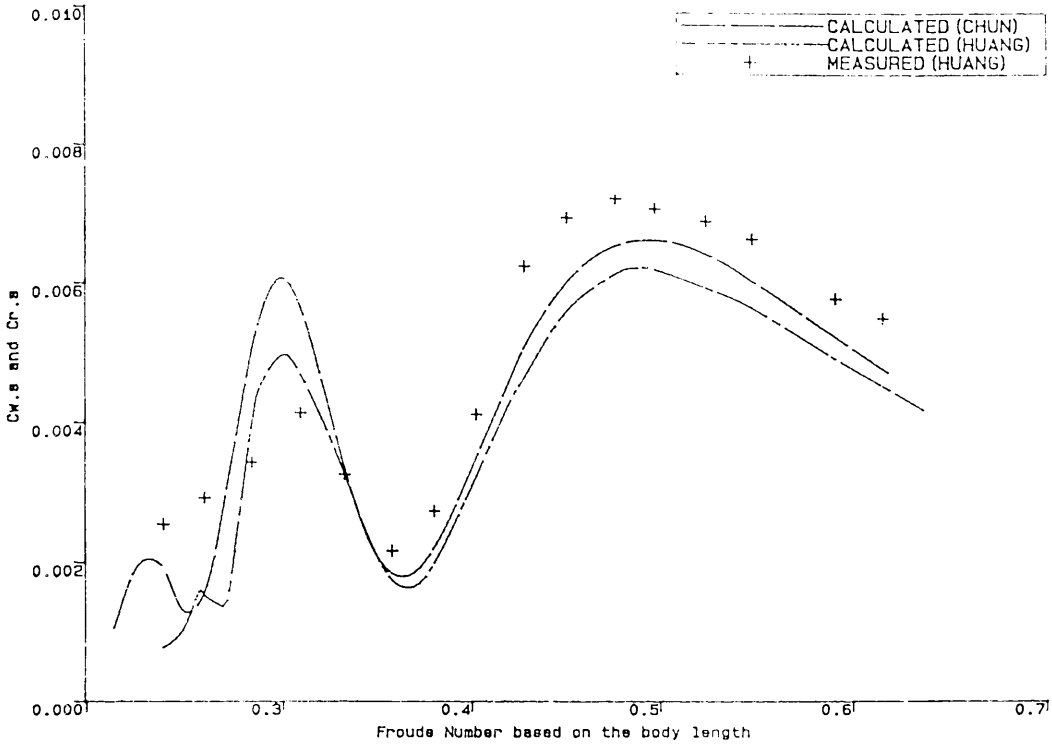

Comparison of Calculated and Measured (Residuary) Resistance Coefficients of SWATH Passenger Vessel M8501

Fig.3.8

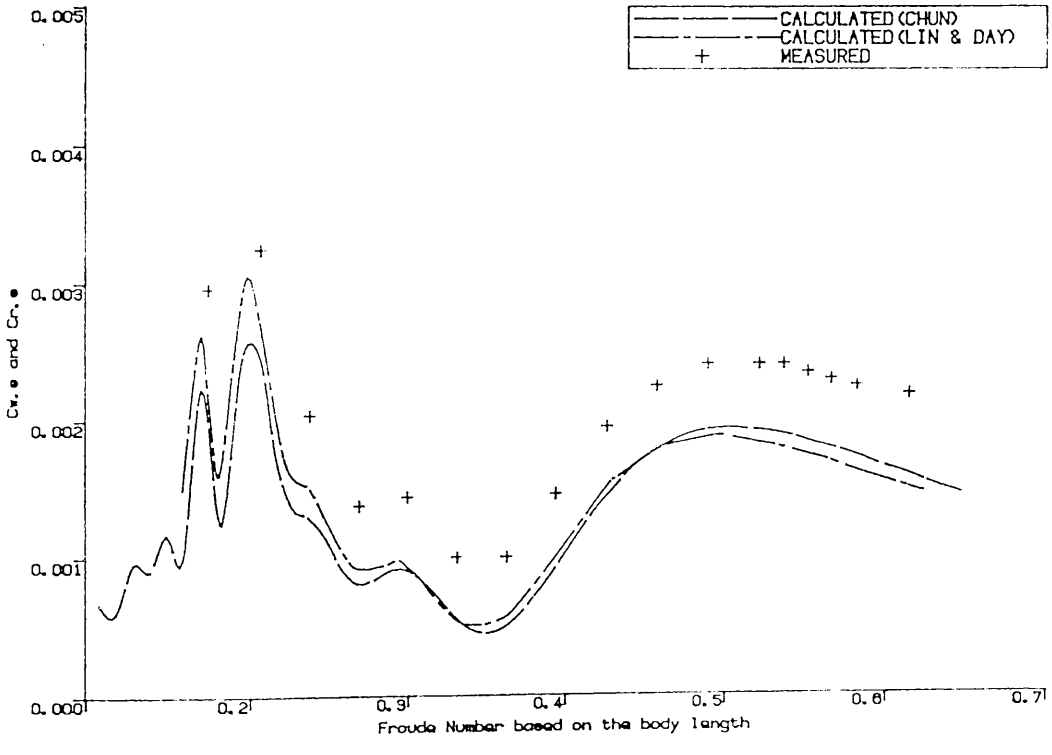

Comparison of Calculated and Measured (Residuary) Resistance Coefficients of SWATH3 NSRDC Model-5278 (Demihull)

Fig.3.9

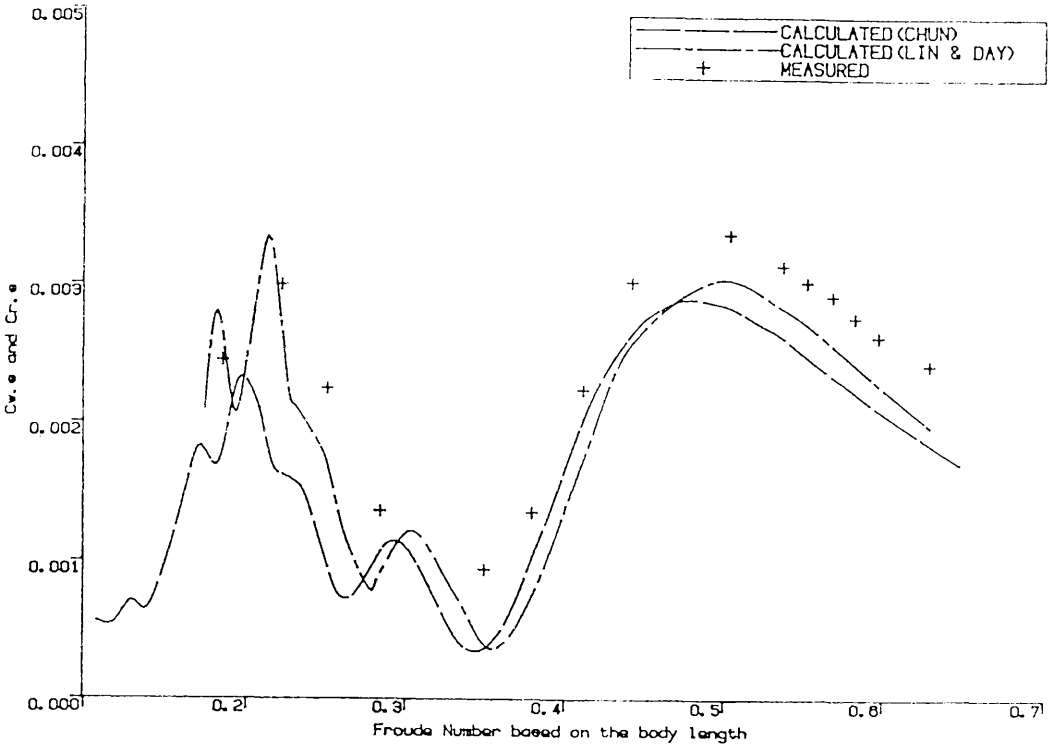

Comparison of Calculated and Measured (Residuary) Resistance Coefficients of SWATH3 NSRDC Model-5278

Fig.3.10

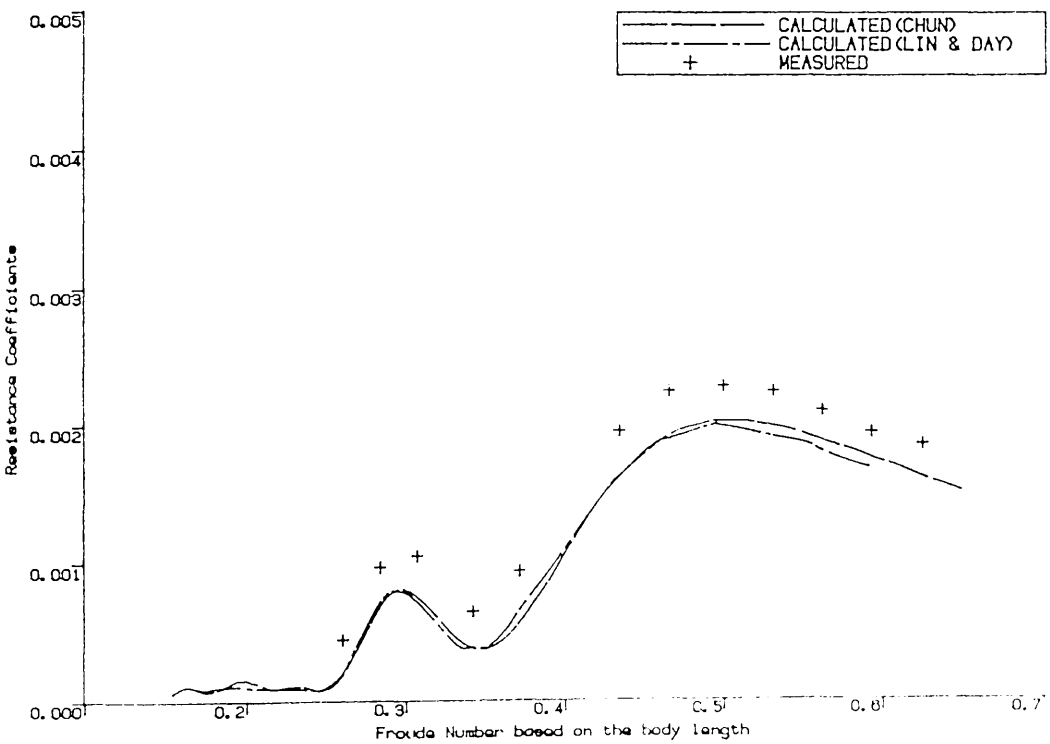

Comparison of Calculated and Measured (Residuary) Resistance Coefficients of SWATH3 NSRDC Model-5278E (DEMIHULL)

Fig.3.11

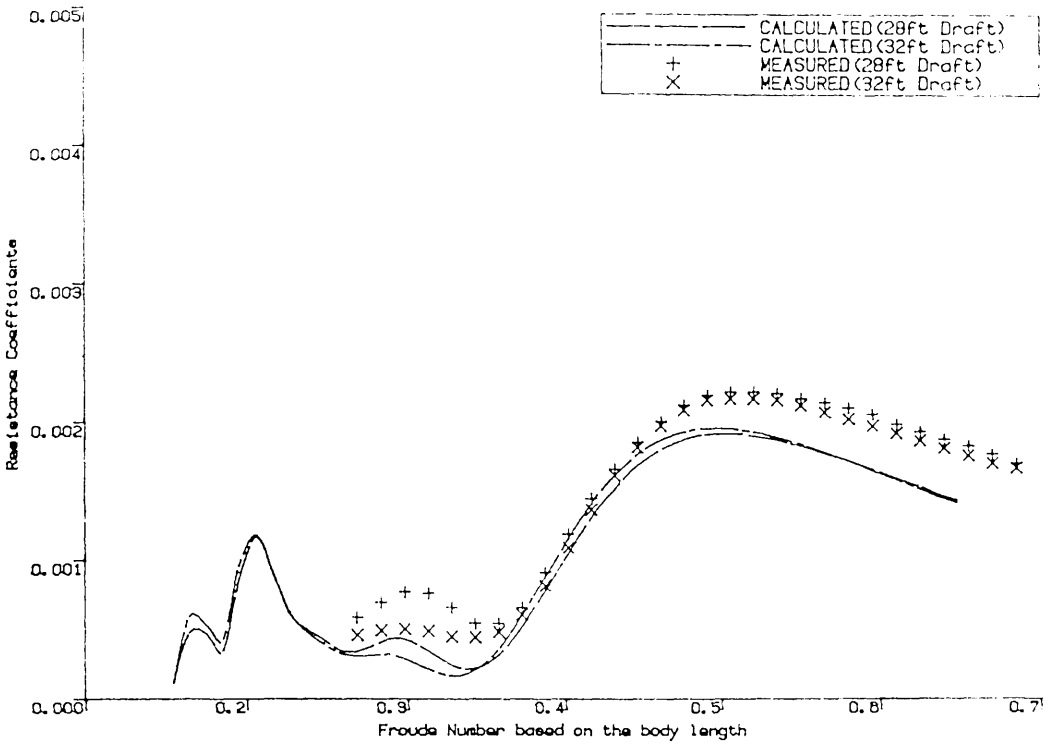

Comparison of Calculated(by CHUN) and Measured(Residuary) Resistance Coefficients of SWATH3 NSRDC Model-5276C(Demihull)

Fig.3.12

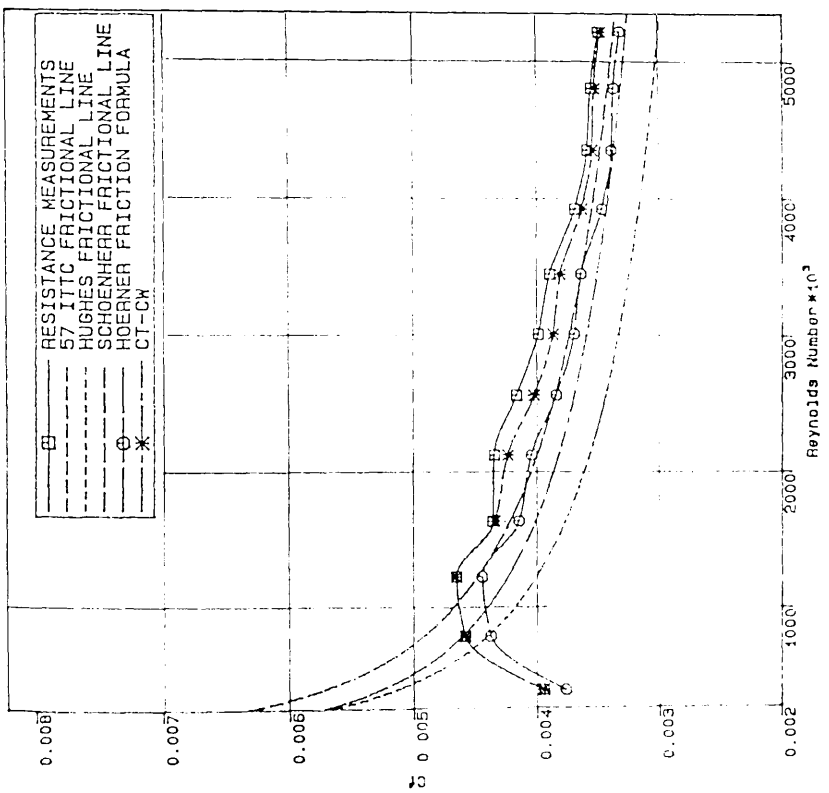

Total Resistance of Submerged Body with Basic Frictional Lines.
MODEL 5067
Depth of Immersion = 5.5B = 0.66M. B=0.12 L=1.3
With Turbulence Stimulation

Fig.3.14

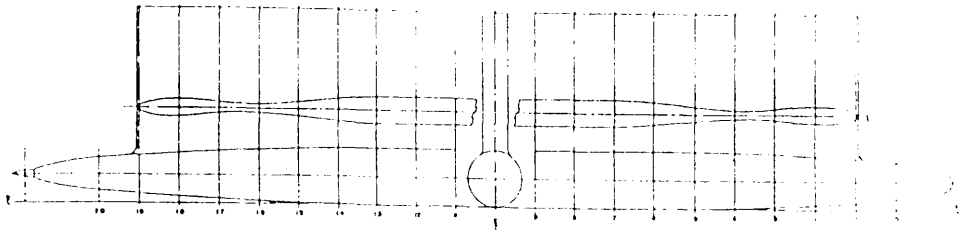

a) Profile and strut section for an LWP catamaran demihull represented by Model 5276

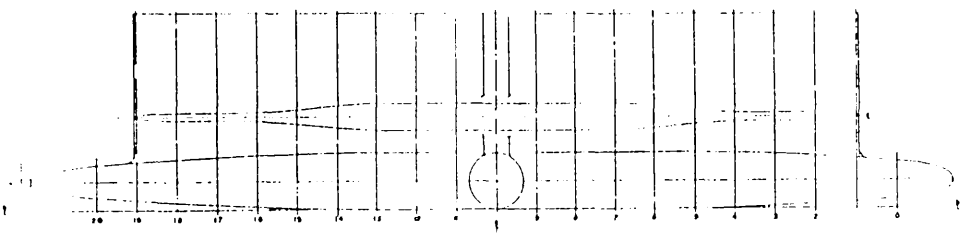

b) Profile and strut section for a single hull, Model 5276-C

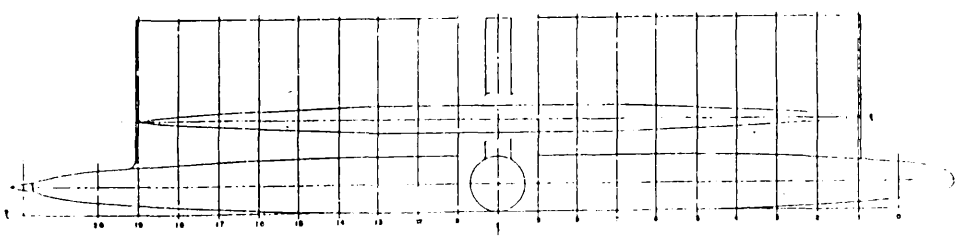

c) Profile and strut section for a single hull, Model 5276-E

Fig. 3.13

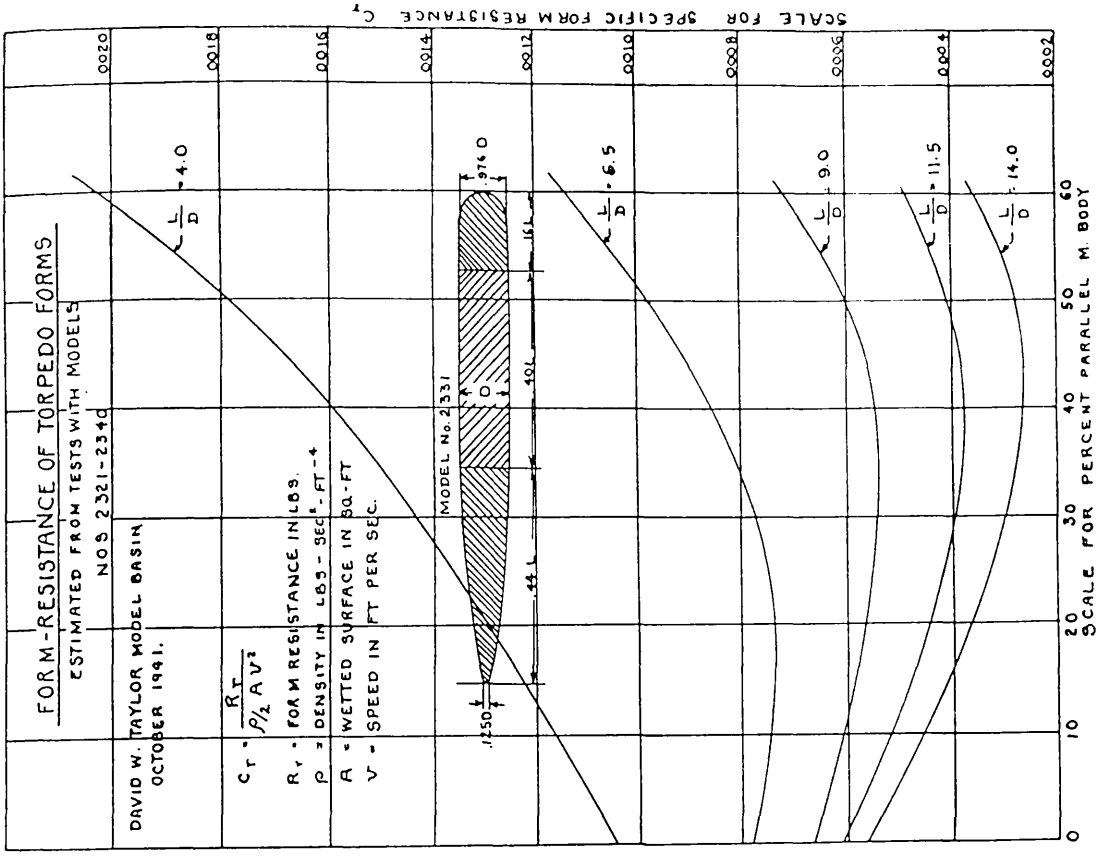

Fig.3.15

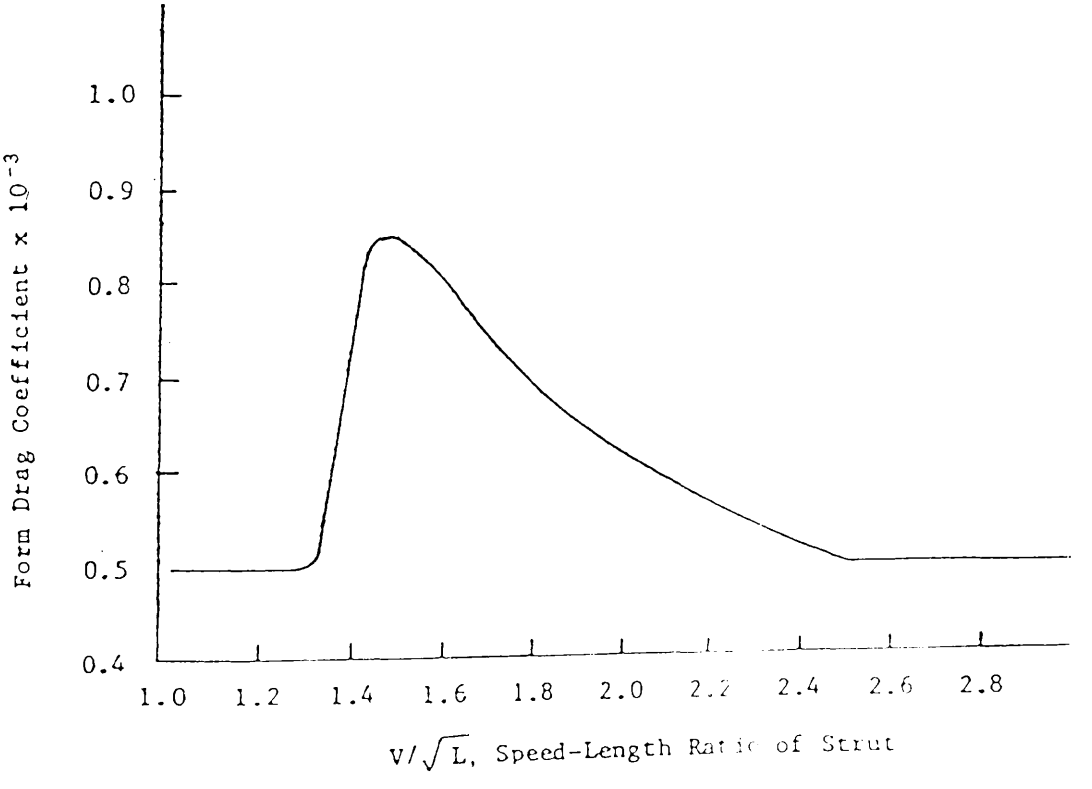

Fig.3.16 Form Resistance Coefficient

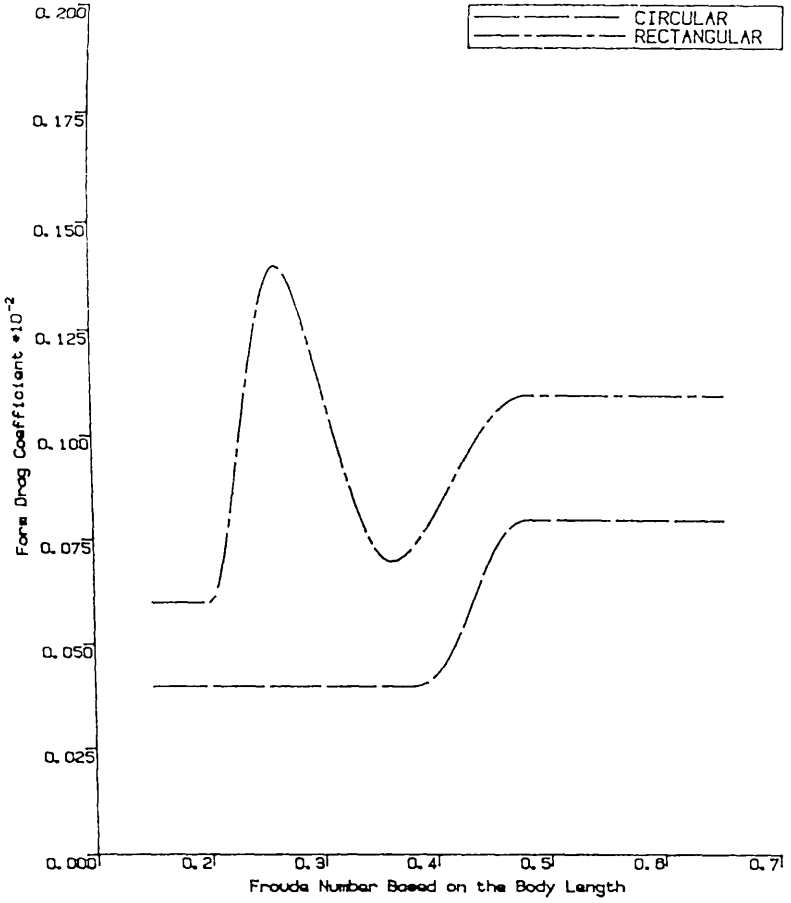

FORM DRAG COEFFICIENT AS A FUNCTION OF FN

Fig.3.17

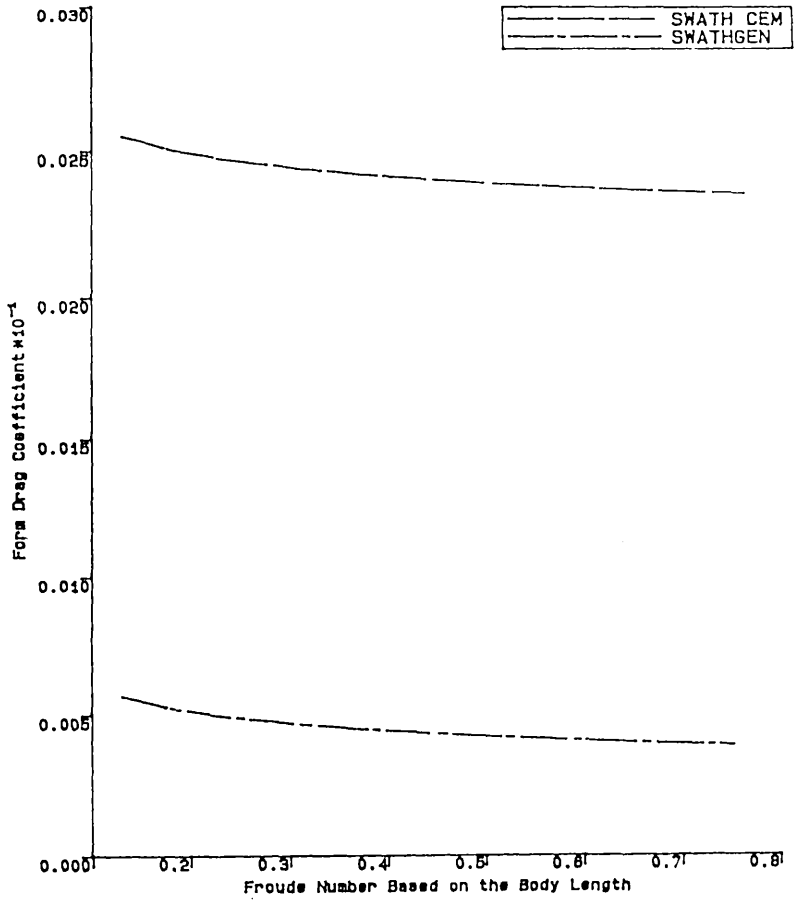

Comparison of Two Form Drag Coefficients for Model SWATH1-C4

Fig.3.18

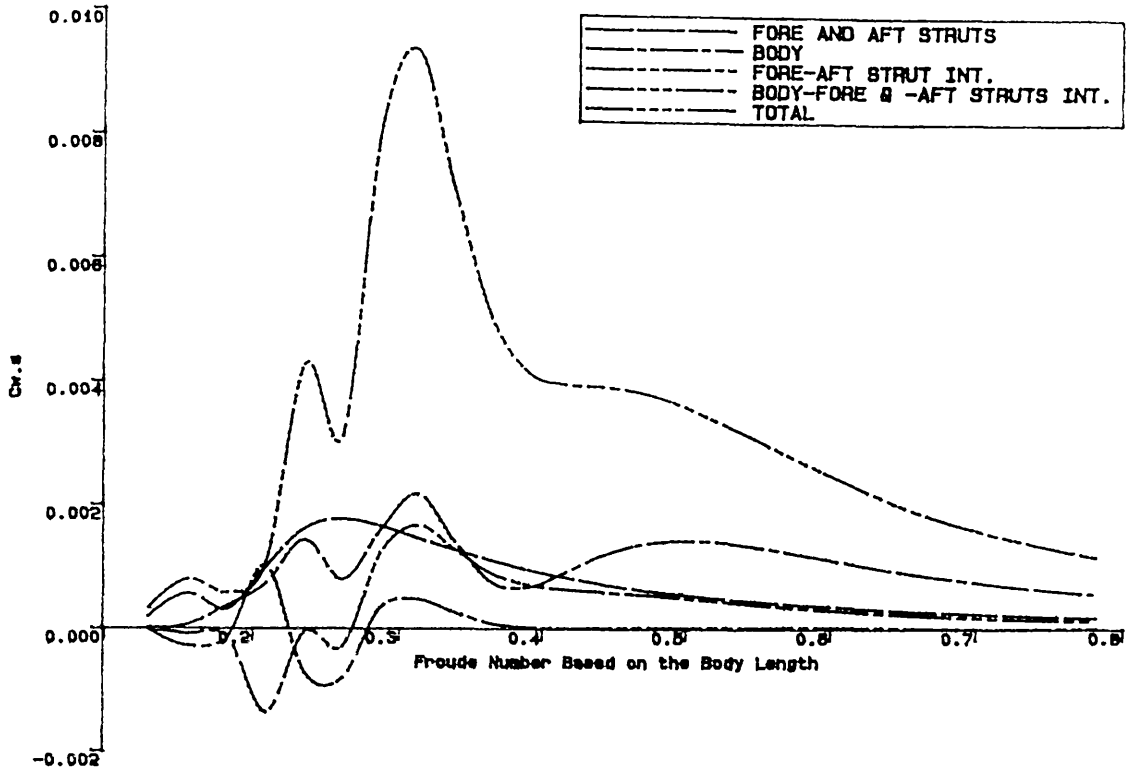

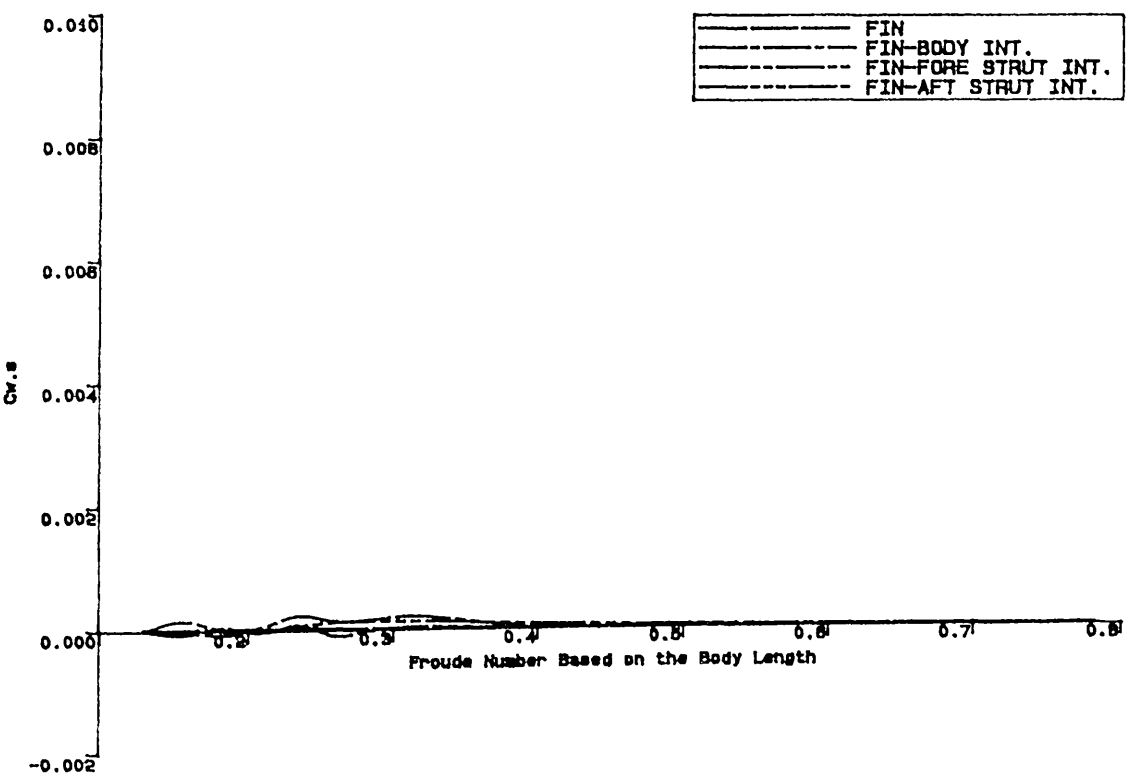

Fig.3.19

Wave Resistance Coefficients of a SWATH(with a pair of fins) and its Components Variations as a Function of Froude Number.

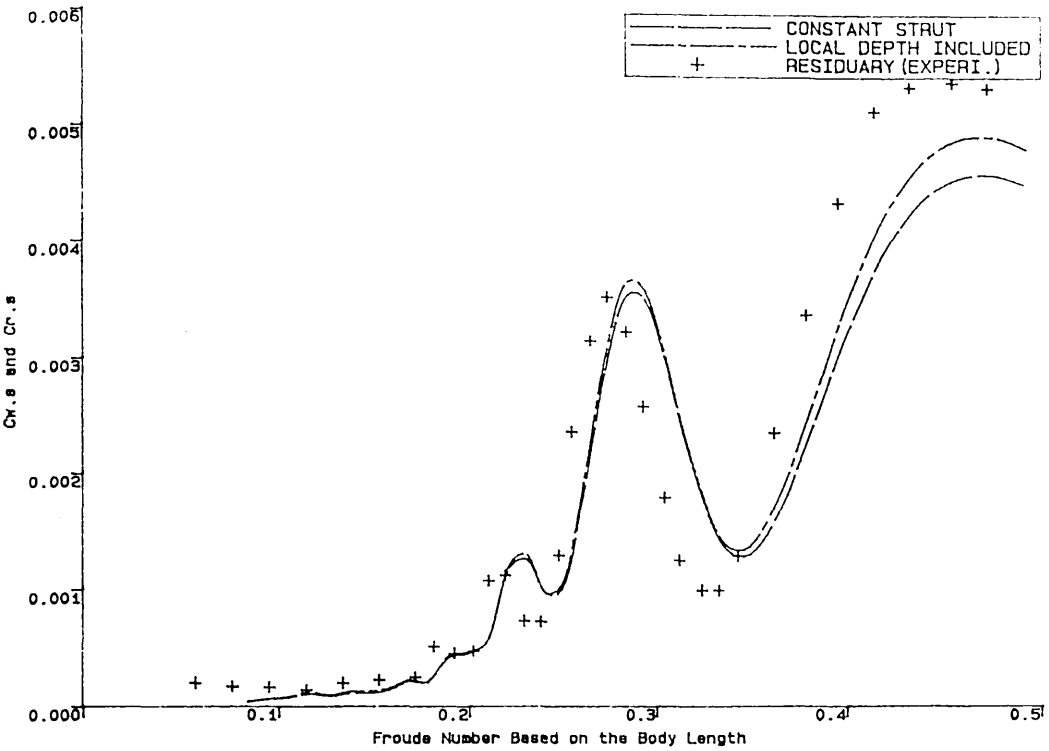

Comparison of Calculated (Using Different Modellings) and Measured (Residuary) Resistance Coefficients for TAGOS Model

Fig.3.20

CHAPTER 4 EXPERIMENTAL WORK WITH FIVE SWATH MODELS IN CALM WATER AND UNIFORM WAVES AS WELL

4.1 INTRODUCTION

There are currently 11 existing SWATH ships operating at sea worldwide. Therefore, experimental data and full scale trial data on SWATH ships are very scarce worldwide. Furthermore, detailed results are not published for confidential reasons. In order to validate the applicability of the computer programs developed in the previous Chapter, systematic calm water resistance, sinkage and trim measurements with three SWATH models(SWATH1, SWATH2 and SWATH3) were conducted at the Hydrodynamics Laboratory of Dept of Naval Architecture and Ocean Engineering, Glasgow University. These results then provided empirical form correlation factors for the total resistance prediction of SWATH ships. Also, using these three models, resistance increase(decrease), motion responses, sinkage and trim in uniform head waves were measured and compared with one another. In addition, the calm water resistance results of two Polish SWATH models(SWATH-386 and SWATH-395) are included in this Chapter to provide a more useful database for theoretical investigations.

Section 4.2 is concerned with the calm water resistance measurements of the SWATH1 model which is a tandem strut configuration with circular cross section hulls. The tests included several parametric changes such as two demihull spacings, draft and struts positions on the demihulls as well as the slenderness ratio of the bodies, resulting in a total of 17 conditions. The test results with this model in uniform head waves are presented in section 4.3. Wave frequencies of 0.3 to 1.6 hz were investigated and several wave heights were varied to study the effect of wave steepness on the hydrodynamic performances of the SWATH model.

The SWATH2 model is also a tandem strut configuration but has rectangular cross section hulls with rounded corners.The resistance, sinkage and trim in calm water and resistance increase(decrease), motion responses, sinkage and trim in waves were measured with this model. The results are presented in Section 4.4. All the results are

compared with those of the SWATH1 circular hulled model in order to find the feasibility of such rectangular hulled SWATH ships which is one of the main objectives of this thesis.

In order to compare the performance of single and tandem struts SWATH ships, a single strut SWATH model, designated as SWATH3, was built and tested in calm water as well as in waves. Rigorous comparisons between the single and tandem struts models are made with regard to resistance(in calm and waves) as well as motion responses in section 4.5.

As part of research collaboration between the Dept of Naval Architecture and Ocean Engineering of Glasgow University(G.U) and the Ship Hydromechanics Division of Gdansk Technical University(G.T.U), Poland, two series of model tests to measure the total resistance in calm water using two models, SWATH-386 and SWATH-395, were carried out at GTU and their analysis and comparison with computational results were conducted at G.U by the author and are presented in section 4.6. The test series included various changes in configurations of strut system, modifications of bow struts as well as of lower hulls and two spacings between the centrelines of the two demihulls which result in a total of 14 conditions. The experiments were aimed at obtaining an optimum strut system in terms of resistance and at finding a hull shape which could help prevent severe bow trim at high speeds and so permit stabilizing fins to be removed. The latter purpose was achieved by introducing a 'sledge bow' concept.

The experimental results with the aforementioned 5 SWATH models including 38 individual configurations are very valuable at this stage of SWATH development. Some of them seem to be extremely important to the further development of SWATH ships as well as to enhancing the performance of SWATH ships. All the calm water results are compared with the theoretical predictions and presented herein. Detailed conclusions are drawn upon at the end of each section and final overall conclusions are addressed at section 4.7.

4.2 SWATH1 MODEL RESISTANCE TESTS IN CALM WATER

In order to study experimentally the performance of a tandem strut SWATH model, designated as SWATH1, systematic resistance measurements were conducted in calm water at the Hydrodynamics Laboratory. The resistance tests consist of parametric changes such as two demihull spacings, draft and struts positions on the demihull as well as the slenderness ratio of the bodies, resulting in a total of 17 conditions with 15-22 speeds for each condition. The experiments were conducted in two modes, model free and model captive. In order to investigate the interference effect between the two demihulls, a single demihull was run in the captive mode.

The main objectives of these tests are to validate the applicability of the computer programs developed in Chapter 3 and to provide empirical correlation form factors for the total resistance prediction as mentioned in Chapter 3. The results are reported in Ref.[64] and this section is taken from the reference.

4.2.1 Description of Model SWATH1

The SWATH1 model is a tandem strut configuration. The lower portion of the demihull, referred to as the submerged body, has circular cross sections with ellipsoidal and tapered ends.The upper portion of the demihull, referred to as the strut, has the same water line at all drafts and is of airfoil section. The forward and aft strut are identical to each other. No camber was introduced in either the struts or the submerged bodies. They are all positioned parallel to the longitudinal centre line. Principal dimensions and coefficients of the SWATH1 model are listed in Table 4.1. Small scale model plans and details are shown in Fig.4.1. The sectional area curve of the lower hull and the waterplane area curves of the struts are shown in Fig.4.95 together with those of the SWATH2 model.

The model was designed in such a way that both the spacings between the hulls and between the struts can be systematically varied over a wide range. The spacing change between the struts can be achieved by inserting small lengths of parallel section

at the midlength of the submerged bodies, thus changing their slenderness as well. The draft can be changed by placing weights(lead shot) in the ballast tanks which are located inside the struts. A pair of stabilising fins(NACA0015) can be fitted near the stern of the model and these should be preset at a particular angle of attack for a range of tests. Turbulence stimulation devices were not introduced for this model.

Table 4.1. Some Dimensions and Principal Coefficients of SWATH1-C5 demihull

GUH Model	SWATH1
Length of Body(m), L_b	1.51
Diameter of Body(m), Di_b	0.0892
Length of Strut(m), L_s	0.4
Maximum Beam of Strut, T_m	0.05
L_b/Di_b	16.93
C_p of Body	0.9
C_{wp} of Strut	0.665
Slenderness of Strut, T_m/L_s	0.125
Draft(m), T	2.0 Di_b=0.1784
Depth of Strut(m), D_s	0.0892
SDBC(m), h	0.1338
Wetted Area(m^2), S	0.5125
Displaced Volume(m^3), ∇	0.0109
$H_1=2h/Di_b$	3.0
Natural Periods*	
Heave(sec), T_z	1.701
Pitch(sec), T_θ	2.252
Roll(sec), T_ϕ	2.778

* Note ; SWATH1-C8 Experimentally determined.

4.2.2 Experimental Arrangements

Model experiments were carried out at the Hydrodynamics Laboratory of Glasgow University, which is 77 m in length, 4.6 m in width and 2.4 m in water depth. The details of the tank can be found in Ref.[67].

In general resistance testing, the towing force should be aligned with the total resistance vector acting on the underwater body[95]. Otherwise, the moment applied to

the model will cause a different model behaviour, such as sinkage and trim etc, which could lead to faulty resistance measurements. Hence, the towing point should be, in general, around the propulsion point of the ship, which is near the stern of the model in longitudinal direction and below the waterline in height. However, because of the larger beam and different geometry characteristics of the SWATH concept, it is unlikely that a 'standard' dynamometer as used for monohull testing can be used for SWATH ships. As a result, different test techniques have been used in the various towing tanks worldwide and a description of the techniques is presented together with advantages and drawbacks in Ref.[96].

The best way to obtain an ideal towing point is to reach through the struts to the submerged body using a special U-type device. In order to obtain this objective, however, the model should be relatively large (so that the device can be installed inside the struts as well as the bodies) and accordingly, the size of the tank should be big. In general, the size of the model is decided by the tank dimensions such as length, width and water depth. This is due to the fact that the tank wall and bottom effects(called blockage effect) should be eliminated and its length should be long enough to obtain a certain time of steady state run for the resistance record. Because the size of the tank of the Hydrodynamics Laboratory is relatively small(the available run length is less than 60m), the construction of a large model is practically not desirable. Since the research into SWATH ships and semisubmersibles has been started at the Hydrodynamics Laboratory in 1978, a similar and consistent towing method[70,71,72,73,101] has been used with some minor modifications from time to time. For the present resistance measurements, the model was towed in the following way.

Towing of the model was effected by attaching a nylon cord yoke to the two fore struts, located in the vicinity of the waterline(2cm above the still water level). The yoke was led to a load cell via a tow point from which the tension was automatically recorded, amplified and displayed at the pen recorder. The experimental arrangement is shown in Fig.4.2 in which the suspension wires and the weights were used in the captive mode explained below. Also, the model placed in the water at the towing carriage is shown in Fig.4.3. This arrangement might, however, reduce the tendancy to trim by bow, especially at higher speeds. It is reported that the effect of towing height

on resistance and mean sinkage is not significant for the speeds tested, but trim is significantly affected by different towing heights[95]. Also, the effect of towing height on resistance was found negligible with the SWATH1 model for the two different towing heights tested and this is shown in Figs.4.49 and 4.50(explained in detail in section 4.3)

Because of the small waterplane area of the model, severe trim and sinkage(rise) are expected with corresponding effects on the measured resistance. In part to check this and in part to check the validity of the experimental arrangement, the total resistance was measured with a captive model in a number of conditions. The captive model condition was achieved in the following way.

The model was weighted(that is, over ballasted) by placing four masses on the deck above the struts. To fix the running depth of the model, the vessel was suspended by four wires from the carriage longitudinal girders. The main source of error in the experiment was expected to be the displacement from the vertical of the suspension wires as tension was taken in the towing yoke. Any displacement from the vertical of these wires would lead to some component of the resistance not being registered by the load cell. To compensate for this error, the model was positioned slightly forward of its normal position at speed, thus allowing the suspension wires to form an obtuse angle in relation to the still water. Therefore, when the carriage moved, viz tension is applied to the towing yoke, the vessel moved aft and the angle between the suspension wires and the towing plane(still waterplane) returned to approximately 90 degrees so that the error involved should be diminished. The arrangement is shown in Fig.4.2 and the model placed in the water with this captive condition at the towing carriage is shown in Fig.4.4.

For all the experiments, the model was restricted in yaw and sway using four vertical guiding rods in order to keep the model on course with minimum restraint, each fixed to the carriage longitudinal girders and passing through the apex of a right angle formed by the transverse and longitudinal deck frames of the model(see Figs.4.3 and 4.4)

4.2.3 Measurements

As shown in Table 4.2, the resistance tests consist of parametric changes including four different spacings between two demihulls, three different drafts and two different spacings between fore and aft struts on the demihull. The last was achieved in such a way that a parallel middle part of 0.2m length was inserted at the centre of the hull so that the relative positions of the struts on the demihull were changed, altering the body length from 1.51m to 1.71m. Therefore, the ratio(L_b/Di_b) is changed as well from 16.9 to 19.2.

Table 4.2 Experimental Conditions Tested(Total 17 Conditions)

Hull Length 1.51m

Spacing(2b) / Draft(t)\	0.427m (B_1=0.566)		0.575m (B_1=0.762)		0.715m (B_1=0.947)
1.5Di_b	C1	C1C	C4	C4C	C7
2.0Di_b	C2	C2C	C5	C5C	C8
2.5Di_b		C3C	C6		

Hull Length 1.71m

Spacing(2b) / Draft(T)\	0.575m (B_1=0.673)	0.651m (B_1=0.762)		
1.5Di_b	C9			
2.0Di_b	C10	C11	C11C	C11CS

Note; C1– Condition 1, C1C– Condition 1 Captive
C11CS – Condition 11 Captive Single Hull(one Demihull)

The experiments were conducted in two modes as follows:

A) free to heave and trim but restricted in yaw, sway and surge (C1,C2,C4, C5,C6,C8,C9,C10 and C11).

B) captive, rigidly fixed at zero trim and heave, and restricted in yaw, sway and surge as well (C1C,C2C,C3C,C4C,C5C and C11C). In addition, in order to investigate the interference effect on the resistance between the two demihulls, one demihull was run in the captive condition(C11CS), resulting in a total of 17 conditions.

The experiments were all carried out without turbulence stimulation devices and control fins. The water temperature in the towing tank was measured at the depth of two-thirds of the model draft every hour and the mean value of these readings was taken for each condition. Between runs, an interval of about 15 to 30 minutes, depending on the velocity and immersed depth of model, was required to allow the water to calm down. Just prior to each run, the tide of the tank water was taken at the mid-tank using a float and accounted for in the model speed.

4.2.4 Discussion

The total resistances, residuary resistances and their coefficients are presented in Tables 4.3 to 4.19 for all the conditions tested. As mentioned in Chapter 3, the residuary resistance was obtained by subtracting the frictional resistance from the total resistance. The frictional resistance is calculated using the ITTC'57 frictional line, in which Reynolds number is calculated based on the lengths of the body and strut individually. The resistance is non-dimensionalised by the factors $0.5\rho U^2S$ and $0.5\rho U^2\nabla^{2/3}$, where S and ∇ are the wetted surface area and displaced volume of the model, respectively. The latter is for the purpose of comparing the resistance of the models having different displacements.

Also, the results are presented in Figs.4.5 to 4.14 which shows the total, residuary and frictional resistances against Froude number for the model free conditions. It can be seen from the figures that the portion of the skin frictional resistance is considerable even at the higher speeds which is in contrast to the expected behaviour in monohulls. This is due to the slenderness ratio of each component of the SWATH1 being so large that the wave-making resistance component is greatly reduced and thus the wetted area of the model is large compared to the equivalent monohull.

This fact is much exaggerated for the conditions C9 to C11, as shown in Figs.4.12 to 4.14, where slenderness ratio(L_b/Di_b=19.2) is larger than that(16.9) of the other conditions. This portion due to friction will, however, be reduced in the full size SWATH ship, depending on its length, due to the decrease in frictional coefficient with Reynolds Number.

Figs.4.15 through 4.24 show comparisons between the calculated wave-making resistance(using OSWATH) and measured residuary resistance coefficients versus Froude Number for the model free conditions. The larger predictions at the slow speeds can be explained in the following way. From Figs.4.5 to 4.14, it should be noted that the measured total resistance is lower than the predicted frictional resistance at the slow speeds. This might be due to the fact that no turbulence stimulation devices were used for the measurements and possibly laminar flow occurred. Another reason for this is that the viscosity of water is ignored in the theory and hence the wave system can be exaggerated over the viscous dominant speed range(slow speeds) due to the absence of the viscous damping. In particular, this phenomenon can be seen over the hump speed range at the slow speed. Apart from the lower speed range, the theory gives good qualitative agreements with the measurements. The difference between the two curves is accounted for by additional resistances such as viscous pressure, form(3-D effect), eddying, wave-breaking and spray resistances as well as some non-linearity effects. It is known from the analysis of several SWATH designs that the quantity, Cr.s - Cw.s, oscillates about zero, being usually bounded within a difference of $\pm 1.0\times10^{-3}$[5]. As mentioned in Chapter 3.5.1, these differences are used to produce an empirical form factor in the computer program MSWATH and OSWATH.

In addition, Figs.4.15 through 4.24 illustrate the contribution of each component of the model to the total wave-making resistance as well as two times one demihull wave-making resistance. From these figures, it is easily understood how the total wave-making resistance is affected by the components of the model as well as by the parametric changes such as draft, spacing between the two demihulls, slendernesses of the body and strut, and relative position of the strut on the demihull.

The discussion is divided into 4 sections, each of which describes the results

caused by variations in two different experimental techniques (model captive and model free to sinkage and trim), draft, two demihull spacings and strut position on the demihull as well as the body slenderness ratio.

4.2.4.1 Two different experimental techniques

As shown in Figs.4.25 to 4.29, the difference in the resistances measured by the two different techniques(model captive and model free to sinkage and trim) is very considerable. Although the sinkage and trim were not measured for this set of experiments, as the speed increases, severe trim and sinkage were observed in the free mode which might contribute to the measured resistance increase. As seen in Figs.4.15 to 4.24, the abrupt increase in the coefficient curves above around Fn=0.65 was due to the green water. This phenomenon occurrs at lower speeds as the draft increases. In condition C6, as shown in Fig.4.19, where freeboard is the smallest among the conditions tested, the resistance measurements could not be conducted above Fn=0.6 due to the severe bow trim and hence, water flowing over the deck(green water). Fig.30 shows that green water occurred in the free mode(C2) at around Fn=0.75, but only the spray sheet can be seen in the captive mode at the same speed but at the different spacing(C8C).

Below the speed where the green water occurs or the severe spray sheets develop, it appears that sinkage and trim only affect the resistance by a small amount(see Figs.4.15 to 4.24). This is supported by the statement that ' the effect of towing height on resistance and mean sinkage is not significant for the speeds tested, but trim is significantly affected by the towing height[95] '. This means that the the effect of the towing height on the trim does not contribute much to the resistance increase. The effect of towing height on resistance was also found negligible with the SWATH1 model which will be mentioned in section 4.3.

Therefore, the large resistance difference between the two techniques suggested that the setting up of the captive model led to error in the measured resistance. In order to prove this, the suspension wires, as mentioned in section 3.2.2, were moved forward and backward by 1 cm each and the resistance was again measured. Large

differences were found between the three conditions and so, it was concluded that the resistance values measured using the captive setting are unreliable. However, the pattern of the resistance curves caused by variations in the draft, spacing and strut position on the demihull followed the same pattern as in the free mode and hence, these results can be used for a comparative study of such parametric changes.

4.2.4.2 Draft variations

Figs.4.31 through 4.36 show the effect of draft variations on the total resistance coefficient, which is non-dimensionalised by the displaced volume, against Froude number. A resistance benefit is not expected from the draft increase in terms of total resistance per tonnage with this model. From Figs.4.15 to 4.24, it is easily understood that the large peak around Fn=0.31, independent of the draft as well as the spacing, is a combination of large wave-making contributions by the struts and bodies coupled with unfavourable interferences between the body and the two struts and between the forward and aft struts. In addition, the contribution of one strut to the total wave-making is very large compared to the body contribution up to moderately high speeds because that the breadth to length ratio is so much larger. As a result, as the draft increases, the increased strut depth results in a considerable increase of the strut wave-making resistance which outweighs the decrease of the body wave resistance, resulting in the increased total wave-making resistance. At higher speeds, the total wave-making resistance coefficient(non-dimensionalised by the wetted area) decreases slightly due to the wave-making resistance of the bodies reducing as the draft increases. This is scarcely measurable if the coefficient is non-dimensionalised by the displaced volume. However, owing to the increased frictional resistance arising from the increased wetted area, the total resistance per displaced volume becomes worse with the increase of the draft throughout the speed tested, as shown in Figs.4.31 to 4.36. This phenomenon is mostly due to the fact that as mentioned earlier, the proportion of the skin frictional resistance is larger than that of the residuary resistance over the most speeds, as shown in Figs.4.5 to 4.14. This result occurs independently of the spacing between the two demihulls, and also in the captive mode.

4.2.4.3 Two demihull spacing effect

Fig.4.38 shows the effect of spacing between the two demihulls on the resistance at the draft of 2.0 times the body diameter. The result show that at higher speeds the wider the spacing distance, the better are the resistance characteristics. However, the trend is reversed in the moderately high speed range(Fn=0.35–0.44). This phenomenon is observed at the other conditions tested as well as in the mode captive as shown in Fig.4.37 and Figs 4.39 to 4.41. This may be due to the complicated hydrodynamic interference effect between the two demihulls.

During the experiments, it was observed that one or two standing waves/cusps were developed in between the two demihulls, and this was independent of the spacing and draft. The two standing waves/cusps started to develop at around a speed of 0.9 m/s(Fn=0.22); one at the middle of the forward struts and the other at the middle of the aft struts. As the speed increases, the two cusps move backwards. At the speed of 1.25 m/s(Fn=0.3) as seen in Fig.4.43-a and b, the first cusp developed at the middle of the model and the second cusp was behind the model. As the speed increases further, the two cusps occur behind the model, as seen in Fig.4.43-c.

This interference wave-making resistance can be seen from the predicted results in nearly the same speed range, as shown in Figs.4.15 to 4.24. From these figures, it can be also seen that in this speed range, the narrower the spacing distance is, the larger the resistance benefit from the interference, which is exactly the same as the experimental finding.

Fig 4.42 shows the comparison between single- and twin-hull ships. Both conditions were conducted in the captive mode. As mentioned earlier, although the results are not reliable, for the most speeds measured (except the speed range above mentioned), the twin ship give more resistance than two times the resistance of the demihull due to the unfavourable interference effect between the two demihulls except in the range of Fn=0.35–0.44. Fig.4.44 shows the condition of the single hull running(C11CS) in the captive mode where the diverging wave system created by the fore strut can be seen.

4.2.4.4 Strut position on the demihull and body slenderness variations

As mentioned in section 4.2.3, a parallel middle part of 0.2m length was inserted at the centre of the original hull so that the relative positions of the struts on the demihull were changed and at the same time, the slenderness ratio(L_b/Di_b) is changed from 16.9 to 19.2. Fig.4.45 shows the comparison between the two versions(C5 and C11) at the same non-dimensional spacing(B_1=0.762). In the condition C11, another minor hump occurs mostly due to the large contribution from the interference effect between the aft and fore struts which can be understood from the computational results as shown in Fig.4.24. Except in that minor hump speed range, the resistance coefficient of C11 becomes lower than that of C5 because of a combination of the different struts interference and less body resistance(larger slenderness). This result is also observed in the captive mode as shown in Fig.4.46.

4.2.5 Conclusions

From the experimental study with the SWATH1 model and comparison with the computational results using the computer program OSWATH developed in Chapter 3, some conclusions can be drawn:

1) It is reported in the ITTC meeting[97] that there is little scatter of total resistance between different tanks in the world for the model-free condition. However, the amount of scatter between tanks is very great for the fixed models probably due to the different way of fixing the captive model. To improve the accuracy of the measurements in the present captive condition, it would have been better to have used a sliding bearing system which would be very sensitive to the longitudinal movements of the model.

2) The strut only wave-making resistance of the SWATH1 model is considerably large compared to the body due to the large breadth to length ratio of the strut compared to that of the body. Coupled with the interferences between the components, the large wave-making resistance of the struts contributes to creating a very large hump at around Fn=0.31, which cannot be expected in single strut SWATH ships.

3) As the draft increases, the increased strut depth results in a considerable increase in the strut wave-making resistance which outweighs the decrease in the body wave-making resistance, resulting in the increased total resistance at all the speeds tested.

4) An interference wave system created by the two demihulls affects the resistance favourably or unfavourably, depending on the speed. Due to the favourable interference between the two demihulls around Fn=0.35-0.44, the resistance decreases as the spacing becomes narrower. However, at higher speeds, the result is reversed.

5) When the positions of the struts on the demihull are changed, the hollow and hump of the resistance coefficient curve is changed due to the different interference effects.

6) The measured resistance variations caused by the parametric changes(spacing between the demihulls, draft and strut positions on the demihull as well as the slenderness ratio of the body) are well predicted by the computational results. Therefore, the computer program OSWATH can be used, with confidence, to carry out parametric studies.

7) During the experiments, severe sinkage and trim by the bow occurred at the higher speeds with the SWATH1 model, hence, creating green water. Therefore, stabilising fins for the SWATH1 model seem to be necessary with regard to seakeeping as well as propeller emergence.

8) In conclusion, favourable interference effects are dependent upon the relative distance between the components of a SWATH design as well as the operating speed. Hence, a SWATH arrangement which will give favourable interference characteristics at all speeds is unlikely to be attained. However, reductions in wave resistance at certain speeds can be obtained by a proper location of the struts on the hulls and a well chosen spacing between the hulls. Most importantly, at a certain draft, a proper distribution of the volume on the struts and bodies, keeping the breadth to length ratio of the strut as low as possible, seems to be essential.

U(m/s)	FN	RN/10^6	RT(N)	CT.V	CT.S	RR (N)	CR.V	CR.S
0.495	0.129	0.656	0.539	0.0611	0.0050	-0.077	-0.0087	-0.0007
0.707	0.184	0.937	1.177	0.0653	0.0054	0.023	0.0013	0.0001
0.899	0.234	1.192	2.452	0.0842	0.0069	0.686	0.0235	0.0019
1.104	0.287	1.464	6.276	0.1429	0.0117	3.733	0.0850	0.0070
1.196	0.311	1.586	8.826	0.1712	0.0140	5.894	0.1143	0.0094
1.306	0.339	1.731	7.502	0.1220	0.0100	4.072	0.0662	0.0054
1.407	0.366	1.865	6.375	0.0893	0.0073	2.457	0.0344	0.0028
1.497	0.389	1.985	7.208	0.0892	0.0073	2.832	0.0351	0.0029
1.600	0.416	2.121	9.268	0.1004	0.0082	4.339	0.0470	0.0039
1.707	0.444	2.263	11.033	0.1051	0.0086	5.499	0.0524	0.0043
1.900	0.494	2.519	14.220	0.1093	0.0090	7.517	0.0578	0.0047
2.086	0.542	2.765	16.034	0.1022	0.0084	8.110	0.0517	0.0042
2.094	0.544	2.776	16.182	0.1024	0.0084	8.202	0.0519	0.0043
2.286	0.594	3.031	18.143	0.0963	0.0079	8.803	0.0467	0.0038
2.486	0.646	3.296	20.202	0.0907	0.0074	9.344	0.0420	0.0034
2.664	0.692	3.532	22.801	0.0891	0.0073	10.505	0.0411	0.0034
2.860	0.743	3.792	26.724	0.0907	0.0074	12.752	0.0433	0.0035

Table 4.3 SWATH1-C1 Tem.=15.1°C

U(m/s)	FN	RN/10^6	RT(N)	CT.V	CT.S	RR (N)	CR.V	CR.S
0.498	0.129	0.660	0.686	0.0711	0.0054	-0.090	-0.0093	-0.0007
0.704	0.183	0.933	1.373	0.0712	0.0054	-0.050	-0.0026	-0.0002
0.901	0.234	1.194	3.776	0.1195	0.0091	1.578	0.0499	0.0038
1.099	0.286	1.457	8.287	0.1763	0.0134	5.164	0.1099	0.0084
1.205	0.313	1.597	12.210	0.2161	0.0164	8.534	0.1510	0.0115
1.251	0.325	1.658	12.847	0.2109	0.0160	8.919	0.1464	0.0111
1.306	0.339	1.731	12.112	0.1825	0.0139	7.872	0.1186	0.0090
1.402	0.364	1.859	9.905	0.1295	0.0098	5.096	0.0666	0.0051
1.448	0.376	1.920	9.415	0.1154	0.0088	4.322	0.0530	0.0040
1.509	0.392	2.000	10.101	0.1140	0.0087	4.620	0.0521	0.0040
1.597	0.415	2.117	11.131	0.1121	0.0085	5.068	0.0511	0.0039
1.704	0.443	2.259	13.141	0.1163	0.0088	6.336	0.0561	0.0043
1.906	0.495	2.527	16.525	0.1169	0.0089	8.215	0.0581	0.0044
2.102	0.546	2.787	18.731	0.1089	0.0083	8.835	0.0514	0.0039
2.299	0.597	3.048	21.036	0.1023	0.0078	9.420	0.0458	0.0035
2.505	0.651	3.321	23.880	0.0978	0.0074	10.336	0.0423	0.0032
2.710	0.704	3.593	28.685	0.1004	0.0076	13.091	0.0458	0.0035
2.895	0.752	3.838	34.325	0.1052	0.0080	16.770	0.0514	0.0039

Table 4.4 SWATH1-C2 Tem.=14.3°C

U(m/s)	FN	RN/10^6	RT(N)	CT.V	CT.S	RR (N)	CR.V	CR.S
0.501	0.130	0.664	0.539	0.0596	0.0049	-0.090	-0.0099	-0.0008
0.702	0.182	0.931	1.030	0.0580	0.0047	-0.110	-0.0062	-0.0005
0.906	0.235	1.201	2.354	0.0796	0.0065	0.563	0.0190	0.0016
1.104	0.287	1.464	6.129	0.1395	0.0114	3.586	0.0816	0.0067
1.194	0.310	1.583	8.777	0.1708	0.0140	5.853	0.1139	0.0093
1.309	0.340	1.735	7.453	0.1207	0.0099	4.009	0.0649	0.0053
1.401	0.364	1.857	6.914	0.0977	0.0080	3.026	0.0428	0.0035
1.511	0.393	2.003	7.698	0.0936	0.0077	3.249	0.0395	0.0032
1.604	0.417	2.126	9.219	0.0994	0.0081	4.268	0.0460	0.0038
1.708	0.444	2.264	10.641	0.1012	0.0083	5.101	0.0485	0.0040
1.903	0.495	2.523	13.239	0.1014	0.0083	6.517	0.0499	0.0041
2.104	0.547	2.789	15.593	0.0977	0.0080	7.545	0.0473	0.0039
2.290	0.595	3.036	17.505	0.0926	0.0076	8.136	0.0430	0.0035
2.532	0.658	3.357	20.251	0.0876	0.0072	9.029	0.0391	0.0032
2.677	0.696	3.549	22.850	0.0885	0.0072	10.446	0.0404	0.0033
2.895	0.752	3.838	27.754	0.0919	0.0075	13.473	0.0446	0.0037

Table 4.5 SWATH1-C4 Tem.=14.6°C

U(m/s)	FN	RN/10^6	RT(N)	CT.V	CT.S	RR (N)	CR.V	CR.S
0.501	0.130	0.664	0.736	0.0754	0.0057	-0.048	-0.0049	-0.0004
0.699	0.182	0.927	1.226	0.0645	0.0049	-0.180	-0.0095	-0.0007
0.899	0.234	1.192	3.678	0.1169	0.0089	1.488	0.0473	0.0036
1.103	0.287	1.462	8.385	0.1771	0.0135	5.242	0.1107	0.0084
1.200	0.312	1.591	11.866	0.2117	0.0161	8.218	0.1466	0.0111
1.256	0.326	1.665	12.259	0.1997	0.0152	8.302	0.1352	0.0103
1.306	0.339	1.731	11.768	0.1773	0.0135	7.528	0.1134	0.0086
1.403	0.365	1.860	10.543	0.1376	0.0105	5.727	0.0748	0.0057
1.452	0.377	1.925	9.930	0.1210	0.0092	4.811	0.0586	0.0045
1.499	0.390	1.987	10.739	0.1228	0.0093	5.322	0.0609	0.0046
1.596	0.415	2.116	11.425	0.1152	0.0088	5.369	0.0542	0.0041
1.690	0.439	2.240	12.847	0.1156	0.0088	6.142	0.0553	0.0042
1.902	0.494	2.521	15.691	0.1114	0.0085	7.413	0.0526	0.0040
2.069	0.538	2.743	17.653	0.1060	0.0081	8.032	0.0482	0.0037
2.106	0.547	2.792	18.094	0.1048	0.0080	8.164	0.0473	0.0036
2.305	0.599	3.056	20.350	0.0984	0.0075	8.680	0.0420	0.0032
2.442	0.635	3.237	22.066	0.0951	0.0072	9.126	0.0393	0.0030
2.506	0.651	3.322	22.948	0.0939	0.0071	9.395	0.0384	0.0029
2.697	0.701	3.575	26.479	0.0935	0.0071	11.019	0.0389	0.0030
2.909	0.756	3.856	31.873	0.0968	0.0074	14.166	0.0430	0.0033

Table 4.6 SWATH1-c5 Tem.=14.6°C

U(m/s)	FN	RN/10^6	RT(N)	CT.V	CT.S	RR (N)	CR.V	CR.S
0.493	0.128	0.654	0.637	0.0629	0.0045	-0.276	-0.0272	-0.0019
0.703	0.183	0.932	1.422	0.0690	0.0049	-0.275	-0.0133	-0.0010
0.914	0.238	1.212	4.756	0.1366	0.0097	2.066	0.0593	0.0042
1.096	0.285	1.453	10.199	0.2036	0.0145	6.495	0.1297	0.0093
1.205	0.313	1.597	14.612	0.2414	0.0172	10.233	0.1690	0.0121
1.296	0.337	1.718	14.907	0.2129	0.0152	9.925	0.1417	0.0101
1.400	0.364	1.856	12.798	0.1566	0.0112	7.087	0.0867	0.0062
1.499	0.390	1.987	12.504	0.1335	0.0095	6.057	0.0647	0.0046
1.600	0.416	2.121	12.994	0.1217	0.0087	5.757	0.0539	0.0039
1.695	0.440	2.247	14.318	0.1195	0.0085	6.300	0.0526	0.0038
1.897	0.493	2.515	16.917	0.1127	0.0080	7.122	0.0475	0.0034
2.097	0.545	2.780	20.742	0.1131	0.0081	9.033	0.0493	0.0035
2.307	0.600	3.058	25.743	0.1160	0.0083	11.862	0.0535	0.0038

Table 4.7 SWATH1-C6 Tem.=14.6°C

U(m/s)	FN	RN/10^6	RT(N)	CT.V	CT.S	RR (N)	CR.V	CR.S
0.492	0.128	0.652	0.539	0.0618	0.0051	-0.070	-0.0080	-0.0007
0.702	0.182	0.931	1.079	0.0607	0.0050	-0.061	-0.0034	-0.0003
0.900	0.234	1.193	2.354	0.0806	0.0066	0.584	0.0200	0.0016
1.102	0.286	1.461	6.007	0.1372	0.0112	3.472	0.0793	0.0065
1.204	0.313	1.596	8.434	0.1614	0.0132	5.466	0.1046	0.0086
1.298	0.337	1.721	8.091	0.1332	0.0109	4.698	0.0774	0.0063
1.403	0.365	1.860	7.355	0.1037	0.0085	3.457	0.0487	0.0040
1.508	0.392	1.999	7.993	0.0975	0.0080	3.559	0.0434	0.0036
1.605	0.417	2.128	9.071	0.0977	0.0080	4.115	0.0443	0.0036
1.699	0.442	2.252	10.199	0.0980	0.0080	4.712	0.0453	0.0037
1.932	0.502	2.561	13.190	0.0981	0.0080	6.284	0.0467	0.0038
2.095	0.544	2.777	15.054	0.0952	0.0078	7.068	0.0447	0.0037
2.300	0.598	3.049	17.113	0.0898	0.0074	7.670	0.0402	0.0033
2.503	0.650	3.318	20.153	0.0893	0.0073	9.161	0.0406	0.0033
2.682	0.697	3.556	23.046	0.0889	0.0073	10.600	0.0409	0.0033
2.807	0.729	3.721	25.253	0.0889	0.0073	11.744	0.0414	0.0034
2.945	0.765	3.904	28.735	0.0919	0.0075	14.006	0.0448	0.0037

Table 4.8 SWATH1-C7 Tem.=14.3°C

U(m/s)	FN	RN/10^6	RT(N)	CT.V	CT.S	RR (N)	CR.V	CR.S
0.501	0.130	0.664	0.637	0.0653	0.0050	-0.147	-0.0150	-0.0011
0.694	0.180	0.920	1.226	0.0654	0.0050	-0.162	-0.0086	-0.0007
0.896	0.233	1.188	3.580	0.1146	0.0087	1.403	0.0449	0.0034
1.103	0.287	1.462	8.287	0.1750	0.0133	5.144	0.1086	0.0083
1.196	0.311	1.586	11.474	0.2061	0.0157	7.847	0.1410	0.0107
1.256	0.326	1.665	11.866	0.1933	0.0147	7.910	0.1288	0.0098
1.298	0.337	1.721	11.376	0.1735	0.0132	7.182	0.1095	0.0083
1.417	0.368	1.879	10.641	0.1362	0.0103	5.740	0.0734	0.0056
1.448	0.376	1.920	10.248	0.1256	0.0095	5.155	0.0632	0.0048
1.509	0.392	2.000	10.739	0.1212	0.0092	5.258	0.0593	0.0045
1.595	0.414	2.114	11.278	0.1139	0.0087	5.229	0.0528	0.0040
1.710	0.444	2.267	13.190	0.1159	0.0088	6.343	0.0557	0.0042
1.906	0.495	2.527	15.054	0.1065	0.0081	6.744	0.0477	0.0036
2.096	0.545	2.779	17.260	0.1009	0.0077	7.414	0.0434	0.0033
2.324	0.604	3.081	20.006	0.0952	0.0072	8.164	0.0388	0.0030
2.501	0.650	3.316	21.821	0.0896	0.0068	8.315	0.0342	0.0026
2.716	0.706	3.601	25.253	0.0880	0.0067	9.597	0.0334	0.0025
2.892	0.752	3.834	30.157	0.0926	0.0070	12.635	0.0388	0.0030

Table 4.9 SWATH1-C8 Tem.=14.2°C

U(m/s)	FN	RN/10^6	RT(N)	CT.V	CT.S	RR (N)	CR.V	CR.S
0.499	0.122	0.749	0.539	0.0554	0.0044	-0.145	-0.0149	-0.0012
0.598	0.146	0.898	0.785	0.0561	0.0044	-0.157	-0.0112	-0.0009
0.698	0.170	1.048	1.128	0.0592	0.0047	-0.109	-0.0057	-0.0005
0.806	0.197	1.210	1.618	0.0637	0.0050	0.022	0.0009	0.0001
0.900	0.220	1.351	3.187	0.1007	0.0079	1.246	0.0394	0.0031
0.998	0.244	1.498	4.021	0.1033	0.0081	1.688	0.0434	0.0034
1.066	0.260	1.600	4.119	0.0928	0.0073	1.496	0.0337	0.0027
1.098	0.268	1.648	4.658	0.0989	0.0078	1.894	0.0402	0.0032
1.204	0.294	1.808	8.042	0.1420	0.0112	4.784	0.0845	0.0067
1.242	0.303	1.865	9.415	0.1562	0.0123	5.971	0.0991	0.0078
1.313	0.321	1.971	9.758	0.1448	0.0114	5.955	0.0884	0.0070
1.382	0.337	2.075	8.875	0.1189	0.0094	4.708	0.0631	0.0050
1.500	0.366	2.252	7.944	0.0903	0.0071	3.120	0.0355	0.0028
1.605	0.392	2.410	8.679	0.0862	0.0068	3.234	0.0321	0.0025
1.696	0.414	2.546	10.003	0.0890	0.0070	3.993	0.0355	0.0028
1.892	0.462	2.840	13.141	0.0939	0.0074	5.830	0.0417	0.0033
2.088	0.510	3.135	15.887	0.0933	0.0073	7.161	0.0420	0.0033
2.306	0.563	3.462	18.878	0.0909	0.0072	8.447	0.0407	0.0032
2.508	0.612	3.765	20.693	0.0842	0.0066	8.561	0.0348	0.0027
2.695	0.658	4.046	23.145	0.0815	0.0064	9.335	0.0329	0.0026
2.907	0.710	4.364	26.675	0.0808	0.0064	10.847	0.0328	0.0026

Table 4.10 SWATH1-C9 Tem.=14.4°C

V(m/s)	FN	RN/10^6	RT(N)	CT.V	CT.S	RR (N)	CR.V	CR.S
0.499	0.122	0.749	0.736	0.0706	0.0052	-0.106	-0.0101	-0.0007
0.702	0.171	1.054	1.471	0.0713	0.0053	-0.060	-0.0029	-0.0002
0.901	0.220	1.353	4.413	0.1299	0.0096	2.036	0.0599	0.0044
0.939	0.229	1.410	5.394	0.1462	0.0108	2.837	0.0769	0.0057
1.001	0.244	1.503	6.375	0.1520	0.0112	3.511	0.0837	0.0062
1.048	0.256	1.573	6.227	0.1355	0.0100	3.122	0.0679	0.0050
1.100	0.269	1.651	6.669	0.1317	0.0097	3.285	0.0649	0.0048
1.204	0.294	1.808	10.543	0.1738	0.0128	6.570	0.1083	0.0080
1.258	0.307	1.889	12.602	0.1903	0.0140	8.308	0.1254	0.0092
1.301	0.318	1.953	13.485	0.1904	0.0140	8.926	0.1260	0.0093
1.393	0.340	2.091	12.896	0.1588	0.0117	7.749	0.0954	0.0070
1.503	0.367	2.256	11.131	0.1177	0.0087	5.238	0.0554	0.0041
1.552	0.379	2.330	10.788	0.1070	0.0079	4.549	0.0451	0.0033
1.619	0.395	2.431	11.278	0.1028	0.0076	4.551	0.0415	0.0031
1.711	0.418	2.569	12.602	0.1029	0.0076	5.178	0.0423	0.0031
1.905	0.465	2.860	15.446	0.1017	0.0075	6.453	0.0425	0.0031
2.104	0.514	3.159	18.094	0.0977	0.0072	7.353	0.0397	0.0029
2.333	0.570	3.503	20.595	0.0904	0.0067	7.672	0.0337	0.0025
2.500	0.610	3.753	22.752	0.0870	0.0064	8.125	0.0311	0.0023
2.718	0.664	4.081	26.087	0.0844	0.0062	9.093	0.0294	0.0022
2.890	0.706	4.339	29.421	0.0842	0.0062	10.448	0.0299	0.0022

Table 4.11 SWATH1-C10 Tem.=14.1°C

V(m/s)	FN	RN/10^6	RT(N)	CT.V	CT.S	RR (N)	CR.V	CR.S
0.493	0.120	0.740	0.736	0.0723	0.0053	-0.088	-0.0087	-0.0006
0.703	0.172	1.055	1.373	0.0664	0.0049	-0.162	-0.0078	-0.0006
0.901	0.220	1.353	4.266	0.1256	0.0093	1.889	0.0556	0.0041
0.946	0.231	1.420	5.492	0.1466	0.0108	2.901	0.0775	0.0057
1.001	0.244	1.503	6.129	0.1462	0.0108	3.266	0.0779	0.0057
1.098	0.268	1.648	6.669	0.1322	0.0097	3.296	0.0653	0.0048
1.192	0.291	1.790	9.954	0.1674	0.0123	6.052	0.1018	0.0075
1.262	0.308	1.895	12.308	0.1847	0.0136	7.989	0.1199	0.0088
1.314	0.321	1.973	13.239	0.1832	0.0135	8.600	0.1190	0.0088
1.404	0.343	2.108	12.602	0.1528	0.0113	7.382	0.0895	0.0066
1.506	0.368	2.261	11.523	0.1214	0.0089	5.610	0.0591	0.0044
1.605	0.392	2.410	11.768	0.1092	0.0080	5.145	0.0477	0.0035
1.709	0.417	2.566	12.798	0.1047	0.0077	5.390	0.0441	0.0032
1.898	0.463	2.849	15.299	0.1015	0.0075	6.365	0.0422	0.0031
2.097	0.512	3.148	17.947	0.0975	0.0072	7.270	0.0395	0.0029
2.347	0.573	3.524	20.399	0.0885	0.0065	7.336	0.0318	0.0023
2.510	0.613	3.768	22.801	0.0865	0.0064	8.069	0.0306	0.0023
2.694	0.658	4.044	26.234	0.0864	0.0064	9.508	0.0313	0.0023

Table 4.12 SWATH1-C11 Tem.=14.6°C

U(m/s)	FN	RN/10^6	RT(N)	CT.V	CT.S	RR (N)	CR.V	CR.S
0.496	0.129	0.658	0.490	0.0552	0.0045	-0.129	-0.0145	-0.0012
0.708	0.184	0.939	0.736	0.0407	0.0033	-0.422	-0.0233	-0.0019
0.903	0.235	1.197	1.471	0.0501	0.0041	-0.308	-0.0105	-0.0009
1.104	0.287	1.464	4.904	0.1115	0.0091	2.359	0.0537	0.0044
1.204	0.313	1.596	7.257	0.1389	0.0114	4.290	0.0821	0.0067
1.301	0.338	1.724	5.884	0.0965	0.0079	2.479	0.0407	0.0033
1.400	0.364	1.856	4.707	0.0666	0.0055	0.823	0.0116	0.0010
1.500	0.390	1.989	5.492	0.0677	0.0055	1.099	0.0135	0.0011
1.600	0.416	2.121	6.718	0.0728	0.0060	1.790	0.0194	0.0016
1.703	0.443	2.258	8.189	0.0783	0.0064	2.677	0.0256	0.0021
1.896	0.493	2.514	10.592	0.0818	0.0067	3.914	0.0302	0.0025
2.096	0.545	2.779	11.327	0.0715	0.0059	3.334	0.0211	0.0017
2.328	0.605	3.086	13.141	0.0673	0.0055	3.491	0.0179	0.0015
2.505	0.651	3.321	13.828	0.0611	0.0050	2.820	0.0125	0.0010
2.670	0.694	3.540	14.711	0.0573	0.0047	2.364	0.0092	0.0008
2.867	0.745	3.801	16.427	0.0555	0.0045	2.393	0.0081	0.0007

Table 4.13 SWATH1-C1C Tem.=15.0°C

U(m/s)	FN	RN/10^6	RT(N)	CT.V	CT.S	RR (N)	CR.V	CR.S
0.497	0.129	0.659	0.637	0.0663	0.0050	-0.136	-0.0141	-0.0011
0.700	0.182	0.928	1.079	0.0566	0.0043	-0.330	-0.0173	-0.0013
0.902	0.234	1.196	2.452	0.0774	0.0059	0.249	0.0079	0.0006
1.101	0.286	1.460	6.571	0.1393	0.0106	3.438	0.0729	0.0055
1.199	0.312	1.589	10.003	0.1788	0.0136	6.361	0.1137	0.0086
1.253	0.326	1.661	10.297	0.1685	0.0128	6.358	0.1041	0.0079
1.300	0.338	1.723	9.513	0.1447	0.0110	5.309	0.0808	0.0061
1.353	0.352	1.794	8.091	0.1136	0.0086	3.576	0.0502	0.0038
1.401	0.364	1.857	7.355	0.0963	0.0073	2.552	0.0334	0.0025
1.499	0.390	1.987	7.453	0.0852	0.0065	2.037	0.0233	0.0018
1.603	0.417	2.125	8.483	0.0848	0.0064	2.380	0.0238	0.0018
1.702	0.442	2.256	9.709	0.0861	0.0065	2.918	0.0259	0.0020
1.901	0.494	2.520	11.817	0.0840	0.0064	3.547	0.0252	0.0019
2.102	0.546	2.787	13.239	0.0770	0.0059	3.343	0.0194	0.0015
2.299	0.597	3.048	14.514	0.0706	0.0054	2.899	0.0141	0.0011
2.503	0.650	3.318	15.642	0.0642	0.0049	2.117	0.0087	0.0007
2.704	0.703	3.585	17.898	0.0629	0.0048	2.366	0.0083	0.0006
2.919	0.759	3.870	19.614	0.0591	0.0045	1.797	0.0054	0.0004

Table 4.14 SWATH1-C2C Tem.=14.9°C

U(m/s)	FN	RN/10^6	RT(N)	CT.V	CT.S	RR (N)	CR.V	CR.S
0.504	0.131	0.668	0.785	0.0741	0.0053	-0.165	-0.0155	-0.0011
0.705	0.183	0.935	1.471	0.0710	0.0051	-0.234	-0.0113	-0.0008
0.895	0.233	1.187	3.923	0.1175	0.0084	1.330	0.0398	0.0028
1.098	0.285	1.456	9.121	0.1814	0.0130	5.404	0.1075	0.0077
1.199	0.312	1.590	12.455	0.2078	0.0148	8.114	0.1354	0.0097
1.253	0.326	1.661	13.387	0.2045	0.0146	8.694	0.1328	0.0095
1.309	0.340	1.735	12.847	0.1798	0.0128	7.777	0.1089	0.0078
1.399	0.364	1.855	10.641	0.1304	0.0093	4.937	0.0605	0.0043
1.499	0.390	1.987	9.317	0.0994	0.0071	2.870	0.0306	0.0022
1.601	0.416	2.122	9.954	0.0931	0.0066	2.709	0.0253	0.0018
1.698	0.441	2.251	11.131	0.0926	0.0066	3.088	0.0257	0.0018
1.897	0.493	2.515	13.288	0.0886	0.0063	3.493	0.0233	0.0017
2.098	0.545	2.781	14.956	0.0815	0.0058	3.236	0.0176	0.0013
2.301	0.598	3.050	16.427	0.0744	0.0053	2.609	0.0118	0.0008
2.491	0.647	3.302	18.290	0.0707	0.0050	2.370	0.0092	0.0007
2.696	0.701	3.574	20.938	0.0691	0.0049	2.601	0.0086	0.0006
2.908	0.756	3.855	23.390	0.0663	0.0047	2.394	0.0068	0.0005

Table 4.15 SWATH1-C3C Tem.=14.9°C

U(m/s)	FN	RN/10^6	RT(N)	CT.V	CT.S	RR (N)	CR.V	CR.S
0.508	0.132	0.673	0.441	0.0474	0.0039	-0.203	-0.0219	-0.0018
0.702	0.182	0.931	0.736	0.0414	0.0034	-0.404	-0.0228	-0.0019
0.903	0.235	1.197	1.373	0.0467	0.0038	-0.407	-0.0138	-0.0011
1.100	0.286	1.458	4.511	0.1034	0.0085	1.984	0.0455	0.0037
1.204	0.313	1.596	6.522	0.1248	0.0102	3.554	0.0680	0.0056
1.295	0.337	1.717	5.737	0.0949	0.0078	2.358	0.0390	0.0032
1.409	0.366	1.868	5.394	0.0754	0.0062	1.466	0.0205	0.0017
1.502	0.390	1.991	5.688	0.0700	0.0057	1.286	0.0158	0.0013
1.622	0.421	2.150	6.963	0.0734	0.0060	1.912	0.0202	0.0017
1.717	0.446	2.276	8.091	0.0761	0.0062	2.499	0.0235	0.0019
1.902	0.494	2.521	9.317	0.0715	0.0059	2.601	0.0199	0.0016
2.096	0.545	2.779	10.641	0.0672	0.0055	2.648	0.0167	0.0014
2.304	0.599	3.054	11.965	0.0625	0.0051	2.492	0.0130	0.0011
2.505	0.651	3.321	13.043	0.0577	0.0047	2.035	0.0090	0.0007
2.703	0.702	3.583	14.220	0.0540	0.0044	1.598	0.0061	0.0005
2.891	0.751	3.833	15.838	0.0526	0.0043	1.593	0.0053	0.0004

Table 4.16 SWATH1-C4C Tem.=15.0°C

U(m/s)	FN	RN/10^6	RT(N)	CT.V	CT.S	RR (N)	CR.V	CR.S
0.501	0.130	0.664	0.637	0.0653	0.0050	-0.147	-0.0150	-0.0011
0.699	0.182	0.927	1.030	0.0542	0.0041	-0.376	-0.0198	-0.0015
0.898	0.233	1.190	2.059	0.0656	0.0050	-0.126	-0.0040	-0.0003
1.112	0.289	1.474	5.982	0.1243	0.0094	2.794	0.0581	0.0044
1.203	0.313	1.595	8.875	0.1576	0.0120	5.210	0.0925	0.0070
1.303	0.339	1.727	8.385	0.1269	0.0096	4.162	0.0630	0.0048
1.403	0.365	1.860	7.944	0.1037	0.0079	3.128	0.0408	0.0031
1.505	0.391	1.995	7.993	0.0907	0.0069	2.538	0.0288	0.0022
1.600	0.416	2.121	8.728	0.0876	0.0067	2.645	0.0266	0.0020
1.709	0.444	2.266	9.268	0.0815	0.0062	2.427	0.0214	0.0016
1.920	0.499	2.545	11.327	0.0790	0.0060	2.908	0.0203	0.0015
2.120	0.551	2.810	12.357	0.0706	0.0054	2.308	0.0132	0.0010
2.306	0.599	3.057	13.534	0.0654	0.0050	1.855	0.0090	0.0007
2.510	0.652	3.328	15.299	0.0624	0.0047	1.706	0.0070	0.0005
2.673	0.695	3.544	16.819	0.0605	0.0046	1.605	0.0058	0.0004
2.899	0.753	3.843	18.584	0.0568	0.0043	0.986	0.0030	0.0002

Table 4.17 SWATH1-C5C Tem.=15.1°C

U(m/s)	FN	RN/10^6	RT(N)	CT.V	CT.S	RR (N)	CR.V	CR.S
0.492	0.120	0.739	0.588	0.0581	0.0043	-0.232	-0.0229	-0.0017
0.595	0.145	0.893	0.785	0.0530	0.0039	-0.360	-0.0243	-0.0018
0.702	0.171	1.054	0.932	0.0452	0.0033	-0.599	-0.0291	-0.0021
0.800	0.195	1.201	1.324	0.0494	0.0036	-0.603	-0.0225	-0.0017
0.905	0.221	1.359	3.383	0.0987	0.0073	0.988	0.0288	0.0021
1.007	0.246	1.512	3.923	0.0924	0.0068	1.029	0.0242	0.0018
1.101	0.269	1.653	4.315	0.0851	0.0063	0.926	0.0182	0.0013
1.203	0.294	1.806	7.600	0.1255	0.0092	3.634	0.0600	0.0044
1.268	0.310	1.904	9.170	0.1363	0.0100	4.815	0.0716	0.0053
1.310	0.320	1.967	10.150	0.1413	0.0104	5.536	0.0771	0.0057
1.401	0.342	2.103	9.317	0.1134	0.0084	4.117	0.0501	0.0037
1.508	0.368	2.264	8.336	0.0876	0.0065	2.408	0.0253	0.0019
1.597	0.390	2.398	8.826	0.0827	0.0061	2.261	0.0212	0.0016
1.695	0.414	2.545	9.317	0.0775	0.0057	2.016	0.0168	0.0012
1.726	0.421	2.591	9.856	0.0791	0.0058	2.316	0.0186	0.0014
1.902	0.464	2.855	10.984	0.0726	0.0053	2.016	0.0133	0.0010
2.105	0.514	3.160	13.141	0.0709	0.0052	2.391	0.0129	0.0010
2.300	0.562	3.453	14.318	0.0647	0.0048	1.721	0.0078	0.0006
2.492	0.609	3.741	15.789	0.0608	0.0045	1.246	0.0048	0.0004
2.691	0.657	4.040	17.358	0.0573	0.0042	0.666	0.0022	0.0002
2.906	0.710	4.363	20.742	0.0587	0.0043	1.580	0.0045	0.0003

Table 4.18 SWATH1-C11C Tem.=14.2°C

U(m/s)	FN	RN/10^6	RT(N)	CT.V	CT.S	RR (N)	CR.V	CR.S
0.511	0.125	0.767	0.392	0.0359	0.0026	-0.485	-0.0443	-0.0033
0.607	0.148	0.911	0.588	0.0382	0.0028	-0.597	-0.0387	-0.0029
0.705	0.172	1.058	0.686	0.0330	0.0024	-0.856	-0.0411	-0.0030
0.803	0.196	1.206	1.275	0.0472	0.0035	-0.665	-0.0246	-0.0018
0.897	0.219	1.347	3.040	0.0903	0.0067	0.682	0.0202	0.0015
0.949	0.232	1.425	3.236	0.0859	0.0063	0.631	0.0167	0.0012
1.000	0.244	1.501	3.531	0.0844	0.0062	0.672	0.0161	0.0012
1.099	0.268	1.650	3.923	0.0776	0.0057	0.544	0.0108	0.0008
1.204	0.294	1.808	7.355	0.1212	0.0089	3.383	0.0558	0.0041
1.248	0.305	1.874	8.336	0.1279	0.0094	4.102	0.0629	0.0046
1.302	0.318	1.955	9.415	0.1327	0.0098	4.850	0.0684	0.0050
1.312	0.320	1.970	10.003	0.1389	0.0102	5.376	0.0746	0.0055
1.405	0.343	2.109	9.807	0.1187	0.0087	4.581	0.0555	0.0041
1.510	0.369	2.267	9.022	0.0946	0.0070	3.081	0.0323	0.0024
1.625	0.397	2.440	9.219	0.0834	0.0061	2.447	0.0221	0.0016
1.694	0.414	2.543	9.317	0.0776	0.0057	2.024	0.0169	0.0012
1.905	0.465	2.860	10.984	0.0723	0.0053	1.991	0.0131	0.0010
2.095	0.512	3.145	12.063	0.0657	0.0048	1.404	0.0076	0.0006
2.306	0.563	3.462	13.926	0.0626	0.0046	1.270	0.0057	0.0004
2.505	0.612	3.761	15.691	0.0598	0.0044	1.011	0.0039	0.0003
2.728	0.666	4.096	17.162	0.0551	0.0041	0.056	0.0002	0.0000
2.893	0.706	4.343	20.006	0.0571	0.0042	0.998	0.0028	0.0002

Table 4.19 SWATH1-C11CS Tem.=15.0°C

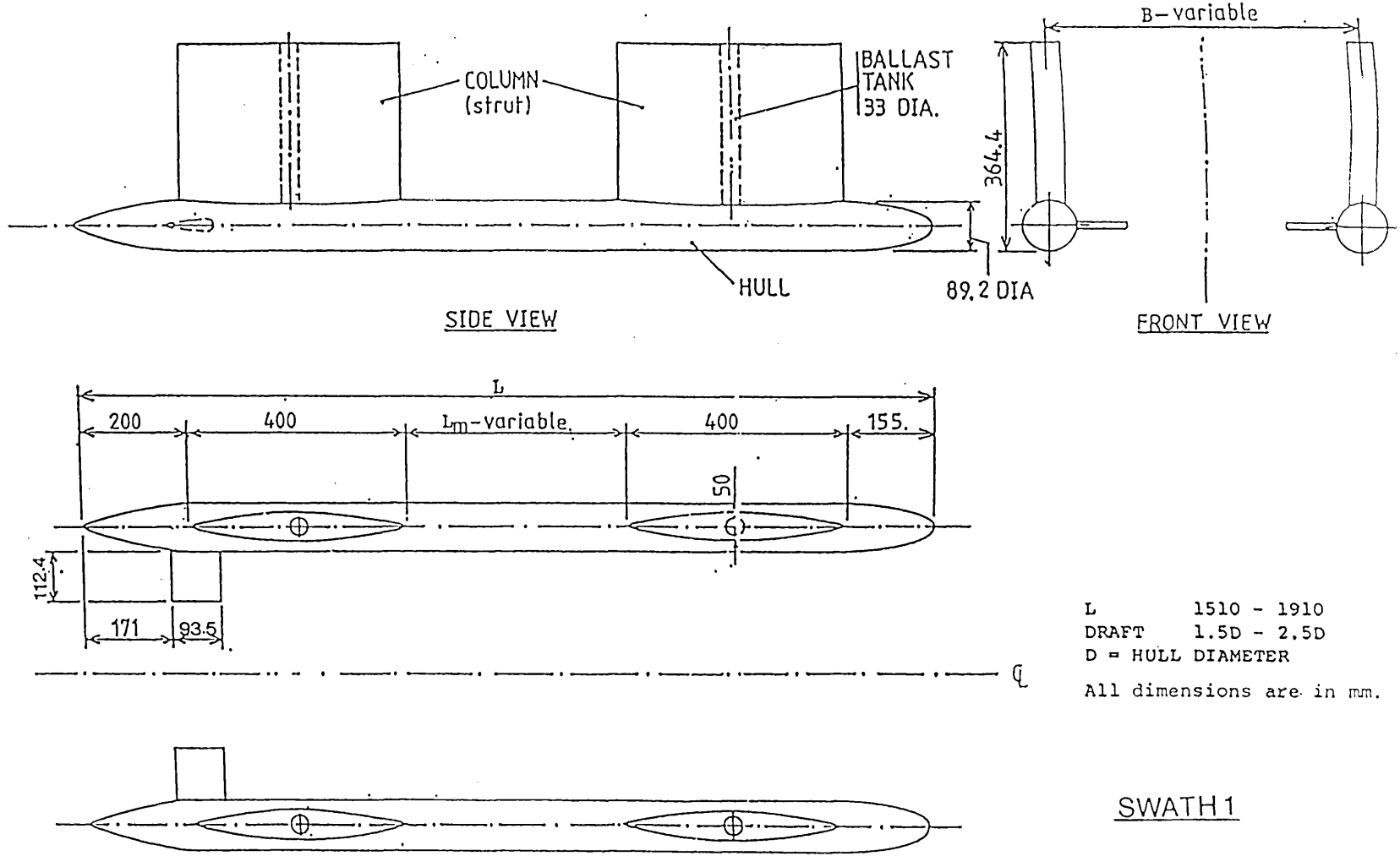

Fig.4.1
Plans and details of SWATH1 model

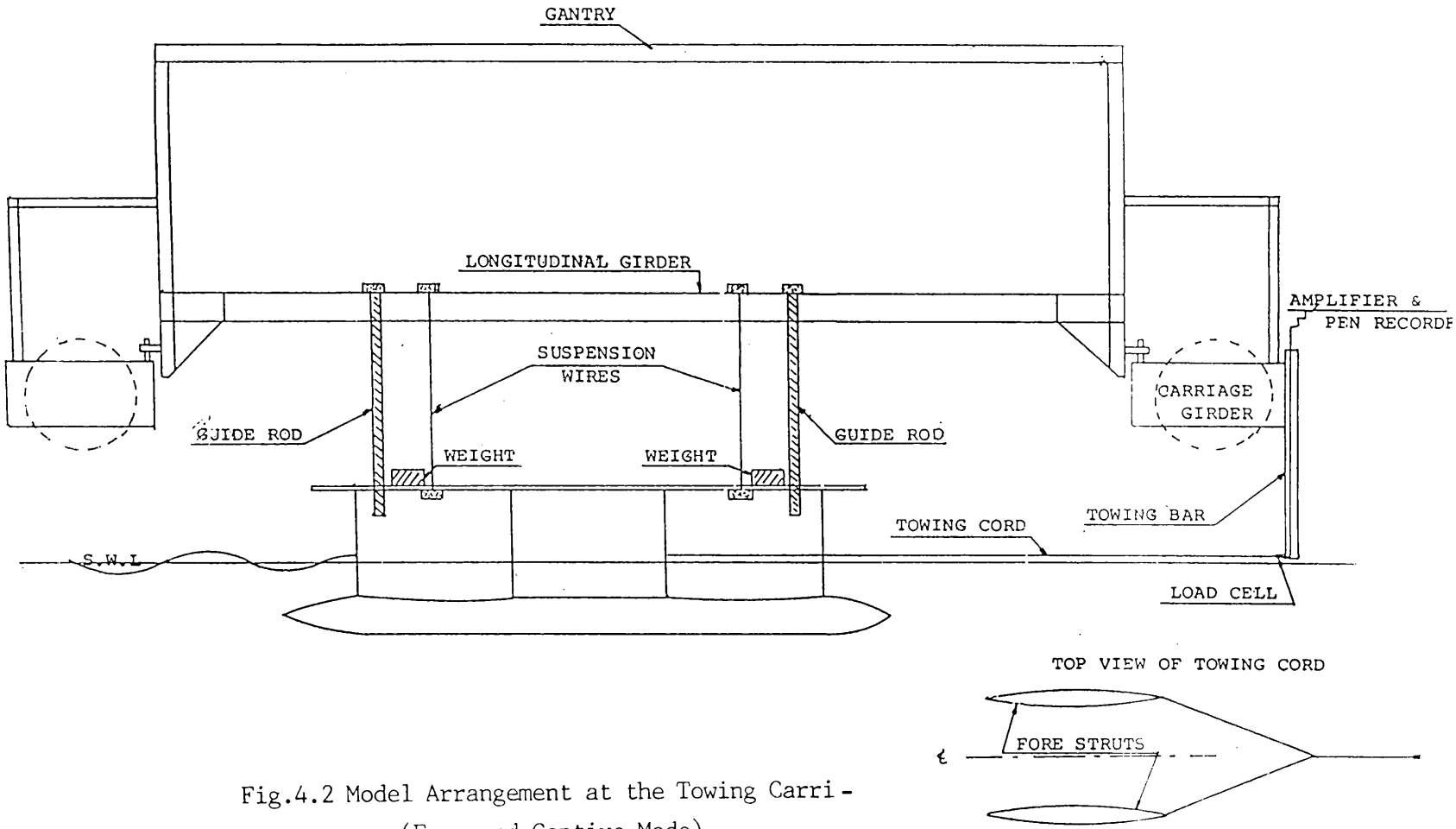

Fig.4.2 Model Arrangement at the Towing Carriage (Free and Captive Mode)

Fig 4.3 The Model in the Water under the Towing Carriage (in the Free Mode)

Fig4.4 The Model in the Water under the Towing Carriage (in the Captive Mode)

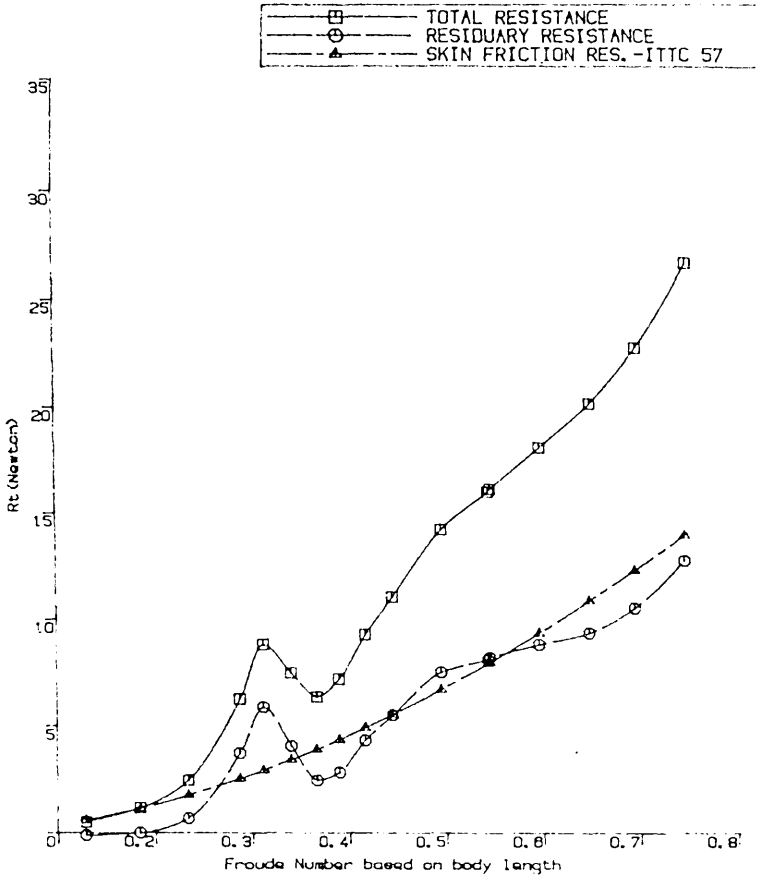

Total, residuary and skin-frictional resistance variations of SWATH1-C1 versus Froude Number(FN)

Fig.4.5

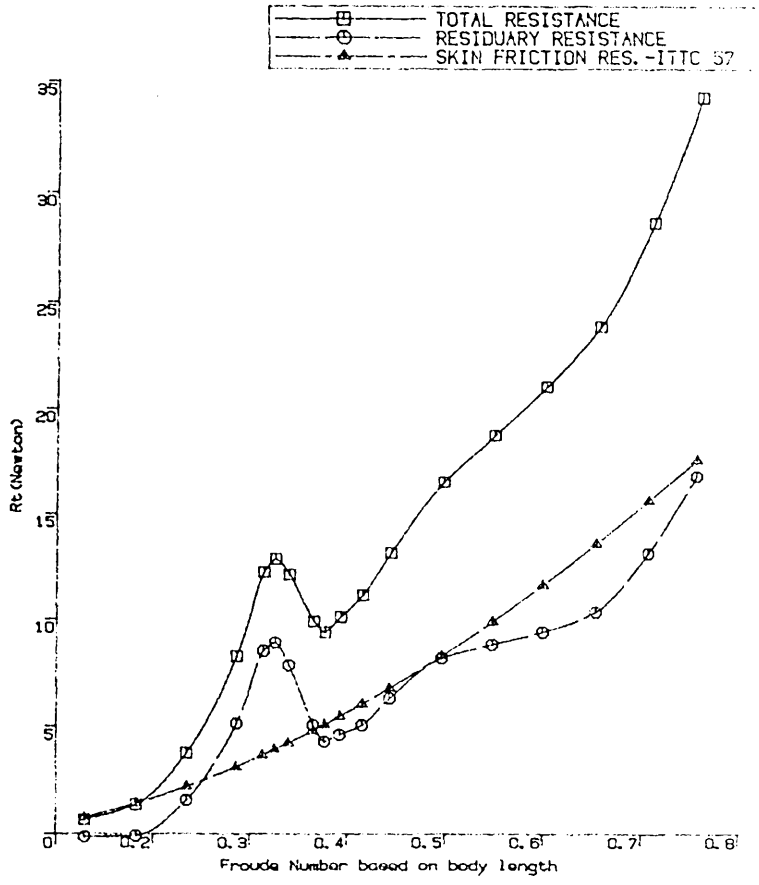

Total, residuary and skin-frictional resistance variations of SWATH1-C2 versus Froude Number(FN)

Fig.4.6

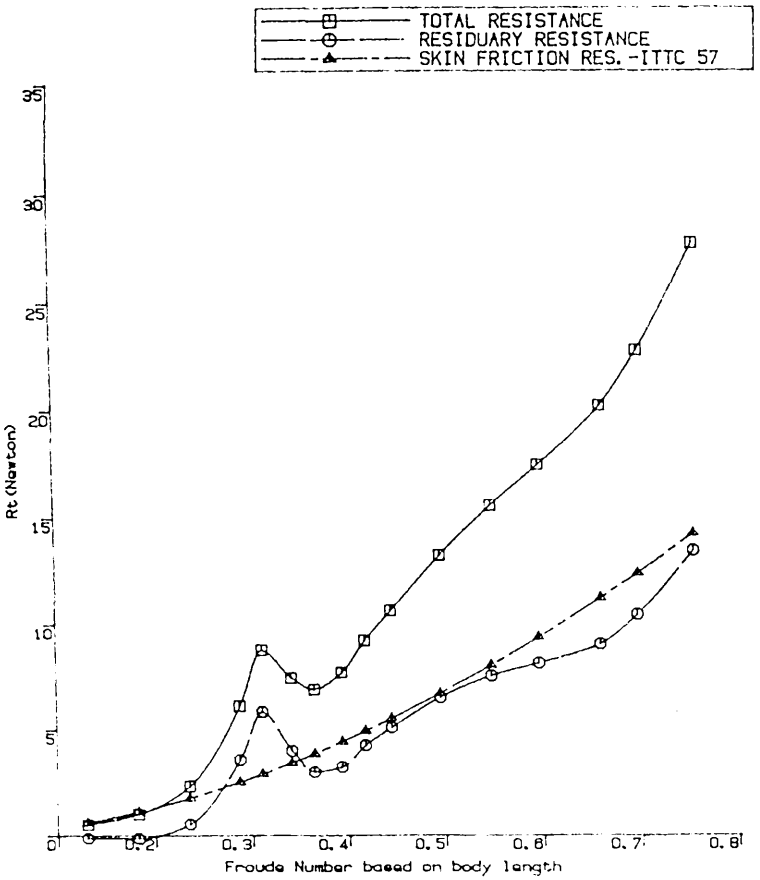

Total, residuary and skin-frictional resistance variations of SWATH1-C4 versus Froude Number (FN)

Fig.4.7

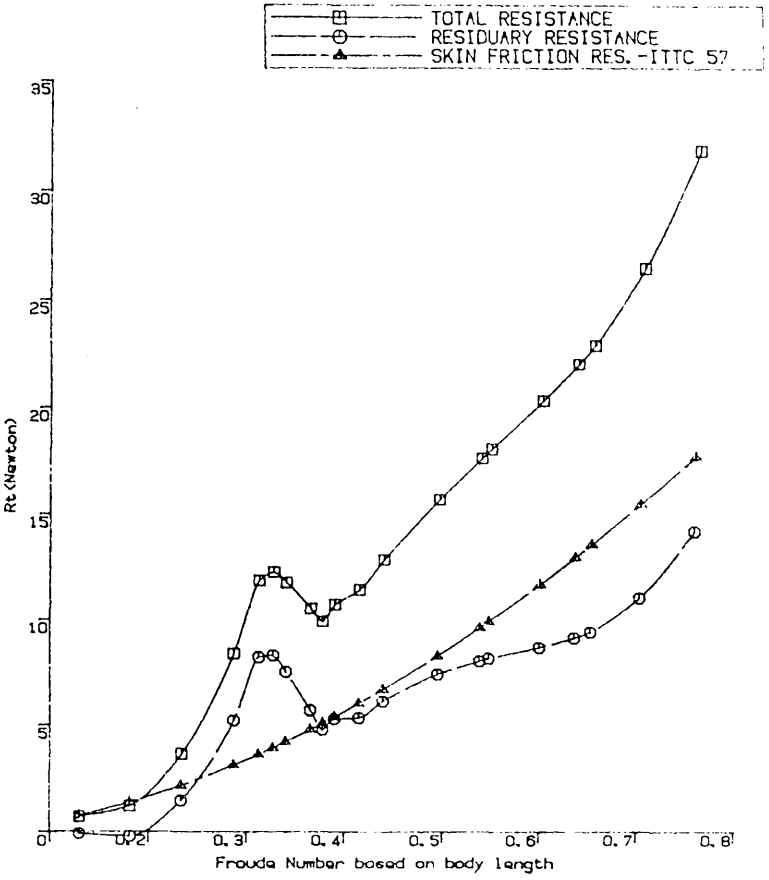

Total, residuary and skin-frictional resistance variations of SWATH1-C5 versus Froude Number (FN)

Fig.4.8

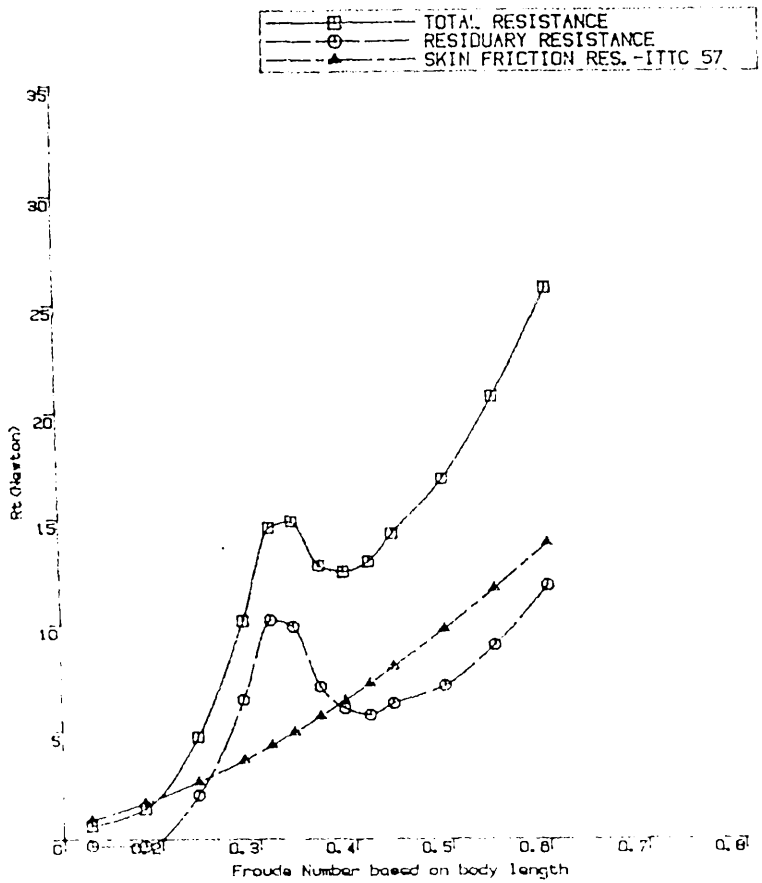

Total, residuary and skin-frictional resistance variations of SWATH1-C6 versus Froude Number (FN)

Fig.4.9

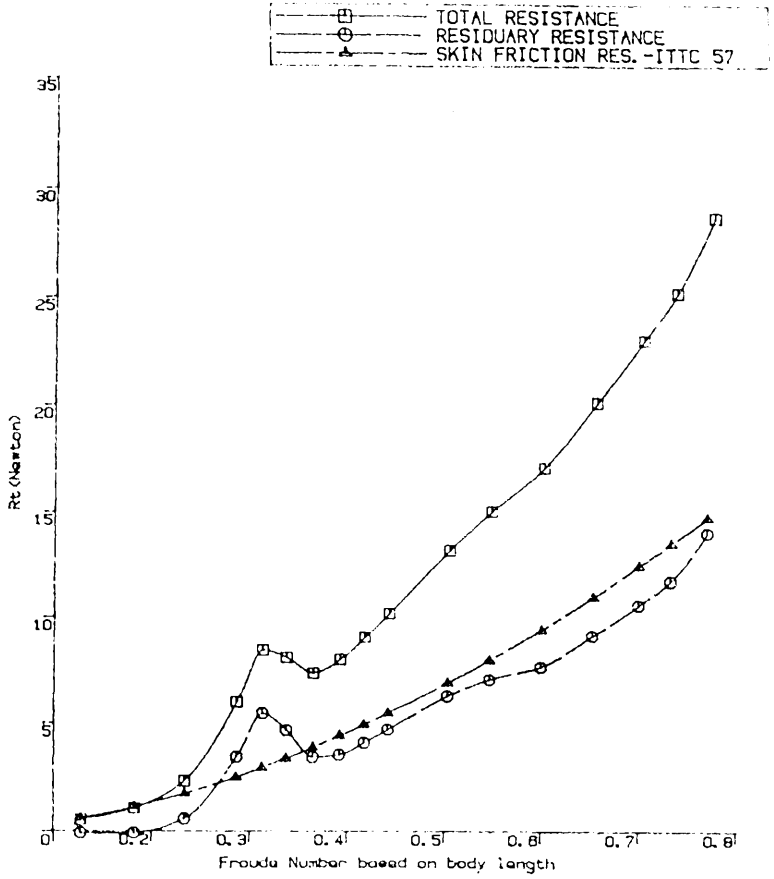

Total, residuary and skin-frictional resistance variations of SWATH1-C7 versus Froude Number (FN)

Fig.4.10

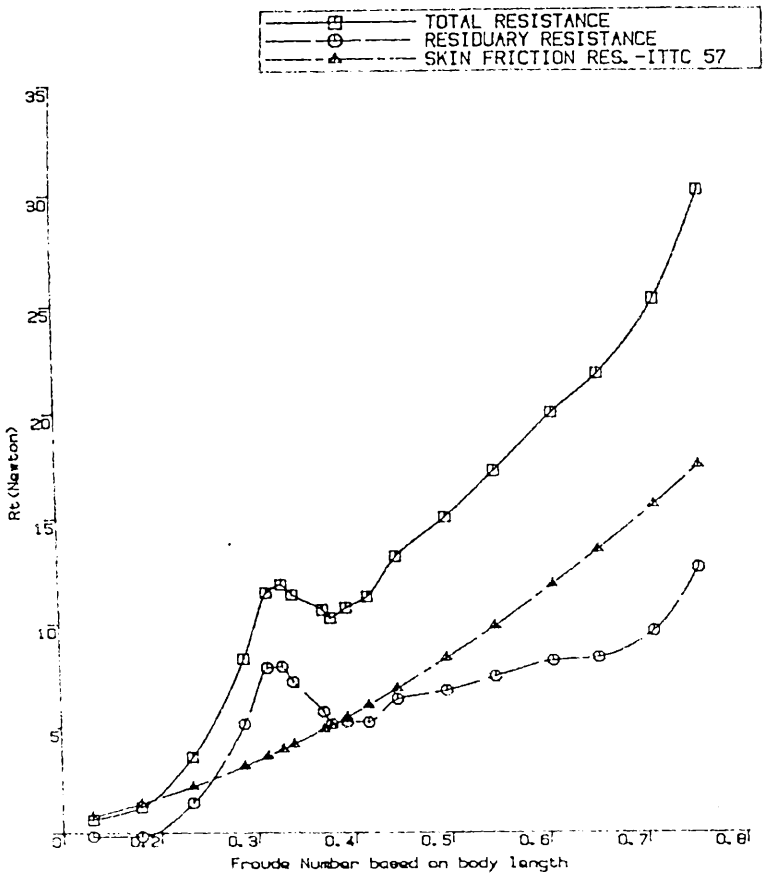

Total, residuary and skin-frictional resistance variations of SWATH1-C8 versus Froude Number (FN)

Fig.4.11

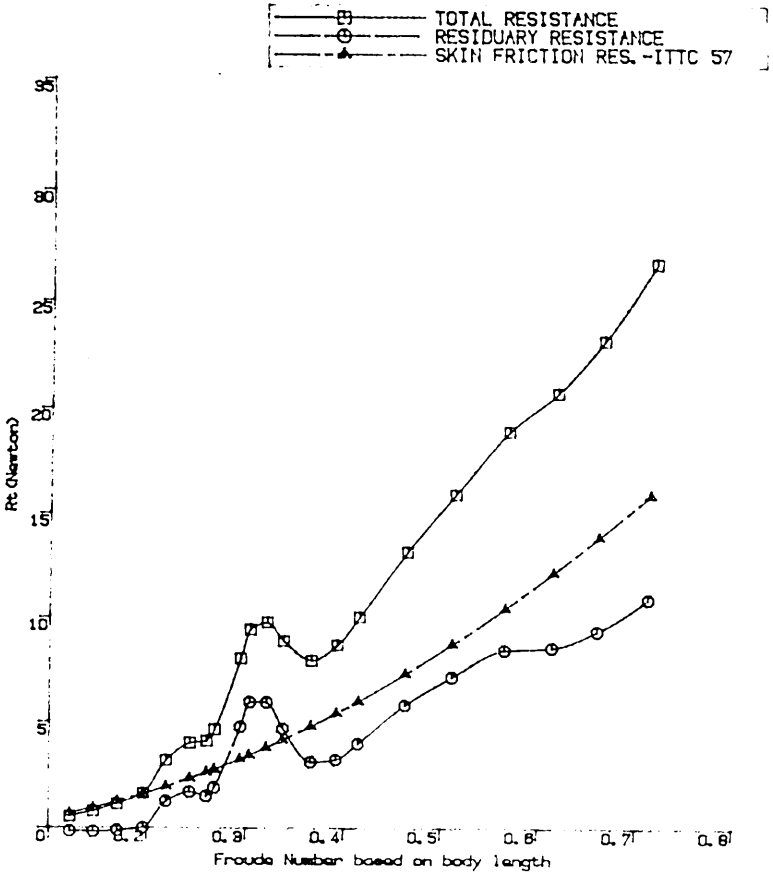

Total, residuary and skin-frictional resistance variations of SWATH1-C8 versus Froude Number (FN)

Fig.4.12

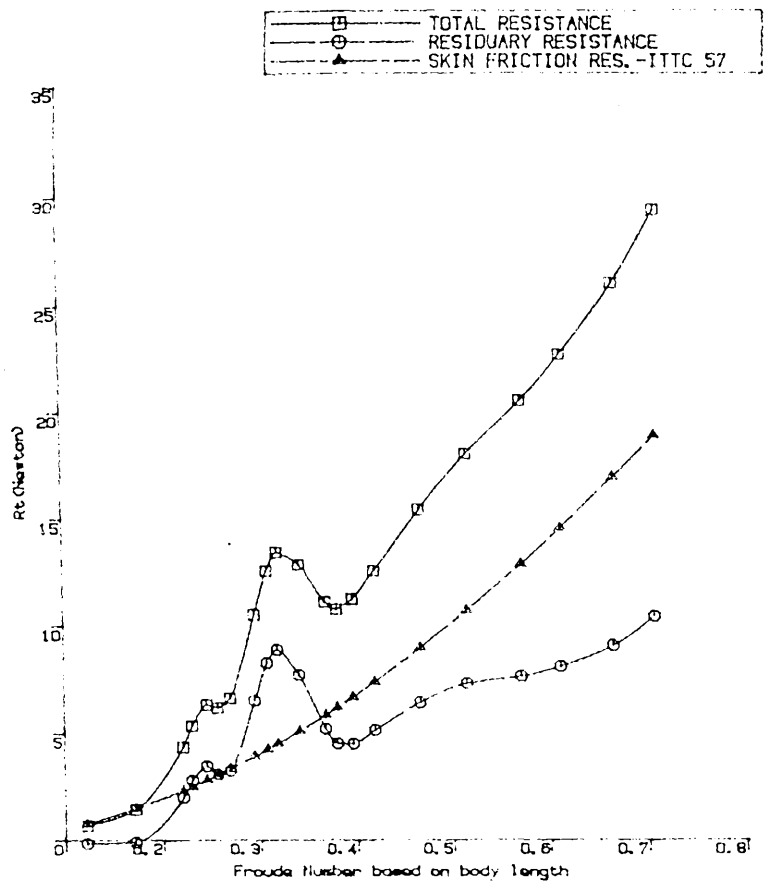

Total, residuary and skin-frictional resistance variations of SWATH1-C10 versus Froude Number (FN)

Fig.4.13

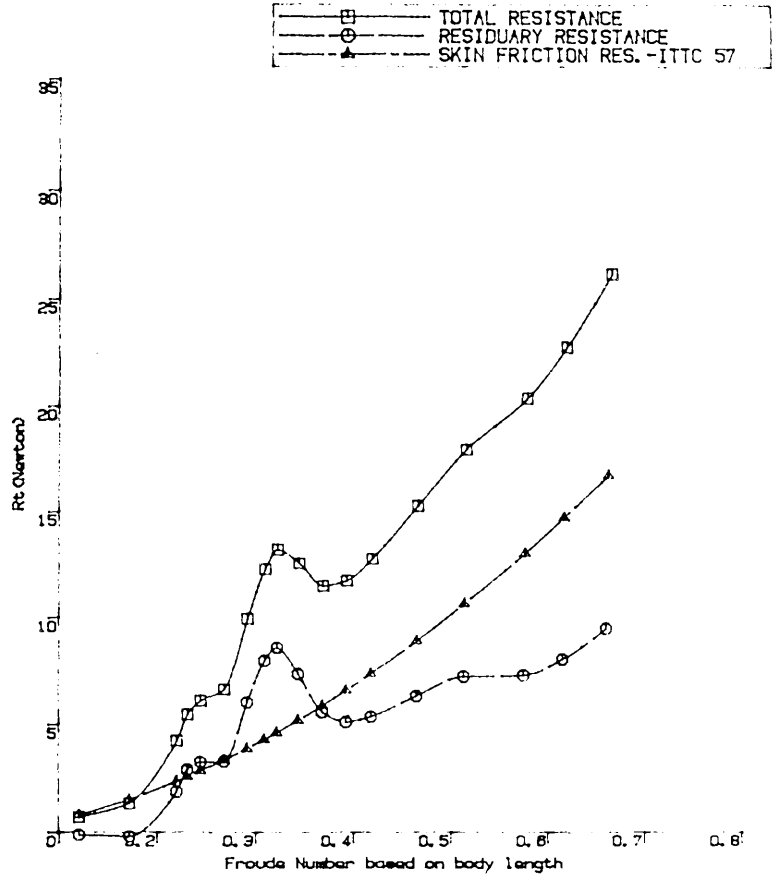

Total, residuary and skin-frictional resistance variations of SWATH1-C11 versus Froude Number (FN)

Fig.4.14

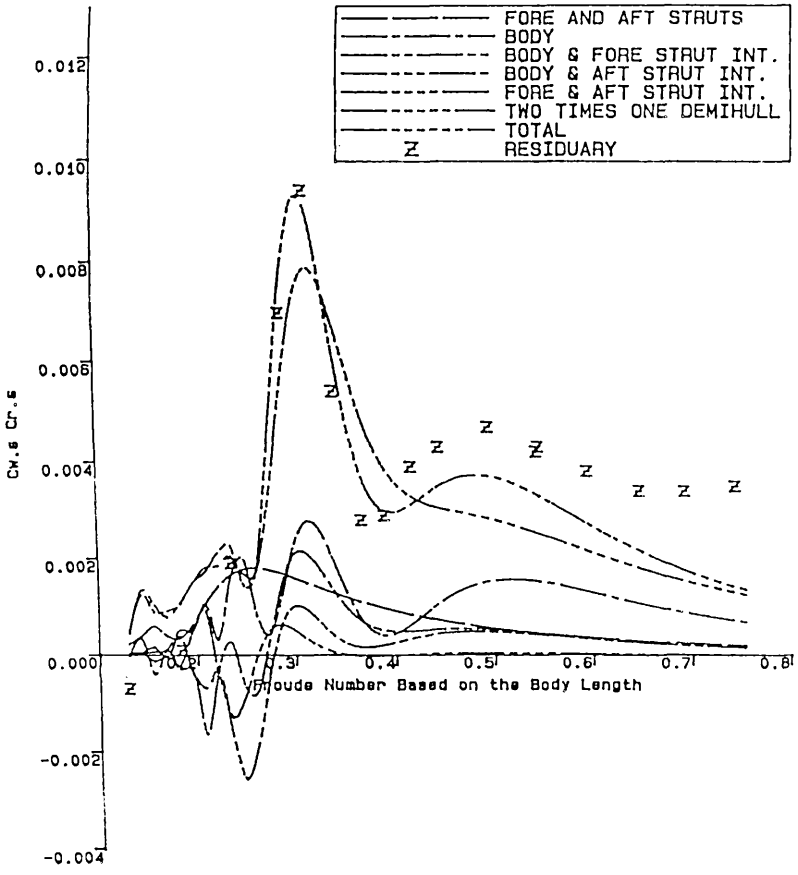

Wave Resistance Coefficients of SWATH1-C1 and its Component Variations together with Residuary Resistance Coefficient as a Function of froude Number.

Fig.4.15

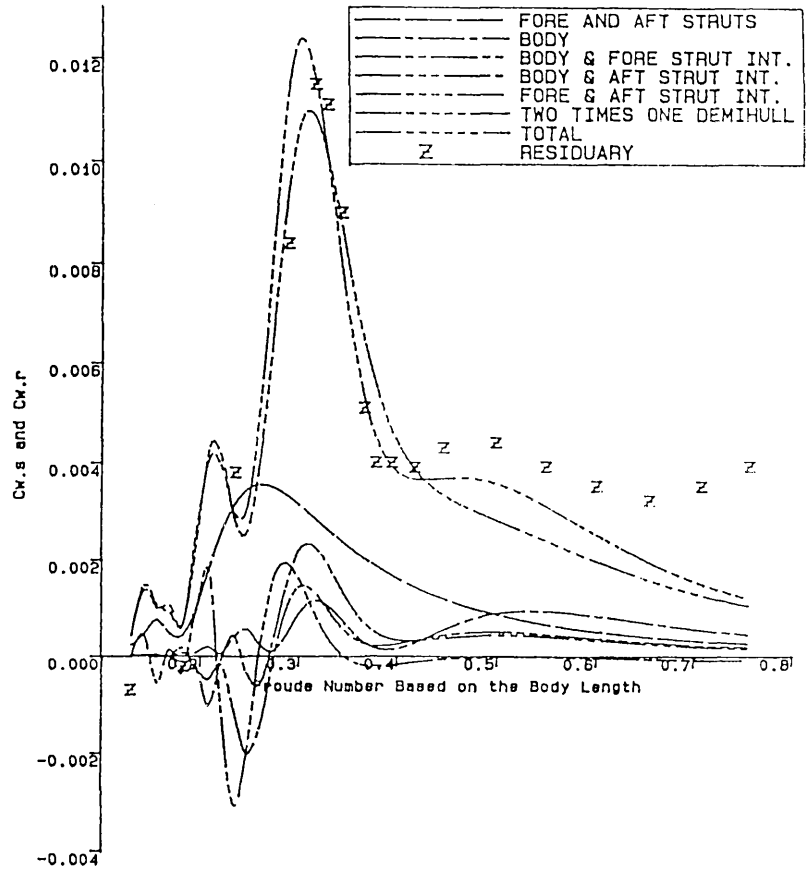

Wave Resistance Coefficients of SWATH1-C2 and its Component Variations together with Residuary Resistance Coefficient as a Function of Froude Number.

Fig.4.16

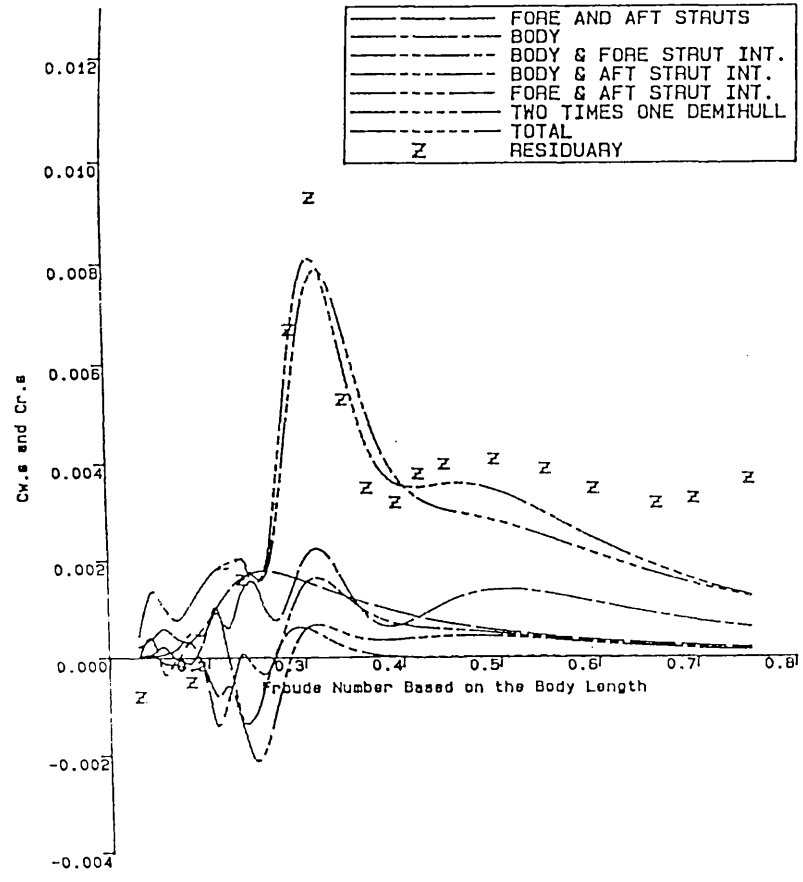

Wave Resistance Coefficients of SWATH1-C4 and its Component Variations together with Residuary Resistance Coefficient as a Function of Froude Number

Fig.4.17

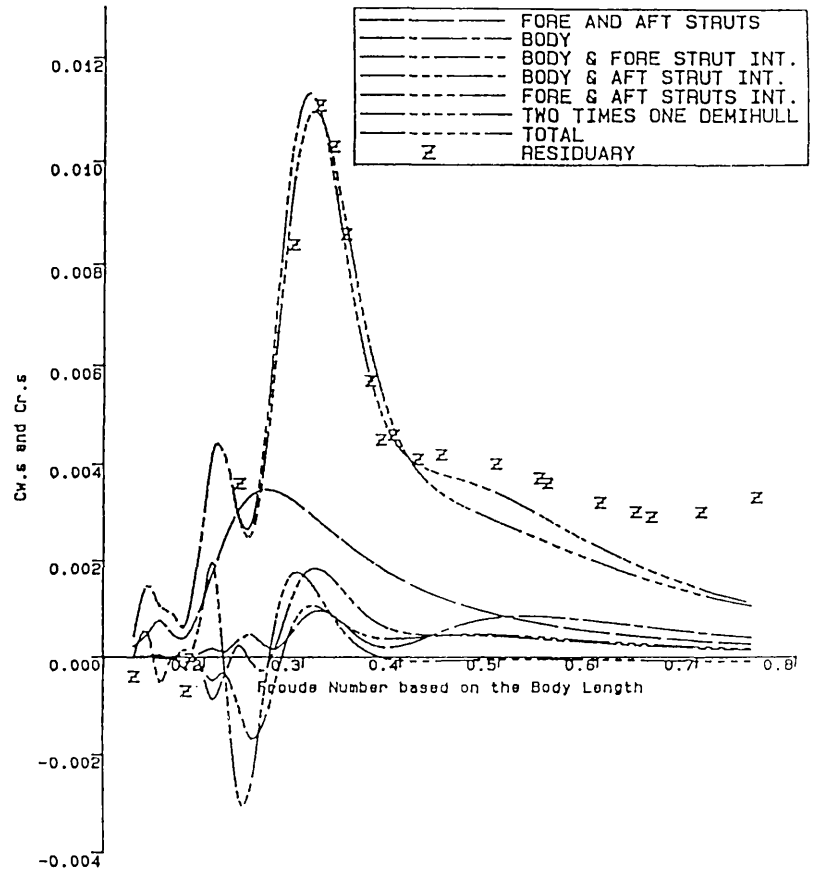

Wave Resistance Coefficients of SWATH1-C5 and its Component Variations together with Residuary Resistance Coefficient as a Function of Froude Number

Fig.4.18

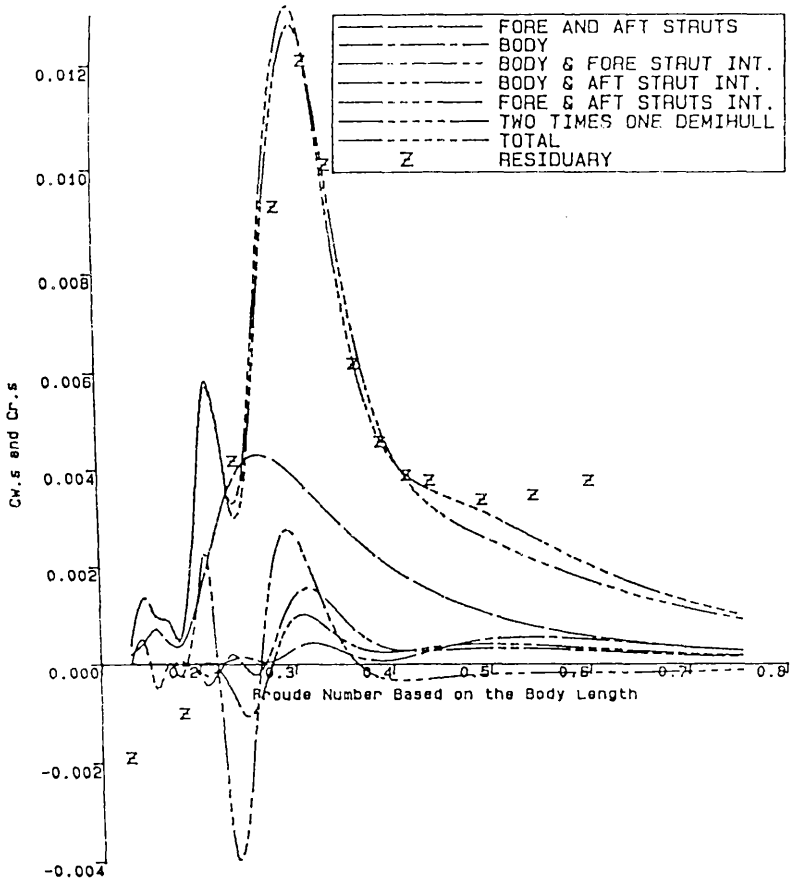

Wave Resistance Coefficients of SWATH1-C6 and its Component Variations together with Residuary Resistance Coefficient as a Function of Froude Number.

Fig.4.19

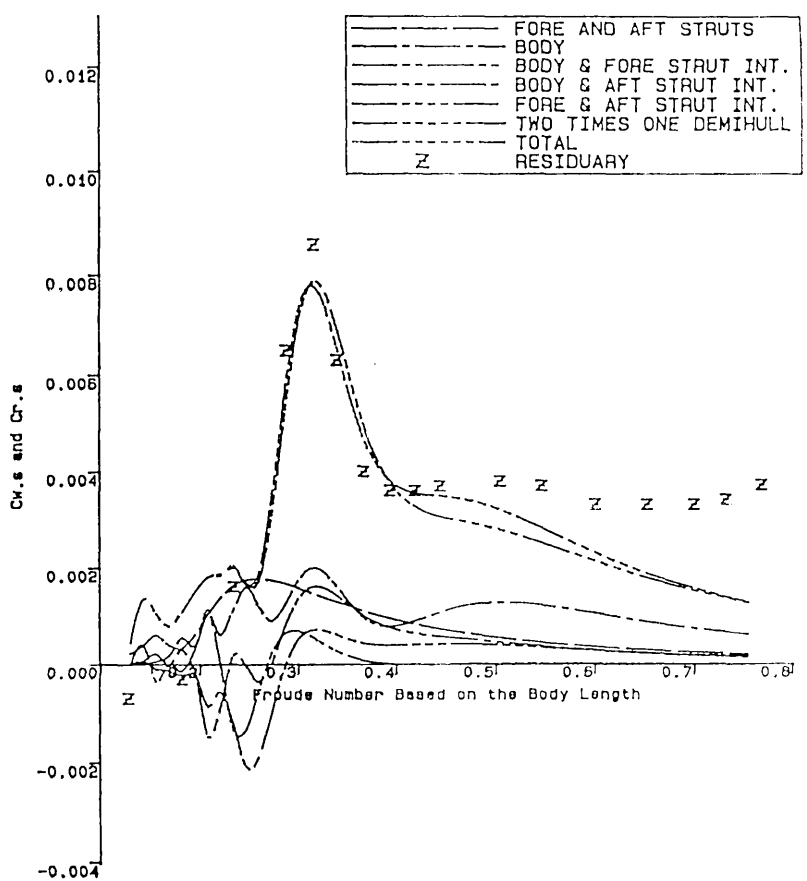

Wave Resistance Coefficients of SWATH1-C7 and its Component Variations together with Residuary Resistance Coefficient as a Function of Froude Number

Fig.4.20

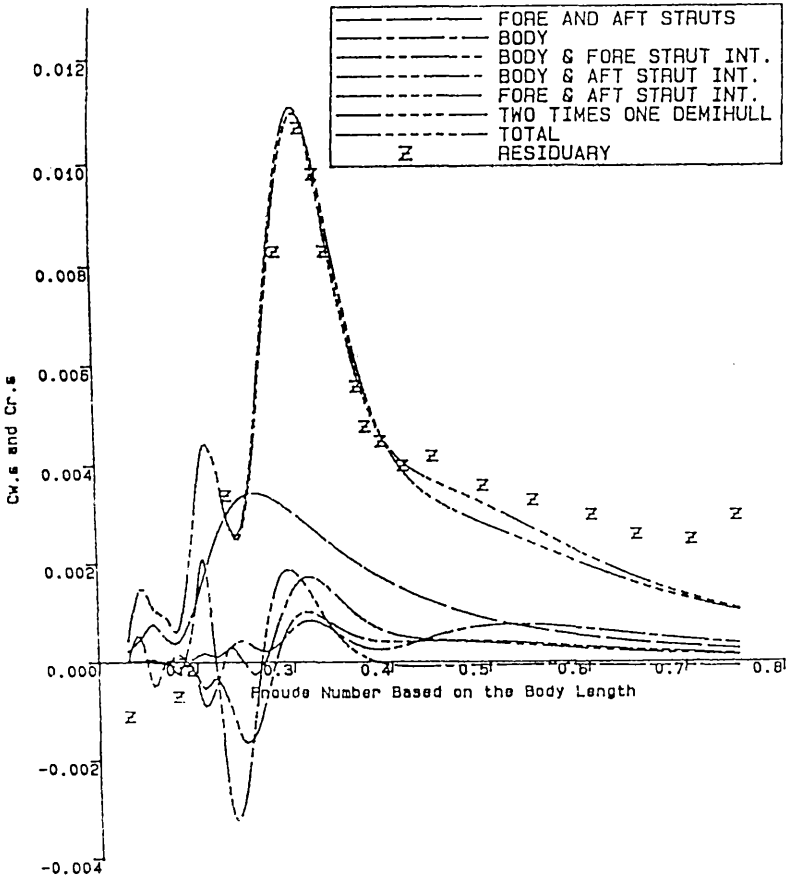

Wave Resistance Coefficients of SWATH1-C8 and its Component Variations together with Residuary Resistance Coefficient as a Function of Froude Number

Fig.4.21

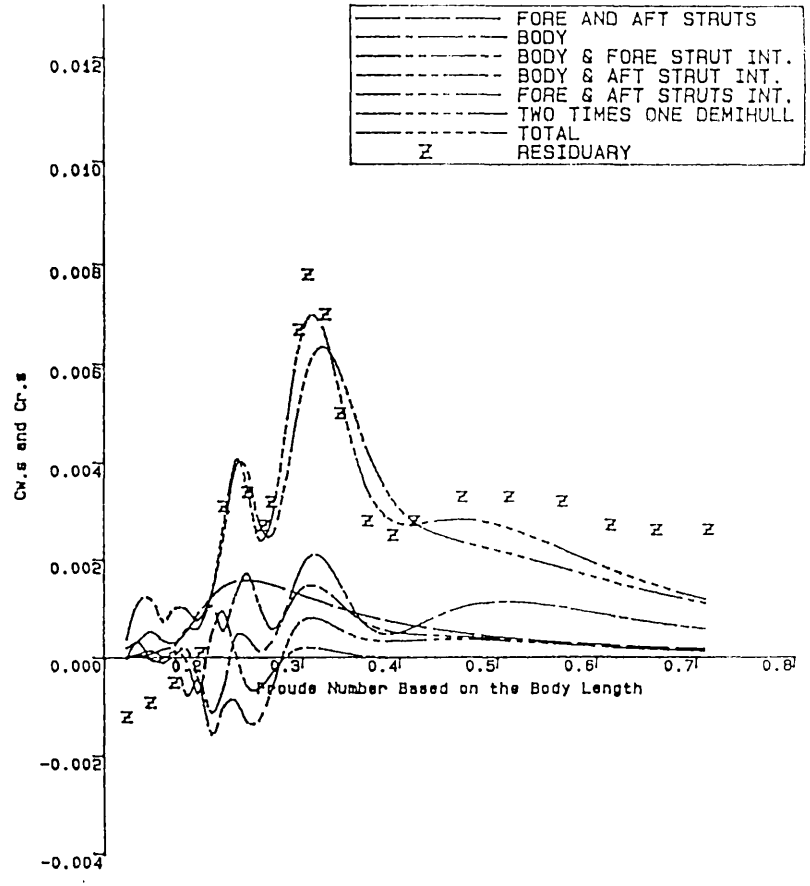

Wave Resistance Coefficients of SWATH1-C9 and its Component Variations together with Residuary resistance Coefficient as a Function of Froude Number.

Fig.4.22

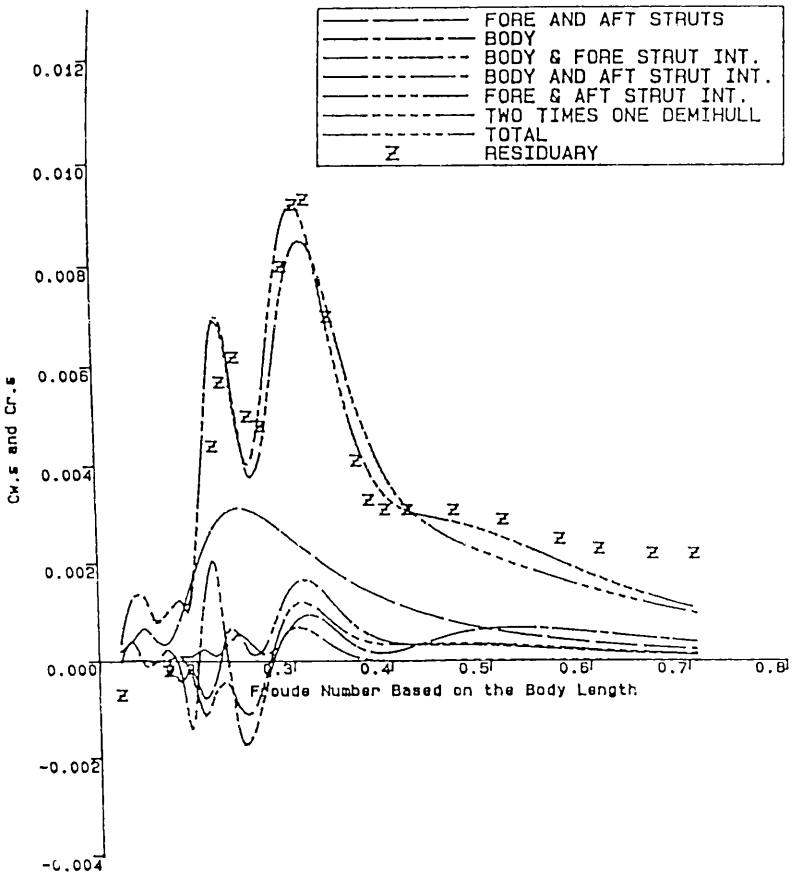

Wave Resistance Coefficients of SWATH1-C10 and its Component Variations together with Residuary Resistance Coefficient as a Function of Froude Number.

Fig.4.23

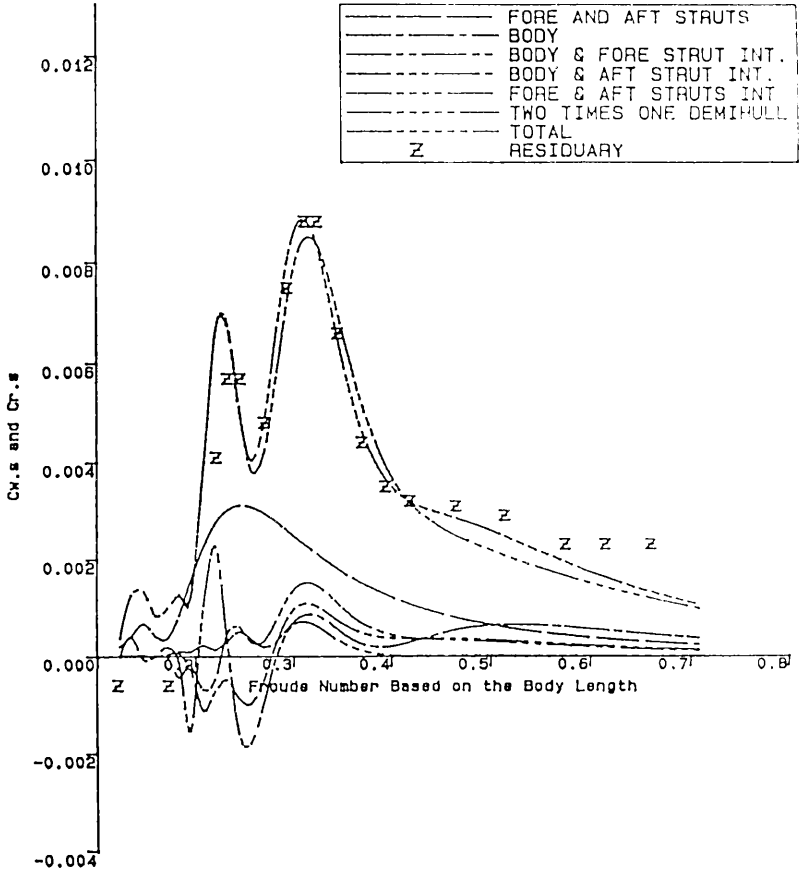

Wave Resistance Coefficients of SWATH1-C11 and its Component Variations together with Residuary Resistance Coefficient as a Function of Froude Number.

Fig.4.24

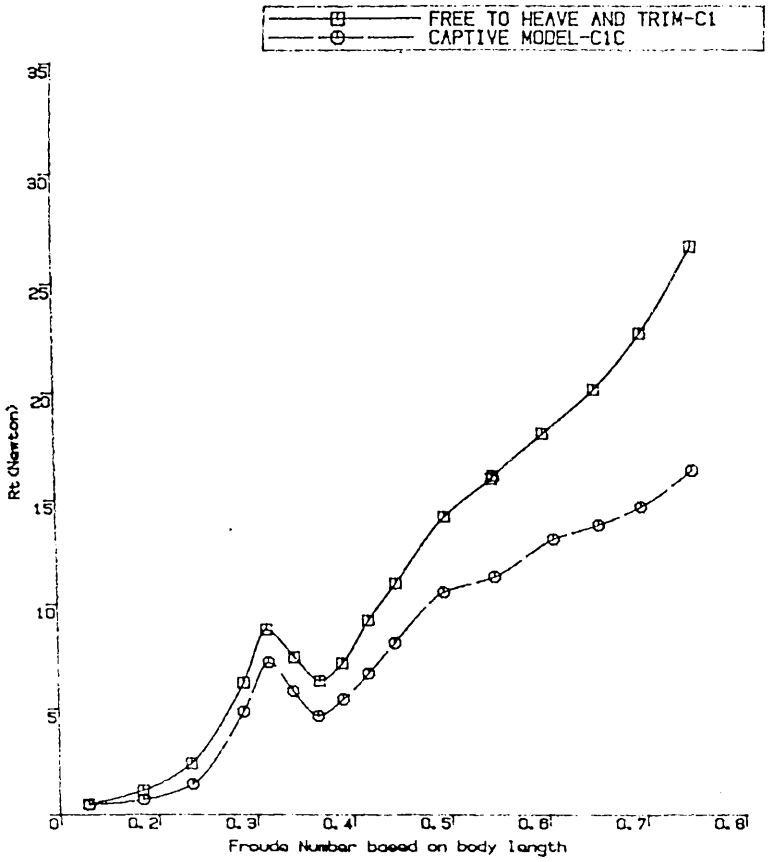

Comparison of two different experimental techniques
- total resistance -

Fig.4.25

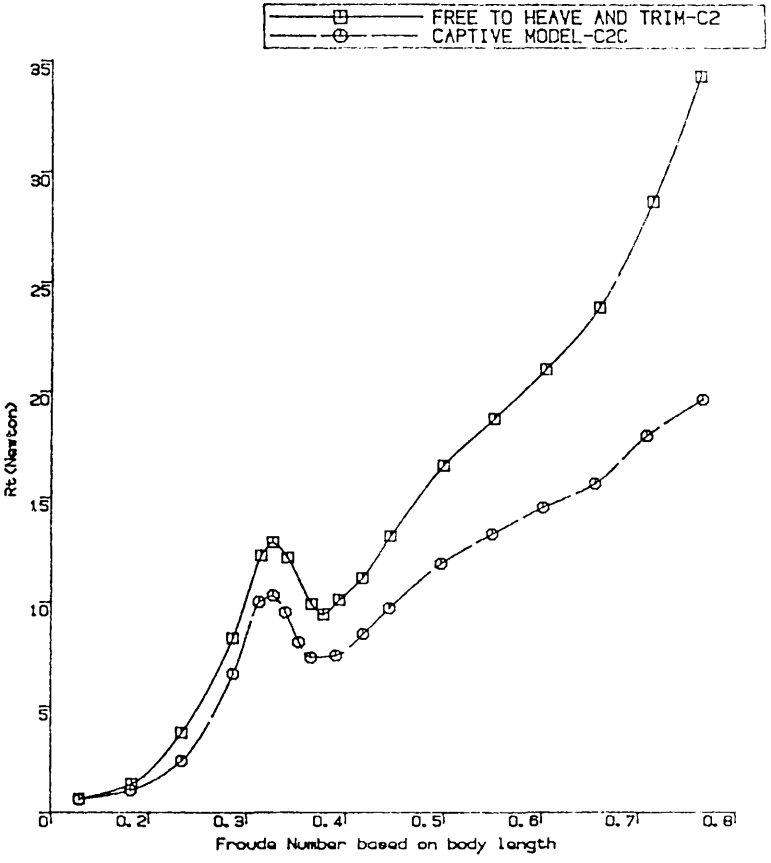

Comparison of two different experimental techniques
- total resistance -

Fig.4.26

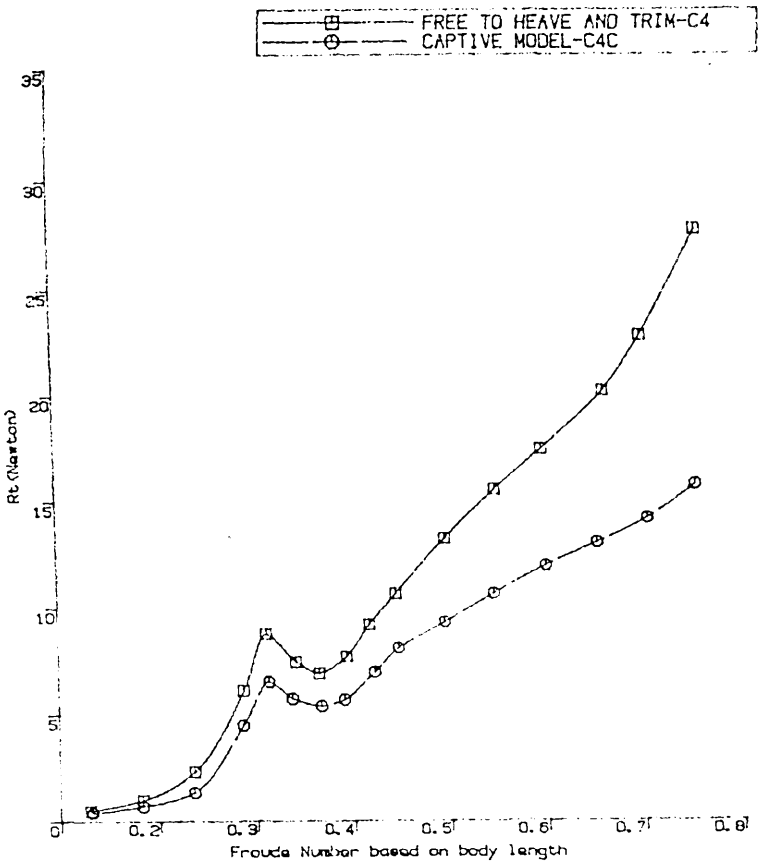

Comparison of two different experimental techniques
- total resistance -

Fig.4.27

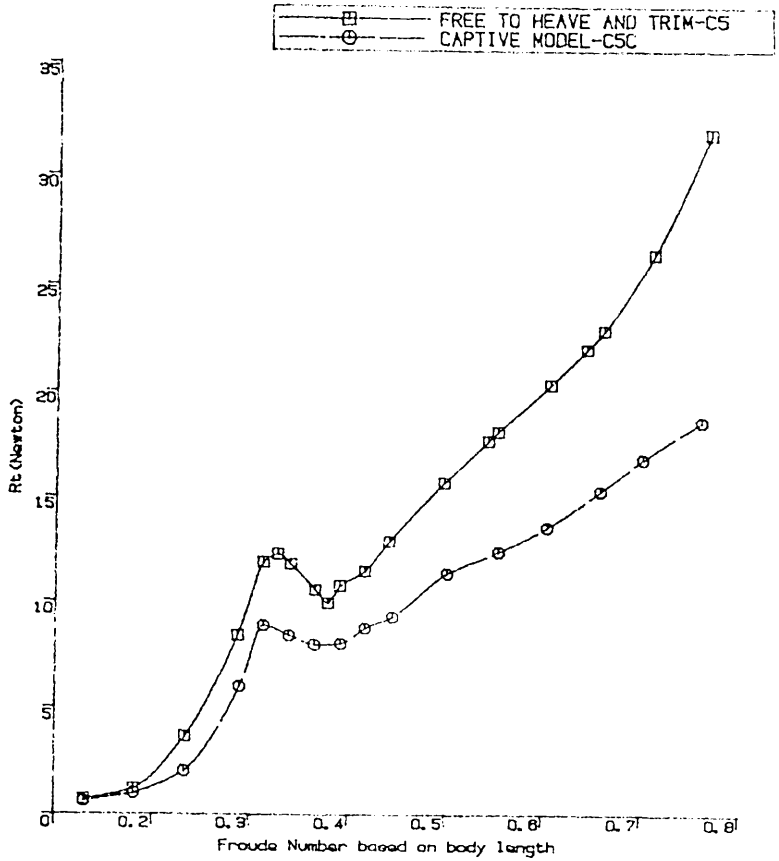

Comparison of two different experimental techniques
- total resistance -

Fig.4.28

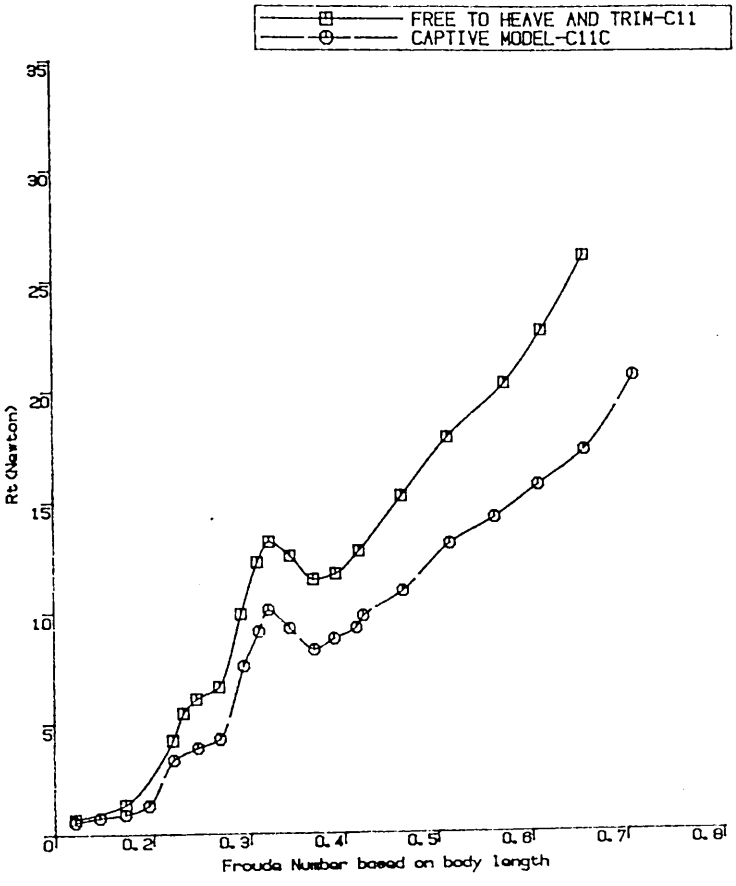

Comparison of two different experimental techniques
- total resistance -

Fig.4.29

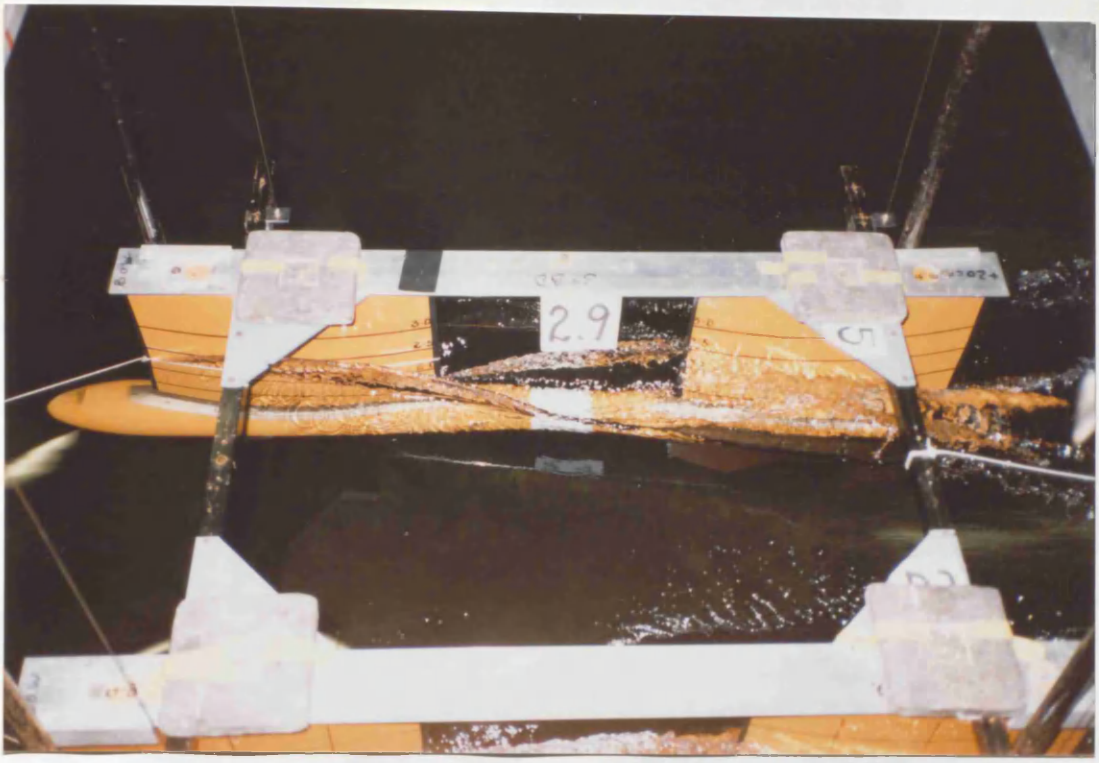

a) Model Captive C8C Speed=2.9m/s

b) Model Free C2 Speed=2.9m/s

Fig 4.30 Comparison of Two Different Experimental Techniques

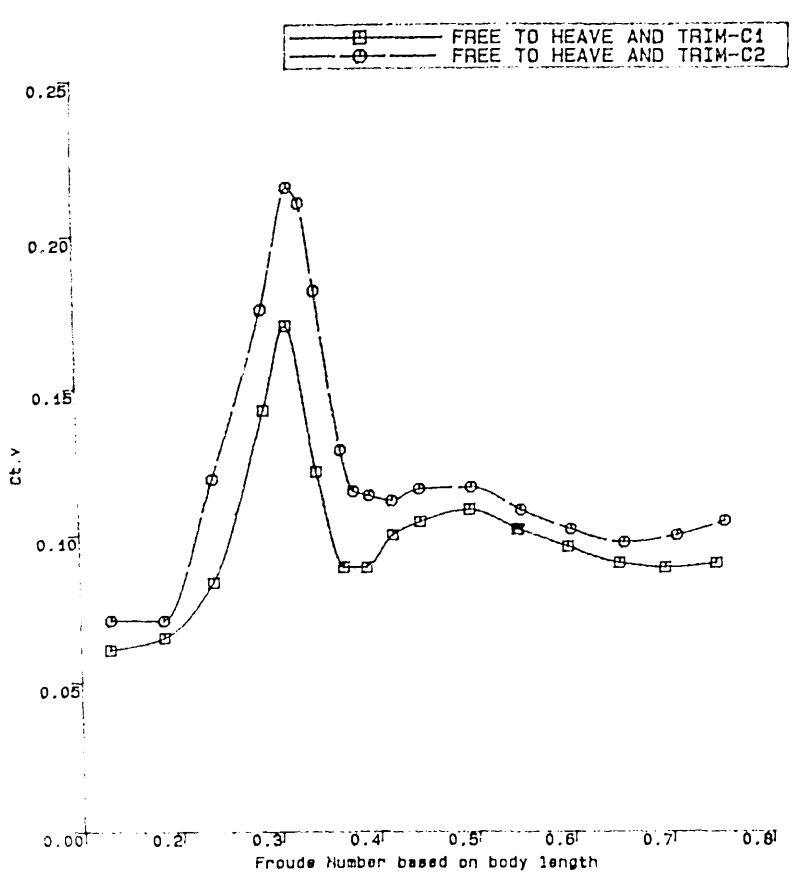

Total resistance coefficient variations SWATH1 versus Froude Number

Fig.4.31

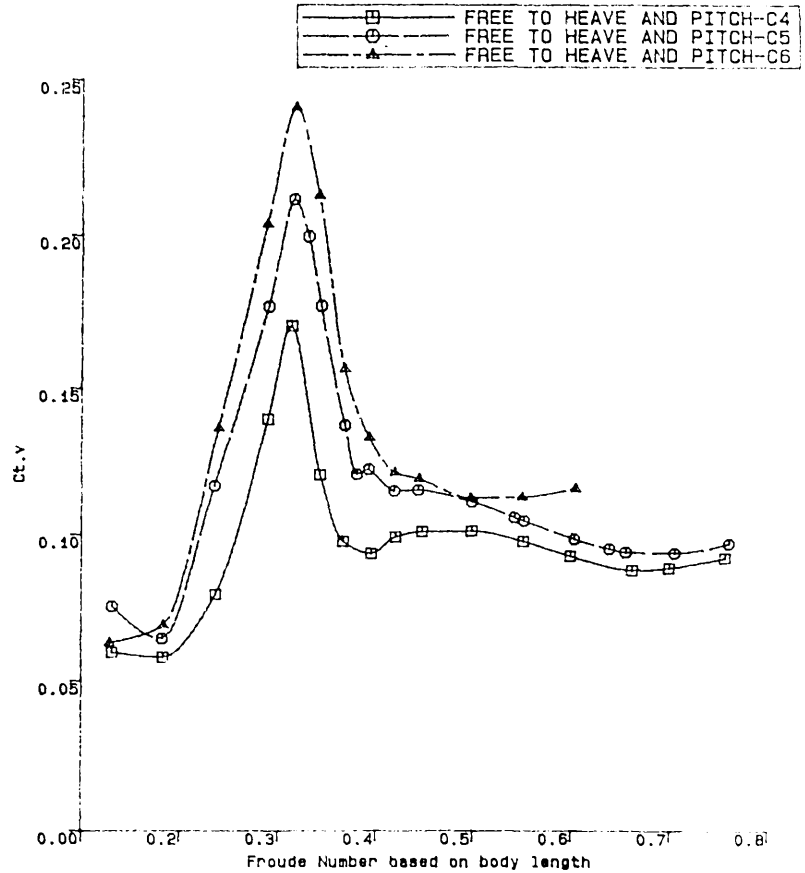

Total resistance coefficient variations of SWATHs with three different drafts versus Froude Number based on the SWATH1 body length

Fig.4.32

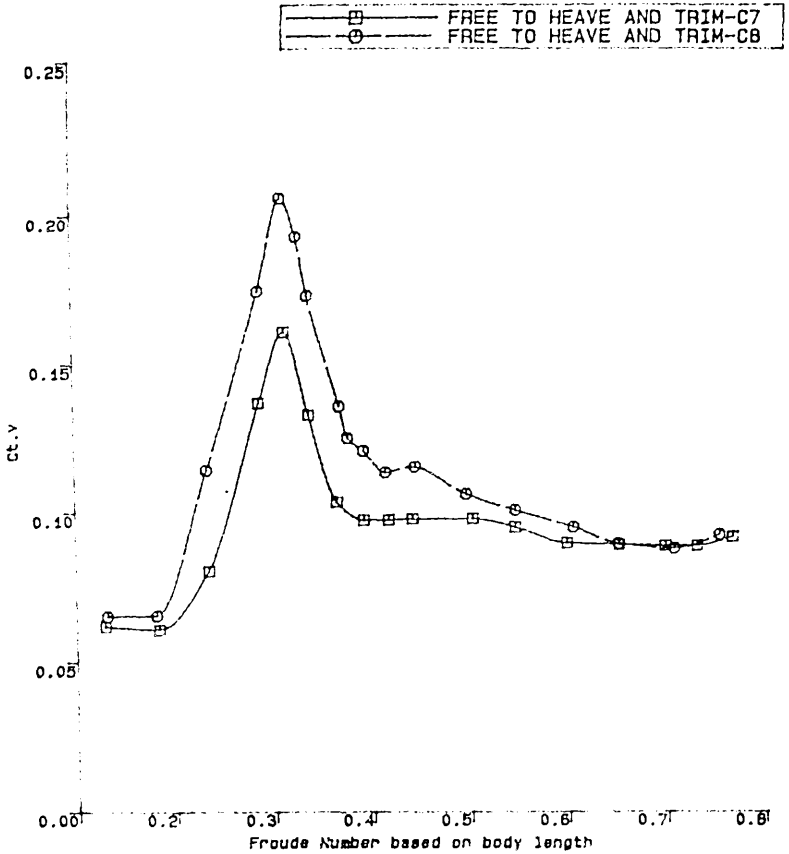

Total resistance coefficient variations SWATH1 versus Froude Number

Fig.4.33

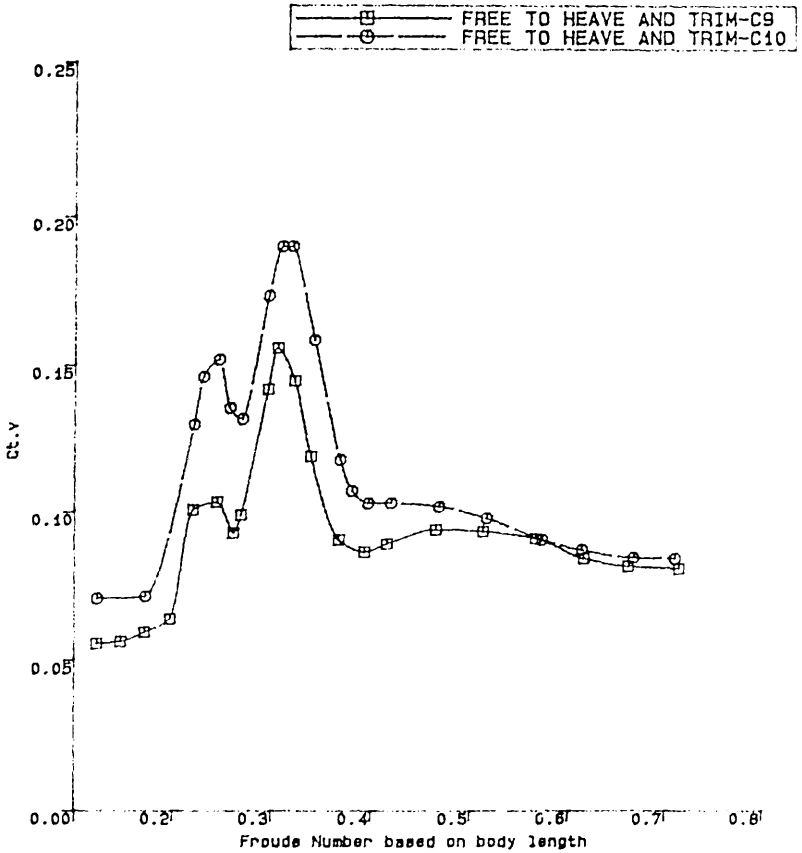

Total resistance coefficient variations SWATH1 versus Froude Number

Fig.4.34

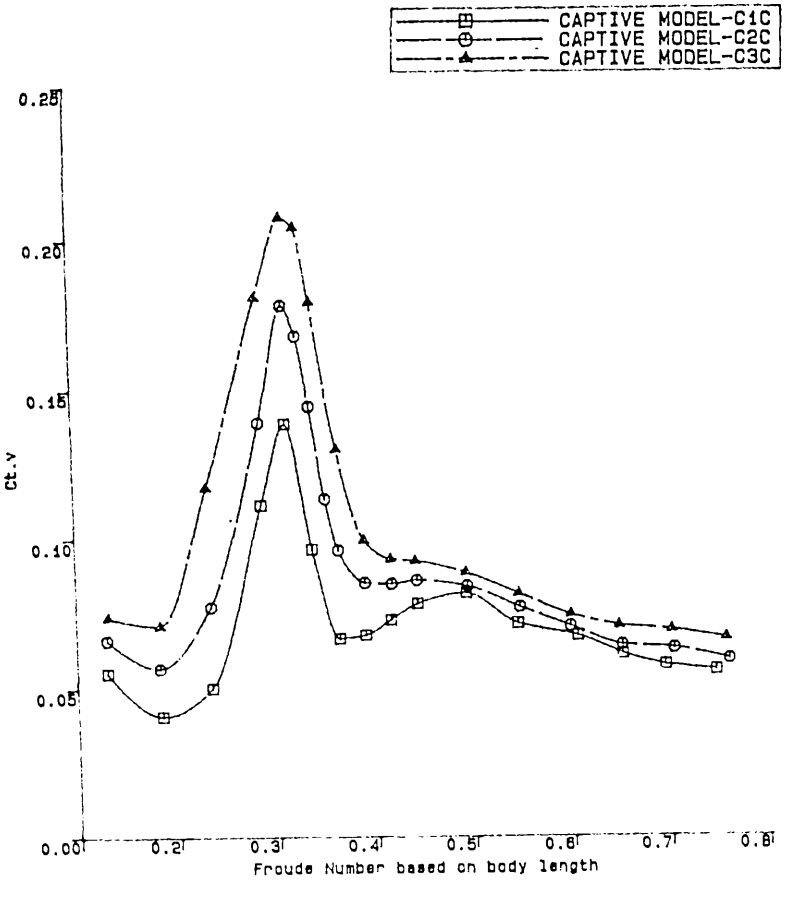

Total resistance coefficient variations of SWATHs with three different drafts versus Froude Number based on the SWATH1 body length

Fig.4.35

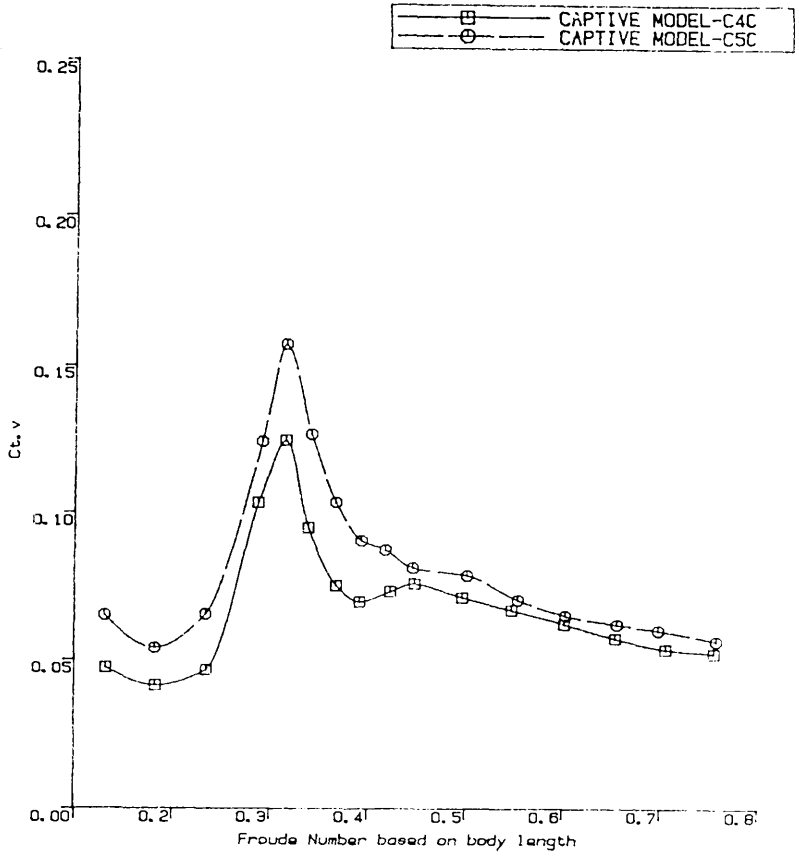

Total resistance coefficient variations SWATH1 versus Froude Number

Fig.4.36

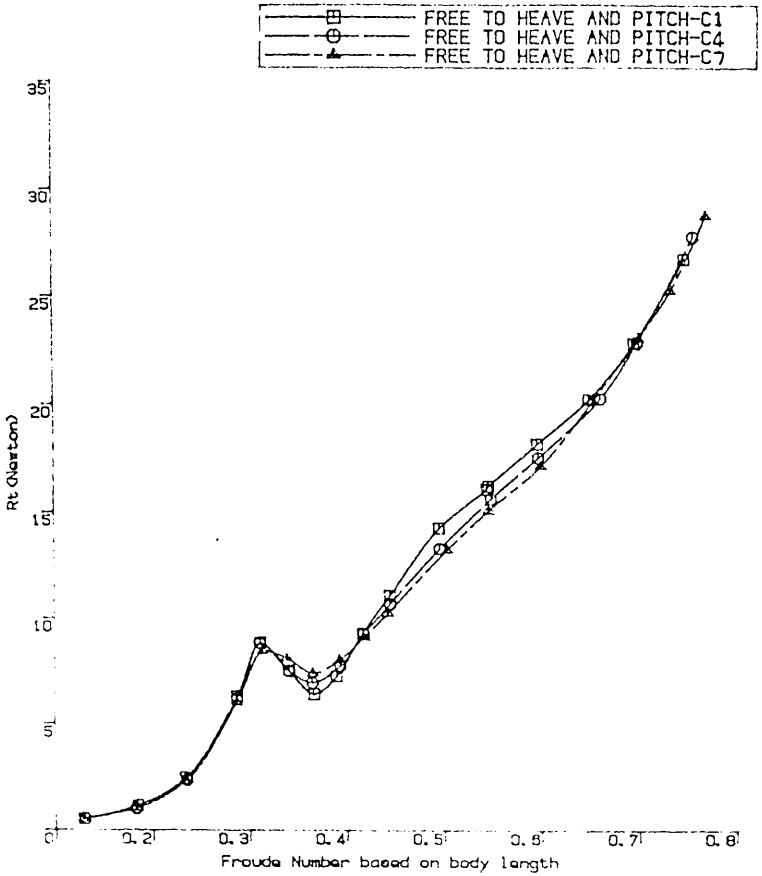

Total resistance variations of SWATH1 with three different spacings versus Froude Number

Fig.4.37

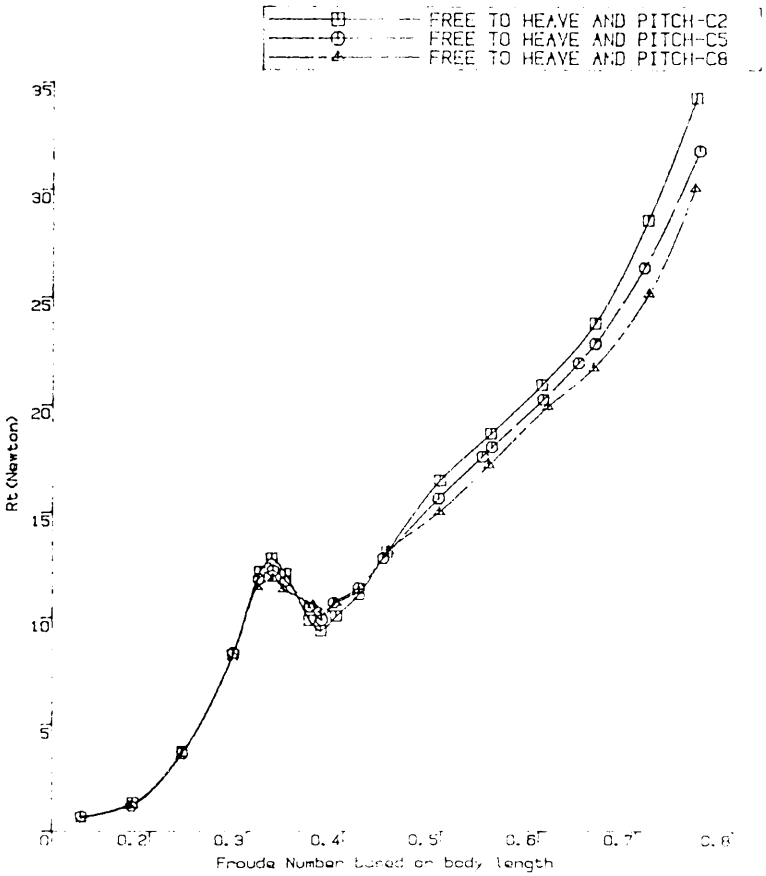

Total resistance variations of SWATH1 with three different spacings versus Froude Number

Fig.4.38

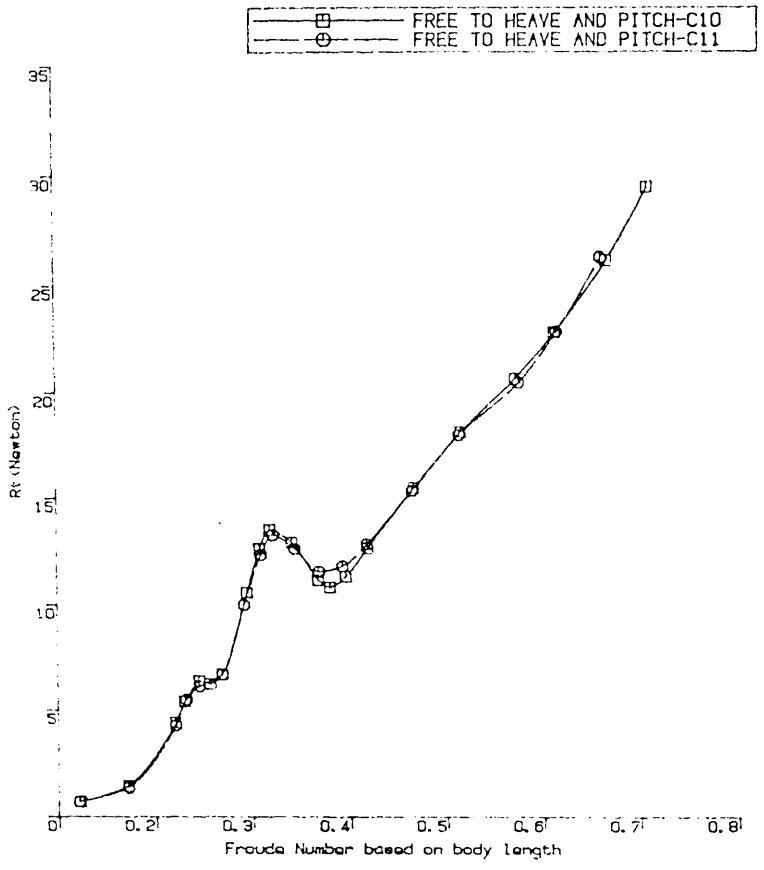

Total resistance variations of SWATH1 with two different spacings versus Froude Number

Fig.4.39

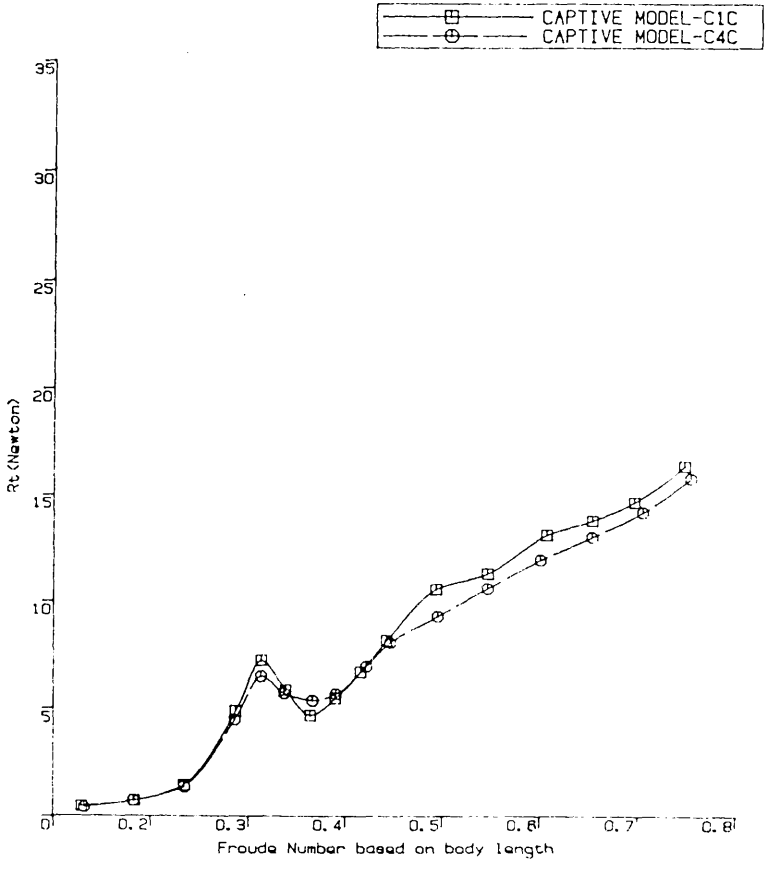

Total resistance variations of SWATH1 with two different spacings versus Froude NumberC

Fig.4.40

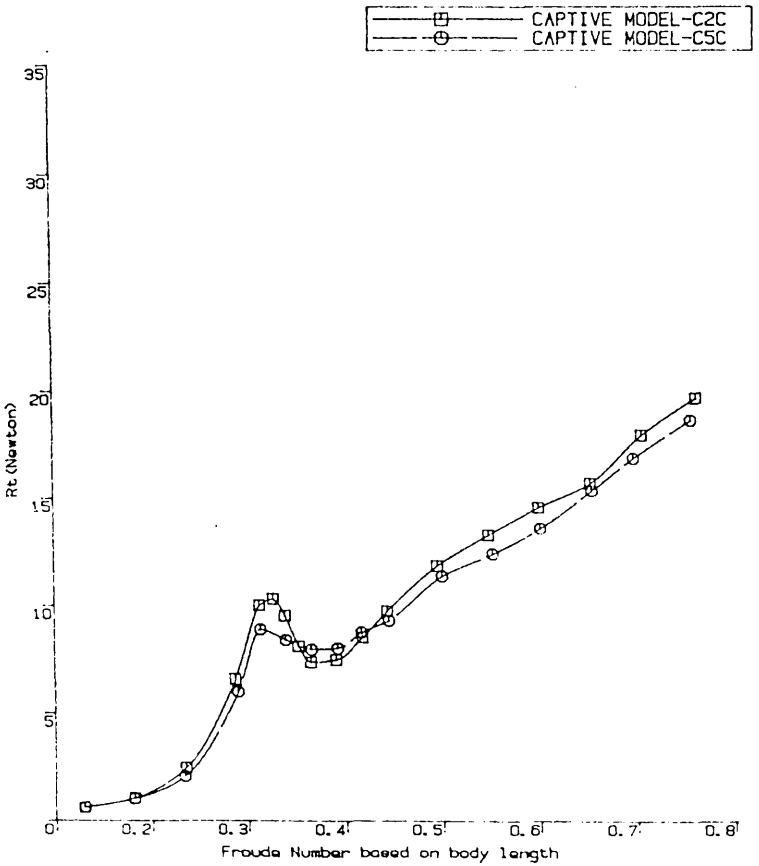

Total resistance variations of SWATH1 with two different spacings versus Froude Number

Fig.4.41

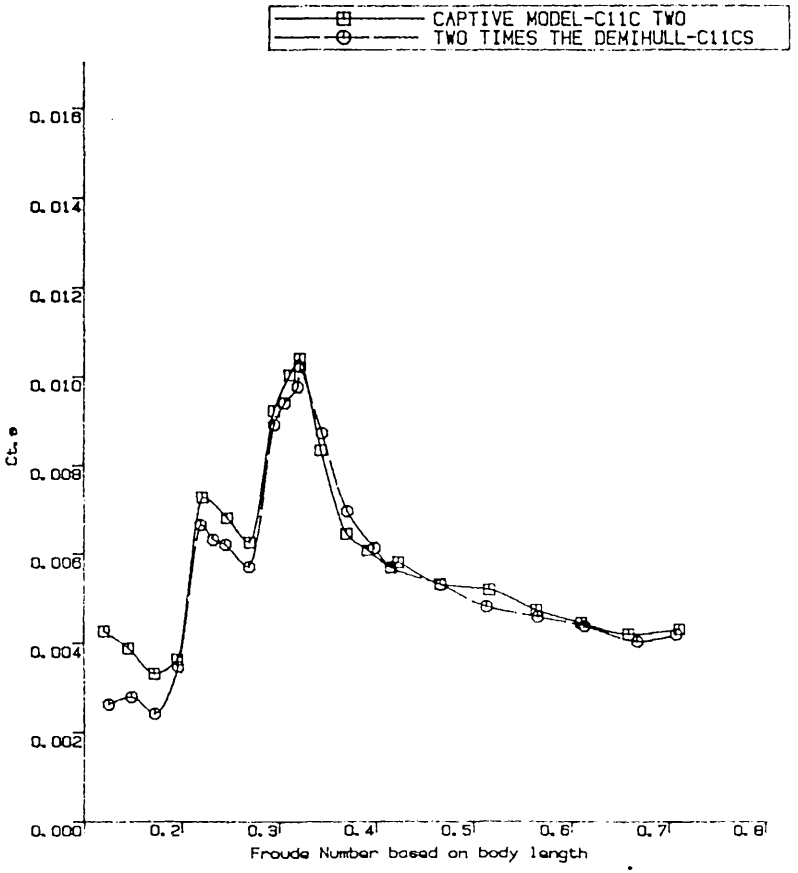

Twin hull interference effect on the resistance
- resistance coefficients -

Fig.4.42

Fig 4.43-a SWATH1-C2 under way(1.25m/s)

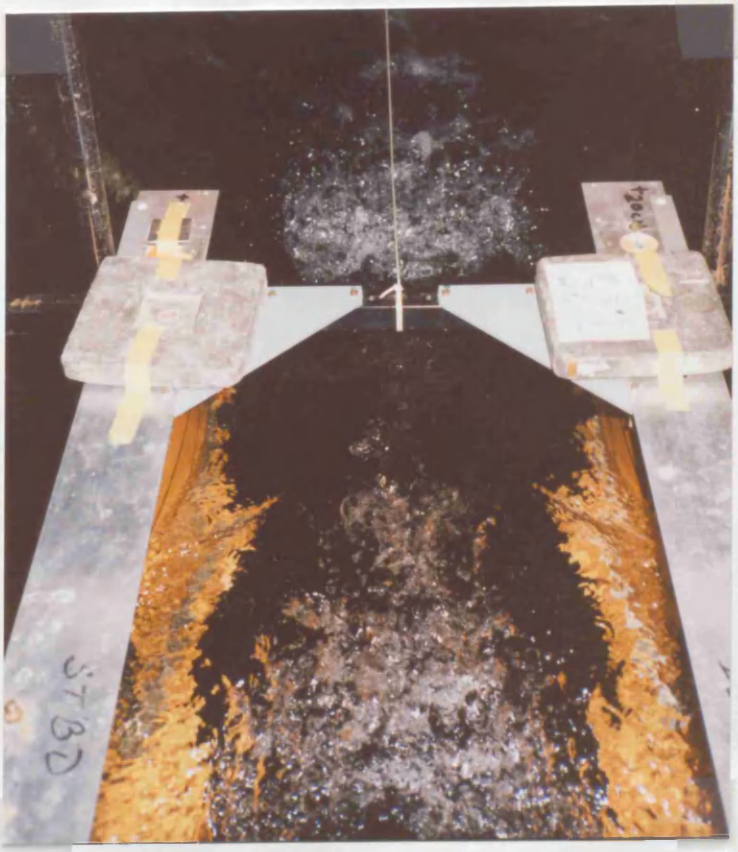

Fig.4.43-b SWATH1-C1C under way(1.25m/s)

Fig 4.43-c SWATH1-C5 under way(1.6m/s)

Fig 4.43-a,b,c Interference Wave Systems

Fig 4.44 Single Hull C11CS under way(1.5m/s)

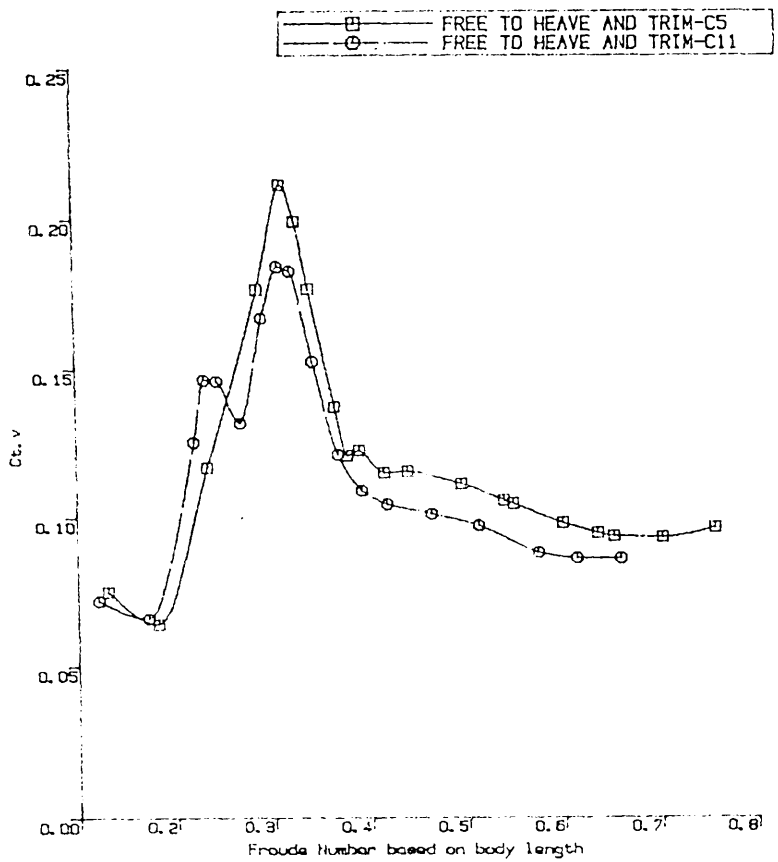

Total resistance coefficient variations SWATH1 versus Froude Number

Fig.4.45

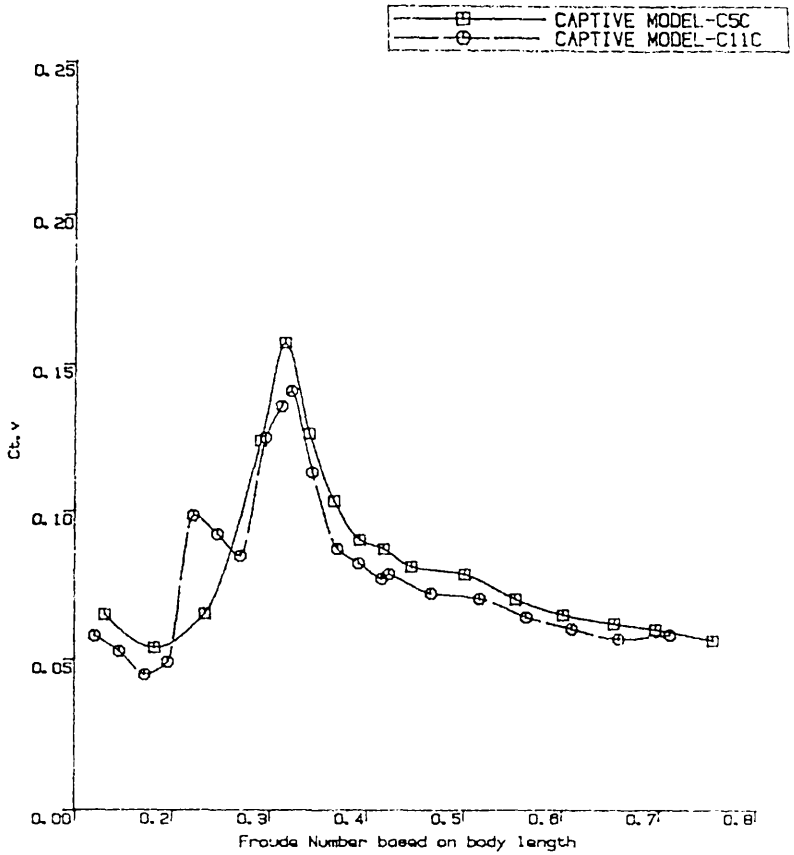

Total resistance coefficient variations SWATH1 versus Froude Number

Fig.4.46

4.3 SWATH1 MODEL RESISTANCE AND MOTION IN UNIFORM WAVES

One of the most publicised merits of SWATH ships is their ability to sustain speed without much loss in rough weather. However, due to the lack of design data, an exact estimation of power increase or speed loss due to the resistance augmentation in rough weather is hardly possible at the present time. There are very few papers published concerning the power increase of SWATH ships in rough weather.

Based on full scale test results at service power, it is reported that the speed loss of the 'MESA 80' was less than 2 percent of maximum in sea state 4[66,75]. Using the SWATH6-DTNSRDC Model 5737-A, Yeh et al[76] predicted both mean added resistance and mean added power in rough water from measurements in regular, head waves based on the linear superposition principle at three speeds. Also, they proved the validity of the predictions by showing close agreement with irregular wave experimental data. According to the results, it can be seen that the added resistance and the added power are both nearly proportional to the wave height with a slope which increases with the speed. This indicates that they are both functions of the speed and wave height. Based on the DTNSRDC results, MacGregor[77] estimated the power increase in rough weather of a 2400 tonne SWATH ship designed at the Dept. According to his results, the power increase is significant as the wave height increases, ie, more than 10 percent in sea state of 4(See Fig.4.47).

Since the two above results are contradictory and this added power is of prime importance in estimating the design power margin of SWATH ships in rough weather, studies into the added resistance in regular waves were conducted with the SWATH1 model which was used for the calm water resistance study as presented in section 4.2. Total resistances as well as motions were measured in uniform, head waves at two settings of the spacing between the centrelines of two demihulls (SWATH1-C5 and C8). C5 and C8 are the condition numberings for the equivalent calm water tests as shown in Table 4.2. Both conditions have the same draft (twice the diameter of the body) and the non-dimensional spacings between the centrelines of two demihulls are B_1=0.762 for C5 and 0.947 for C8.

Regular wave experiments were conducted with SWATH1-C5 at 4 wave frequencies of 0.45, 0.83, 1.02 and 1.17hz which correspond to ratios of wave length to body length of 5.11, 1.5, 1.0 and 0.75, respectively. Two to four wave heights were used for each wave length to study the effect of wave steepness on the resistance of the SWATH model. 5 to 15 speeds were run at each condition. Heaving, pitching and surging were measured and compared with the computational results from the computer program SWATHL which was developed at the Laboratory[85]. Mean sinkages and trims were also measured and compared with the results in calm water.

Tests with SWATH1-C8 were jointly conducted with Djatmiko as part of a seakeeping investigation[73] and the results were made available for the present purpose. These tests covered a range of frequencies from 0.3 to 1.6hz, which correspond to ratios of wave length to model length of 11.5 to 0.4. The speeds covered are 0.5, 1.0, 1.5 and 2.0m/s which correspond to Froude number based on the body length of 0.13, 0.26, 0.39 and 0.52. Two sets of wave heights were used to find a relationship between motion responses and the wave height as well as between the added resistance and the wave height.

Instead of using the load cell towing system used for the previous calm water tests of the SWATH1 model which was not free to surge(as mentioned in section 4.2.2), a pendulum type of dynamometer was used to allow the model to move back and forth in waves. Using this system, still water resistances were measured again for SWATH1-C5 and C8 and compared to those tested previously.

It is reported that there is little difference in added resistance between that obtained by the constant towing force technique and that obtained by the constant speed technique. The latter is much easier to perform and the results are more reliable and accurate[78,79]. Hence, the constant speed technique was used to measure the resistances in waves. The added resistance is then derived by subtracting the still water resistance from the resistance in waves.

From the present study with the tandem strut SWATH1 model, very interesting and important results are found. There is little increase in the added resistance as speed increases. Further, in the supercritical zone, as the wave height increases, the resistance decreases(by as much as 24%) over the speed range of Fn=0.31-0.39 due to the

complicated hydrodynamic interferences. These findings seem to be very valuable in the applications of SWATH ships to naval combatants where the speed loss is of prime importance. All the results are reported in Ref.[65] and this section is taken from the reference.

4.3.1 Description of Model SWATH1

The description of the SWATH1 model are made in section 4.2.1. In order to keep consistency with the calm water tests, turbulence stimulation devices were not introduced for this model.

4.3.2 Instrumentation

Instead of using the load cell towing system used previously for the calm water tests of SWATH1 model which was not free to surge, a pendulum type of dynamometer was used to allow the model to move back and forth in waves. The model was towed using a nylon cord yoke which was attached to two fore struts at 5 cm above the still water level which was 3cm higher than the previous one in order to avoid the waves touching the towing pulley. Resistances were transmitted via the pulley to the paper placed on the rotating drum of the dynamometer by a piano wire attached to the end of the yoke. The model was free to heave, trim and surge, but restricted in yaw and sway using four vertical guiding rods in order to keep the model on course with minimum restraint. The model towing arrangement is illustrated in Fig.4.48.

Since the different towing systems and different towing heights would result in different resistance measurements, the calm water resistances were again measured using the new system and compared with the previous results. Figs.4.49and 4.50 show that there is little difference in the two results for both SWATH1-C5 and C8. Sinkages and trims were not recorded in the previous tests and consequently no comparison is possible. However, the trims for the both towing systems may be different from each other due to the two different towing heights. Therefore, as mentioned in section 4.2, it can be concluded that below the speed where green water

occurs or severe spray sheets develop, sinkage and trim do not affect much to the increase in resistance .

Two LVDT(Linear Variable Differential Transformer) vertical displacement transducers attached to the gantry of the carriage above the model were used to measure the heave and pitch responses. As can be seen in Fig.4.48, one LVDT was positioned above the bow of the model and the other above the stern of the model. Both of these were connected by piano wires to the centres of the bow and stern transverse beams, respectively, so that the distance between the two transducers was 0.785m. These LVDTs were positioned vertically and their weights were balanced so that any acceleration being induced on the transformers during the model motions could be eliminated. The heave and pitch responses were recorded on the pen recorder through a special amplifier which sums and differences the signals from the two transducers to produce outputs proportional to the heave and pitch movements of the model. In order to remove any error in heave due to surge, the model was kept oscillating(surging) around the original stationary position(LVDTs positioned vertically) by placing the proper weights on the pendulum. This was achieved without any difficulty since the calm water resistance was already known. However, in some cases, the run was repeated so as to place the proper weights in waves. The surge response was read off from the magnitude of the resistance curve oscillation due to the oncoming wave.

The regular waves were created by a parabolic plunger type of wave maker driven by an electronically controlled hydraulic pump and measured by capacitance wave probes.There is inevitably some tank wall effects due to the finite tank width and accordingly waves are slightly attenuated as they travel along the tank. Hence, three wave probes were placed on a bridge across the tank located close to the wave maker and arranged in such a way (B/2, B/3 and B/4 from the tank wall side where B is the tank width) that any changes in the wave patterns due to the finite tank width can be noted. Mean wave height was taken from the three readings. Typical records of wave probes, pitching, heaving, surging and resistance in waves are shown in Fig.4.51.

4.3.3 Calibration Procedures

4.3.3.1 Calibration of LVDTs

Using the pen recorder, zero readings were taken from the still water condition. The piano wires connected to the front and stern of the model were then displaced ±5 cm using calibration gauges attached to the vertical tubes of the transducers and the new readings were recorded. Thus, calibration factors for the pitch and heave were calculated from the pen recorder.

4.3.3.2 Calibration of wave probes

Zero readings were obtained with the wave probes in still water. The bridge mounting the wave probes was then lifted by 5 cm on both sides of the tank and a new reading for each probe was taken. Thus a calibration factor for each probe was found.

Before the first test run of each day, calibrations for the two LVDT transducers as well as for the wave probes were performed to account for changes due to the atmosphere surrounding the devices, ie temperature, humidity, current and voltage etc.

The water temperature in the towing tank was measured at the depth of two-thirds of the model draft once every hour and the mean value of these readings was taken for each condition. Between runs, an interval of about 15 to 30 minutes, depending on the velocity and immersed depth of the model and the wave frequency, was required to allow the water to calm down. Just prior to each run, the tide in the tank water was measured at midtank using a float and taken account of in the carriage speed.

4.3.4 Analysis and Discussions

4.3.4.1 Record analysis

The pitch angle θ is calculated as $\theta = \tan^{-1}$(amplitude of the pitch from the pen

recorder/78.5cm) where 78.5 cm is the distance between the front and stern LVDT transducers.

The surge, heave and pitch are nondimensionalised as follows:

$$X' = \frac{x_a}{\zeta_a} \qquad Z' = \frac{z_a}{\zeta_a} \qquad \Theta' = \frac{\theta_a}{\zeta_a \omega_e^2/g} \tag{4.1}$$

where x_a, z_a and θ_a are the amplitudes of the surge and heave in metres and pitch in degrees, respectively, and ω_e is the encounter wave frequency in rad/sec.

The wave frequency is non-dimensionalised as

$$\omega' = \frac{\omega}{\sqrt{g/L}} \tag{4.2}$$

where L is the characteristic length of the model and the body length(L_b) is used.

The added resistance is nondimensionalised as

$$\sigma_{AW} = \frac{R_{AW}}{\rho g \zeta_a^2 \nabla^{1/3}} \tag{4.3}$$

where R_{AW} is the added resistance due to the oncoming waves. Instead of using the breadth of the model as usually used for monohull ships, the displacement volume is used for the purpose of the present study.

4.3.4.2 Discussions

The still water resistance of SWATH1-C5 is plotted versus Froude Number in Fig.4.52 through 4.55 together with the resistances in waves. In long waves(λ/L_b=5.11), see Fig.4.52, the resistance increases are very small for the two waves whose steepnesses are both comparatively small. The resistance increase is about 0.5% at Fn=0.548 for λ/ζ_w=171.0 and about 2.5% at Fn=0.543 for λ/ζ_w=98.4. At λ/L_b=1.0 as shown in Fig.4.54, it can be seen that the resistance decreases around Fn=0.31-0.39 as the wave height increases. It is worthwhile noting that the resistance decreases by as much as 24% at Fn=0.326 for λ/ζ_w=15.0. This decrease can be also seen in the same speed range at λ/L_b=1.5 and 0.75, respectively, as shown in

Figs.4.53 and 4.55. Fig.4.56 is redrawn from Fig.4.54 over the speed range where the resistance decrease occurs. From the figure, it can be seen that as the wave height increases, the resistance decreases systematically with the tendancy that the resistance peak shifts to the slower speeds and that the hollow and hump are flattened.

These decreases seem to be caused by very complicated hydrodynamic effects between the many components of the model and the oncoming waves, and it is not easy to clearly identify the cause. However, some possible reasons are given below, but a full explanation will require a considerable theoretical investigation of first and second order wave effects.

There are some reports[102,103] that an airfoil(s) attached to the hull can create propulsive energy which moves the ship forward. By the same principle, the complicated hydrodynamic interferences between the many components of the tandem strut SWATH model combined with some motion aspects would create some propulsive forces. This is supported by the fact that with the single strut SWATH 3, the decrease in resistance did not occur as will be described in section 4.5. In addition, with the tandem strut SWATH2 model which has rectangular cross section bodies with rounded corners, the same resistance decrease occurs over nearly the same speed range as above. This will be shown in section 4.4 following.

As mentioned in Fig.4.18(see section 4.2.4.2), the large peak around Fn=0.31 is caused mostly by the interference wave systems between the fore and aft struts and between the struts and the body. These interferences are a function of not only the relative distance between the components but also speed. As the model is towed at a constant speed through waves, its apparent speed will be increased due to the speed of the encountering wave. Hence, this changed speed would possibly affect the wave interference systems and consequently, shift the peak to the slower speed as shown in Fig.4.53 through 4.55. In addition,the phase shift towards the slower speeds with increasing wave height may possibly be attributed to the changed(increased) speed of water particles near the model due to the increased surge motion with the increase of the wave height.

In addition, the decrease in resistance may possibly be understood from the curves of sinkage and trim as shown in Figs.4.57 through 4.64. From these figures it

can be seen that the trim decreases by up to 50% (depending on the speed) as the wave height increases. The negative resistance increases over Fn=0.31-0.39 could be partly due to the considerably decreased trims over that speed range. At higher speeds above Fn=0.39, the resistances are not reduced despite the much reduced trims. This can be possibly explained by the fact that the mean sinkages are increased at the higher speeds as shown in Figs.4.57 to 4.60, hence creating more resistance. In general, the sinkage in waves decreases up to Fn=0.3, and then increases relative to the still water value. However, this postulation seems to be less justifiable than the earlier explanations. The sinkage and trim are brought about by the ship wanting to keep the forces, caused by the pressure distribution around the hull, to be balanced by the internal weight. Therefore, in the author's opinion, the decreased resistance caused the different sinkage and trim rather than the changed sinkage and trim reduced the resistance. Of course, if the ship is towed in a trim condition by force, the resistance will be different from that of the ship towed in free mode.

The decrease in resistance cannot be seen at a wave length of λ/ζ_w=5.11 as shown in Fig.4.52. This may be explained by the fact that the motions of the model are large due to its closeness to the natural frequencies of heave and pitch, 0.588 and 0.444hz, respectively. These motion responses are shown in Fig 4.71 through 4.82 together with the surge response.

For comparison, Figs.4.65 and 4.66, taken from ref[84], show the resistances of destroyer DE-1006 and series 60(C_B=0.6) in calm water and waves as a function of Froude Number at four wave lengths. From the comparison of the two figures and the results of SWATH1 model, it can be understood that the resistance increase of the SWATH model in waves is very much less than those of the monohull ships.

It is generally found for monohulls that added resistance is propotional to the square of wave height[80]. However, a number of papers which are opposed to the square law have been published[81,82,83]. If the square law is correct, then all the resistances of a given model at various wave heights but constant wave length can be reduced to a single curve when divided by the square of the wave heights.

The non-dimensional added resistance coefficients are plotted versus Froude Number in Figs.4.67 to 4.70 for the four wave lengths tested. The added resistance is obtained by subtracting the calm water resistance from the resistance in waves. If the speeds tested in calm water and in waves are different from each other, the calm water resistance is read off from the curve of measured resistance at the speed tested in waves. For convenience of comparing the added resistance of SWATH ships having different displacements, the added resistance is non-dimensionalised by $\rho g \zeta_a^2 \nabla^{1/3}$ where one third of the power of displacement(∇) is used instead of the breadth as usually used for the monohull. Also, the concept of breadth for a SWATH is different from that of the conventional monohull. From these figures it is difficult to justify the use of the square law between the wave height and added resistance for the SWATH1 model. The discrepancy is larger at the low frequency of 0.45hz, which is close to the pitch resonance, than the other frequencies. This might also be due to the fact that the wave steepnesses tested at 0.45hz are comparatively small . In general, it is known that the square law is less applicable as wave steepness decreases. At the wave length of λ/L_b=1.0 as shown in Fig.4.69, the big increase in the added resistance at the top speeds for λ/ζ_w=19.6, 16.7 and 15.0 are due to green water on the deck and front cross beam of the model which was observed during the experiments. Except that, it is worthwhile noticing that there is little increase in the added resistance in waves as the speed increases, even up to the high speed of Fn=0.5. The greatest resistance decreases among the tested wave lengths occur at the shortest wave length of λ/L_b=0.75.

The non-dimensional motion responses (heaving, pitching and surging) are plotted against Froude number in Figs.4.71 through 4.82. Excepting the frequency of 0.45hz, the motion responses can be seen to be linear with wave height if the ordinate scales are kept the same as those in Figs.4.88 through 4.90

The calm water resistance of SWATH1-C8 is presented versus Froude number in Fig.4.83 together with the result of SWATH1-C5. It can be seen from the figure that the narrow spacing(C5) is worse at higher speeds, as expected, with little difference at slow speeds. It is interesting to observe the results over the hump and hollow part of the speed range. As the spacing decreases, the interference between the two demihulls seems to intensify both favourably and unfavourably. Over the hump speed range, C5

is worse than C8 and the result is reversed over the hollow speed range due to a favourable interference between the two demihulls. This spacing effect is stated in more detail in the previous calm water experiments. Also, the spacing effect is well illustrated in the trim curves as shown in Fig.4.85. The narrow spacing model trims more than the wide spacing model and the hump and hollow occur in the same manner as in the curve of the resistance but shift to slower speed with the peaks biased. There is little difference in the sinkages between the two conditions as shown in Fig.4.84.

The added resistance coefficients of the SWATH1-C8 are presented against the non-dimensional encounter wave frequency for the four speeds tested in Fig.4.86. At Fn=0.39, the negative resistance increase can be seen for the first set of wave heights and virtually zero increase for the second set. The speed of Fn=0.39 is at the upper end of the range where the negative resistance increase occurs, as shown in the earlier Fig.4.56 for the SWATH1-C5. It can be seen from Fig.4.56 that the negative or nearly zero increase occurs around the same speed as it does for SWATH1-C8. The worst resistance increase occurs around pitch resonance from which it can be concluded that the pitch motion dominantly effects the resistance increases of the SWATH1 model at all the tested speeds. As in the case of SWATH1-C5, it can be seen from the figure that there does not appear to be a square law between the added resistance and wave height.

The heaving, pitching and surging motion responses of the SWATH1-C8 are plotted versus the non-dimensional encounter wave frequency at the four speeds tested in Fig.4.87-a, b and c. Figs.4.88 to 4.89 show the comparisons of the results obtained for the two sets of wave heights together with the computational results for heaving and pitching. The predictions of the 2D-strip theory are higher in the critical zone because the damping due to viscosity in the theory is ignored. In the supercritical zone, the two results accord well with each other. The heaving and pitching responses as shown in Fig 4.88 and 4.89 seem to be linear with wave height (independent of λ/ζ_w) except in the resonance region. However, it is unlikely that the linearity can be applied to the surge motion of the SWATH1 as shown in Fig.4.90.

Fig 4.91 and 4.92 show the sinkage and trim variations against wave frequency in rad/sec which reveals that they are nearly independent of the wave length. This result is also reported for the same model but at a wider spacing[72].

The interference wave systems between the two demihulls affected the resistance depending on their closeness to each other as mentioned earlier. Figs.4.93 and 4.94 show the heave and pitch responses at the three different spacings with the four forward speeds. SWATH-Wu, taken from Ref[72], has the widest nondimensional spacing (B_1=1.132). Since the results of only two to four frequencies were tested for SWATH1-C5 at the four speeds, a clear comparison between them can not be made. However, it can be seen from the comparison between the SWATH1-C8 and-Wu that the wide spacing model is subject to less motion responses compared to the narrow one, in particular, at the slow speed(Fn=0.130) and at the re-sonance region for all the tested speeds.

4.3.5 Conclusions

From the present studies, the following important conclusions can be drawn.

A) The resistance increase of the SWATH model in waves is very much smaller than those of the monohull ships. There is little increase in the added resistance as speed increases.

B) In the supercritical zone, as the wave height increases, the resistance decreases systematically over the speed range of Fn=0.31-0.39 with the tendancy that the resistance peak shifts to slower speeds and that the humps and hollows are flattened.

C) The added resistance is not proportional to the square of the wave height. The added resistance divided by the square of the wave height decreases as the wave height increases.

D) The worst resistance increase in waves occurs around pitch resonance.

E) The sinkage and trim are independent of the wave length but dependent on the wave height.

F) The trim in waves becomes lower than that in calm water and decreases with increasing wave height. The sinkage in waves decreases up to Fn=0.30 and then increases compared to that in calm water.

G) The narrow spacing model trims more than the wide spacing one with little difference in the sinkages between them.

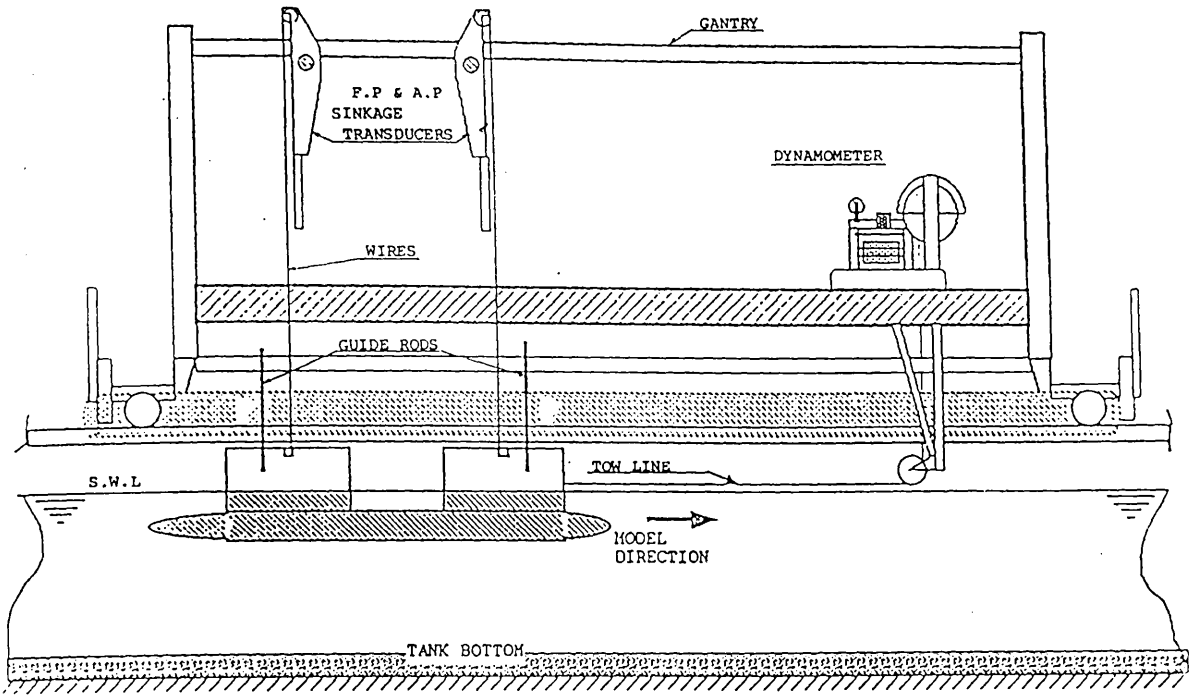

Towing arrangement at the carriage

Fig.4.48

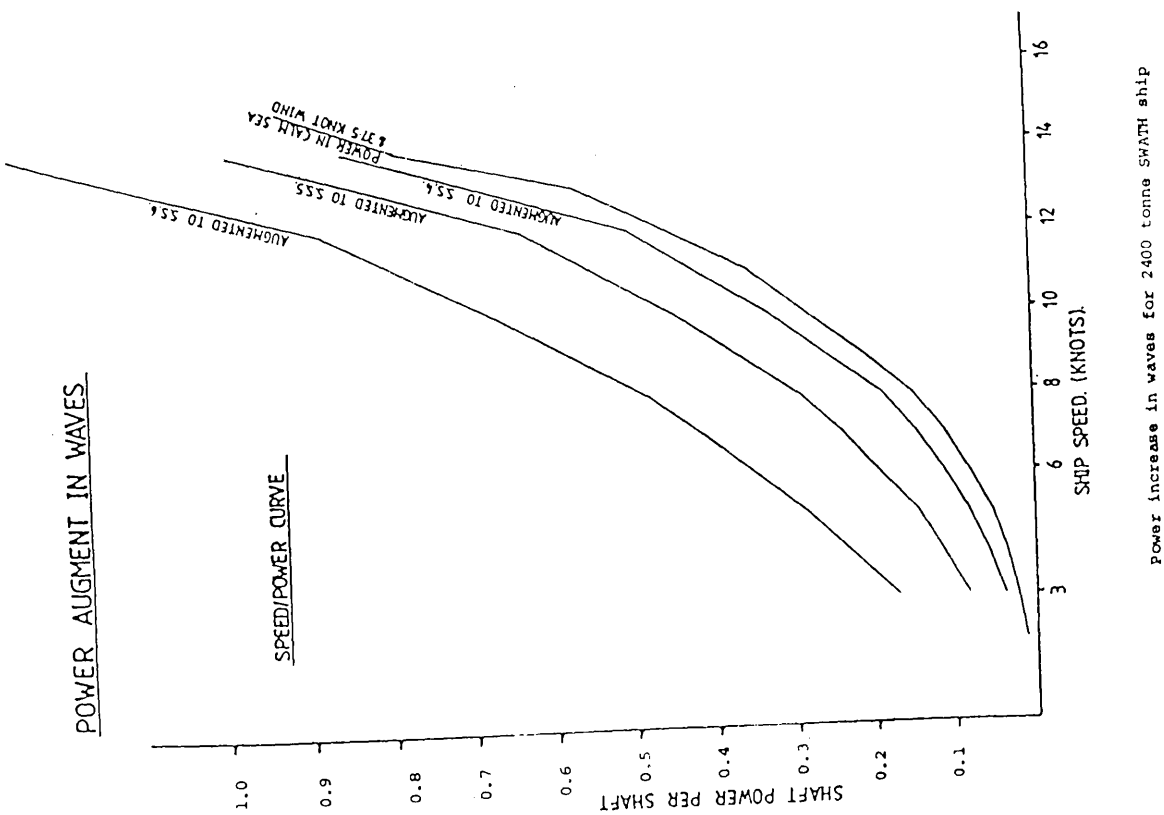

Power increase in waves for 2400 tonne SWATH ship

Fig.4.47

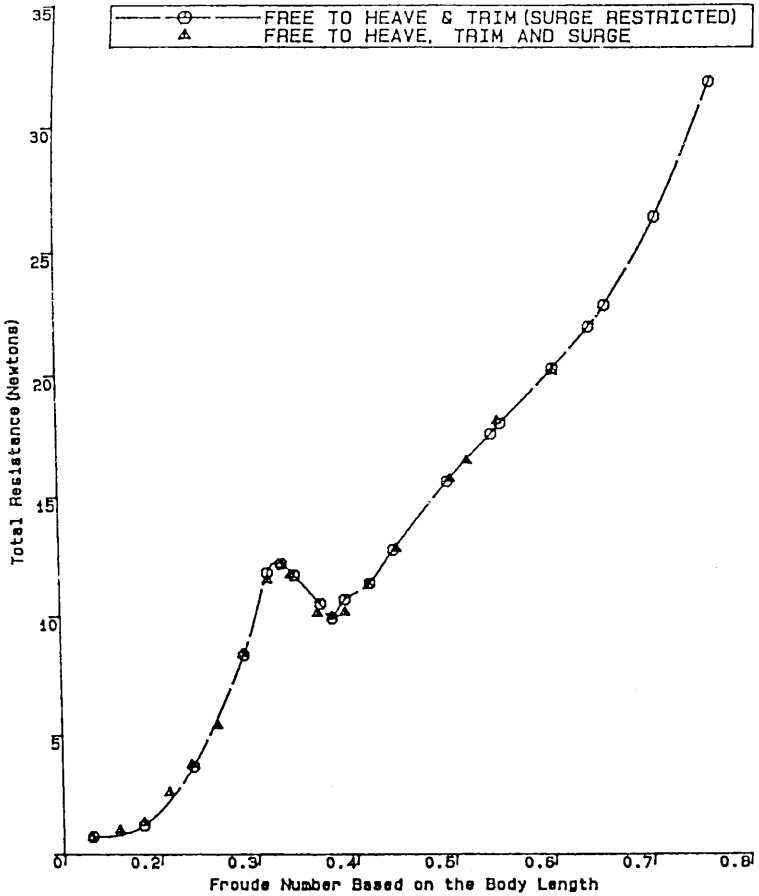

Comparison of different experimental techniques (SWATH1-C5)

Fig.4.49

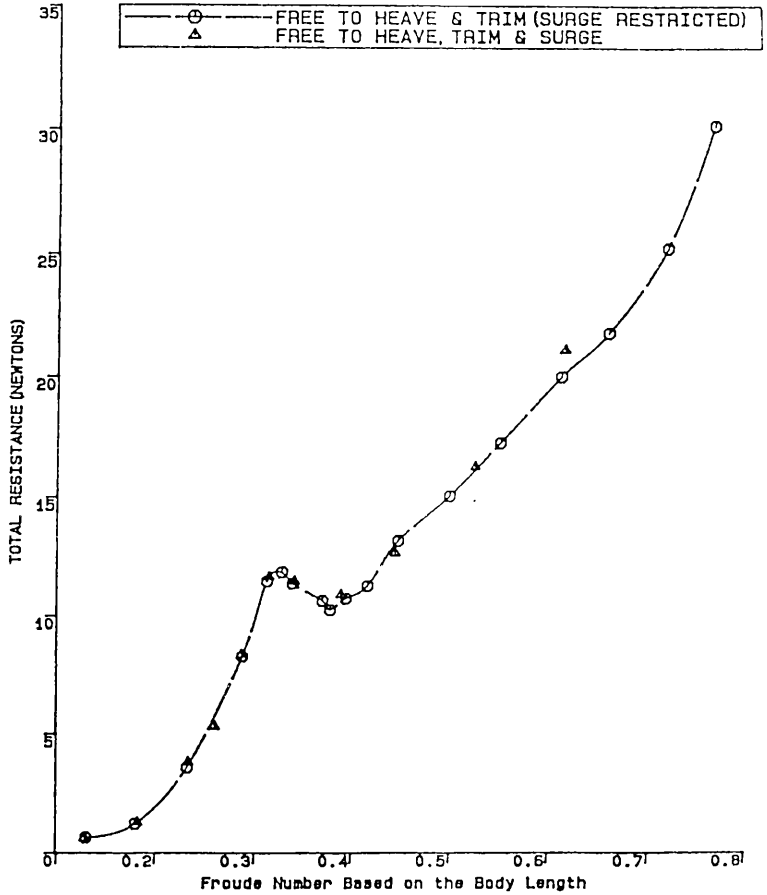

Comparison of two different experimental techniques (SWATH1-C8)

Fig.4.50

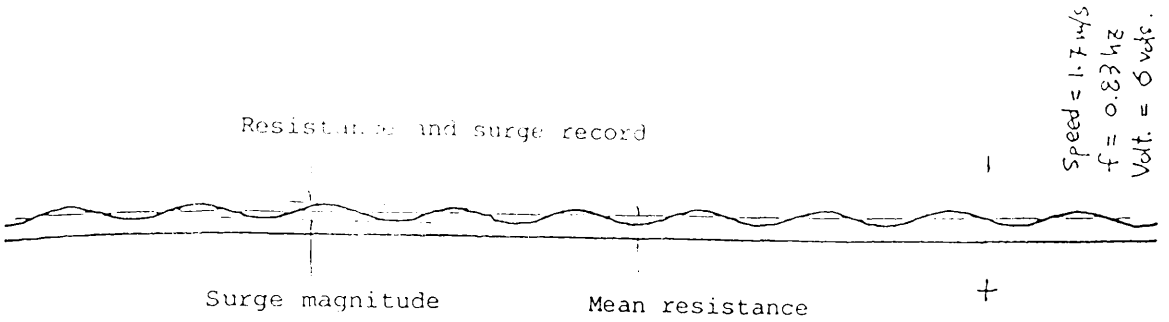

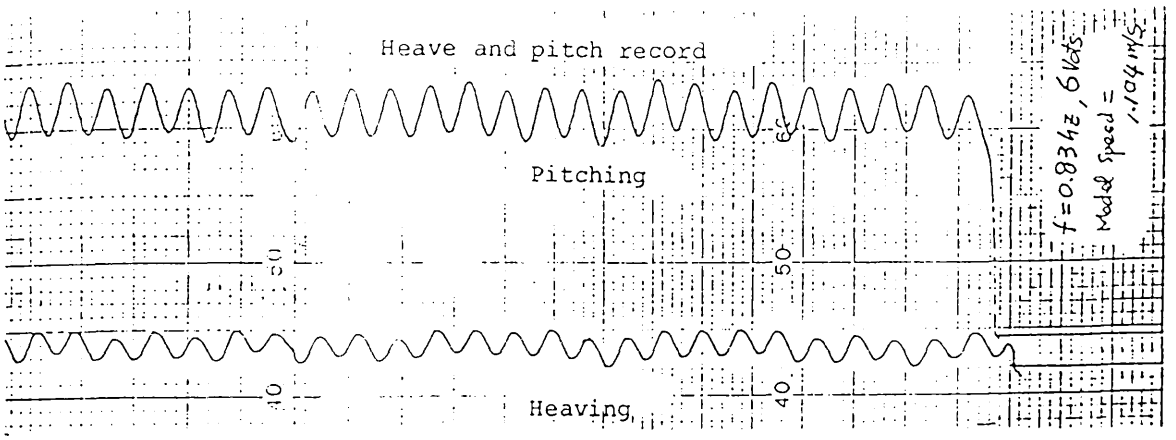

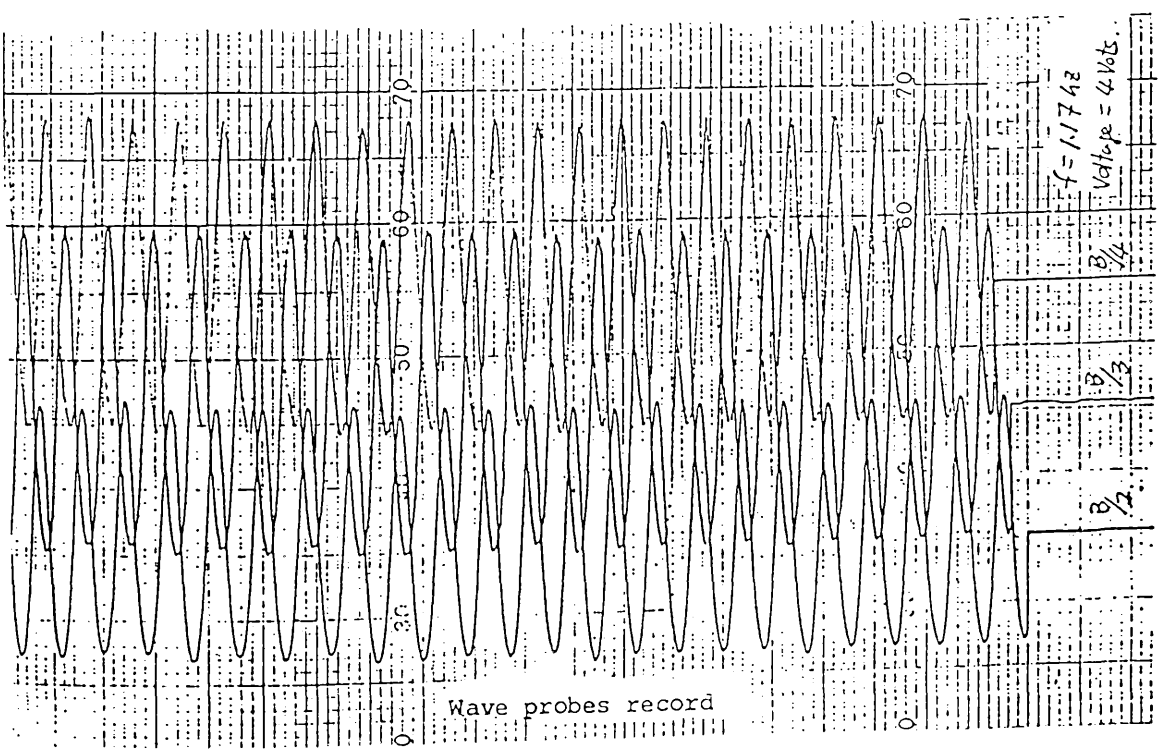

Typical Recordings of Surging, Heaving, Pitching, resistance and Wave Heights.

Fig.4.51

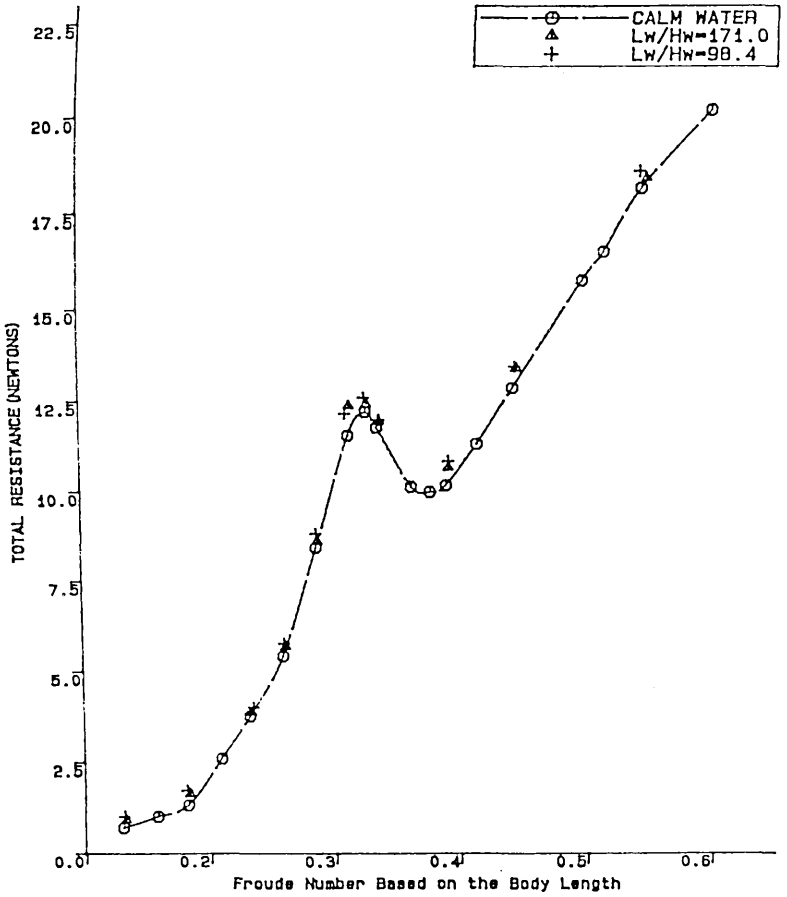

SWATH1 Model-C5 Total Resistance as a Function of Froude Number (Wave Frequency=0.45Hz, Lw/Lb=5.11)

Fig.4.52

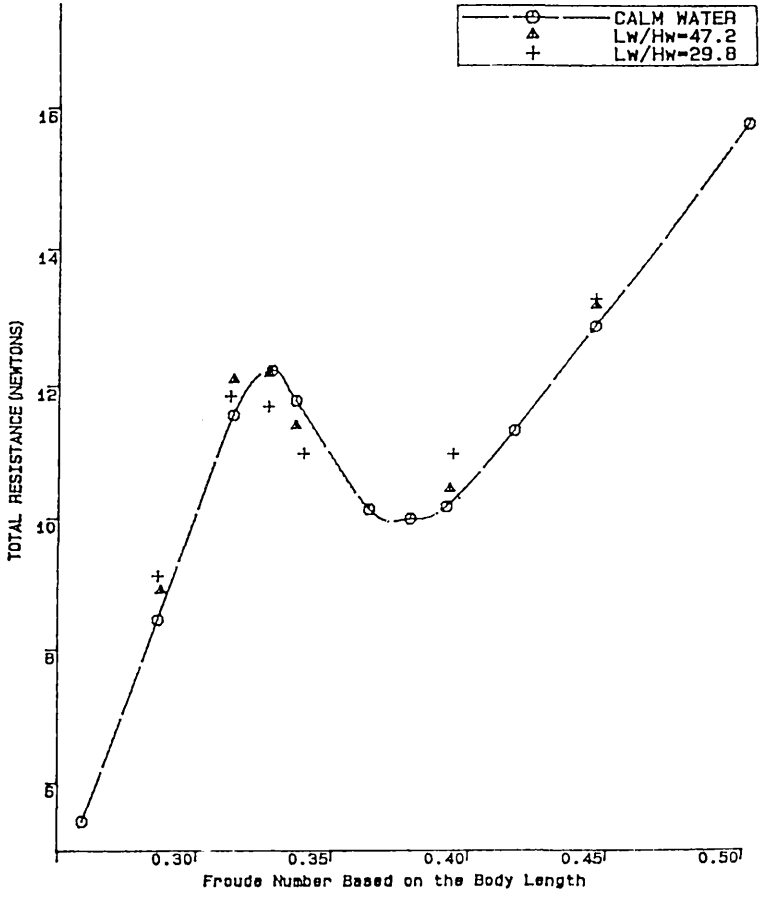

SWATH1 Model-C5 Total Resistance as a Function of Froude Number (Wave Frequency=0.83Hz, Lw/Lb=1.5)

Fig.4.53

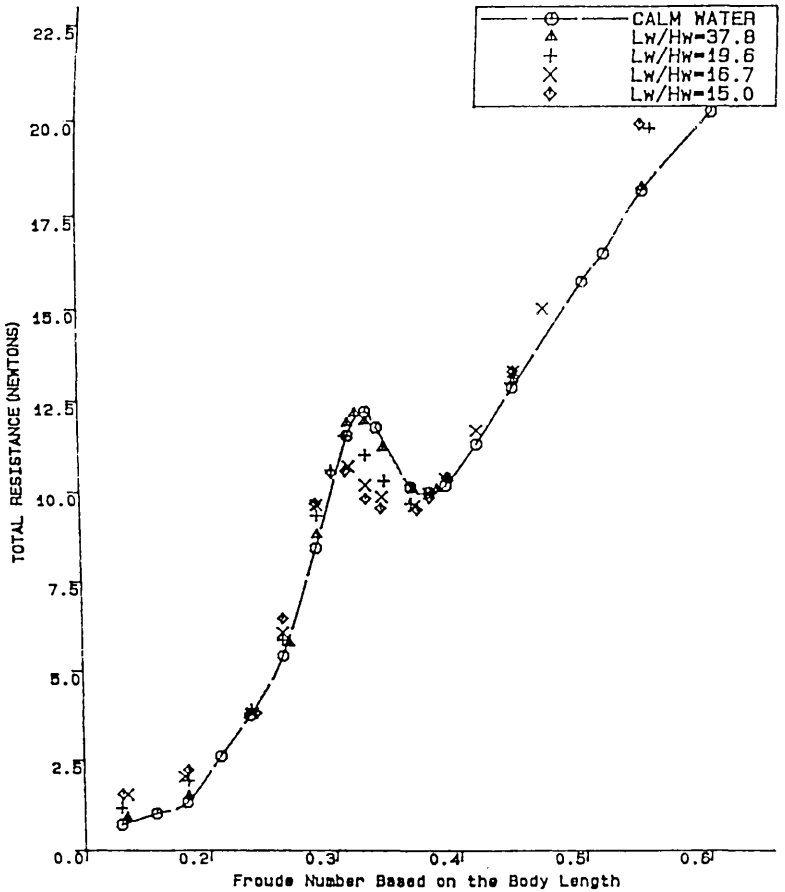

SWATH1 Model-C5 Total Resistance as a Function of Froude Number (Wave Frequency=1.02Hz, Lw/Lb=1.0)

Fig.4.54

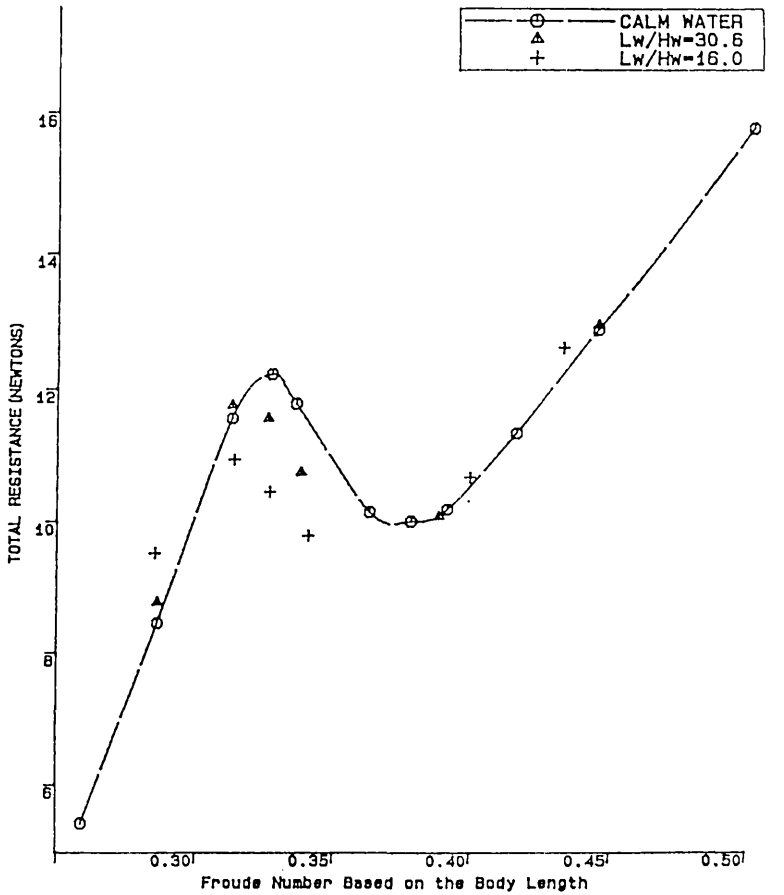

SWATH1 Model-C5 Total Resistance as a Function of Froude Number (Wave Frequency=1.17Hz, Lw/Lb=0.75).

Fig.4.55

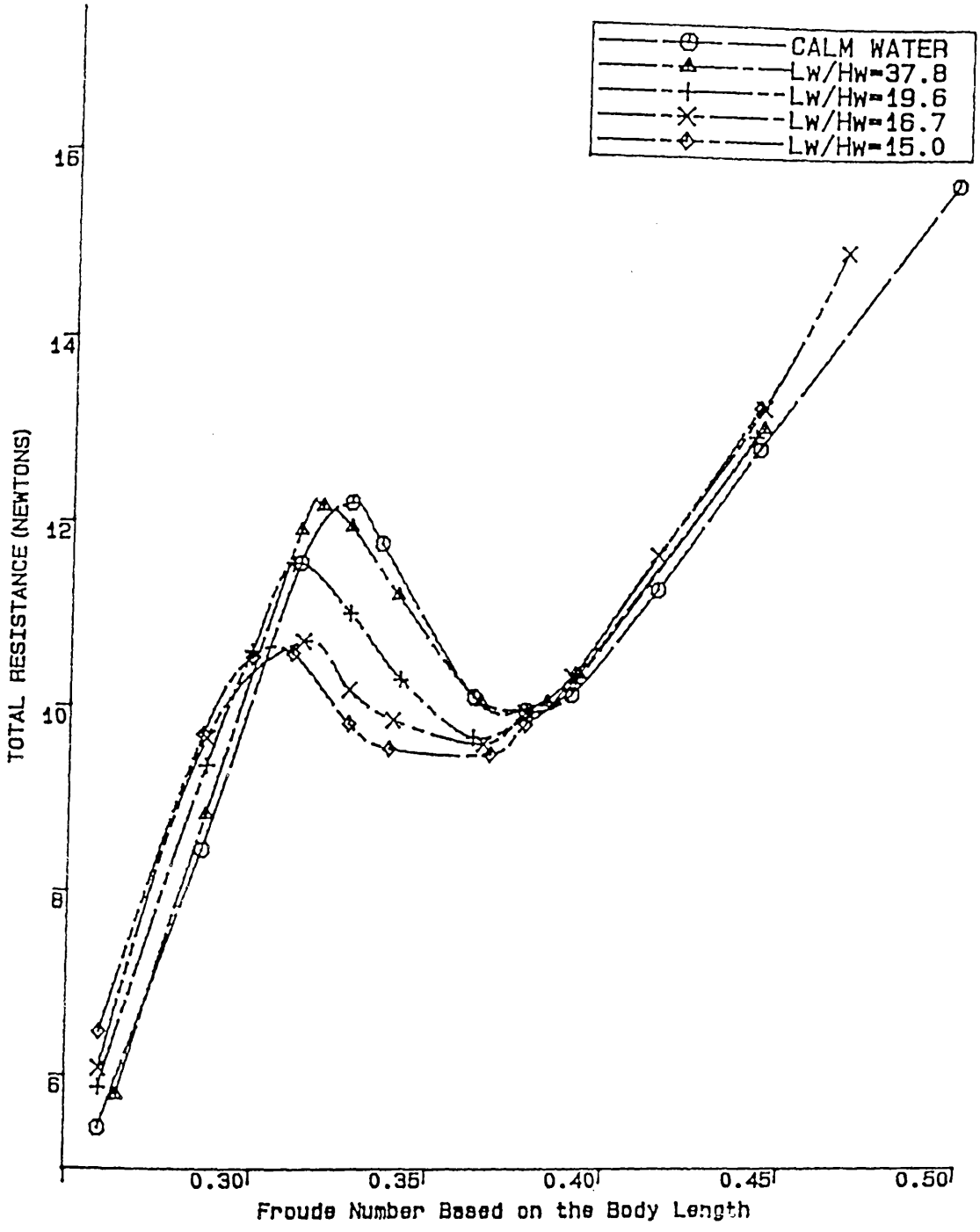

SWATH1 Model-C5 Total Resistance as a Function of Froude Number (Wave Frequency=1.02Hz, Lw/Lb=1.0)

Fig.4.56

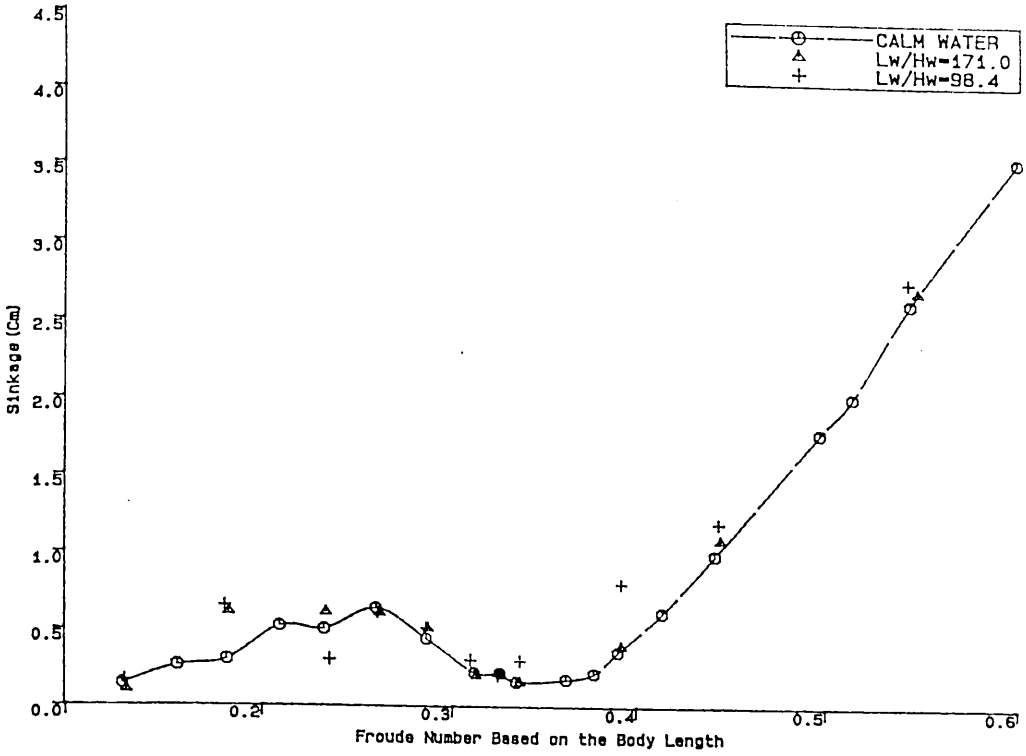

SWATH1 Model-C5 Sinkages vs Froude Number (f=0.45Hz, Lw/Lb=5.1)

Fig.4.57

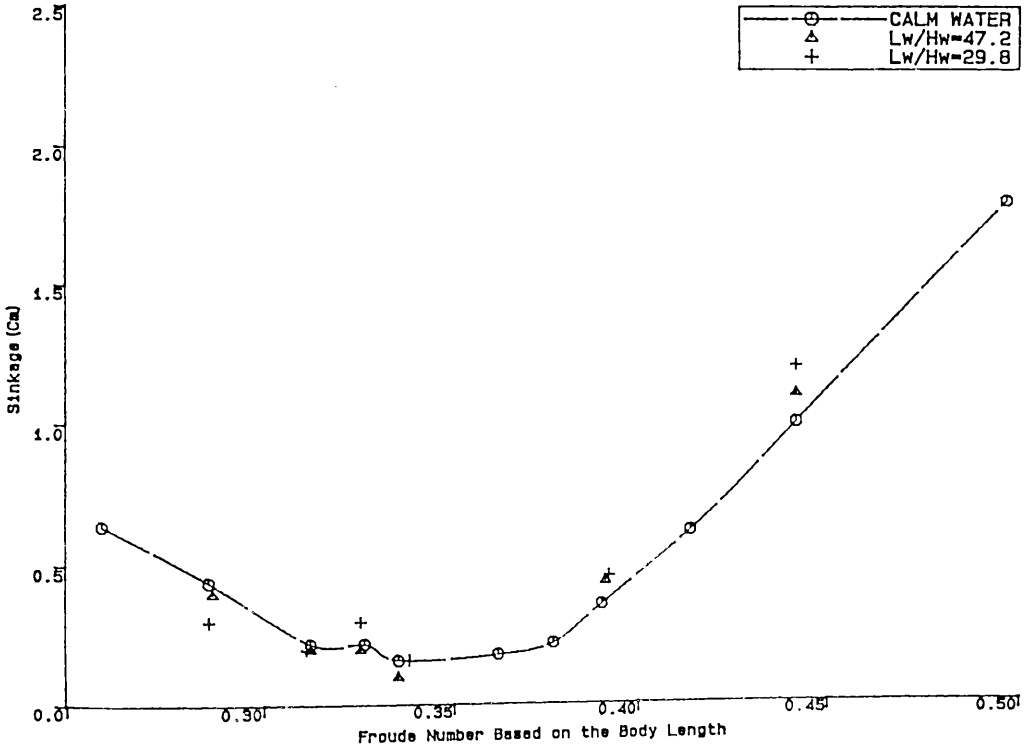

SWATH1 Model-C5 Sinkages vs Froude Number (f=0.83Hz, Lw/Lb=1.5)

Fig.4.58

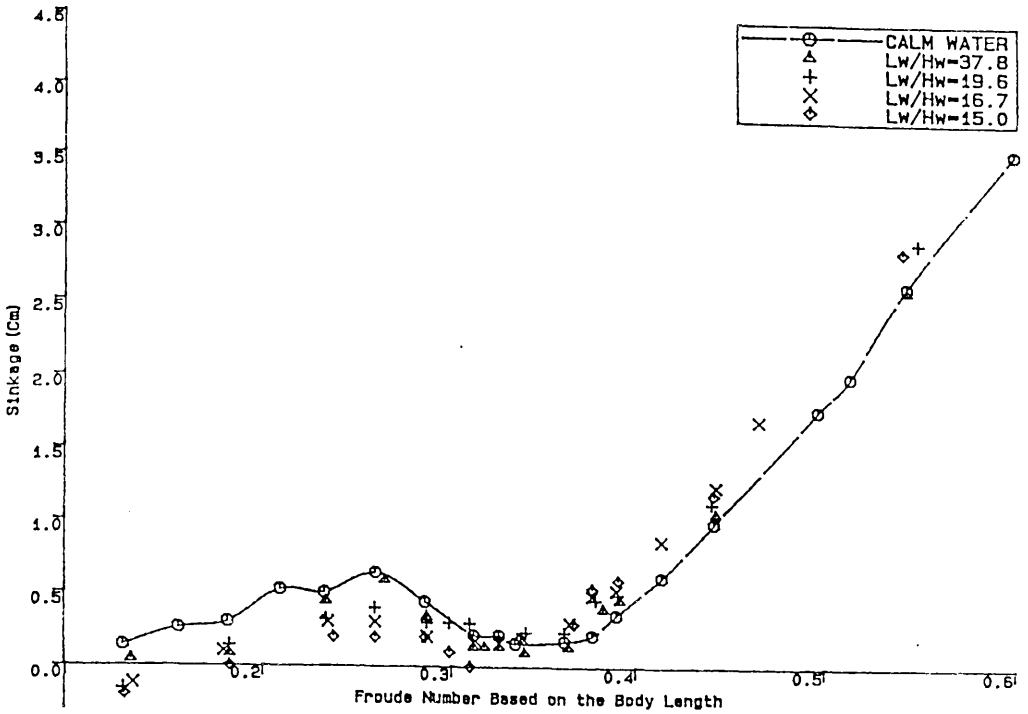

SWATH1 Model-C5 Sinkages vs Froude Number (f=1.02Hz, Lw/Lb=1.0)

Fig.4.59

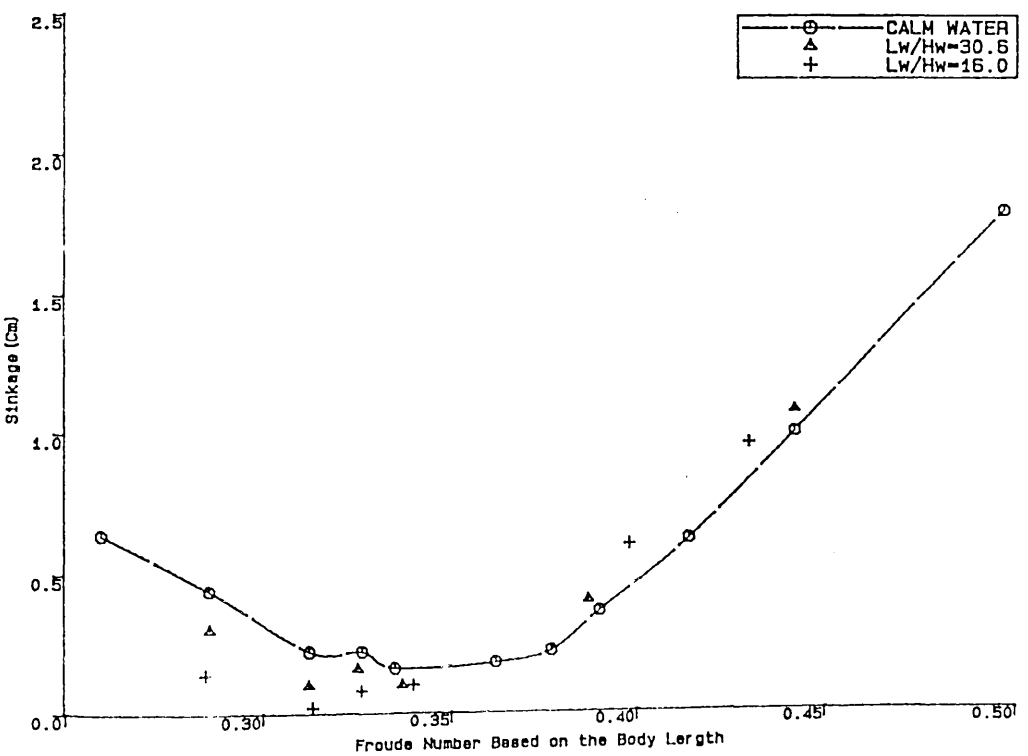

SWATH1 Model-C5 Sinkages vs Froude Number (f=1.17Hz, Lw/Lb=0.75)

Fig.4.60

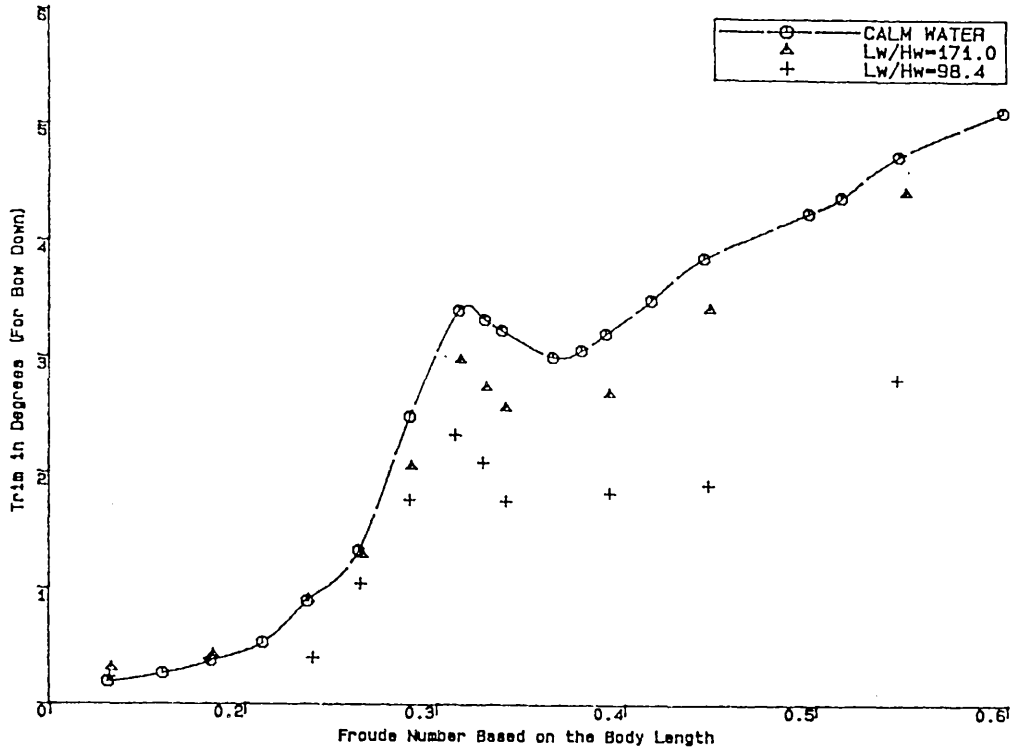

SWATH1 Model-C5 Trims vs Froude Number (f=0.45Hz, Lw/Lb=5.1)

Fig.4.61

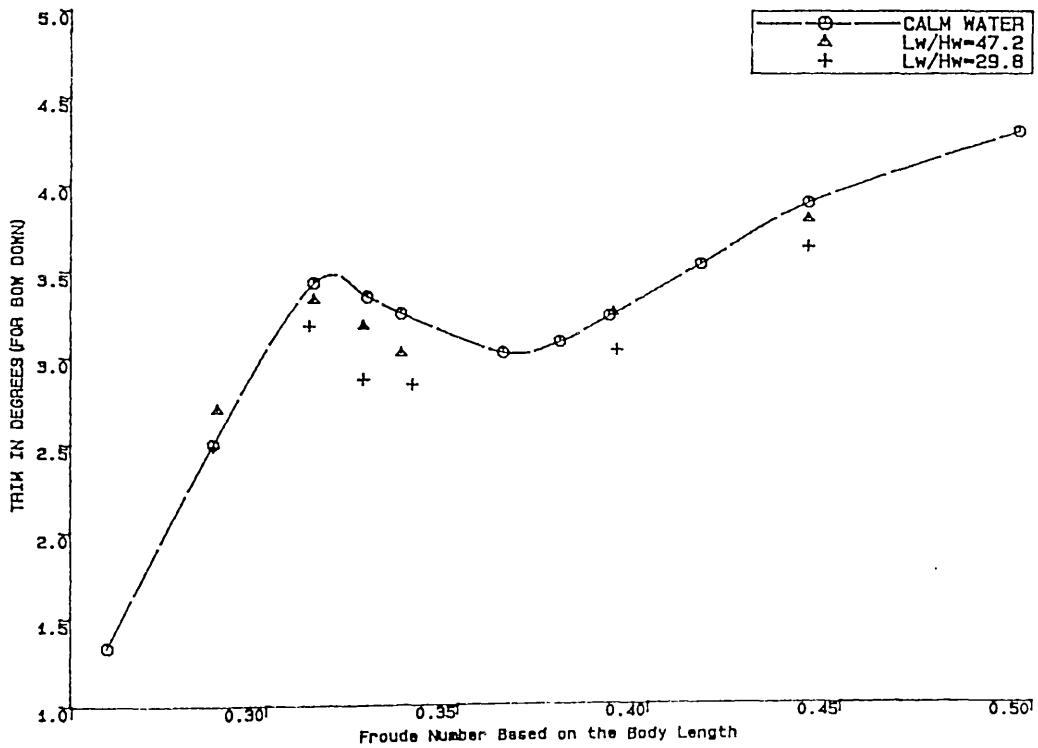

SWATH1 Model-C5 Trims VS Froude Number (F=0.83Hz, Lw/Lb=1.5)

Fig.4.62

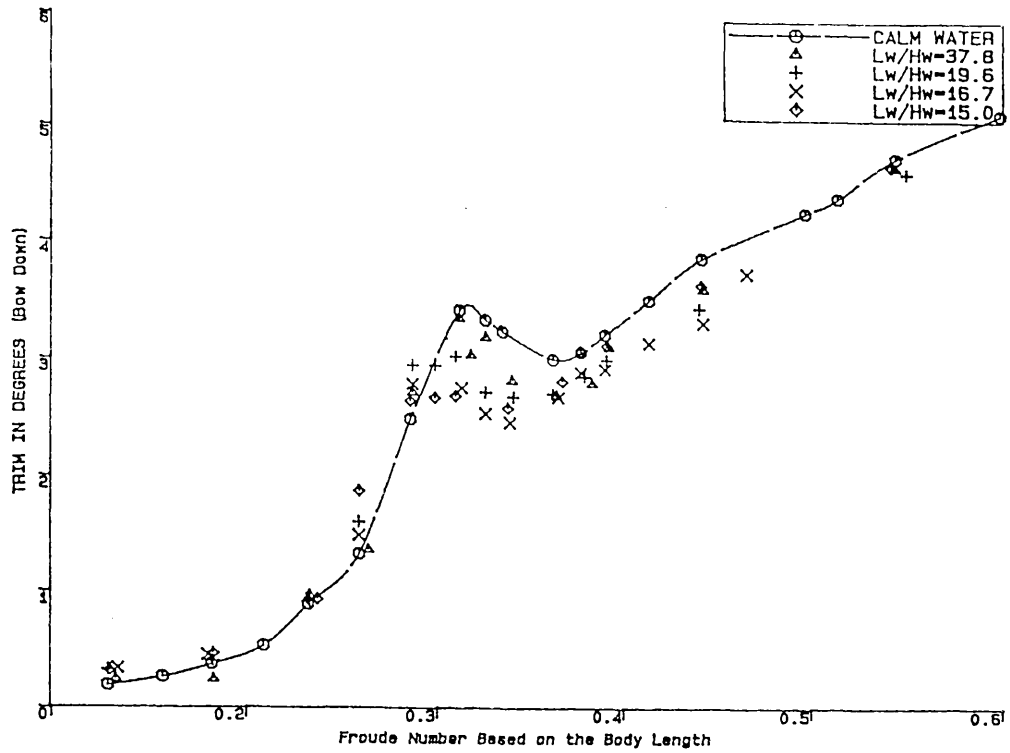

SWATH1 Model-C5 Trims vs Froude Number (f=1.02Hz, Lw/Lb=1.0)

Fig.4.63

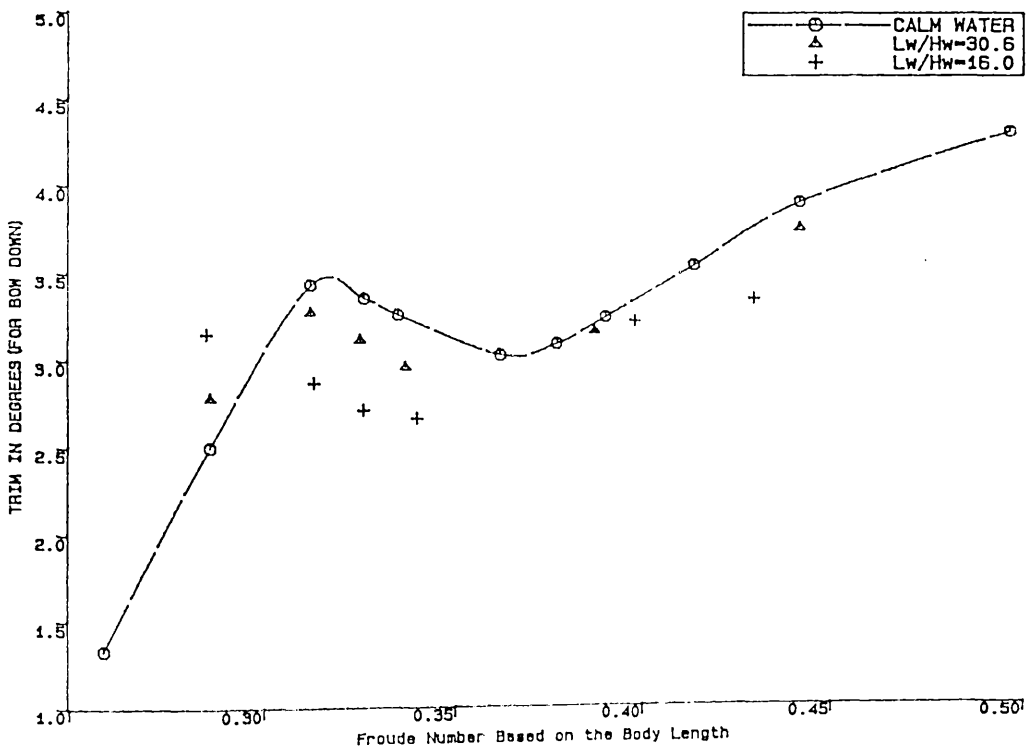

SWATH1 Model-C5 Trims vs Froude Number (f=1.17Hz, Lw/Lb=0.75)

Fig.4.64

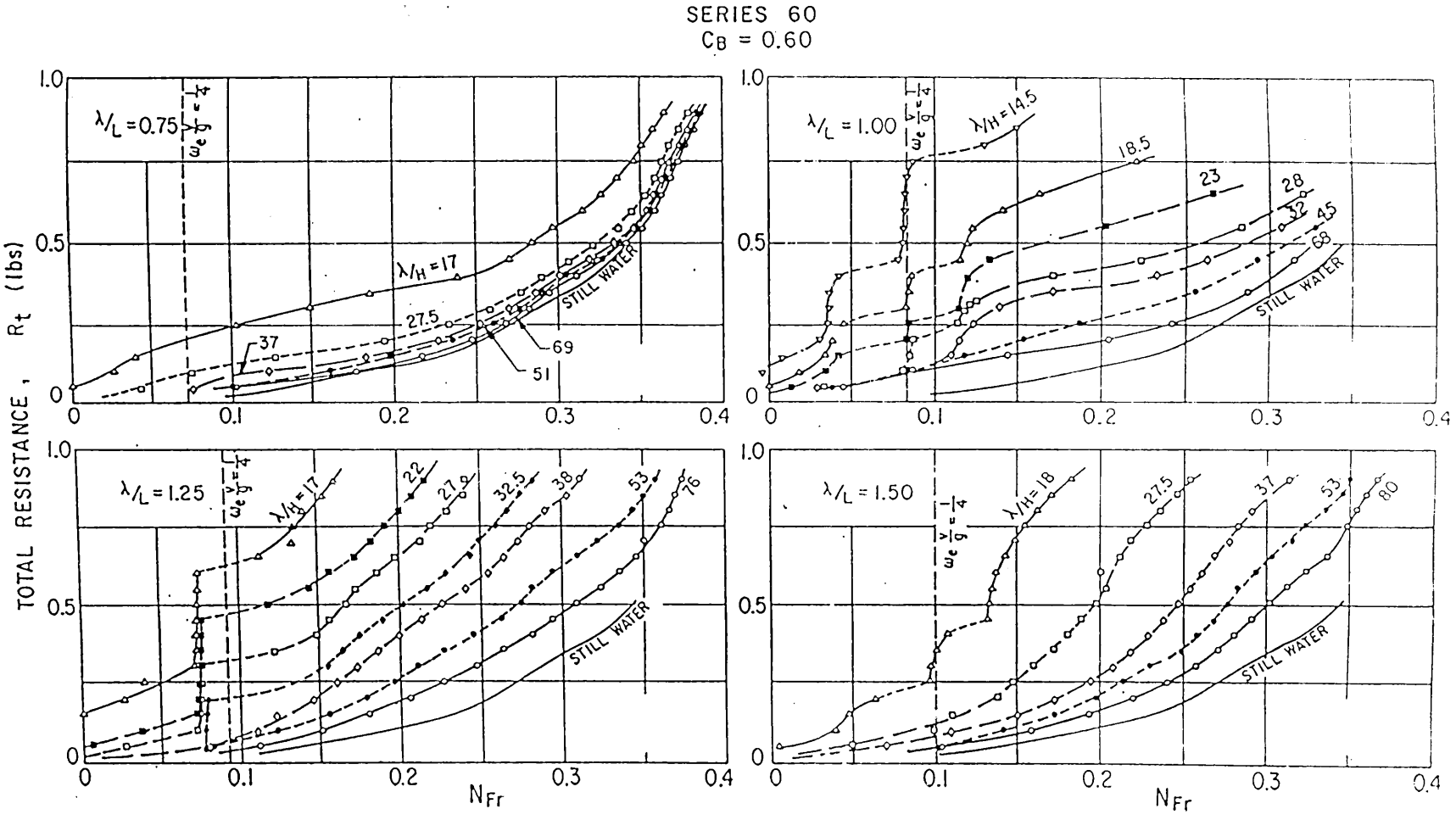

TOTAL RESISTANCE AS A FUNCTION OF FROUDE NUMBER

Fig.4.65

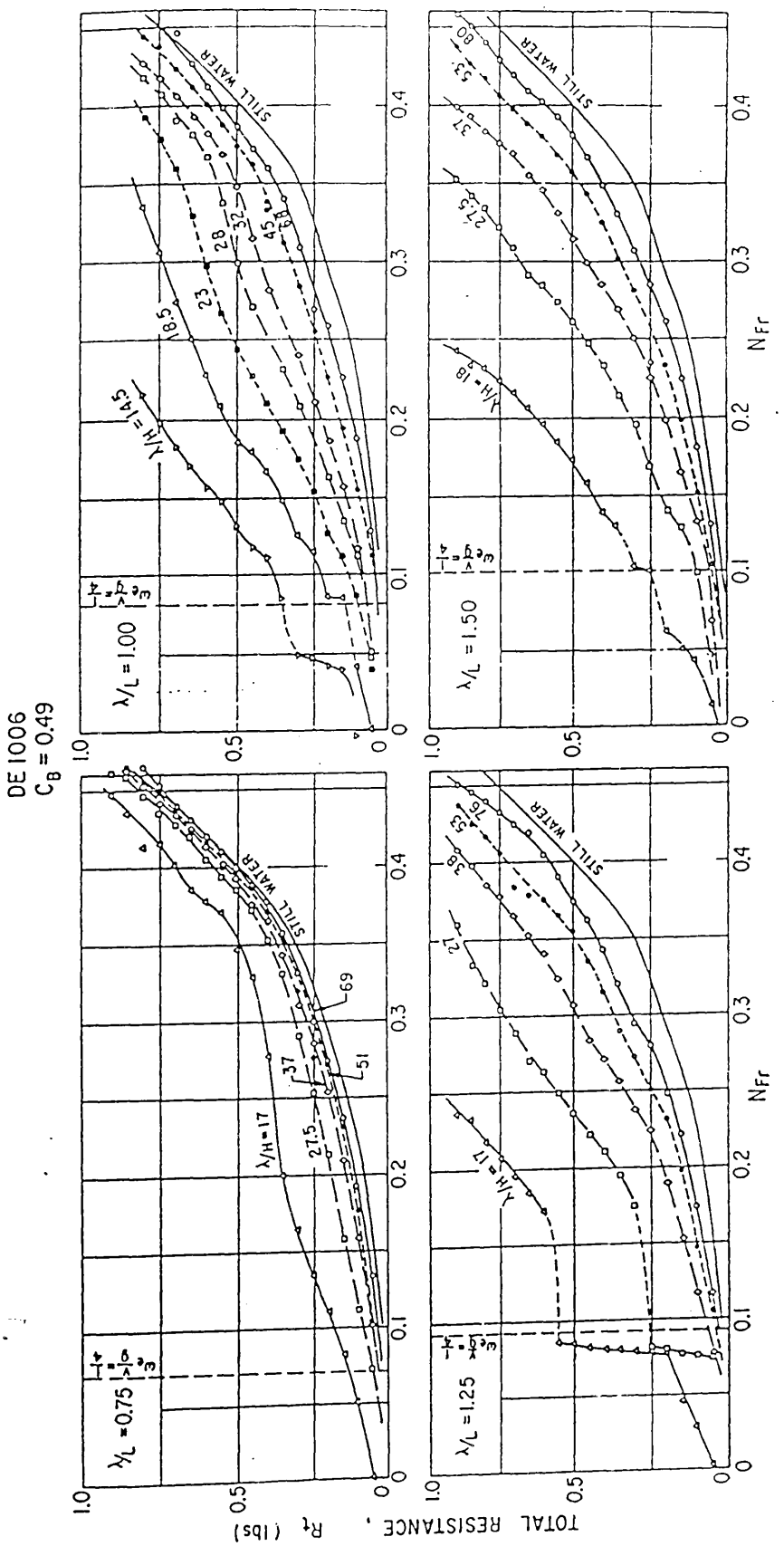

TOTAL RESISTANCE AS A FUNCTION OF FROUDE NUMBER

Fig.4.66

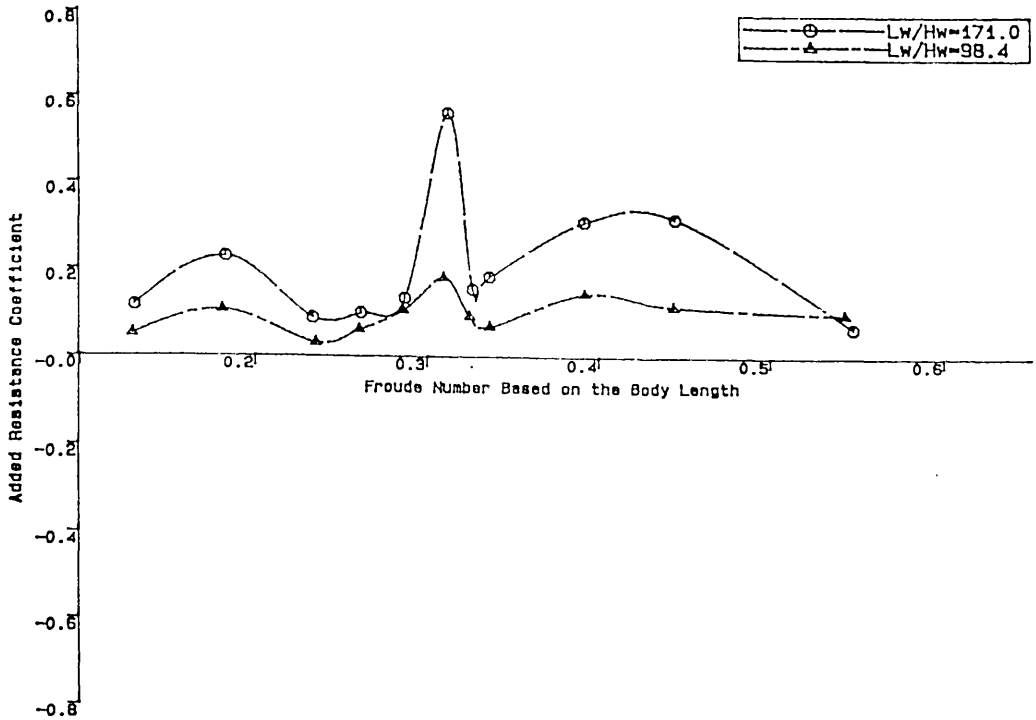

SWATH1 Model-C5 Added Resi. Coefficient vs Fn (f=0.45hz, Lw/Lb=5.1)

Fig.4.67

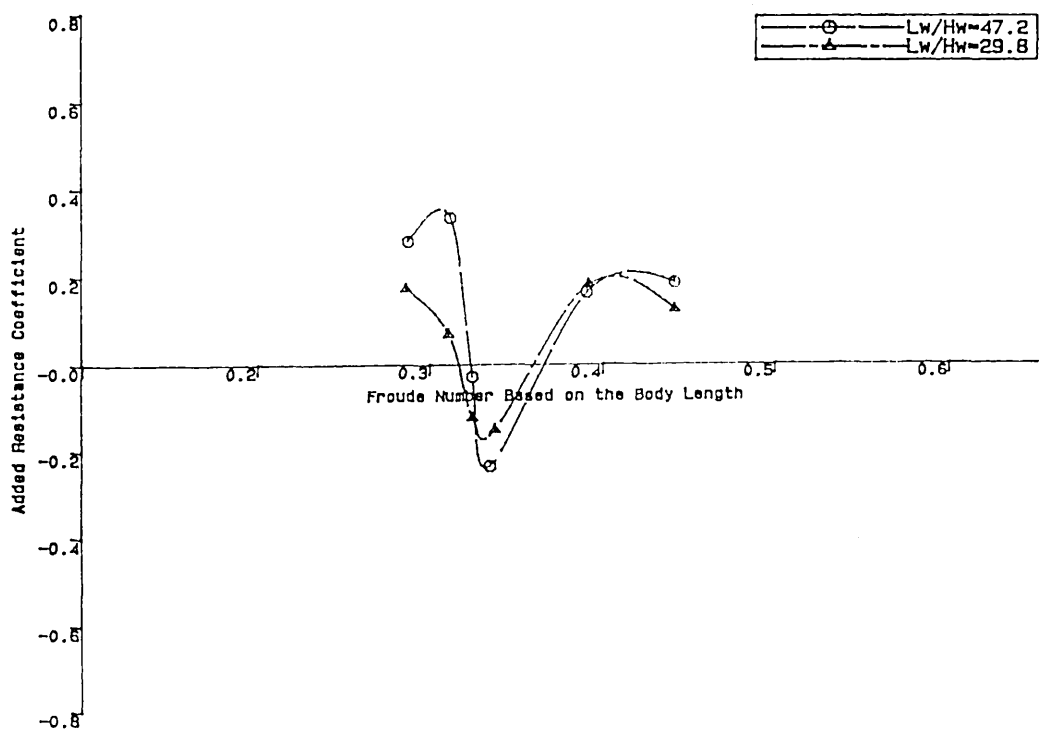

SWATH1 Model-C5 Added Resi. Coefficient vs Fn (f=0.83Hz, Lw/LB=1.5)

Fig.4.68

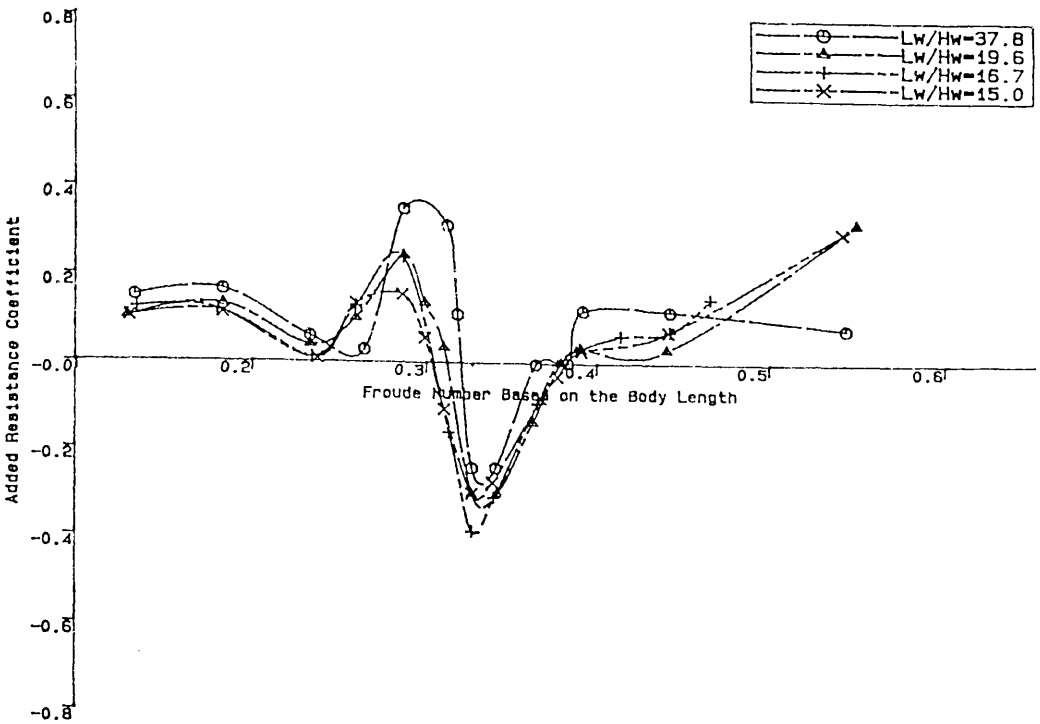

SWATH1 Model-C5 Added Resi. Coefficient vs Fn (f=1.02Hz, Lw/Lb=1.0)

Fig.4.69

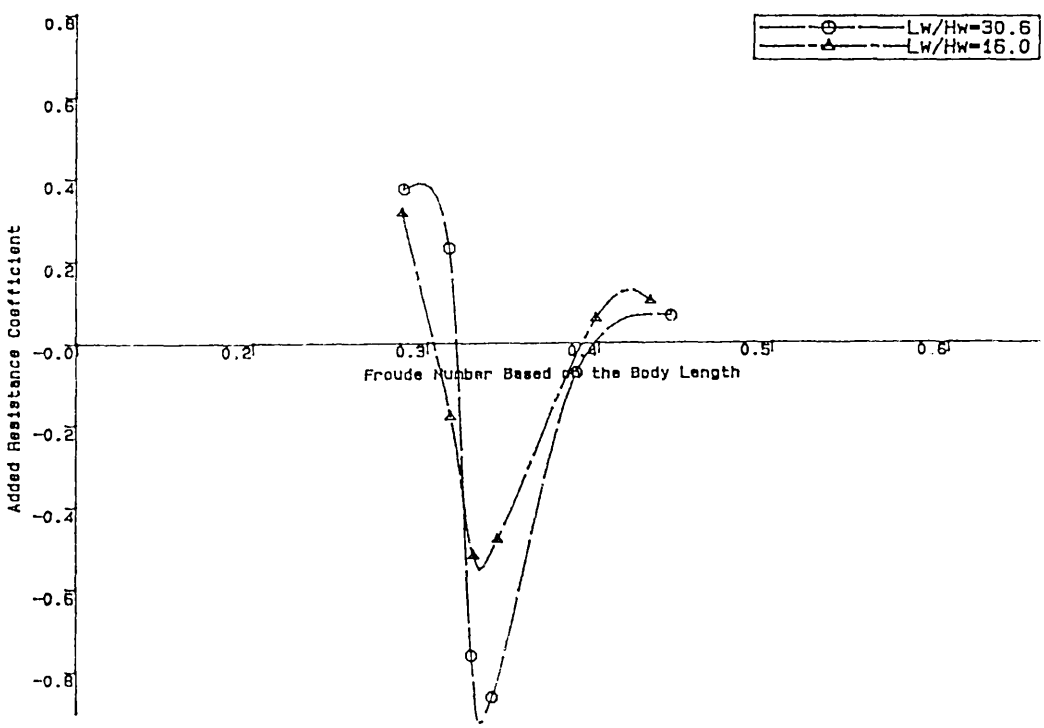

SWATH1 Model-C5 Added Resi. Coefficient vs Fn (f=1.17Hz, Lw/LB=0.75)

Fig.4.70

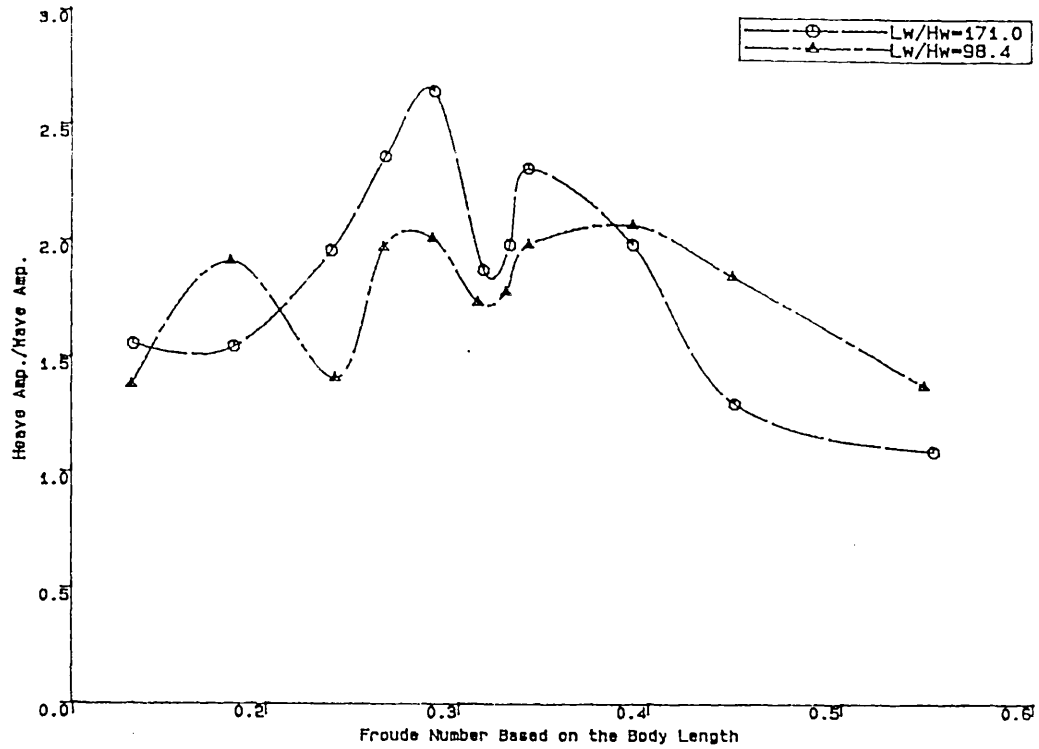

SWATH1 Model-C5 Heave Responses in Head Seas as Functions of Froude Number and Wave Steepness (Wave Frequency=0.45Hz, Lw/Lb=5.1).

Fig.4.71

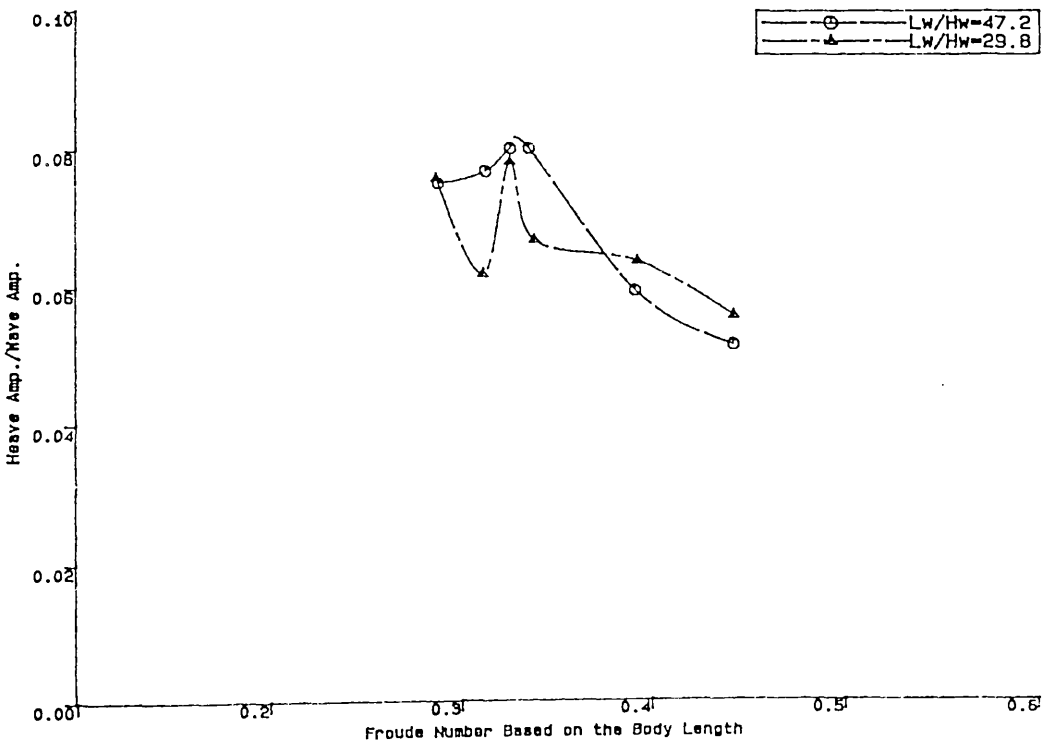

SWATH1 Model-C5 Heave Responses in Head Seas as a Function of Froude Number and Wave Steepness (Wave Frequency=0.83Hz, Lw/Lb=1.5)

Fig.4.72

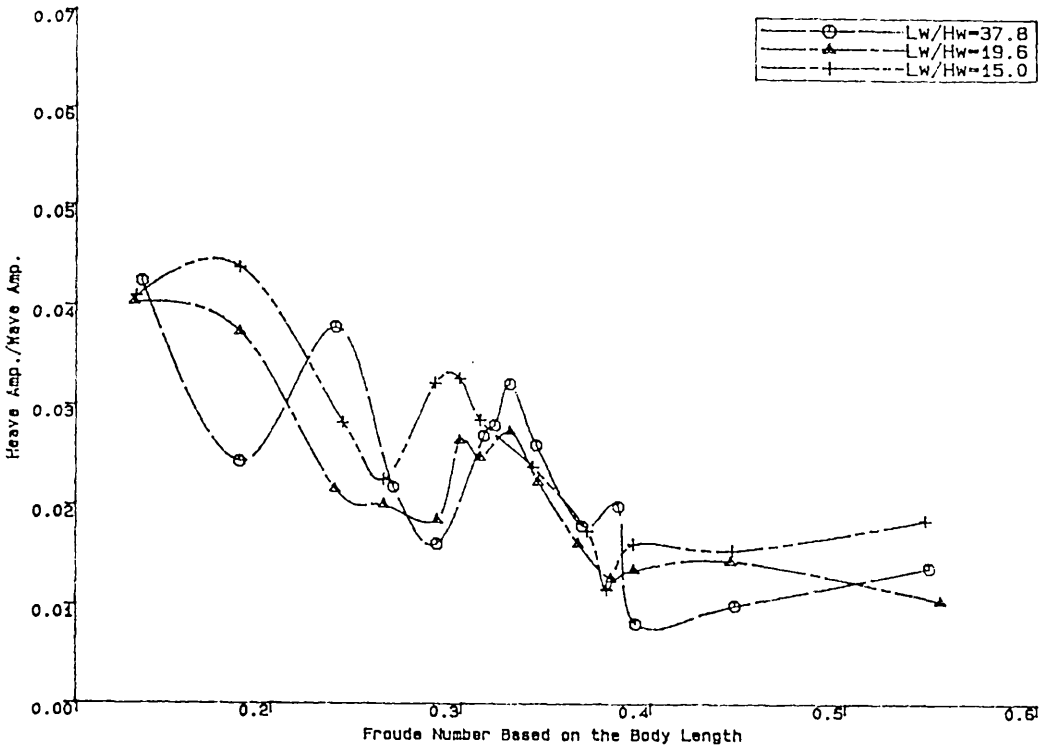

SWATH1 Model-C5 Heave Responses in Head Seas as a Function of Froude Number and Wave Steepness (Wave Frequency=1.02Hz, Lw/Lb=1.0)

Fig.4.73

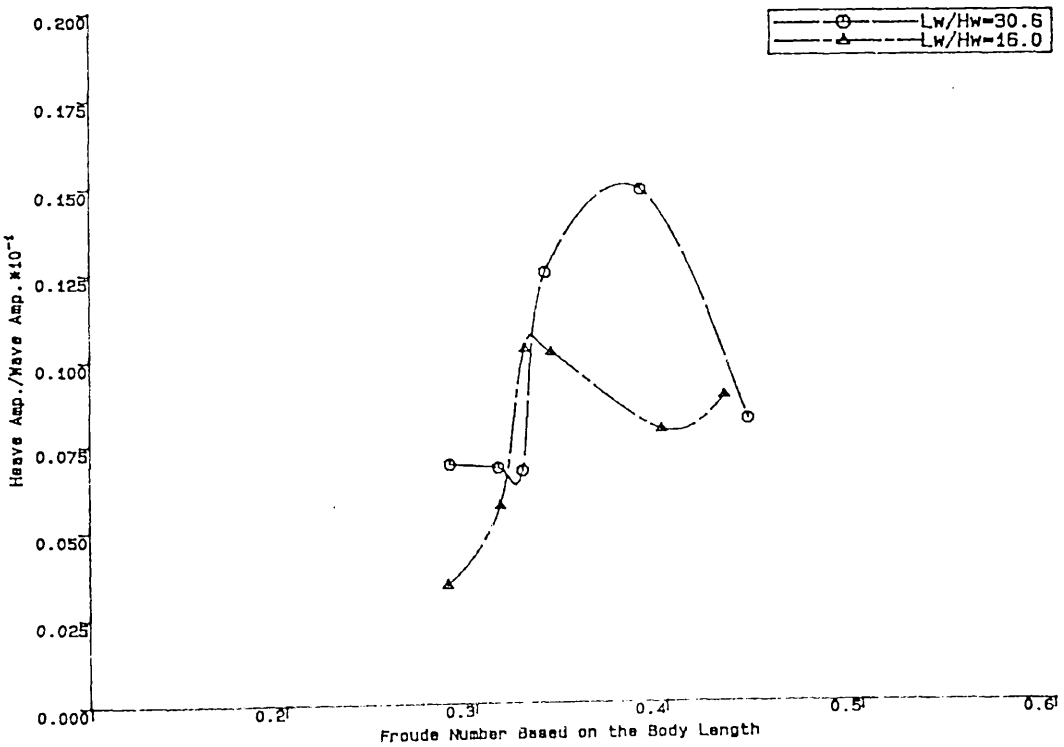

SWATH1 Model-C5 Heave Responses in Head Seas as a Function of Froude Number and Wave Steepness (Wave Frequency=1.17Hz, Lw/Lb=0.75)

Fig.4.74

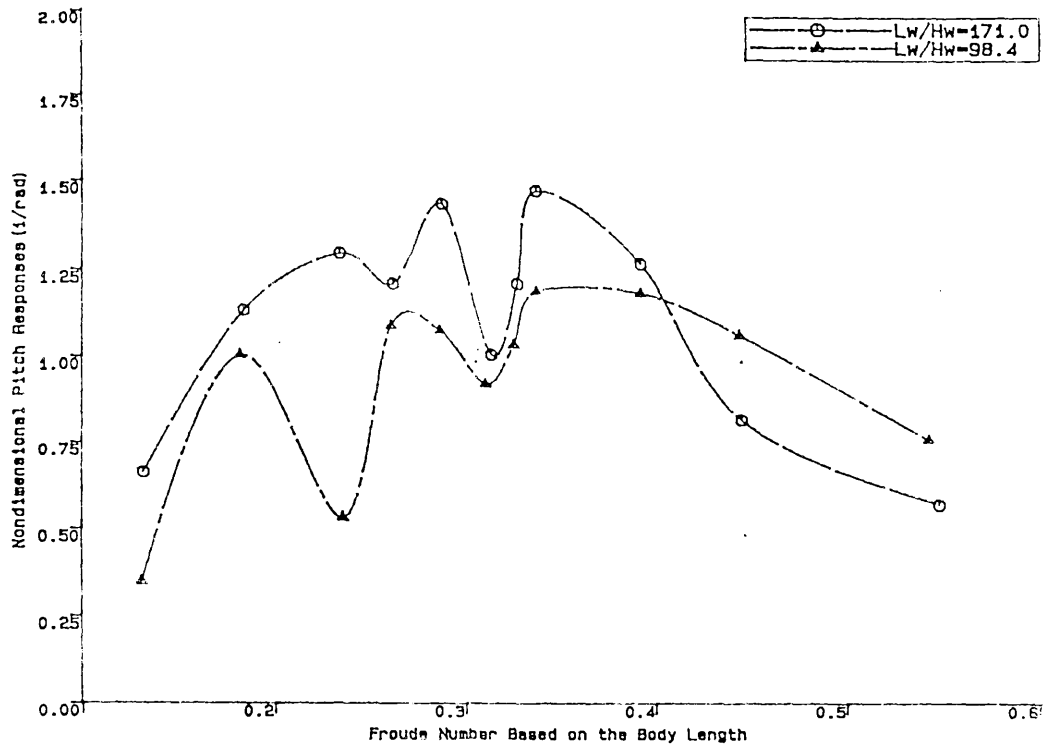

SWATH1 Model-C5 Pitch Responses in Head Seas as a Function of Froude Number and Wave Steepness (Wave Frequency=0.45Hz, Lw/Lb=5.1)

Fig.4.75

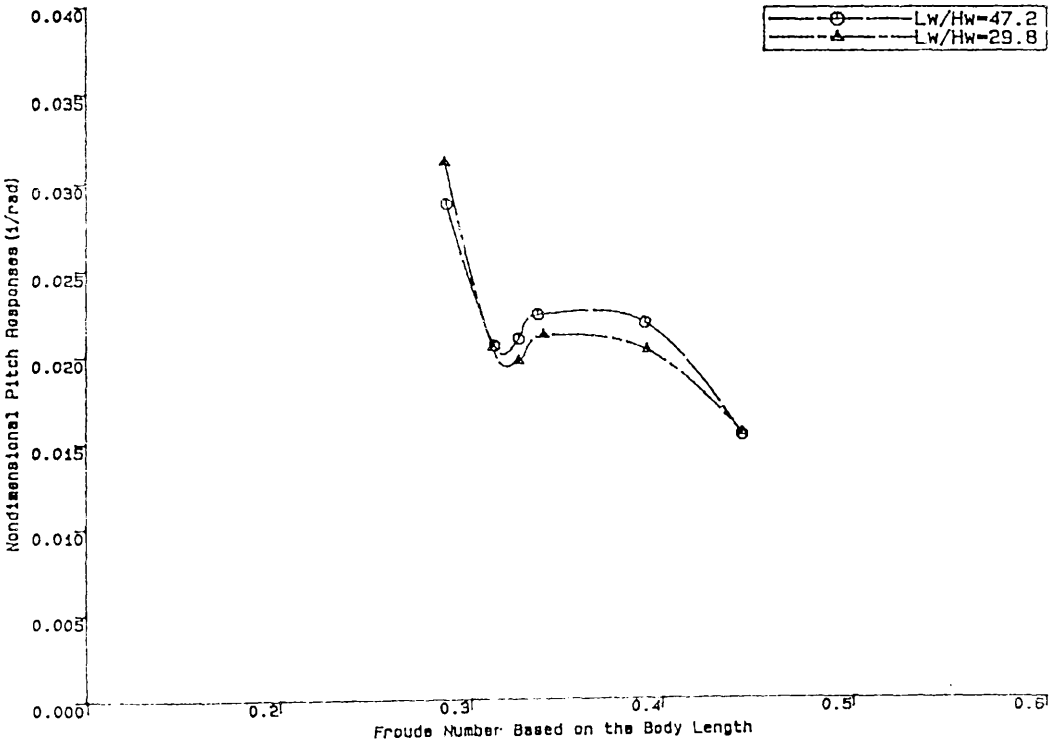

SWATH1 Model-C5 Pitch Responses in Head Seas as a Function of Froude Number and Wave Steepness (Wave Frequency=0.83Hz, Lw/Lb=1.5)

Fig.4.76

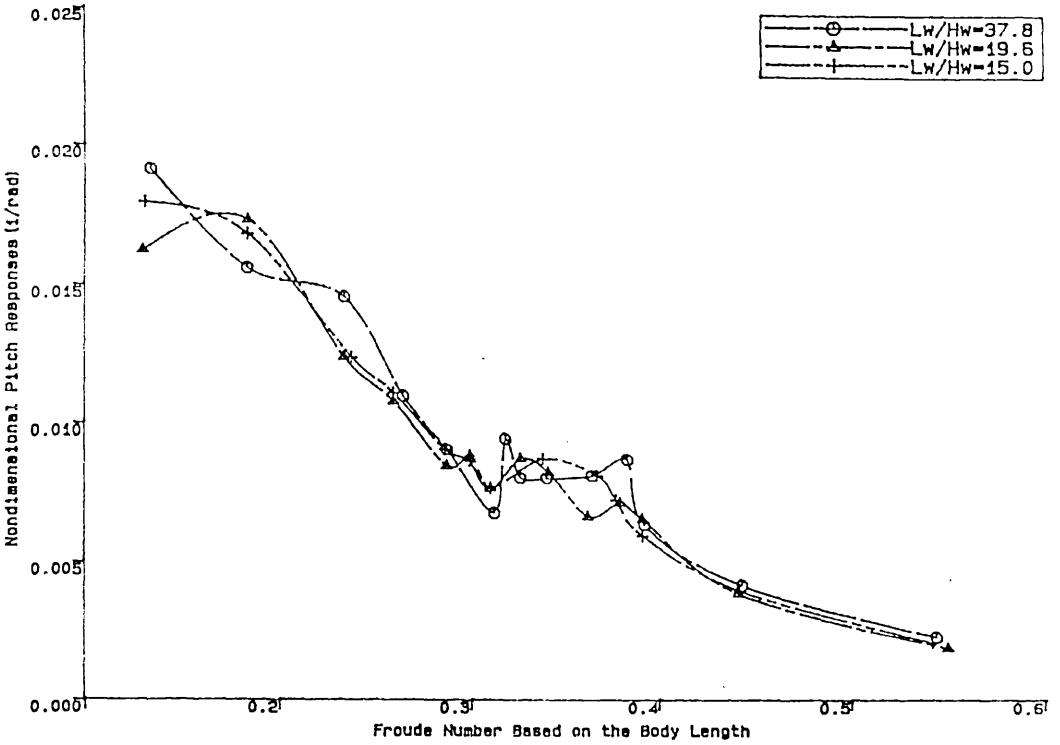

SWATH1 Model-C5 Pitch Responses in Head Seas as a Function of Froude Number and Wave Steepness (Wave Frequency=1.02Hz, Lw/Lb=1.0)

Fig.4.77

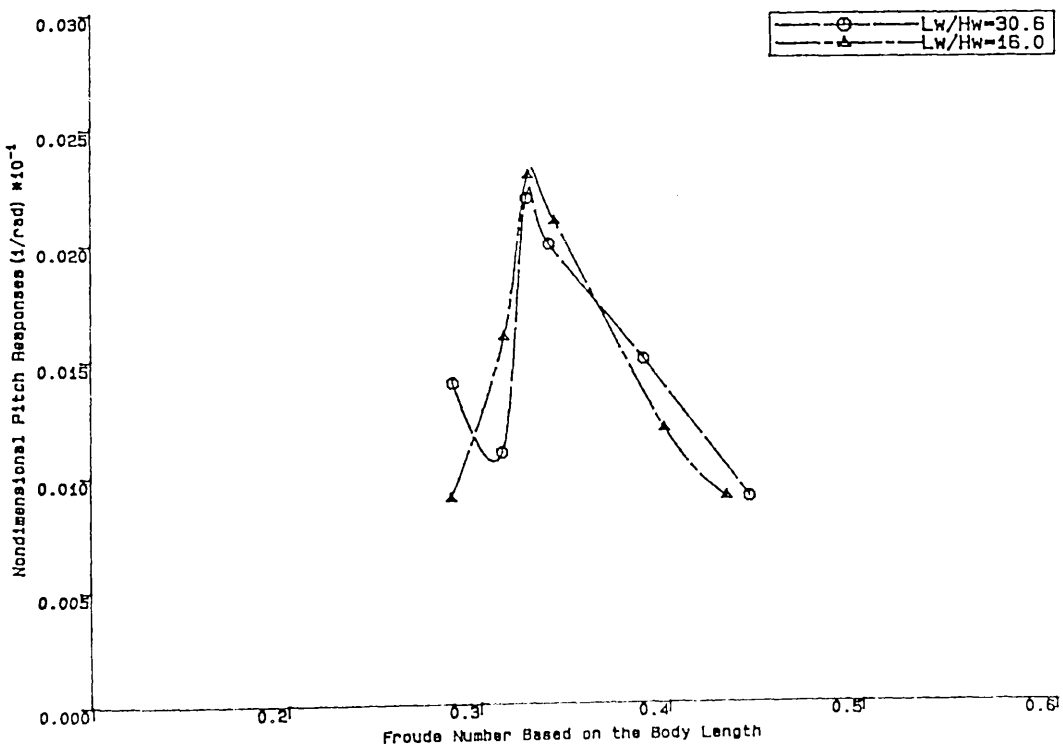

SWATH1 Model-C5 Pitch Responses in Head Seas as Functions of Froude Number and Wave Steepness (Wave Frequency=1.17Hz, Lw/Lb=0.75)

Fig.4.78

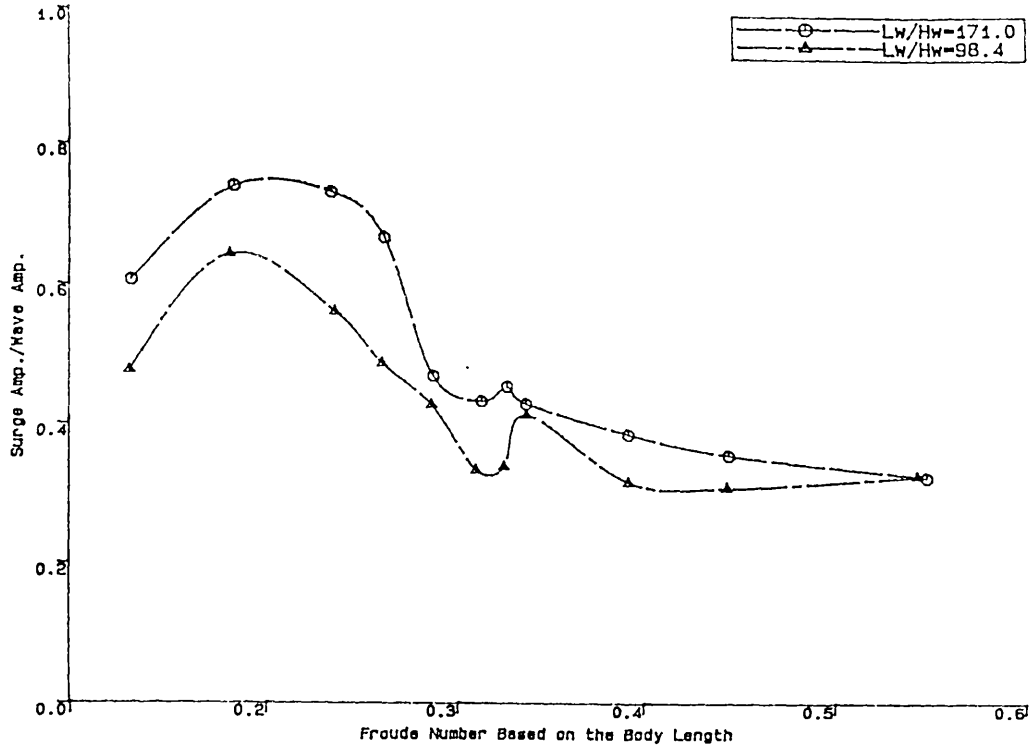

SWATH1 Model-C5 Surge Responses in Head Seas as Functions of Froude Number and Wave Steepness (Wave Frequency=0.45Hz, Lw/Lb=5.1)

Fig.4.79

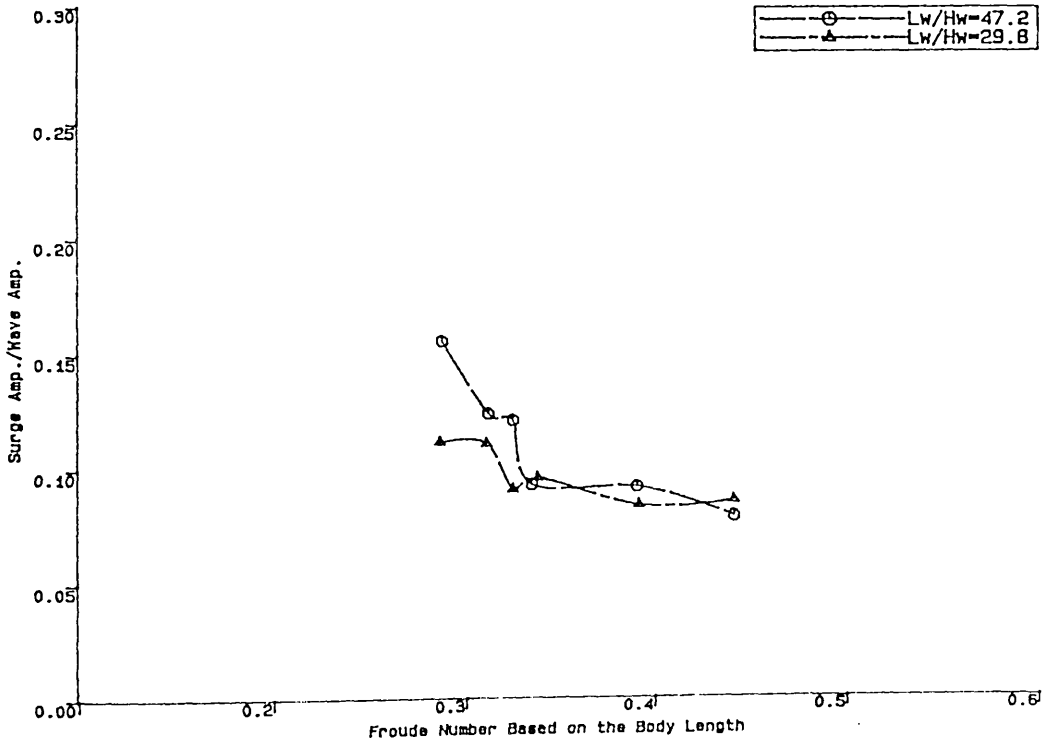

SWATH1 Model-C5 Surge Responses in Head Seas as a Function of Froude Number and Wave Steepness (Wave Frequency=0.83Hz, Lw/Lb=1.5)

Fig.4.80

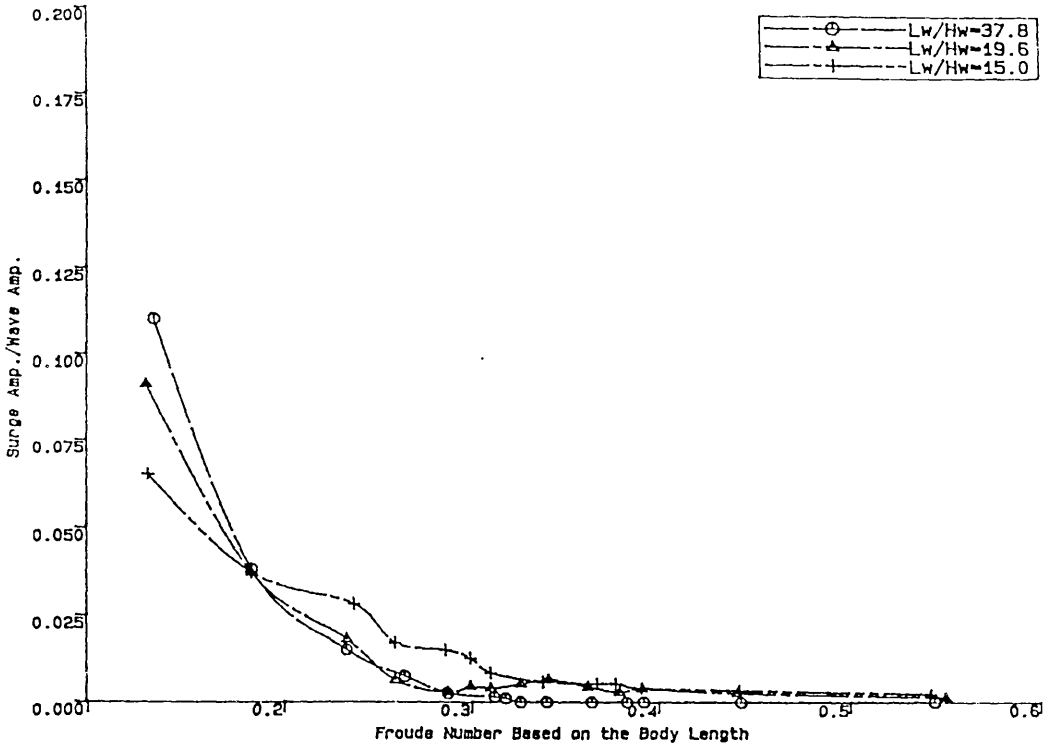

SWATH1 Model-C5 Surge Responses in Head Seas as a Function of Froude Number and Wave Steepness (Wave Frequency=1.02Hz Lw/Lb=1.0)

Fig.4.81

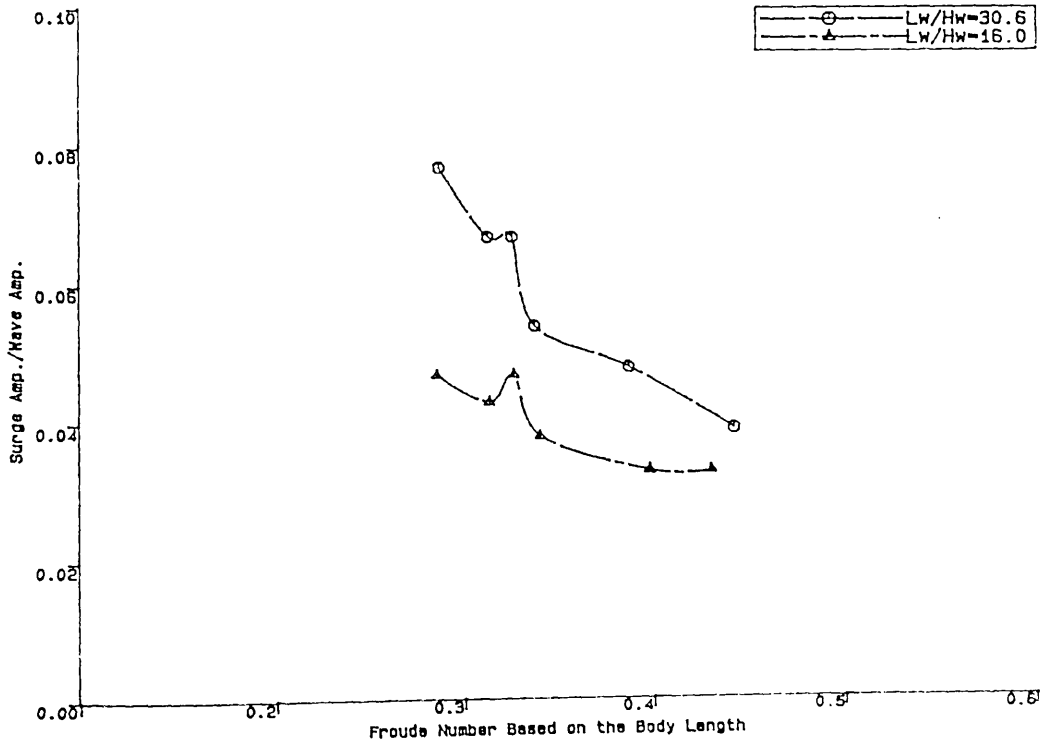

SWATH1 Model-C5 Surgee Responses in Head Seas as a Function of Froude Number and Wave Steepness (Wave Frequency=1.17Hz Lw/Lb=0.75)

Fig.4.82

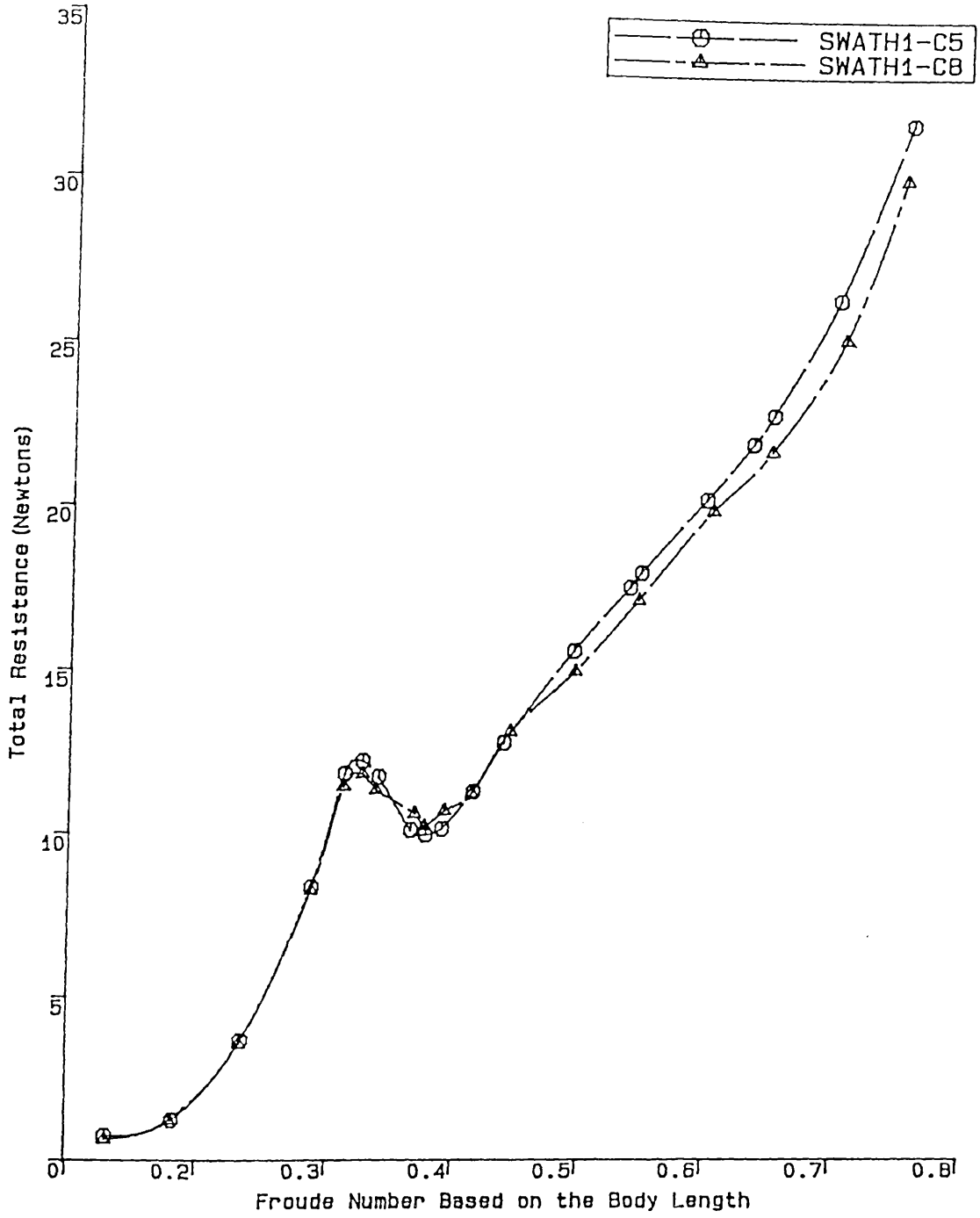

Comparison of the Calm Water Resistances of SWATH1-C5 and SWATH1-C8 versus Froude Number

Fig.4.83

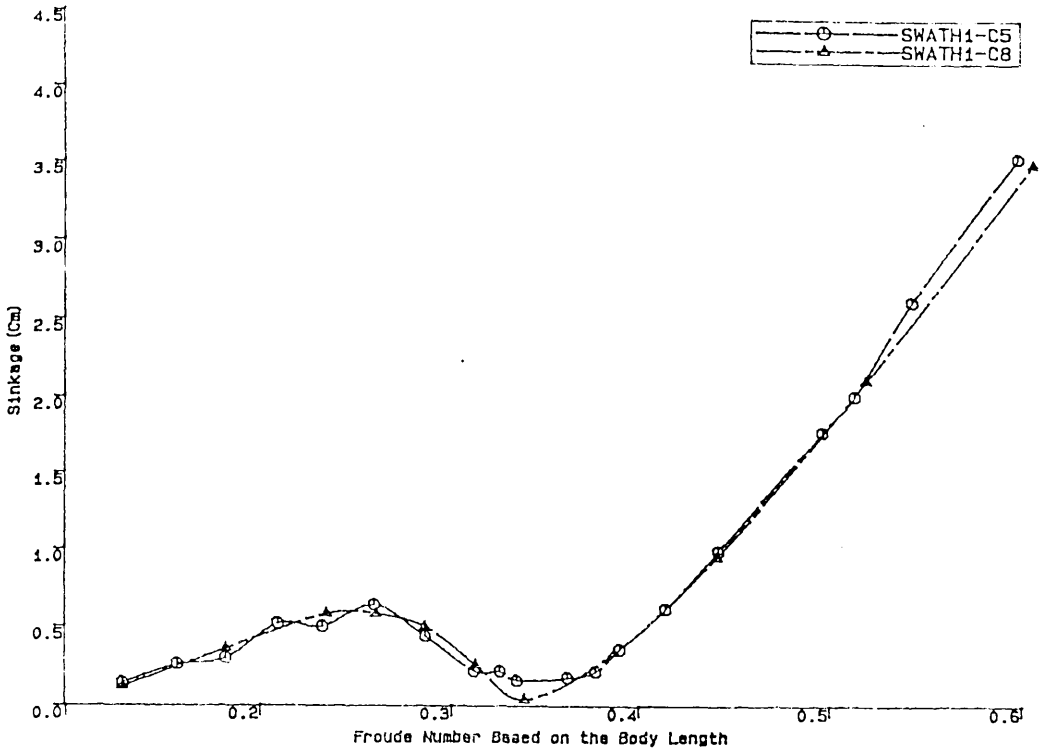

SWATH1 Model Sinkage in Calm Water as a Function of Froude Number

Fig.4.84

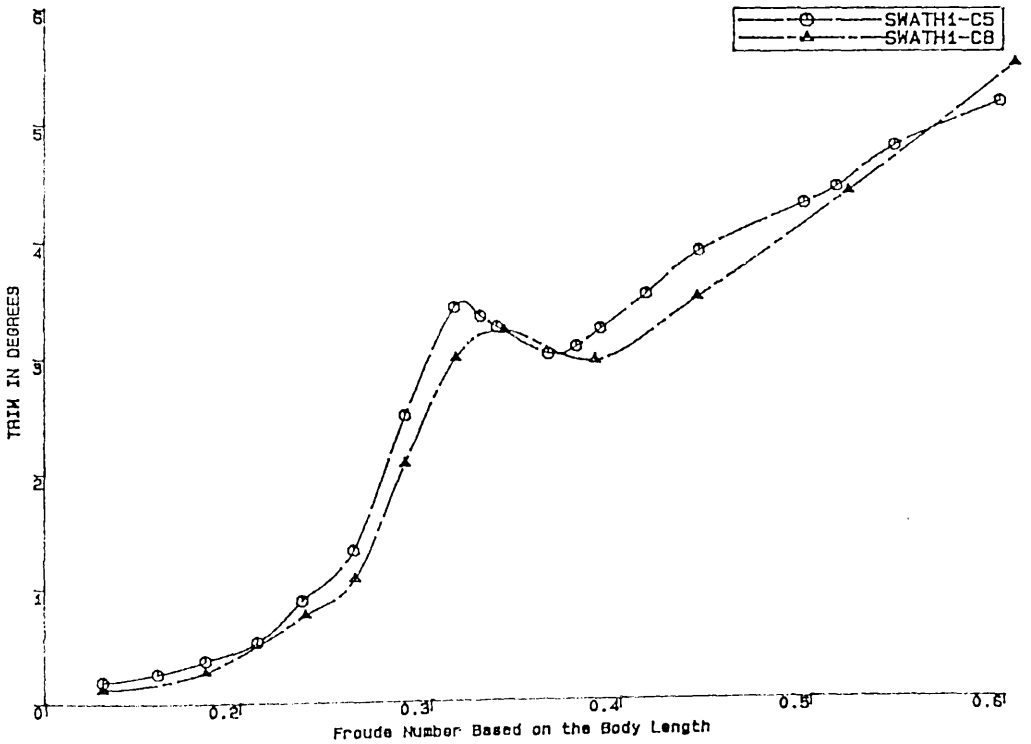

SWATH1 Model Trim in Calm Water as a Function of Froude Number

Fig.4.85

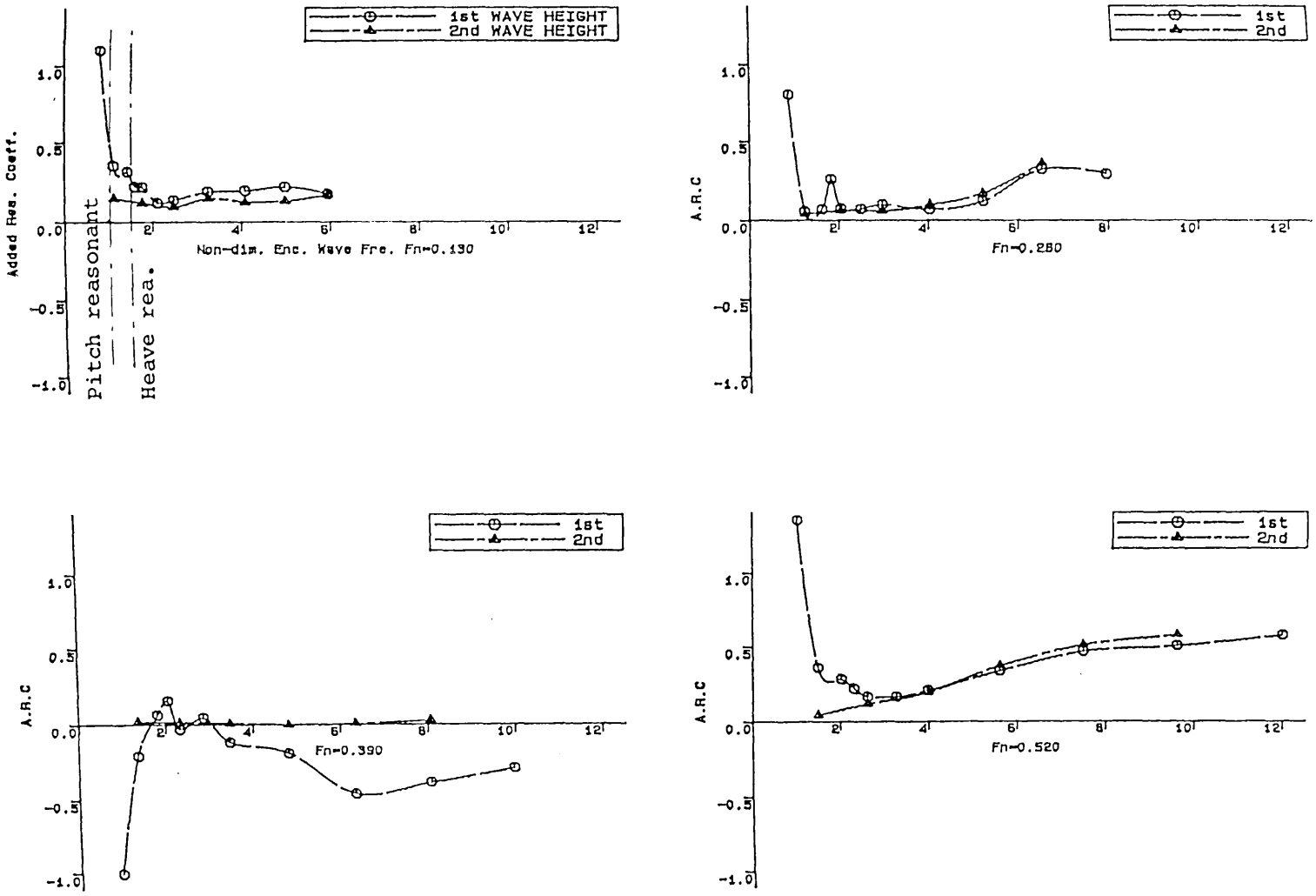

Fig.4.86
SWATH1-C8 Added Resi. Coeffi. vs Non-dim. Encounter Wave Fre. for Four Speeds

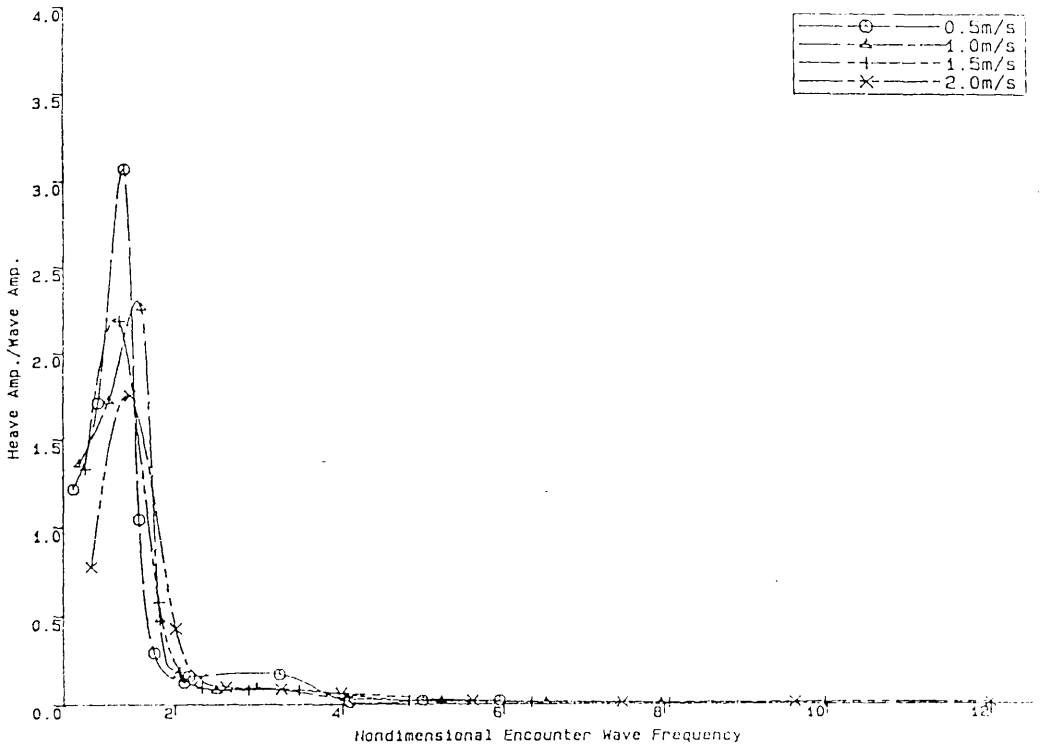

SWATH1-C8 Heave Responses in Head Seas With 4 Forward Speeds

Fig.4.87-a

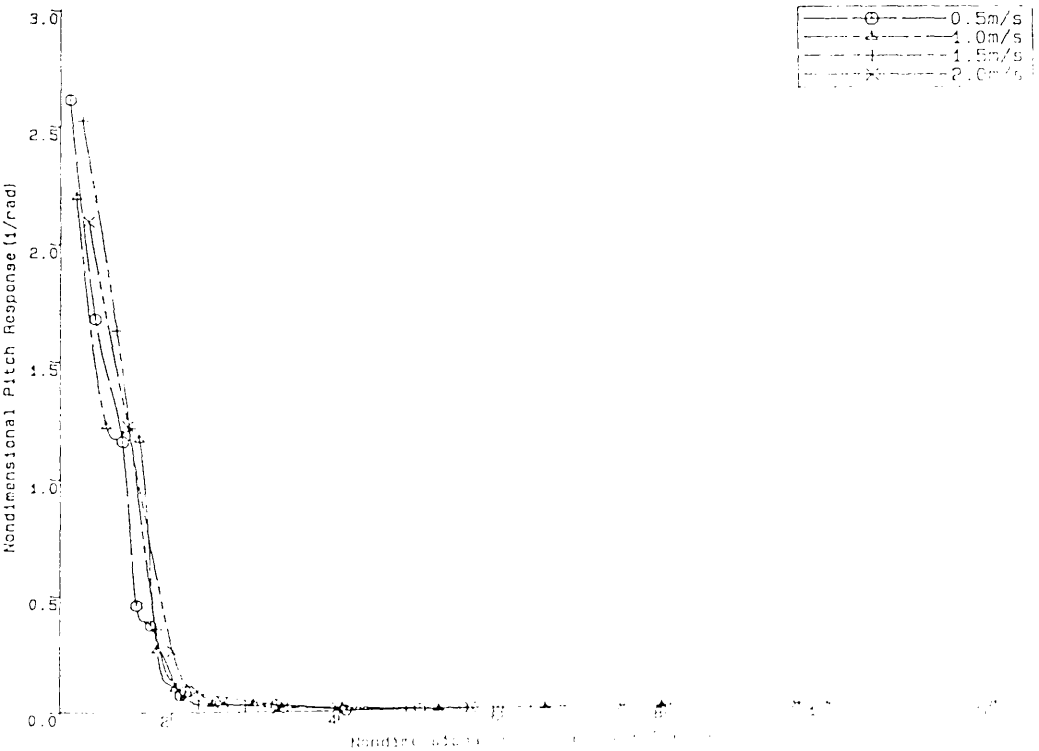

SWATH1-C8 Pitch Responses in Head Seas with 4 Forward Speeds

Fig.4.87-b

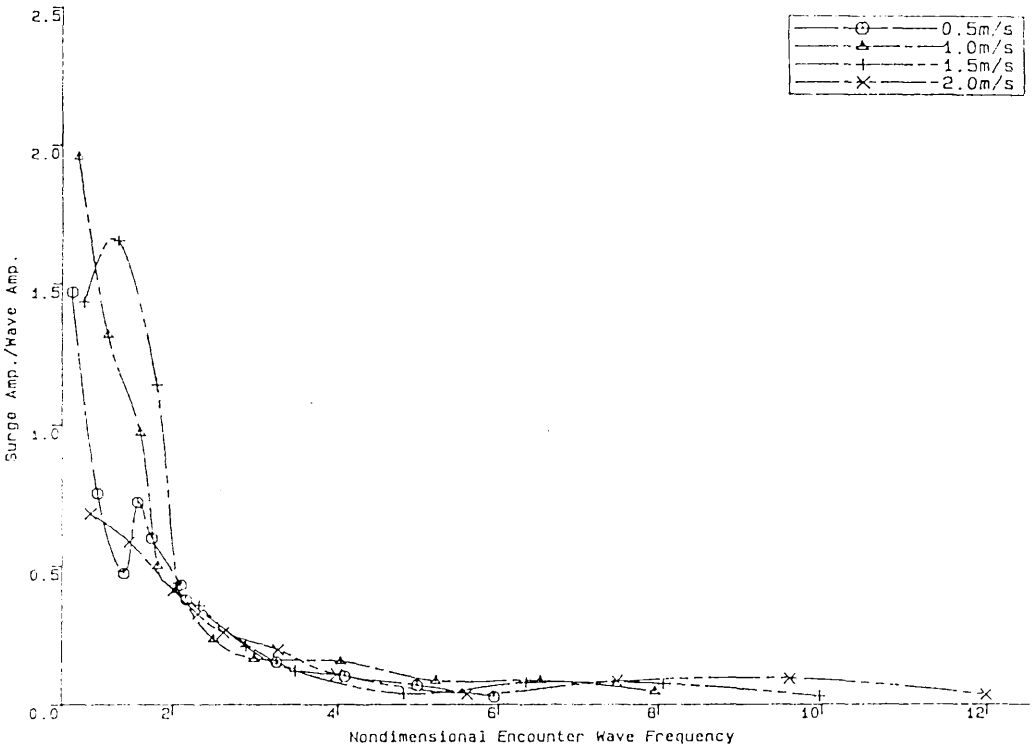

SWATH1-C8 Surge Responses in Head Seas With 4 Forward Speeds

Fig.4.87-c

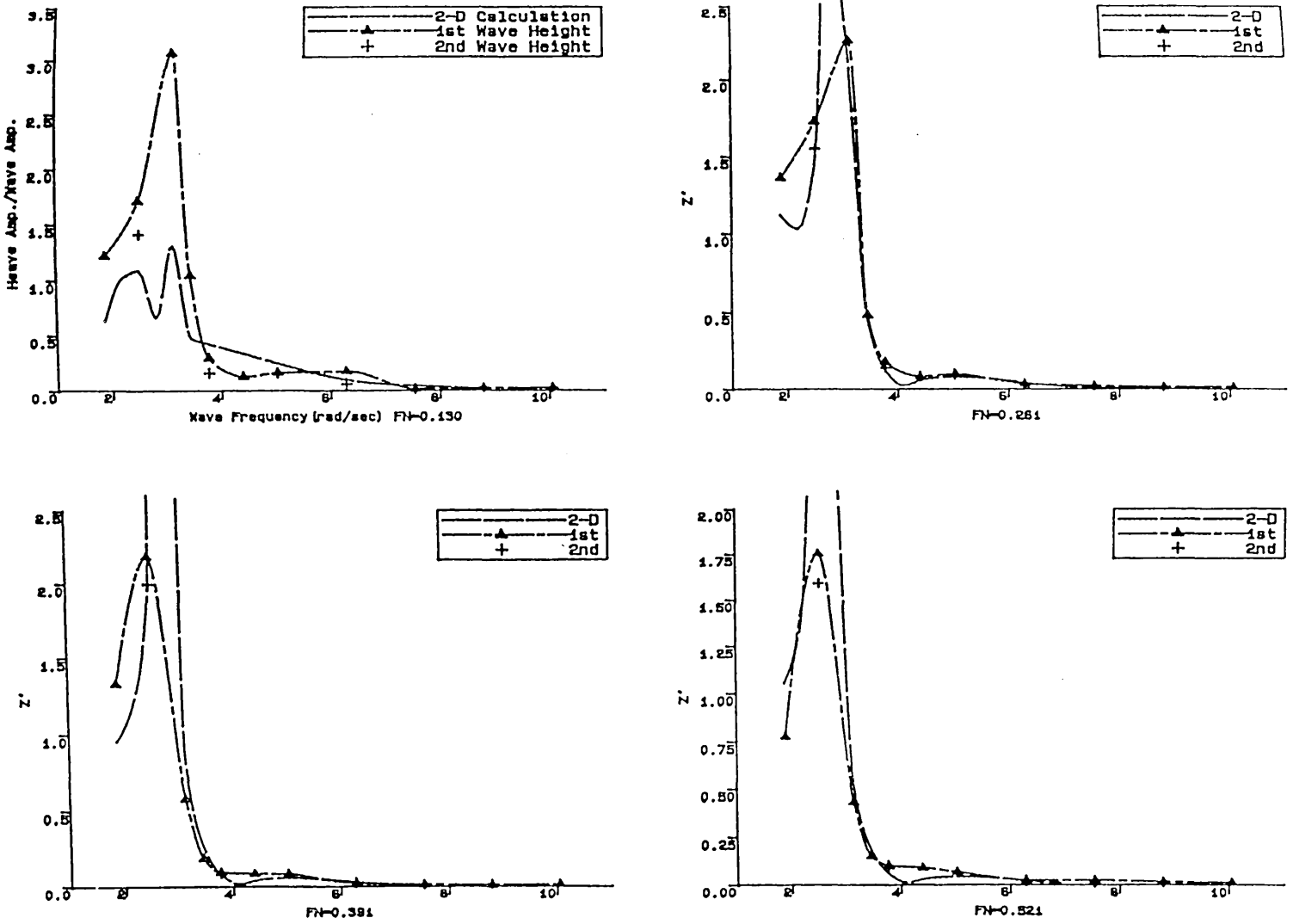

Fig. 4.88
SWATH1-C8 Heave Responses in Head Seas With Different Wave Heights

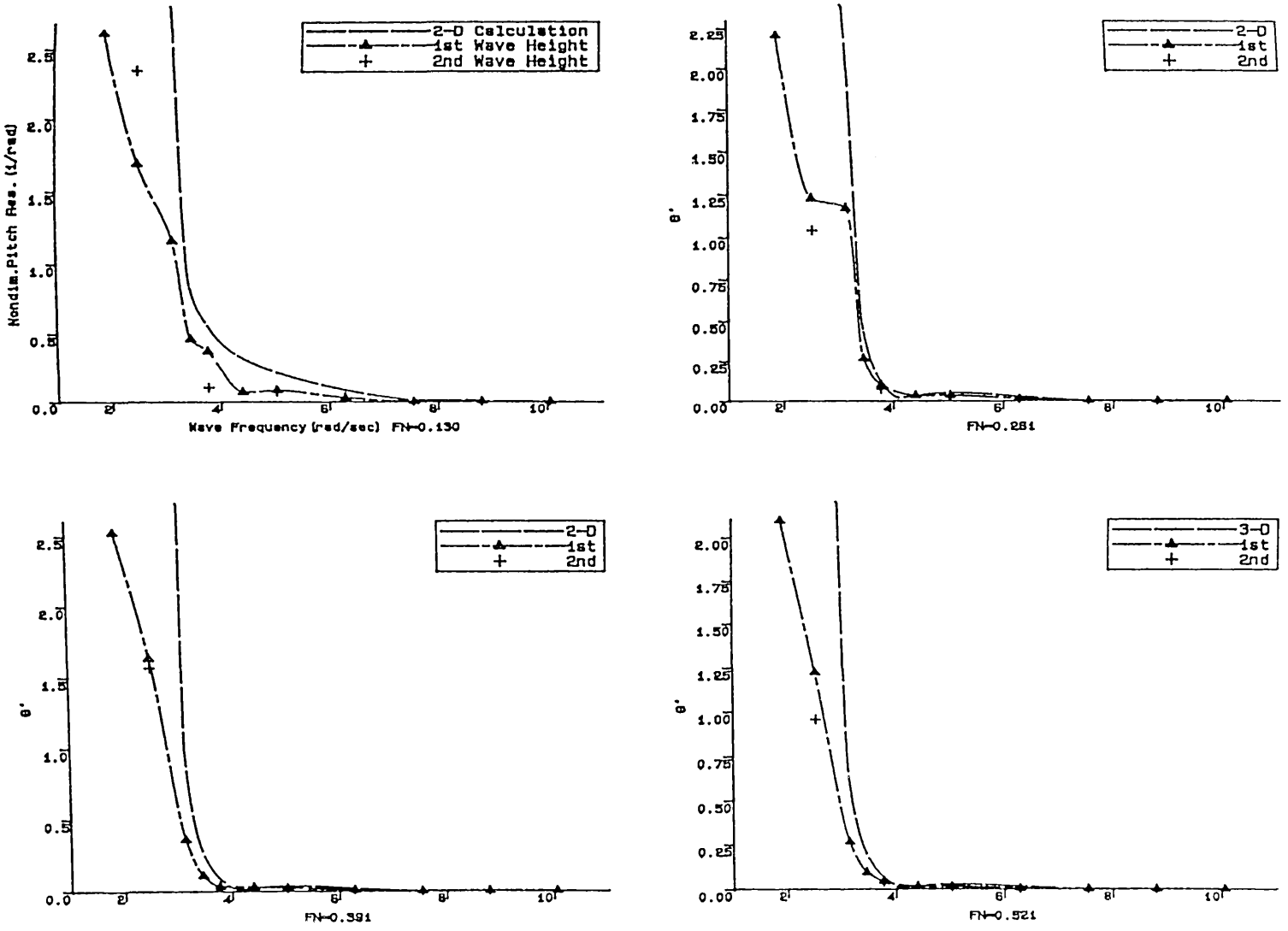

Fig.4.89

SWATH1-C8 Pitch Responses in Head Seas With Different Wave Heights

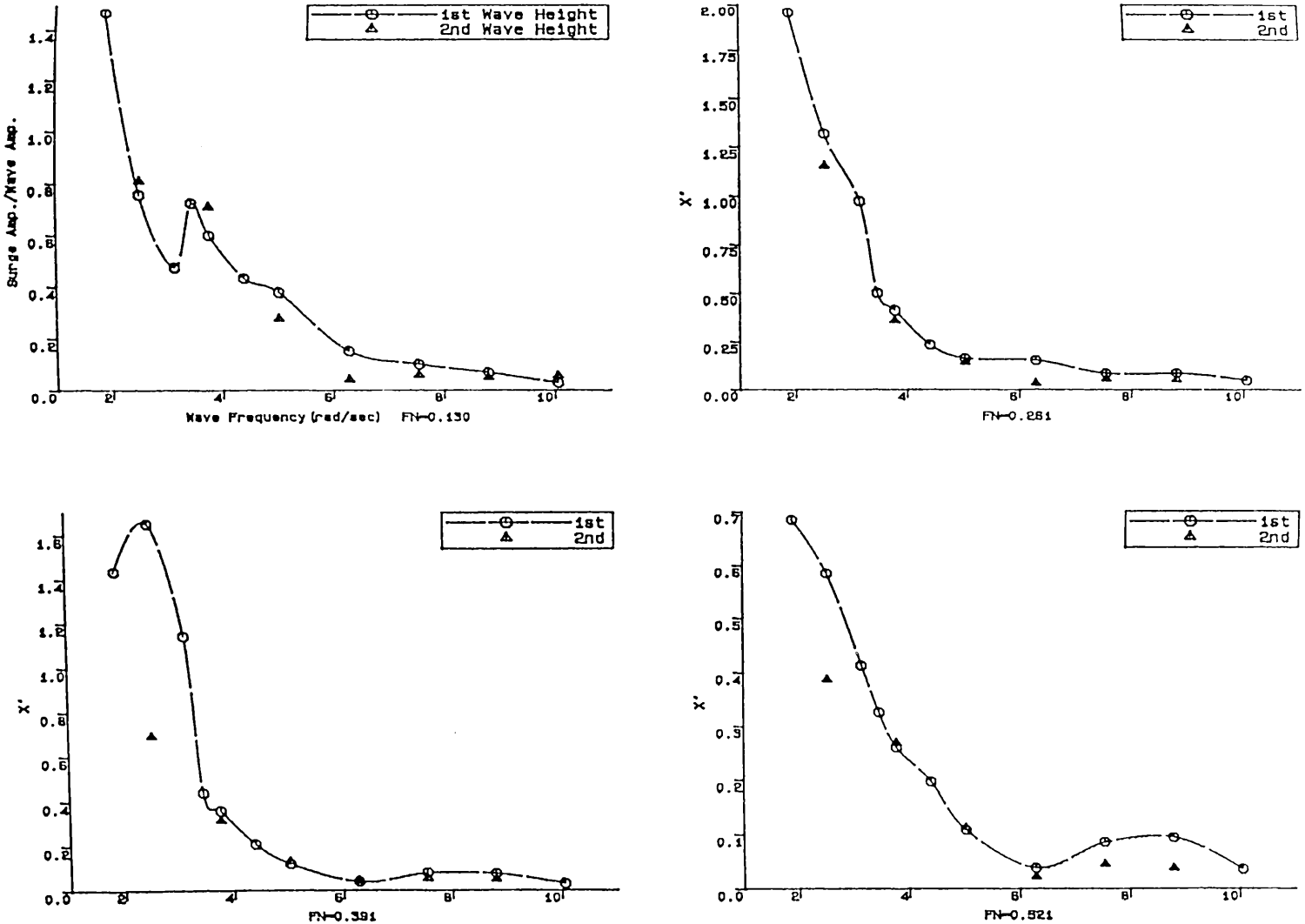

Fig.4.90

SWATH1-C8 Surge Responses in Head Seas With Different Wave Heights

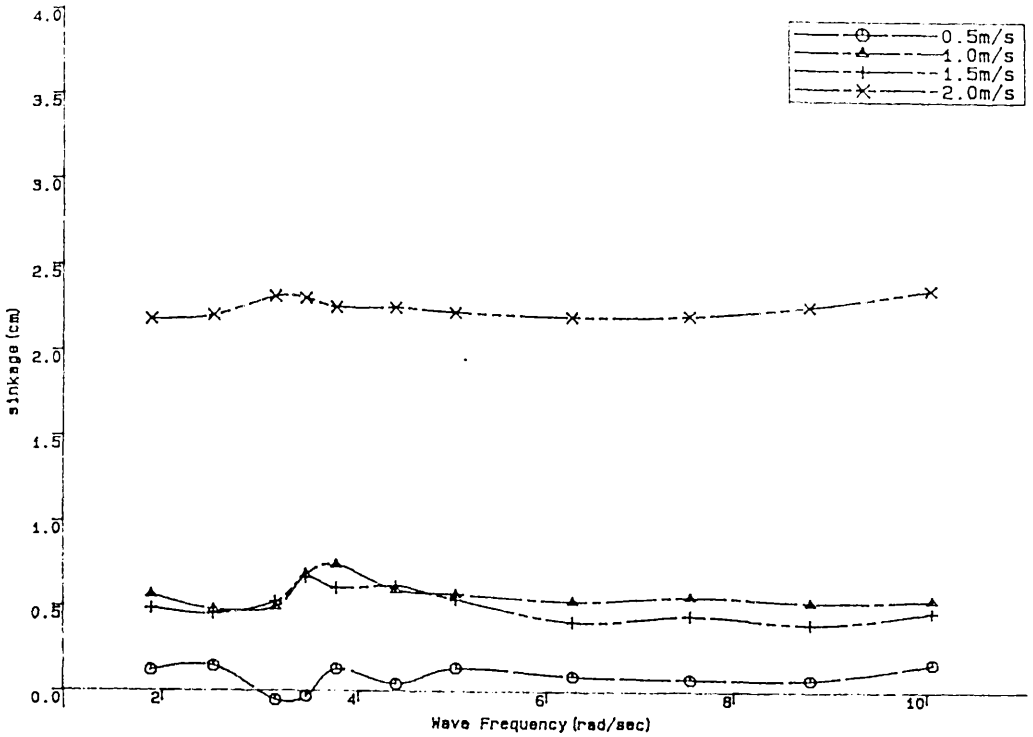

SWATH1-C8 Sinkages in Waves as a Function of Wave Frequency and Speed.

Fig.4.91

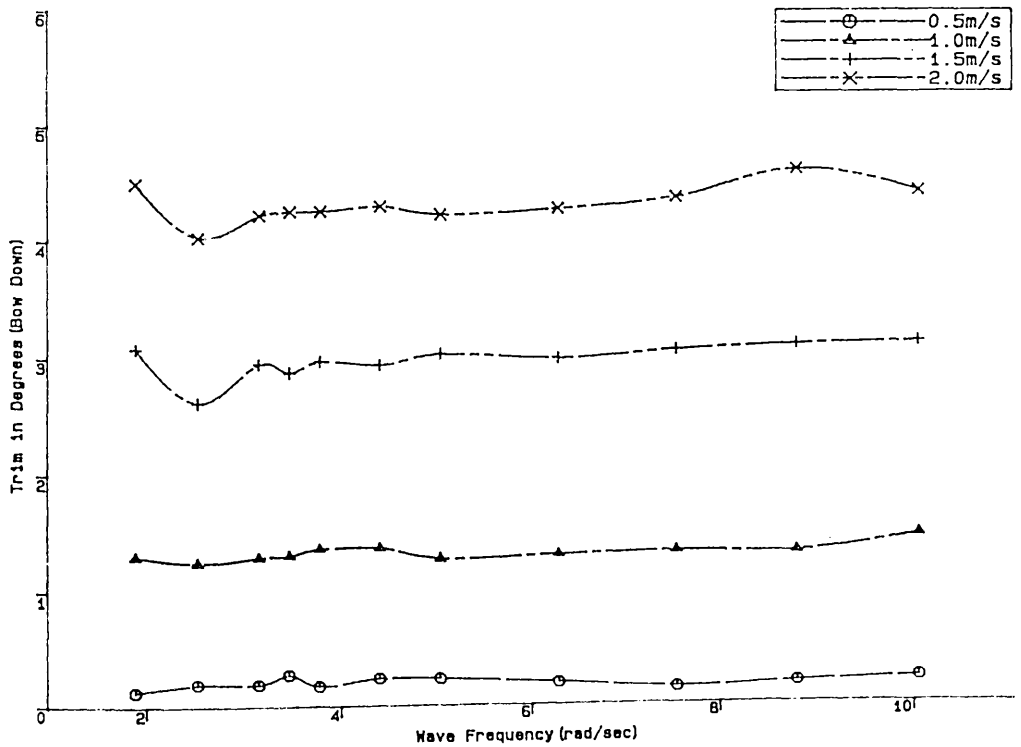

SWATH1-C8 Trims in Waves as a Function of Wave Frequency and Speed.

Fig.4.92

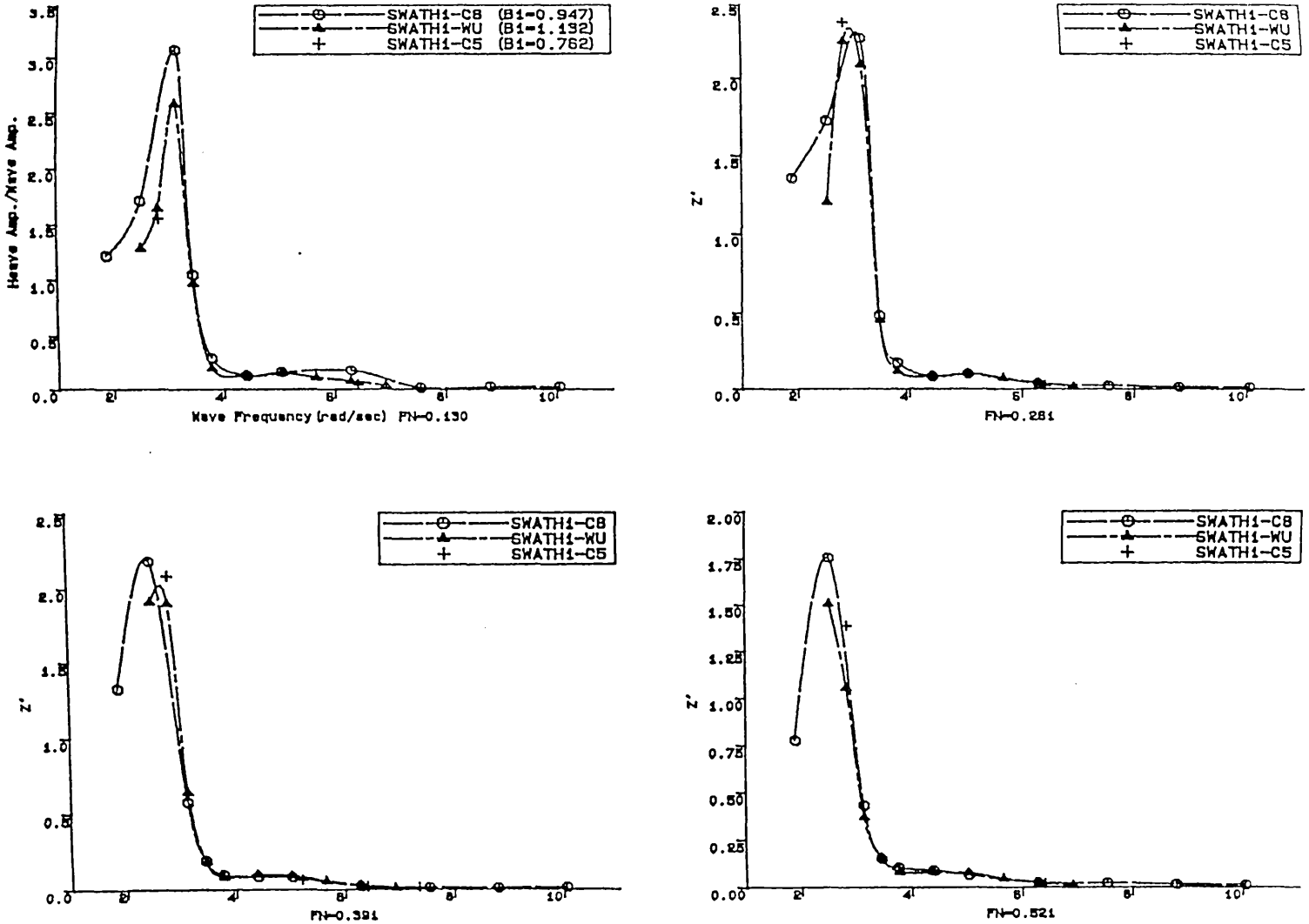

Fig.4.93

SWATH1 Model Heave Responses in Head Seas For Three Spacings Between Demihulls

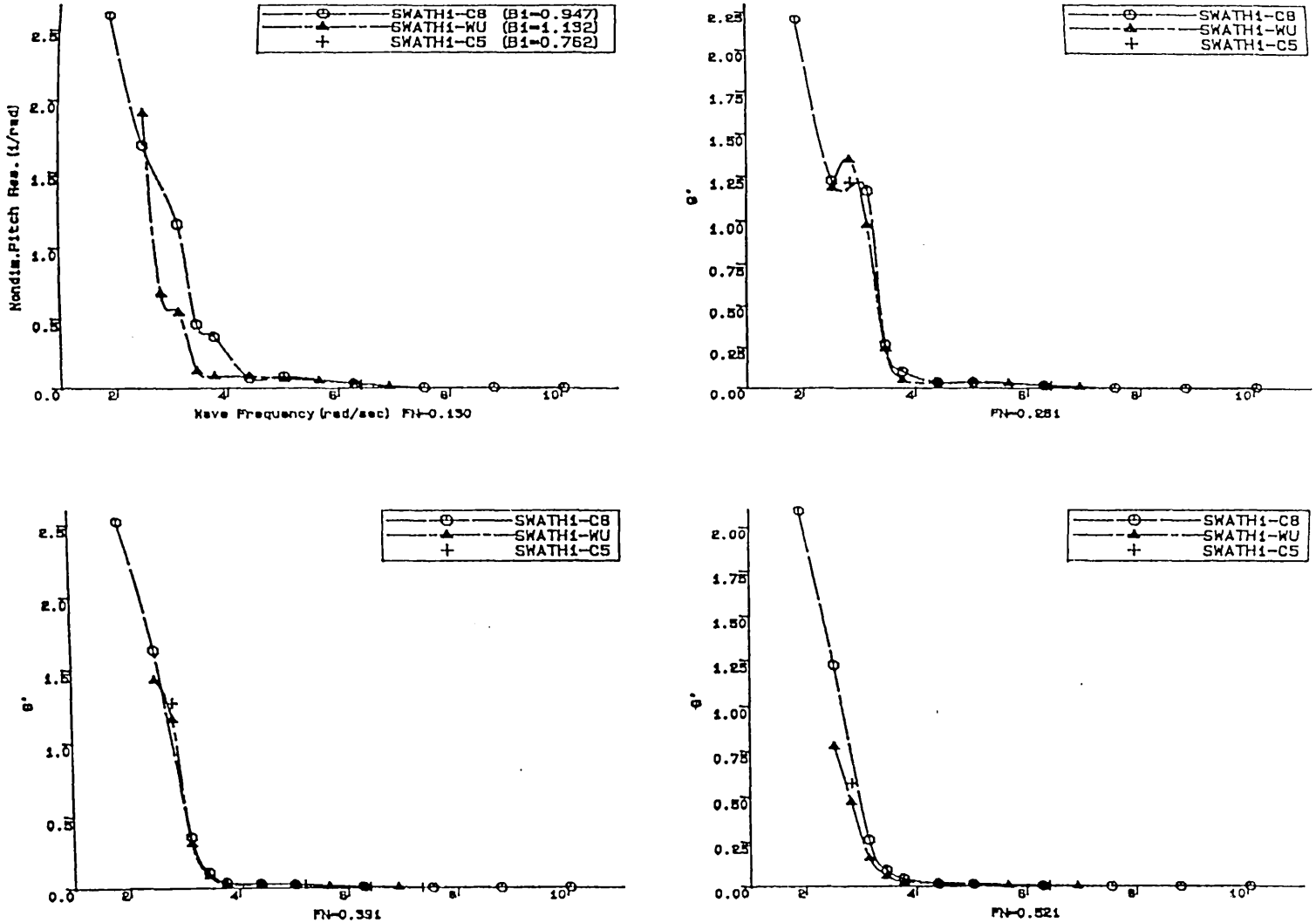

Fig.4.94

SWATH1 Model Pitch Responses in Head Seas For Three Spacings Between Demihulls.

4.4 SWATH2 MODEL CALM WATER RESISTANCE, AND RESISTANCE AND MOTION IN UNIFORM WAVES

The SWATH2 model has hulls of rectangular cross sections with rounded corners and is a tandem strut configuration. A SWATH ship with rectangular cross section hulls with rounded corners is considered to be promising in terms of draft reduction, construction cost and payload which are all drawbacks of the conventional SWATH ships. Some improvements in motion characteristics may also be expected compared to circular cross section hulls. However, a resistance penalty is expected on the rectangular hulled SWATH ship and hence, most SWATH designers take the view that this is too large to offset the benefits. Therefore, in this section, special attention is paid to two points. One is to measure the total resistance of this rectangular hulled model and to compare it with theoretical results in order to validate the computer program previously developed. The other is to compare the test results of the SWATH2 model with those of the SWATH1 circular hulled model.

Parametric changes of spacing between the centrelines of the two demihulls, the spacing between forward and aft struts, the slenderness ratio of the submerged body and the draft etc which were conducted with the SWATH1 model were not performed with the SWATH2 model because of the tank time limit. Also, it was not felt necessary to conduct these parametric studies with SWATH2 because the computer program OSWATH had been proved successful in predicting the resistance variations caused by such changes with the SWATH1 model. Parametric studies for SWATH2 can therefore be efficiently carried out by the computer program.

For the purpose of comparing with the test results of SWATH1, three drafts were selected and tested at a spacing between demihull centrelines which corresponds to one of the spacings tested with the SWATH1 model(See Table 4.20). In addition, the model was towed in the astern direction at the first draft condition in order to check the difference between the results towed in the two different directions. Therefore, a total of four conditions of resistance measurements in calm water were performed. In order to help improve our understanding of the resistance -speed characteristics of the SWATH

model, sinkages and trims were measured for each condition.

As mentioned in the previous section 4.3, the added resistance of the SWATH1 model in uniform waves is remarkably small and becomes even negative by as much as up to 24% of that in still water over some speed ranges. Also it was noticed that the added resistance of the model is not proportional to the square of the wave height which is opposed to the generally known square law.

Table 4.20 Experimental Conditions Tested with the SWATH2 model

Draft	Condition Numbering	$H_1=2h/D_b$
1.5 D_b =0.1338 m	C1 , C1SA	2.0
1.87D_b=0.18265 m	C2	2.75
2.0 D_b=0.195 m	C3	3.0

Note; C1 = Condition 1, C1SA = Condition 1 Stern Ahead; Spacing between the centrelines of two demihull 2b=0.863 (B_1=4b/L_b=0.762) for all conditions.

In order to check these points with the SWATH2 model, model tests in uniform waves were carried out at the deepest draft-C3 to measure the total resistances, motion responses, sinkages and trims as in the calm water. As used in the previous experiments with the SWATH1 model, the measurements were conducted using the constant speed method due to its simplicity and accuracy compared to the constant thrust method. The added resistance due to the oncoming waves is derived by subtracting the still water resistance from the total resistance in waves. Three wave heights of λ/ζ_w=50.0, 32.3 and 22.3 were varied at one frequency of 0.83hz corresponding to the ratio of wave length to model length(λ/L_b) of 1 to check relationships between the motion responses and the wave height as well as between the added resistance and the wave height squared.

In addition, experiments were jointly carried out with Djatmiko[73] in a range of frequency 0.3 to 1.6 hz, which corresponds to the ratios of the wave length to the model length of 7.66 to 0.27, as part of a seakeeping investigation.

The calm water test results were compared with the theoretical predictions using the computer program developed in the previous Chapter and detailed discussions are presented herein. The experimental motion responses are also compared with the theoretical calculations using the existing computer program in the Laboratory[85]. All the experimental results in calm water as well as in the waves are compared with those of the SWATH1 circular hulled model previously tested.

Based on the present studies, a rectangular cross section hull can be applied to the design of practical SWATH ships up to moderately high speeds without any penalty in the resistance compared to the circular counterpart. Detailed result are reported in Ref.[90] and this section is taken from the reference.

4.4.1 Description of Model SWATH2

The SWATH2 model is a tandem strut configuration as is the SWATH1 model. The lower portion of the demihull, referred to as the submerged body, has rectangular cross sections with rounded corners whereas SWATH1 has circular cross sections.The upper portion of the demihull, referred to as the strut, has the same water line with the draft consisting of an airfoil shape as with SWATH1. The model was made of a combination of PVC and GRP. The struts and the parallel parts of the submerged bodies were made of PVC and the ends of the submerged bodies were of GRP. The lengths of the struts and of the submerged bodies for the SWATH2 model are one and half times those of the SWATH1 model. In order to be able to make a comparison between these two models, basic coefficients such as waterplane area coefficients, ratio of strut length to thickness, relative lengths of the ends of submerged bodies,and relative positions of forward and aft struts on the demihull were kept the same; the major difference being the prismatic coefficients of the bodies. Fig.4.95 shows the sectional area curve of the body and the waterplane area curves of the struts for the SWATH2 as well as for SWATH1. The sectional area curve of the body of SWATH2 is slightly different from that of SWATH1. Principal dimensions and coefficients of the SWATH2 model are listed in Table 4.21. Small scale model plans and details are

shown in Fig.4.96-a and the side and front view of the model are shown in Fig.4.96-b and -c, respectively.

As with the SWATH1, the model was designed so that the spacings both between the hulls and between the struts can be systematically varied over a wide range. The spacing change between the struts can be achieved by inserting small lengths of parallel parts at the centre of the submerged bodies, thus changing their slenderness ratio as well. The draft can be changed by adding weights into the ballast tanks which are located inside the struts. Stabilising fins were not considered for this model. Turbulence stimulation devices were not introduced for the model as for the SWATH1 model.

Table 4.21. Some Dimensions and Principal Coefficients of SWATH2 demihull

GUH Model	SWATH2		
Length of Body(m), L_b	2.265		
Depth of Body(m), D_b	0.0975		
Breadth of Body(m), B_b	0.15		
Length of Strut(m), L_s	0.6		
Maximum Beam of Strut(m), t_m	0.075		
Slenderness of Body	L_b/D_b=23.23, L_b/B_b=15.1		
C_p of Body	0.909		
C_{wp} of Strut	0.665		
Slenderness of Strut, t_m/L_s	0.125		
Draft(m), T	1.5 D_b=0.146	1.87D_b=0.183	2.0 D_b=0.195
Depth of Strut(m), D_s	0.04875	0.08515	0.0975
SDBC(m)*, h	0.0975	0.1339	0.14625
Wetted Area(m^2), S	0.95375	1.04202	1.07197
Displaced Volume(m^3), ∇	0.032025	0.03422	0.03496
$H_1=2h/D_b$	2.0	2.75	3.0
Natural Periods*			
Heave(sec), T_z	2.24		
Pitch(sec), T_θ	2.638		
Roll(sec), T_ϕ	2.498		

* Note; Experimentally determined for SWATH2-C3.

Model arrangements, instrumentation, towing system, calibration procedures

(LVDTs and wave probes) are exactly the same as those for the SWATH1 model experiments in waves, as described in sections 4.3.1 to 4.3.3. The only difference was that the distance between the two trancducers was changed to 112.5 cm since the length of the model SWATH2 is longer than that the SWATH1 model.

4.4.2 Results and Discussion

4.4.2.1 In calm water

A) Draft variation

Figs. 4.97 through 4.99 present the total, residuary and skin frictional resistances as a function of Froude Number for conditions C1,C2 and C3. The patterns of the curves are nearly the same as for the circular hulled model-SWATH1 regardless of the different shapes in cross sections of the bodies and their different cross sectional curves with each other. From the figures, it is seen that the portion of the skin frictional resistance is significant even above the Froude Number of 0.4 which would not be expected in a monohull type of ship. The reason for this was explained in detail in section 4.2.4 with the SWATH1 model. The total resistances, residuary resistances and their coefficients are presented in tables 4.23 to 4.26 for the four conditions tested.

Figs. 4.100 compares the resistance coefficients non-dimensionalised by the displaced volume for the three conditions. As with the SWATH1 model, the results show that a large hump and hollow commonly occurs around Fn=0.3-0.4 independent of the draft, its magnitude increasing with increase of the draft. This hollow and hump is caused by interference wave effects between each component of the model as well as the wave resistance characteristics of its components, as explained in detail later. Also, the figure illustrates that a resistance benefit from the increase of the draft cannot be expected in terms of the resistance per the displacement volume , which is the same as with SWATH1 model. This is due partly to the increased strut depth and partly to the increased additional resistances as stated later despite the increased submergence of the body with the draft.

B) Towed in opposing directions(bow and stern)

As far as potential theory is concerned, the resistances of a body towed in the directions of the bow and stern are exactly the same as each other, giving the minimum wave resistance for the fore and aft symmetrical body. In practice this does not apply to real fluids. Several model test results for surface vessels have shown that the optimum position of the LCB, in general, moves from forward to backward of the longitudinal centre of the ship with increase of speed[68]. Over the wave-making speed range, the length of the entrance of a surface running vessel is, in general, recommended to be longer than its run length to reduce wave-making resistance. On the other hand, over a viscous dominant speed range, a longer run is preferable to avoid separation of flow.

T. Byquist carried out experiments with a series of bodies of revolution which were towed in the two different directions as well as varying their submergence[19]. The experiments revealed, in general, that for higher speeds a submerged body having longer entrance than run results in less resistance than that of the reversed case, varying with submergence. For slower speeds, the result becomes reversed, the difference in the measured resistance between the two directions of tow being scarcely measurable. However, over the speed range where the wave-making resistance coefficient causes a hump, the wave-making resistance of the body with the longer entrance is higher than that of the body having the short entrance. This magnitude decreases with the submergence of the body.

Although the SWATH ship is composed of submerged bodies associated with surface piercing struts, this aforementioned general trend can be observed from the comparison of the results of the SWATH2 model towed in the two directions as demonstrated in Fig.4.103. As can be seen in the figure, the two results are nearly the same as each other at slower speeds, but at higher speeds condition-C1SA gives lower resistance than condition-C1 despite its slightly higher bow trim as shown in Fig.4.102. There is no difference in the sinkage between the two conditions as shown in Fig.4.101. Again, the humps and hollows of the resistance curve are exaggerated for condition-C1SA which has a longer entrance than condition C1. Although this fact is

found from only one set of experiments, the conclusion drawn from the experiments can be applied to the design of the volume distribution of the submerged bodies of SWATH depending on the speed of interest.

C) Sinkage and trim

A vessel travelling through water responds to changes in pressure distribution and friction induced trimming moments by changing position vertically in the water, called sinkage, and changing trim until a balance of forces is obtained by nature. Such sinkage and trim are both influenced by such parameters as the length-breadth ratio, the breadth-draft ratio and speed, and by environmental conditions such as shallow water, restricted channel and density etc as well as by hull conditions such as type of propulsion, hull fittings and appendage etc. With regard to the relationship between sinkage, trim and resistance, Ferguson concluded that the principal influencing factors are hull shape as well as speed with special emphasis on the effect of shallow water which is of prime importance to safe navigations[69]. Seren investigated in detail this shallow water problem with several mathematical and physical models of monohulls as well as semisubmersibles[71].

Figures 4.101 and 4.102 show the sinkage and trim as a function of Froude Number for all conditions tested. Although the results are not compatible to those measured by self-propulsion, they can be used to help improve our knowledge of the resistance-speed characteristics as well as the relationships between the sinkage, trim and resistance for SWATH ships. According to the figures, it is apparent that the sinkage and trim, in general, increase with speed, resulting in a severe sinkage and trim by bow at higher speeds due to the small waterplane area of the model and due to the Munk moment which is proportional to the heave added mass times the square of the model speed[72]. The sinkage and trim also increase with the draft with some exceptions at slower speeds as seen in the figures. The hump and hollow which appear in the curves of the total resistances in Figs.4.97 to 4.99 can be seen in the curves of the sinkages in such a way that the peaks of the humps and hollows are commonly shifted to slower speeds for all conditions tested. It is interesting to see that a simple

arithmetical summing of the sinkage and the trim produces a curve with a character rather more similar to the curve of the total resistance(with some undulations) than to the residuary resistance curve for the monohull ship[69]. Hence, it can be expected for the bare SWATH ship that there would be a relationship between some combination of the changes in sinkage and trim due to forward speed and changes in resistance which was discussed in Ref[69].

It seems that the severe sinkage and trim of the rectangular hulled SWATH2 model at higher speeds caused an increase in the total measured resistance. Thus, it is recommended that controllable fins are necessary in terms not only of seakeeping problem but also of the resistance increase problem for non-circular hulled SWATH ships(mentioned later in more detail). It was found that fixed fins can reduce trim at higher speeds considerably, up to zero level according to the angle of attack, while they have little effect on the sinkage[72]. It is inevitable that a resistance increase will be caused by the attached fins as well as by the fins induced resistance at non zero angle of attack. However, it is not clear at this stage whether the total resistance of a SWATH ship advancing with level trim by means of controllable fins is higher or less than that of a SWATH ship running at a trim without the active fins. Nonetheless, it is certain that such fins are necessary for SWATH ships in light of seakeeping and pitch stability requirements.

D) Comparison with Computational Results

Figures 4.104 to 4.106 show comparisons between the calculated wave-making resistance and measured residuary resistance coefficients. The residuary resistance is obtained by subtracting the skin frictional resistance, using the ITTC'57 model-ship correlation line as mentioned in the previous sections, from the measured total resistance. The figures show good qualitative agreements between the calculated and measured results in that the theory predicts nearly the same hump and hollow pattern with speed as those of the measurements. The differences between the two curves account for additional resistances such as viscous pressure, form, eddying, wave breaking and spray resistances as well as some nonlinear effects ,and in general, their

magnitudes are greater than those in the SWATH1 model as shown in Figs.4.15 and 4.24. In contrast to the behaviour of the SWATH1 model, it can be seen from Figs.4.104 to 4.106 that the difference increases with the draft, which means that the additional resistance increases with draft. This can be understood from the fact, explained earlier, that the sinkage and trim are both increased as the draft increases. It is known from analysis of several SWATH designs that the quantity, Cr.s-Cw.s, oscillates about zero, the usual bound of this difference being within $\pm 1.0\times10^{-3}$[5]. However, large values are obtained for the present rectangular hulled model. It was found during the experiments that the submerged bodies of SWATH2, which has rectangular cross sections with rounded corners, are not so well streamlined at large bow trim angles and hence, creating larger eddy and form resistances. In addition, this phenomenon made the model unstable at higher speeds which is reflected in the curves of resistance and trim. The residuary resistance coefficient curves as shown in Figs 4.104 to 4.106 are not as smooth at higher speeds as those for SWATH1. Also, the trim curves of SWATH2 against speed as shown in Fig.4.102 are undulatory at higher speeds while those of SWATH1 increased smoothly with speed. Therefore, in contrast with the circular hulled SWATH1 model, the trim of the SWATH2 model contributed to some extent to the resistance increase due to its non streamlined shape at trim.

Also, Figures 4.104 to 4.106 illustrate how each component of the model contributes to the total wave-making resistance for the three drafts. From these figures, it is easily understood that the large peak around Fn=0.31, independent of the draft, is a combination of large wave-making contributions by each hull as well as by the struts coupled with unfavourable interferences between the body and the two struts and between the forward and aft struts. At the first draft as seen in Fig.4.104, the total wave-making resistance is even less at slow speeds than that of the submerged body due to the favourable interference effects between each component. This body wave-making resistance decreases with increase of draft due to its increased submergence as seen in Figures 4.105 and 4.106. On the other hand, the strut component increases with the draft since its depth increases accordingly. Owing to these complicated interference effects the total wave making resistance increases up to Fn=0.5 and then slightly (scarcely measurable) decreases above Fn=0.5 with the draft. Further, if the increased

wetted area is taken into account, the total resistance will increase with the draft as has been proved in the experiments.

At the second and third drafts, which are realistic for the practical SWATH ship, the strut only wave making resistance is significantly larger compared to that of the body due to its large breadth to length ratio compared to that of the body. For single strut SWATH ships, this can be reduced to some extent because of the increased breadth to length ratio of single strut which becomes the same order as the diameter-length ratio of the body.

From the three figures, another interference between the two demihulls can be seen. It is noticed that favourable interferences between the two demihulls occur around FN=0.31-0.41 independent of the draft. Except over that speed range, unfavourable interferences are found throughout the speed range and these values approach zero as the speed increases to higher speeds.

From the foregoing results, it is not expected to obtain a SWATH arrangement which will give favourable resistance characteristics at all speeds since such interference effects are dependent upon the relative distances between the components of the SWATH ships as well as operating speed. In conclusion, reductions in wave resistance at certain speeds with a tandem strut SWATH at a given draft may be obtained by a proper location of the struts on the demihull, a well chosen spacing between the hulls and, by lowering the slenderness ratio of the strut as much as possible.

E) Comparison with SWATH1 model

As shown in Table 4.20, all the experiments with SWATH2 were carried out at one spacing which is 0.762 of the non-dimensional spacing between the centrelines of the two demihulls($B_1=4b/L_b$). So, the experimental results of SWATH1-C4 and C5 which are the same non-dimensional spacing as with the SWATH2 are compared herein.

Fig. 4.107 and 4.108 present the total and residuary resistance coefficients of SWATH2 as well as of SWATH1, respectively. As the lengths of the two models are different from each other, it is difficult to find an appropriate criterion of the draft to

compare the two models directly. Hence, relative comparisons are made at the same three draft criteria of 1.5 and 2 times the body depth, and the ratio of $2h/L_b$=0.118. Although the last nondimensional draft is most suitable to compare for the different length of bodies, the strut depths are different from each other as seen in Table 4.22.

Table 4.22. Comparison of drafts for SWATH1 and SWATH2

	SWATH1		SWATH2		
	C4=1.5Di_b	C5=2.0Di_b	C1=1.5D_b	C2=1.87D_b	C3=2.0D_b
Draft	0.1338	0.1784	0.14625	0.18265	0.195
D_S	0.0446	0.0892	0.04875	0.08515	0.0975
h(SDBC)	0.0892	0.1338	0.0975	0.1339	0.14625
$2h/L_b$	0.118	0.177	0.086	0.118	0.129
$D_{S1}=2D_S/L_S$	0.223	0.446	0.1625	0.284	0.325

Therefore, if comparing SWATH2-C1 and SWATH1-C4, and SWATH2-C3 and SWATH1-C5, which correspond to 1.5 and 2 times the depths of the bodies for each model, respectively, it can be seen that SWATH2 is better up to moderately high speed in terms of total resistance per tonne. From the comparisons of the computational results, Figs.4.104 and 4.17, and Figs.4.106 and 4.18, this conclusion is a result of the fact that the contributions of the shorter depth of struts to the total resistance outweigh the increased resistance from the smaller submergence of the body for the SWATH2 compared to its counterpart on SWATH1. At higher speeds, SWATH2, however, becomes worse than SWATH1 due partly to its increased form resistance as mentioned earlier and partly to the smaller submergence of the body than that of SWATH1. This result is seen exaggerated for the residuary resistance coefficient curves as shown in Fig.4.108.

At the same non-dimensional submergence depth of $2h/L_b$=0.118, SWATH2 is worse than SWATH1 throughout the speed range. From the computational results as given in Figs.4.105 and 4.17 for each model, it can be seen that this result is due mostly to the fact that the 27.3% longer depth of struts contribute much more to the

wave-making resistance than those of SWATH1. The contributions of the submerged bodies are seen to be nearly similar to each other from the figures since the submergence ratios of the bodies are the same as each other.

As a result, if careful attention is paid to the strut depth effects on the resistance for the rectangular hulled SWATH model, some of this resistance can be reduced. Hence, a well designed rectangular cross section hull with rounded corners can be implemented for practical SWATH ships up to moderately high speeds without a serious resistance penalty.

In order to compare the sinkage and trim for different lengths of models, The sinkage and trim are non-dimensionalised by the length of bodies for SWATH1 and SWATH2, and these curves are plotted versus Froude Number in Figs.4.109 and 4.110. Unfortunately, the measurements of the sinkage and trim for SWATH1-C4 were not recorded. As seen in the figures, sinkage and trim increase with draft. The submergence ratio of the body for SWATH1-C5 is much deeper than that of SWATH2-C3. Comparing the two models with these points in mind, the sinkages seem to be very similar to each other except in the range Fn=0.3-0.37 where the SWATH2 Model emerges above the still water level. However, the trims of SWATH2 seem to be less than those of the counterpart SWATH1.

4.4.2.2 In head seas

The still water resistances of SWATH2-C3 are plotted as a function of Froude Number in Fig.4.111 together with the resistances in waves of $\lambda/L_b=1.0$ with the three wave heights. The pattern of the resistances of the SWATH2 in waves is nearly the same as that of the SWATH1. The resistance increases in waves are comparatively high at slower speeds which might be due to the increased bow trim compared to that in still water as shown in Fig.4.113.

As was the case with the SWATH1model, the resistance decreases over the speed range of Fn=0.32-0.37 by up to as much as 12% at Fn=0.319 for $\lambda/\zeta_w=22.3$. Although the speed intervals tested with the SWATH2 are not as many as those of the SWATH1, because of limitations in tank time, it can be seen from the figure that the

range giving the negative resistance increases extends over the range of Fn=0.31-0.39 as for SWATH1. Also, it can be seen that as the wave height increases, the resistance decreases systematically with the tendancy that the resistance hump and hollow shift to the slower speeds and are flattened, which also happened in SWATH1. An attempt to explain the reason for this was given in section 4.3.4.2 dealing the SWATH1 model. In summary, this seems to be caused by the complicated interference wave systems between the components of the model and by the reduced trim over that speed range, as shown in Fig.4.113. At the higher speeds above Fn=0.39, the resistances are not reduced despite the greatly reduced trim. This can be understood possibly by the fact that the mean sinkages are increased at the higher speeds as shown in Fig.4.112 hence, creating more resistance.

In general, the sinkage in waves decreases up to Fn=0.35 and then increases compared to that in calm water. The trim in waves becomes high up to Fn=0.29 and then low compared to that in calm water. In addition, the trim increases at slow speeds and decreases at higher speeds as the wave height increases.

The added resistance coefficients are plotted in Fig.4.114 as a function of Froude Number for the three different wave heights. The added resistance is obtained by subtracting the calm water resistance from the resistance in waves. If the speeds tested in the calm water and in the waves are different from each other, the calm water resistance was read off from the resistance curve fitting at the speed tested in the waves as shown in Fig.4.111. As mentioned in the previous section 3.3, in general, it is found for monohulls that the added resistance is proportional to the square of the wave height. However, a number of papers which are opposed to the square law have been published depending on the form. Like the SWATH1 model, also it can be seen from the figure that the square law between the wave height and added resistance can hardly be applied to the SWATH2 model. The added resistance coefficient decreases significantly at the higher speeds with the increasing wave height.

The added resistance coefficient of SWATH2 can be compared with that of the SWATH1-C5 at the same wave-length ratio of λ/L_b=1.0, as shown in Fig.4.69. As mentioned earlier in the comparison of the performance of both models in calm water, it is not possible to compare both results directly since the submergence ratios of the

bodies($2h/L_b$) are different from each other, ie, $2h/L_b$=0.177 for the SWATH1 and 0.129 for the SWATH2 as shown in Table 4.22. Consequently, the SWATH2 is subject to higher motions in waves than those of the SWATH1 due to it being closer to the free surface. Such motion responses of the SWATH2 as heaving, pitching and surging are presented in Figs.4.115 to 4.117 as a function of Froude Number for the three wave heights. The motion responses(heave, pitch and surge) of the SWATH1-C5 at the same wave length ratio of λ/L_b=1.0 are shown in Figs.4.73, 4.77 and 4.81. It can be seen from the comparisons of these figures that the heaving and pitching motions of the SWATH2 are much higher than those of the SWATH1. However, the surge motion of the SWATH1 is higher than that of the SWATH2 up to Fn=0.25 and the reason for this is not understood. At speeds higher than Fn=0.25, the surge of SWATH1 becomes less than that of the SWATH2. With these points in mind, the added resistance coefficients of the SWATH2 can be seen to be less than those of the SWATH1 for the same wave steepness and same submergence ratio of the main body.

Fig.4.118 shows the added resistance coefficients of the SWATH2 versus the non-dimensional wave frequency for the four speeds tested. Fig.4.86 shows the results for the SWATH1-C8 whose non-dimensional spacing(B_1=0.947) is wider than that of the SWATH2-C3 at the same Froude Numbers as for SWATH2 excepting at Fn=0.390. Unlike the SWATH1-C8 for which the worst resistance increases occurred around the pitch resonance, the resistance increases for the SWATH2 is not so exaggerated at the pitch resonance region marked on the figure. Also, a high oscillation in the coefficients can be seen for all four speeds tested and this is intensified as the speed increases. This can be understood from the fact mentioned earlier that the rectangular hulled model is not stable at higher speeds due to the severe turbulence and eddying around the hulls which was reflected in the resistance curves in calm water.

The heaving, pitching and surging responses are presented against the non-dimensional encounter wave frequency in Figs 4.119 to 4.121. Computational results based on the 2-D strip theory[85] are compared with the experimental results and presented in Figs.4.122 and 4.123.

Figs.4.124 to 4.126 show the comparisons of the pitching, heaving and surging responses of the SWATH1-C8 and SWATH2-C3. At the critical zone, the SWATH2

motions are considerably lower than those of the SWATH1 due to its larger added mass and damping compared to the circular hulled model. However, in a range of frequencies just over the critical zone, the SWATH2 becomes worse than the SWATH1. This can be attributed mainly to two factors mentioned earlier. One is that the submergence ratio of the main body for the SWATH1 is much higher that that of the SWATH2. The other is that the non-dimensional spacing between two demihulls for the SWATH1 is wider than that of its counterpart. It was proved in the previous section 3.3 that the narrow spacing model is subject to more motions than the wide one with the SWATH1 model. If these points are taken into account, the rectangular hulled SWATH2 seems to be subject to less motions than the circular hulled counterpart.

The unstableness of the SWATH2 at higher speeds as mentioned earlier can also be seen from the curves of the sinkage and trim as shown in Figs.4.127 and 4.128. At the slowest speeds amongst those tested, the sinkage and trim are both independent of the wave length which was observed throughout the speeds tested with the SWATH1. As the speed increases, undulations are seen in the curves of both sinkage and trim, and these intensify with increasing speed.

4.4.3 Conclusions

Based on the present work, the following conclusions can be drawn:

a) The computational results using computer program OSWATH based on the plane source distributions for the submerged body and for the strut give satisfactory correlations with the experimental results.

b) The patterns of the resistance coefficient curves of the rectangular hulled model-SWATH2 are nearly the same as those of the circular hulled model-SWATH1.

c) A resistance benefit from the increase of the draft cannot be expected due partly to the increased strut depth and partly to the increased additional resistance despite the increased submergence of the body.

d) The form effect which accounts for the difference($C_{r.s}$-$C_{w.s}$) is much higher for the SWATH2 than for SWATH1. This is due to the fact that the rectangular cross section hull is not so well streamlined at large bow trim angles, hence creating large

eddy and form resistances.

e) As was the case with the SWATH1 model, the resistance decreases systematically over the speed range of Fn=0.32-0.37 with the tandancy that the resistance peak shifts to slower speeds and the hump and hollow are flattened. Therefore, tandem strut SWATH ships can be recommended, in confidence, to naval combatants where speed reduction is of prime importance.

f) The motion response of the SWATH2 is much less than that of the SWATH1 model. This fact results in less added resistance for SWATH2 compared to SWATH1 at the same wave steepness and same submergence ratio of the main body.

g) A rectangular cross section hulled SWATH with rounded corners seems to be promising up to moderately high speeds, but at higher speeds, a well streamlined hull seems to be better in terms of the total resistance.

h) When designing a SWATH with tandem struts, careful attention should be paid to the thickness, length and depth of the struts and their relative positions on the demihull, depending on the speed of interest.

i) The trim of SWATH2 is less than that of SWATH1 while there is little difference in the sinkage. However, severe sinkage and bow trim are observed at higher speeds. Therefore, as for the SWATH1 model, stabilising fins for the SWATH2 seem to be necessary with regard to seakeeping as well as to propeller emergence. In addition, in contrast with the circular hulled SWATH1 model, the trim of the SWATH2 model contributes to some extent to the resistance increase due to its non-streamlined geometry at trim.

j) As with SWATH1, the added resistance is not proportional to the square of the wave height. The added resistance divided by the square of the wave height decreases as the wave height increases.

U(m/s)	FN	RN/10^6	RT(N)	CT.V	CT.S	RR (N)	CR.V	CR.S
0.510	0.108	1.071	1.112	0.0535	0.0045	-0.120	-0.0058	-0.0005
0.592	0.126	1.243	1.646	0.0587	0.0049	0.040	0.0014	0.0001
0.709	0.150	1.489	2.446	0.0609	0.0051	0.233	0.0058	0.0005
0.899	0.191	1.888	4.003	0.0620	0.0052	0.621	0.0096	0.0008
1.002	0.213	2.104	5.338	0.0665	0.0056	1.232	0.0153	0.0013
1.115	0.237	2.341	7.940	0.0799	0.0067	2.968	0.0299	0.0025
1.196	0.254	2.511	10.364	0.0906	0.0076	4.726	0.0413	0.0035
1.300	0.276	2.729	16.680	0.1235	0.0104	10.132	0.0750	0.0063
1.397	0.296	2.933	22.418	0.1437	0.0121	14.966	0.0959	0.0081
1.493	0.317	3.135	24.686	0.1385	0.0116	16.288	0.0914	0.0077
1.601	0.340	3.361	22.774	0.1111	0.0093	13.251	0.0647	0.0054
1.697	0.360	3.563	21.395	0.0929	0.0078	10.820	0.0470	0.0039
1.799	0.382	3.777	23.374	0.0903	0.0076	11.626	0.0449	0.0038
1.910	0.405	4.010	26.510	0.0909	0.0076	13.423	0.0460	0.0039
1.993	0.423	4.184	31.136	0.0981	0.0082	17.005	0.0536	0.0045
2.100	0.446	4.409	35.740	0.1014	0.0085	20.210	0.0573	0.0048
2.310	0.490	4.850	42.812	0.1004	0.0084	24.365	0.0571	0.0048
2.514	0.533	5.278	50.262	0.0995	0.0083	28.765	0.0569	0.0048
2.760	0.586	5.795	53.888	0.0885	0.0074	28.433	0.0467	0.0039
2.907	0.617	6.103	62.583	0.0926	0.0078	34.621	0.0513	0.0043

Table 4.23 SWATH2-C1 Tem.=17.1°C

U(m/s)	FN	RN/10^6	RT(N)	CT.V	CT.S	RR (N)	CR.V	CR.S
0.517	0.110	1.085	1.290	0.0578	0.0046	-0.149	-0.0067	-0.0005
0.700	0.149	1.470	2.713	0.0663	0.0053	0.252	0.0062	0.0005
0.895	0.190	1.879	4.670	0.0698	0.0056	0.860	0.0128	0.0010
1.010	0.214	2.121	6.939	0.0814	0.0065	2.211	0.0259	0.0021
1.107	0.235	2.324	10.497	0.1025	0.0082	4.928	0.0481	0.0039
1.206	0.256	2.532	13.944	0.1148	0.0092	7.453	0.0613	0.0049
1.311	0.278	2.753	20.861	0.1453	0.0117	13.323	0.0928	0.0074
1.382	0.293	2.902	28.200	0.1767	0.0142	19.916	0.1248	0.0100
1.507	0.320	3.164	34.027	0.1793	0.0144	24.351	0.1283	0.0103
1.608	0.341	3.376	29.223	0.1353	0.0109	18.352	0.0849	0.0068
1.636	0.347	3.435	26.799	0.1198	0.0096	15.585	0.0697	0.0056
1.715	0.364	3.601	26.377	0.1073	0.0086	14.171	0.0577	0.0046
1.731	0.367	3.634	27.088	0.1082	0.0087	14.677	0.0586	0.0047
1.811	0.384	3.802	30.513	0.1114	0.0089	17.052	0.0622	0.0050
1.890	0.401	3.968	31.269	0.1048	0.0084	16.734	0.0561	0.0045
1.984	0.421	4.166	35.540	0.1081	0.0087	19.677	0.0598	0.0048
2.098	0.445	4.405	39.409	0.1072	0.0086	21.868	0.0595	0.0048
2.261	0.480	4.747	47.371	0.1109	0.0089	27.298	0.0639	0.0051
2.466	0.523	5.178	57.913	0.1140	0.0092	34.438	0.0678	0.0054
2.662	0.565	5.589	64.051	0.1082	0.0087	37.100	0.0627	0.0050
2.867	0.608	6.019	75.104	0.1094	0.0088	44.288	0.0645	0.0052

Table 4.24 SWATH2-C2 Tem.=17.0°C

U(m/s)	FN	RN/10^6	RT(N)	CT.V	CT.S	RR (N)	CR.V	CR.S
0.504	0.107	1.069	1.290	0.0599	0.0047	-0.139	-0.0064	-0.0005
0.598	0.127	1.268	1.824	0.0602	0.0048	-0.109	-0.0036	-0.0003
0.617	0.131	1.309	2.002	0.0620	0.0049	-0.042	-0.0013	-0.0001
0.700	0.149	1.485	2.736	0.0659	0.0052	0.180	0.0043	0.0003
0.806	0.171	1.709	3.425	0.0622	0.0049	0.142	0.0026	0.0002
0.901	0.191	1.911	4.893	0.0711	0.0056	0.889	0.0129	0.0010
1.005	0.213	2.132	7.428	0.0868	0.0069	2.564	0.0300	0.0024
1.098	0.233	2.329	10.675	0.1045	0.0083	4.978	0.0487	0.0039
1.206	0.256	2.558	14.456	0.1173	0.0093	7.719	0.0626	0.0050
1.217	0.258	2.581	15.879	0.1265	0.0100	9.032	0.0720	0.0057
1.306	0.277	2.770	20.528	0.1420	0.0112	12.759	0.0883	0.0070
1.399	0.297	2.967	29.312	0.1767	0.0140	20.525	0.1238	0.0098
1.507	0.320	3.196	37.208	0.1933	0.0153	27.167	0.1412	0.0112
1.606	0.341	3.406	31.870	0.1458	0.0115	20.616	0.0943	0.0075
1.712	0.363	3.631	29.357	0.1182	0.0094	16.734	0.0674	0.0053
1.809	0.384	3.837	30.380	0.1095	0.0087	16.443	0.0593	0.0047
1.909	0.405	4.049	33.747	0.1093	0.0087	18.395	0.0596	0.0047
2.041	0.433	4.329	39.899	0.1130	0.0089	22.584	0.0640	0.0051
2.105	0.447	4.465	41.967	0.1118	0.0088	23.663	0.0630	0.0050
2.198	0.466	4.662	47.060	0.1149	0.0091	27.274	0.0666	0.0053
2.304	0.489	4.887	54.065	0.1202	0.0095	32.527	0.0723	0.0057
2.454	0.521	5.205	57.780	0.1132	0.0090	33.648	0.0659	0.0052
2.694	0.572	5.714	65.853	0.1071	0.0085	37.296	0.0606	0.0048
2.875	0.610	6.098	76.995	0.1099	0.0087	44.880	0.0641	0.0051

Table 4.25 SWATH2-C3 Tem.=17.5°C

U(m/s)	FN	RN/10^6	RT(N)	CT.V	CT.S	RR (N)	CR.V	CR.S
0.498	0.106	1.046	1.112	0.0561	0.0047	-0.070	-0.0035	-0.0003
0.606	0.129	1.272	1.779	0.0606	0.0051	0.105	0.0036	0.0003
0.694	0.147	1.457	2.380	0.0618	0.0052	0.249	0.0065	0.0005
0.795	0.169	1.669	2.892	0.0572	0.0048	0.177	0.0035	0.0003
0.899	0.191	1.888	4.137	0.0640	0.0054	0.755	0.0117	0.0010
1.002	0.213	2.104	5.293	0.0660	0.0055	1.187	0.0148	0.0012
1.106	0.235	2.322	7.295	0.0746	0.0063	2.394	0.0245	0.0021
1.187	0.252	2.492	9.430	0.0837	0.0070	3.867	0.0343	0.0029
1.305	0.277	2.740	18.059	0.1327	0.0111	11.465	0.0842	0.0071
1.494	0.317	3.137	25.398	0.1423	0.0119	16.990	0.0952	0.0080
1.699	0.360	3.567	19.994	0.0866	0.0073	9.396	0.0407	0.0034
1.927	0.409	4.046	26.999	0.0910	0.0076	13.701	0.0462	0.0039
2.103	0.446	4.415	34.650	0.0980	0.0082	19.080	0.0540	0.0045
2.354	0.499	4.942	42.612	0.0962	0.0081	23.524	0.0531	0.0045

Table 4.26 SWATH2-C1SA Tem.=17.6°C

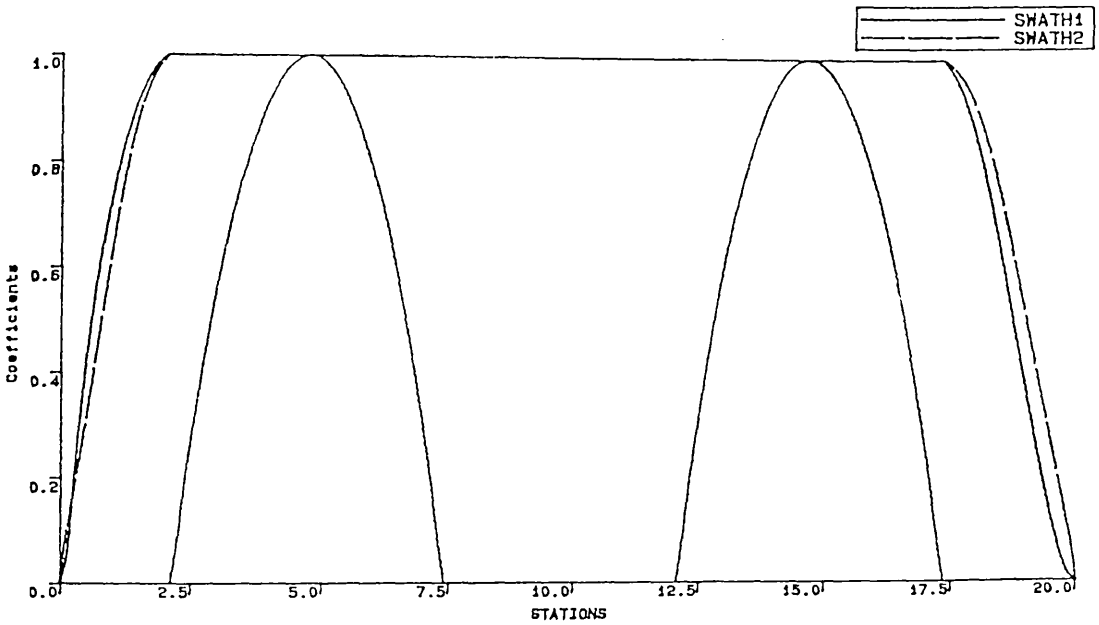

Fig.4.95

SECTIONAL AREA AND WATERPLANE AREA CURVES FOR SWATH1 AND SWATH2

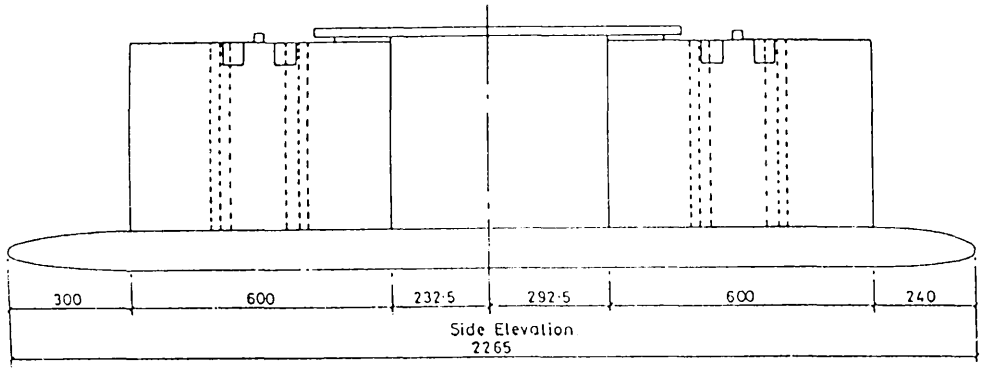

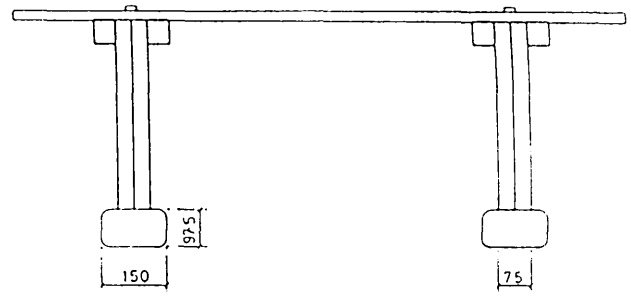

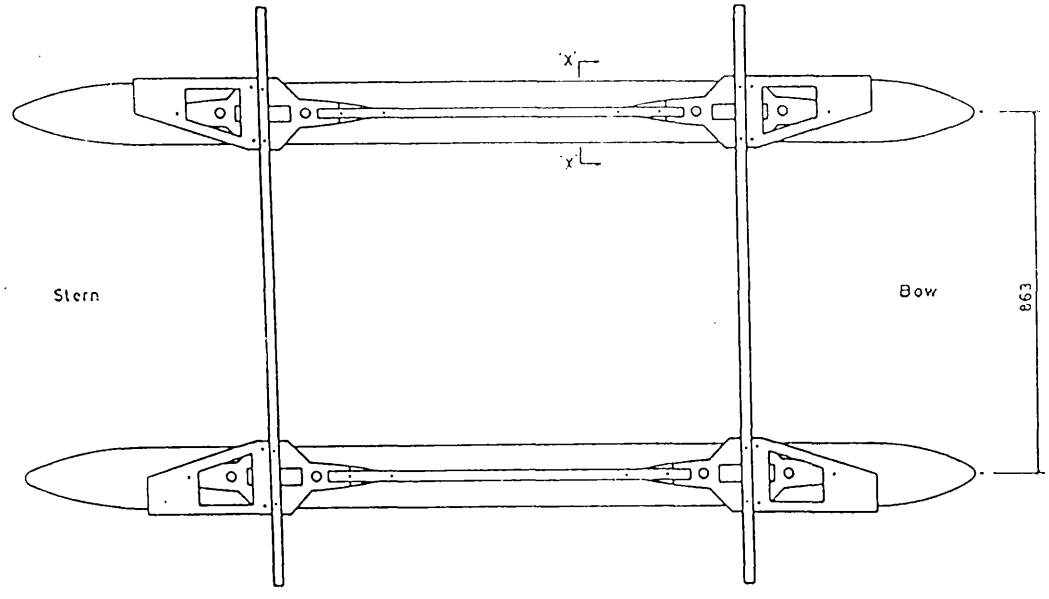

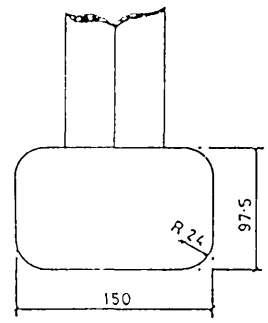

SWATH II

Fig.4.96-a
Plans and details of SWATH2 model

Dimensions in Millimetres.
Drawn by D.T. Sinclair.
September 1987.

Fig.4.96-b Front View of SWATH2 Model

Fig.4.96-c Side View of SWATH2 Model

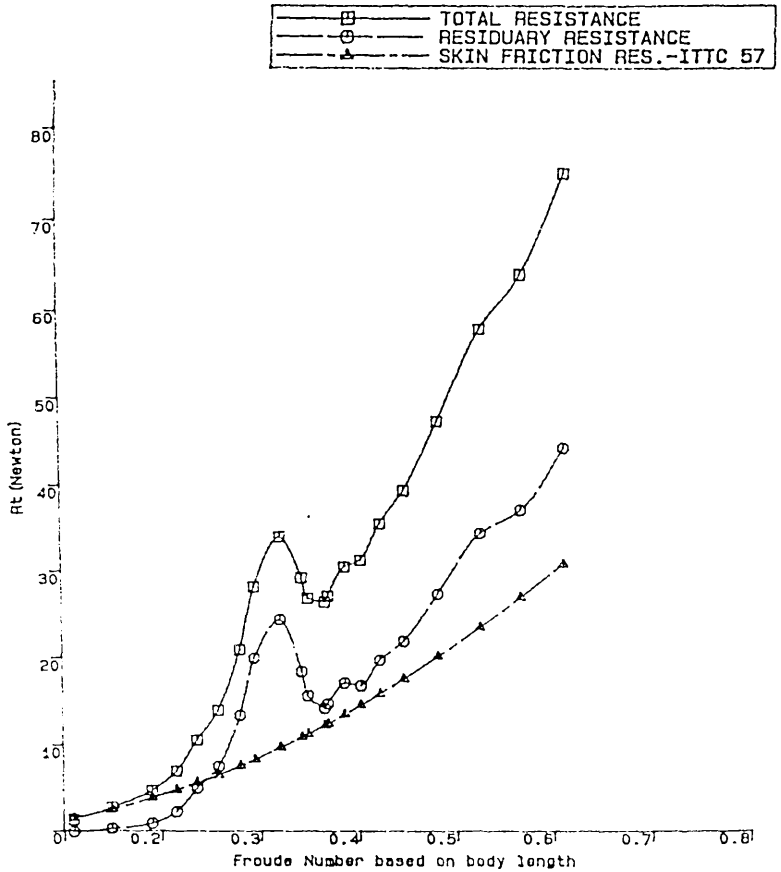

Total, residuary and skin-frictional resistance variations of SWATH2-C2 versus Froude Number (FN)

Fig.4.98

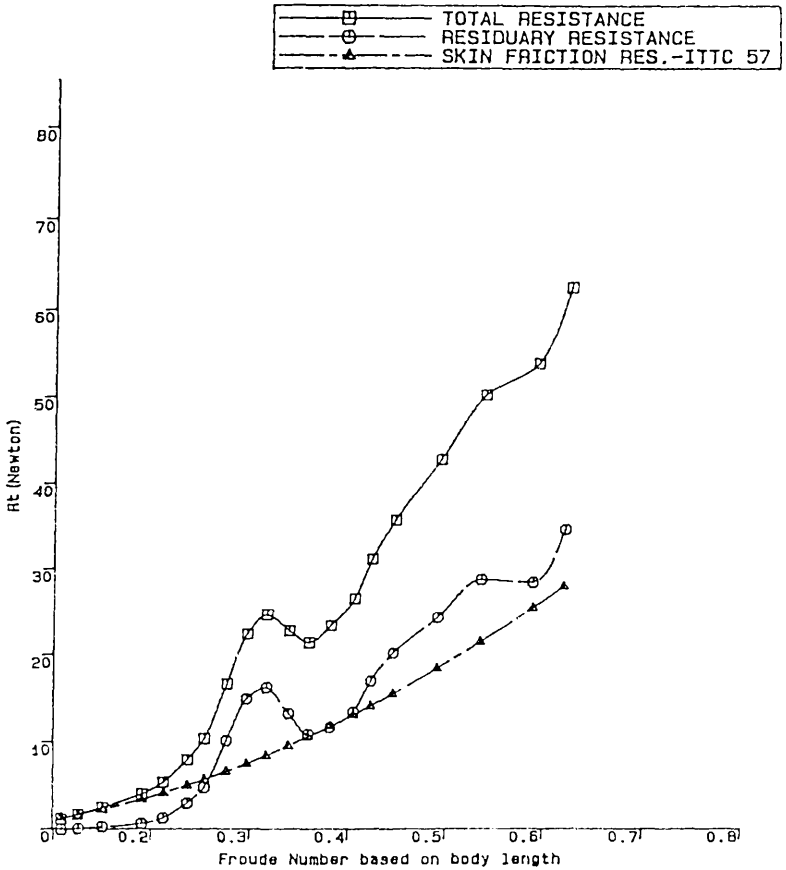

Total, residuary and skin-frictional resistance variations of SWATH2-C1 versus Froude Number (FN)

Fig.4.97

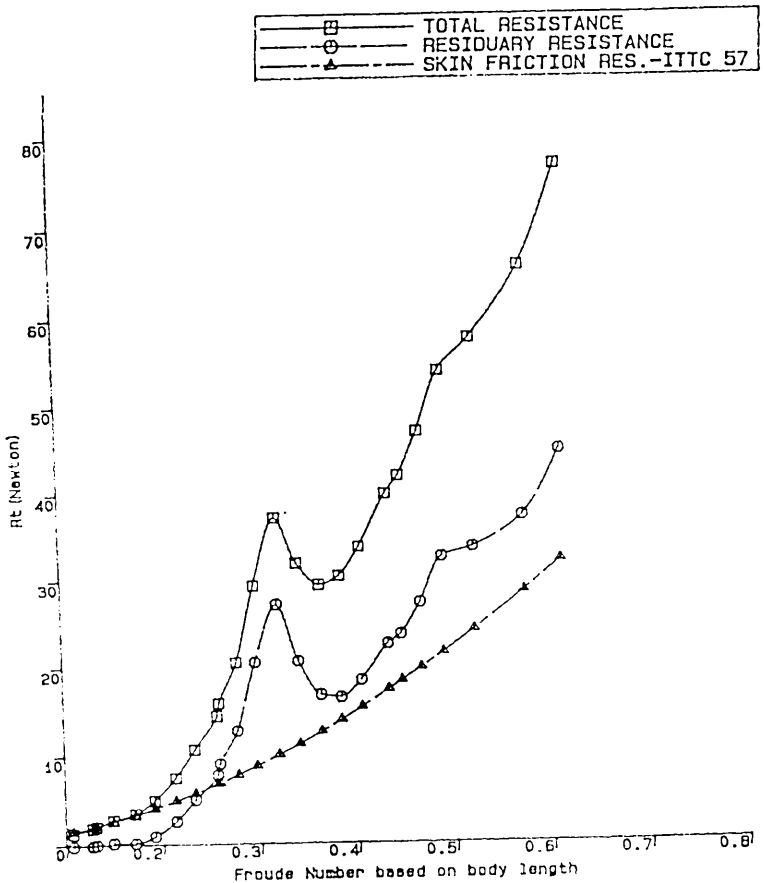

Total, residuary and skin-frictional resistance variations of SWATH2-C3 versus Froude Number (FN)

Fig.4.99

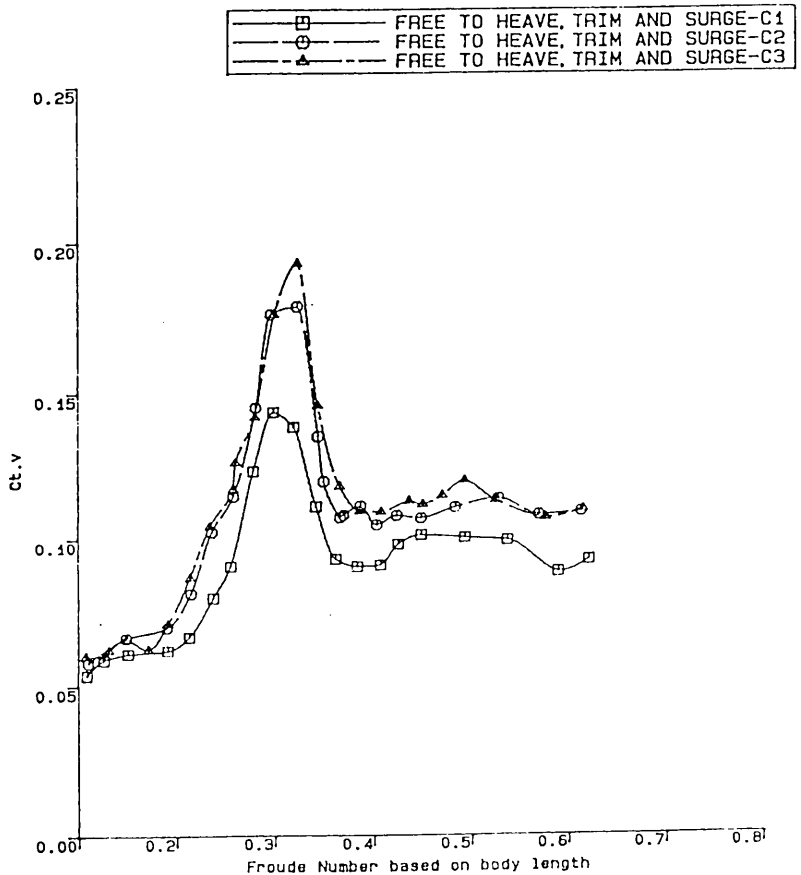

Total resistance coefficient variations of SWATH2 with three different drafts versus Froude Number

Fig.4.100

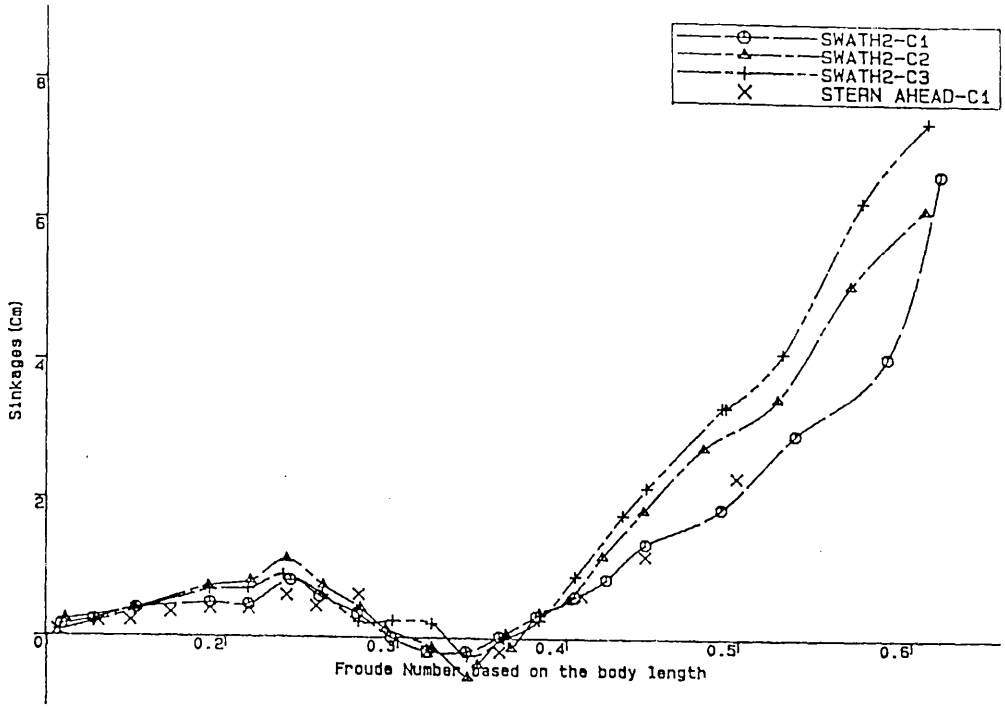

SWATH2 Model Sinkages in Calm Water as a Function of Froude Number.

Fig.4.101

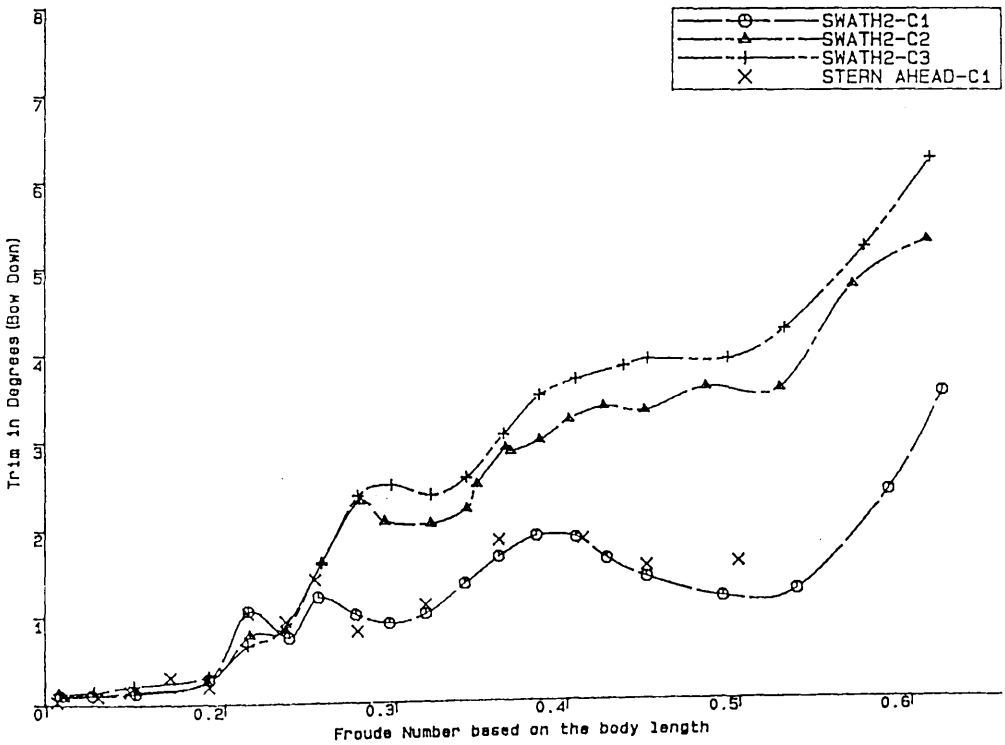

SWATH2 Model Trims in Calm Water as a Function of Froude Number.

Fig.4.102

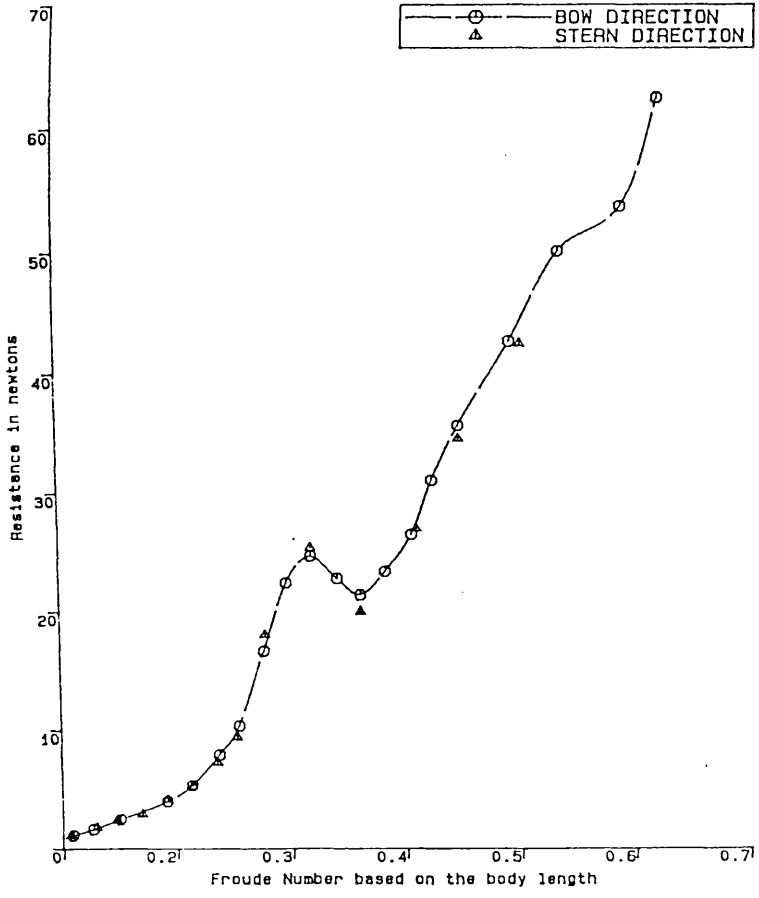

Comparison of Total Resistances of SWATH2-C1 Towed in Two Directions as a Function of Froude Number.

Fig.4.103

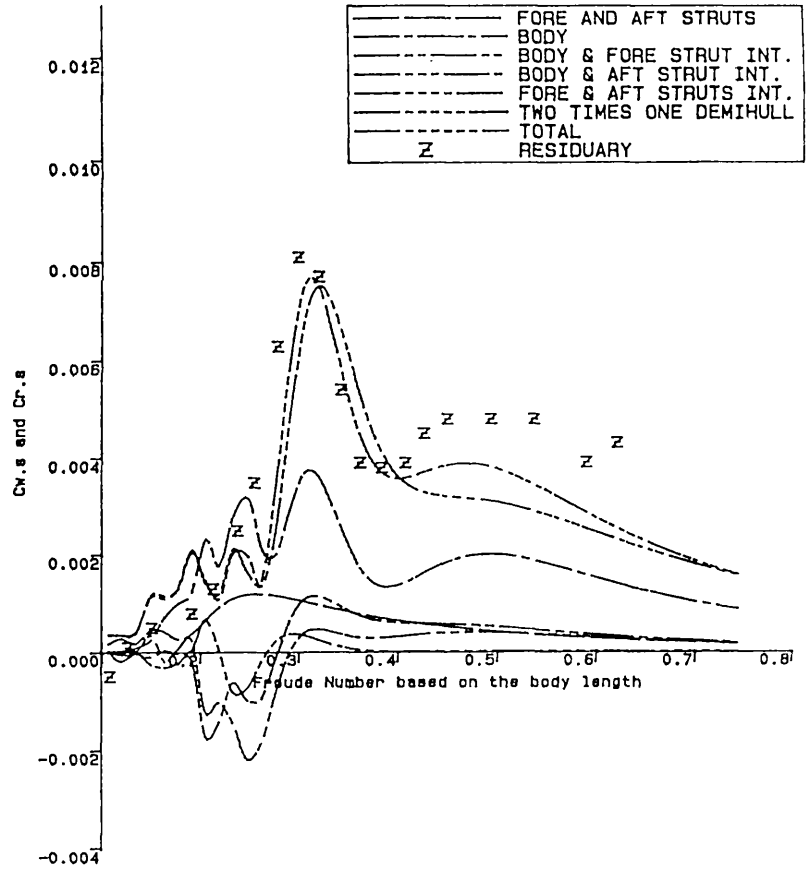

Wave Resistance Coefficients of SWATH2-C1 and its Component Variations together with Residuary resistance Coefficient as a Function of Froude Number.

Fig.4.104

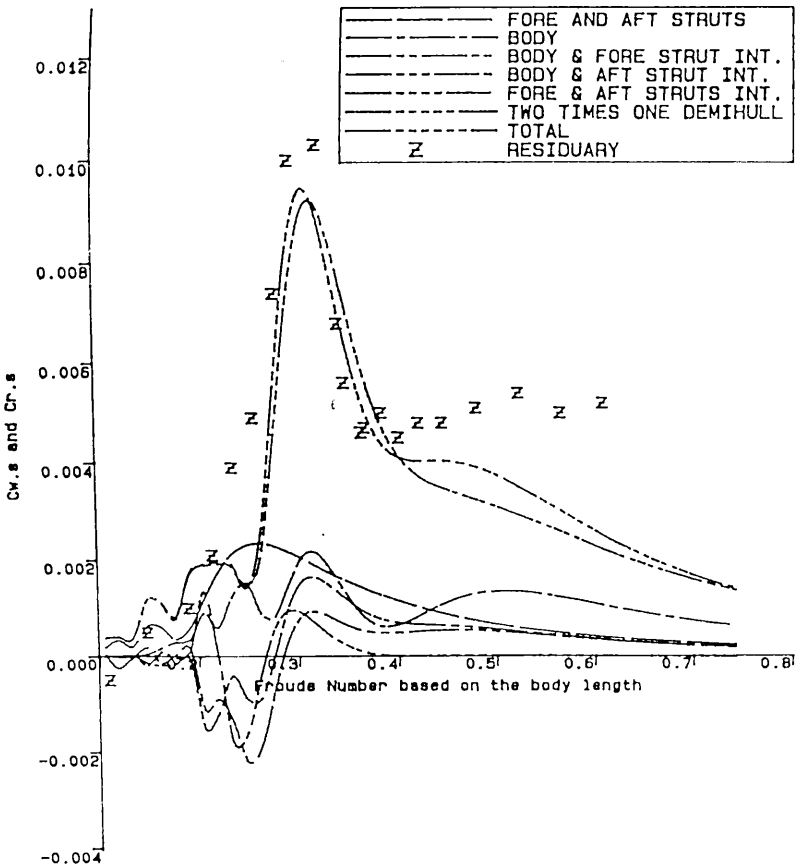

Wave Resistance Coefficients of SWATH2-C2 and its Component Variations together with Residuary Resistance Coefficient as a Function of Froude Number.

Fig.4.105

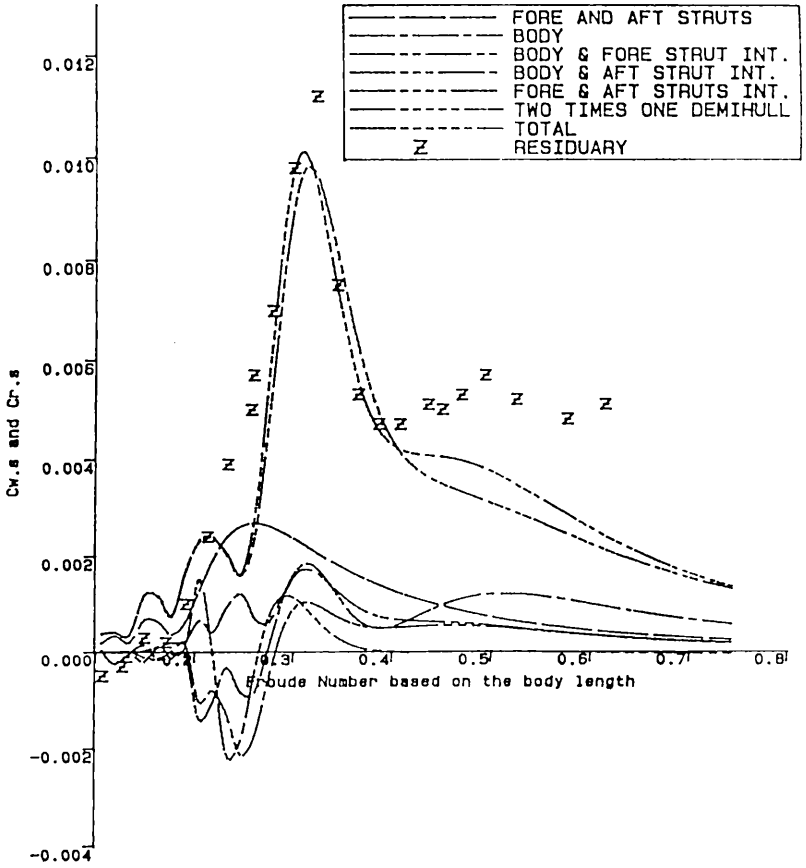

Wave Resistance Coefficients of SWATH2-C3 and its Component Variations together with Residuary Resistance Coefficient as a Function of Froude Number.

Fig.4.106

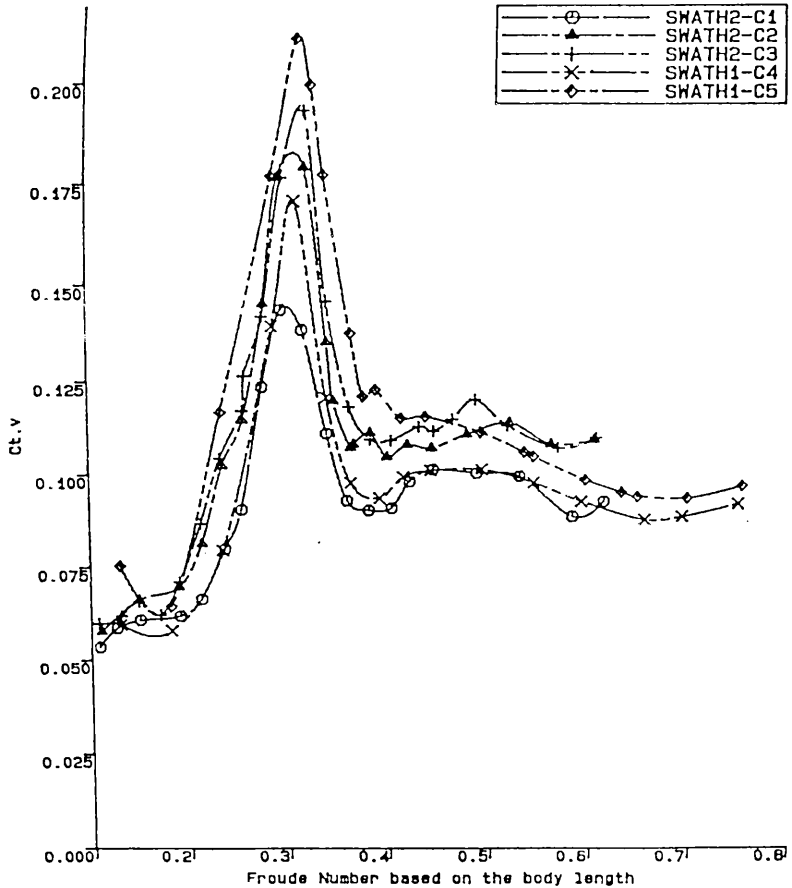

Comparison of the Total Resistance Coefficients of SWATH1 and SWATH2

Fig.4.107

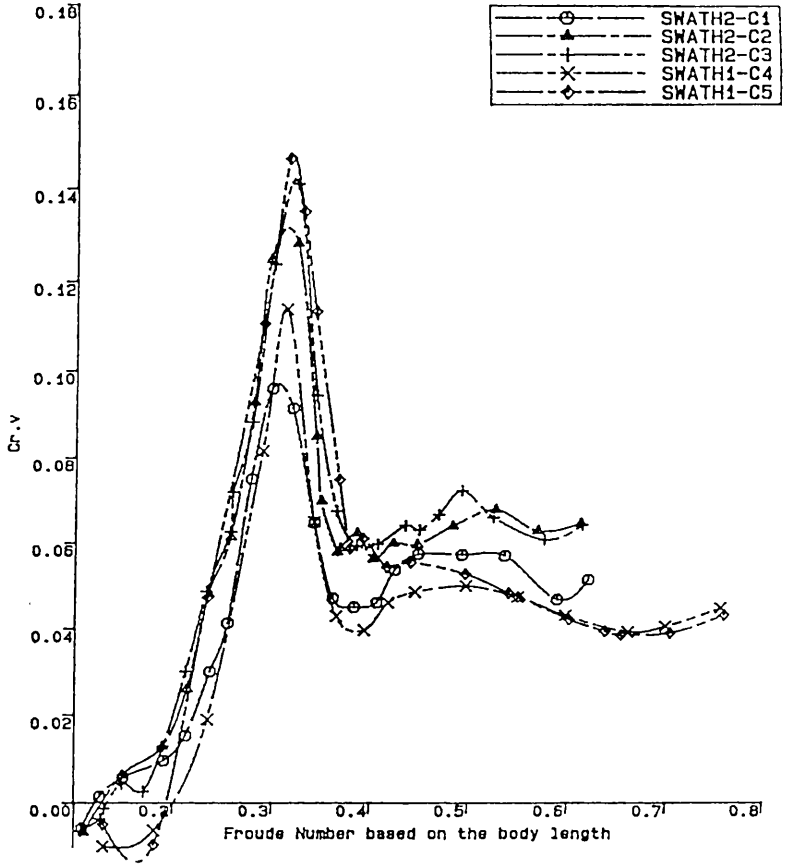

Comparison of the Residuary Resistance Coefficients of SWATH1 and SWATH2

Fig.4.108

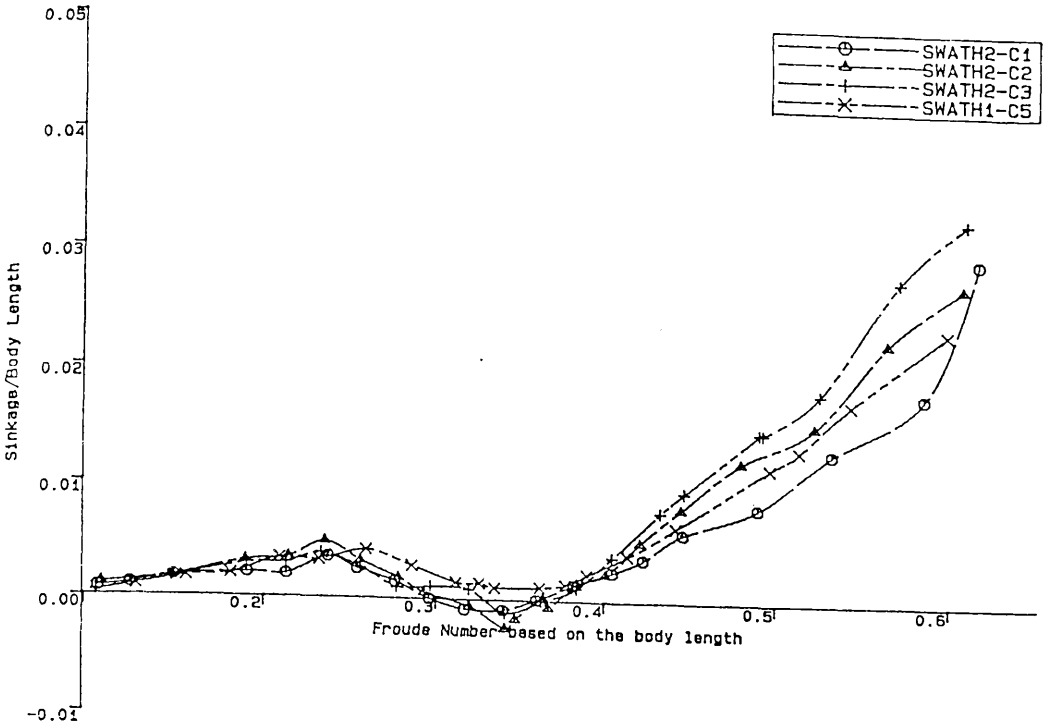

Non-dimensional Sinkage Divided by Body Length in Calm Water as a Function of Froude Number.

Fig.4.109

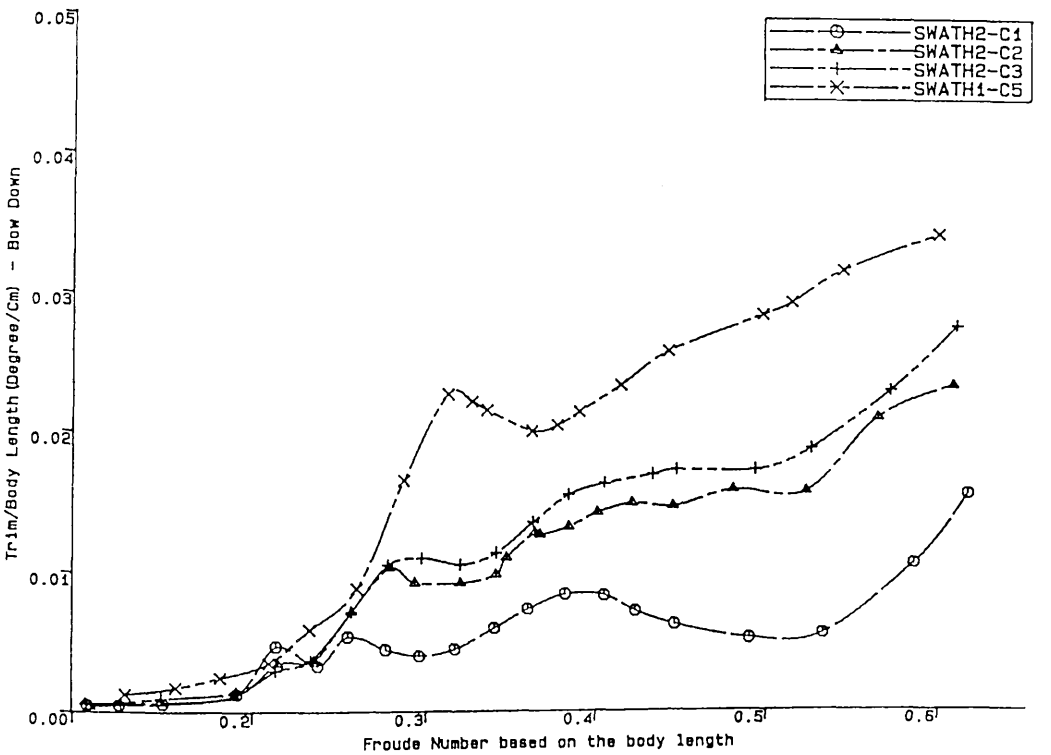

Trim Divided by Body Length in Calm Water as a Function of Froude Number.

Fig.4.110

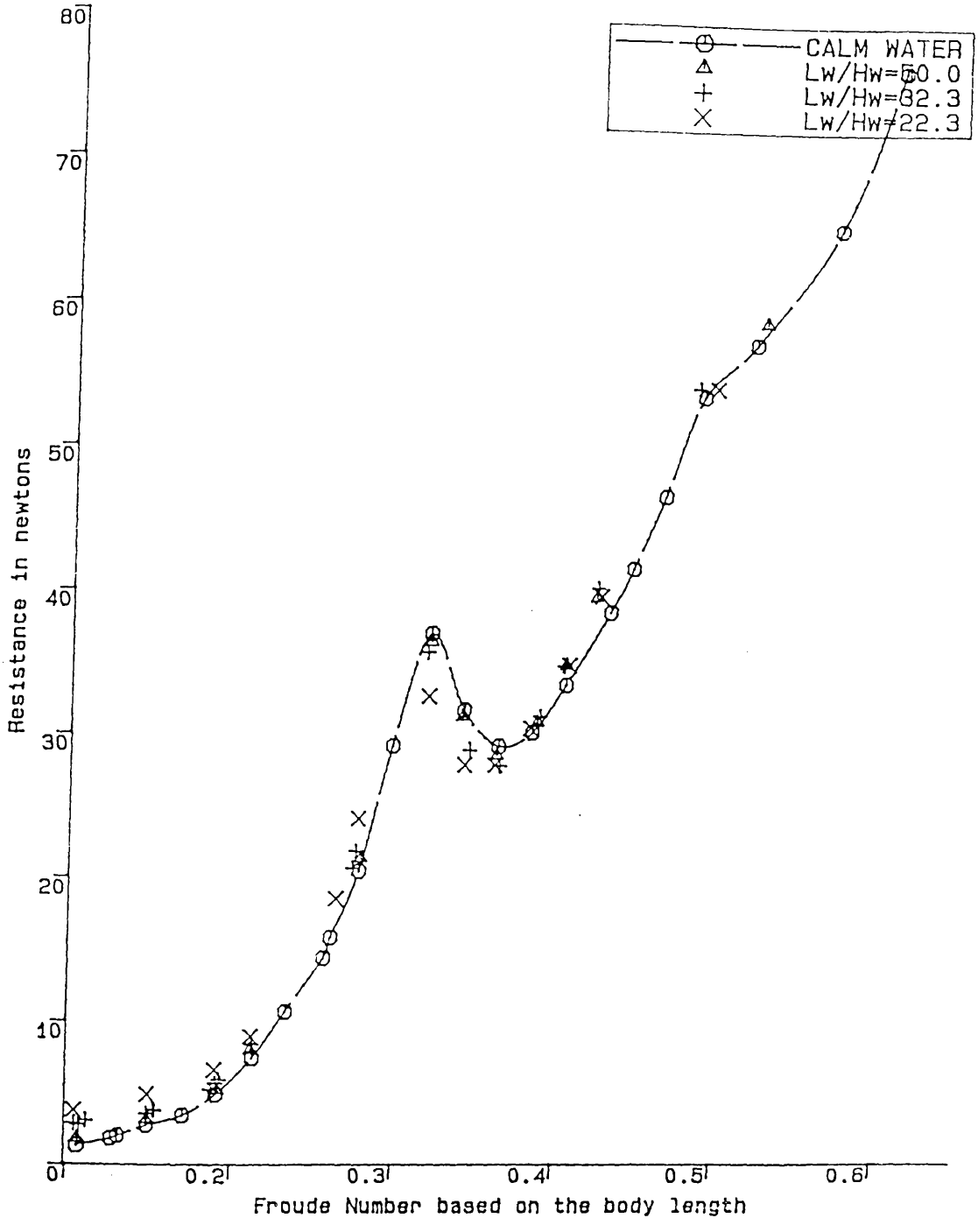

SWATH2 Model-C3 Total Resistances as a Function of Froude Number (Wave Frequency=0.83Hz, Lw/Lb=1.0)

Fig.4.111

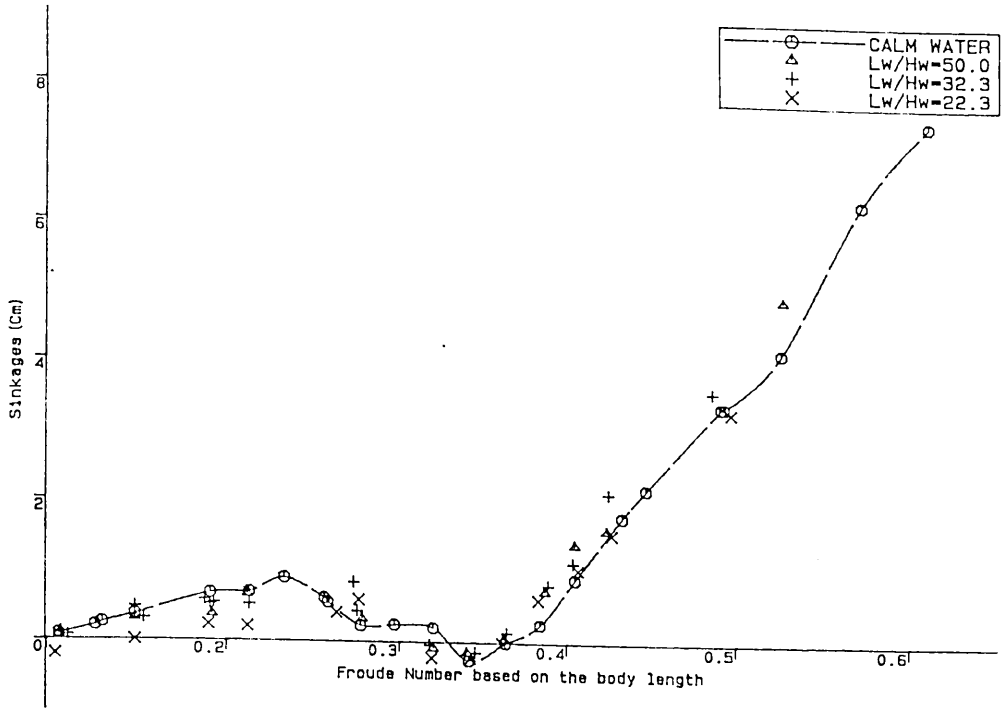

SWATH2-C3 Sinkages vs Froude Number and Wave Steepness (f=0.83hz, Lw/Lb=1.0)

Fig.4.112

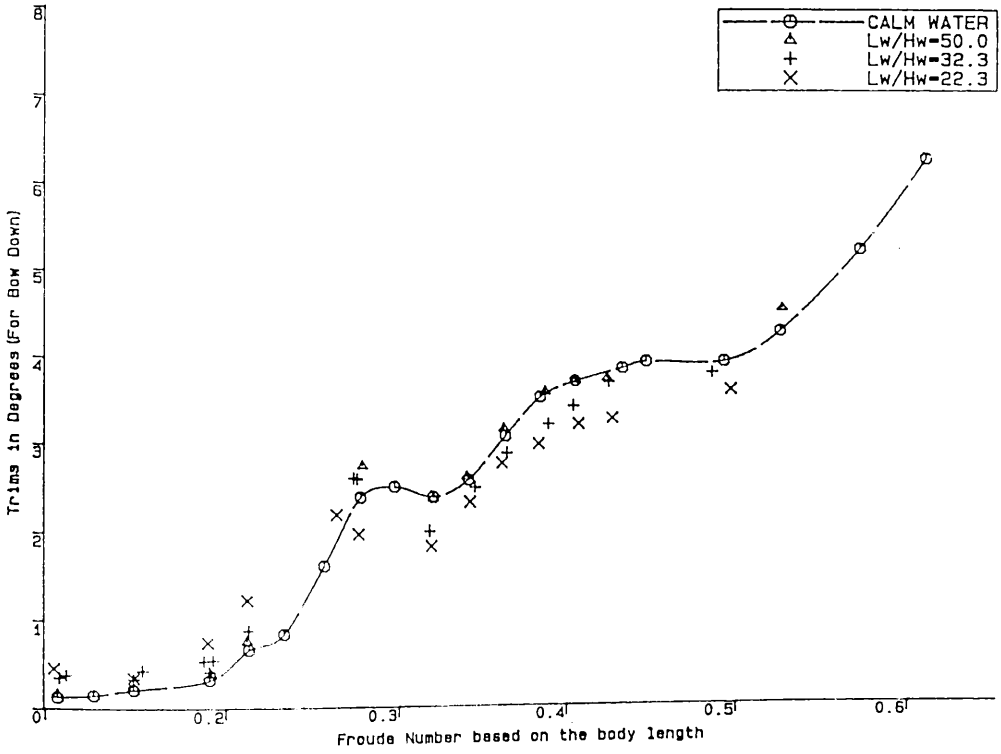

SWATH2-C3 Trims vs Froude Number and Wave Steepness (f=0.83hz, Lw/Lb=1.0)

Fig.4.113

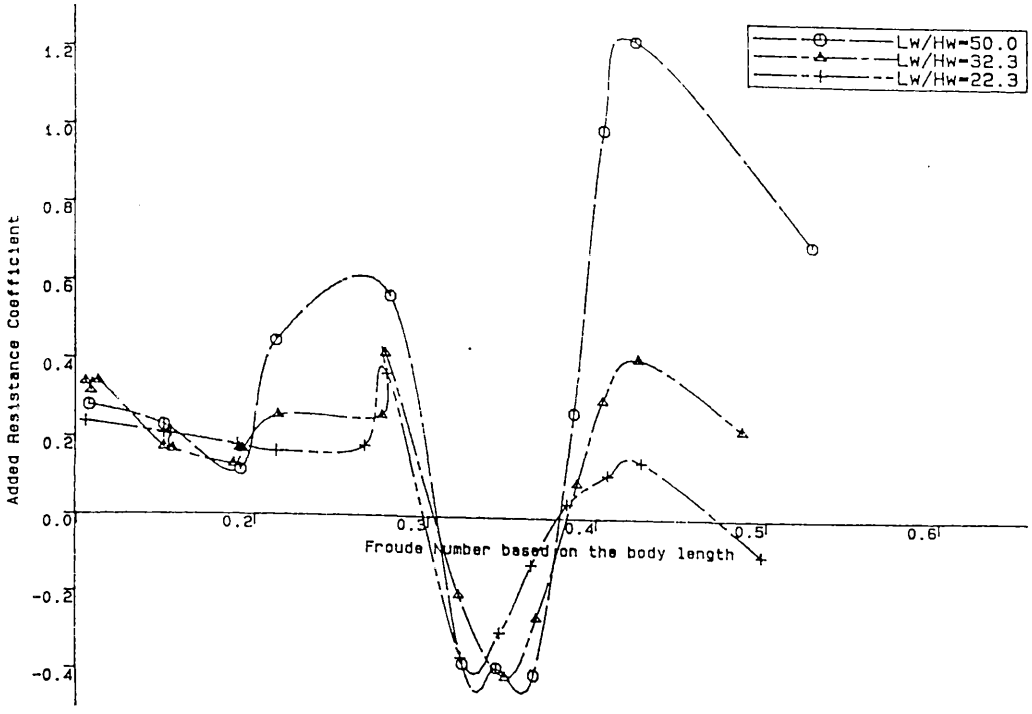

SWATH2 Model-C3 Added Resistance Coefficient as Functions of Froude Number and Wave Steepness (Wave Frequency=0.83Hz, Lw/Lb=1.0)

Fig.4.114

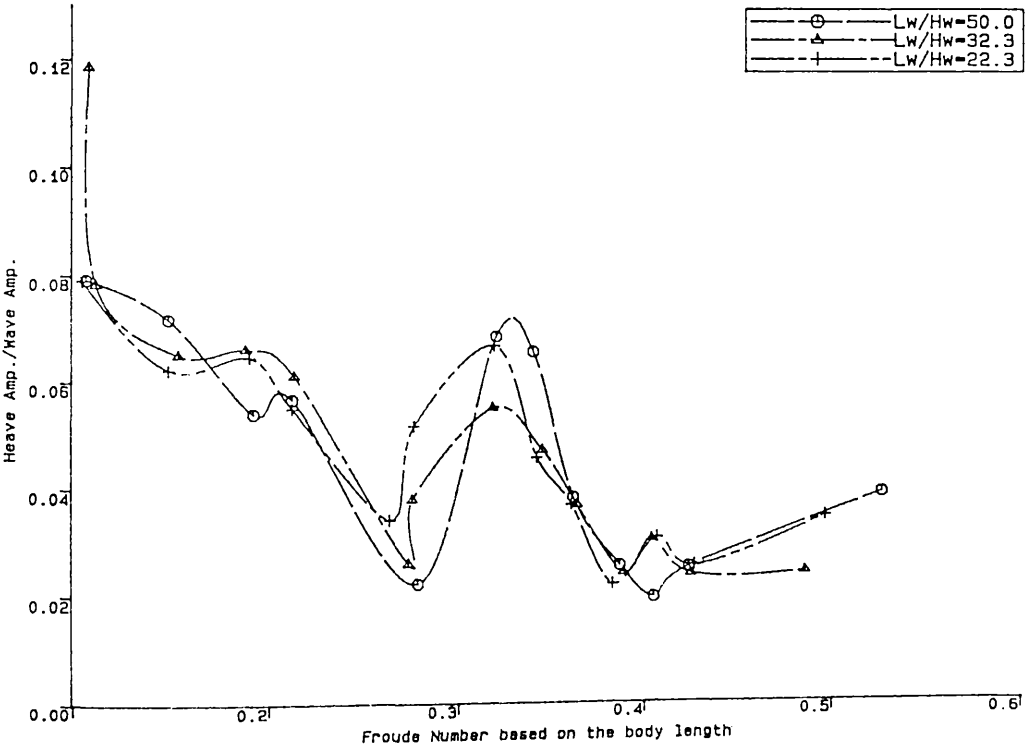

SWATH2 Model-C3 Heave Responses in Head Seas as Functions of Froude Number and Wave Steepness (Wave Frequency=0.83Hz, Lw/Lb=1.0)

Fig.4.115

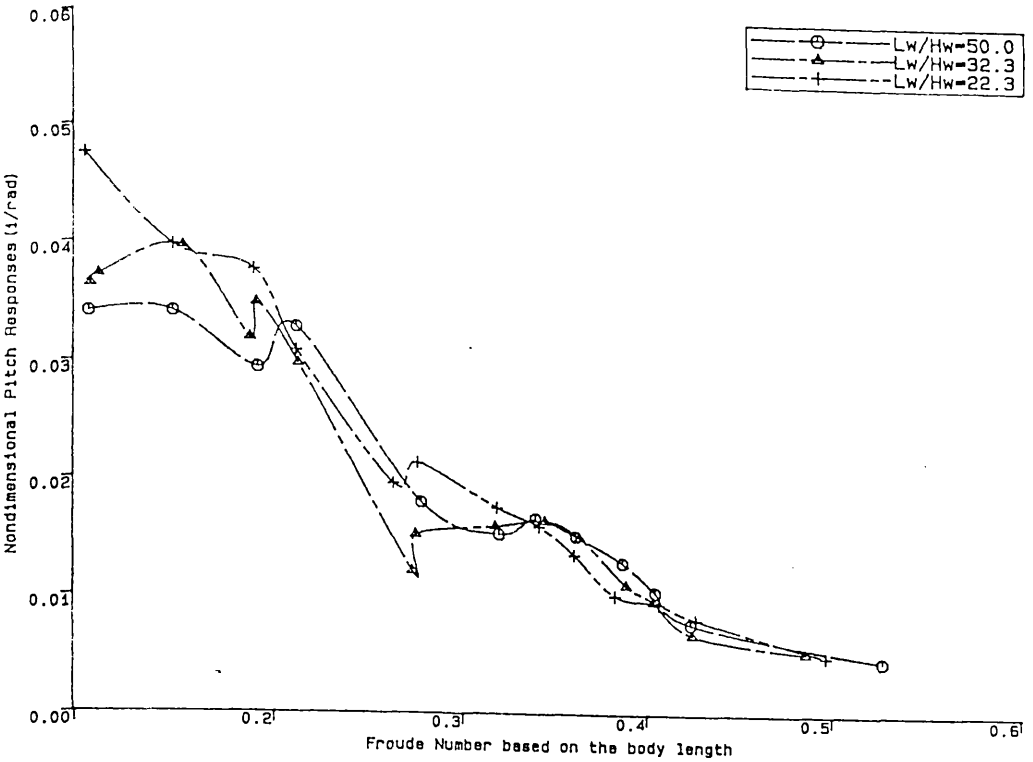

SWATH2 Model-C3 Pitch Responses in Head Seas as Functions of Froude Number and Wave Steepness (Wave Frequency=0.83Hz, Lw/Lb=1.0)

Fig.4.116

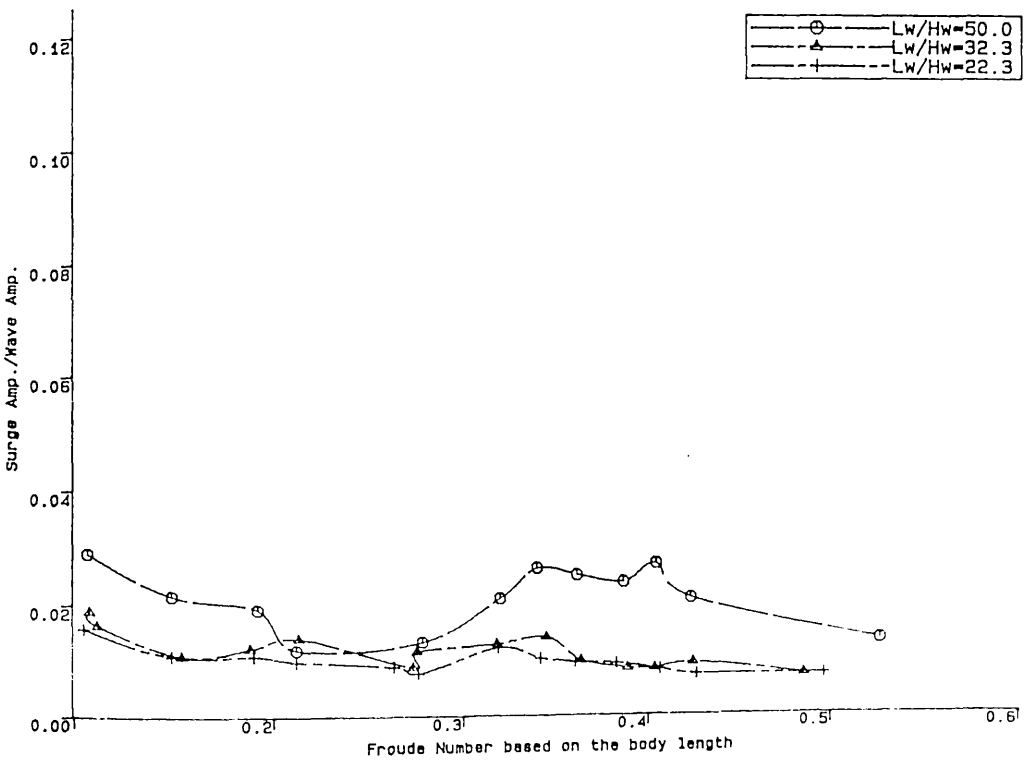

SWATH2 Model-C3 Surge Responses in Head Seas as Functions of Froude Number and Wave Steepness (Wave Frequency=0.83Hz, Lw/Lb=1.0)

Fig.4.117

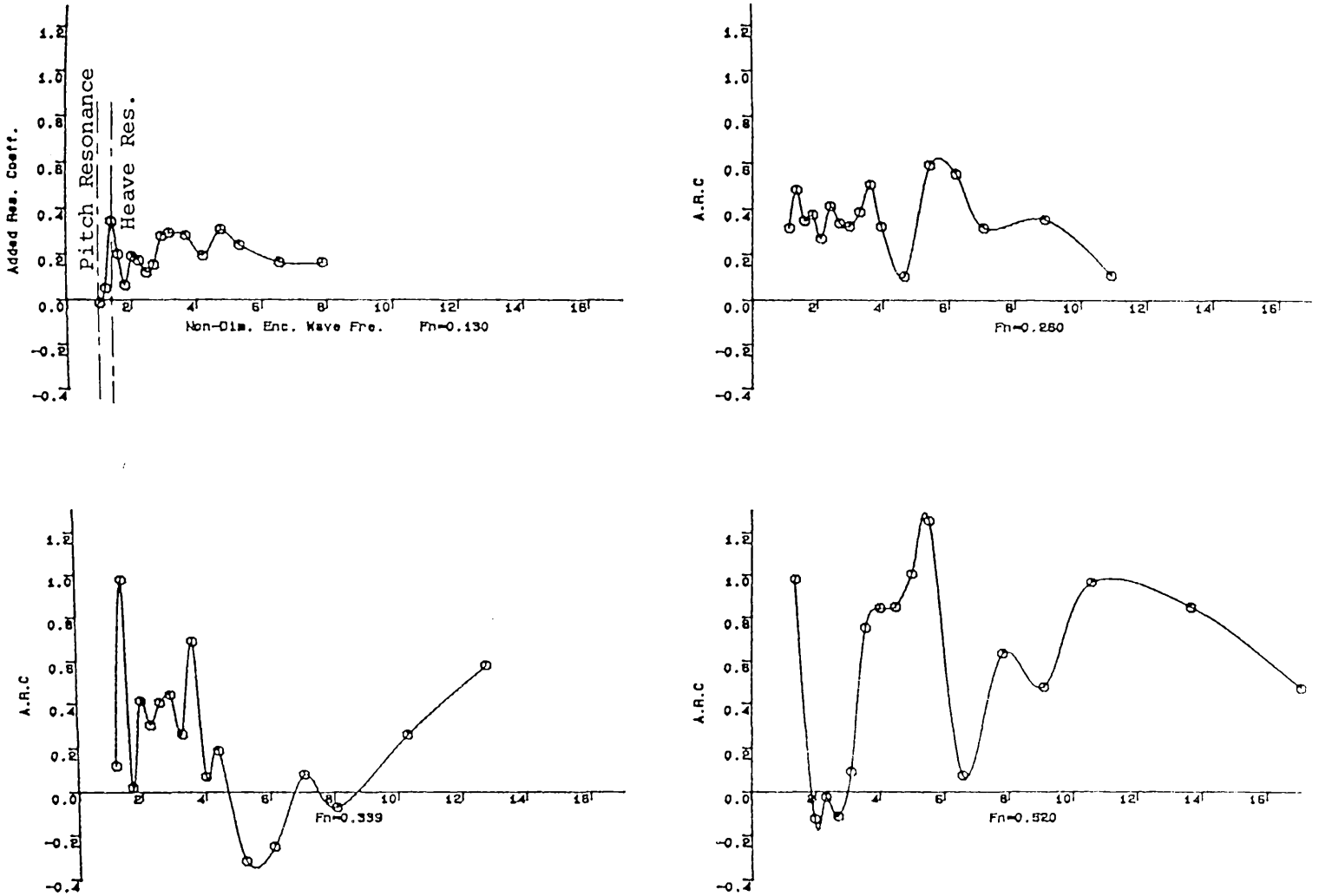

Fig.4.118
SWATH2-C3 Added Resistance Coefficient vs Non-Dimensional Encounter Wave Frequency For 4 Different Speeds

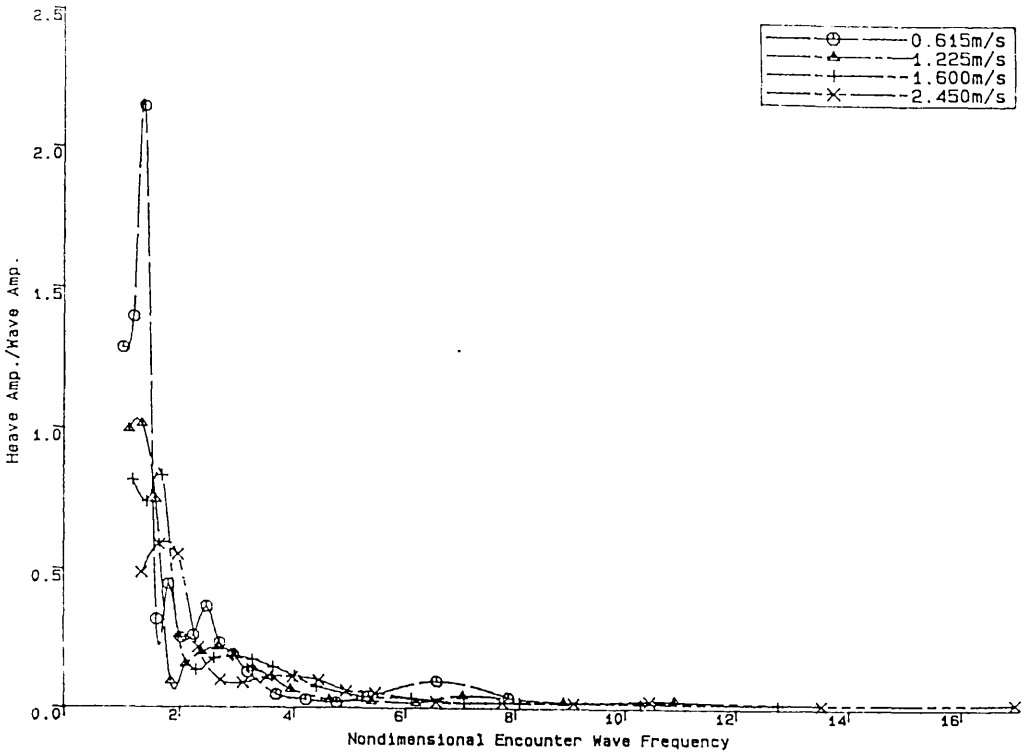

SWATH2-C3 Heave Responses in Head Seas With 4 Forward Speeds.

Fig.4.119

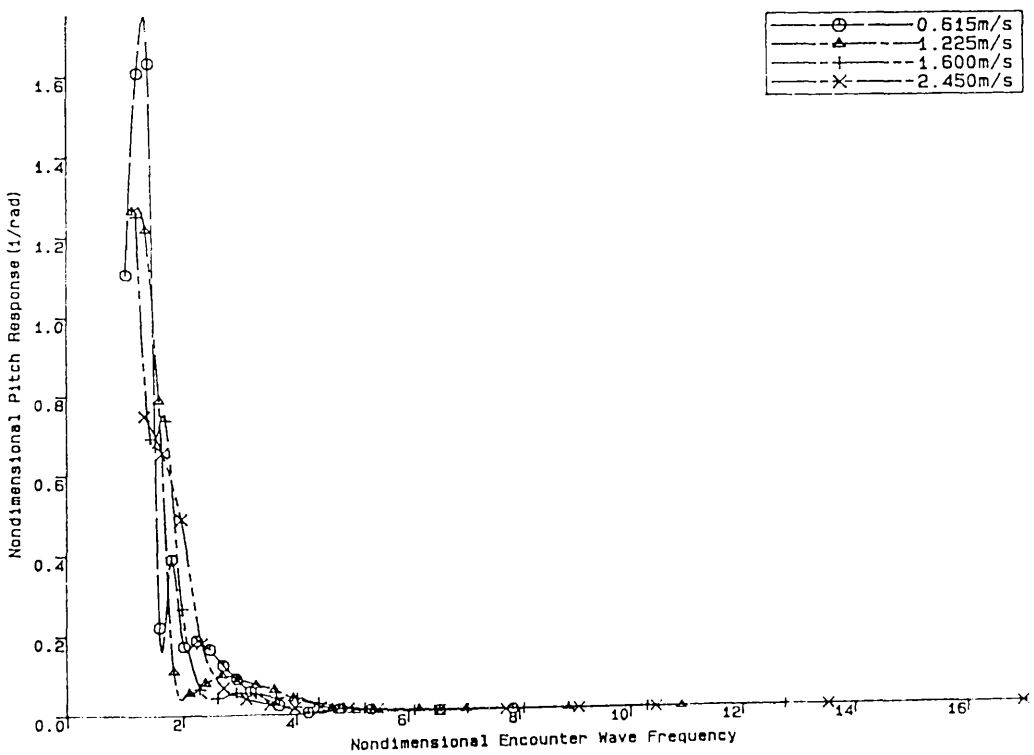

SWATH2-C3 Pitch Responses in Head Seas With 4 Forward Speeds.

Fig.4.120

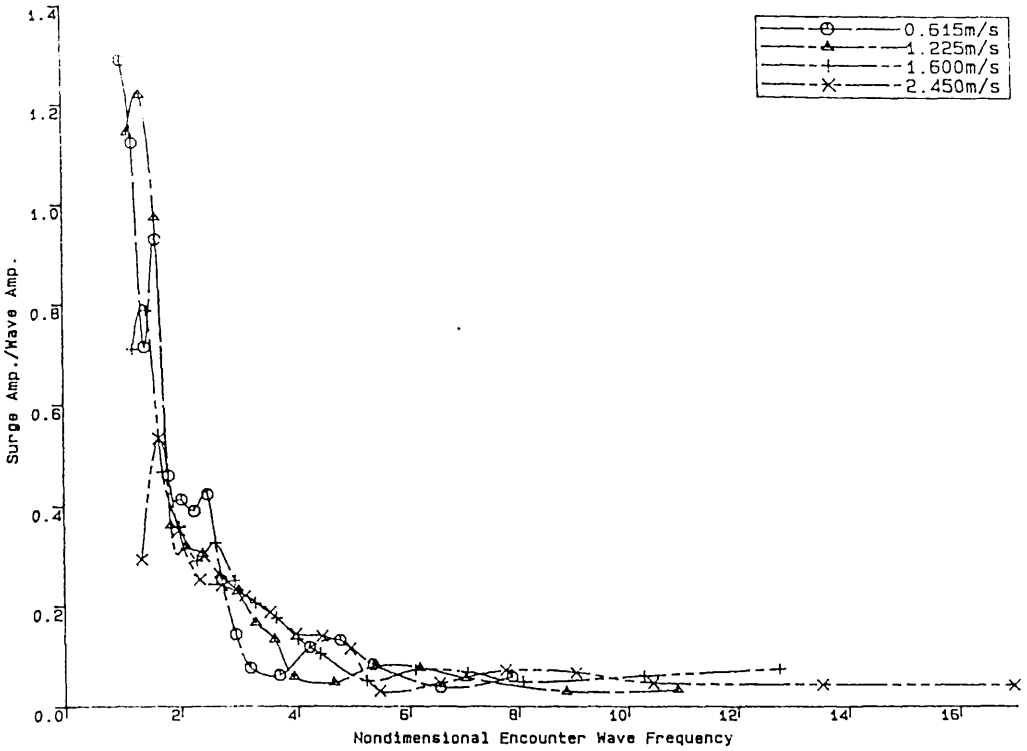

SWATH2-C3 Surge Responses in Head Seas With 4 Forward Speeds.

Fig.4.121

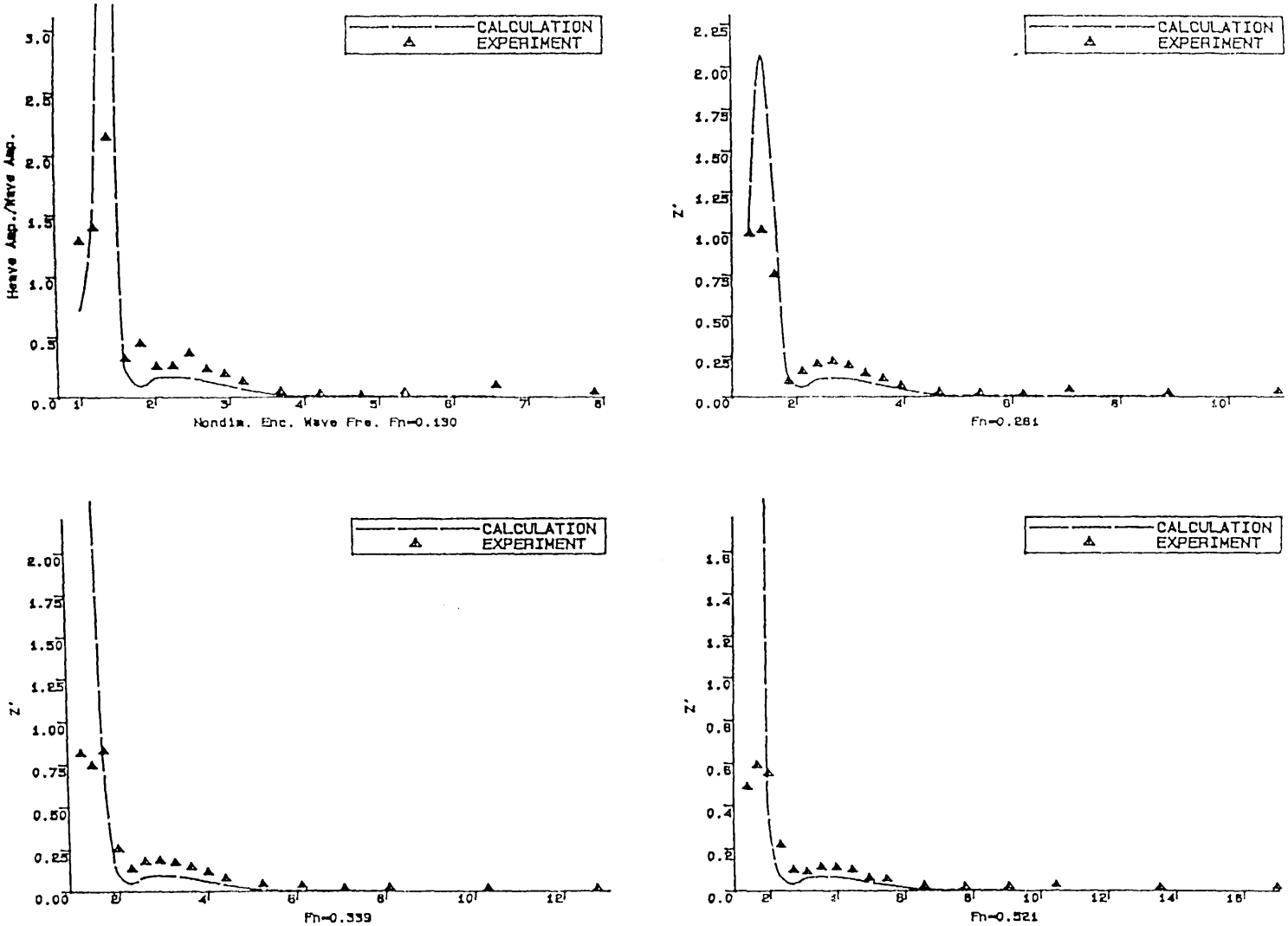

Fig.4.122

Computational(2-D) and Experimental Heave Responses of SWATH2-C3 in Head Seas

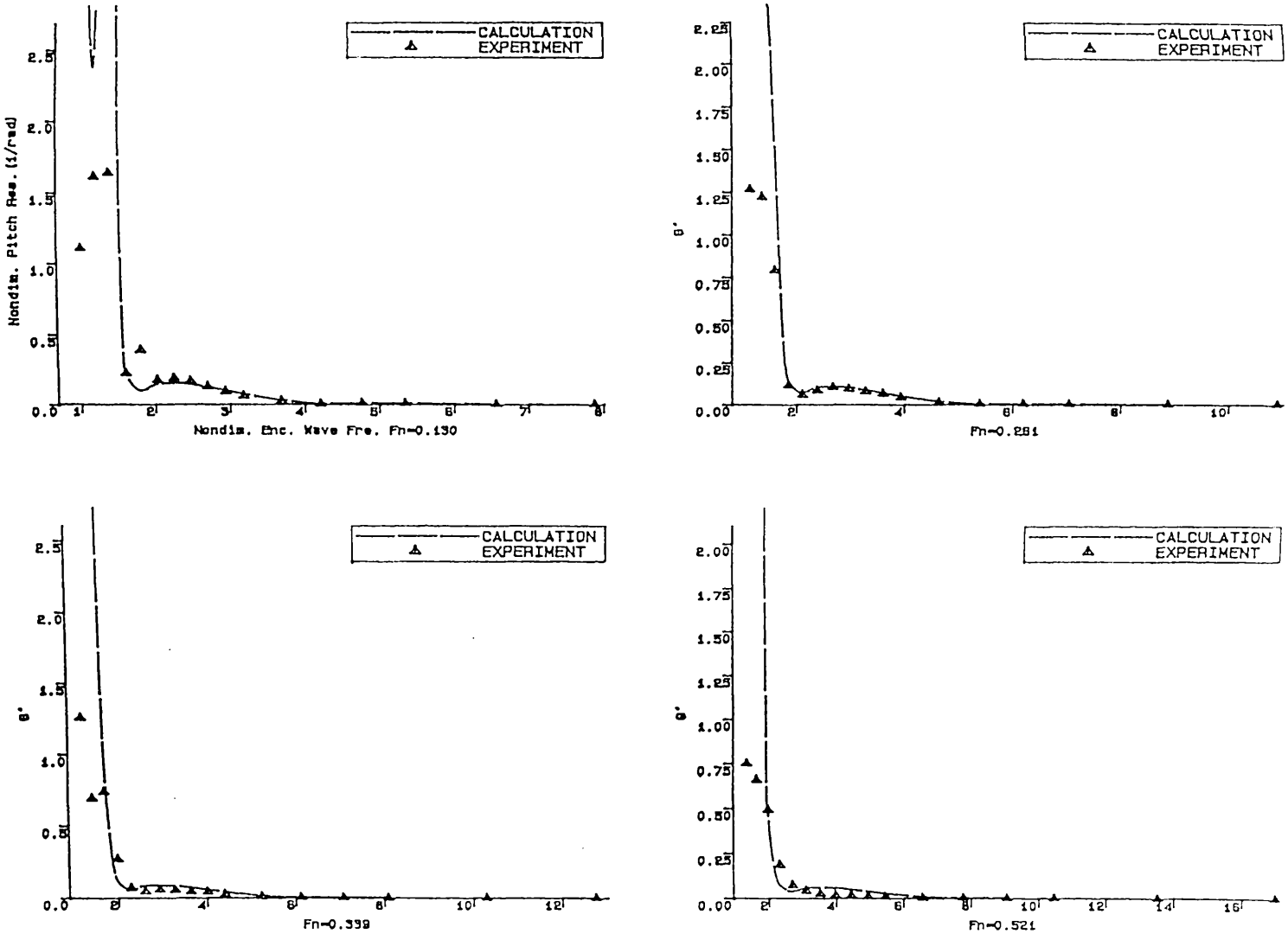

Fig.4.123

Computational (2-D) and Experimental Pitch Responses of SWATH2 in Head Seas

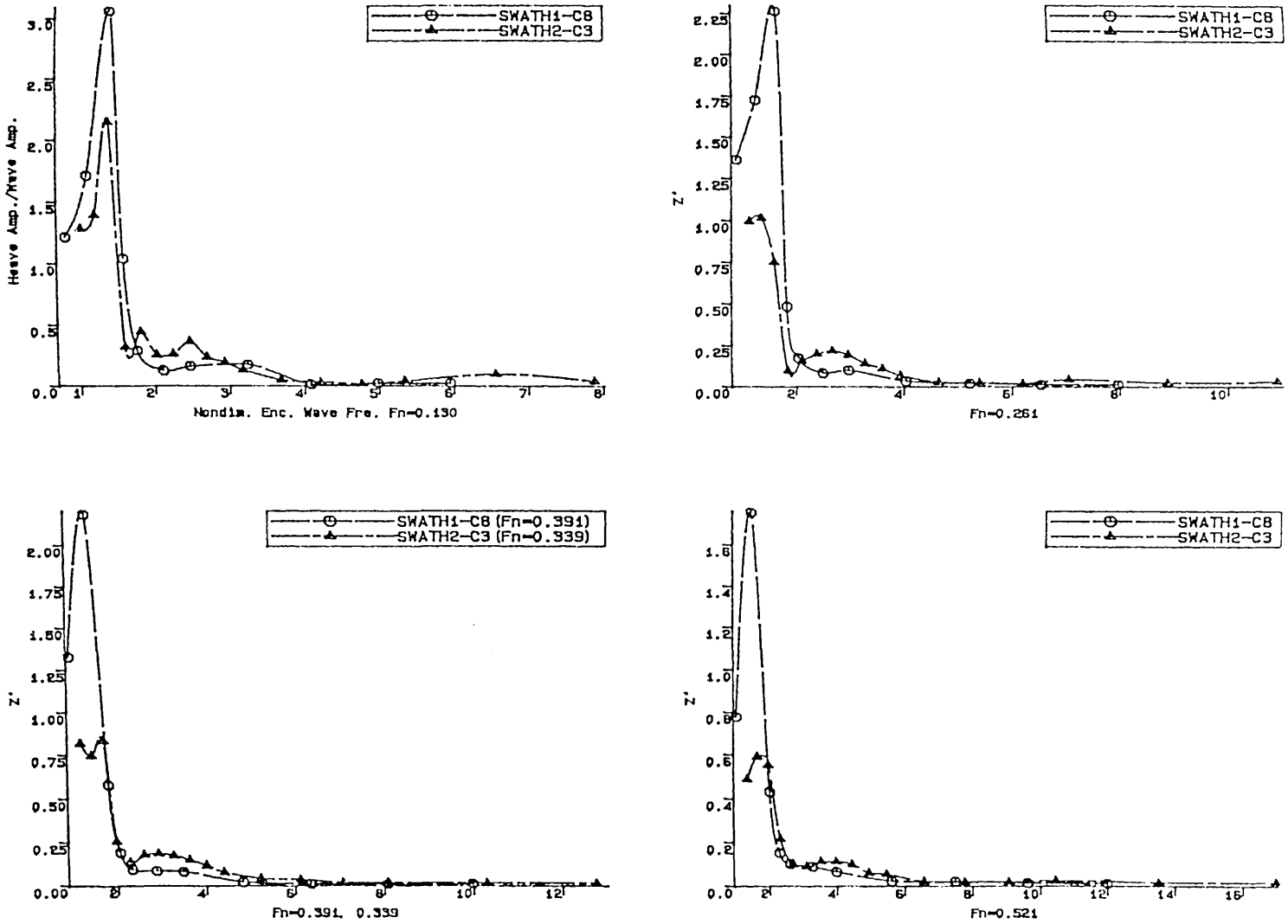

Fig.4.124

Comparison of Heave Responses of SWATH1 and SWATH2 in Head Seas

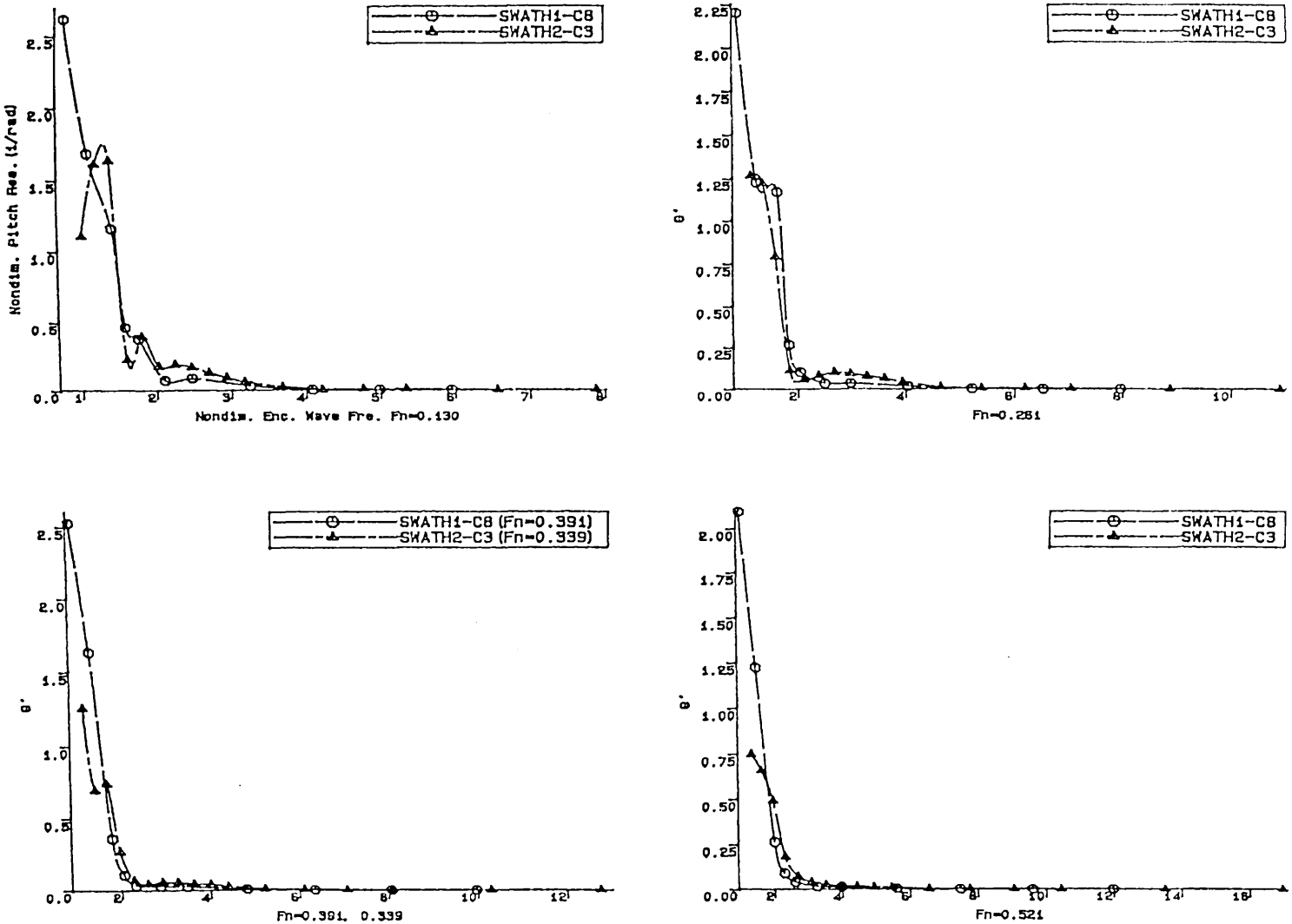

Fig.4.125
Comparison of Pitch Responses of SWATH1 and SWATH2 in Head Seas

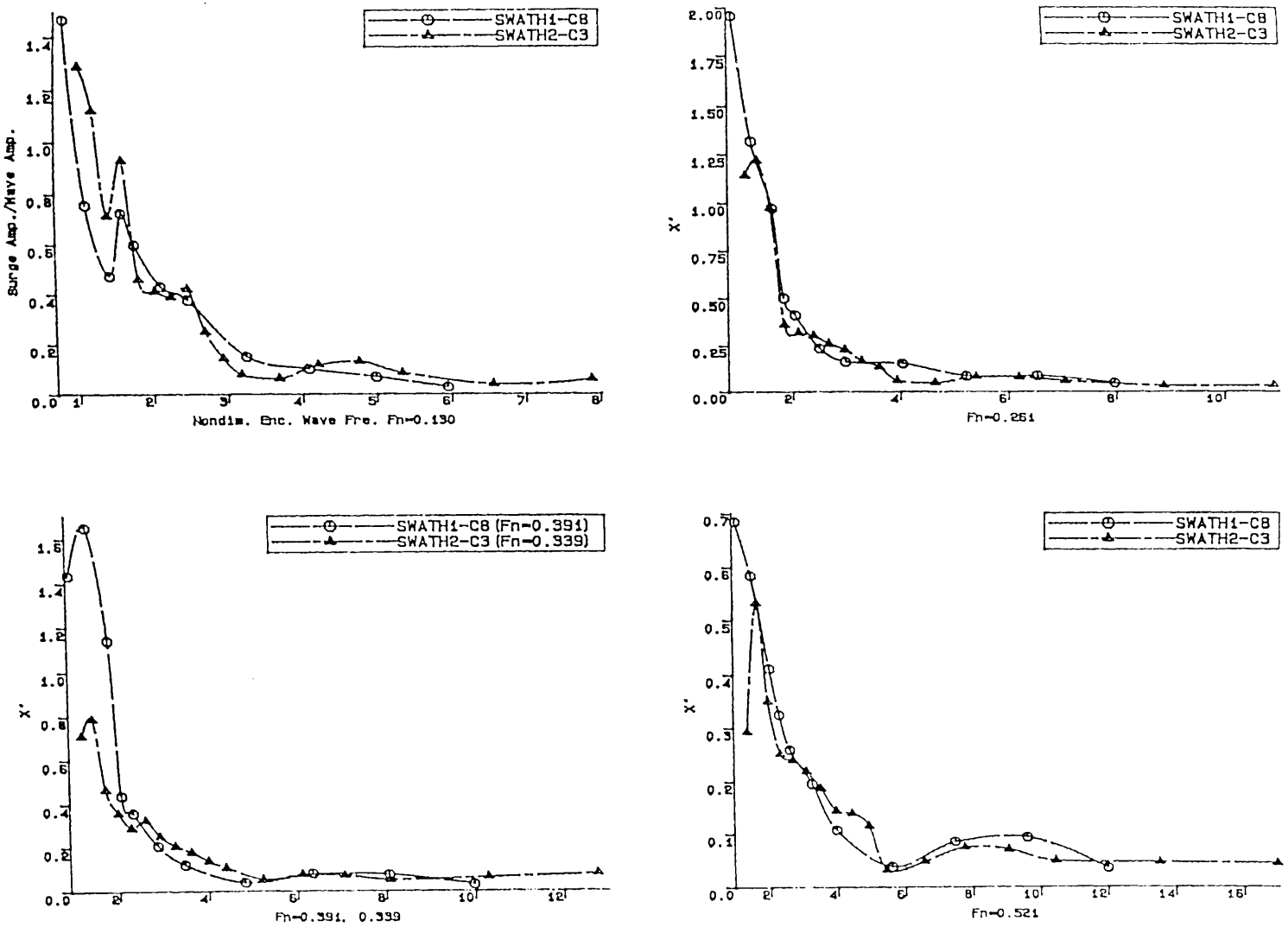

Fig.4.126

Comparison of Surge Responses of SWATH1 and SWATH2 in Head Seas

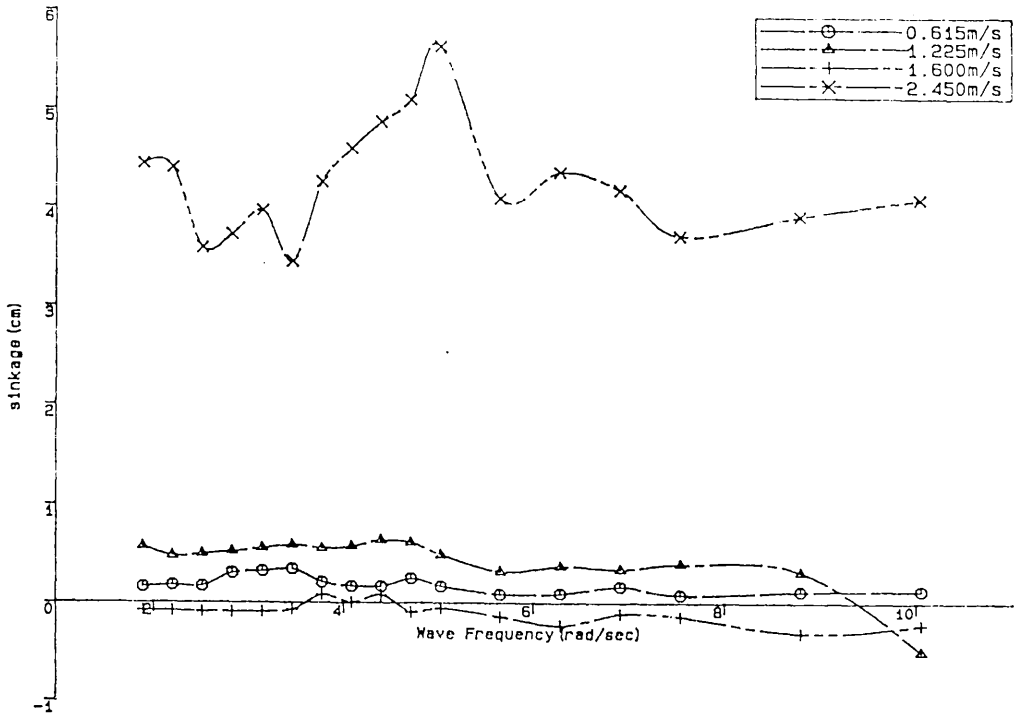

SWATH2-C3 Sinkages in Waves as Functions of Wave Frequency and Speed.

Fig.4.127

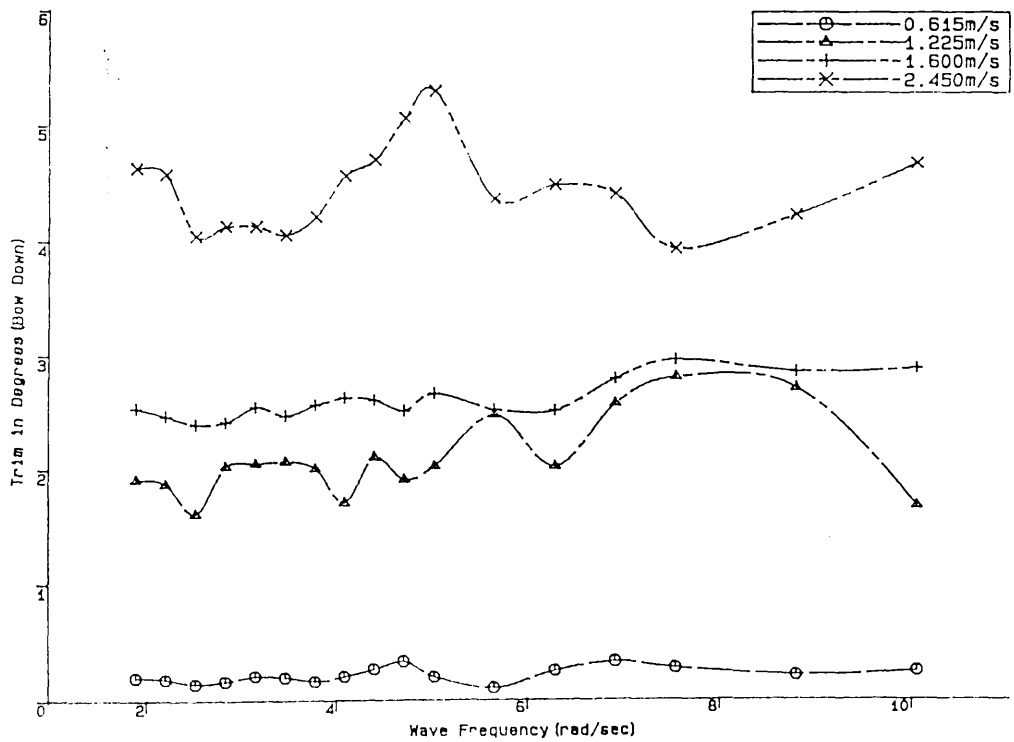

SWATH2-C3 Trims in Waves as Functions of Wave Frequency and Speed.

Fig.4.128

4.5 SWATH3 MODEL(SINGLE STRUT) CALM WATER RESISTANCE, AND RESISTANCE AND MOTION IN UNIFORM WAVES

The choice between single and tandem struts for SWATH ships has been considered in several papers[91,93]. The single strut version has been mostly adopted so far because of various practical aspects such as simplicity in design, better accessibility to the lower hulls for maintenasnce, more storage space in the struts, greater structural strength, large payload and greater static stability. This greater static stability can reduce the risk of possible heeling due to a sudden shift of many passengers(important for passenger ships) or other items of cargo payload.

Mitsui Engineering and Shipbuilding Co., Ltd. built a twin strut SWATH, 'MARINE ACE', and later converted it to a single strut version by filling the gap between the fore and aft struts to make a smooth continuous strut. Extensive sea trials for the both versions were conducted and the results are reported in Ref.[93], without much detail. Table 4.27 shows a comparison of main particulars for both versions of 'MARINE ACE', taken from the reference. The waterplane area of the tandem version is less than one half that of the single version. The reduction in waterplane area changes the restoring force and moment and, consequently, alters the natural periods in heave, pitch and roll motions as shown in the Table. Also, this reduced waterplane area will enhance seakeeping performance at the cost of the TPC and a stiffer roll motion for the single version is expected due to the shorter roll period. In general, the tandem struts version has lower side loads and motions at rest, and a shorter turning radius compared to the single strut version[92,93,94]. Therefore, the choice of either single or tandem struts version , from a seakeeping point of view, will mostly depend on the nature of the operating sea conditions and on the mission of the ship.

With regard to resistance for the single and tandem struts versions, there are contradictory reports: one is that the resistance of the tandem version of 'MARINE ACE' is higher than that of the single one at all the speeds tested due to miscellaneous resistances[93]; the other is that a tandem strut configuration is preferred to a single strut at higher speeds due to favourable interference wave systems[1]. A rigorous

comparison between the two versions is not given in the two papers nor in any other publised papers. Further, there are very few papers concerning the comparison between the performance of the two versions in calm water as well as in waves.

This section has twofold objectives. One is to compare the experimental and computational results of resistance of two models, SWATH1-tandem strut version and SWATH3-single strut version, and to validate the applicability of the computer program OSWATH. The other is to compare the experimental results of both models in waves such as resistance increase and motion responses(heave, pitch and surge). Sinkage and trim were also measured in calm water as well as in waves and compared with each other.

Table 4.27. Main particulars of MARINE ACE two versions

	Twin struts	Single Strut
Length b.p.(m)	11.00	
Breadth,max,(m)	6.50	
Depth (m)	2.70	
Draft (m), fully loaded	1.55	
Displacement at full load(ton)	18.4	22.2
Waterplane area at load line(m^2)	4.9	10.3
Natural periods (sec)		
Heave	5.5	3.9
Pitch	4.8	4.5
Roll	11.2	4.7
GMT (m)	0.5	2.1

In order to achieve the objectives, the SWATH1-tandem strut model was converted to a single strut version, designated SWATH3, in the same manner as was done for 'MARINE ACE': A parallel section between the maximun chord points of the fore and aft struts on the model SWATH1 was inserted to make a continuous, smooth strut with all other dimensions unchanged. Hence, the waterplane area of the SWATH3 is nearly doubled and, consequently, the natural period of heaving, pitching and rolling are all decreased as shown in Table 4.28.

For the purpose of comparing with the previous results of tests on SWATH1, a

total of three conditions consisting of two settings of draft(2.0 and 2.5 times the dimeter of body) and two settings of the spacing between the centrelines of two demihulls were selected as shown in Table 4.29. SWATH3-C1,C2 and C3 are the condition numberings which are equivalent to SWATH1-C5,C6 and C8, respectively, with regard to the spacing and draft.

Table 4.28. Some Dimensions and Principal Coefficients for SWATH1 and SWATH3 Demihull at the Draft of Two Times the Body Diameter

GUH Model	SWATH1	SWATH3
Length of Body(m), L_b	1.51	
Diameter of Body(m), Di_b	0.0892	
Length of Strut(m), L_s	0.4	1.155
Maximum Beam of Strut, t_m	0.05	
L_b/Di_b	16.93	
C_p of Body	0.9	
C_{wp} of Strut	0.665	0.884
L_s/t_m	8.0	23.1
Draft(m), T	2.0 Di_b=0.1784	
Depth of Strut(m), D_s	0.0892	
SDBC(m), h	0.1338	
Wetted Area(m^2), S	0.5125	0.55039
Displaced Volume(m^3), ∇	0.0109	0.01305
$H_1=2h/Di_b$	3.0	
Waterplane Area(m^2)	0.0266	0.0510
Natural Periods*		
Heave(sec), T_z	1.701	1.23
Pitch(sec), T_θ	2.252	2.06
Roll(sec), T_ϕ	2.778	1.717

Note; * at the nondimensional spacing of $B_1(4b/L_b)$=0.762

Table 4.29. Experimental Conditions Tested with SWATH3 Model

	0.575m (B_1=0.762)	0.715 (B_1=0.947)
2.0Di_b (H_1= 3)	C1	C3
2.5Di_b (H_1= 4)	C2	

Total resistance and motion responses(heave, pitch and surge) were also measured in uniform, head waves together with mean sinkage and trim. The added resistance due to the oncoming waves is derived by subtracting the still-water resistance from the total resistance in waves.The constant velocity towing method was used due to its simplicity and accuracy compared to the constant thrust method. Several wave frequencies within a range of 0.4hz to 1.1hz corresponding to wave length to body length ratios of 6.46 to 0.85 were covered for SWATH3-C1 at two forward speeds with two sets of wave height at each speed in order to study the effect of the wave steepness on the added resistance as well as on the motion responses. Ten speeds were used at one wave frequency of 1.02hz with two wave height changes. Further, 8 wave heights were used to investigate in detail the relationship between the added resistance and waveheight as well as between the motion responses and wave height. Lastly, 8 speeds were used for SWATH3-C2 at one wave length of 1.02hz in order to find the submergence effect on both the added resistance and motion responses. Mean sinkage and trim in waves are compared with those in calm water and are used to examine the resistance variations in waves as well as with speed by physical reasoning. All the results are compared with those of SWATH1 and discussed at length. Detailed results are reported in Ref.[100] and this section is taken from that reference.

4.5.1 Description of Model SWATH3

The SWATH1-tandem strut model was converted by inserting a parallel section between the maximum chord of the fore and aft struts on the demihull to make a continuous, smooth strut and designated as SWATH3. Hence, the waterplane area is nearly doubled from that of the SWATH1. Some dimensions and principal coefficients for the both models are listed in Table 4.28 together with the comparison of the natural periods for heave, pitch and roll. A small scale model plan and details are shown in Fig.4.129-a and a front view of the SWATH3 model is shown in Fig.4.129-b.

Model arrangements, instrumentation, towing system and calibration procedures(LVDTs and wave probes) are exactly the same as those for the SWATH1 model experiments as described in sections 4.3.1 to 4.3.3. Turbulence stimulation

devices were not introduced for the model to keep consistency with the previous tests.

4.5.2 Analysis and Discussion

4.5.2.1 In calm water

The total, residuary resistances and their coefficients are listed at Tables 4.30 to 4.32 for conditions C1, C2 and C3 tested, respectively. Figures 4.131 through 4.133 present the total, residuary and skin frictional resistances as a function of Froude Number for these conditions.

Figs.4.136 through 4.138 show comparisons between the calculated wave-making resistance and measured residuary resistance coefficients versus Froude Number. The lower measurements at slow speeds might be due to the fact that no turbulence stimulation devices were used for the measurements and possibly laminar flow occured. Another reason for this is that the viscosity of water is ignored in the wave resistance theory and hence the wave system can be exaggerated over the viscous dominant speed range(slow speeds) due to the absence of the viscous damping. In particular, this phenomenan can be seen over the hump speed range at the slow speed. Apart from the lower speed range, the theory gives good qualitative aggrements with the measurements. The difference between the two curves accounts for additional resistances such as viscous pressure, form(3-D effect), eddying, wave-breaking and spray resistances as well as some non-linearity effects. It is known from the analysis of several SWATH designs that the quantity, $C_{r.s}$ - $C_{w.s}$, oscillates about zero, being usually bounded within a difference of $\pm 1.0 \times 10^{-3}$[5].

Also, these figures illustrate the contribution of each component of the model to the total wave-making resistance as well as two times one demihull wave-making resistance for the three tested conditions. From the figures, it is easily understood how the total wave-making resistance is affected by the components of the model as well as by the parametric changes such as draft, spacing between the two demihulls, slenderness of the body and strut, and relative position of the strut on the demihull, etc. For the two drafts tested(C1 and C2), for example, a resistance benefit is not expected

from the draft increase in terms of resistance per tonne. This is due to the fact that the increased strut depth results in a considerable increase of the strut wave-making resistance which outweighs the decrease of the body wave resistance as the draft increases. If the increased wetted area is taken into account, the total resistance per tonne becomes worse with the increase of the draft as shown in Fig.4.134. The largest hump at around Fn=0.3 for SWATH3-C1(see Fig.4.136) is slightly shifted to Fn=0.29 for SWATH3-C2(see Fig.4.137) due to the increased strut contribution to the total wave-making.

It is noticed from the theoretical calculations that favourable interferences between the two demihulls occur within the range of Fn=0.3-0.38 depending on the spacing and draft. Excepting for that speed range, unfavourable interferences are found throughout the speed range and the worst interference is seen around Fn=0.5 for all the conditions tested. As the speed increases further, these interferences becomes negligible. This spacing effect can be seen from the experimental measurements as shown in Fig.4.135. The interference waves cusps, which appeared in between the demihull of the SWATH1 and SWATH2 models, did not develop with the present single strut model(see Fig.4.130). In general, the wider spacing of the two demihulls, the better at higher speeds in terms of resistance. However, at slow to moderate speeds, in particular, Fn=0.3-0.38, an optimum spacing can be found depending on the arrangement of the components of a SWATH ship.

A) Sinkage and trim

Figures 4.139 and 4.140 show the sinkage and trim as a function of Froude Number for all conditions tested. Although the results are not compatible with those measured by self-propulsion, they can be used to help improve our knowledge of the resistance-speed characteristics as well as of the relationships between the sinkage, trim and resistance for SWATH ships. According to the figures, it is apparent that the sinkage and trim, in general, increase with speed, resulting in severe sinkage and trim by the bow at higher speeds. This is due to the small waterplane area of the model and due to the Munk moment which is proportional to the heave added mass times the

square of the model speed. It is worthwhile noting that the sinkage and trim curves follow the same trends as the resistance curves for the three conditions. Namely, the wider the spacing between the two demihulls, the smaller the sinkage and trim. The sinkage and trim also increase with draft with some exceptions at the slower speeds as seen in the figures. The humps and hollows in the curves of the total resistances in Figs.4.131 to 4.133 can also be seen in the curves of trim. As was mentioned with the SWATH2 tandem strut model, it is interesting to see that a simple arithmetical summing of the sinkage and the trim produces a curve character rather similar to the curve of the total resistance, with some undulations and a gentle slope at higher speeds, rather than to the residuary resistance curve shown for the monohull ship[69].

Owing to the comparatavely small freeboard compared to the other tested conditions, the severe sinkage and trim at higher speeds caused an increase in the measured total resistance due to green water as seen at the last speed for SWATH3-C3 (see Fig.4.137) and the measurements could not be conducted further more at this draft. It is interesting to see that the sinkage and trim of the single strut design are considerably smaller than those of the tandem strut as discussed later.

B) Comparison with tandem strut SWATH1

Figs.4.18, 4.19 and 4.21 show the wave-making resistance coefficients of SWATH1-C5, C6 and C8, which are equivalent to SWATH3-C1, C2 and C3, respectively, with regard to draft and spacing. This diagrams also illustrate the contribution of each component of the model to the total wave-making resistance as well as the residuary resistance coefficient. Compared to the resistance coefficient curves as shown in Figs.4.136 to 4.138 for the single strut version, a very large peak around Fn=0.3-0.31 is seen for the tandem struts. This is easily understood from the figures which show that it is caused by the large wave-making contributions of the struts coupled with unfavourable interferences between the body and the struts and between the forward and aft struts. In particular, the tandem struts, which have low length to thickness ratios compared to the long single strut as shown in Table 4.28, contribute significantly to the large peak at that speed. However, the strut with the low length to

thickness ratio gives low wave-making resistance at higher speeds and hence, the wave resistance of the tandem strut SWATH is lower at higher speeds than its counterpart single strut SWATH. From the comparison of the wave-making resistance between the two models, the single strut version is better up to Fn=0.42 and the tandem strut becomes better above this speed.

On the other hand, if skin-frictional resistance is taken into account, a very interesting result can be seen. It has been thought that an increased wetted area for a single strut SWATH creates more frictional resistance and hence, more total resistance than for a tandem one.Comparing the total resistance coefficients(Ct_V) of SWATH1-C5, C6 and C8 as shown in Figs.4.32 and 4.33, with the equivalent results of the single strut version as shown in Figs. 4.134 and 4.135, it can be seen that the total resistance coefficients of the single strut version is slightly less at higher speeds than those of the tandem for all three conditions despite the aforementioned larger wave-making resistance at the higher speeds. This can be explained by the followings. The characteristic length of the single strut is 2.9 times longer than that of each strut for the tandem struts and hence, the Reynolds number(Rn=UL/v) of the single strut is higher than that of the tandem strut at the same model speed. Therefore, the skin frictional resistance coefficient of the single strut SWATH is smaller than that of the tandem strut SWATH. This can be easily understood from the comparison of the frictional resistance coefficients of SWATH3-C1 and SWATH1-C5 as shown in Figs.4.141 and 4.142. These figures present the total, residuary and frictional resistance coefficients all together in one graph for SWATH3-C1 and SWATH1-C5, respectively. This effect will be decreased for the full size ship depending on its length since the slope of the skin-frictional formula(ITTC'57 line) becomes gentler as Reynolds number increases.

It was reported from the analysis of SWATH-386 model experiments[23](this will also be discussed in the following section 4.6) that both the wave-making and total resistance coefficients of the single strut version are higher at higher speeds than those of all the other tandem strut versions.

As a result, it can be seen that, in general, a single strut SWATH is better up to moderately high speeds and a tandem strut SWATH becomes better at higher speeds from the point of view of resistance.

Fig.4.143 presents a comparison of the sinkages between the single and tandem strut versions. The sinkage of the tandem strut version is lower around Fn=0.29-0.45 than that of the counterpart due to its complicated interference wave systems. Except within that speed range, the single strut SWATH is subject to lower sinkages than the tandem strut SWATH and this is very much exaggerated at higher speeds. The pattern of trim for both versions are similar as shown in Fig.4.144, but the single strut version is subject to less bow trim than the counterpart, especially, at higher speeds.

4.5.2.2 In head waves

The still water resistances of SWATH3-C1 and C2 are plotted as a function of Froude Number in Figs.4.145 and 4.146 together with the resistances in waves. The negative resistance increase, which occurred over the hollow and hump speed range(Fn=0.31-0.39) for the tandem strut versions, SWATH1 and SWATH2, cannot be seen for the single strut version. Therefore, this finding can support the fact that the negative resistance, which occurred with the tandem strut models, is due to the complicated hydrodynamic interferences between the fore and aft struts combined with some motion aspects of the tandem struts models rather than due to the sinkage and trim variations.

As with the tandem strut versions, the sinkages in waves as shown in Fig.4.147 are decreased(but not much compared to the tandem strut versions) at slow speeds and then increased compared to those in calm water. The trim in waves as shown in Fig.4.148 occurs in the opposite way to the tandem version, namely, the trim in waves becomes lower at slow speeds and then higher at high speeds compared to that in calm water. This increased trim results in the resistance increases compared to the tandem version at higher speeds. In addition, unlike the tandem versions, it can be seen that there is little difference in both the sinkage and trim for the two wave steepnesses. The sinkage and trim for SWATH3-C2 in calm water and waves are shown in Figs.4.149 and 4.150.

The non-dimensional added resistance coefficients of SWATH3-C1and C2 are shown in Fig.4.151 as functions of Froude Number and wave steepness. The added

resistance is obtained by subtracting the calm water resistance from the resistance in waves. If the speeds tested in calm water and in the waves are different from each other, the calm water resistance is read off from the curve fitting of the measured results at the speed tested in waves. From the comparison of the results at λ/ζ_W=38.9 and 21.6 for SWATH3-C1, it can be seen that the added resistance coefficient decreases significantly at higher speeds as the wave height increases.

The motion responses(heaving, pitching and surging) of these three conditions are plotted against Froude Number in Figs.4.152 through 4.154. As expected, SWATH3-C2 is subject to less motion responses than SWATH3-C1 due to its deeply submerged body compared to the SWATH3-C1. However, the added resistance has a slightly opposing trend as shown in Fig.4.151 at the similar wave steepness. Because of the relatively small free board for SWATH3-C2, a large amount of green water on deck was observed during the experiments at the wave height tested when the model was under motion. Therefore, it is fairly certain that the green water caused higher resistance increases at the 2nd draft. With this point in mind, it can be believed that the added resistance of the deeper draft SWATH will be less than that of the lighter draft one provided that green water effects don't occur.

The added resistance coefficients of SWATH3-C1 are presented in Fig.4.155 versus the non-dimensional encounter wave frequency for the two speeds tested and two sets of wave heights at each speed. The number of the frequencies tested was not enough to fit a curve smoothly and the pitch resonance frequency range was not included fully in the tests. It can be seen from the figure that the large resistance increase occurs at around the heave resonant region for the two speeds. However, it was found that the greatest resistance increase or decrease occurs at around pitch reasonant region for the SWATH1 as shown in Fig.4.86. A possible reason for this is explained in detail later.

Figs.4.156 to 4.158 show the non-dimensional heaving, pitching and surging responses against the non-dimensional wave frequency. A local peak can be seen in the pitch response as shown in Fig.4.157 which might be due to the interference wave system between the two demihulls. This is well predicted by the 2-D strip theory as shown in Fig.4.160. In the surge mode, a local maximum occurs at the first speed

tested as shown in Fig.4.158. From the results, it can be seen that the pitch and heave motions are linear with the wave height except near the critical zone. However, it is hard to see the linear relationship for the surge mode at the first speed tested.The 2-D strip theory predictions and measurements for the heaving and surging as shown Figs.4.159 and 4.160 agree very well in the supercritical zone, but around the critical zone, the theory predicts higher values possibly because the damping due to the viscosity is ignored in the theory.

Figs.4.161 and 4.162 show the sinkage and trim variations against the encounter wave frequency for the two sets of wave height and two forward speeds. Unlike the SWATH1 tandem strut, the sinkage and trim are both undulatory with wave length, but it can be seen that the mean value is roughly independent of the wave length as with the tandem versions

In order to examine, in more detail, the effect of wave height on the added resistance, tests were carried out at 8 wave heights up to as high as approximately 11centimetres and at two speeds. The results are shown in Fig.4.163. The added resistance coefficient significantly decreases at the lower wave heights, but the decrease is less marked at higher wave heights for the two speeds tested. The heave and pitch motions can be seen to be linear with the wave height as shown in Figs.4.164 and 4.165. The surge motion can be also seen to be linear with the wave height except for the first two wave heights at the speed of 0.7m/s as shown in Fig.4.166. An interesting result is found from the sinkage and trim as shown in Figs.4.167 and 4.168 in that unlike SWATH1 with tandem strut, they are nearly independent of the wave height, as mentioned earlier, with some undulations.

A) Comparison with tandem strut SWATH1

The comparison of different designs of ship in waves is not as simple as that in calm water since the performance of a ship in waves is most influenced by its natural periods of motion and every ship has its own natural frequency of motion. As shown in Table 4.28, the tandem strut SWATH has longer motion periods of heaving and pitching than those of the single strut one which has a waterplane area nearly two times

that of the tandem.

Fig.4.69 shows the added resistance coefficient variations of the SWATH1 as functions of Froude Number and wave steepness at the same wave length as with the SWATH3(see Fig.4.151). From the comparison of these two models, the added resistance of the single strut version is much higher than that of the tandem at higher speeds. Figs.4.73, 4.77 and 4.81 show the non-dimensional heaving, pitching and surging responses of the SWATH1-C5. The heave response of the single strut as shown in Fig.4.152 is higher than that of the tandem version as shown in Fig.4.73 mostly due to its reduced pressure cancellation effect from the upper surface of the submerged body compared to the tandem. The pitch response of the single strut as shown in Fig.4.153 is lower than that of the tandem as shown in Fig.4.77. This can be explained as follows. As shown in Fig.4.144, the trim of the single version in the calm water is much lower than that of the tandem. From this, it can be postulated that the resisting force to the trim of the single version is greater than that of the tandem and consequently, this affects the pitch amplitude in waves. The surge motion of the single strut is much higher than that of its counterpart. It can be partly understood that the bigger displacement and larger waterplane area of the SWATH3 may cause the higher surge motion. Also, the damping associated with two struts is much greater than for a single strut (C_D is higher and is multiplied by two).

Fig.4.86 shows the added resistance coefficients of SWATH1-C8 as functions of the non-dimensional encounter wave frequency and wave height at four forward speeds. Its non-dimensional spacing(B_1=0.947) between the two demihulls is wider than that(0.762) of the SWATH3-C1, but the draft is the same in each case. It was mentioned in section 3.3 that the wider spacing model is subject to less motion responses compared to the narrower one, particulasrly at the slower speeds and in the resonant region. As mentioned earlier in Fig.4.155, the large resistance increase for the single strut occured at around the heave resonant region while the most resistance increase or decrease occurs at around the pitch resonant region for the tandem strut C8. Since the pitch motion of the single strut is appreciably smaller, but its heave motion is larger than the tandem strut. Thus, this larger heave motion would appear to contribute the large resistance increase at the heave resonant area. As seen in Fig.4.156, the heave

response reaches up to three times the wave height at the resonant frequency.

Figs.4.169 through 4.171 compares the motion responses of SWATH1-C8 and SWATH3-C1 at the same speed of 1.0 m/s. As mentioned above, the heave motion of the tandem version-C8 is less than that of the single strut one excepting around its natural resonant region of heave(see Fig.4.169). Again, the pitch motion of the tandem is larger than that of the single strut excepting the local maximum region. The surge motion of the single is larger than that of the tandem.

As mentioned earlier, it is worthwile noting that the sinkage and trim of the single strut are both nearly independent of the wave height while they are both independent of the wave frequency for the tandem strut SWATH.

4.5.3 Conclusions

Based on the single strut SWATH tests, a number of points are worth noting:

a) The computational results from the computer program OSWATH developed by the author gives satisfactory correlations with the experimental results.

b) Both the sinkage and trim follow the same trends as the total resistance associated with parametric changes such as spacing and draft. Namely, the wider the spacing between the two demihulls, the smaller the sinkage and trim, and they are both increased with draft.

c) The sinkage and trim of the single strut are both much smaller than those of the tandem version, but stabilising fins are recommended to control the pitch instability at higher speeds which causes a higher resistance penalty due to green water.

d) The wave-making resistance of the tandem strut is much higher than that of the single one up to moderately high speeds , but at higher speeds, the tandem strut is appreciably better. If the skin-friction and form drag(including additional drag) is taken into account, the difference in the resistance between the two versions is, however, reduced at higher speeds.

e) The resistance increase of the single strut in waves is larger than that of the tandem at higher speeds possibly due to the increased trim and sinkage compared to

those in the calm water(the trim of the tandem strut in waves is significantly reduced as the wave height increases).

f) It can be seen that the heaving, pitching and surging responses are proportional to the wave height, but the added resistance coefficient is not proportional to the square of the wave height. The break in the square law is considerable at lower wave heights compared to at high wave heights.

g) The most resistance increase or decrease of the tandem strut version occurs at around the pitch resonant region while the large resistance increase for the single strut occurs at around the heave resonant frequency possibly due to the much exaggerated heave motion in this region. Unlike the tandem strut, the heave response reaches up to three times the wave height at the resonant frequency.

h) The deep draft model is subject to less motion than that of the light draft and results in less resistance increase in waves.

i) The heave and surge motions of the tandem strut are less than those of the single strut excepting around the resonant regions, but the pitch motion of the tandem is larger than that of its counterpart.

j) The sinkage and trim of the single strut are both nearly independent of the wave height while they are independent of the wave frequency for the tandem strut SWATH.

k) Excepting the various practical aspects of a single strut SWATH compared to a tandem one as mentioned in the introduction, the choice of either single or tandem strut, from a seakeeping point of view, will mostly depend on the nature of the operating sea conditions as well as on the mission of the ship. From a resistance point of view, a single strut is much preferable up to moderately high speed and at higher speeds a tandem strut can be recommended.

U(m/s)	FN	RN/10^6	RT(N)	CT.V	CT.S	RR (N)	CR.V	CR.S
0.511	0.133	0.677	0.667	0.0581	0.0046	-0.094	-0.0081	-0.0007
0.608	0.158	0.806	0.934	0.0575	0.0046	-0.101	-0.0062	-0.0005
0.706	0.183	0.936	1.401	0.0640	0.0051	0.052	0.0024	0.0002
0.807	0.210	1.070	1.877	0.0656	0.0052	0.165	0.0058	0.0005
0.900	0.234	1.193	2.446	0.0687	0.0055	0.367	0.0103	0.0008
1.000	0.260	1.326	3.292	0.0749	0.0060	0.783	0.0178	0.0014
1.106	0.287	1.466	4.839	0.0900	0.0072	1.836	0.0341	0.0027
1.170	0.304	1.551	5.449	0.0906	0.0072	2.127	0.0354	0.0028
1.201	0.312	1.592	5.560	0.0877	0.0070	2.079	0.0328	0.0026
1.303	0.339	1.727	5.645	0.0756	0.0060	1.617	0.0217	0.0017
1.403	0.365	1.860	6.103	0.0705	0.0056	1.504	0.0174	0.0014
1.505	0.391	1.995	7.913	0.0795	0.0064	2.697	0.0271	0.0022
1.610	0.418	2.134	10.342	0.0908	0.0073	4.455	0.0391	0.0031
1.706	0.443	2.262	12.788	0.1000	0.0080	6.255	0.0489	0.0039
1.800	0.468	2.386	14.678	0.1031	0.0082	7.484	0.0526	0.0042
1.911	0.497	2.533	16.555	0.1031	0.0082	8.544	0.0532	0.0043
1.999	0.519	2.650	18.063	0.1029	0.0082	9.375	0.0534	0.0043
2.199	0.571	2.915	20.407	0.0960	0.0077	10.091	0.0475	0.0038
2.374	0.617	3.147	22.809	0.0921	0.0074	10.966	0.0443	0.0035
2.600	0.676	3.447	25.234	0.0849	0.0068	11.278	0.0380	0.0030

Table 4.30 SWATH3-C1 Tem.15.0°C

U(m/s)	FN	RN/10^6	RT(N)	CT.V	CT.S	RR (N)	CR.V	CR.S
0.501	0.130	0.664	0.756	0.0616	0.0046	-0.125	-0.0101	-0.0008
0.600	0.156	0.795	1.179	0.0669	0.0050	-0.033	-0.0019	-0.0001
0.711	0.185	0.943	1.557	0.0630	0.0047	-0.081	-0.0033	-0.0002
0.772	0.201	1.023	2.091	0.0717	0.0054	0.195	0.0067	0.0005
0.869	0.226	1.152	2.624	0.0711	0.0053	0.284	0.0077	0.0006
0.987	0.256	1.308	3.821	0.0802	0.0060	0.884	0.0186	0.0014
1.095	0.285	1.452	5.560	0.0948	0.0071	2.025	0.0345	0.0026
1.197	0.311	1.587	6.227	0.0889	0.0067	2.082	0.0297	0.0022
1.285	0.334	1.704	6.454	0.0799	0.0060	1.748	0.0216	0.0016
1.407	0.366	1.865	7.339	0.0758	0.0057	1.803	0.0186	0.0014
1.507	0.392	1.998	8.896	0.0801	0.0060	2.634	0.0237	0.0018
1.596	0.415	2.116	12.116	0.0973	0.0073	5.176	0.0415	0.0031
1.700	0.442	2.254	14.945	0.1057	0.0079	7.171	0.0507	0.0038
1.793	0.466	2.377	17.169	0.1092	0.0082	8.615	0.0548	0.0041
1.892	0.492	2.508	18.873	0.1078	0.0081	9.450	0.0540	0.0040
2.006	0.521	2.659	20.683	0.1051	0.0079	10.215	0.0519	0.0039
2.198	0.571	2.914	25.220	0.1067	0.0080	12.879	0.0545	0.0041

Table 4.31 SWATH3-C2 Tem.=15.0°C

U(m/s)	FN	RN/10^6	RT(N)	CT.V	CT.S	RR (N)	CR.V	CR.S
0.504	0.131	0.668	0.667	0.0598	0.0048	-0.075	-0.0067	-0.0005
0.604	0.157	0.801	0.943	0.0588	0.0047	-0.080	-0.0050	-0.0004
0.701	0.182	0.929	1.379	0.0638	0.0051	0.046	0.0021	0.0002
0.814	0.212	1.079	2.180	0.0748	0.0060	0.441	0.0152	0.0012
0.902	0.234	1.196	2.357	0.0659	0.0053	0.270	0.0076	0.0006
1.014	0.264	1.344	3.558	0.0787	0.0063	0.986	0.0218	0.0017
1.114	0.289	1.477	4.893	0.0897	0.0072	1.850	0.0339	0.0027
1.209	0.314	1.603	5.596	0.0871	0.0070	2.073	0.0323	0.0026
1.301	0.338	1.725	5.898	0.0793	0.0063	1.881	0.0253	0.0020
1.412	0.367	1.872	6.338	0.0723	0.0058	1.687	0.0192	0.0015
1.498	0.389	1.986	7.562	0.0767	0.0061	2.389	0.0242	0.0019
1.575	0.409	2.088	8.976	0.0823	0.0066	3.316	0.0304	0.0024
1.697	0.441	2.250	11.475	0.0907	0.0072	5.005	0.0395	0.0032
1.807	0.470	2.396	14.056	0.0979	0.0078	6.811	0.0475	0.0038
1.947	0.506	2.581	16.284	0.0977	0.0078	7.999	0.0480	0.0038
2.001	0.520	2.653	17.192	0.0977	0.0078	8.488	0.0482	0.0039
2.215	0.576	2.936	20.016	0.0928	0.0074	9.564	0.0444	0.0035
2.410	0.626	3.195	22.396	0.0877	0.0070	10.226	0.0401	0.0032
2.652	0.689	3.516	25.064	0.0811	0.0065	10.601	0.0343	0.0027
2.837	0.737	3.761	27.311	0.0772	0.0062	10.973	0.0310	0.0025

Table 4.32 SWATH3-C3 Tem.=15.0°C

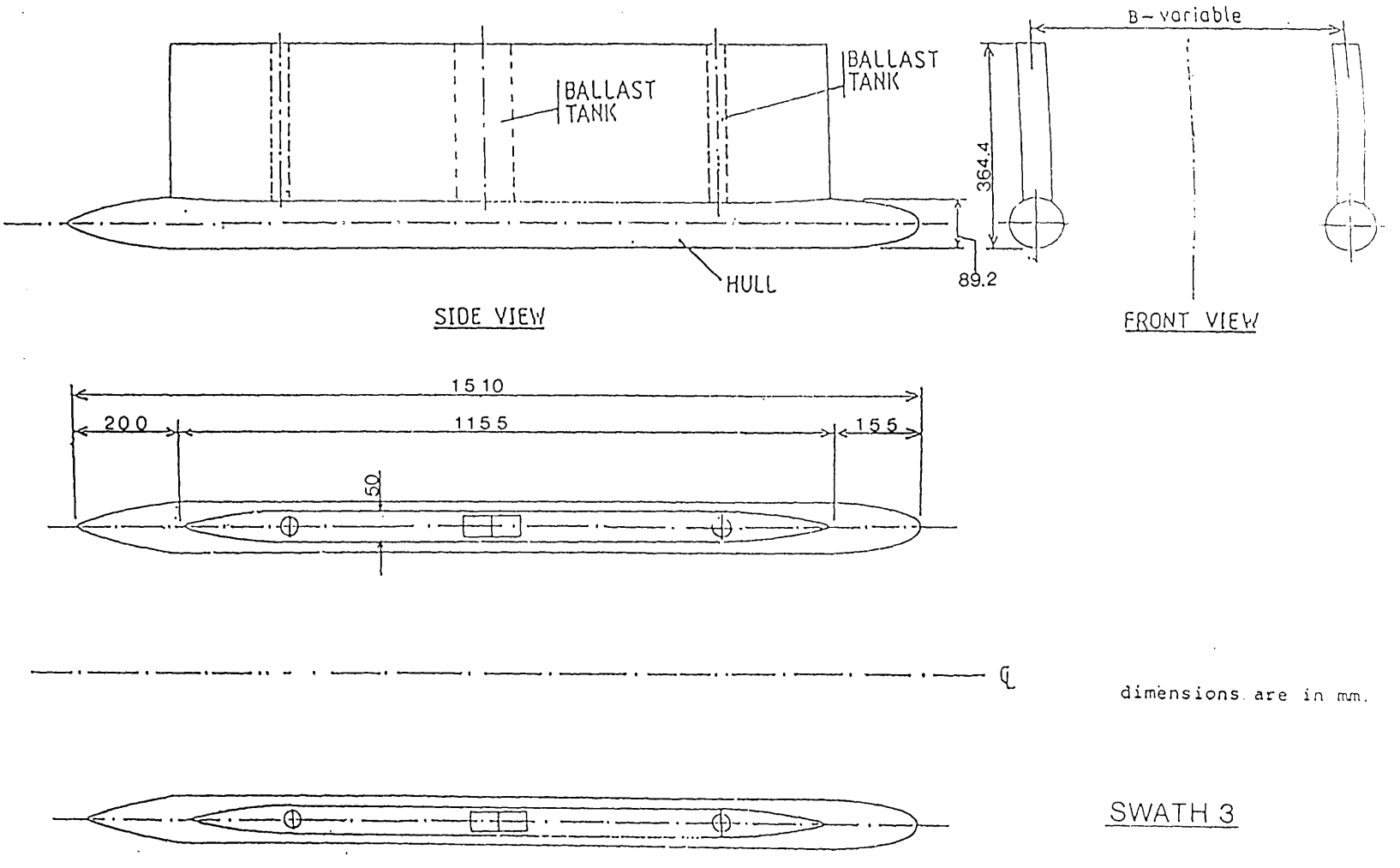

Fig.4.129-a Plans and details of model SWATH3

Fig.4.129-b Front View of the SWATH3 Model

Fig 4.130 SWATH3-C2 under way Speed=1.1m/s

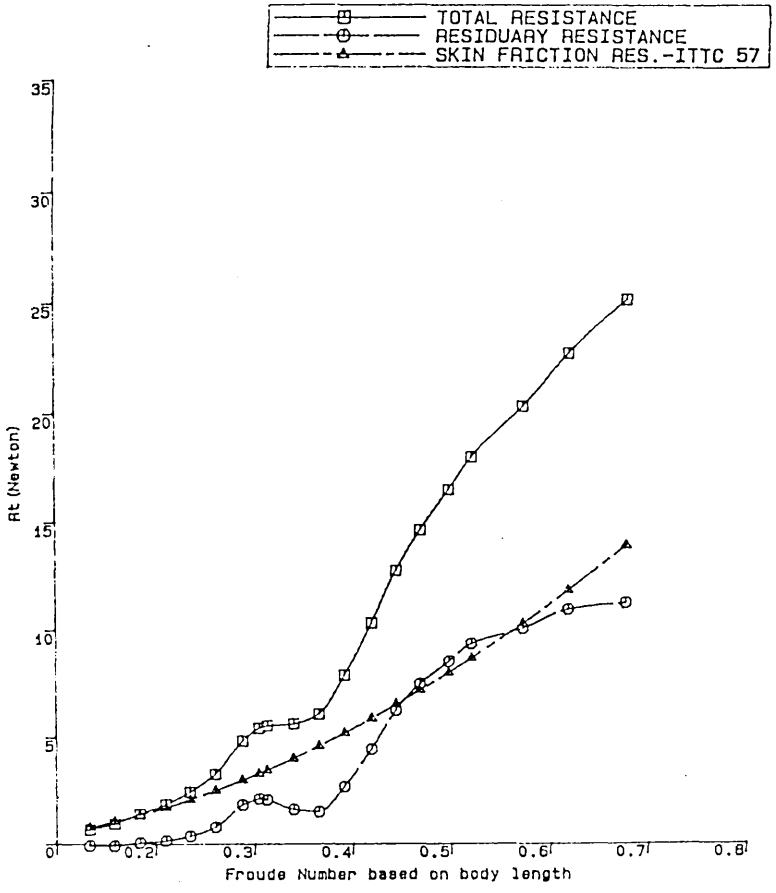

Total, residuary and skin-frictional resistance variations of SWATH3-C1 versus Froude Number (FN)

Fig.4.131

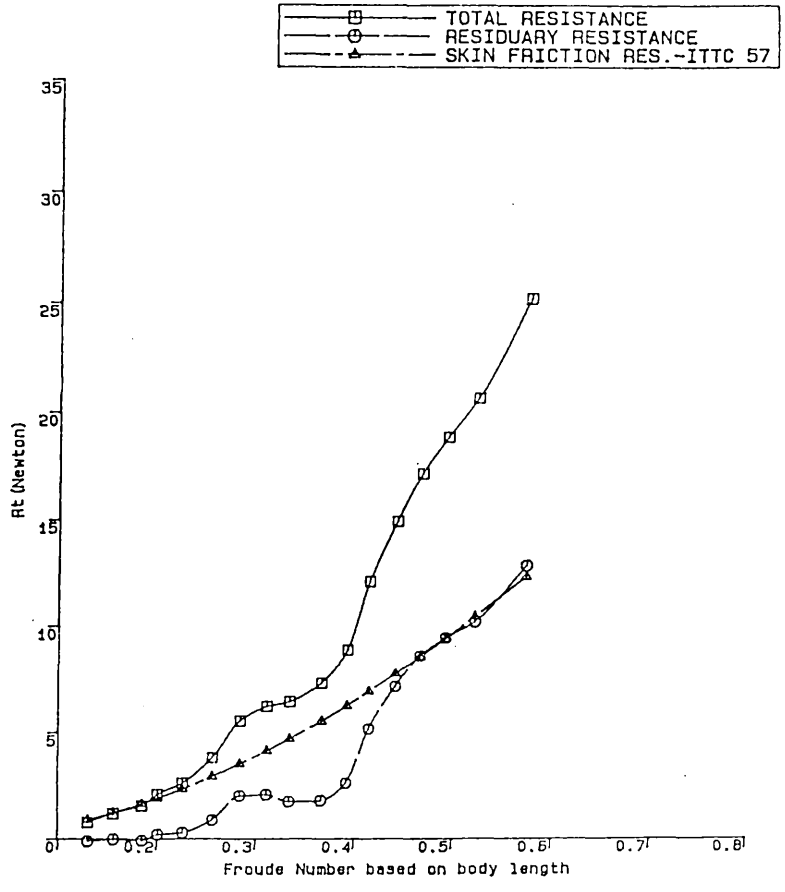

Total, residuary and skin-frictional resistance variations of SWATH3-C2 versus Froude Number (FN)

Fig.4.132

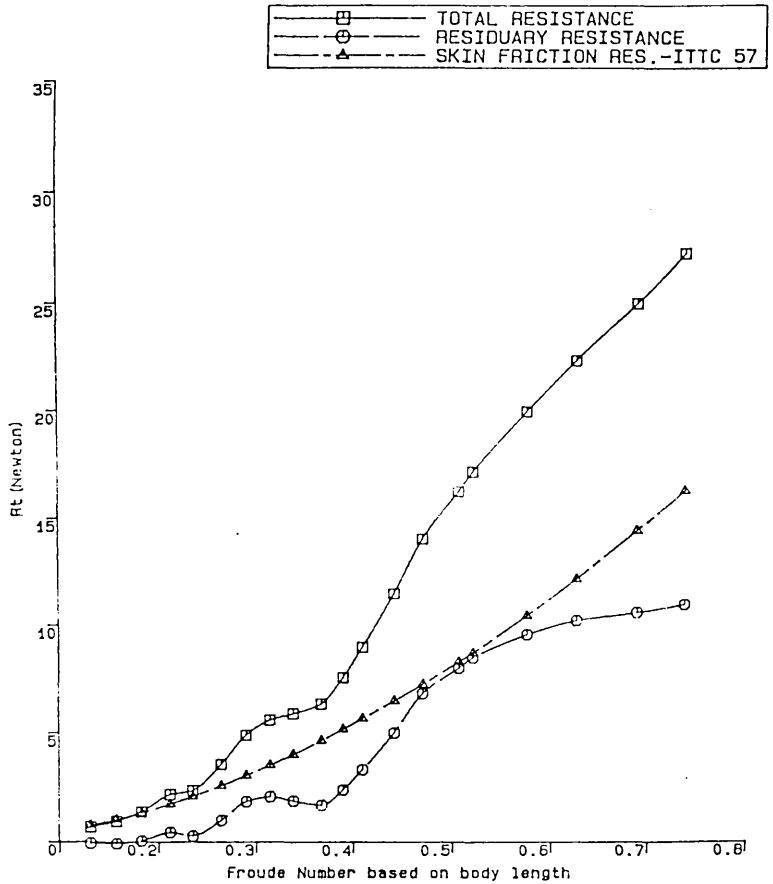

Total, residuary and skin-frictional resistance variations of SWATH3-C3 versus Froude Number (FN)

Fig.4.133

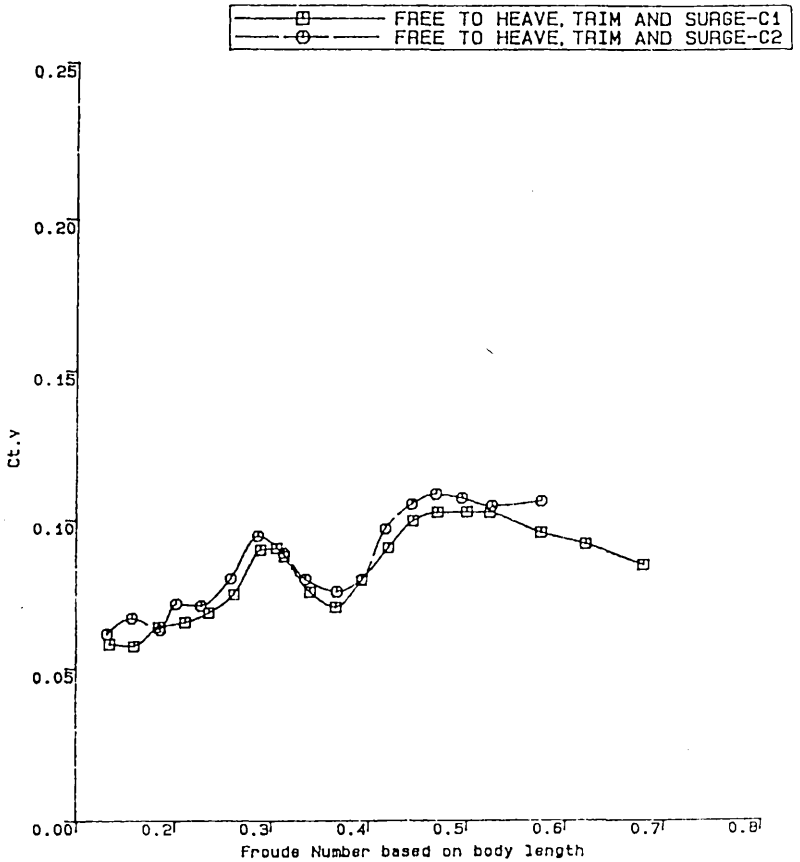

Total resistance coefficient variations SWATH3 versus Froude Number

Fig.4.134

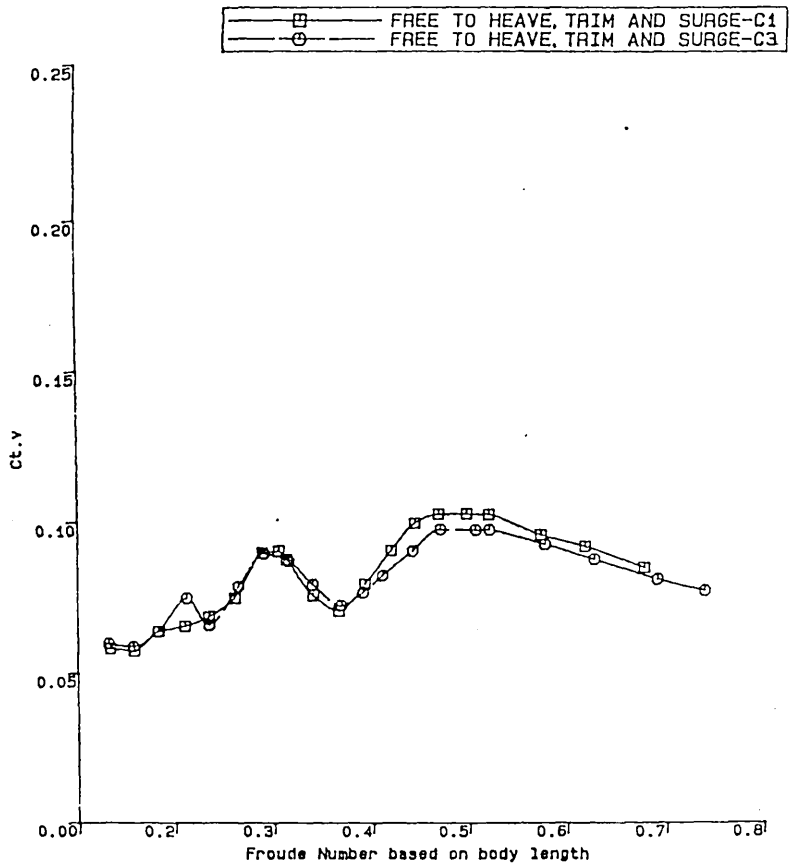

Total resistance coefficient variations of SWATH3 with two different spacings versus Froude Number based on the body length

Fig.4.135

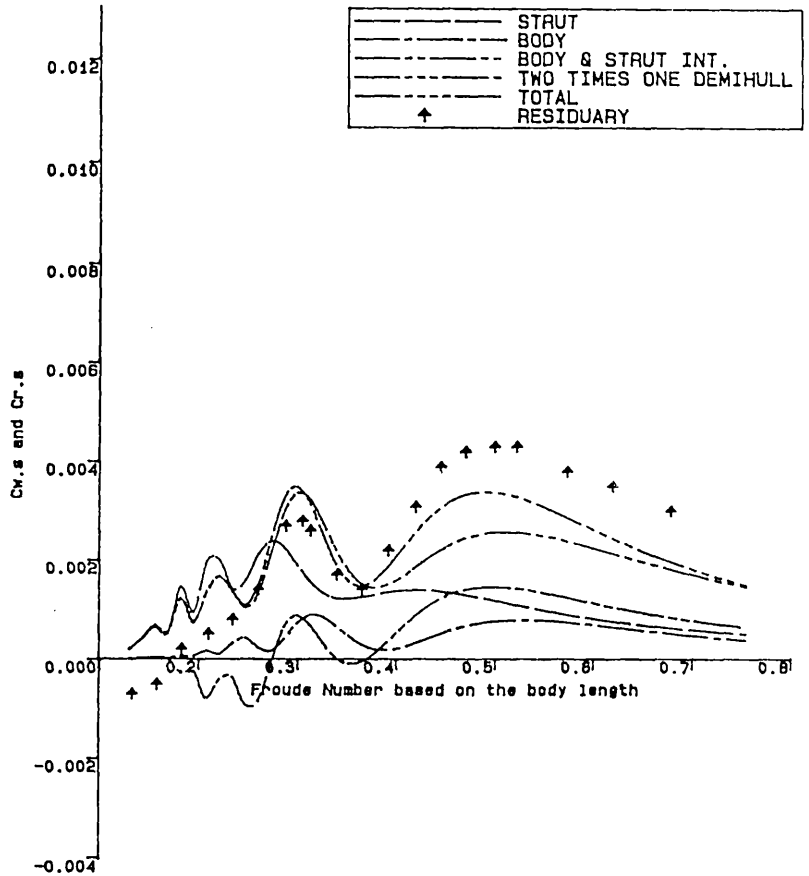

Wave Resistance Coefficients of SWATH3-C1 and its Component Variations together with Residuary Resistance Coefficient as a Function of Froude Number.

Fig.4.136

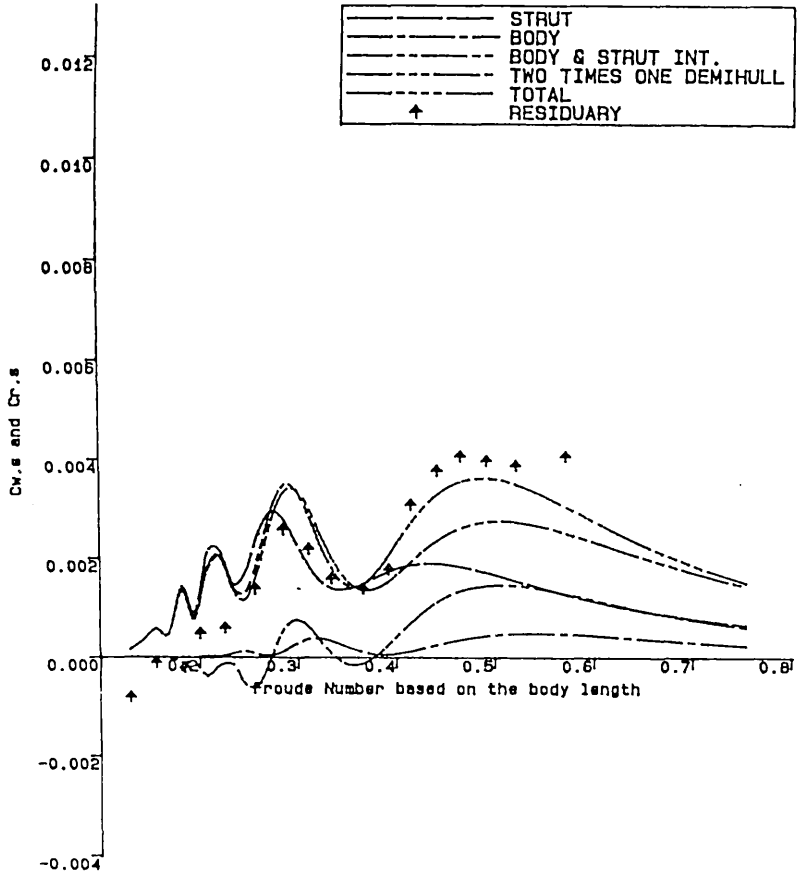

Wave Resistance Coefficients of SWATH3-C2 and its Component Variations together with Residuary Resistance Coefficient as a Function of Froude Number.

Fig.4.137

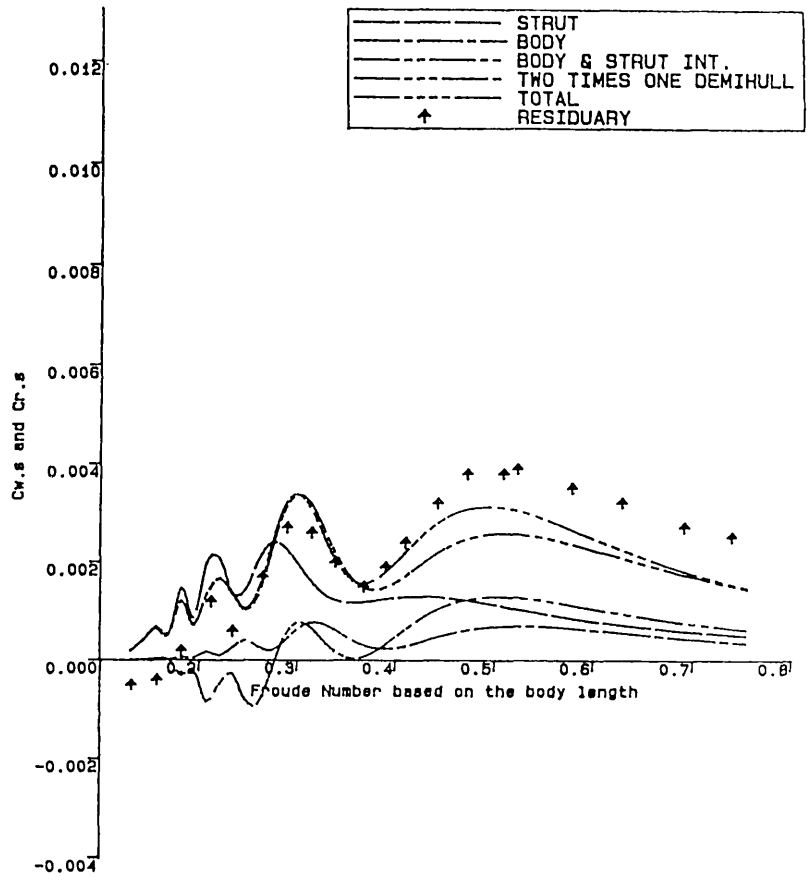

Wave Resistance Coefficients of SWATH3-C3 and its Component Variations together with Residuary Resistance Coefficient as a Function of Froude Number.

Fig.4.138

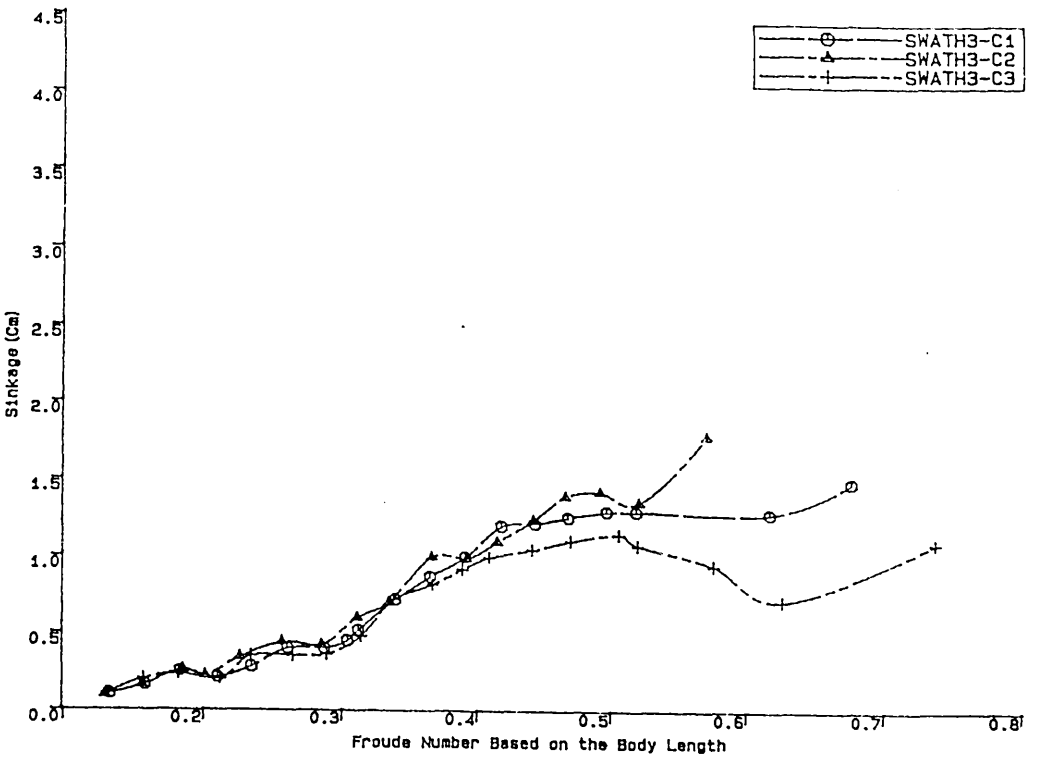

SWATH3 Model Sinkages as a Function of Froude Number.

Fig.4.139

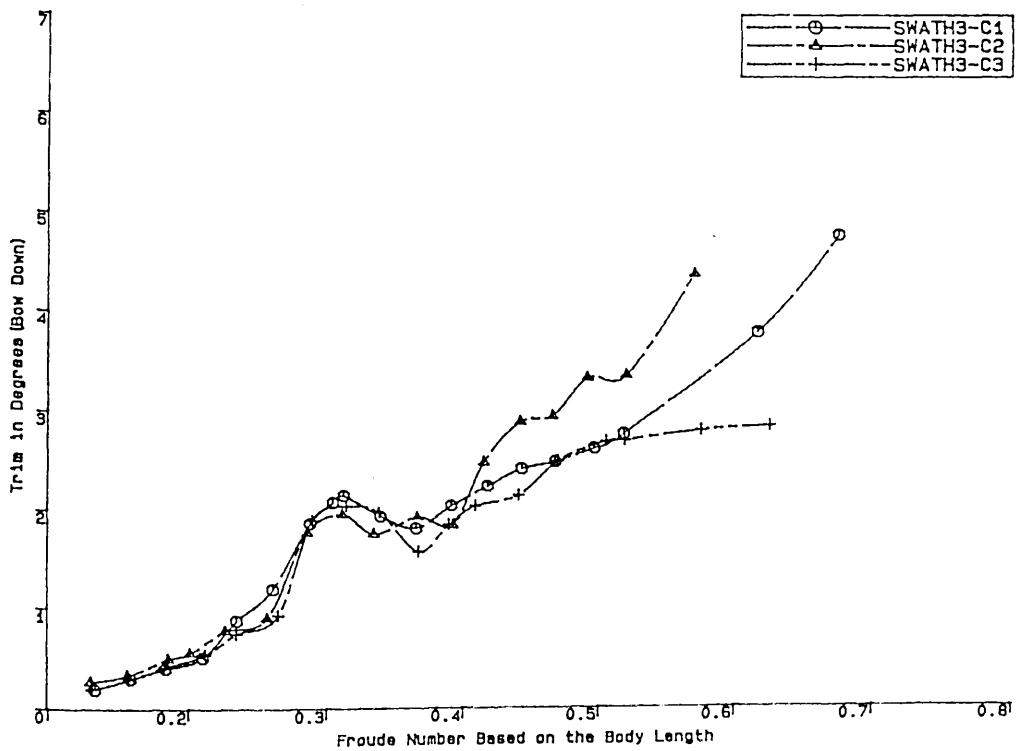

SWATH3 Model Trims as a Function of Froude Number.

Fig.4.140

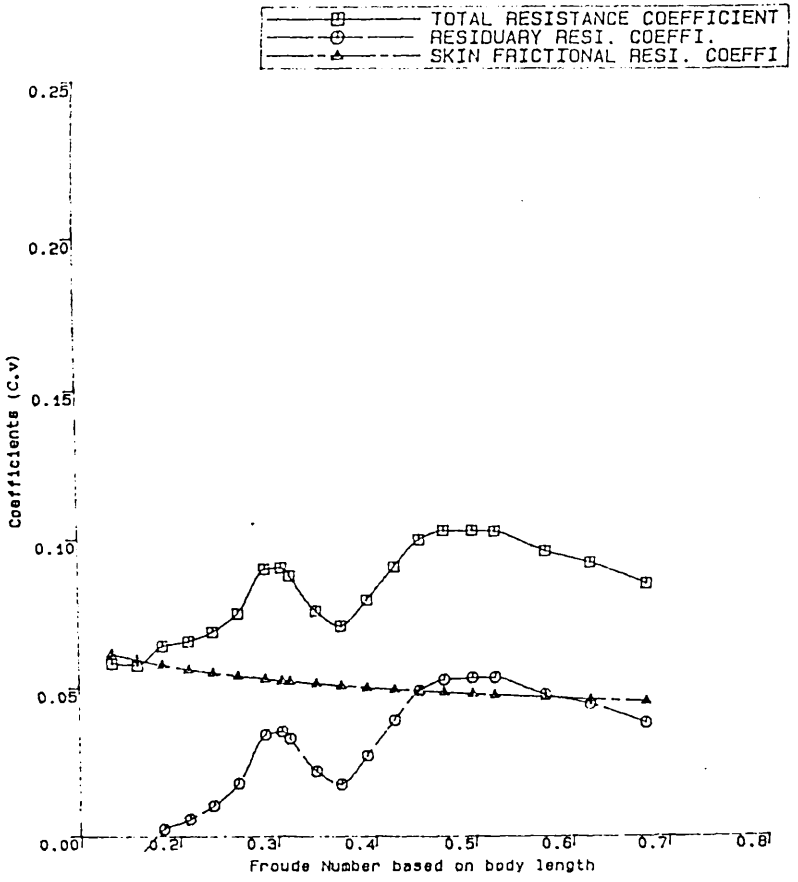

Total, residuary and skin-frictional resistance coefficients variations of SWATH3-C1 as a function of Froude Number (FN)

Fig.4.141

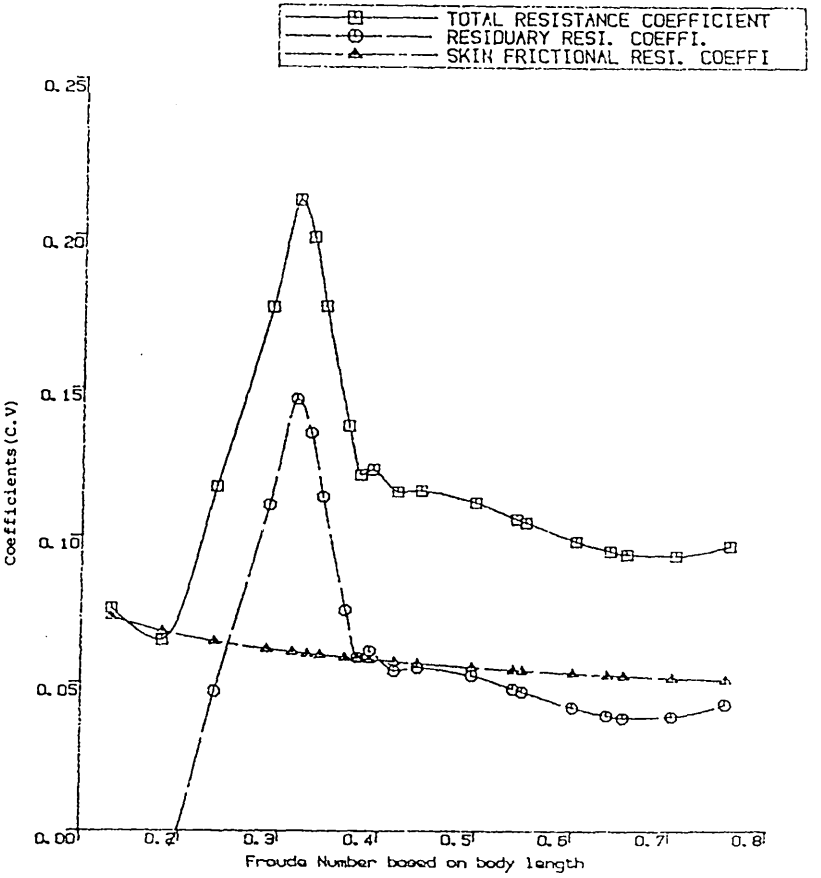

Total, residuary and skin-frictional resistance coefficients variations of SWATH1-C5 as a function of Froude Number (FN)

Fig.4.142

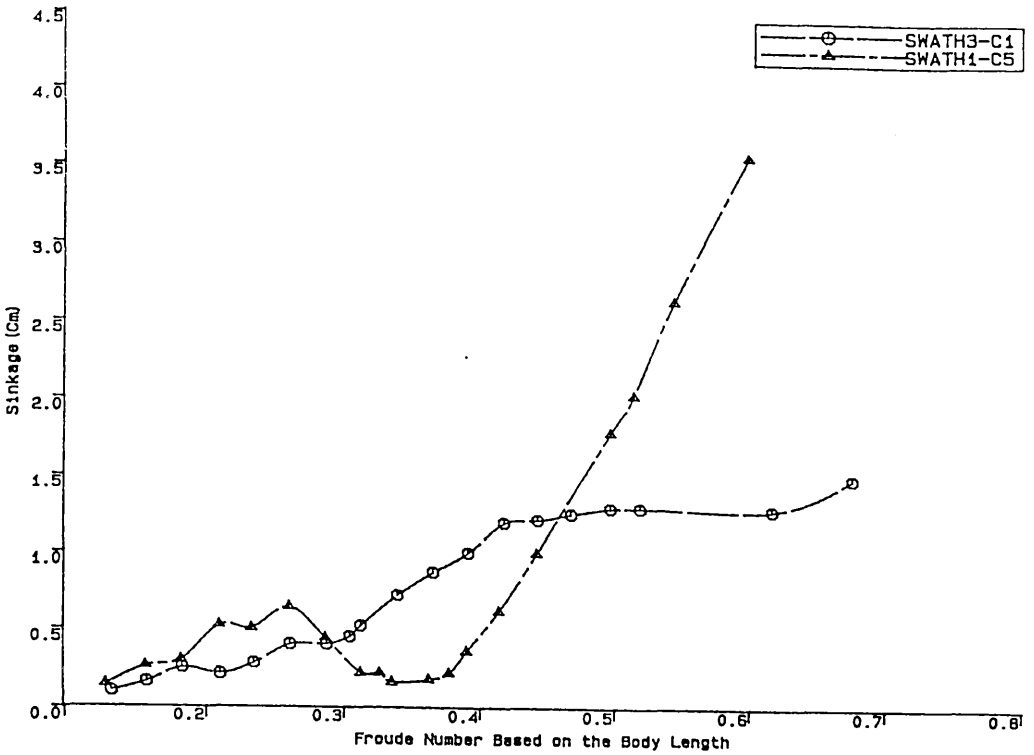

Comparison of SWATH3-C1 and SWATH1-C5 Sinkages vs Froude Number.

Fig.4.143

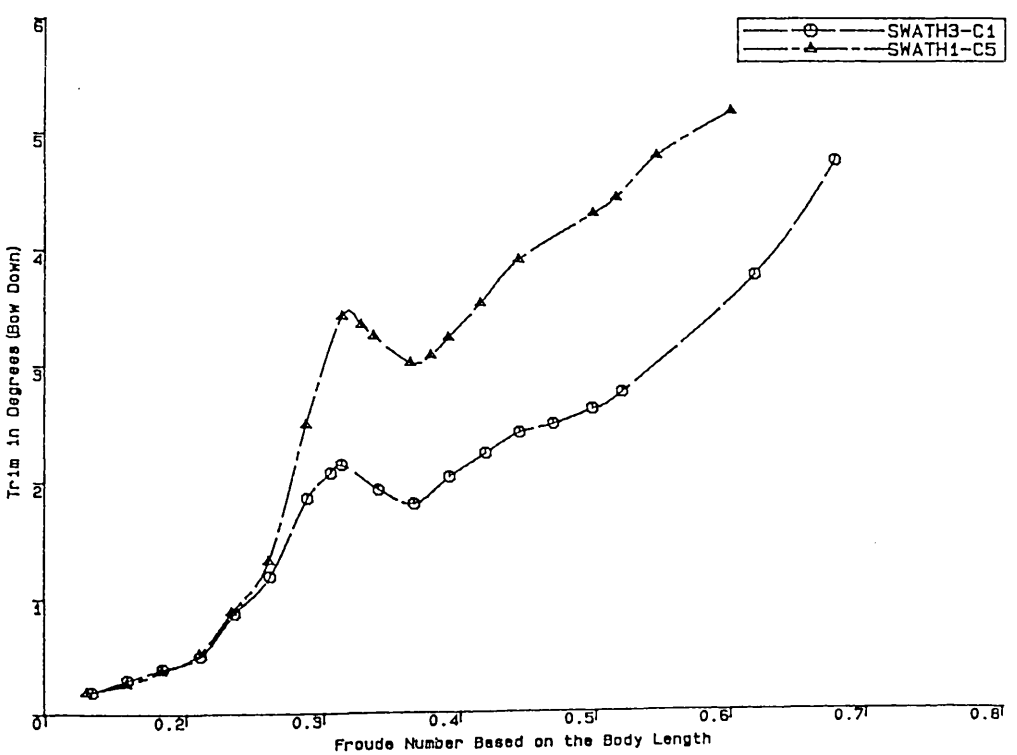

Comparison of SWATH3-C1 and SWATH1-C5 Trims vs Froude Number.

Fig.4.144

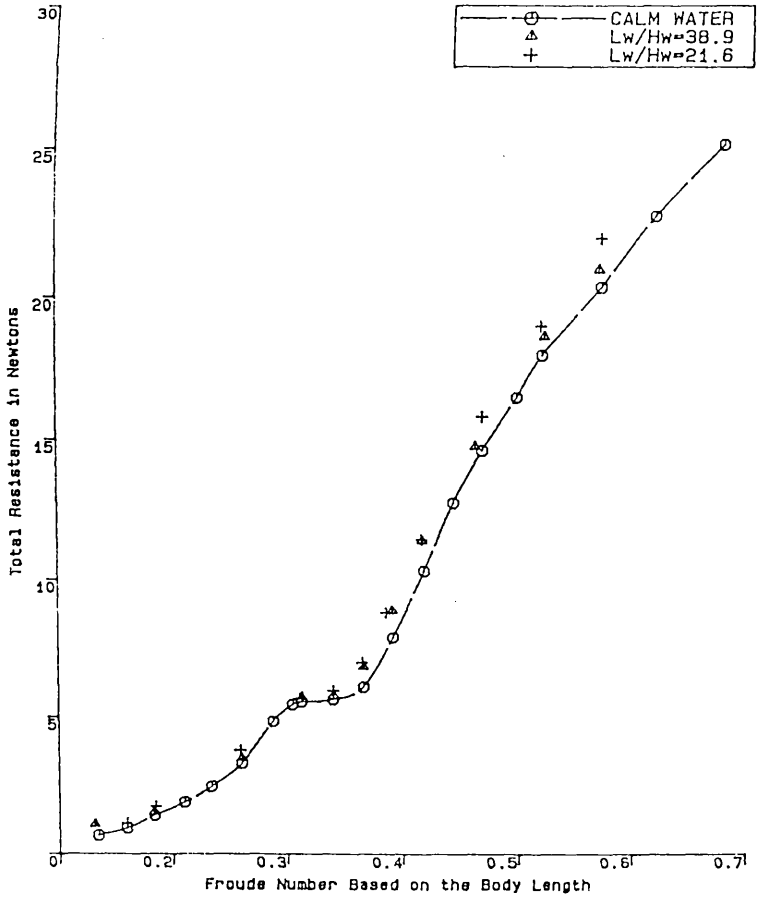

SWATH3 Model-C1 Total Resistance as a Function of Froude Number as well as Wave Steepness (Wave Frequency=1.02Hz Lw=1.51m Lw/Lb=1.0)

Fig.4.145

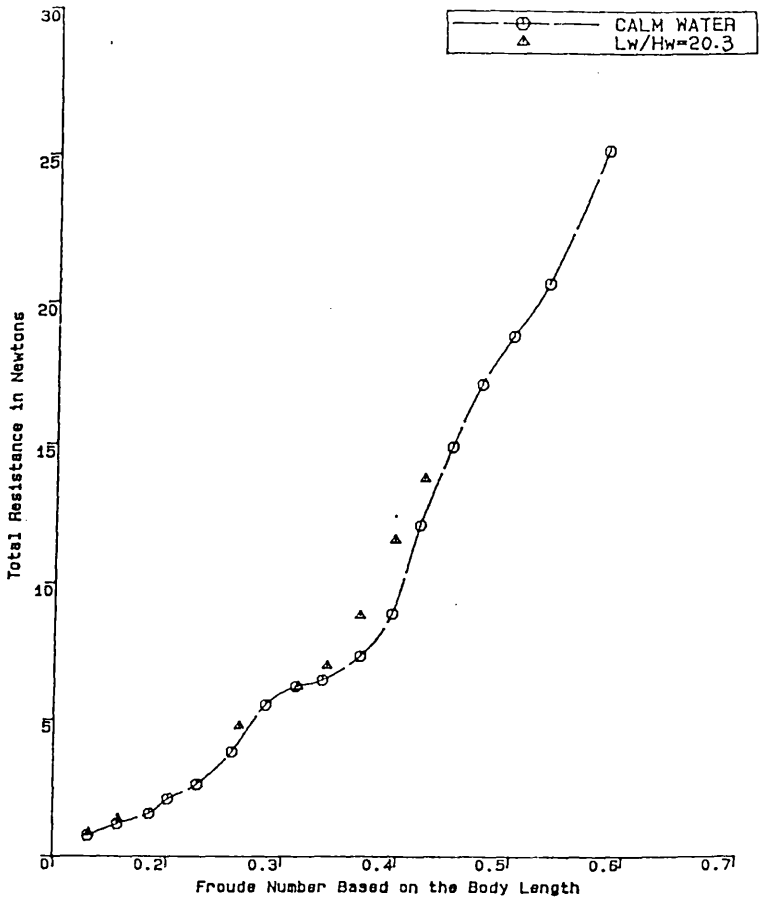

SWATH3 Model-C2 Total Resistance as a Function of Froude Number as well as Wave Steepness (Wave Frequency=1.02Hz Lw=1.51m Lw/Lb=1.0)

Fig.4.146

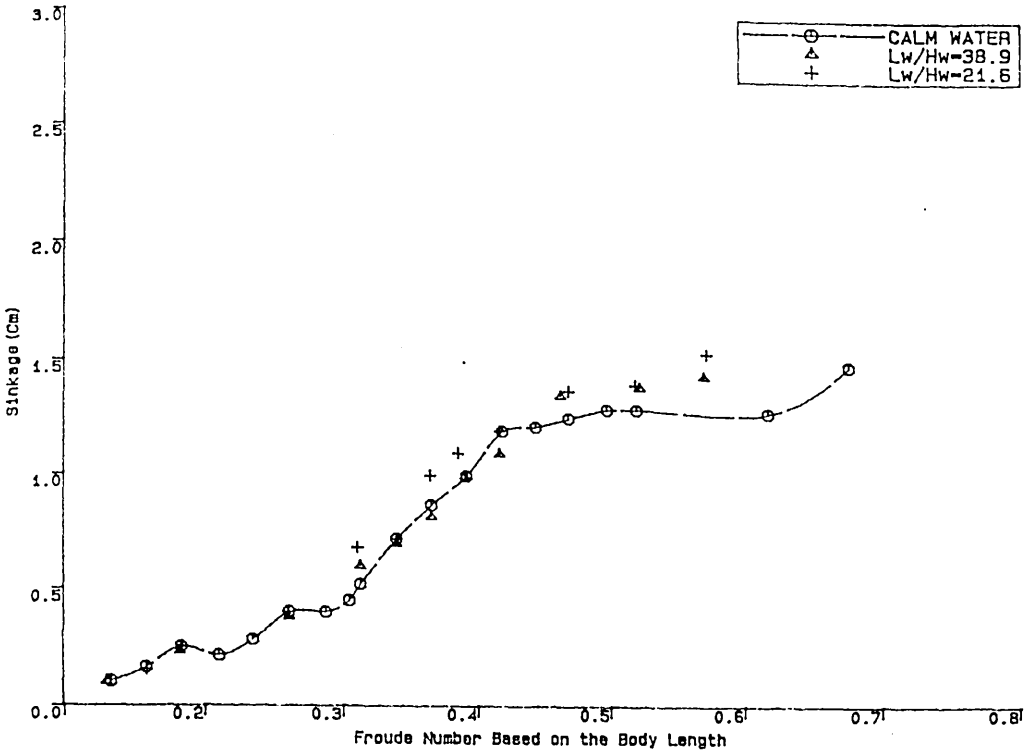

SWATH3-C1 Sinkages as a Function of Froude Number as well as Wave Steepness (Wave Frequency=1.02Hz Lw/Lb=1.0)

Fig.4.147

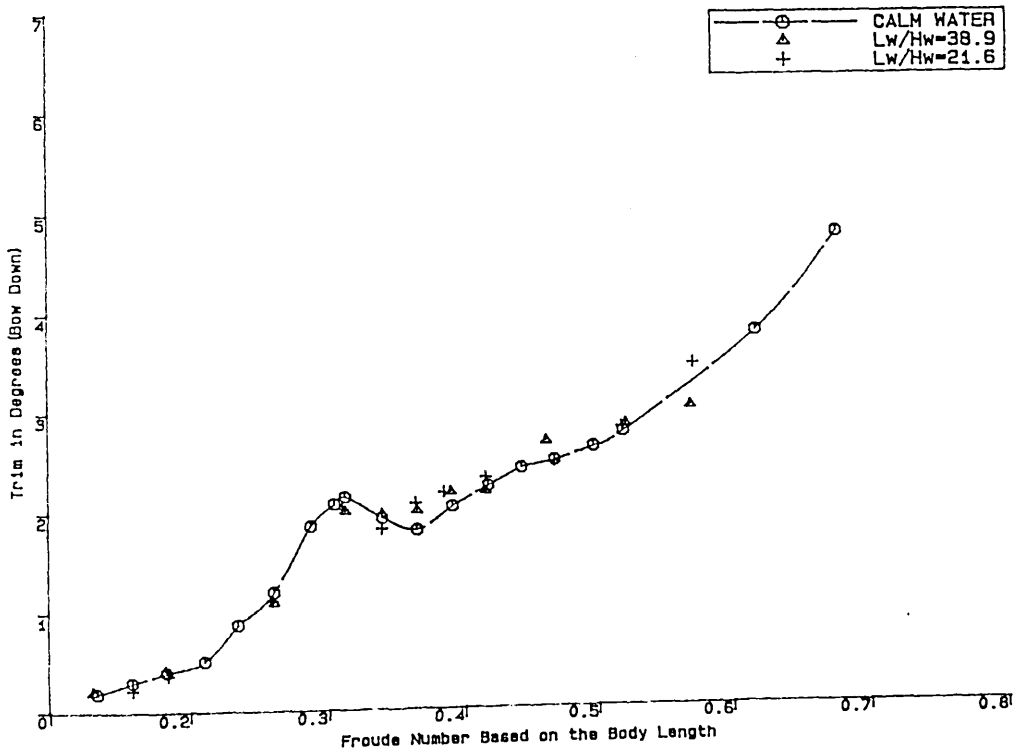

SWATH3-C1 Trims as a Function of Froude Number as well as Wave Steepness (Wave Frequency=1.02Hz Lw/Lb=1.0)

Fig.4.148

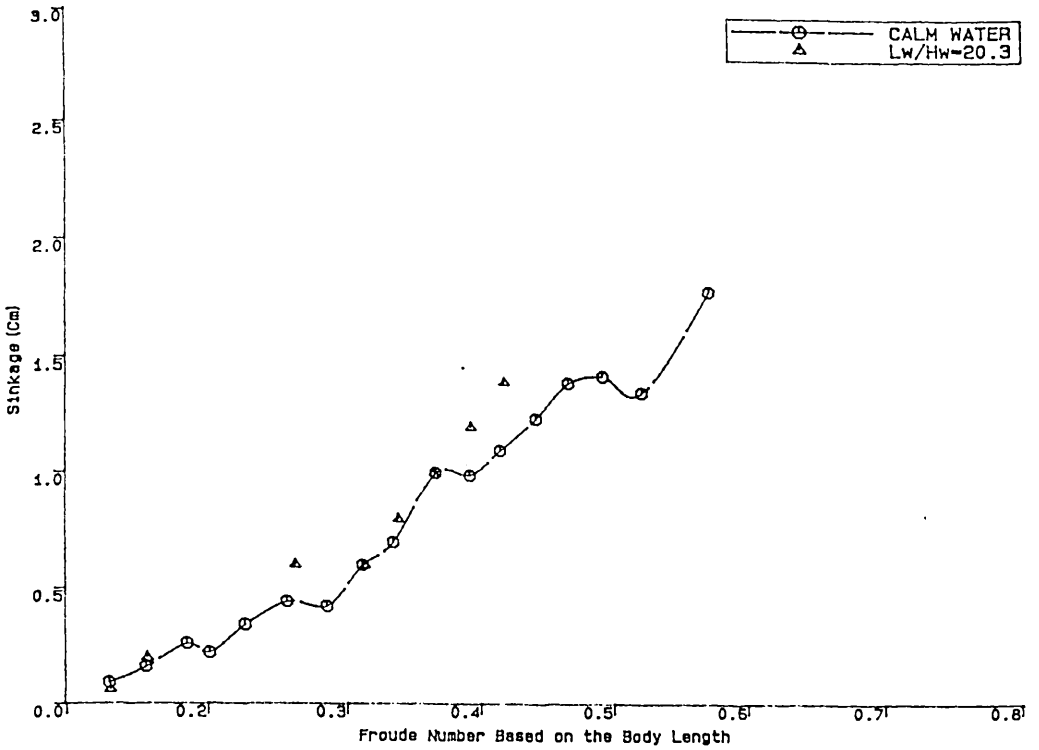

SWATH3-C2 Sinkages as a Function of Froude Number as well as Wave Steepness (Wave Frequency=1.02Hz Lw/Lb=1.0)

Fig.4.149

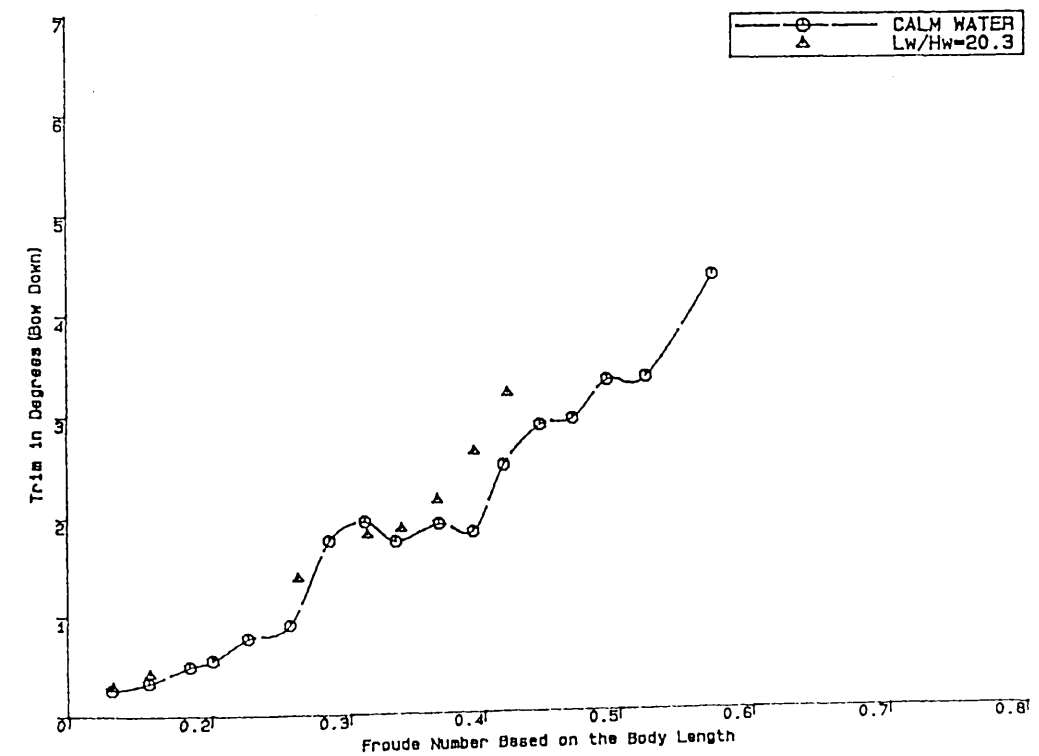

SWATH3-C2 Trims as a Function of Froude Number as well as Wave Steepness (Wave Frequency=1.02Hz Lw/Lb=1.0)

Fig.4.150

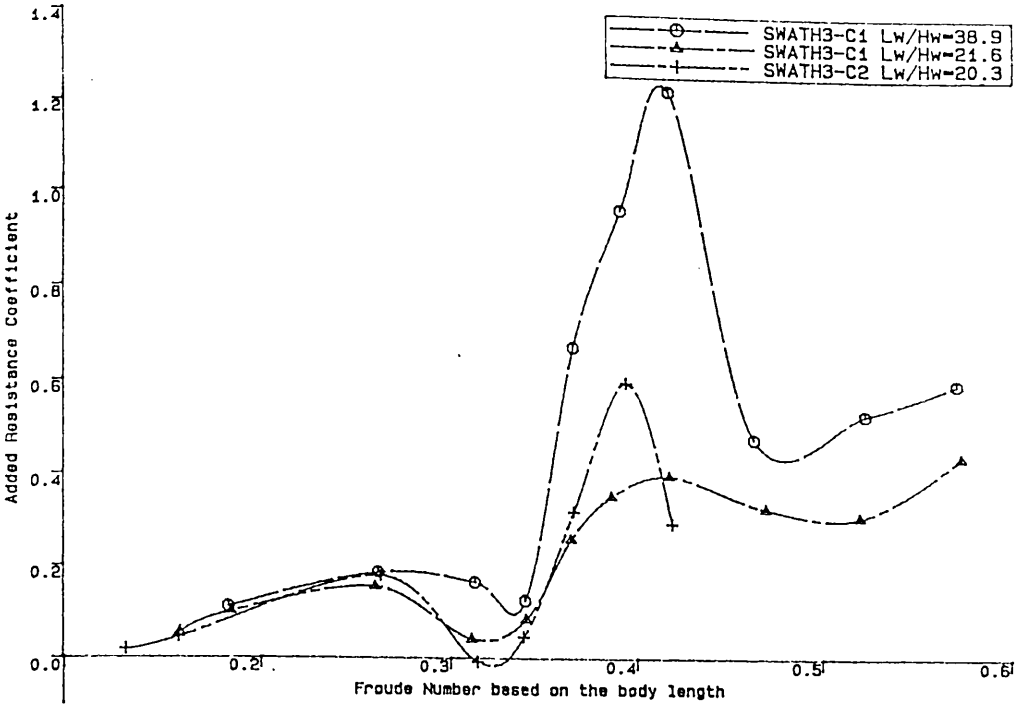

SWATH3 Model Added Resistance Coefficients in Head Seas as Functions of Froude Number and Wave Steepness (Wave Frequency=1.02Hz Lw/Lb=1.0)

Fig.4.151

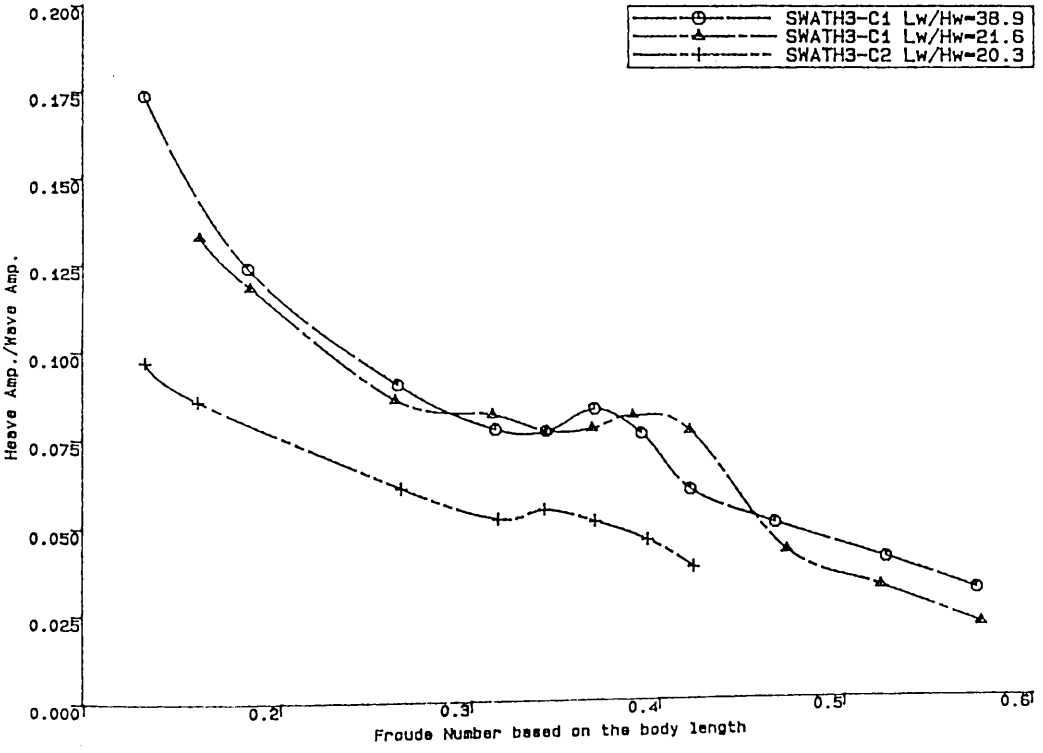

SWATH3 Heave Responses in Head Seas as Functions of Froude Number and Wave Steepness (Wave Frequency=1.02Hz Lw/Lb=1.0)

Fig.4.152

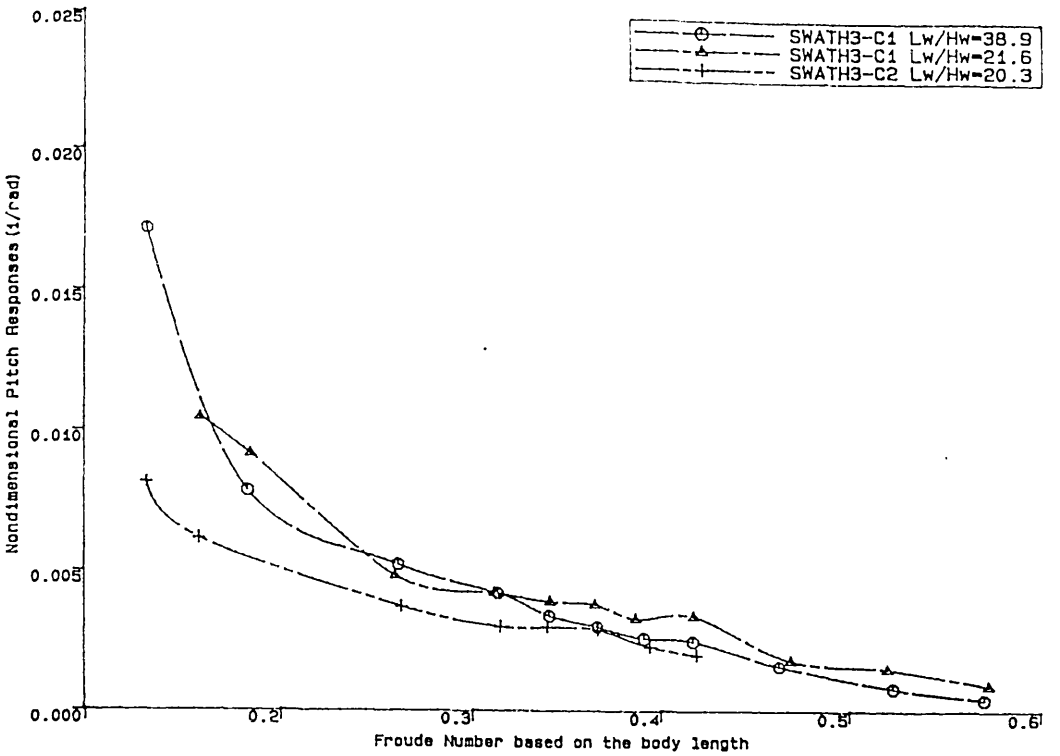

SWATH3 Pitch Responses in Head Seas as Functions of Froude Number and Wave Steepness (Wave Frequency=1.02Hz Lw/Lb=1.0)

Fig.4.153

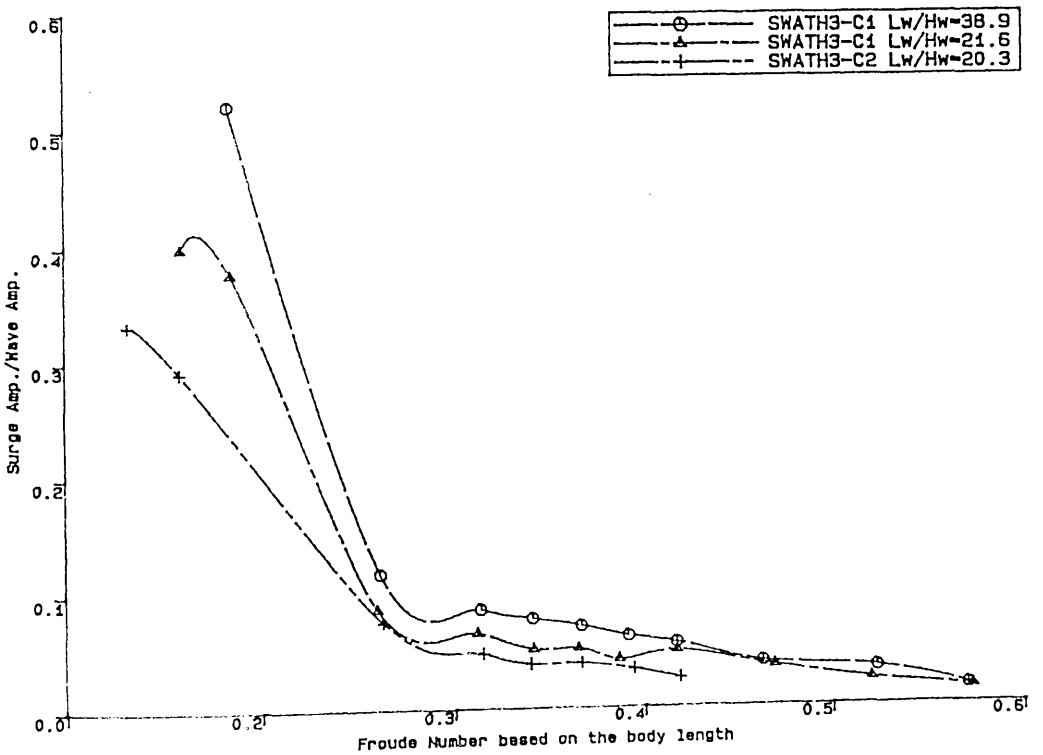

SWATH3 Surge Responses in Head Seas as Functions of Froude Number and Wave Steepness (Wave Frequency=1.02Hz Lw/Lb=1.0)

Fig.4.154

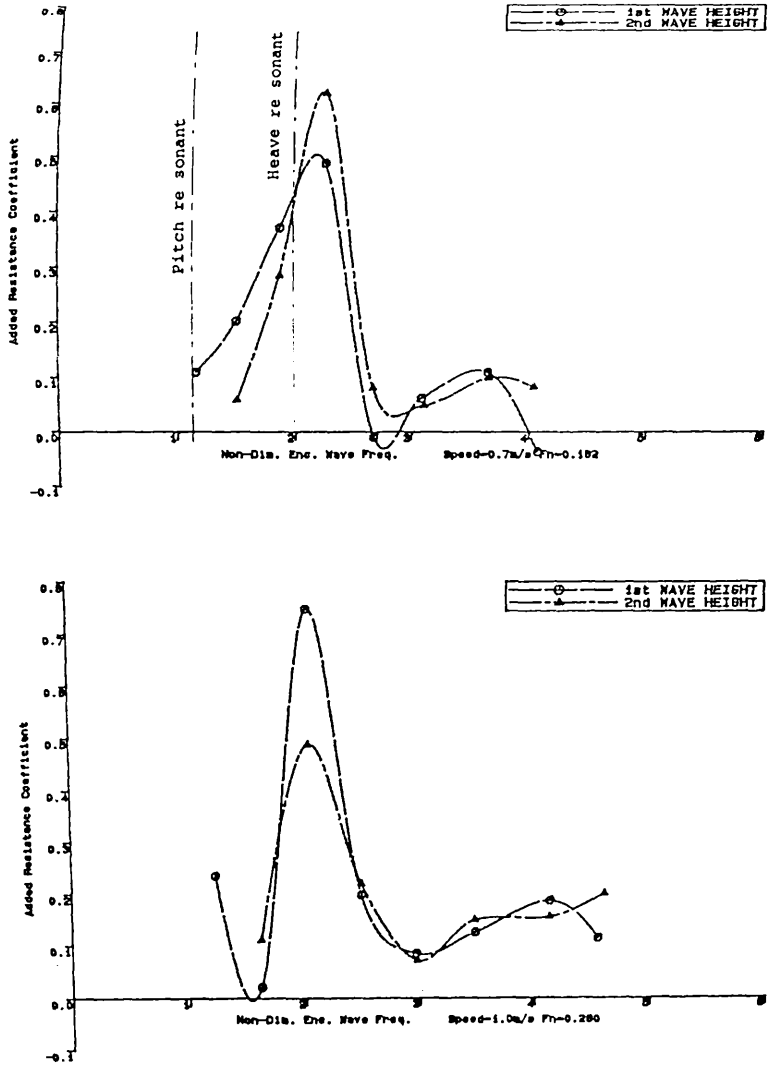

SWATH3-C1 Added Resistance Coefficient vs Non-dimensional Encounter Wave Frequency with 2 Wave Height at 2 Speeds

Fig.4.155

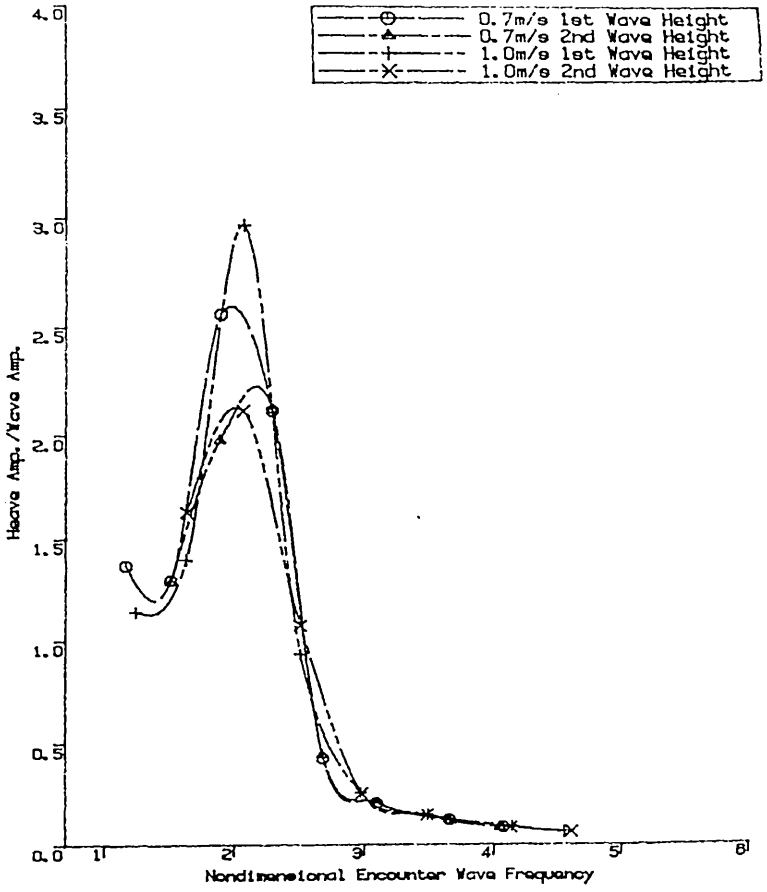

SWATH3-C1 Heave Responses in Head Seas with 2 Forward Speeds and 2 Wave Heights.

Fig.4.156

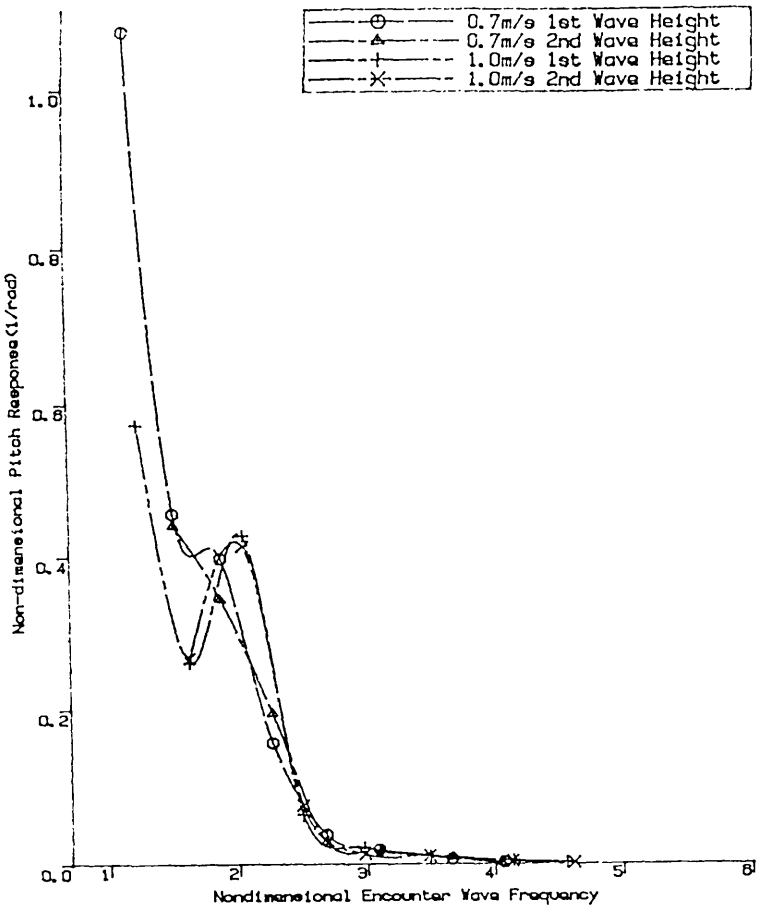

SWATH3-C1 Pitch Responses in Head Seas with 2 Forward Speeds as well as 2 Wave Heights

Fig.4.157

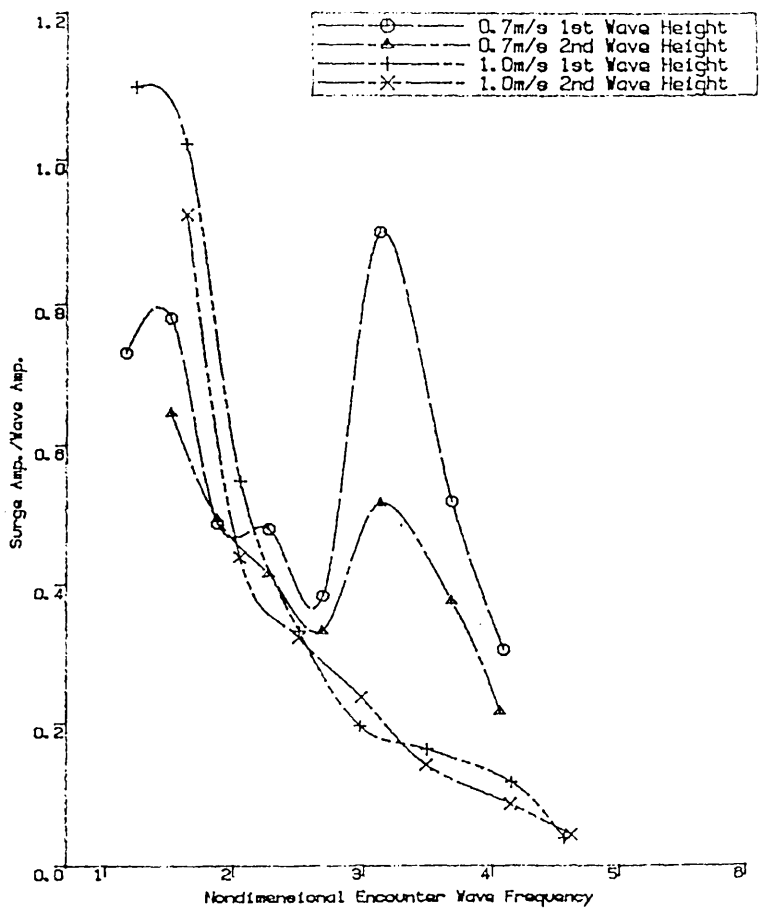

SWATH3-C1 Surge Responses in Head Seas with 2 Forward Speeds as well as 2 Wave Heights

Fig.4.158

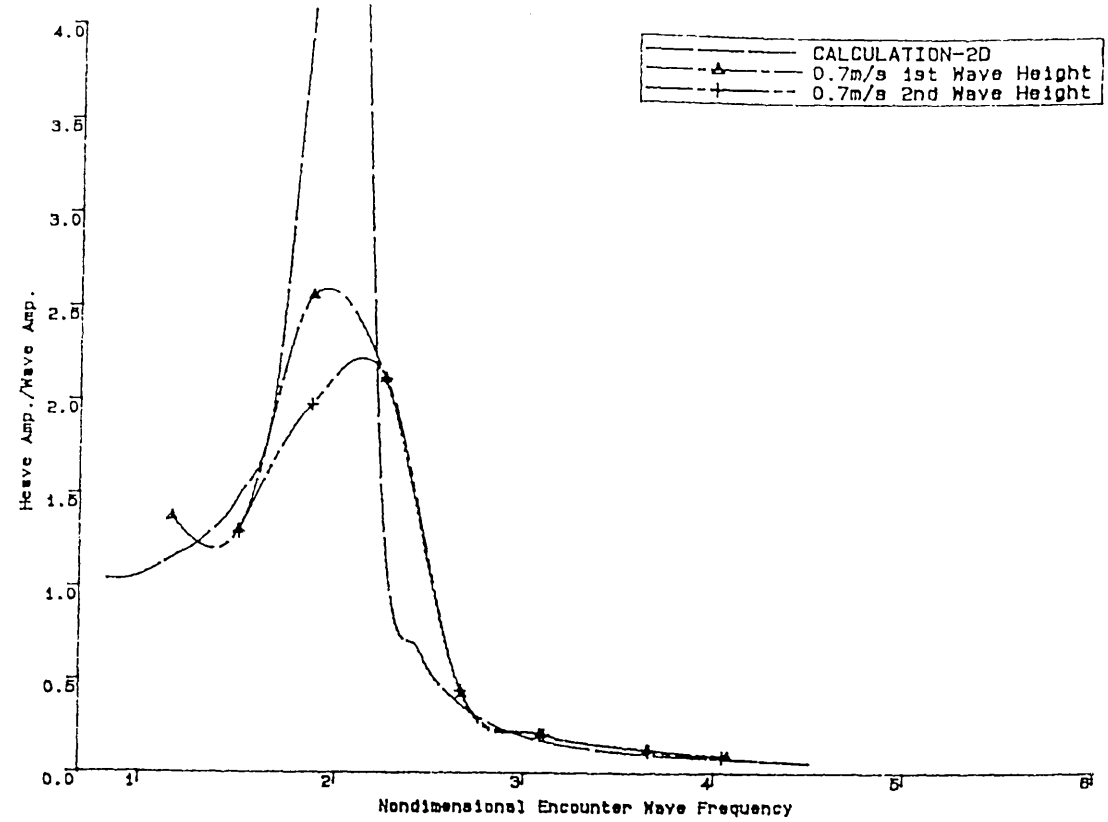

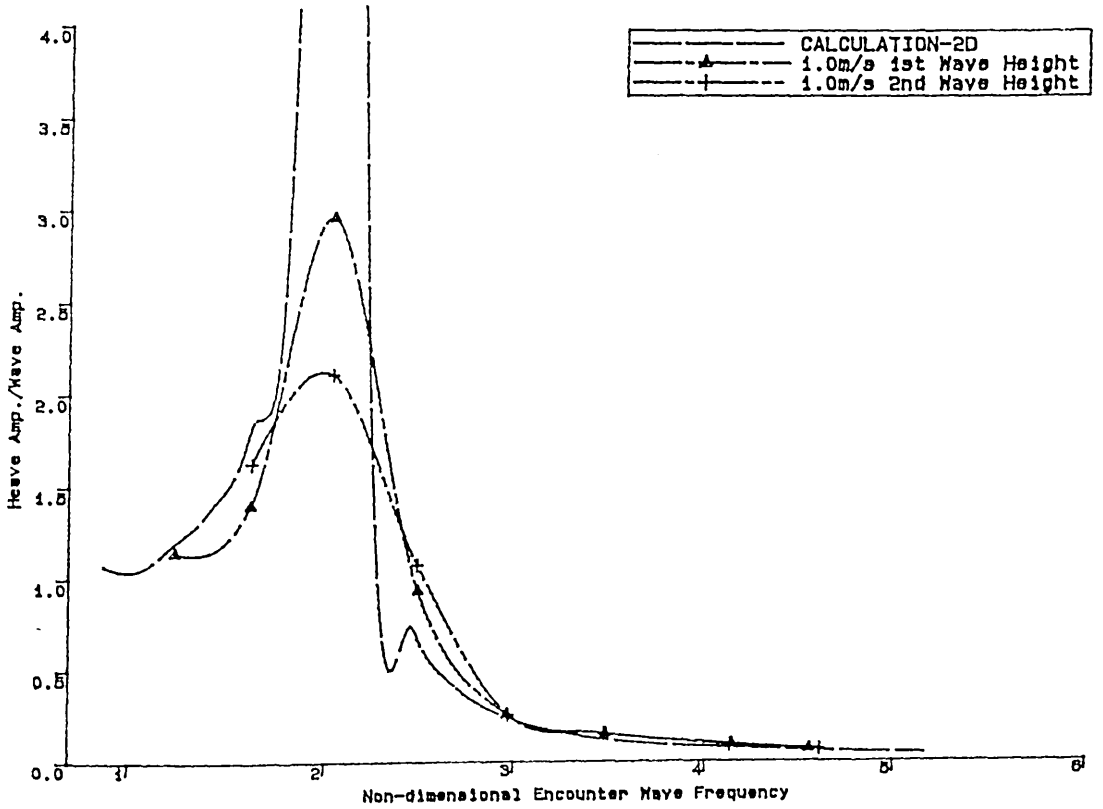

Fig.4.159

Computational and Experimental Heave Responses of SWATH3-C1 in Head Seas with 2 Forward Speeds

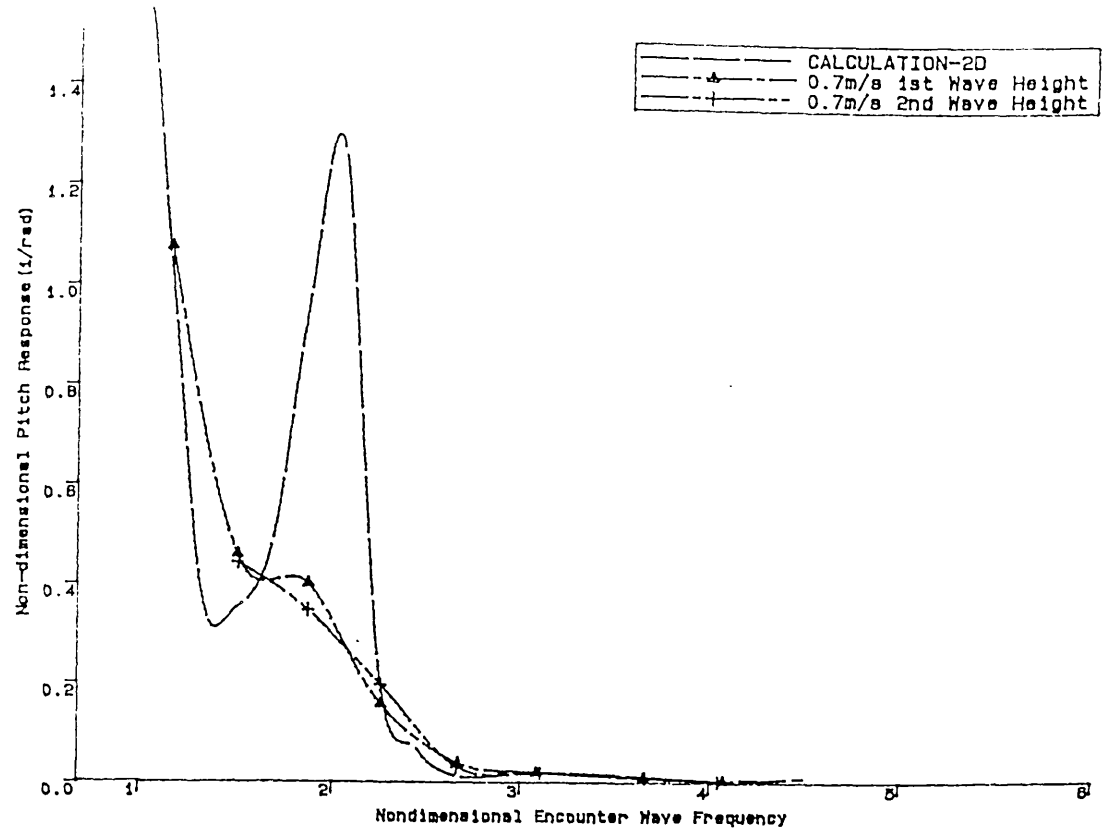

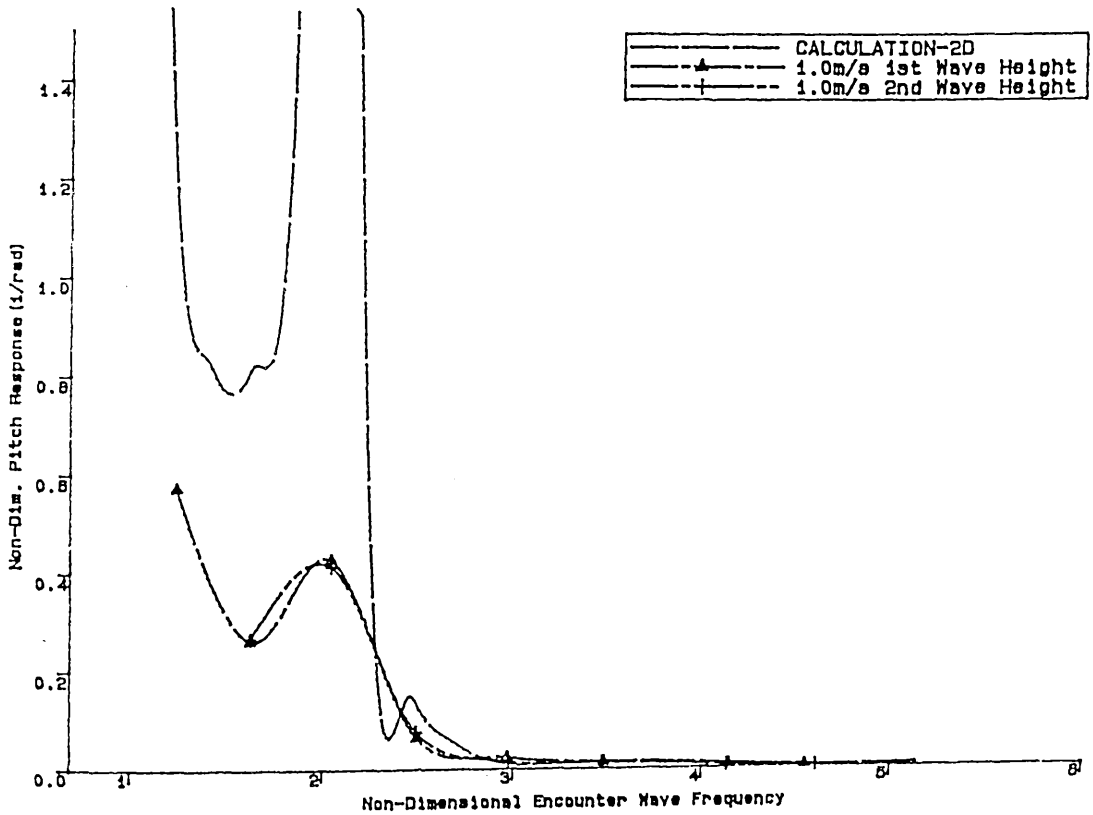

Fig.4.160
Computational and Experimental Pitch Responses of SWATH3-C1 in Head Seas with 2 Forward Speeds

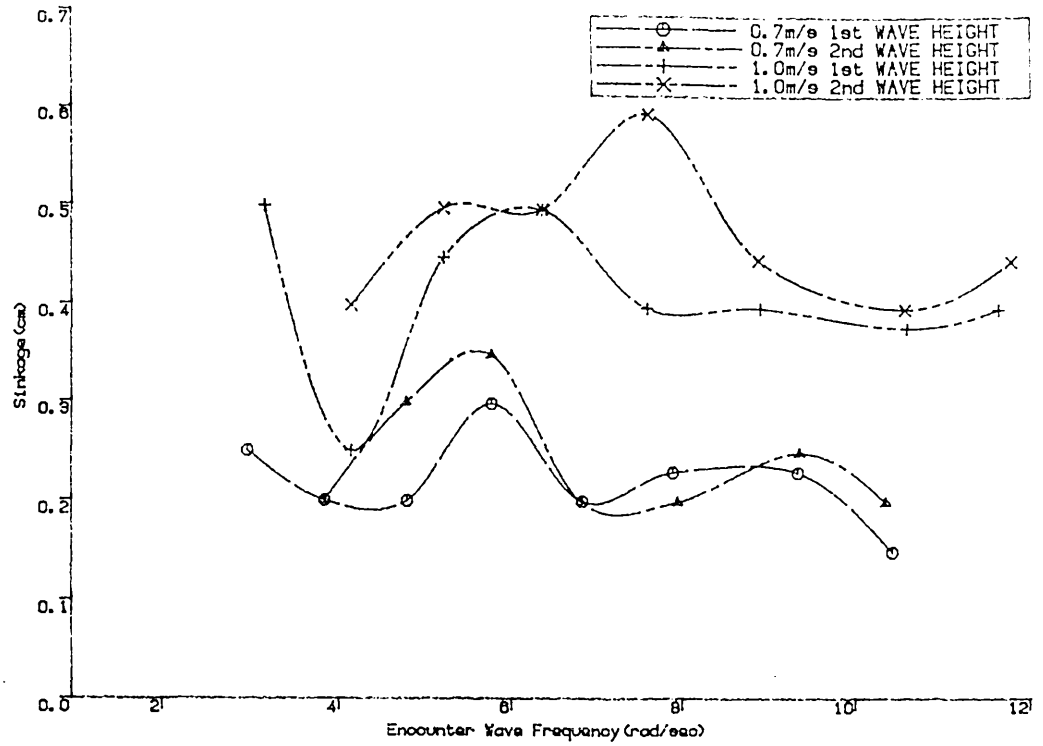

SWATH3-C1 Sinkages in Waves as a Function of Wave Frequency

Fig.4.161

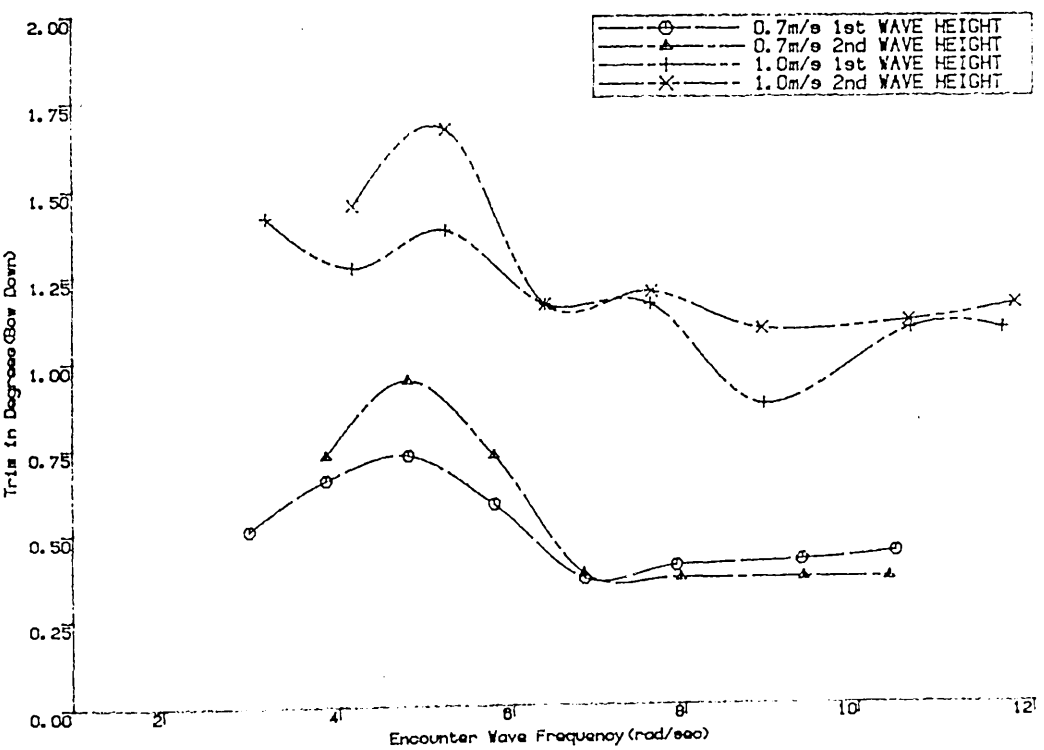

SWATH3-C1 Trims in Waves as a Function of Wave Frequency

Fig.4.162

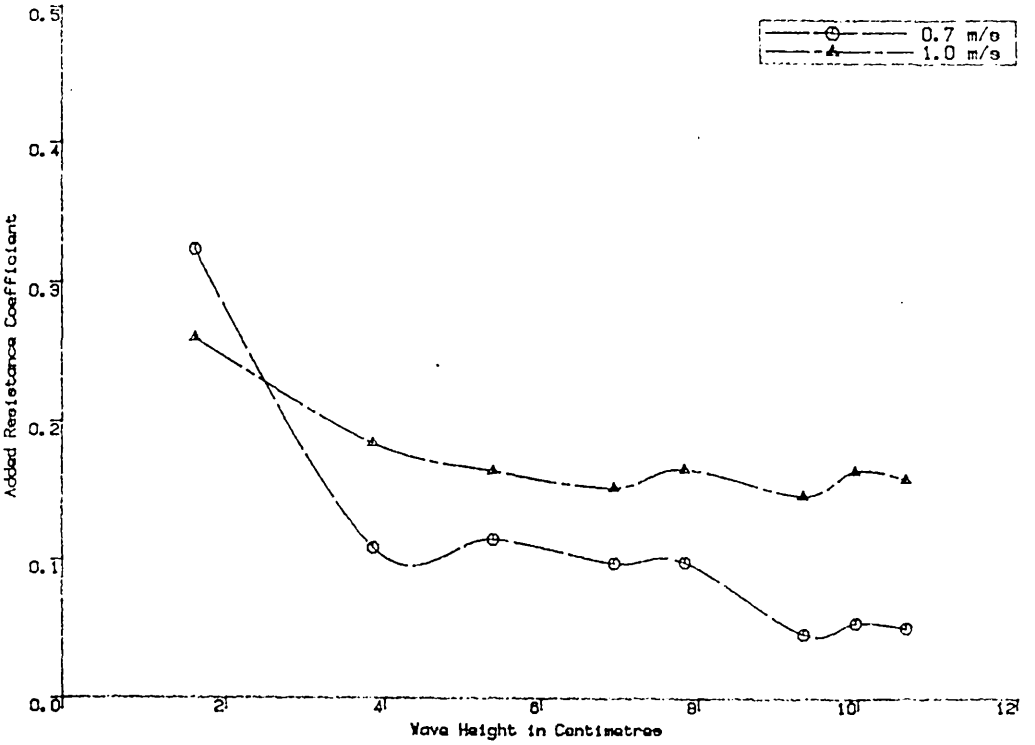

SWATH3-C1 Added Resistance Coefficient as a Function of Wave Height at Two Different Forward Speeds (Wave Freq. =1.02Hz Lw/Lb=1.0)

Fig.4.163

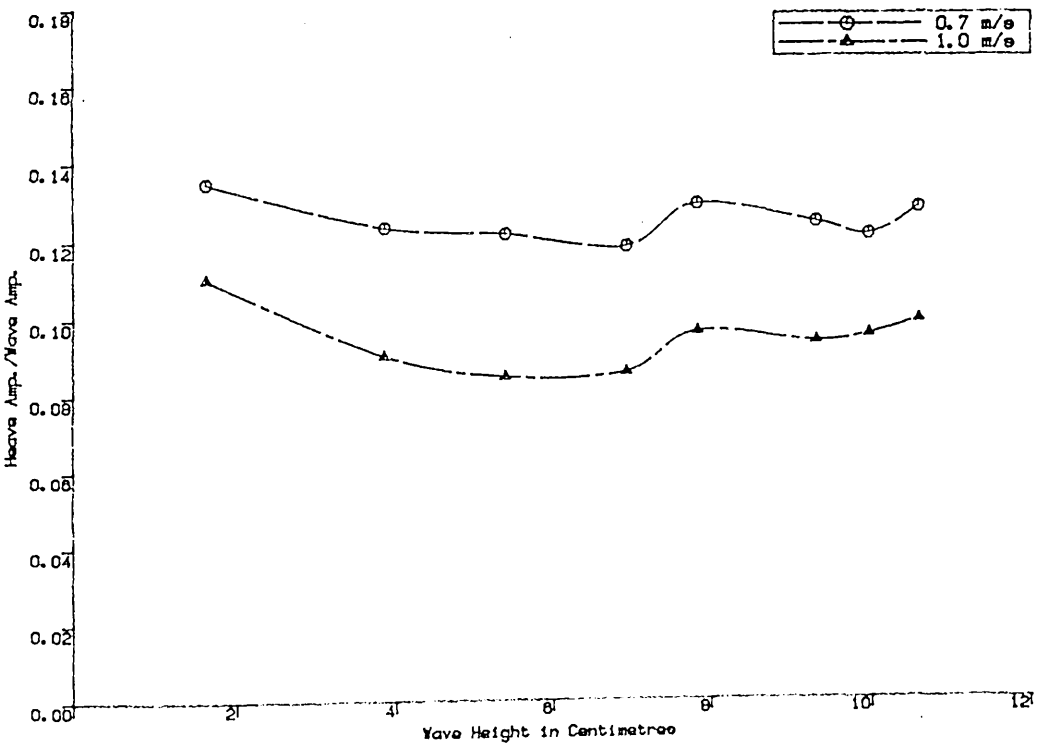

SWATH3-C1 Heave Responses as a Function of Wave Height at Two Different Forward Speeds (Wave Freq. =1.02Hz Lw/LB=1.0)

Fig.4.164

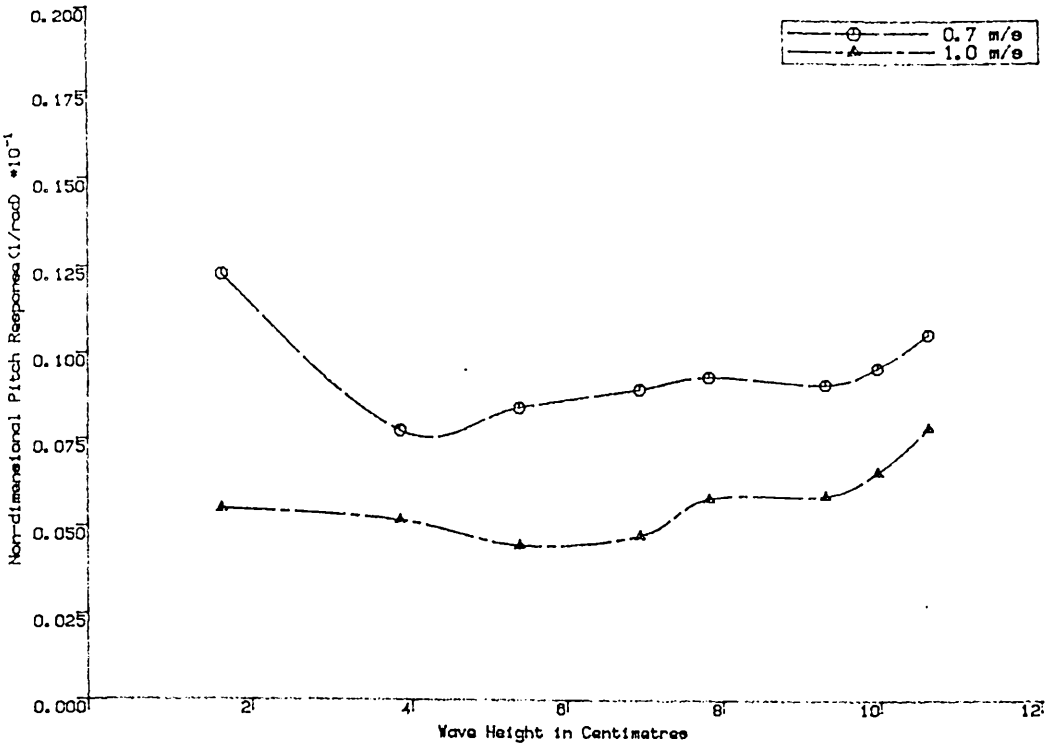

SWATH3-C1 Pitch Responses as a Function of Wave Height at Two Different Forward Speeds (Wave Freq.=1.02Hz Lw/Lb=1.0)

Fig.4.165

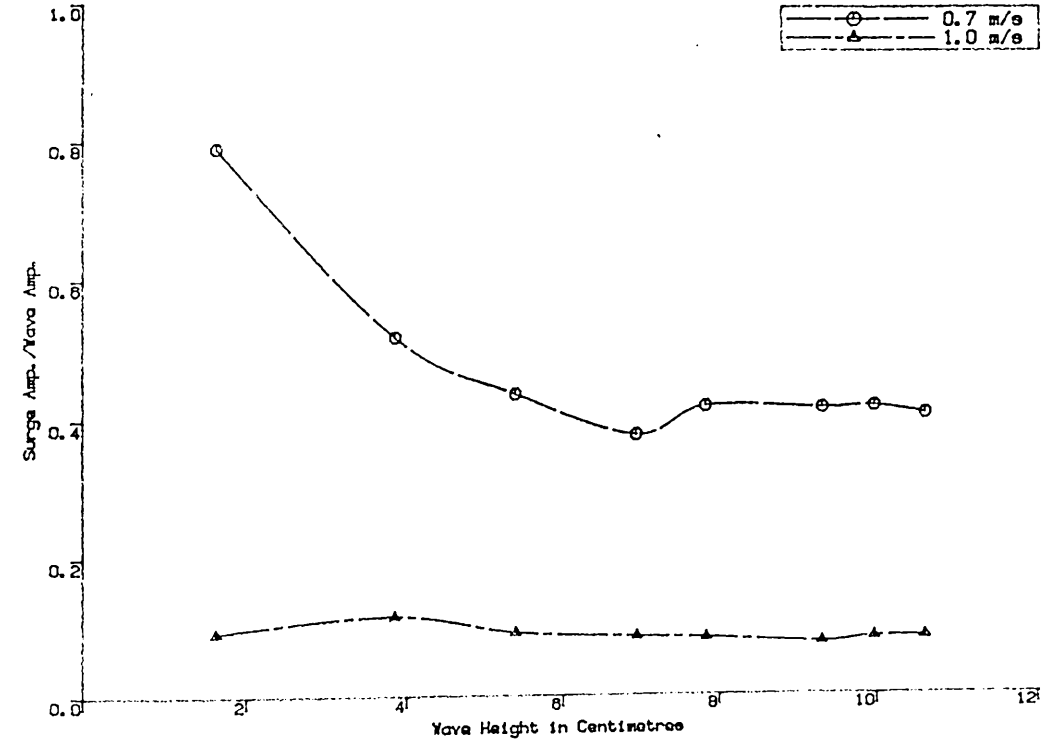

SWATH3-C1 Surge Responses as a Function of Wave Height at Two Different Forward Speeds (Wave Freq.=1.02Hz Lw/Lb=1.0)

Fig.4.166

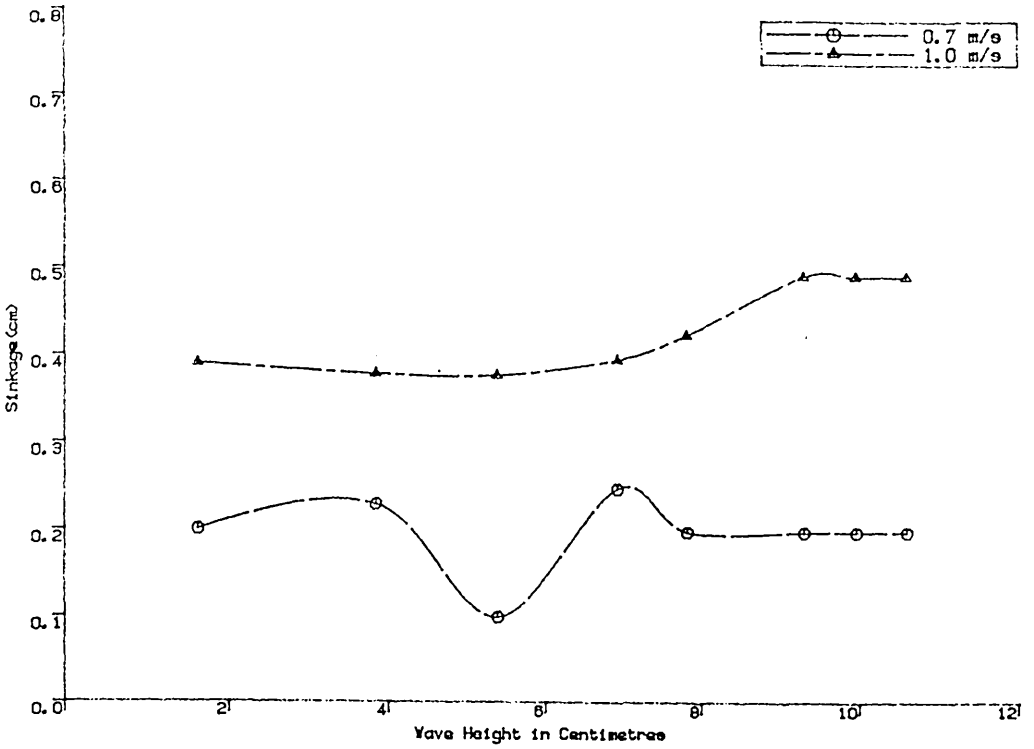

SWATH3-C1 Sinkages as a Function of Wave Height at Two Different Forward Speeds (Wave Freq.=1.02Hz Lw=1.51m Lw/Lb=1.0)

Fig.4.167

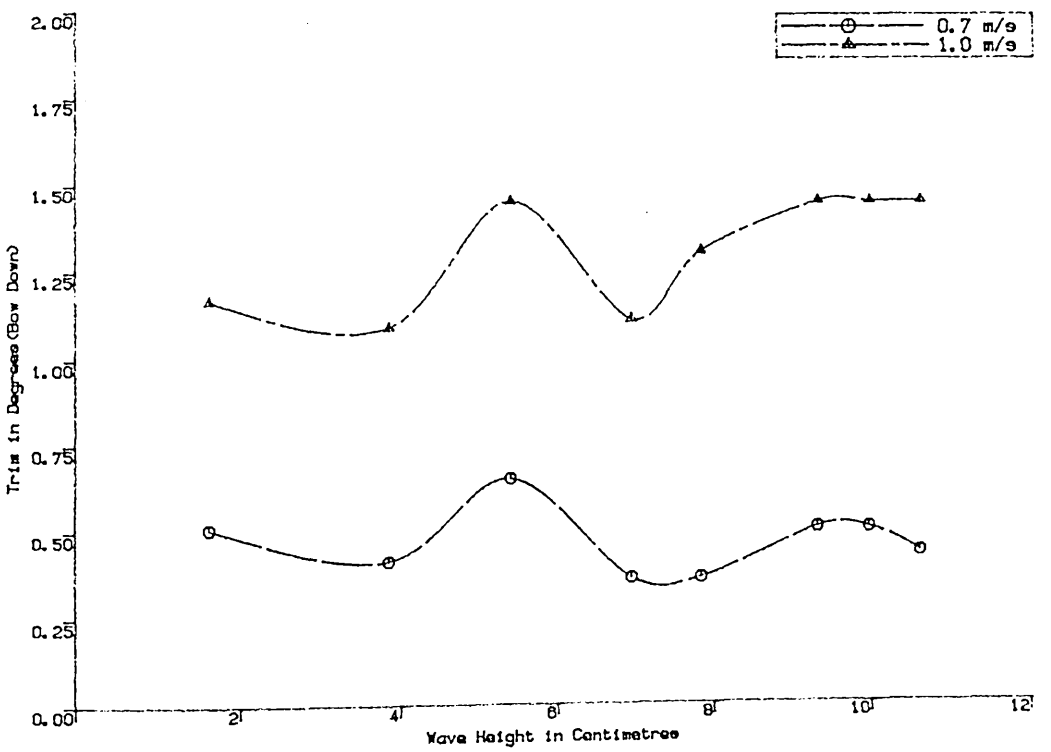

SWATH3-C1 Trims as a Function of Wave Height at Two Different Forward Speeds (Wave Freq.=1.02Hz Lw=1.51m Lw/Lb=1.0)

Fig.4.168

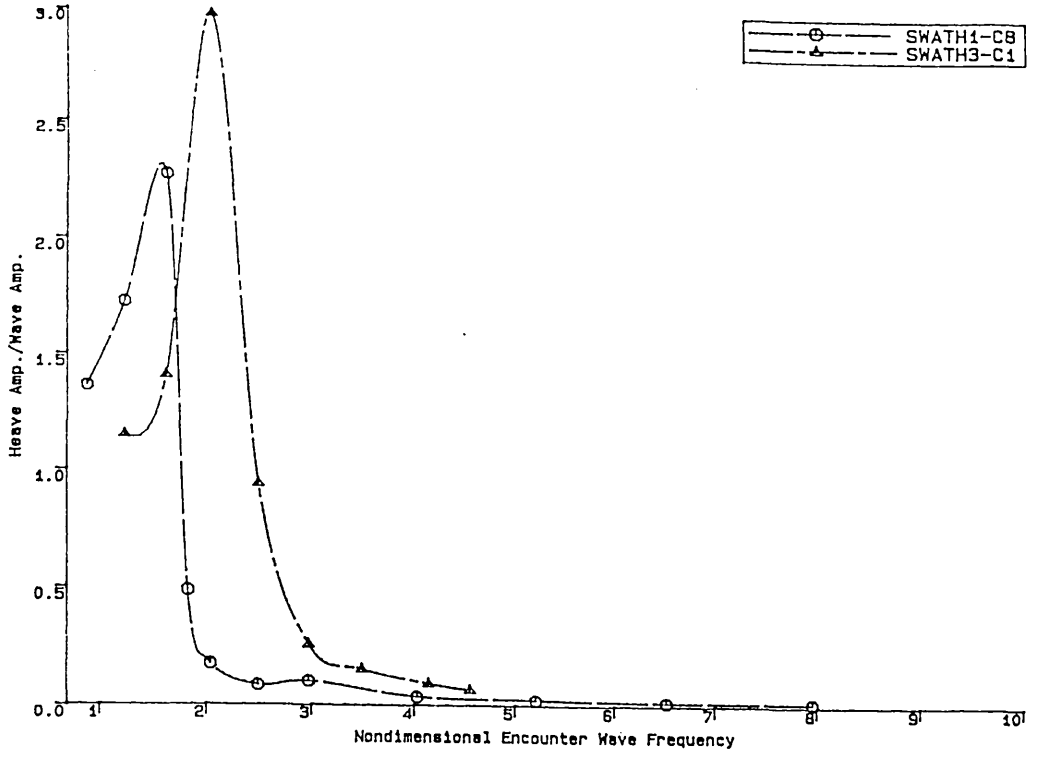

Heave Responses in Head Seas at Speed of 1.0 m/s

Fig.4.169

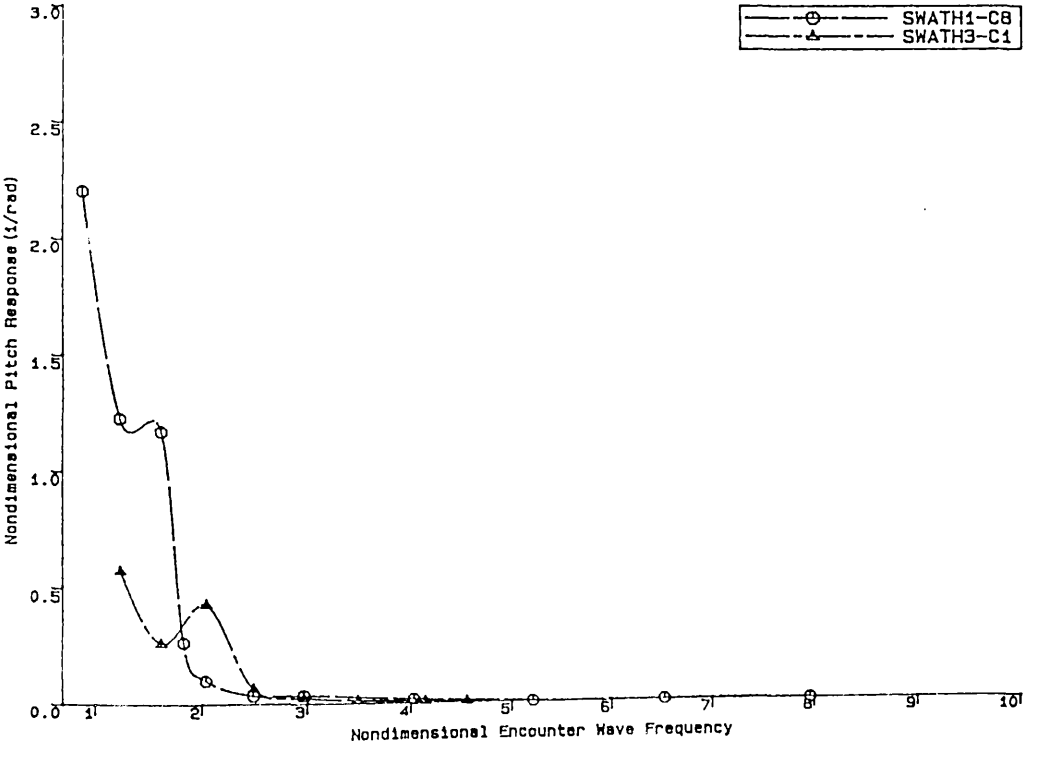

Pitch Responses in Head Seas at Speed of 1.0 m/s

Fig.4.170

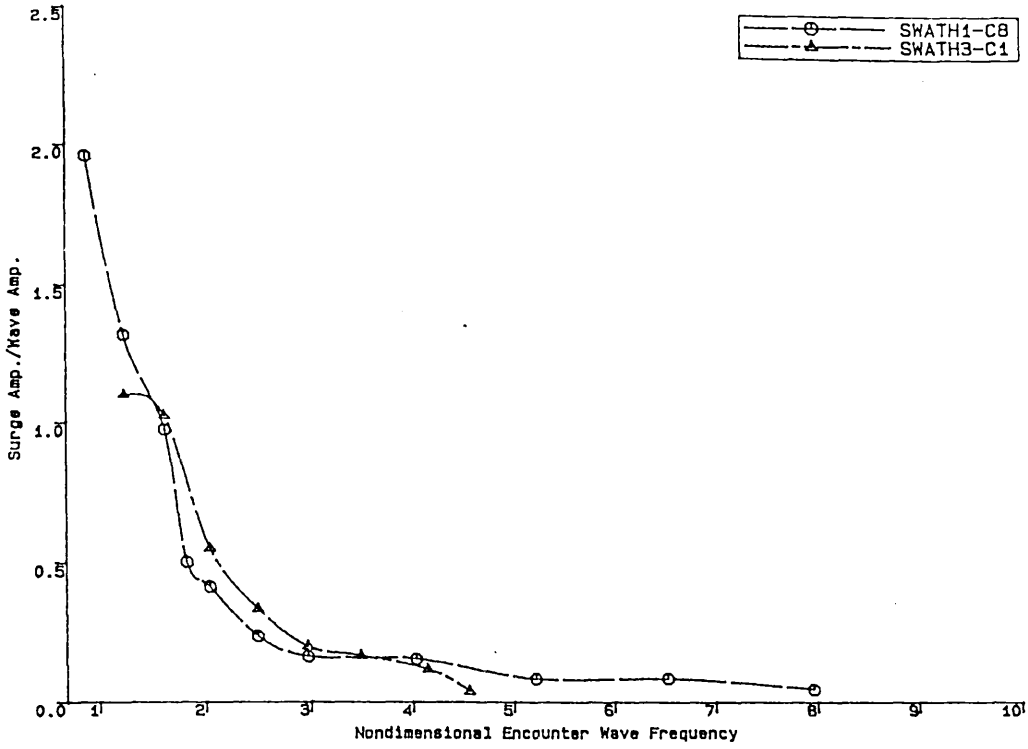

Surge Responses in Head Seas at Speed of 1.0 m/s

Fig.4.171

4.6 ANALYSIS OF THE EXPERIMENTS ON TWO POLISH MODELS (SWATH-386 AND -395) AND COMPARISON WITH COMPUTATIONAL RESULTS

As part of research collaboration between Dept of Naval Architecture and Ocean Engineering of Glasgow University(G.U) and Ship Hydromechanics Division of Gdansk Technical University(G.T.U), Poland, a series of model tests to measure the total resistance in calm water using SWATH-386, 0.833m in length, were carried out at GTU and their analysis and comparison with computational results were conducted at G.U by the author and reported in Ref.[23]. Some important results are discussed in this section, taken from that reference. In addition, open water test results of the SWATH-395 model were sent to the author[98] and compared with computational results herein.

4.6.1 Test Conditions and Description of the Models

The test series with the SWATH-386 model included various changes in configurations of strut system, modifications of bow struts as well as of lower hulls and two spacings between the centrelines of the two demihulls etc., which result in a total of 12 conditions(See Fig.4.172 and 4.173). All the measurements were performed at one draft of 0.167m and the principal dimensions and basic coefficients are listed in Table 4.33. No turbulence devices were introduced for the measurements. Instrumentation, towing system and facilities etc were not provided to the author and so, can not be mentioned herein in detail. The experiments were aimed at obtaining an optimum strut system in terms of resistance and at finding a hull shape which could help prevent severe bow trim at high speeds and so permit stabilizing fins to be removed. The latter purpose was achieved by introducing a 'sledge bow' concept which is mentioned below.

All the configurations of SWATH 386 tested are shown in Figs.4.172 and 4.173. Series A and B indicate the spacing of 0.5 and 0.433 metres between the centreplanes

of the two demihulls, respectively, both of which are comparatively wide compared to the hull length. SWATH 386 is a tandem strut configurations and its submerged hull has circular cross sections with the a hemispherical entrance as well as with a tapered run. Model 386-1 is a version that had a parallel middle block of 0.1m length inserted at the longitudinal centre of the aft strut of the original model 386. Forward and aft struts were both changed in the same way for Model 386-2(also, see Fig.174-b, the model under test at the tank) and forward strut only was changed for Model 386-3. Model 386-4 is a single strut configuration that was constructed by adding a parallel section between the maximum chord points of struts on Model 386. This version is shown in Fig.4.174-c where the model is under test at the tank. All the versions mentioned thus far have two pair of stabilising fins (NACA0012) as seen in Fig.4.174-a.

Table 4.33 Some Dimensions and Principal Coefficients of SWATH-386 Demihull

GTU Model	SWATH 386
Length of Body(m), L_b	0.833
Diameter of Body(m), Di_b	0.08
Length of Strut(m), L_S	0.2
Maximum Beam of Strut(m), t_m	0.033
L_b/Di_b	10.4125
L_S/t_m	6.061
Draft(m), T	0.167
SDBC(m), h	0.127
Wetted Area(m^2), S	0.255732
Displaced Volume(m^3),∇	0.00445
C_p of Body	0.88
C_{wp} of Strut	0.65
$H_1=2h/Di_b$	3.175

Note ; Dimensions are calculated by the computer program OSWATH

In order to obtain a hull shape which can prevent severe bow trim at higher speeds which is a severe problem with conventional SWATH ships, a sledge bow was introduced for Models 386-APW1, APW2 and APW2 by removing a portion of the underside of the original hull nose so that the bottom of the hull becomes a flat

surface. Also, flare and rake were introduced to the upper part of the strut entrance for all the versions. The tail part of the forward strut was replaced by a parallel block for 386-APW3. Two pairs of stabilizing fins were fitted to 386-APW2 and -APW3 alike. The SWATH-386-APW2 configuration is shown in Fig.4.174-a.

After having confirmed the benefits resulting from the introduction of a 'sledge' bow to the SWATH-386 configurations, the second model SWATH-395, 2.03m in body length, was built with this concept. The total resistance and trim with this model were measured at one spacing(0.75m) and one draft(0.19m) with and without stabilising fins(NACA0012). The principal dimensions and basic coefficients of this model are listed at Table 4.34 and a side view of the model is shown in Fig.4.175. The experiments were conducted at Lake Ilawa Test Station, Poland, and again, no detailed description of the testing procedure can be made herein.

Table 4.34 Principal Dimensions of SWATH-395 Demihull

GTU Model	SWATH-395
Length of Body(m), L_b	2.03
Diameter of Body(m) Di_b	0.145
Length of strut(m) L_S	2.05
Maximum Beam of Strut(m) T_S	0.09
L_b/Di_b	14.0
L_S/T_S	22.8
Draft(m), T	0.19
SDBC(m), h	0.118
Wetted area(m^2), S	1.72
Displaced Volume(m^3)	0.070
C_p of Body	0.798
C_{wp} of Strut	0.917
$H_1=2h/di_b$	1.6

4.6.2 Discussion

Fig.4.182 shows one(Model-386-A) of the comparisons between the calculated wave-making and measured residuary resistances for all the versions tested and illustrates its component contributions to the total wave-making resistance. In general, the comparisons between the measurements and predictions for all the tested conditions are in good aggrement excepting the high form effect of the model 386, as mentioned in detail in Ref.[23]. Including the empirical form factor and fin drag mentioned in Chapter 3, the total resistance is calculated for this condition and compared with the measurements(see Fig.4.183). For this purpose, the angle of attack of fins is uniformly assumed 2 degrees for all the speeds. However, practically, it is nearly impossible to obtain an uniform angle of attack of fins to the flow when the model is under way at different speeds.

Fig. 4.176 and 4.177 show comparisons of the total and residuary resistance coefficients nondimensionalised by the displacement for the five configurations. From Fig.4.176, it is noticed that all the tandem strut configurations result in much higher resistances than the single strut version up to around Fn=0.45 but above this speed they become better in terms of total resistance per displaced volume. This high penalty is caused by the large wave-making contributions of the struts and unfavourable interferences between the struts and between the struts and the body as can be seen in Fig.4.182. The short struts configuration version of 386-A is the worst up to Fn=0.3 and the best among the configurations at higher speeds which is caused by the strut wave-making characteristics[23]. In general, the wave-making resistance coefficient of a short strut reaches its maximum earlier than a long strut does and then, the coefficient of the short strut becomes lower than the other at higher speeds(Detailed parametric studies are conducted in the following Chapter 5). Also, it can be clearly seen that 386-2A, which has two long struts, is subject to the least resistance up to moderate speeds and is then the largest amongst the tandem strut configurations. It is of interest to compare 386-1A and 3A. The resistance of 386-1A is larger than that of 386-3A up to moderate speeds, but at higher speeds, the result is reversed. This is due to the fact that the interference between the body and longer fore strut with 386-3A contributes to

making the wave-making resistance larger at higher speeds compared to the counterpart configuration[23].

Fig.4.178 and 4.179 show the total and residuary resistance coefficients for the four tandem strut configurations at the second spacing. The results shows the same patterns as in the first spacing configurations. As results, the five configurations tested shows that by changing the strut position on the hull, a better performance can be achieved over a particular speed region but it is impossible to select a combination which will give a better performance over the whole speed range. In general, a short strut-body combination give less resistance than a long strut-body combination at higher speed but at slow speeds, the result is reversed.

Fig.4.180 shows the spacing effects. At higher speeds, the wider spacing versions are all better in terms of resistance, but at slower speed this is not always the case as mentioned in the previous sections.

Fig.4.181 shows a comparison between the original version(386-A) and the modified sledge versions with and without fins. There is little difference between 386-APW1 and the original 386-A upto Fn=0.29, but the sledge version becomes worse than the original version above that speed. Mr. Paul and Mr. Grygorowicz(visitors from G.T.U) explained that they observed during the experiments a much reduced bow trim with the sledge version of APW1 compared to the original one, but failed to reduce the resistance at higher speeds which might be due to the flare and rake. It seems to be certain that the flare introduced to the fore struts of APW1 creates more waterplane area at trim, resulting in the large resistance increase. In general, stabilizing fins cause an increase in the resistance in calm water(compare 386-APW1 and -APW2). The largest resistance of APW3 seems to be caused by the parallel tail part of the forward strut with square end(see Fig.4.173).

The measured residuary resistance coefficient of the SWATH-395 model(no fins) is shown in Fig.4.185 together with the calculated wave-making resistance. The two results are in good agreement excepting the large predicted value at around Fn=0.31. It can be seen that the body contribution to the total wave making resistance is comparatively large due to its shallow submergence as seen in Table 4.33. Fig.4.184

shows the measured total resistances(in newtons) of the model with two pair of fins and without fins as a function of Froude number. Again, including the present form factor and fin drag, the total resistance is calculated assuming a 2 degree of angle of attack of the fins. It seems that this angle is high at slow speeds and low at higher speeds. However, the agreement is excellent excepting at around Fn=0.31 which is caused by the larger predicted wave-making resistance as seen in Fig.4.185.

Fig.4.186 shows a comparison of the trims between two single strut SWATH models, SWATH3-C1 and SWATH-395, both of which have no fins. The result of SWATH3-C1 is taken from Fig.4.144. In order to compare the trims of different lengths of model, as usual, the trims are non-dimensionalised by each body length. In general, trim is very sensitive to the towing system and towing height so that a direct comparison cannot be made. However, the trim of the sledge bow SWATH is significantly smaller and further this model runs at level trim at much higher speeds. This kind of performance has not been observed with numerous SWATH models worldwide. As mentioned in section 4.5, the measurements with the SWATH1 model could not be conducted further beyond the last speed tested due to the severe bow trim and hence, green water effects. Consequently, a 'sledge' bow, if well designed, might give a possibility of removing stabilising fins which previously had been considered essential to all conventional SWATH ships. As seen above, these fins cause a large resistance increase and also produce control problems.

4.6.3 Conclusions

a) In general, the comparison between the predictions and measurements is in good agreement, in particular, with the large SWATH 395 model.

b) As mentioned in the previous sections with the three SWATH models(SWATH1, 2 and 3), it is not expected to obtain a SWATH configuration which will give favourable resistance characteristics at all speeds since such interference effects are dependent upon the relative distance between the components of the SWATH ships as well as the operating speeds. The present configurations of

changing the strut systems on the demihull proved that statement by showing that one gives better result than the other depending on the speed. In general, a short strut-body combination give less resistance than a long strut-body combination at higher speeds, but the result is reversed at slow speeds. Therefore, a single strut SWATH is recommended upto moderately high speeds, but at higher speeds a tandem strut configuration is better from the point of view of resistance.

c) At higher speeds, the wider spacing versions between two demihull all give less resistance than the narrower spacing versions tested. However, in the moderate speed range, the result is reversed due to favourable interferences between the two demihulls.

d) A 'sledge' bow seems to be promising in terms of reducing the bow trim and hence, a resistance reduction can be expected. The contribution of fin drag to total resistance is substantial. If controllable fins can be removed from the SWATH concept, this will be a great breakthrough to the further development of SWATH ships. It is therefore recommended that further research should be followed on the 'sledge' concept.

e) Flare introduced to the strut creates a substantial resistance increase, especially at higher speeds.

4.7 CONCLUDING REMARKS

The experimental results with 5 SWATH models including 38 individual configurations presented in this Chapter are very valuable at this stage of SWATH developmemt. Some of them seem to be of extreme importance to the further development of SWATH ships. Detailed conclusions have been drawn at the end of each section and some general and important remarks are made below:

a) One of the most important things is that the present analytical method gives excellent correlations with the various SWATH configurations including single and tandem struts, circular and non-circular hulls, with and without fins and such parametric changes as spacing of the two demihulls, draft, strut position on the demihull and slenderness ratioes of body as well as strut etc. Therefore, this tool can be used, with good confidence, for parametric studies and for an optimisation process in selecting hull form with regard to resistance.

b) A resistance benefit from an increase of draft cannot be obtained for all the SWATH models(SWATH1, SWATH2 and SWATH3). This is due to the fact that since the slenderness ratio of the bodies for the three models are comparatively small, the increased strut depth results in a subtantial increase of the strut wave-making resistance which outweighs the decrease of the body wave-making resistance. This result reveals that at a given displacement, the proper distribution of the displacement on struts and bodies is essential depending on the draft as well as the speed of interest.

c) An interference wave system created by the two demihulls affects the resistance favourably or unfavourably, depending on speed. Owing to the unfavourable interferences at higher speeds the wider the spacing between two demihulls, the better the resistance. However, up to moderately high speeds, there are some favourable interference effects betwen two demihulls.

d) The hollow and hump in the resistance curve is significantly changed by the strut(s) position on the demihull. In particular, this is much exaggerated with the tandem strut SWATH designs. Therefore, when designing a SWATH with tandem struts, careful attention should be paid to the position of the struts on the demihull

depending on speed.

e) As results, interference effects are dependent upon the relative distance between the components of a SWATH design as well as the operating speed. Hence, a SWATH arrangement which will give favourable interference characteristics at all speeds is not to be expected at all. However, reductions in wave resistance at certain speeds can be obtained by a proper location of the struts on the hulls and a well chosen spacing between the hulls. Most importantly, at certain drafts, a proper distribution of the displacement on the struts and bodies, keeping the breadth to length ratio of the strut as low as possible, seems to be essential. In general, a short strut-body combination give less resistance than a long strut-body combination at higher speeds, but the result is reversed at slow speeds. Therefore, a single strut SWATH is recommended up to moderately high speeds, but at higher speeds a tandem strut configuration is better from the point of view of resistance.

f) The sinkage and trim of the tandem strut models are independent of the wave length but dependent on the wave height. However, with the single strut SWATH3, they are both nearly independent of the wave height.The sinkage and trim of the single strut SWATH are both much smaller than those of the tandem versions. Both the sinkage and trim follow nearly the same trends as the total resistance variations associated with parametric changes such as spacing and draft. Namely, the wider the spacing between the two demihulls, the smaller the sinkage and trim, and they are both increased with draft. In general, the sinkage and trim are both increased with increasing speed which creates severe bow trim and accordingly green water at higher speeds. In particular, the resistance of the SWATH2 model with rectangular hulls with rounded corners is substantially increased by the trim at high speeds. Thus, stabilising fins are needed for the SWATH models with regard to resistance increase, sea-keeping and propeller emergence problems.

g) The resistance increase of the SWATH models in waves is very much smaller than those of monohull ships. There is little increase in added resistance as speed increases. Further, in the supercritical zone, as the wave height increases, the resistance of the tandem strut models systematically decreases by as much as 24 % of the calm water resistance over the speed range of Fn=0.31-0.39 with the tendency that

the resistance peak shifts to the slower speeds and that the hump and hollow are flattened. This seems to be due to the combination of several complicated hydrodynamic interferences such as trim and sinkage changes in waves relative to those in calm water, increased apparent speed of the models due to the oncoming waves and changed speed of water particles near the models due to the increased surge motion with the increase of wave height etc. However, this negative resistance increase does not occur with the single strut SWATH3 model. Therefore, the resistance decrease is mostly due to the interference effects between the twin struts combined with some motion aspects of the tandem strut SWATH models. As a result, the tandem strut SWATH ship can be recommended to apply to naval combatants where speed reduction is of prime importance. In order to confirm the resistance decrease in regular waves, experiments in random waves will be desirable.

h) It can be seen that the heaving, pitching and surging responses are proportional to the wave height. However, the added resistance for the three models tested is not proportional to the square of the wave height. The added resistance divided by the square of the wave height decreases as the wave height increases. The break in the square law is more significant in lower wave heights compared to in high wave heights

i) The motion response of the SWATH2 is much less than that of the SWATH1 model. This fact results in less added resistance for SWATH2 compared to SWATH1 at the same wave steepness and same submergence ratio of the main body. A rectangular cross section hulled SWATH with rounded corners seems to be promising up to moderately high speeds, but at higher speeds, a well streamlined hull seems to be better in terms of the total resistance.

j) The resistance increase of the single strut SWATH in the waves is larger than that of the tandem versions at higher speeds possibly due to the increased trim and sinkage compared to those in calm water(the trim of the tandem strut in waves is significantly reduced as the wave height increases). The most resistance increase or decrease of the tandem strut versions occurs at around the pitch resonant region while the large resistance increase for the single strut occurs at around the heave resonant region possibly due to the much exaggerated heave motion at the resonant

frequency. Unlike the tandem strut, the heave response reaches up to three times the wave height at the resonant frequency. The heave and surge motions of the tandem strut are less than those of the single strut excepting around the resonant regions, but the pitch motion of the tandem is larger than that of its counterpart.

k) A 'sledge' bow seems to be promising in terms of reducing the bow trim and hence, a resistance reduction can be expected. The contribution of fin drag to total resistance is substantial. If controllable fins can be removed from the SWATH concept, this will be a great breakthrough to the further development of SWATH ships. In regard of this, it can be recommended that further research should be followed on the 'sledge' concept.

l) In conslusion, a SWATH ship with rectangular cross section hulls with rounded corners can be recommended for the next generation of SWATH development in terms of less motion responses, less resistance increase in waves, draft reduction and construction cost compared to circular hulled SWATH ships. The trim of the SWATH2 model is less than that of the SWATH1 circular hulled model. In addition, the 'sledge' bow can be easily introduced to rectangular hulled SWATH ships. Therefore, a rectangular cross section hull can be applied to the design of practical SWATH ships up to moderately high speeds without any serious penalty in resistance compared to the circular counterpart. However, at higher speeds, a well streamlined hull is better in terms of the total resistance.

CONFIGURATIONS OF STRUTS UKŁADY WSPORNIKÓW	PARAMETERS PARAMETRY
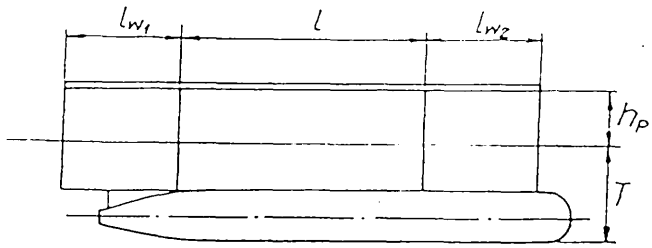 386-A, B	D = 8,92 kg T = 167 mm $l_{W1,2}$ = 200 mm l = 433 mm h_P = 83 mm
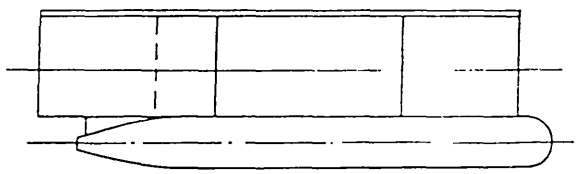 386-1A, 1B	D = 9,50 kg T = 170 mm l_{W1} = 300 mm l_{W2} = 200 mm l = 333 mm h_P = 80 mm
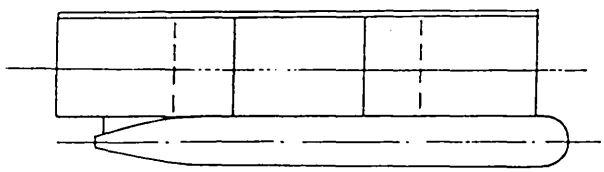 386-2A, 2B	D = 10.36 kg T = 175 mm $l_{W1,2}$ = 300 mm l = 233 mm h_P = 80 mm
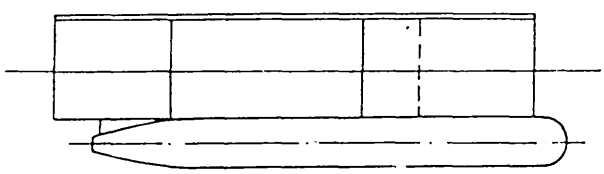 386 - 3A, 3B	D = 9,50 kg T = 170 mm l_{W1} = 200 mm l_{W2} = 300 mm h_P = 80 mm
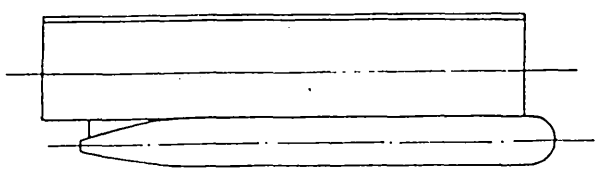 386 - 4A	D = 12,90 kg T = 175 mm l_W = 833 mm h_P = 75 mm

Fig.4.172 Configurations of SWATH model-386

MODEL	CONSIDERATIONS UWAGI
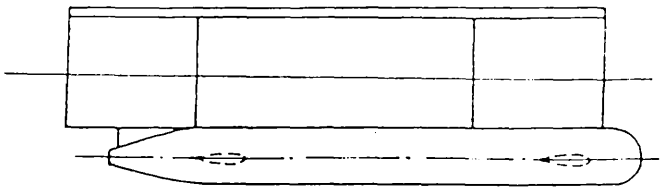 386 -A,B - podstawowy fundamental	- 2 pary płetw stabilizacyjnych ; - bez podcięcia dolnych kadłubow ; 2 pair of stabilizing fins
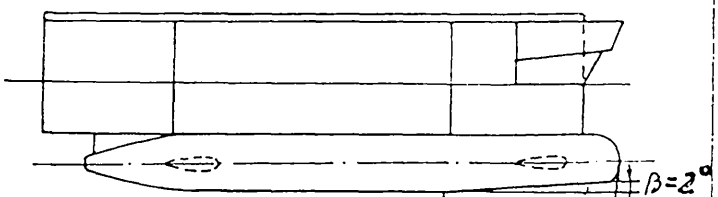 β=2° 386 - APW1 230	- 2 pary płetw stabilizacyjnych ; - β = 2° - podcięcie dolnych kadłubow ; - modyfikacja kształtu wsporników dziobowych nad linią wodną ; 2 pair stabilizing fins
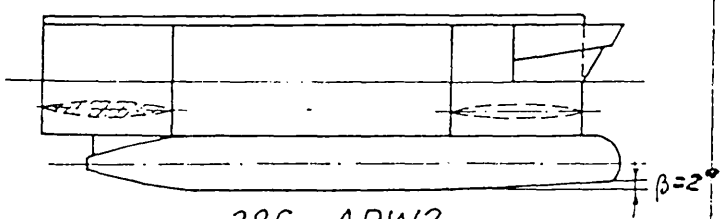 β=2° 386 - APW2	- bez płetw stabiliz. ; pozostałe zmiany jak wyżej ; without of stabilizing fins
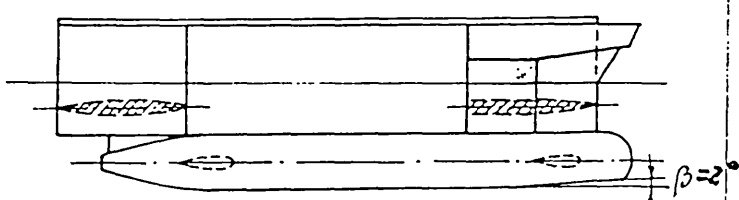 β=2° 386 - APW3	- 2 pary płetw stabiliz. ; - całkowita modyfik. kształtu wsporników dziobowych ; - β = 2° ; 2 pair of stabilizing fins

Fig.4.173 Configurations of SWATH model-386

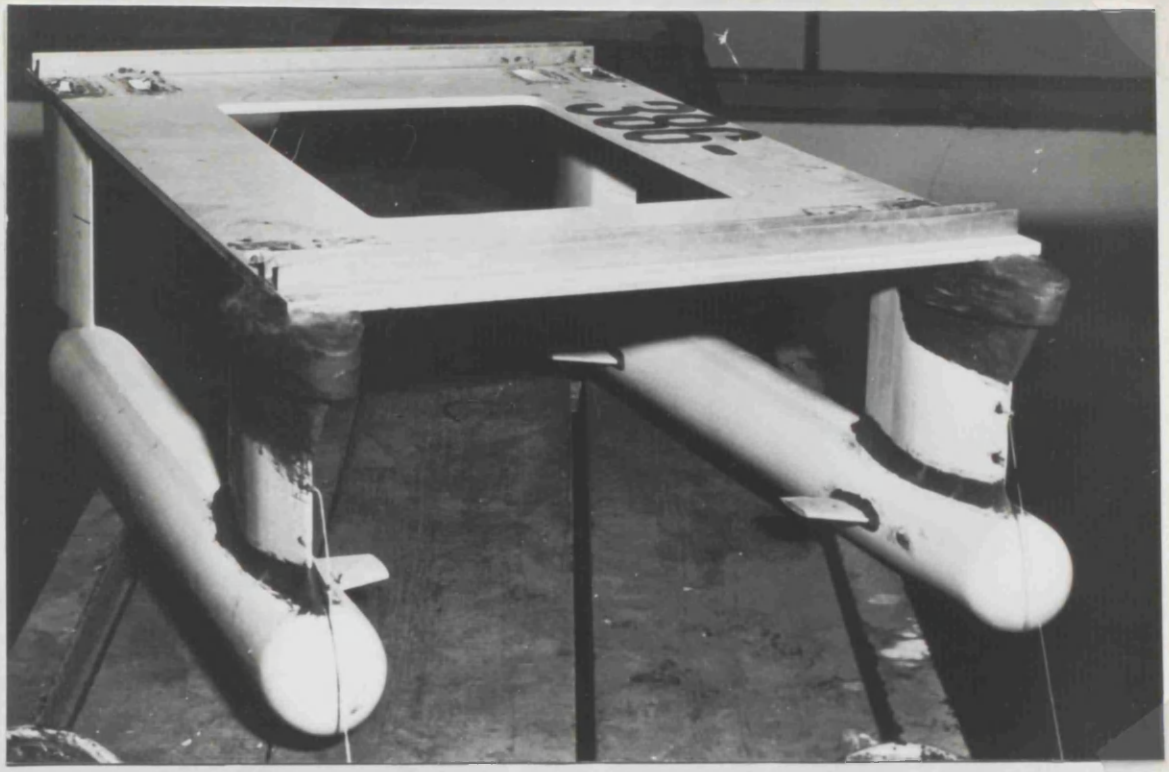

Fig 4.174-a Front View of Model 386-APW2

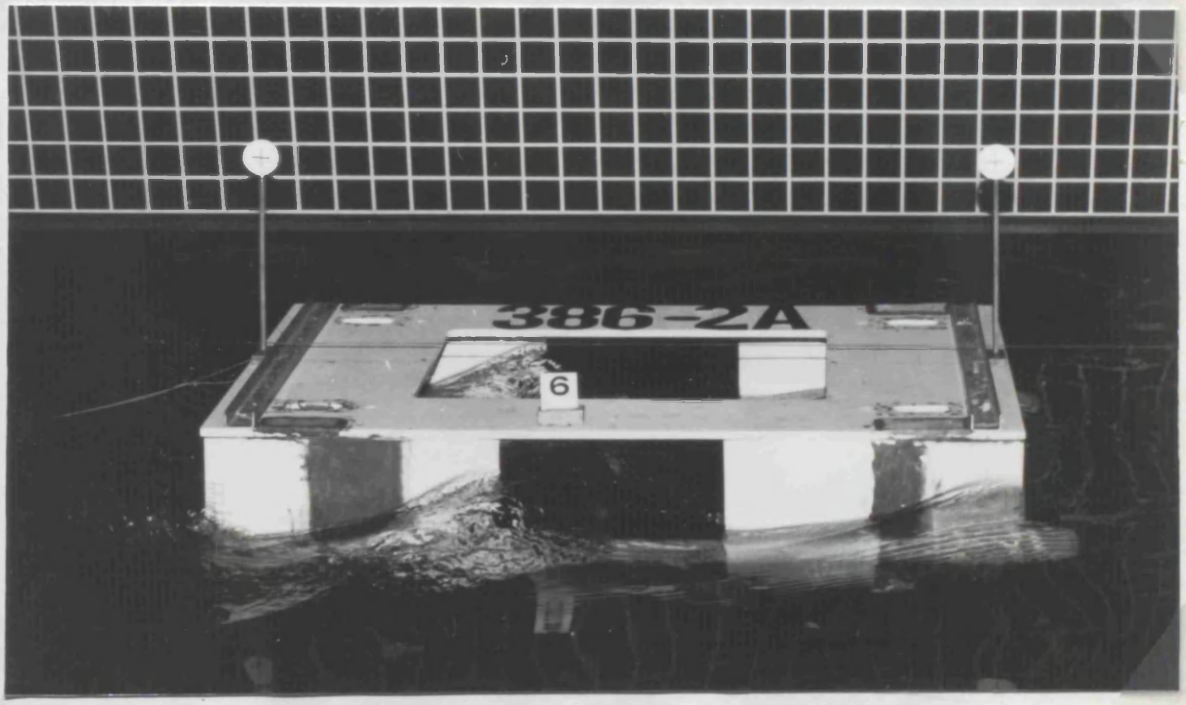

Fig 4.174-b Model 386-2A under way in Water

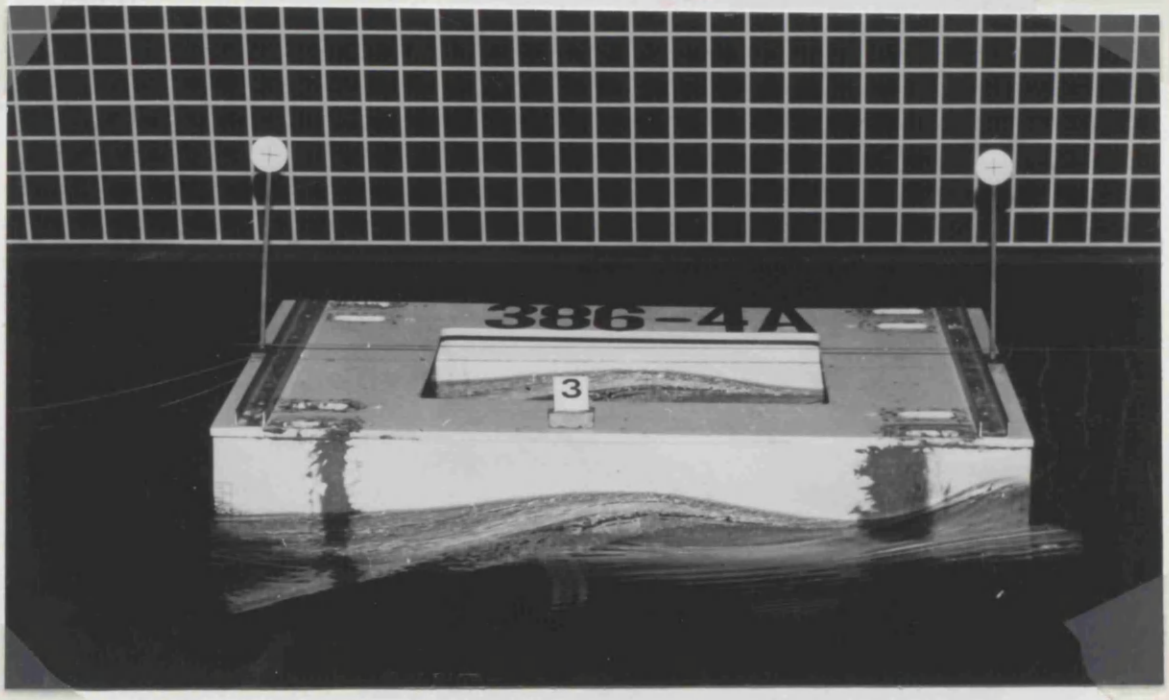

Fig 4.174-c Model 386-4A under way in Water

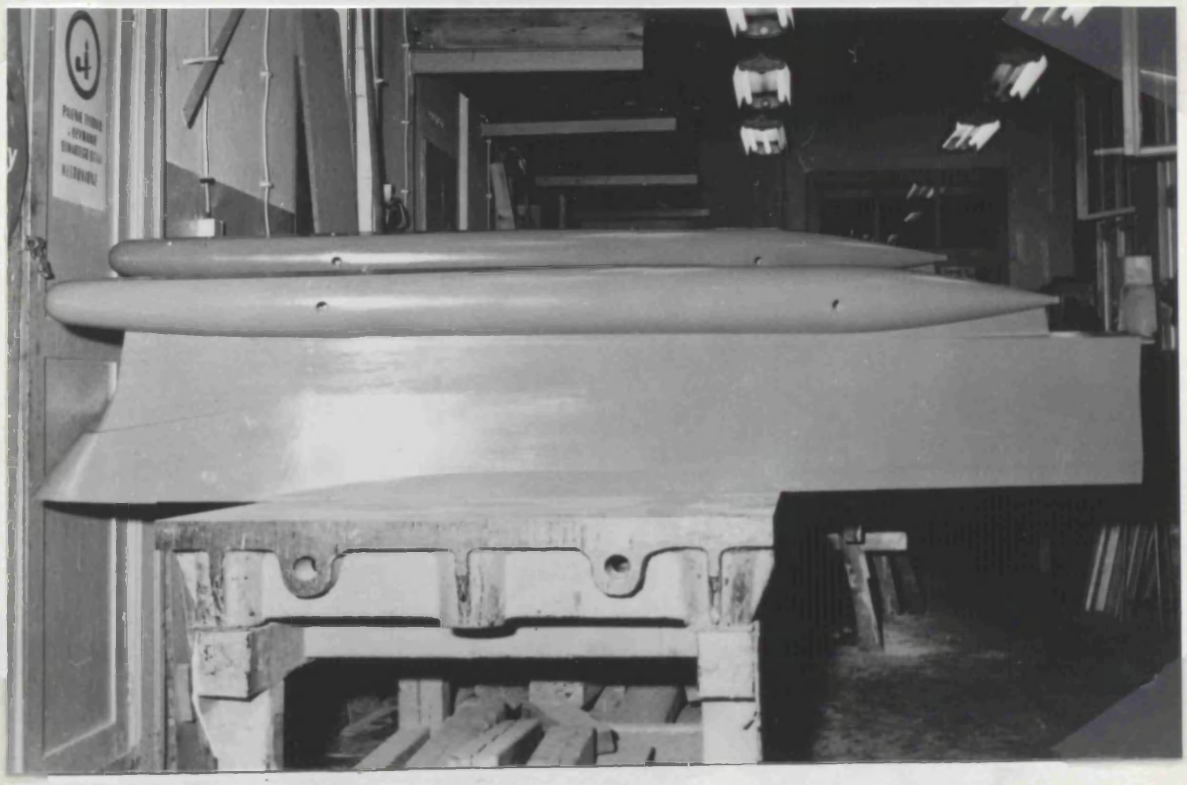

Fig 4.175 Side View of Model-395(Up Side Down)

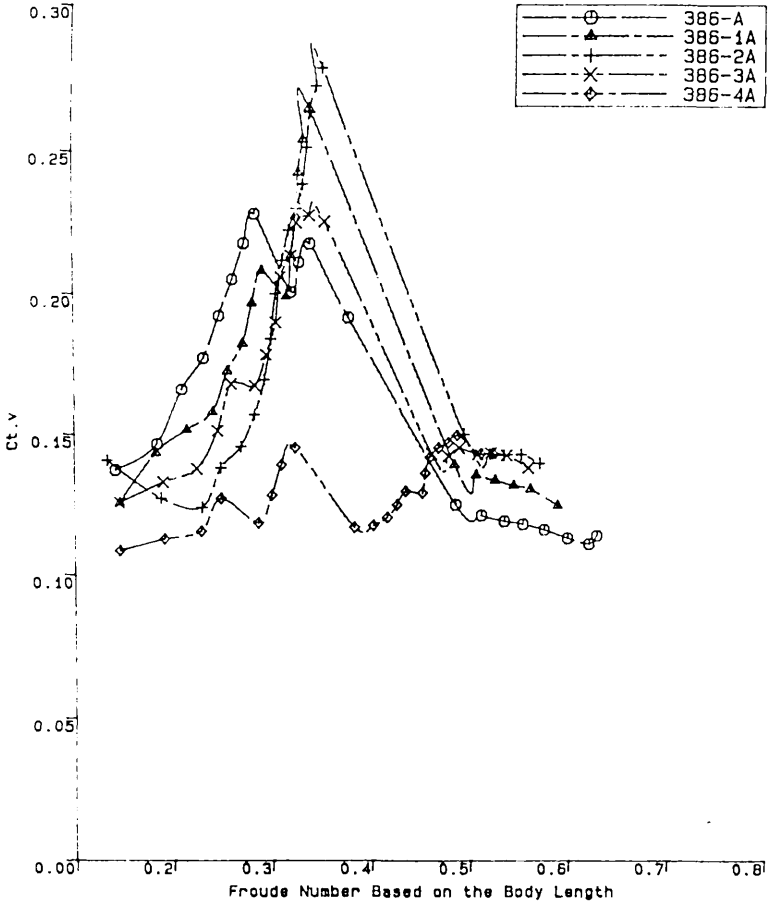

Comparison of Total Resistance Coefficients of 5 SWATH Configurations as a Function of Froude Number.

Fig.4.176

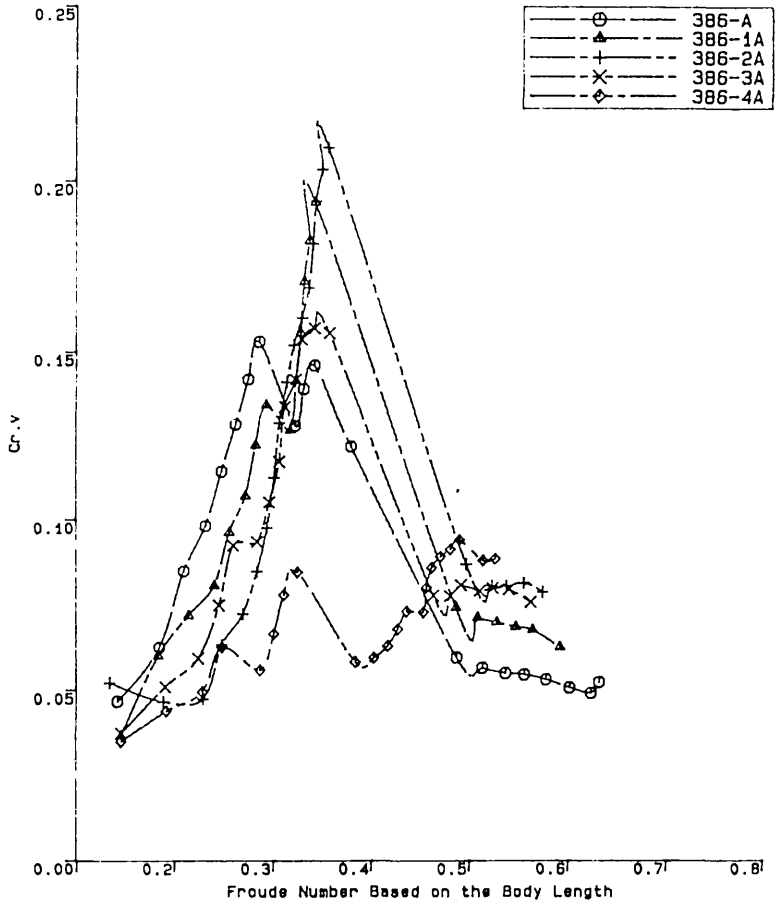

Comparison of Residuary Resistance Coefficients of 5 SWATH Configurations as a Function of Froude Number.

Fig.4.177

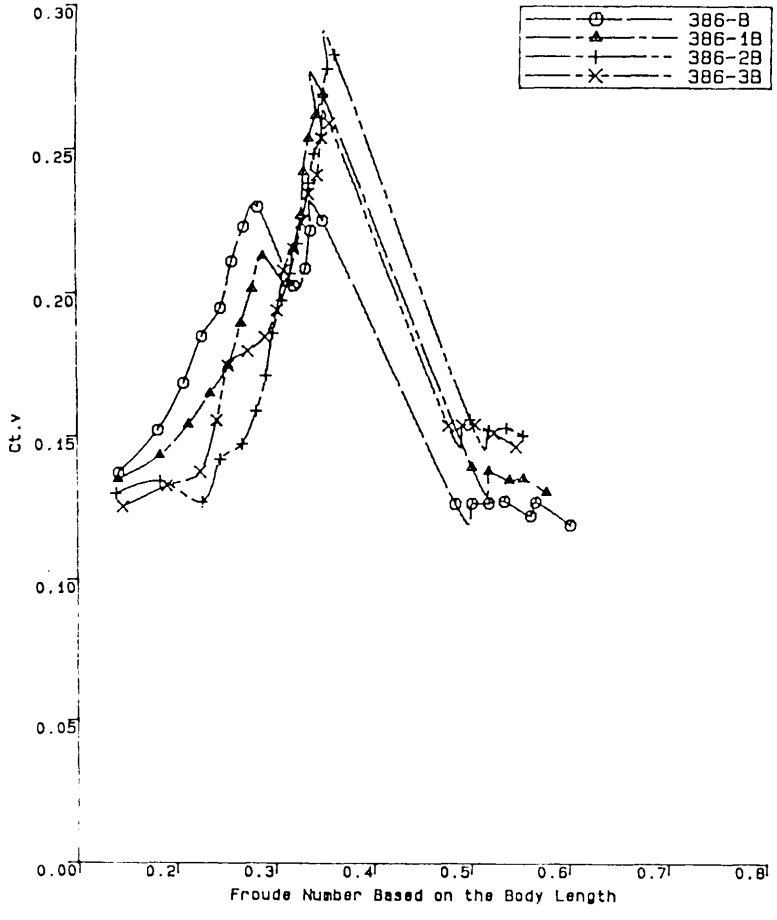

Comparison of Total Resistance Coefficients of 4 SWATH Configurations as a Function of Froude Number.

Fig.4.178

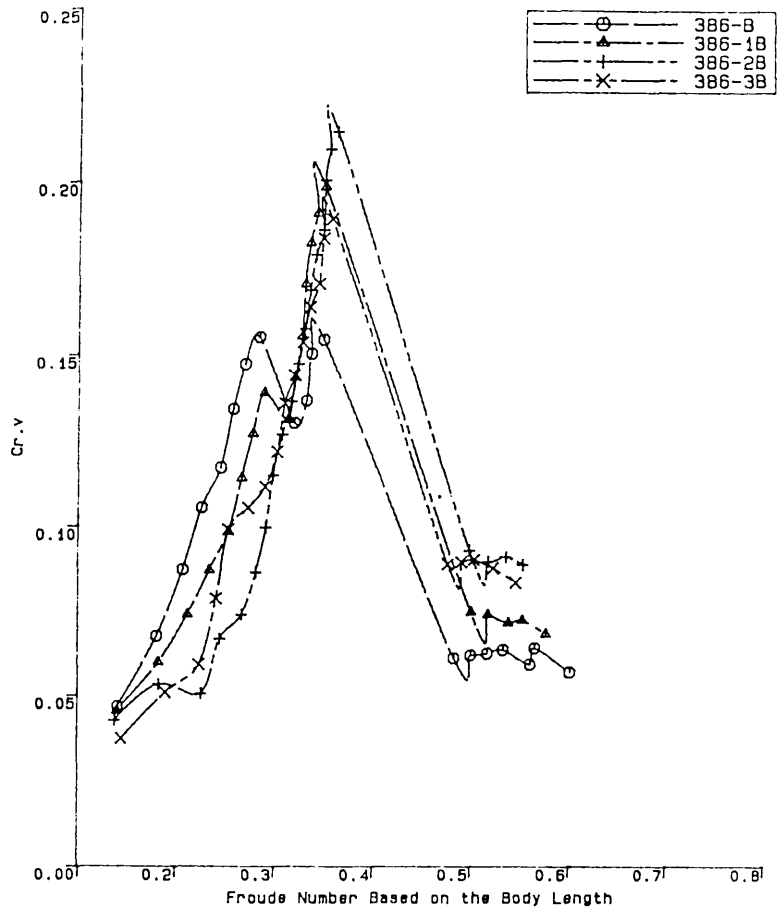

Comparison of Residuary Resistance Coefficients of 4 SWATH Configurations as a Function of Froude Number.

Fig.4.179

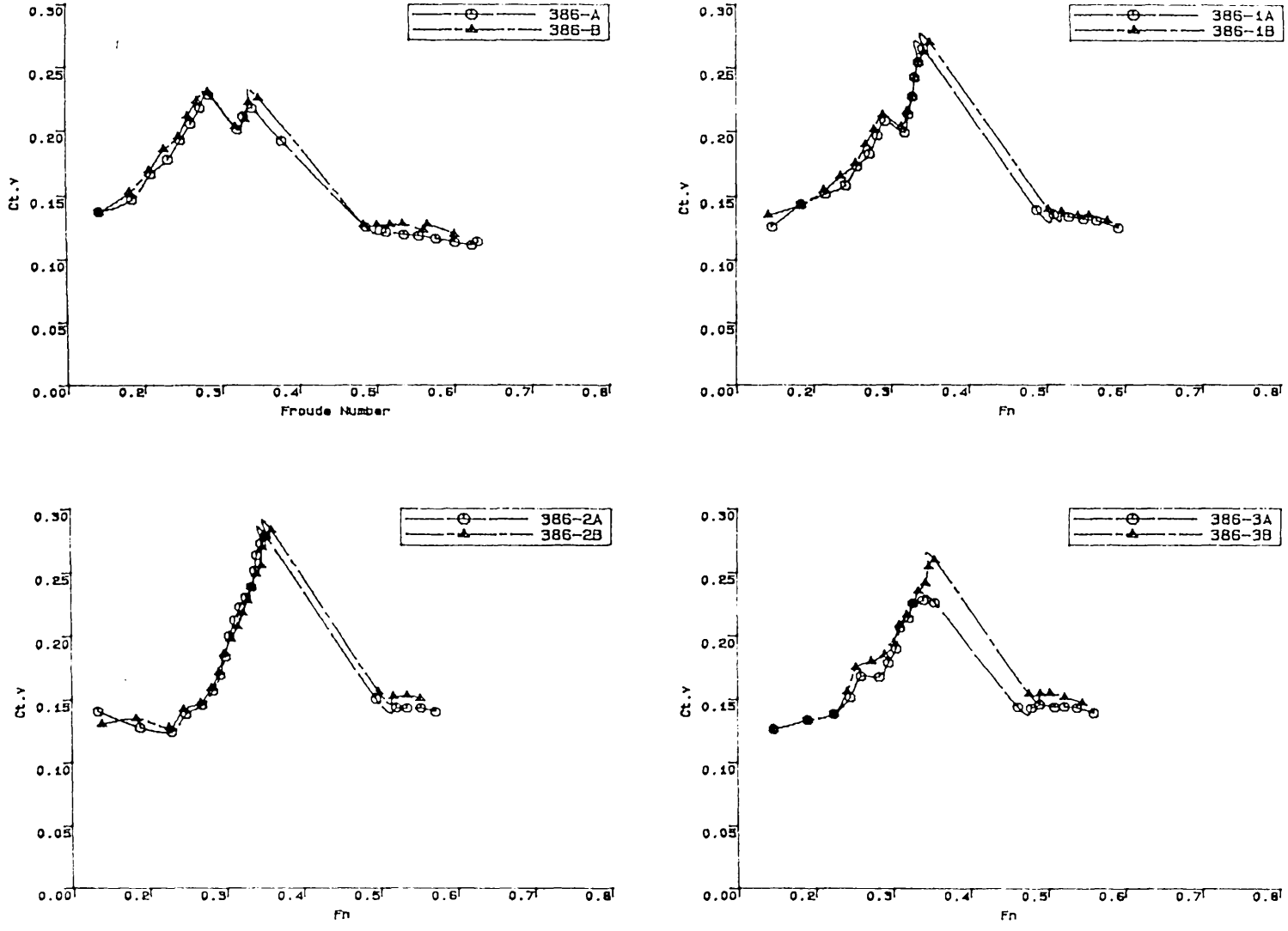

Fig.4.180
Comparison of Total Resistance Coefficients of 4 SWATH Configurations as a Function of Froude Number as well as Spacing.

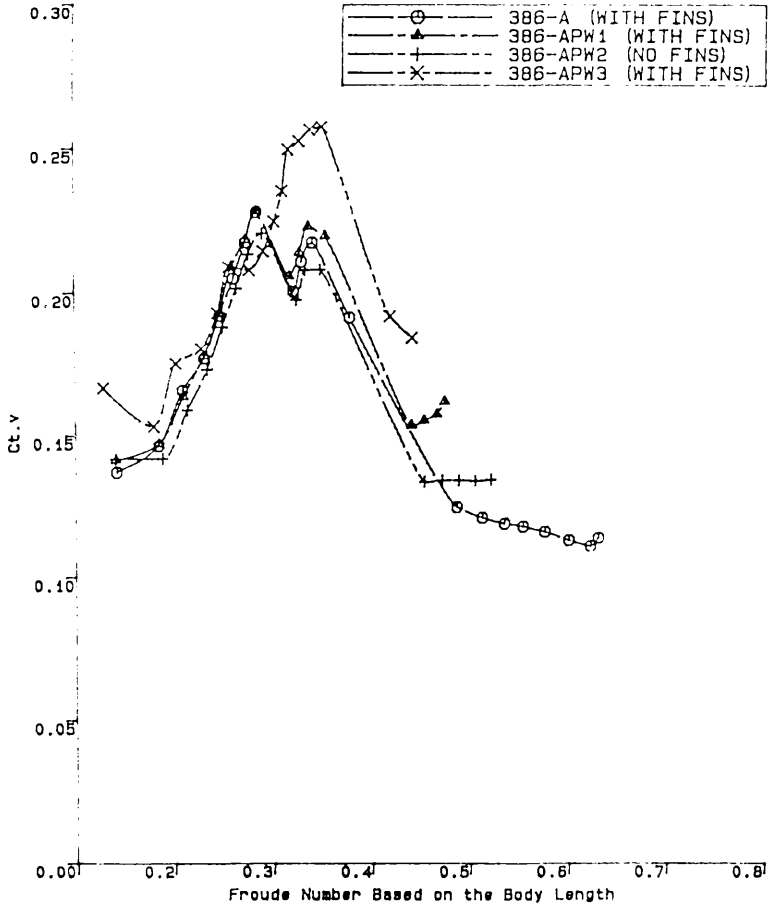

Comparison of Total Resistance Coefficients of 4 SWATH Configurations as a Function of Froude Number.

Fig.4.181

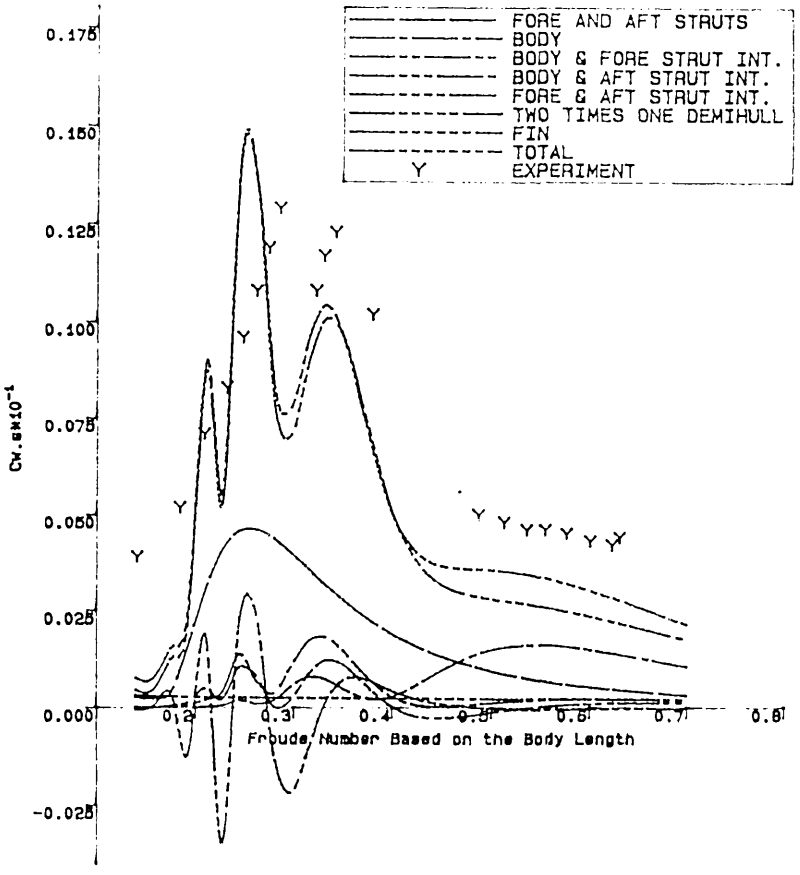

Wave Resistance Coefficients of SWATH-386-A and its Components Variations together with Residuary Resistance Coefficient as a Function of Froude Number.

Fig.4.182

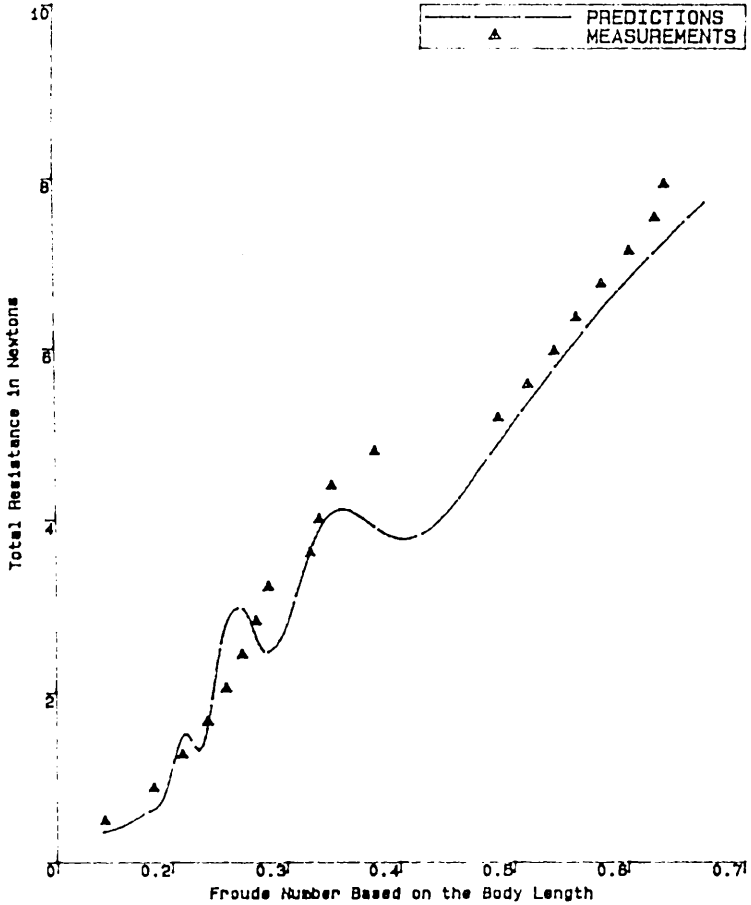

Comparison of the Predicted and Measured Total Resistances of SWATH-386-A versus Froude Number

Fig.4.183

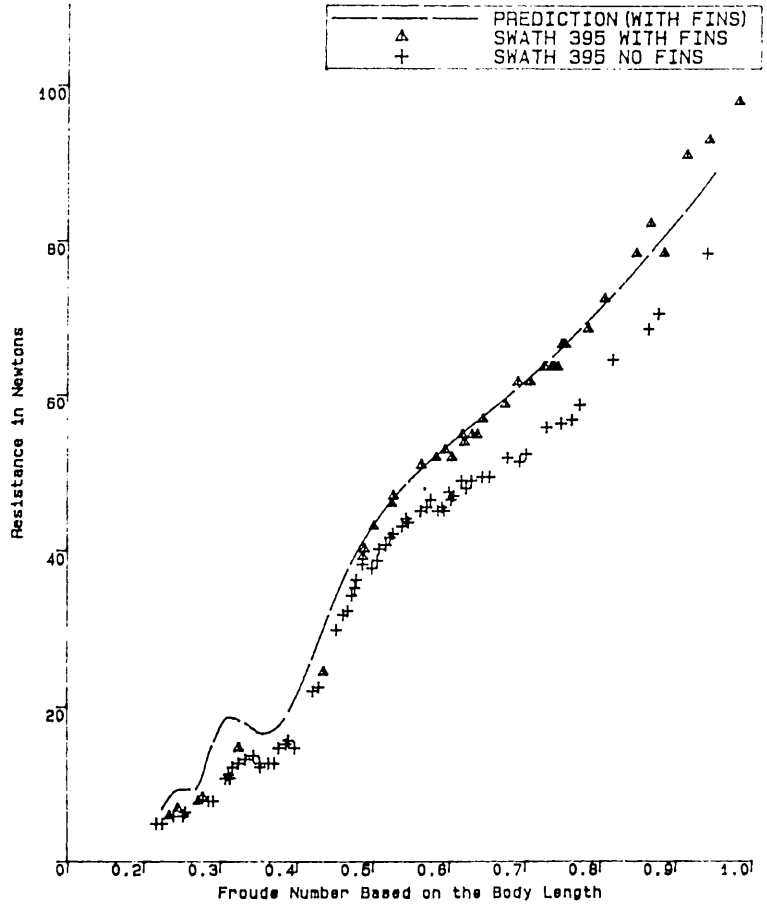

Comparison of Total Resistance of SWATH-395 Model With and Without Fins vs Froude Number

Fig.4.184

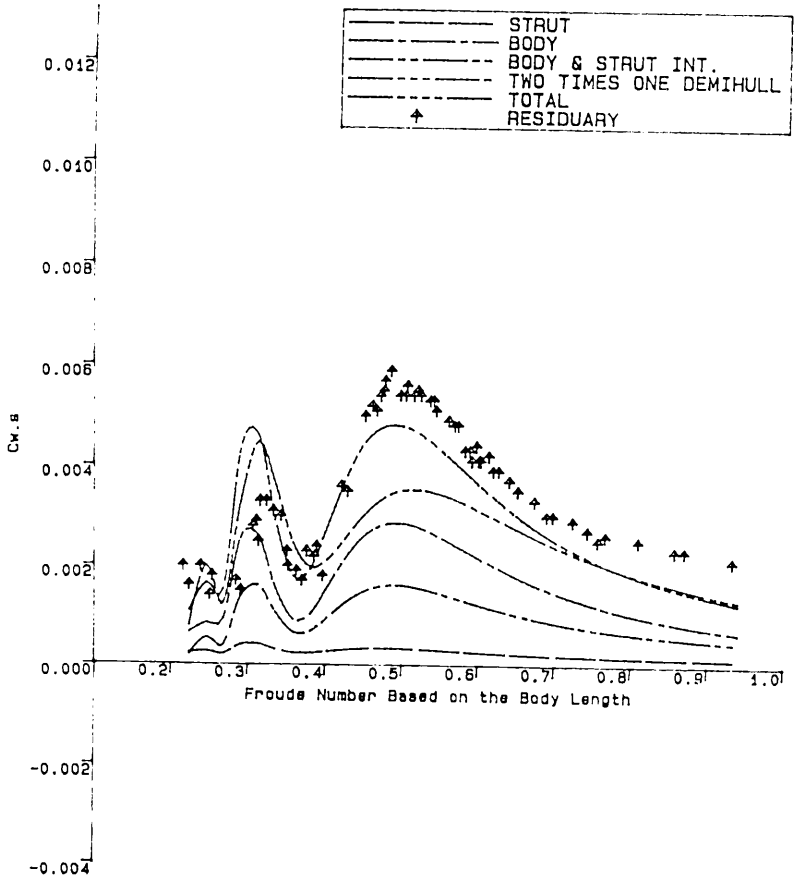

Wave Resistance Coefficients of SWATH-395(No Fins) and its Components Variations together with Residuary Resistance Coefficient as a Function of Froude Number.

Fig.4.185

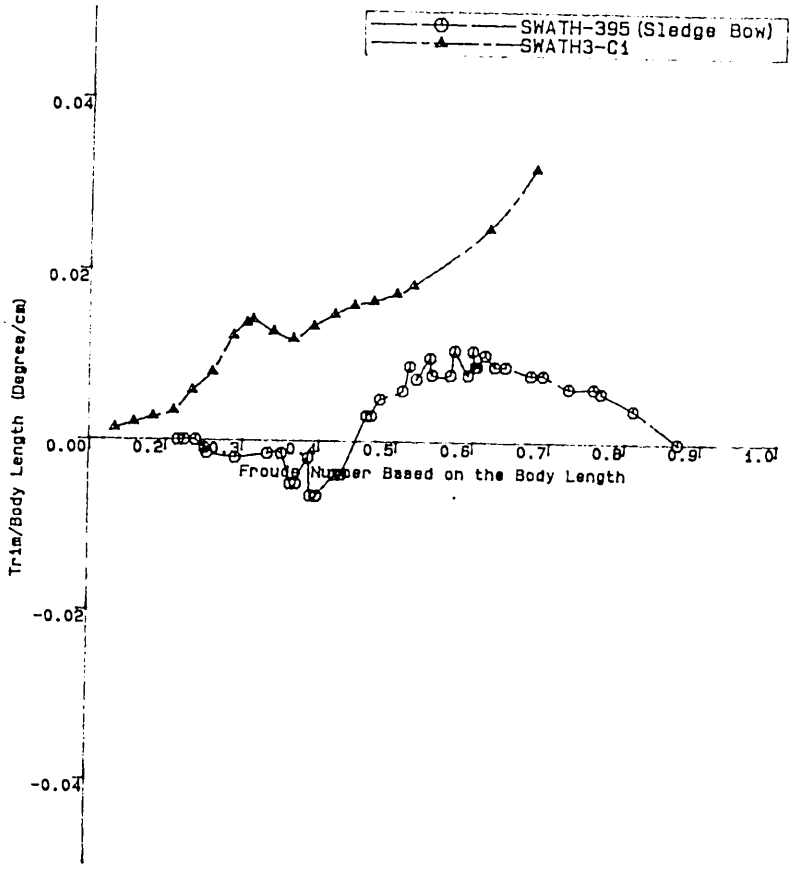

SWATH Models Trim Variation vs Froude Number

Fig.4.186

CHAPTER 5 SOME PARAMETRIC STUDIES, OPTIMISATION EXAMPLE AND SWATH RESISTANCE COMPARISON WITH EQUIVALENT MONOHULLS

5.1 INTRODUCTION

In this Chapter, some parametric studies which were not covered in the experimental work are systematically performed. In order to investigate the resistance changes caused by variations in SWATH geometry, a variety of parameters which are mostly important to the design of SWATH ships with regard to resistance are covered: spacing of the two demihulls, strut position on the demihull, strut numbers(up to three) on the demihull, strut length and shape(simple and contoured), body shape(simple and contoured) and its cross section shape(circular, elliptical and rectangular with rounded corners), body breadth to depth ratio, radius of rounded corners for the rectangular cross section and draft etc. Also, the contribution of controllable fins to total resistance is investigated in detail.

In order to demonstrate the capability of the present analytical tool, it is used to find 'optimum' configurations for a 2405 tonne SWATH ship at the two speeds of 8 knots(operating speed) and 14 knots(maximum speed). This work demonstrates the state-of-the-art of the present thesis.

Finally, the resistance performance of the SWATH3 model is compared with those of equivalent monohulls(Destroyer DE-1006(C_b=0.49), Series-60(C_b=0.6 and C_b=0.7) in calm water as well as in waves. It is demonstrated how well the SWATH ship can perform in waves compared to equivalent monohulls in terms of speed reduction and of power increase.

These results together with the experimental results(in Chapter 4) provide practical and very valuable design guidance for the high performance of SWATH ships with regard to resistance.

5.2 INVESTIGATION OF SOME PARAMETERS MOSTLY AFFECTING RESISTANCE

5.2.1 Two Demihull Spacing Effect on Wave-Making Resistance

From the experimental results discussed in the previous Chapter 4, it has been seen that some favourable interference effects between the two demihulls occur in the moderately high speed range of Fn=0.35-0.44(slightly changing with model configurations), resulting in less resistance as the spacing becomes narrower. This spacing effect is due to the presence of the interference factor, $[1+\cos(k_1 B_1 \sec^2\theta \sin\theta)]$, in the integrand of eq.(3.1). This was discussed in detail in section 2.8.4. This factor is a function of the speed(k_1) and spacing distance(B_1) of two demihulls, and varies from 0 to 2. Consequently, the wave-making resistance of twin hulls, which travel abreast of each other, is between zero and four times that of single hull.

Fig.5.1 illustrates the interference effects between the two demihulls of the SWATH1-model(at draft of 1.5 times of the body diameter). The corresponding experimental results are shown in Fig.4.37 at the three spacings tested. Fig.5.1 shows the ratio of C_W to $C_{W.\infty}$(at infinite separation, ie, two times one demihull) as a function of non-dimensional spacing distance for a number of Froude numbers. The mathematical condition of the two demihulls merging together, ie B_1=0.0, apparently becomes 2 as the derived formula is based on the linear superposition principle as mentioned above. As seen in Fig.4.37, a resistance benefit from the two demihull spacing occurs over the hump speed range, Fn=0.35–0.45, and is well predicted by the computational results. According to Fig.5.1-a, the largest saving in the resistance (around 40%) takes place at Fn=0.390 and at B_1=0.53. For reference, the non-dimensional spacing of SWATH1-C1, C4 and C7 are 0.566, 0.762 and 0.947, respectively, as shown in Table 4.2. Beyond Fn=0.46, no reduction in the wave resistance with the varying spacing distance is expected and the ratio converges to unity as the spacing increases

Fig.5.2 shows the spacing effect of the SWATH1 model at the draft of two times the body diameter, for which experimental results are shown in Fig.4.38 for SWATH1-C2, C5 and C8. Again, the resistance savings can be seen over nearly the

same speed range as at the previous draft conditions but the spacing distance giving most savings becomes narrower compared to the previous results as shown in Fig.5.1. The spacing effect of the SWATH3 model(at the draft of 1.5 times the body diameter) is shown in Fig.5.3. From the figure, nearly the same pattern as observed with the tandem strut model SWATH1 can be seen with a slight difference at the speeds and spacings where most resistance savings occur. The experimental results of the SWATH3 model(at a draft of two times the body diameter) at the two different spacings are shown in Fig.4.135.

It can be seen form all these figures that the speed range giving a resistance benefit from the spacing of the two demihulls does not vary greatly with the geometry changes of the SWATH ships. This can be further justified from the Polish SWATH model experimental results as shown in Fig.4.180. Also, there is not much deviation from Everest's conclusion for catamaran ships[104] that the most important speed range giving a resistance reduction from the two demihull spacing is approximately Fn=0.3–0.4.

In conclusion, a well chosen spacing of the present SWATH models results in a considerable resistance reduction(up to around 40% the resistance of twin hull at infinity) around Fn=0.35-0.45. Thus, special attention should be paid to the two demihull spacing for SWATH ships whose operating speed is within the range of Fn=0.35-0.45 in order to get optimum performance.

5.2.2 Interference Effects Between Body and Strut and Between Struts in Tandem

According to the experimental results in Chapter 4, the total wave-making resistance is significantly influenced by the composition of the components of SWATH models. Fig. 5.6 shows the total resistance coefficient curves of the SWATH1 model at five different strut combinations on the demihull. Amongst these, CS=0.3 and CS1=-0.355(where CS and CS1 are the distances between the centre of the fore strut and the centre of the body and between the centre of the aft strut and the body, respectively) is the configuration of SWATH1-C4 whose calculated and experimental results are shown in Fig.4.17.

The total resistance coefficient with CS=0.2 and CS1=-0.2(the trailing edge of the fore strut and leading edge of the aft struts are touching one another, resulting in a

single strut) is remarkably reduced as compared with SWATH1-C4 at all the speeds above Fn=0.26. This is due to the fact that the interferences between the struts and body(see Fig.5.4-a) become favourable and also the interference between the fore and aft struts(see Fig.5.5-a) becomes favourable over the speed range. However, the resistance coefficient of this configuration is significantly increased below the speed of Fn=0.26 compared with the SWATH1-C4.

As seen in Fig.5.4, the strut located on the longitudinal centre of the demihull(CS=0.0) gives rise to favourable interferences Fn=0.19-0.22 and Fn=0.28-0.48 while it gives unfavourable interferences Fn=0.22-0.28 and at higher speeds. As the strut position moves forward, the pattern of the body-strut interference effects is changed in such a way that the former negative part becomes positive and that the unfavourable interference is reduced at higher speeds. This fact results in the overhanging strut combination(CS=0.6 and CS1=-0.6) being subject to less wave-making resistance than that of SWATH1-C4 at higher speeds as seen in Fig.5.6.

As seen in Fig.5.5 which shows the interference effects between the fore and aft struts as a function of Froude number, the interference effects change with the distance between the two struts, particularly at slow speeds. However, the two strut interference effects becomes negligible above Fn=0.4 if the two strut are displaced from one another by a strut chord length.

When designing a tandem strut SWATH ship, well chosen struts positions on the demihull can reduce significantly the wave-making resistance depending on its operating speeds. In general, from the resistance point of view, it is desirable to place the two struts near the ends of the lower demihull. This combination benefits from favourable body-strut interference as well as favourable strut interference. In addition, it is essential to keep the ratio of strut thickness to length as low as possible which reduces the strut wave-making resistance, particularly, over the hump speed range.

5.2.3 Draft Effect on Wave-making Resistance

Fig.5.7 systematically illustrates how the total wave-making resistance coefficient of the SWATH1 model varies with the immersion depth together with its components variations. Three immersion depths are varied which correspond to SWATH3-C1, C2

and C3, respectively. One of the interesting results that can be seen from the figure is that the shape of the coefficient curve for each component is nearly independent of the immersion depth, but its magnitude is decreased or increased with the increase of the immersion depth. The body–strut interferences decreases in magnitude with the immersion depth and also, the body wave-making resistance is considerably decreased due to its increased submergence. However, the wave-making resistances of the struts are considerably increased due to their increased depth and the two struts interference intensifies both favourably and unfavourably.

These two facts result in a large total wave-making resistance increase over the prime hump speed range as the draft increases. By virtue of the reduced body wave resistance and the favourable interference between the struts, the total wave-making resistance coefficient is reduced at higher speeds. However, as mentioned in section 4.2.4.2, if the increased wetted area and thus frictional resistance is taken into account, the total resistance per displaced volume becomes worse with the increase of the draft even at high speeds.

This total resistance increase with the draft can be also seen with the SWATH3 single strut model, as shown in Fig.5.8. According to the figure, the strut wave-making resistance increase with draft is so large that it outweighs the resistance decrease of the body, resulting in the increase of the total wave-making resistance.

However, this is not always the case with SWATH ships. This resistance increase with the draft is mostly attributable to the fact that the slenderness ratio of the body of the present model SWATH1 and SWATH3(L_b/Di_b=16.93) is comparatively large so that the contribution of the body to the total wave-making resistance is relatively small. When this ratio becomes smaller, the wave-making resistance of the body becomes larger so that the total wave-making resistance will be decreased with the draft at certain speeds, especially wave-making speed range. This is shown in section 5.3.

5.2.4 Strut Length Effect on Wave-making Resistance

It has been experimentally and computationally shown in Chapter 4 that in general, a short strut-body combination gives less resistance than a long strut-body

combination at higher speeds while the result is reversed at slow speeds. Therefore, a single strut SWATH ship is subject to less resistance up to moderately high speeds, but at higher speeds a tandem strut configuration is better from the resistance point of view. Also, it is reported from the systematic series of tests results on single strut SWATH models[2] that short strut configurations are superior to long strut configurations with respect to resistance with some exceptions at certain speed ranges.

In order to clarify this fact, the strut length of the SWATH3 model is enlarged and shortened by inserting and removing a parallel section(0.3m in length) at the longitudinal centre of the strut, resulting in the total length of 1.455m and 0.855m, respectively. The strut set back on the body is kept unchanged at 0.155m(see Fig.4.129-a). As a result, the enlarged strut overhangs beyond the end of the body. The wave-making resistance coefficients(non-dimensionalised by $0.5\rho U^2\nabla^{2/3}$) of these two models are calculated and plotted against Froude number in Fig.5.9 together with the result of the original model SWATH3-C1. It can be seen that the short strut is subject to the least wave-making resistance of the three configurations at higher speeds. This is due to the fact that the body-strut interference of this configuration leads to a larger reduction in resistance at higher speeds. In addition, the wave-making resistance of this short strut configuration is significantly decreased over the moderate speed range compared to the others due to the favourable body-strut interference over that speed range. However, this configuration is the worst around Fn=0.22–0.27.

The original strut SWATH3-C1 is subject to the largest wave-making resistance at higher speeds and the wave-making resistance of the overhanging strut configuration is largest over the moderate speed range among the three configurations calculated. As a result, it is not easy to generalise that a short strut configuration is always superior to a long strut configuration with regard to resistance. This is due to the fact that the interferences between body and strut, and between the entance and run of the strut vary significantly with the shape of the entrance and run, the length of parallel section as well as the distance between the centres of body and strut. In general, a short strut-body combination seems to be superior to a long strut-body combination with regard to resistance above moderate speeds and particularly at higher speeds, .

5.2.5 The Effect of The Number of Struts on the Demihull and Strut Shape(Contoured) on Wave-making Resistance

Since the wave-making resistance of SWATH ships is very much dependent upon the relative compositions of the components as well as their shapes, it is not easy to generalise that a particular SWATH design is always better than others at all speeds with regard to resistance. Even for the fixed shapes of the components of a SWATH ship, its wave-making resistance is significantly varied with the relative distances between the components and vice versa. Therefore, a SWATH designer will have great difficulty in selecting candidate hull forms at the very early stage of design process due to his large freedom of choice compared to monohulls.

However, a relative comparison between several SWATH designs can be made within some restrictions. In order to investigate the effect of the number of struts and the contoured strut on the wave-making resistance, four struts configurations on the same body geometry are changed, as shown in Fig.5.10. The body(1.7m in length) has an ellipsoidal entrance and paraboloidal end which are joined together by a straight mid section with circular cross sections. A simple long strut(1.7m in length, 0.05m in maximum thickness) has a parabolic entrance and end, both of which are 0.25m in length. This strut is placed on the body with a set back of 0.15m, which results in the strut overhanging the body end(see Fig.5.10-a). Two parabolic struts(both 0.5m in length and 0.05m in maximum thickness) are placed in the manner as shown in Fig.5.10-b. The entrance of the forward strut is in line with that of the long strut in Fig.5.10-a and the run of the second strut coincides with the run of the long strut. Another parabolic strut(0.2m in length and 0.02m in maximum thickness) is placed on the longitudinal centre of the simple long strut, resulting in the triple strut configuration as in Fig.5.10-b. Last, the original long strut is changed to a contoured shape, as shown in Fig.5.10-c, where the maximum thickness of the middle parallel section is kept 0.02m which is the maximum thickness of the middle strut of the triple strut configuration.

Figs.5.11 through 5.14 shows the wave-making resistance coefficients of the above four strut configurations. As expected, the total wave-making resistance coefficient is considerably varied with the configurations, particularly in the moderate

speed range, due to the different interference effects between the components. The wave-making resistance of the triple strut configuration(see Fig.5.13) is the lowest of the four models at higher speeds(slightly lower than those of the simple single strut(see Fig.5.11) and tandem strut(see Fig.5.12) configurations and appreciably lower than that of the contoured strut configuration(see Fig.5.14)). Both the tandem and triple strut configurations are worse than the two single strut configurations up to moderately high speeds with regard to resistance per displaced volume. It is interesting to see that the wave-making resistance of the contoured strut configuration is significantly increased at the moderate speed range compared to the original simple strut.

It should be noted that none of these are designed or optimised for specific speeds, but a relatively easy selection is made in order to demonstrate the effect of the different strut configurations on wave-making resistance. Further, any of the above four configurations can be designed to be superior to the other configurations at certain speeds with regard to resistance.

5.2.6 Fin Contribution to Resistance

Owing to its pitch instability at higher speeds, stabilising fins seem to be inevitable for a SWATH ship design and all existing and proposed SWATH ships have a pair of fins fitted near either one end of the submerged bodies or in some cases a pair of fins near both ends. As seen in Fig.4.184 and Figs.5.15 to 5.19, the fin resistance contribution is substantial.

As discussed in section 3.5.2 the wave-making resistance contribution of a fin including the interferences with the other components to total resistance is negligibly small since its submergence is so much deep compared to its thickness. On the other hand, as seen in Fig.5.19, the profile drag (friction+pressure) is the highest of the components up to moderately high speeds and then, the induced drag becomes the highest for the present SWATH1 C4. This induced drag is very dependent on the angle of attack of the fin, as given by eq.(3.130). Therefore, when the entrance angle of local flow over the fin is increased, the contribution of this component will increase. Also, the present wave-making approximation(given by eq.3.127) used for the computer program OSWATH is dependent upon the angle of attack of the fin.

However, in practice, it is nearly impossible to obtain a precise angle of attack of

the fin to the local flow when the model is under way. For the present calculation as seen in Fig.4.184 and Figs.5.15 to 5.19, 2 degrees of angle of attack of the fin is throughout used. For the SWATH-386 model as seen in Fig.4.184, it seems that this assumption is high at slow speeds and low at higher speeds. Also, some scatter can be seen for the SWATH1 model as seen in Figs.5.15 to 5.19.

Although the contribution of the fin to the total resistance is dependent upon the chord, span and maximum thickness of the fin as well as the angle of attack of the fin, it can be seen that the contribution of a pair of fins is around 5-7% the total resistance(see Figs.5.15 to 5.19) and 10-14% for two pair of fins(see Figs.4.184). Both these figures are based on the model results, but the proportion will be decreased for full scale ships due to lower frictional effect. However, in view of this size of these figures, the 'sledge' bow concept, as mentioned in Chapter 4, should therefore be investigated in detail as a means of removing these fins while maintaining the pitch stability requirement.

5.3 AN OPTIMUM STUDY OF A 2405 TONNE SWATH SHIP AT TWO SPEEDS OF 8 AND 14 KNOTS

The objective of this section is

a) to find optimum or near optimum shapes for a 2405 tonne SWATH ship with regard to resistance at two operating speeds of 8 and 14 knots(corresponding to Fn=0.166 and 0.290, respectively, based on the body length(63m)) and

b) to demonstrate the effectiveness of the present analytical tool for an optimisation process.

The objective is achieved by contouring the submerged bodies as well as changing draft within the basic geometry restrictions given:

- displacement(2405 tonne),

- body length(63m), entrance(8.55m) with elliptical profile, run(18.8m) with parabolical profile, cross section is rectangular with rounded corners whose radius(RC) is 1m(maximum),

- strut length(48m), maximum thickness(2.7m), strut set back(4.35m), minimum strut depth(1.5), waterplane area(194.40m^2, C_{wp}=0.75) and shape are fixed,

- maximum draft(7.4m),

- minimum depth(height,D2)) of the first parallel section of body(1.0m), minimum depth(D1) of the second parallel section of body(3.5m),

- length of first parallel section of body(l1) plus length of transition section (l2) to be less than 20m,

- spacing between the centrelines of demihulls(20.50m).

The general configuration of this shape is given in Fig.5.21[1] together with the symbols used in this section. The computer program OSWATH was used to calculate the resistance in sea water at a temperature of 15 degrees in celsius. For this purpose, a subroutine, which automatically(by interactive manner on the monitor) generates the input offset data of the SWATH configurations with the aforementioned restrictions. was written and built into the OSWATH as an option[107].

5.3.1. General Statements

Before proceeding forward to find an 'optimum' geometry at each speed, it will be very useful to understand how the wave-making and frictional resistance of the present type of SWATH ship varies with speed and then, the task may be carried out in an efficient way as quickly as possible.

Fig.5.22 illustrates the wave-making resistance coefficient variations against Froude number of a 2405 tonne SWATH ship, which has the aforementioned geometry restrictions but circular non-contoured hulls, together with its component contributions to the total wave-making resistance. As marked in the figure, two speeds of 8(service speed) and 14 kts(maximum speed) are of primary interest. The first speed is within the range of viscous dominant speed and the second is in the wave-making speed range. In order to understand this statement more clearly, the proportions of the residuary(wave-making + form) and frictional resistances of this SWATH design are drawn at each speed in Fig.5.24 and also the figure illustrates their variations with draft (All values are for a single demihull from here onwards).

At the speed of 8 knots, it can be seen that the proportion of the frictional resistance is very much higher than that of the residuary resistance. As draft increases,

[1] shown in page 362

the total resistance increases mostly because of the increased wetted area. According to Fig.5.24-a, as draft increases, the residuary resistance decreases, but the increase in the frictional resistance outweighs the decrease in the residuary, resulting in an increase in the total resistance. Therefore, in order to find the optimum configurations at this speed, we have to reduce the wetted area as far as possible and then take a compromise between the residuary resistance by changing body shape and the frictional resistance.

However, at the speed of 14 knots, the trend is reversed as compared with the previous speed. As seen in Fig.5.24-b, the residuary resistance is larger than the frictional resistance. Further, as draft increases, the total resistance is reduced because the decrease in the residuary resistance outweighs the increase in the frictional resistance. Therefore, for this speed, it is desirable to find a way of reducing the residuary resistance by means of increasing draft as well as changing body shape.

The resistance variations caused by changing body shape with this circular hulled SWATH at the two speeds can be seen in Fig.5.25 which show the effect of length (l1,l2) on the resistance for the fixed ratio of hull diameters(R1/R2=1.1, where R1 and R2 are radius of the second and first parallel sections, respectively) and fixed Submerged body Depth to Body Centreline(SDBC=4.023m). In the figure, (0,0) indicates non-contoured body. For this condition, it can be seen that the optimum length proportion(7m, 5m) is for 8 kts and (10m,5m) for 14 kts. As a matter of interest, at a higher speed of 27.2 kts as seen in Fig.5.25-c, it is expected to have a significant resistance penalty by contouring the body. It is worthwhile mentioning that (7, 5) and (5, 7) are preferrable for the two design speeds, but this varies with the hull diameter ratio as will be mentioned later.

Fig.5.26 shows the effect of hull diameter ratio on the resistance for the fixed l1(10m), l2(5m) and SDBC(4.901m). In the figure, R1/R2=1 indicates non-contoured hull. At 8kts, as the ratio increases, the resistance decreases, but there is a dramatic decrease of more than 30% at 14 kts However, at 8 kts, the ratio of around 2 is the best.

5.3.2. Optimisation Procedure For the Rectangular Hull

5.3.2.1 Service speed of 8 knots

As viscous resistance is dominant at this speed, it is desirable to reduce the frictional resistance to as low a value as possible which means that draft should be reduced as far as possible. Therefore, the minimum strut depth(1.5m) is chosen. Since the perimeter of a square is shorter than that of a rectangle for the same cross sectional area and accordingly wetted area is smaller, a square cross section is chosen with 1m of corner radius.

As start, D1/D2=2.0 is selected since around this value has given the smallest resistance for the circular hulled SWATH at 8 kts as shown in Fig.5.26. Fig.5.27 shows the resistance variation with various lengths(l1, l2) at the two speeds. At 8 knots, (5, 7) is the best with little difference around this range. Therefore, l1=5m and l2=7m are chosen for further investigation at 8 kts. As a reference, it can be ssen that at 14 knots, (10,5) is the best among the range investigated

With (l1,l2)=(5,7), depth ratio(D1/D2) is varied and drawn in Fig.5.28. In contrast to Fig.5.26-a where around R1/R2=2 was the best at 8 kts for the previous circular hulled SWATH as shown in Fig.5.26-a, around the ratio of 3.5 is the best for this condition. However, at 14 kts, the ratio of 2 is the best for the present square hulled SWATH with rounded corners whose radius is 1m.

With (l1,l2)=(5,7) and D1/D2=3.5, the radius of the rounded corners of the square is reduced as far as 0.5m and the result is shown in Fig.5.29 for the two speeds. For the same cross sectional area, as the radius of corner increases, the perimeter decreases and hence, the wetted area decreases. The figure shows that as the radius increases, the total resistance decreases at the two speeds. . For the present case, 1m is the maximum and hence, this is chosen.

With (l1,l2)=(5,7), D1/D2=3.5 and RC=1m B/D ratio is varied and the result is drawn in Fig.5.30 for the two speeds. As expected, as the ratio increases, the resistance increases mostly due to the increased wetted area at the first speed and in addition, the increased breadth creates a larger wave-making resistance at the second speed.

Finally, with these optimum conditions, in order to confirm that resistance

increases with the increase of draft as mentioned earlier,draft is varied by changing the strut depth and the result is shown in Fig.5.31. As expected, at 8 kts, the resistance is increased as draft increases, and the resistance is decreased at 14 kts. The details of the 'optimum' configuration at 8 kts are given in Table 5.1.

5.3.2.2, 14 knots (maximum speed)

At this speed, since the resistance decreases with draft, the approach should be different from that of the previous speed case. Instead of fixing the strut depth, the draft is fixed at the maximum value of 7.4m. Since a square cross section and RC(1m) has been proved the best, these are used for the present speed investigation. As it was found that the resistance decreases with increase of the ratio R1/R2 at this speed for the circular cross section hulled SWATH, the investigation is started with maximum ratio D1/D2 =5.0 since at this draft, D2 approaches to the limit(1m).

With these conditions, Fig.5.32 shows the resistance variations against some values of (l1,l2) where most resistance reduction occurs. From the figure, (10,9) is the best at this speed. Then, in order to find an optimum value of ratio D1/D2, the ratio is varied and the result is shown in Fig.5.33. As the ratio decreases, resistance increases. Therefore, D1/D2=5.0 and(l1,l2)=(10,9) are the best at this speed and details are given in Table 5.1.

Table 5.1, Optimum Configuration and EHP at Two Speeds

Speed	D_S	SDBC	Draft	D1	D2	RC	(l1,l2)	EHP*
8 kts	1.5	4.10	6.70	5.20	1.485	1.0	(5,7)	147.06
14 kts	1.94	4.67	7.40	5.46	1.093	1.0	(10,9)	994.63

* For Demihull

Fig.5.23 shows the wave-making resistance coefficient of the optimum configuration at 14 kts versus Froude number together with its component contributions to the total wave-making resistance. From the comparison between this figure and

Fig.5.22, it can be seen that at 14 kts, the wave-making resistance of the optimum configuration is reduced by as much as around 70% that of an equivalent non-optimised configuration. However, it should be noted that the wave-making resistance of the optimised SWATH is very much increased at higher speeds compared to the original design.

5.3.3 Discussion

Since there is very little existing form effect data for rectangular shapes which have different rounded corners and different breadth to depth ratios, the same form factor described in Chapter 3 is used for all the SWATH configurations investigated. For the same cross sectional area, in general, a rectangular cross section hull with rounded corners has larger form resistance than for a circular and as the radius of corner increases, the form effect will be decreased. Also, for the rectangular cross section, as B/D approaches to unity(square), the form effect would be reduced. When a final design decision is made based on the present analysis, this fact should be borne in mind.

According to the present results, in the wave-making speed range, the wave-making resistance of the optimum configuration is reduced by as much as around 70% of that of an equivalent non-optimised configuration. This fact explains why contoured hulls are introduced to U.S. Navy SWATH-TAGOS 19(9.6 kts of operating speed) which has been claimed to be the "state–of–the–art" in U.S. Navy SWATH ship design[105]. In addition, there is another benefit in that the machinery of SWATH-TAGOS 19 is installed inside this section of the hull with increased cross sectional area[106]

5.4 EFFECT OF BODY CROSS SECTION SHAPE ON RESISTANCE

The effect of the cross section shapes on the wave-making resistance was investigated with a single slender body in section 2.7.2 and the results are shown in Fig.2.5. According to the results, a horizontal elliptical cross section body is subject to less wave-making resistance than a circular cross section at all the speeds investigated.

However, the result for a SWATH ship may be different from that of a single body due to the existence of the strut(s).

Fig.5.34 illustrates the wave-making resistance coefficient variations of a 2405 tonne SWATH ship, which is used in the optimisation example in the previous section 5.3 but with different draft, as a function of Froude number. The circular cross section shape of the submerged body is changed to an elliptical cross section, while SDBC(4.901) and the displacement are kept constant. Accordingly, the depth of the strut for the elliptical cross section SWATH is increased from 2.5m to 2.94m(17.6% increase) and the draft of the elliptical hulled SWATH is reduced from 7.30m to 6.86m(6% reduction). As seen in Fig.5.34–a, the wave-making resistance of the long depth strut is larger than that of the short. As expected, the elliptical cross section body has less wave-making resistance than has the circular one at all the speeds. The wave-making resistance caused by the elliptical cross section body-strut interference is larger than that of its circular counterpart at higher speeds, as seen in Fig.5.34–c. As a result of these three combinations, the wave-making resistance of the elliptical cross section hulled SWATH ship is worse compared to its counterpart over most speeds excepting some speeds around Fn=0.3.

When the increased wetted area with the elliptical cross section hulled SWATH is taken into account, its total resistance is larger than that of the circular one. When this elliptical cross section is changed to the rectangular cross section with rounded corners(radius=1.0m) while keeping the depth(height) unchanged, the body breadth will be slightly reduced. As a result, the wave-making resistance of the rectangular hulled SWATH is slightly reduced compared to that of the elliptical hulled SWATH. Again, when the increased wetted area is considered, the total resistance of the rectangular hulled SWATH is larger than that of the elliptical one. As an example, Fig.5.35 shows the effective horse power of the demihulls for these three different cross section hulled SWATH ships. At this speed, the EHP of the elliptical and rectangular cross section hulls is increased by 0.9% and 1.2% that of the circular hull, respectively.

The draft of the elliptical cross section hulled SWATH was then increased to 7.21m, and the result is also shown in Fig.5.35(E2). It can be seen that the EHP is reduced by 5% compared to the circular hulled SWATH. In addition, the draft is still

less than that of the circular one(7.30m). Therefore, at certain speeds, a well designed SWATH ship which has non-circular cross section hulls might have a possibility of less resistance than that of a circular hulled SWATH at a certain draft. In general, a circular hulled SWATH ship is superior to a non-circular hulled SWATH ship with regard to resistance. However, as investigated in Chapter 4, when such benefits as less motion responses, less resistance increase in waves, construction cost, draft reduction and easy fabrication of 'sledge' bow, etc compared to circular hulled SWATH ships are brought into consideration, non-circular(in particular rectangular) hulled SWATH ships is recommended, particularly, up to the medium speed range without serious compromise in resistance.

5.5 COMPARISON OF SWATH SHIP RESISTANCE WITH MONOHULLS IN CALM WATER AND WAVES

In most published literature associated with SWATH ship performance, the comparison of the seakeeping performance between SWATH ships and equivalent monohulls have been repeatedly treated. However, a qualitative comparison of resistance between two types of vessel has not been treated either in calm water or in waves. In general, it has been known that the calm water resistance of a SWATH ship is (without giving detailed figures) greater than that of a monohull of the same displacement as the SWATH and that the speed reduction of a SWATH ship in waves is considerably less(again not giving detailed figures) than that of an equivalent monohull. Owing to the limited experimental and sea trial data on SWATH ships, a rigorous comparison between them seems to be unlikely at the present time. Using the available data on monohull models in regular waves, a relative(but rigorous) comparison of two types of vessel on resistance in calm water as well as in waves is made below.

Fig.5.36 shows the comparison of total resistances(per unit displacement) in calm water and in waves of three models, the single strut SWATH3–C1, Destroyer DE-1006(C_b=0.49) and Series–60(C_b=0.7). The results of DE-1006 and Series-60 which are shown in Fig.4.65 are taken from Ref.[84], in which for both model tests the model length(1.52m) was nearly the same as that of the SWATH1 model(1.51m). This coincidence enables the present comparison to be much more reliable because the Reynolds number is nearly the same at the same speed for all models.

As seen in the figure, the calm water resistance of the SWATH model is greater than those of the Destroyer and Series-60 at all the speeds tested. However, the resistance of the Series-60 may be greater that that of the SWATH above Fn=0.31 which is generally known as the wave 'barrier'. Beyond that speed, the resistance increase of such type of vessels is so steep that practically, they are not economical. Except with the hump speed range which is caused by the interference effects between the body and strut as mentioned in section 4.5, the resistance per unit displacement of the SWATH model is 8-10% greater than that of DE-1006 at high speeds and 10-20% at slow speeds.

However, in waves, the story is dramatically changed. At the nearly same wave steepness as for the SWATH model, the resistance increase of DE-1006 is so much that for instance, by the same power marked on the figure, the SWATH runs at speed of Fn=0.285 while DE-1006 runs at speed of Fn=0.14. In other words, when the Destroyer DE-1006 enters from calm water to waves which have wave steepness(λ/ζ_W=18.5), her speed will be involuntarily reduced from Fn=0.36 to Fn=0.14(more than 61% reduction). Or, in order to keep this speed constantly, the power should be increased up to more than 500 newtons per unit displacement(more than 270% increase). However, at this speed, there is little resistance increase for the SWATH3 due to the waves. Therefore, in order to keep the speed of Fn=0.285 at sea whose condition is similar to that given here, the power of the SWATH is around 60% less than that of the Destroyer.

As mentioned in Ref.[84], the larger the block coefficient, the smaller the added resistance per unit displacement. This result can be seen from the resistance increase of Series-60 at the same wave steepness as for the DE-1006 in the same figure 5.36. Nevertheless, the total resistance of Series-60 in the waves is considerably larger than that of the SWATH at the tested speeds.

Fig.5.37 shows the comparison of residuary resistances(per unit displacement) of four models where the result of Series-60(C_b=0.6) is added from Ref.[84]. The residuary resistance of the model having larger block coefficient is higher than that of the smaller one, resulting in a steep increase beyond a certain speed. For that reason, SWATH ships benefit from the wave-making resistance point of view at higher speeds compared to fuller monohulls. However, the residuary resistance of the Destroyer DE-

1006 having a sharp hull form is still less than that of the SWATH3 at high speeds.

As seen above, the power requirement of the SWATH model in calm water is slightly greater than that of the equivalent displacement monohull(having sharp hull shape). However, its power requirement in waves is very much smaller than that of the equivalent monohull. Although the added resistance is only a part of the total resistance, ships mostly operate in wave conditions. With regard to this, the slightly higher calm water resistance of the SWATH ship is trivial compared to the power increase of the equivalent monohull in waves. In conclusion, it can be said that the power requirement of a SWATH ship is much less than that of equivalent displacement monohulls at sea(not only in rough sea).

However, the added resistance changes from wave condition to wave condition and there is another problem of scaling . The present results are based on the model experiments and in uniform waves. In the worst case, assuming that there is at most 50% difference at full scale, nevertheless, the power requirement of a SWATH ship is still much less than that of an equivalent monohull in rough seas. However, it is worthwhile mentioning that since added resistance is considered to be a result of the radiated waves(viscous effect negligible), the added resistance obeys Froude's law: that is, the added resistance of a full scale vessel can be predicted by multiplying the added resistance of the model by the cube of the scale factor(no scale effect)[80]. Thus scale effects are belived to be much less than the above suggested figure.

5.6 CONCLUSIONS

In this Chapter, some parametric studies which were not covered in the experimental work have been systematically carried out. In order to demonstrate the capability of the present analytical tool, it is used to find the optimum configuration for a 2405 tonne SWATH ship for two speeds, changing a wide range of parameters which seem to be of practical importance in constructing such SWATH ships. Finally, it is (qualitatively and quantitatively) demonstrated how well a SWATH ship can advance through waves compared with equivalent monohulls in terms of speed reduction as well as of power increase. The results can be summarised below.

a) A well chosen spacing between the two demihulls of a SWATH results in a considerable resistance reduction(for the present model SWATH1, 2 and 3, up to

around 40% of the resistance of the twin hull at infinite spacing) around Fn=0.35-0.45. This range is not much changed with the geometry changes and draft variations.

b) A short strut located on the longitudinal centre of the demihull gives rise to favourable interferences over the moderate speed range, while being unfavourable at higher speeds. On the other hand, this result is reversed with an overhanging strut, significantly reducing the unfavourable interference at higher speeds. The interference effect between the fore and aft struts (placed in tandem) changes depending on the distance between them, particularly at slow speeds. As two struts are placed more than a distance of the strut chord length apart, the two strut interference becomes negligible at high speeds. As a result, when designing a tandem strut SWATH ship, well chosen strut positions on the demihull significantly reduces the wave-making resistance depending on its operating speed. In general, at higher speeds, it is desirable to place two struts near the ends of the lower demihull.

c) In general, a short strut-body combination gives less resistance than a long strut-body combination beyond moderately high speeds while the result is reversed at slow speeds. By changing the longitudinal thickness distribution of a strut(contoured strut), the wave-making resistance can be considerably varied depending on the speed of interest, giving a serious resistance penalty at other speeds. By the same principle, a triple strut configurations can be beneficial at certain speeds (in particular, higher speeds) from the wave-making resistance point of view, as compared to single and tandem strut configurations.

d) As the draft of a SWATH ship increases, the wave-making resistances of its components including several interference effects between them are decreased or increased in magnitude while the patterns of the coefficients remain nearly unchanged. As a result of these changes in magnitude, it is possible to have an optimum draft for a certain SWATH design. Over the viscous dominant speed range, the lighter the draft, the smaller the resistance. However, over the wave-making speed range, there are two patterns. SWATH ships having large slenderness ratio(L_b/Di_b) are unlikely to have a resistance benefit from the increase of draft because the contribution of the bodies to total wave-making resistance is relatively small which cannot counteract the increase of frictional resistance. This is the case with the SWATH1, SWATH2 and SWATH3 models(both SWATH1 and SWATH3 have the ratio of 16.93 and the rectangular hulled

SWATH2 has L_b/D_b=23.23 and L_b/B_b=15.1). On the other hand, a SWATH ship having a small slenderness ratio(less than around 12) will have a draft at which total resistance is the least.

e) The contribution of controllable fins to total resistance is substantial and is mostly caused by induced drag(at non-zero angle of attack) and frictional resistance plus pressure component. The component of wave-making resistance is negligibly small but, at high angles of attack, the amount is considerably increased at higher speeds. Although the magnitude is dependent upon the fin size(chord, maximum thickness and span) and angle of attack to the local flow, in general, the contribution of a pair of fins is around 5-7% the total resistance and 10-14% for two pair of fins.

f) In general, a circular hulled SWATH ship is superior to a non-circular hulled SWATH ship with regard to resistance. However, at certain speeds(medium range), a well designed SWATH ship having non-circular cross section bodies can have less resistance than that of a circular hulled SWATH at a certain draft. When considering such benefits as less motion responses, less resistance increase in waves, construction cost, draft reduction and easy fabrication of 'sledge' bow, etc compared to circular hulled SWATH ships, non-circular(in particular rectangular) hulled SWATH ships are recommended, particularly, up to the medium speed range without serious compromise at resistance.

g) For rectangular cross section bodies with rounded corners, in general, a B/D of unity(square) is better in terms of total resistance. Also, the larger the radius corners, the better the resistance per unit displacement.

h) By contouring submerged bodies, a great proportion of the wave-making resistance can be reduced over the medium speed range. For the present 2405 tonne SWATH ship investigated in this Chapter, the wave-making resistance of the optimum configuration at 14 knots is reduced by as much as 70% compared to that of an equivalent non-optimised configuration. There is another benefit in that the machinery can be placed inside the enlarged cross section. It is, however, worthwhile noting that the SWATH ship optimised at 14 knots is subject to a significant resistance increase at higher speeds.

i) The calm water resistance per unit displacement of the SWATH3 model is 8-10% greater than that of destroyer DE-1006(C_b=0.49) at high speeds and 10-20% at

slow speeds. However, in waves(at λ/ζ_W=18.5 investigated), the powering requirement of the SWATH is around 60% less than that of the Destroyer. A speed reduction of as much as 65% can occur for the destroyer in the wave conditions while less than 1% speed reduction is observed with SWATH3. Although the added resistance is only a part of the total resistance, ships usually operate in wave conditions and thus the reduced speed loss in the SWATH is of great importance.The slightly higher calm water resistance of the SWATH ship is negligible compared to the power increase of the equivalent of monohull in waves. In conclusion, it can be said that the powering requirement of a SWATH ship is very much less than that of equivalent displacement of monohulls at sea (not only in rough seas).

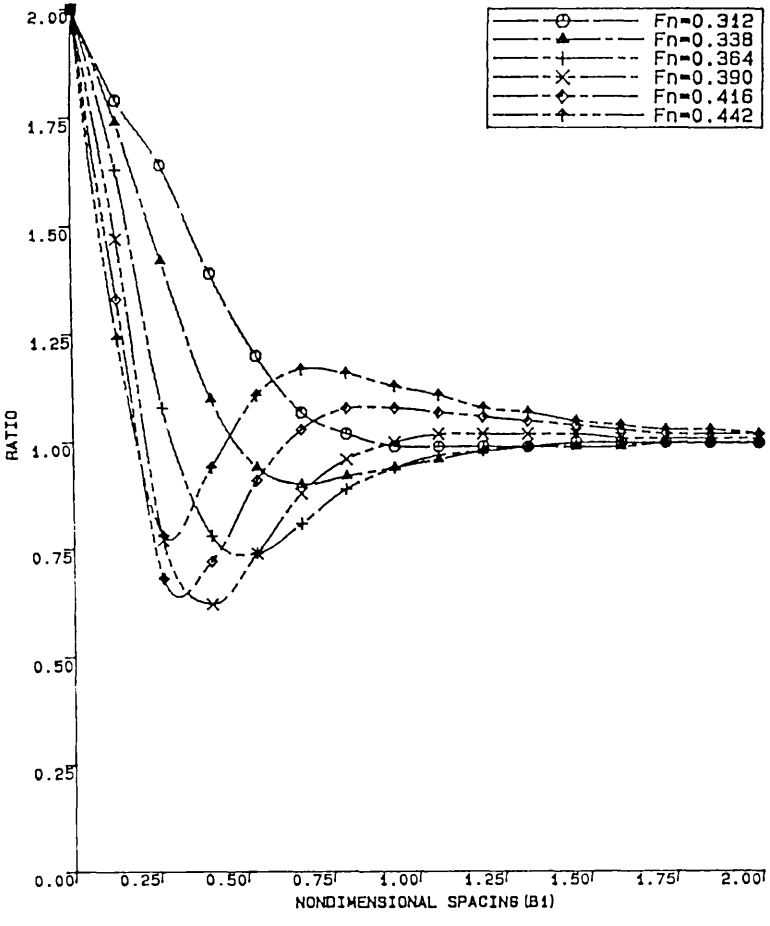

Ratio of Twin Hull- to Two Times One Demihull- Wave Resistance Variation Versus Non-Dimensional Spacing SWATH1 Model (Draft of 1.5 Times Diameter)

Fig.5.1-a

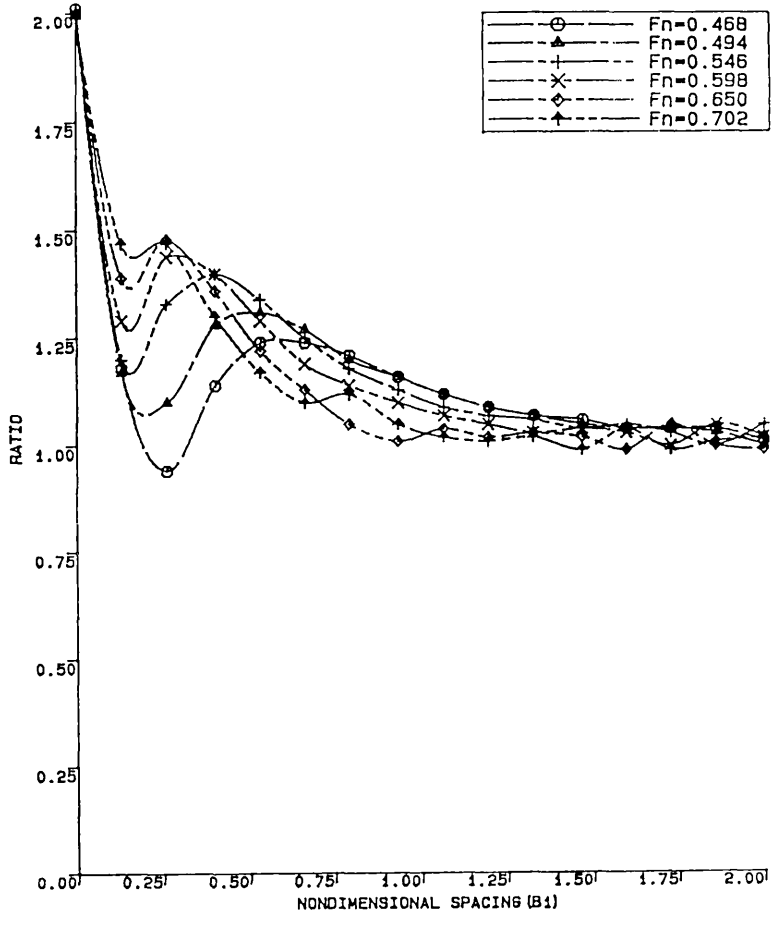

Ratio of Twin Hull- to Two Times One Demihull- Wave Resistance Variation Versus Non-Dimensional Spacing SWATH1 Model (Draft of 1.5 Times Diameter)

Fig.5.1-b

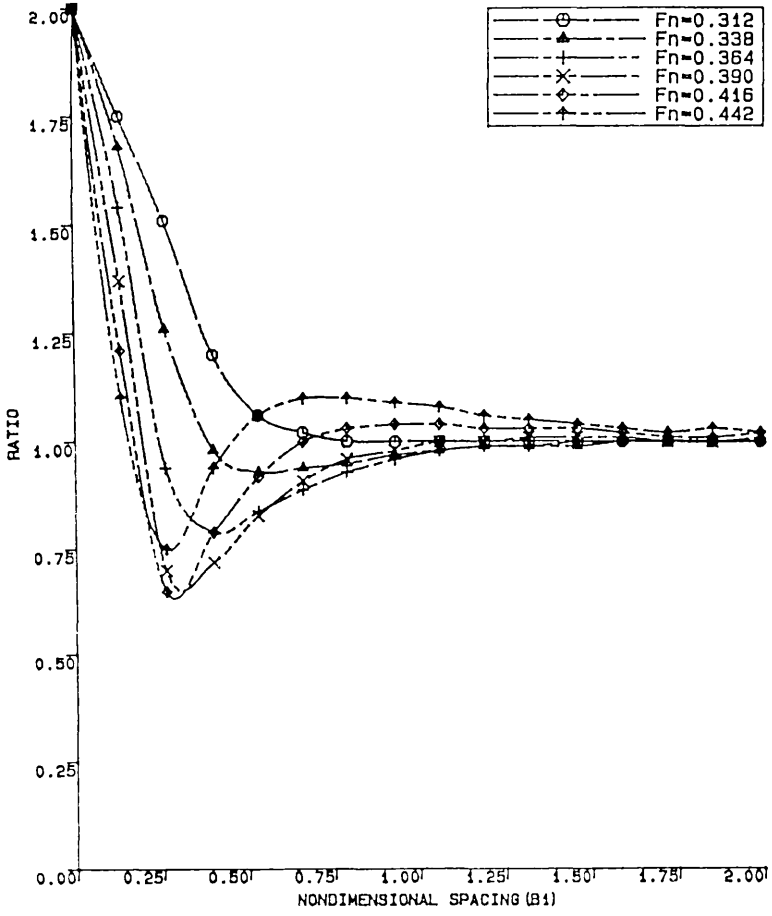

Ratio of Twin Hull- to Two Times One Demihull- Wave Resistance Variation Versus Non-Dimensional Spacing SWATH1 Model (Draft of 2. Times Diameter)

Fig.5.2-a

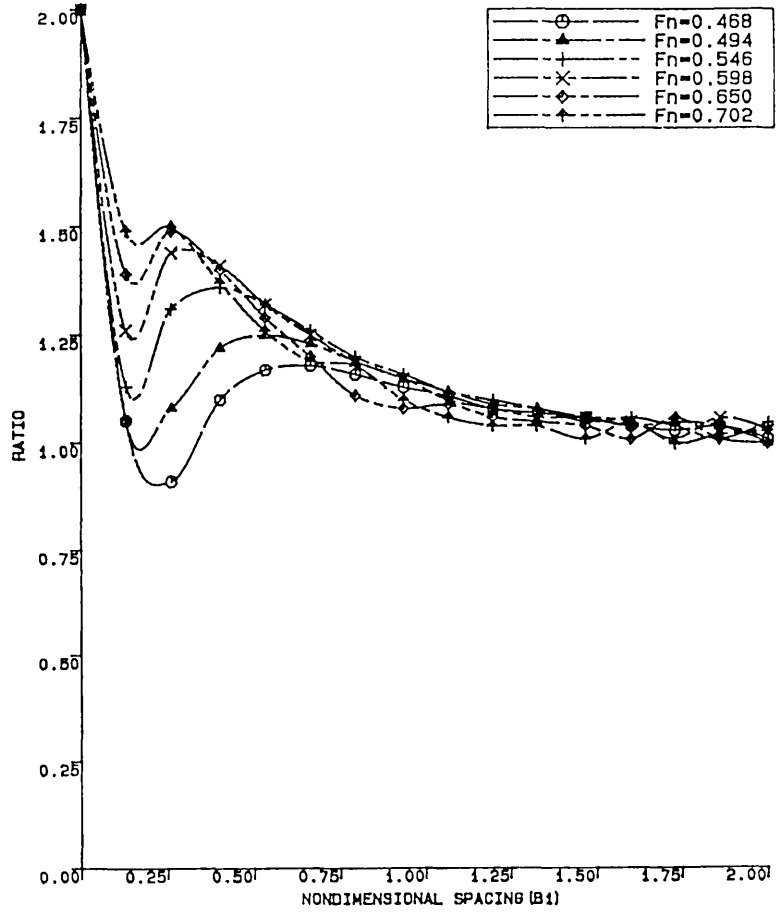

Ratio of Twin Hull- to Two Times One Demihull- Wave Resistance Variation Versus Non-Dimensional Spacing SWATH1 Model (Draft of 2. Times Diameter)

Fig.5.2-b

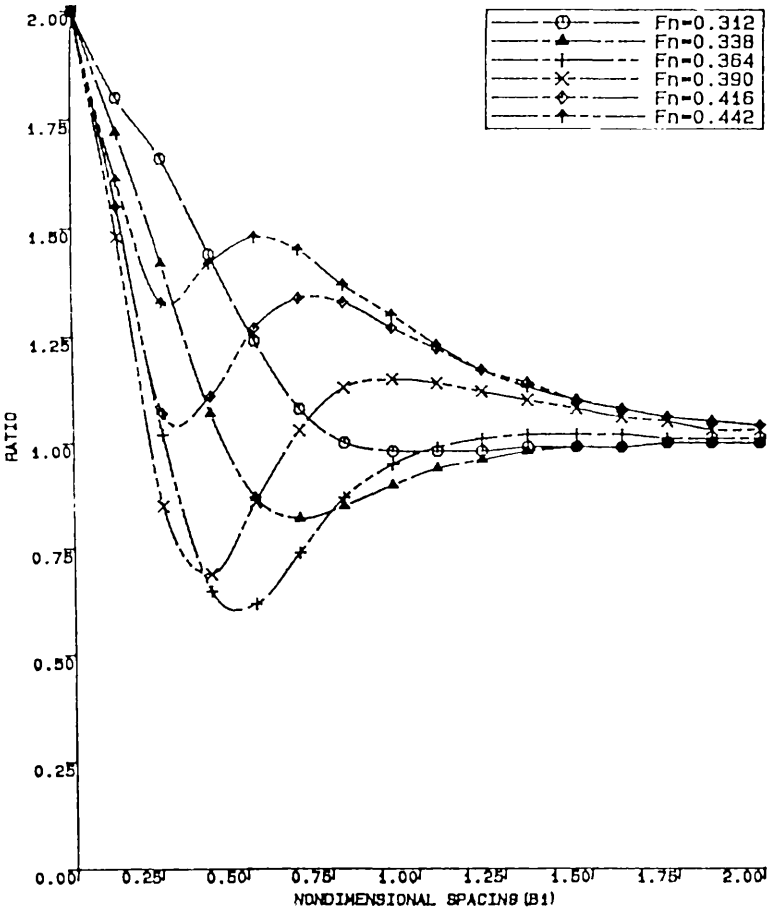

Ratio of Twin Hull- to Two Times One Demihull- Wave Resistance Variation Versus Non-Dimensional Spacing SWATH3 Model (Draft of 1.5 Times Diameter)

Fig.5.3-a

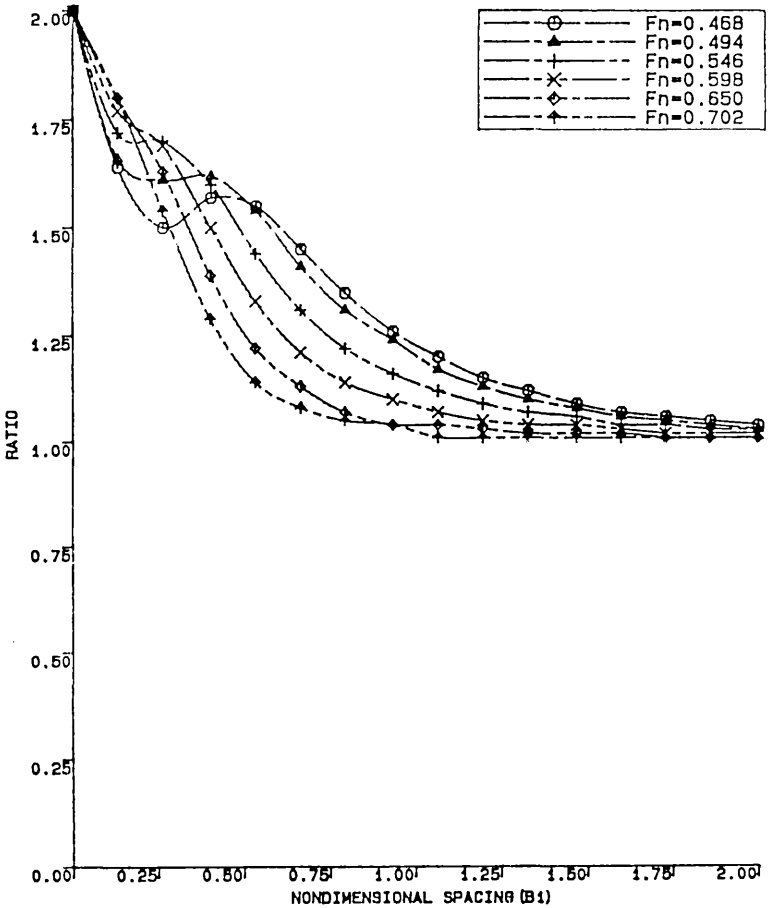

Ratio of Twin Hull- to Two Times One Demihull- Wave Resistance Variation Versus Non-Dimensional Spacing SWATH3 Model (Draft of 1.5 Times Diameter)

Fig.5.3-b

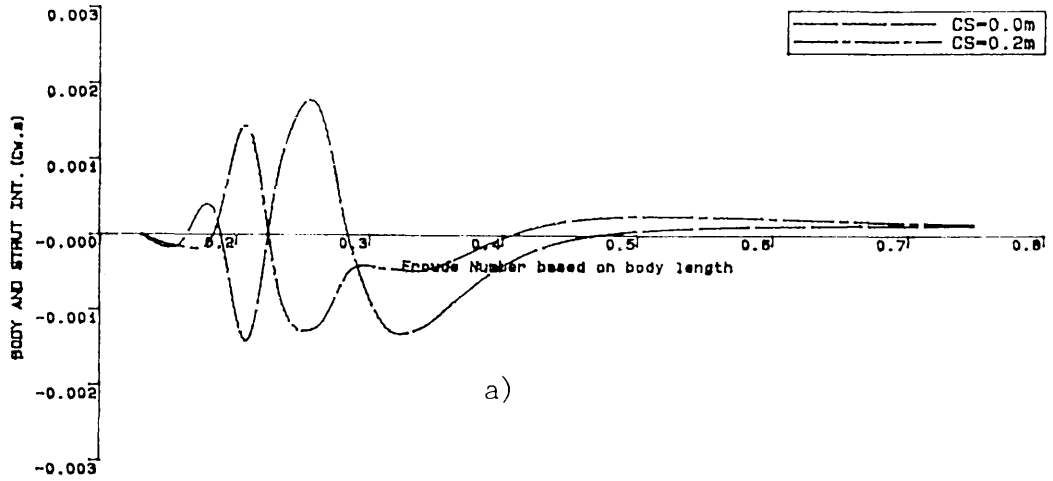

a)

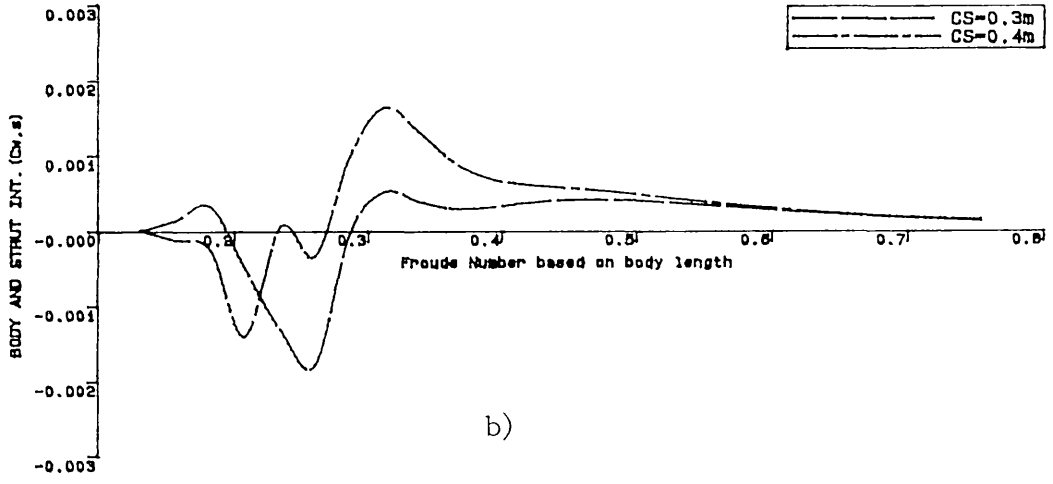

b)

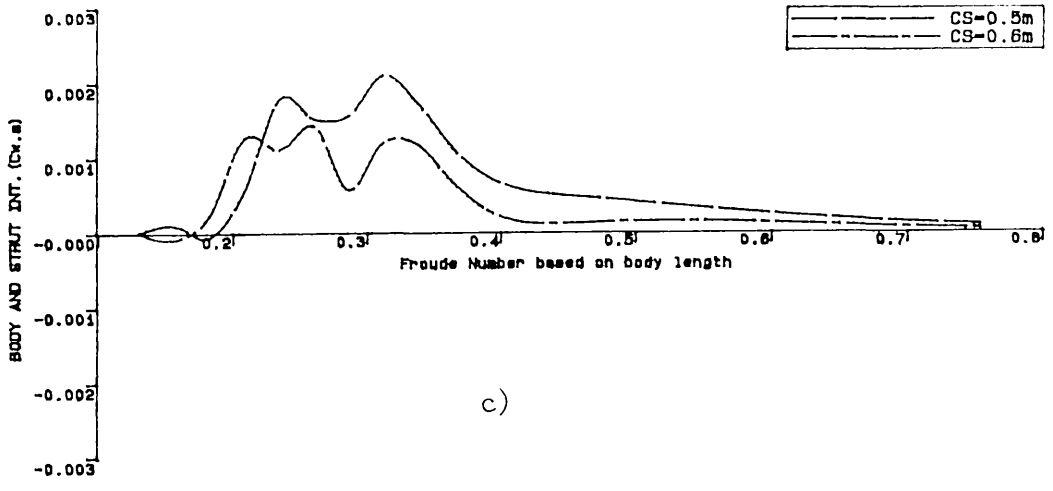

c)

Fig.5.4
Body and Strut Interference Variation with Strut Position On Demihull

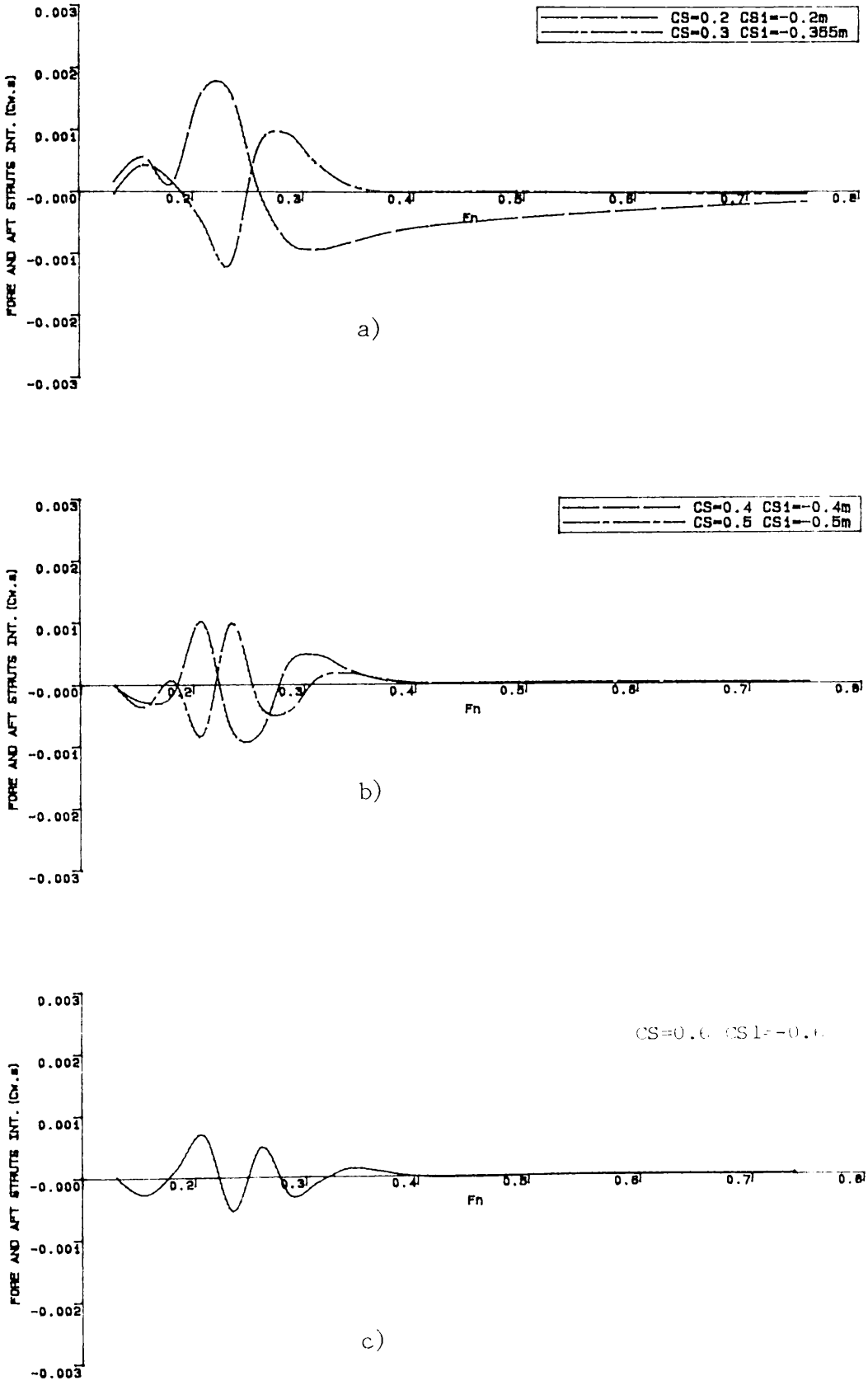

Fig.5.5
Fore and Aft Struts Interference Variations

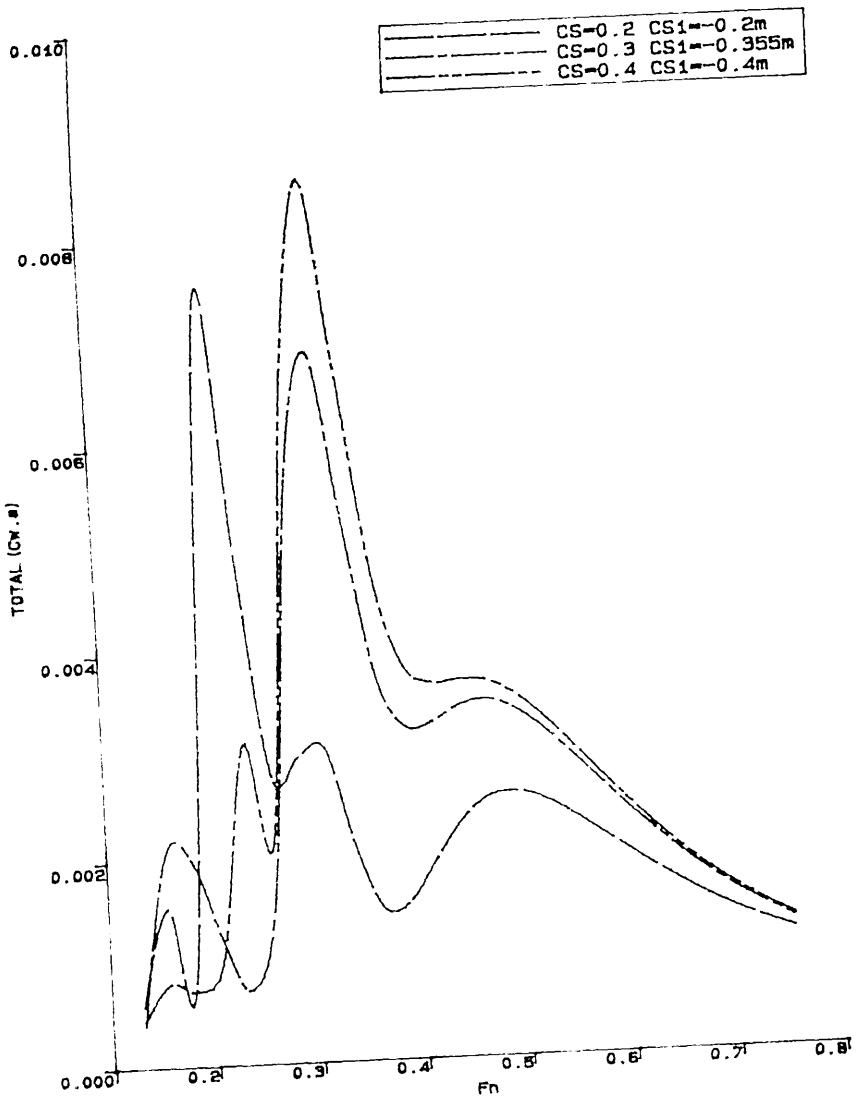

Fig.5.6-a

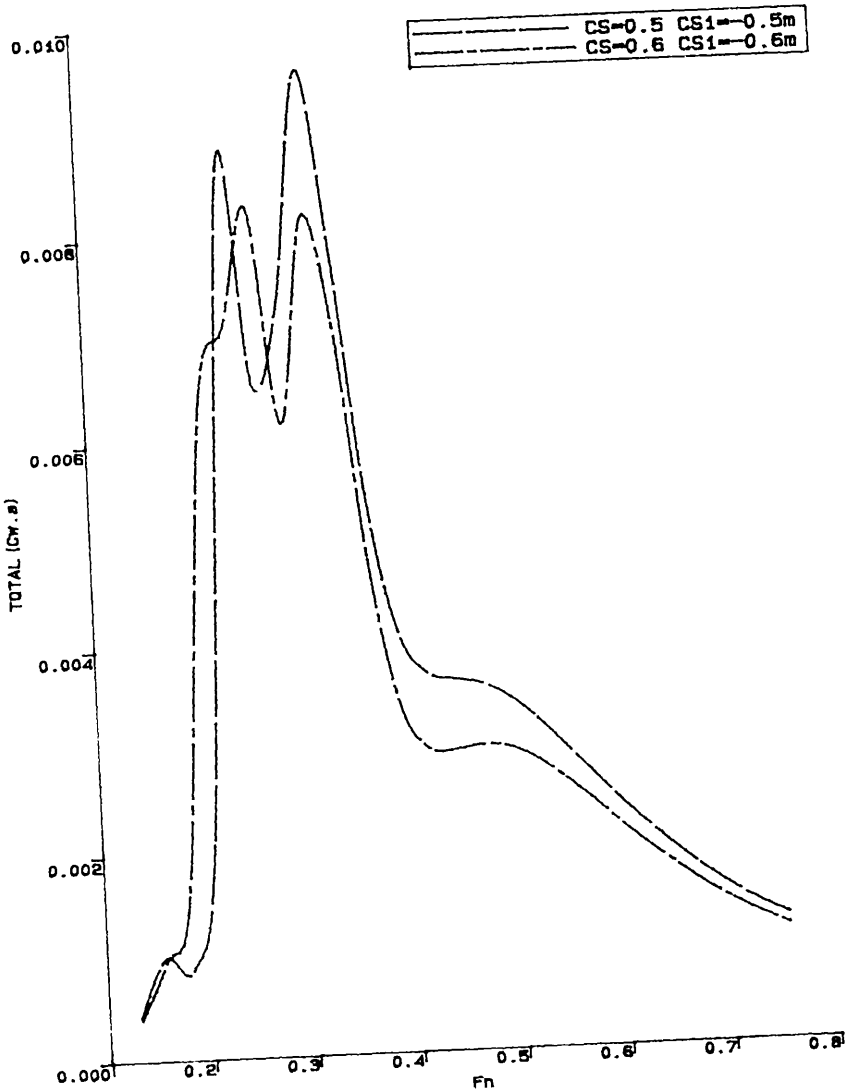

Fig.5.6-b

Total Wave Making Resistance Coefficient of SWATH1 Model

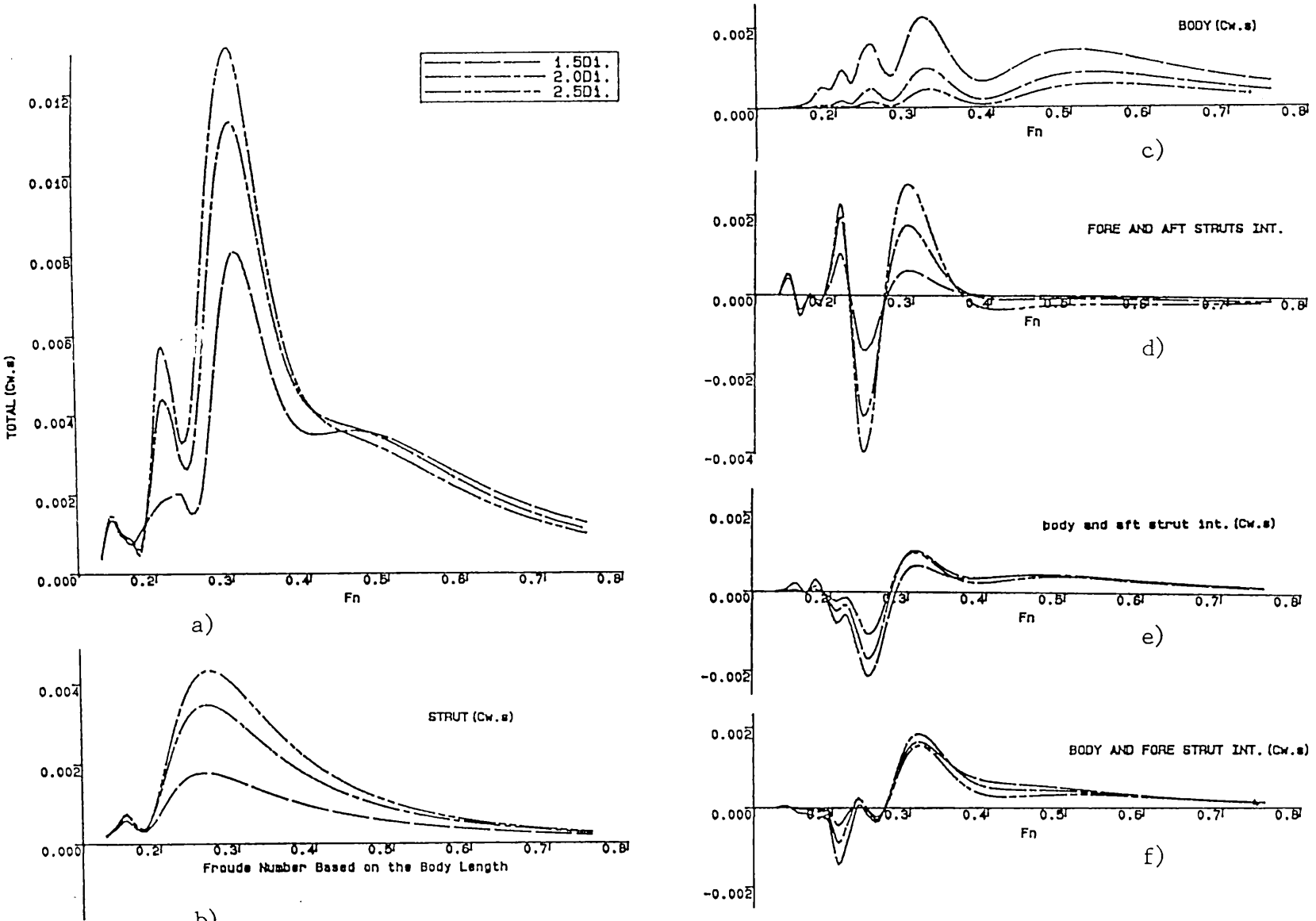

Fig.5.7 The Effect of Immersion Depth of SWATH1 Model on the Wave Resistance Coefficient

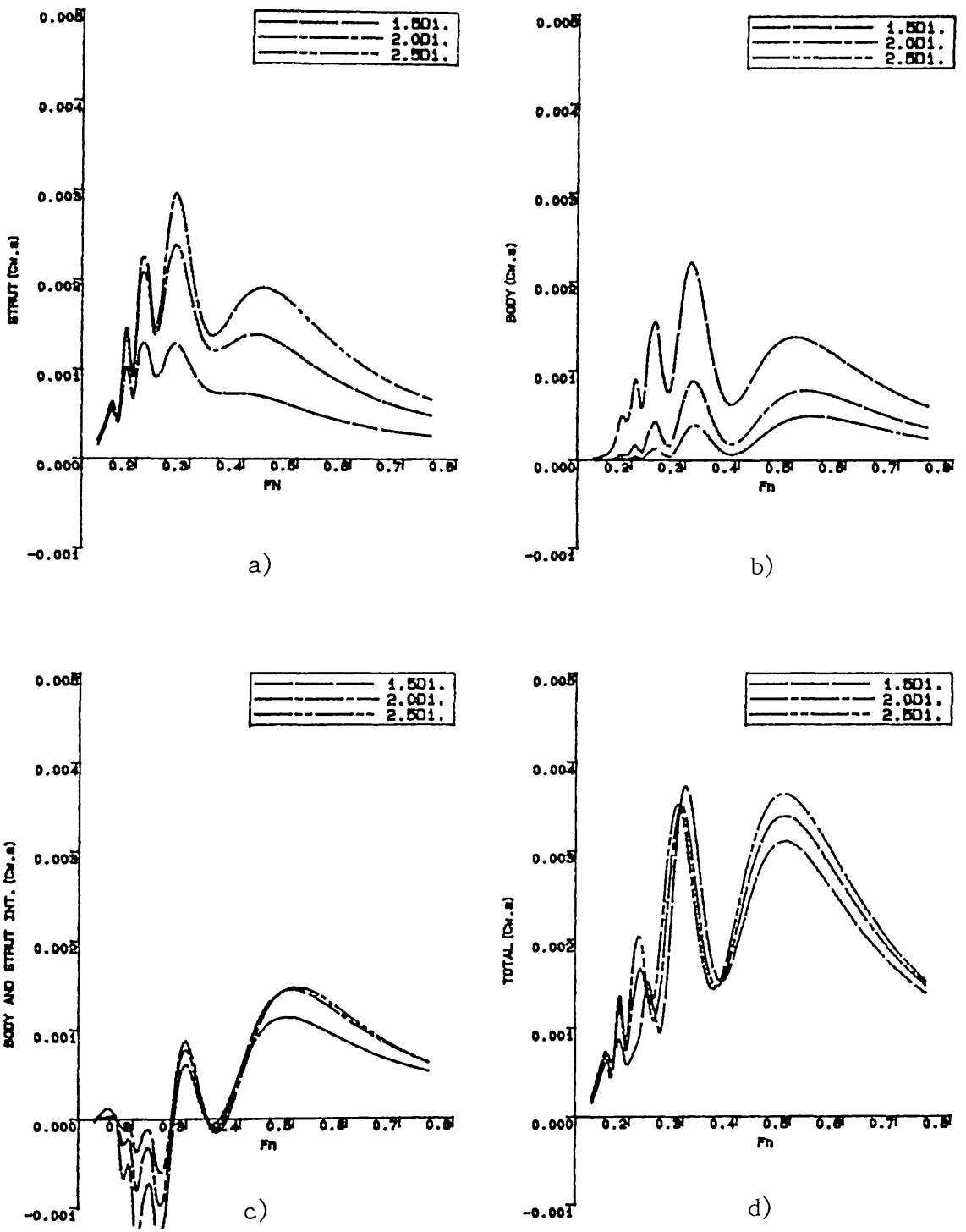

Fig.5.8

Variation of Wave resistance Coefficients of SWATH3 Model and its Components vs Froude Number together with Draft.

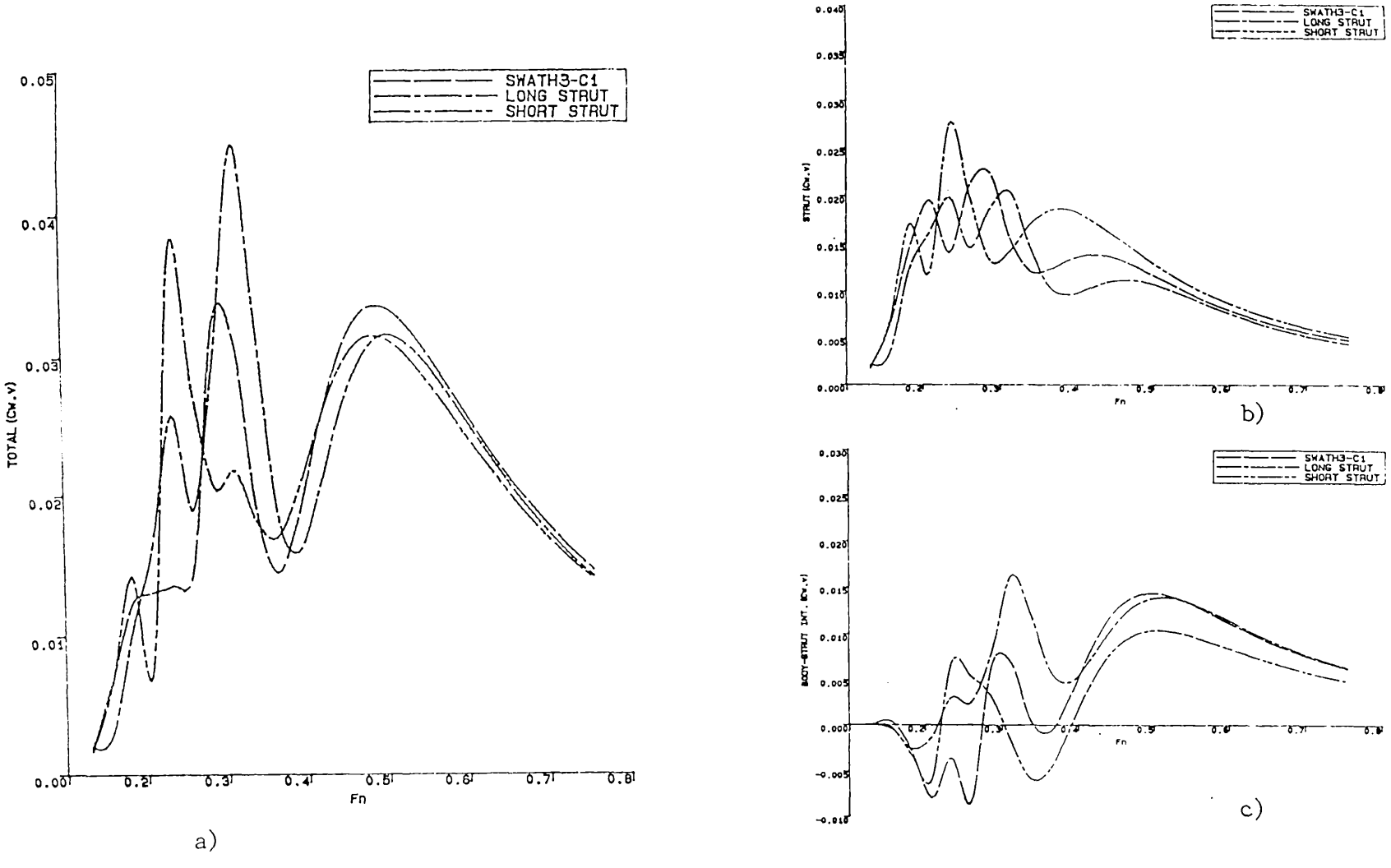

Comparison of Wave-making Resistance Coefficients
for Three Strut Configurations.

Fig.5.9

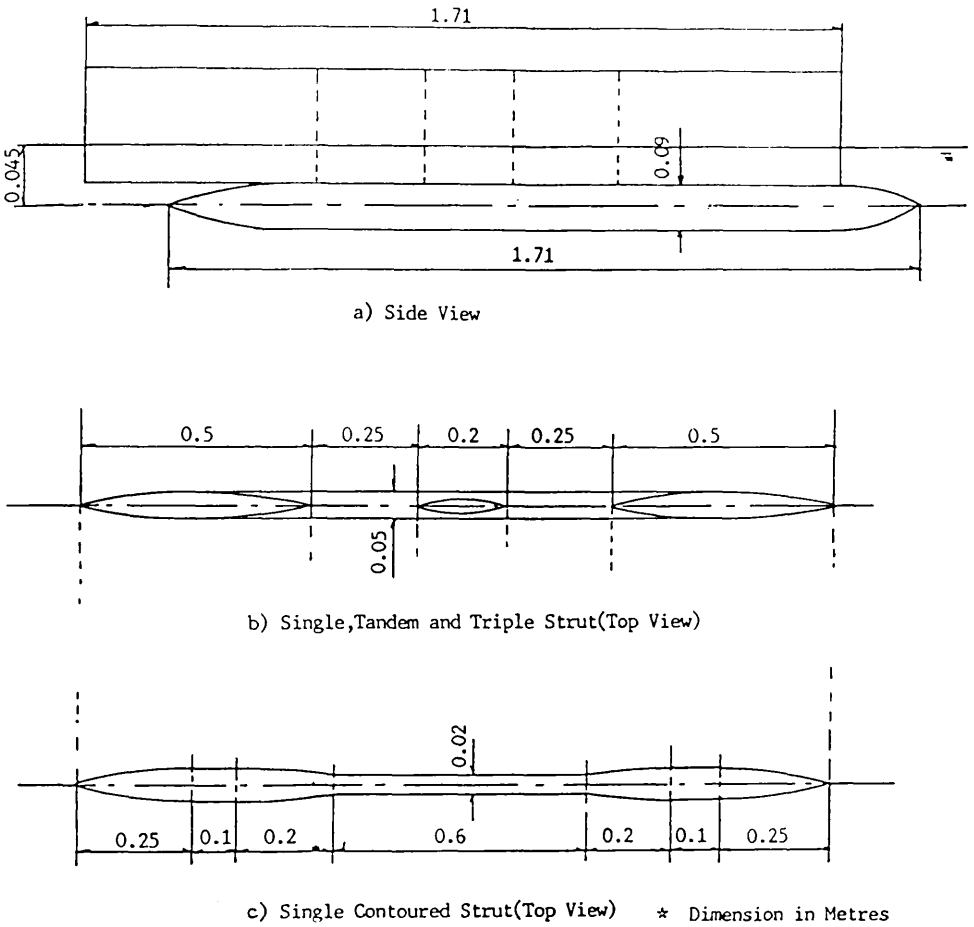

Fig.5.10 Four Struts Configurations Considered for Parametric Study

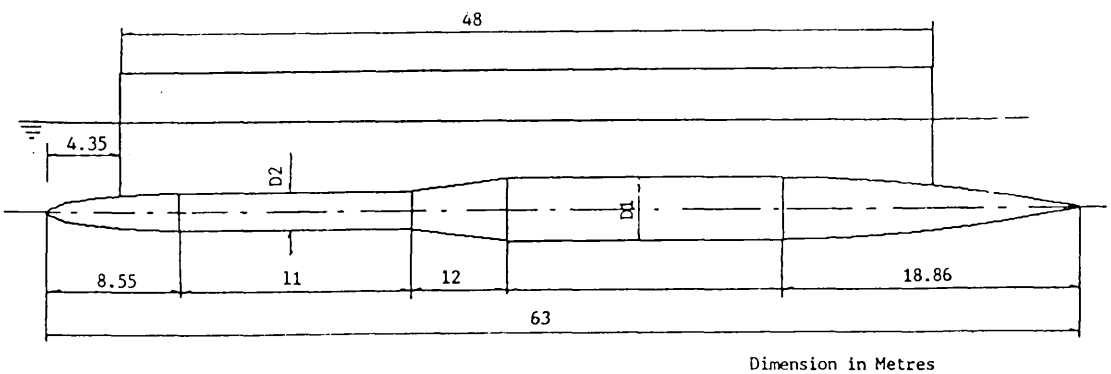

Fig.5.21 2405 tonne SWATH Ship Body and Strut Details together with Symbols

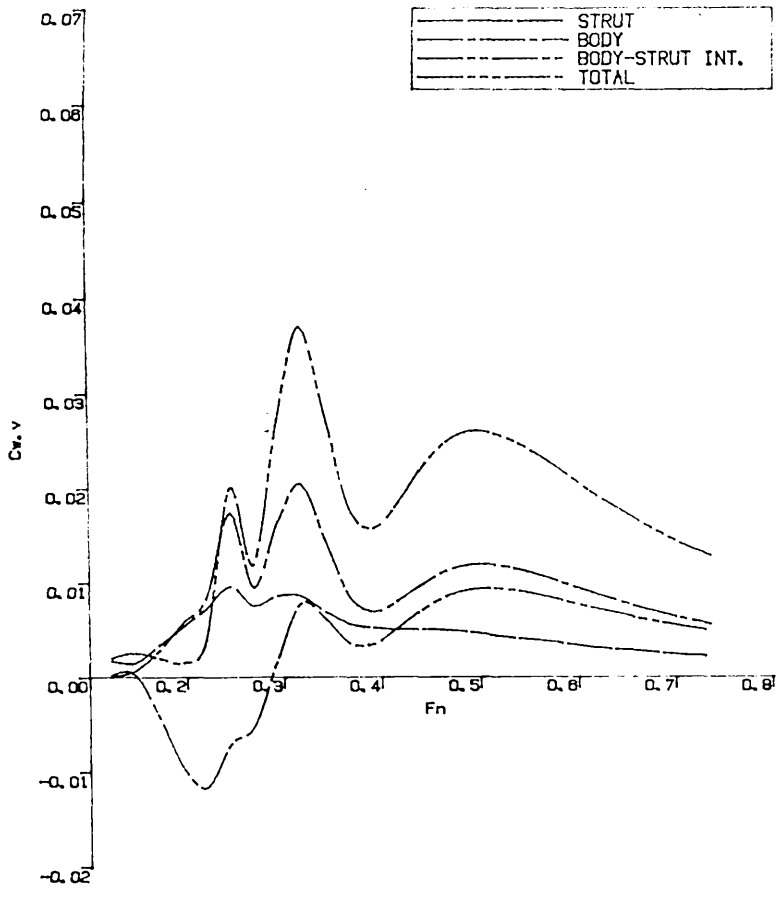

Wave-Making Resistance Coefficient of the Single Strut Configuration against Froude Number

Fig.5.11

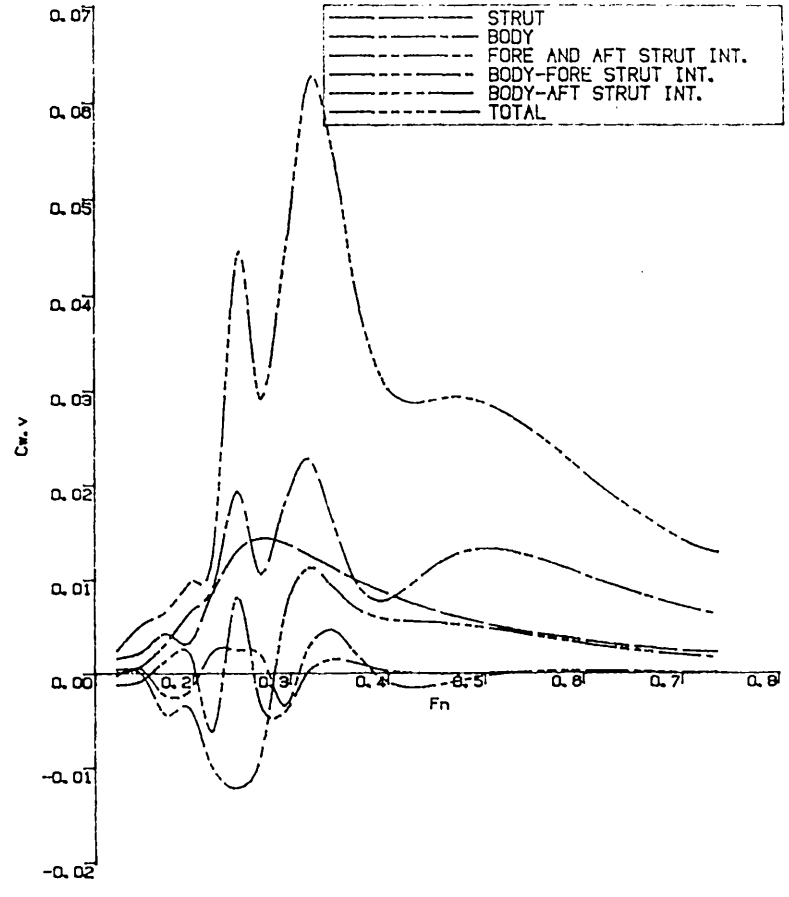

Wave-Making Resistance Coefficient of The Tandem Strut Configuration against Froude Number

Fig.5.12

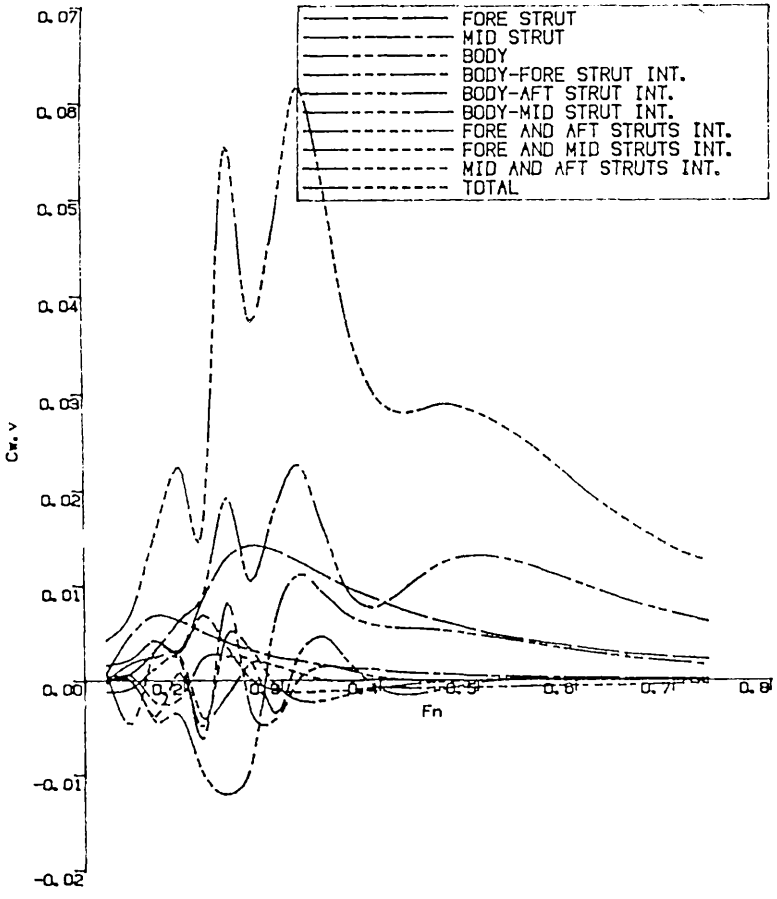

Wave-Making Resistance Coefficient of The Three Struts Configuration against Froude Number

Fig.5.13

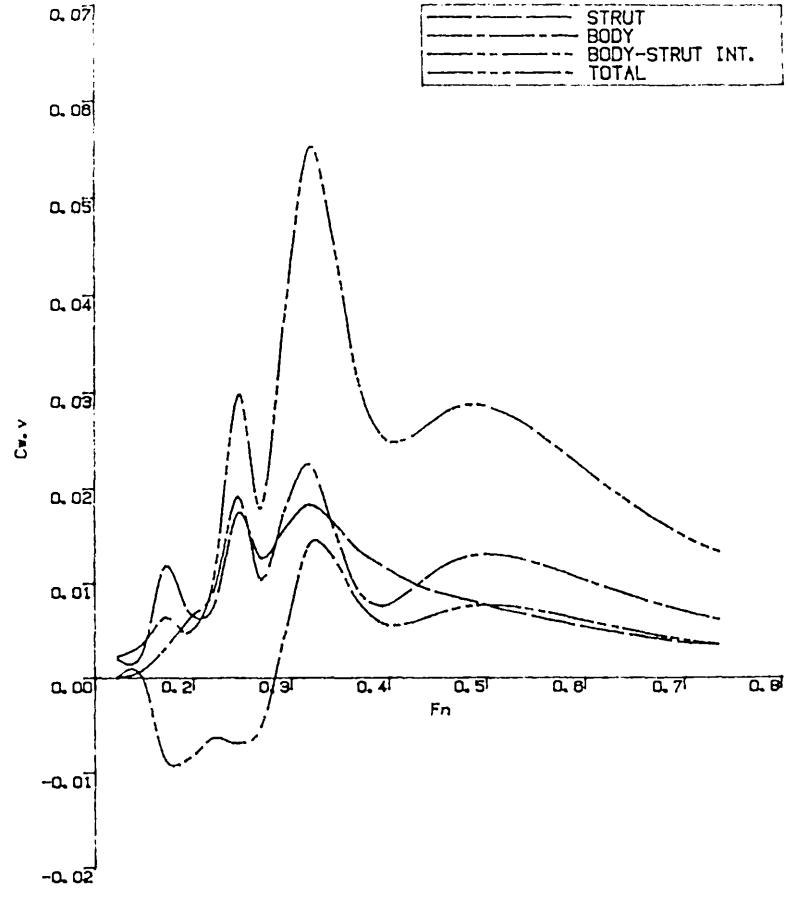

Wave-Making Resistance Coefficient of The Single Contoured Strut Configuration against Froude Number

Fig.5.14

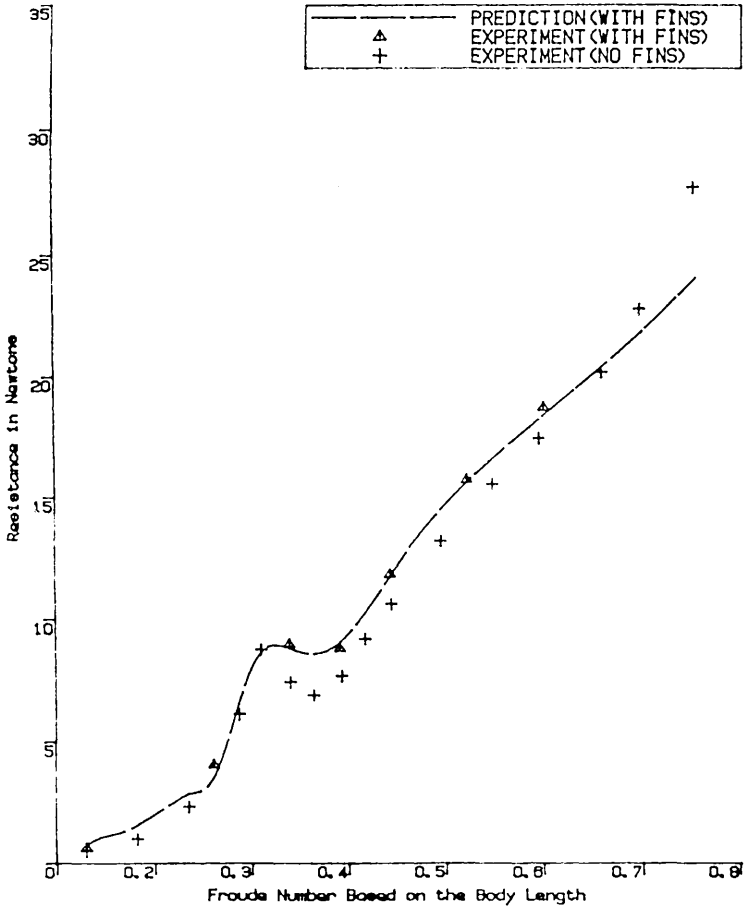

Comparison of Estimated and Measured Total Resistances of SWATH1-C4 with a pair of Controllable Fins

Fig.5.15

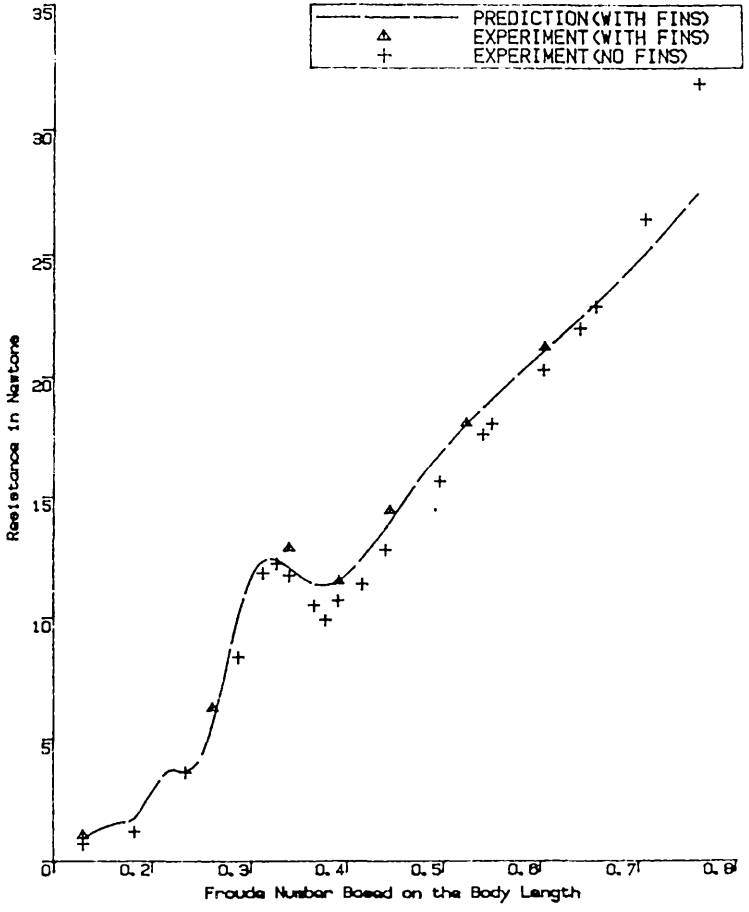

Comparison of Estimated and Measured Total Resistances of SWATH1-C5 with a pair of Controllable Fins

Fig.5.16

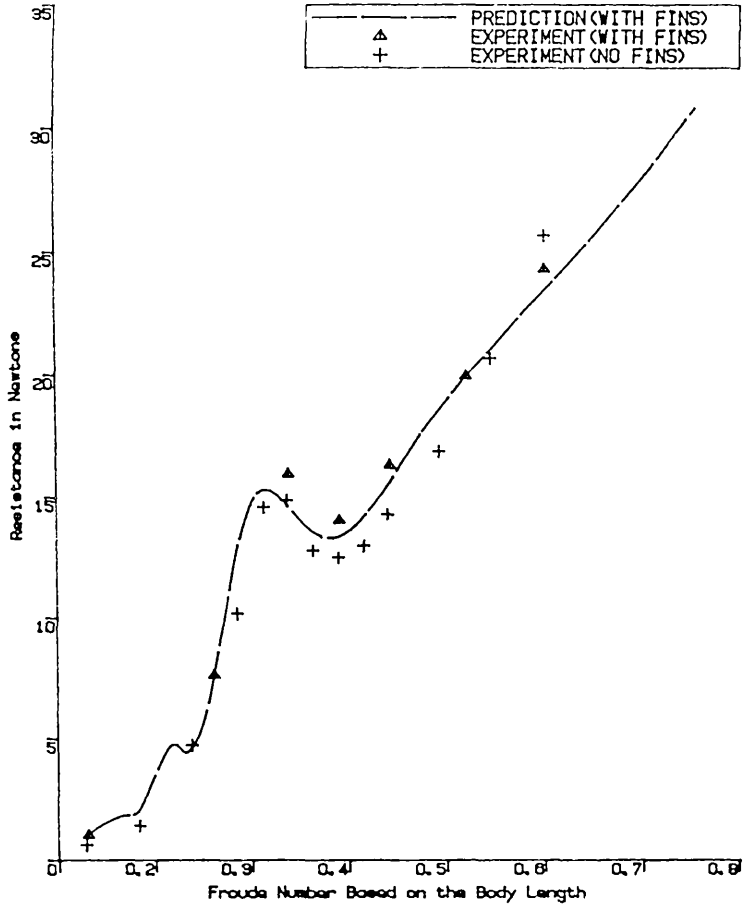

Comparison of Estimated and Measured Total Resistances of SWATH1-C8 with a pair of Controllable Fins

Fig.5.17

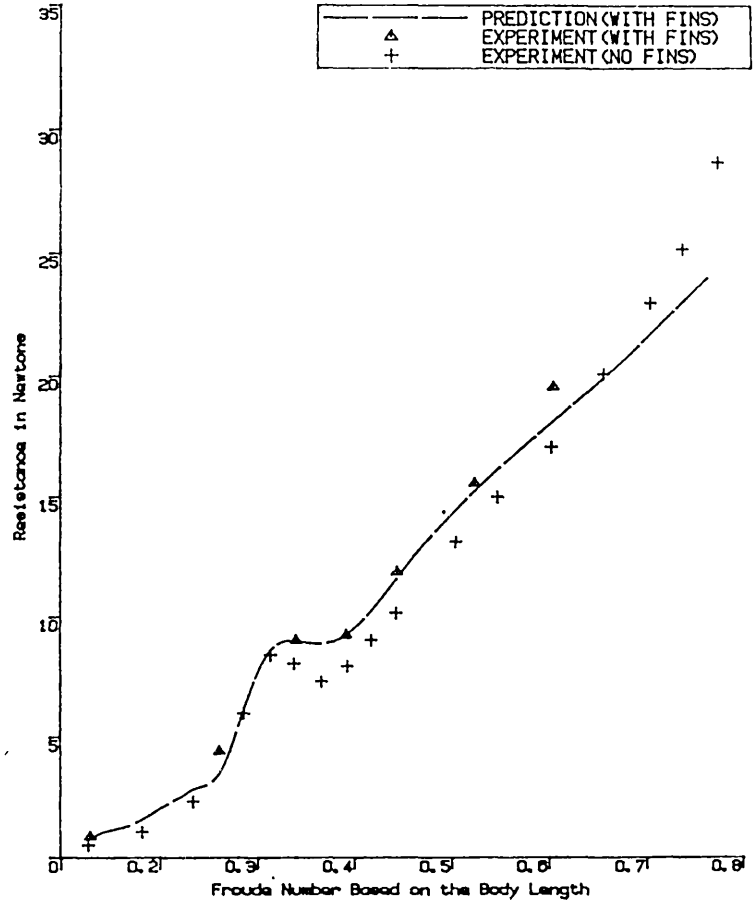

Comparison of Estimated and Measured Total Resistances of SWATH1-C7 with a pair of Controllable Fins

Fig.5.18

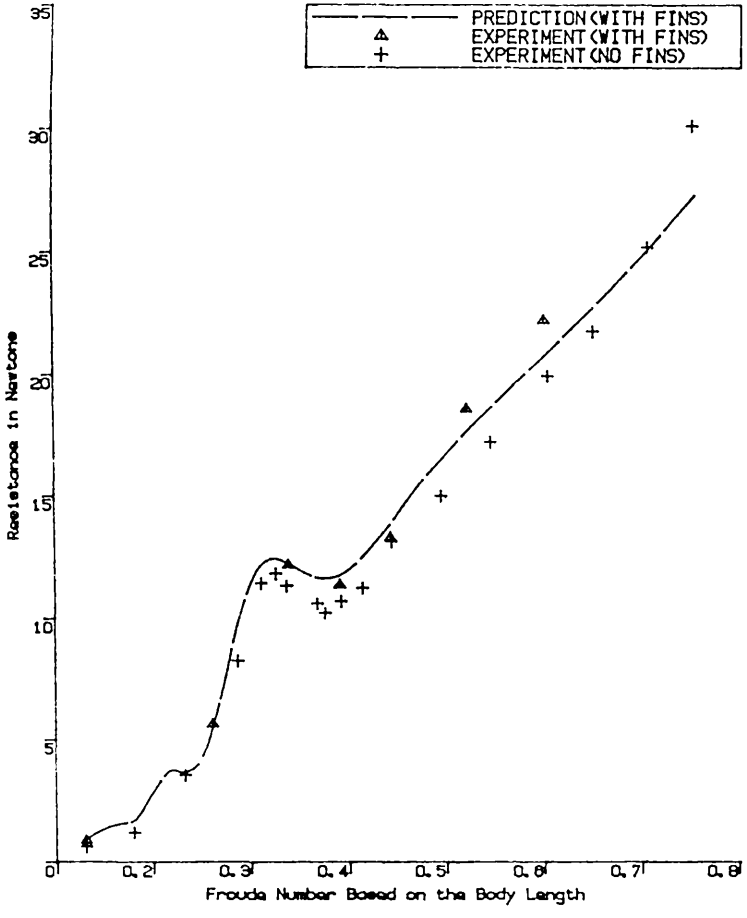

Comparison of Estimated and Measured Total Resistances of SWATH1-C8 with a pair of Controllable Fins

Fig.5.19

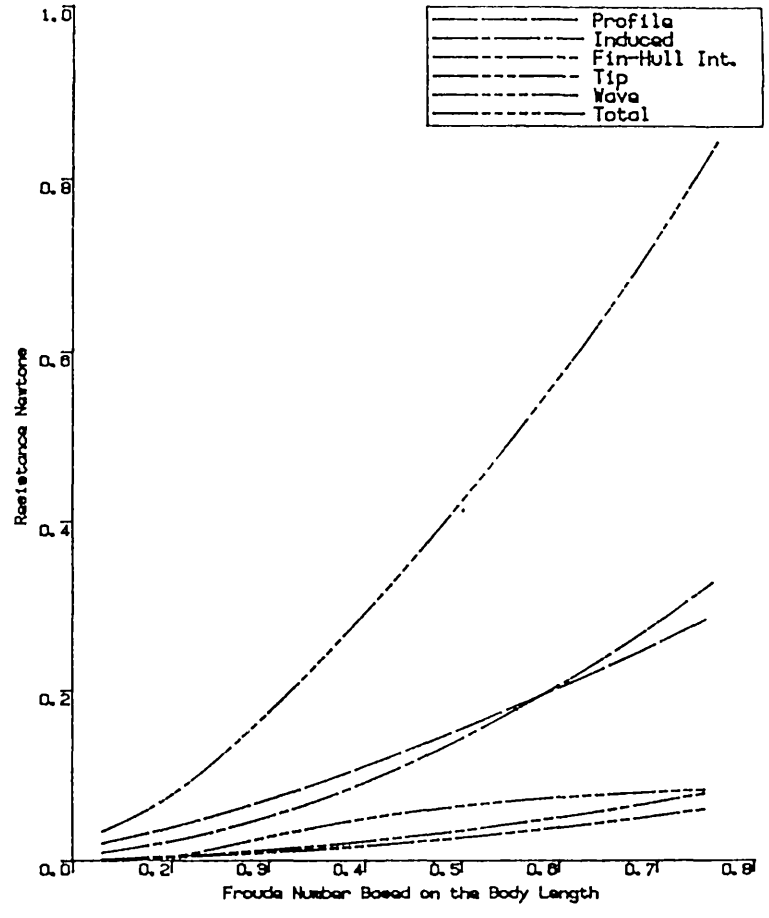

Drag Component Variations of a Fin Attached to the Damihull(SWATH1-C4) with Froude Number together with its Total Drag

Fig.5.20

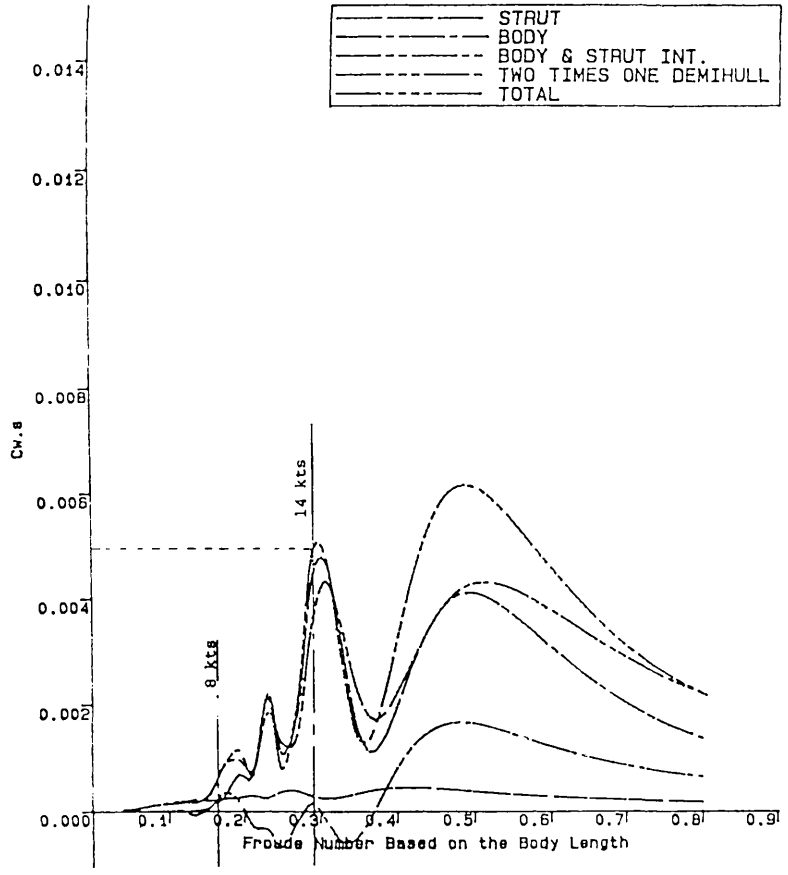

Wave Resistance Coefficients of a 2405 tonne SWATH vs Fn
Draft (6.55m), SD (1.5m), Non-Contoured Circular Cross Sec.

Fig.5.22

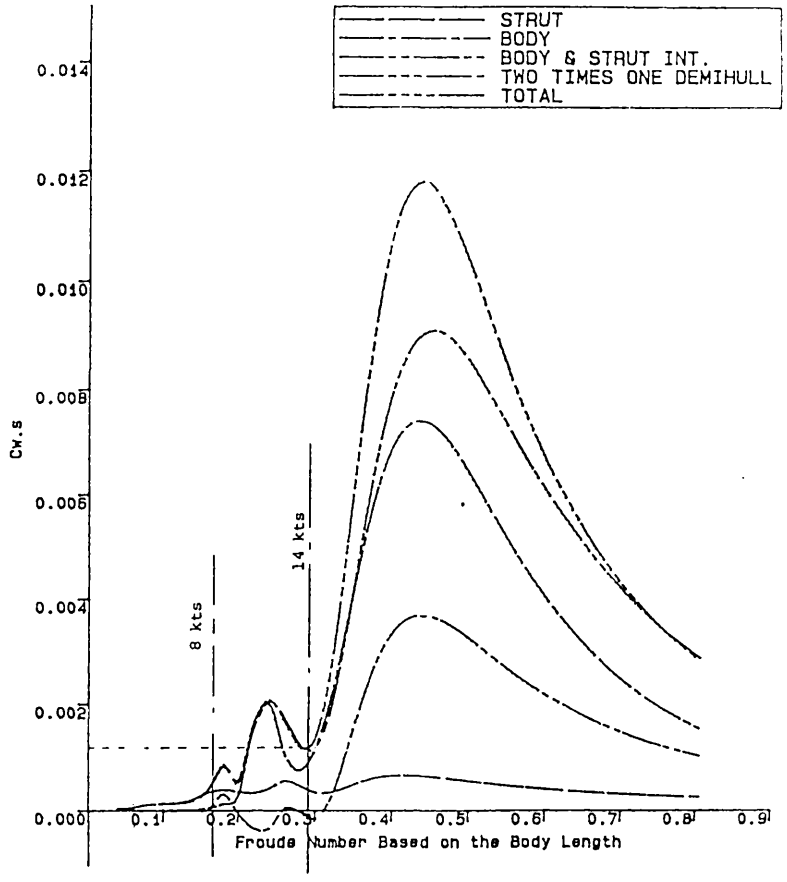

Wave Resistance Coefficients of a 2405 tonne SWATH vs Fn
Draft (7.40m), SD (1.94M), Contoured Square Cross Sec. Hull

Fig.5.23

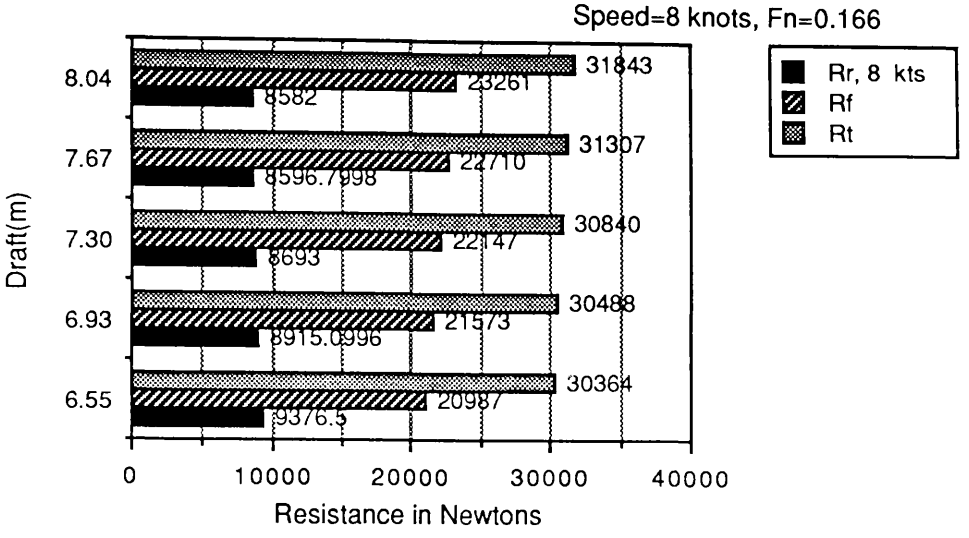

Fig.5.24-a

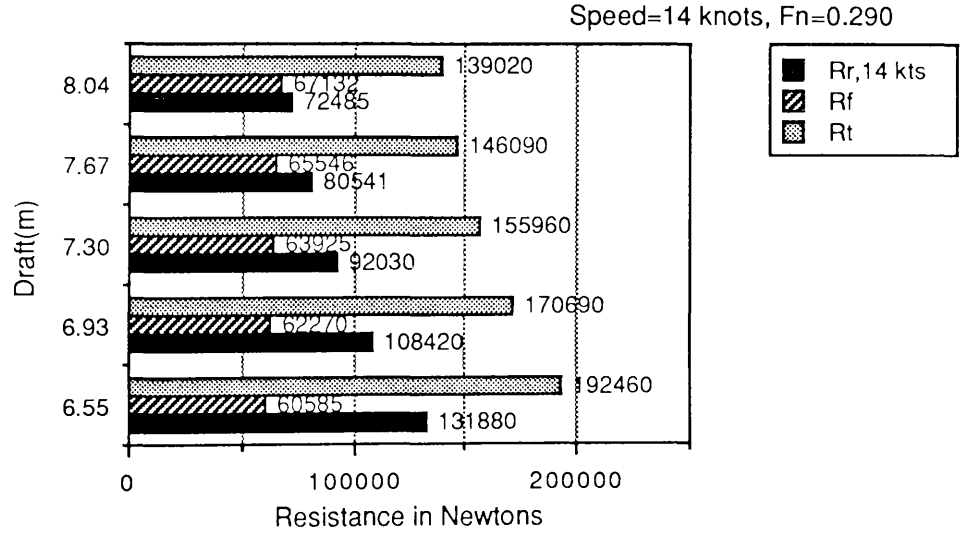

Fig.5.24-b

Fig.5.24 Residuary, Frictional and Total Resistance Variations of a 2405 tonne SWATH ship Demihull with Draft

Fig.5.25-a

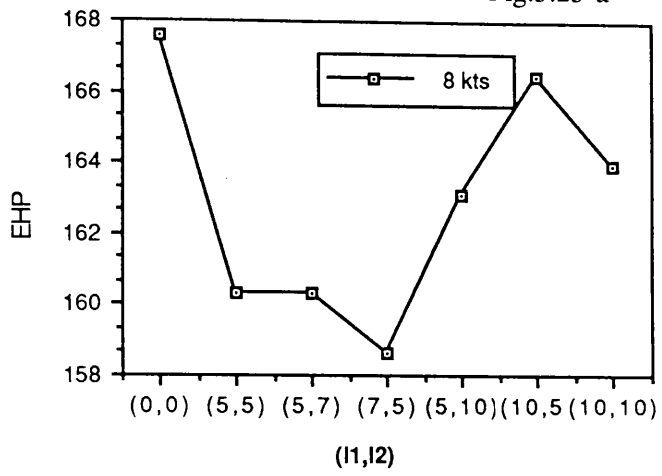

Fig.5.25-b

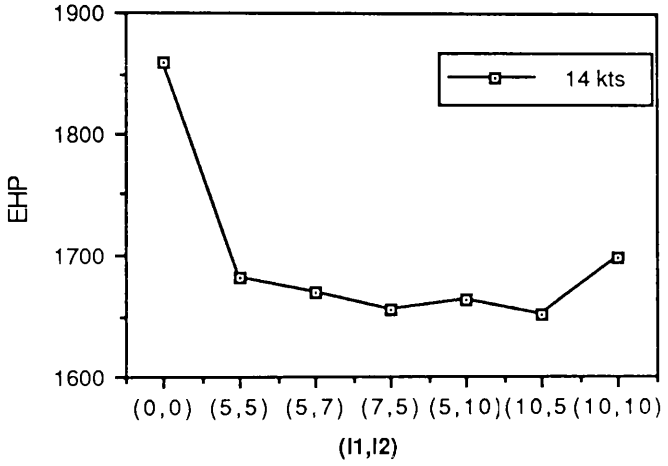

Fig.5.25-c

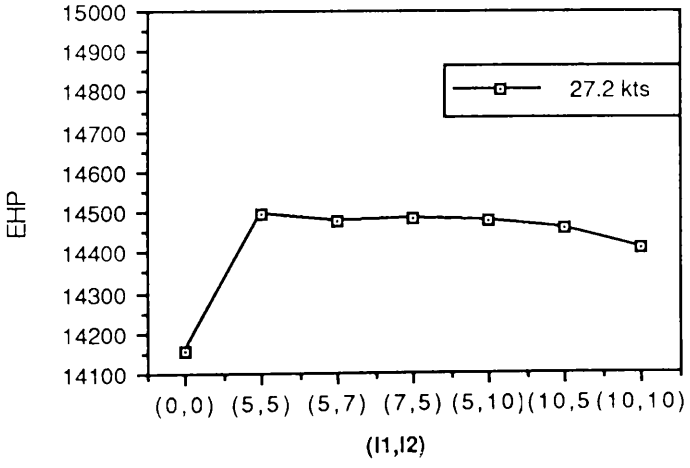

Fig.5.25 EHP Variation of a 2405 tonne SWATH Demihull with(l1,l2) at Three Speeds(SDBC(4.023m) and R1/R2(1.1) fixed)

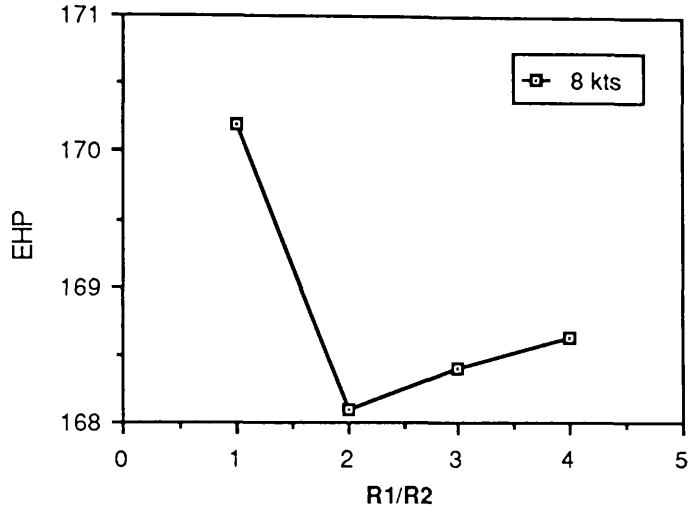

Fig.5.26-a

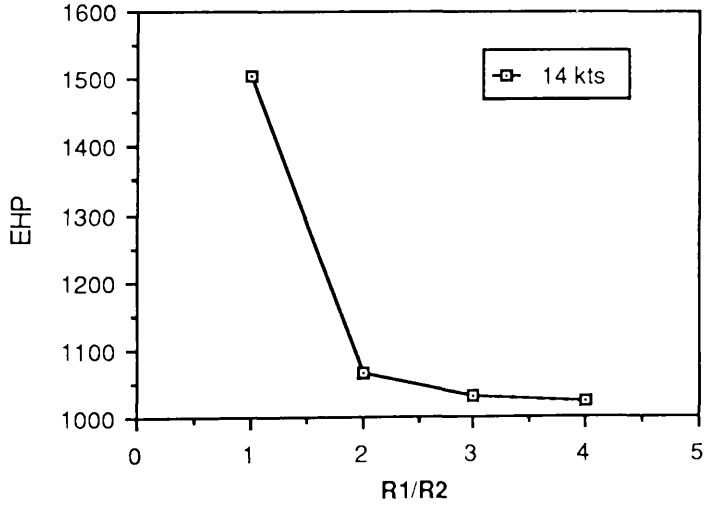

Fig.5.26-b

Fig.5.26 EHP Variation of a 2405 tonne SWATH demihull with R1/R2 ((l1,l2)=(10,5) and SDBC=4.901 Fixed)

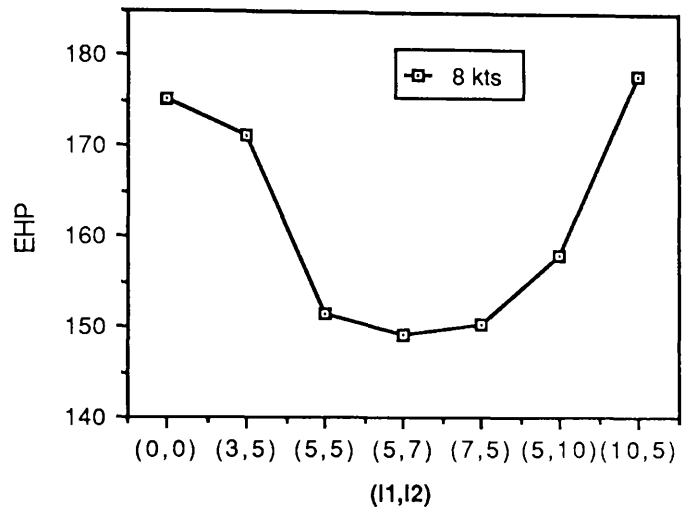

Fig.5.27-a

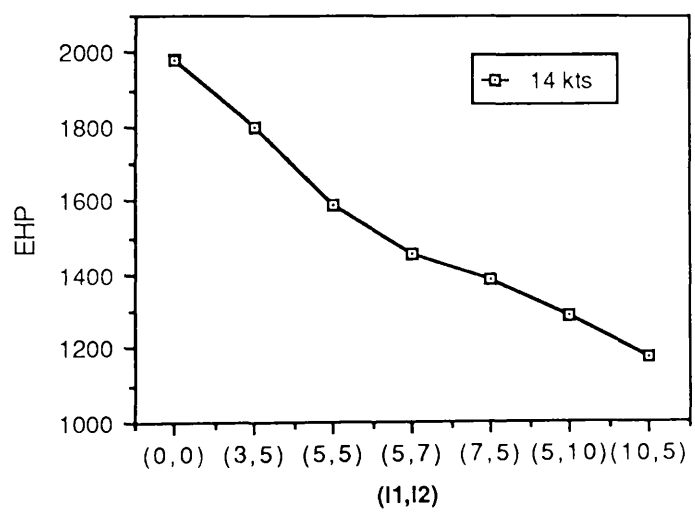

Fig.5.27-b

Fig.5.27 EHP Variation of a 2405 tonne SWATH Demihull with(l1,l2)
(Square Cross Section, RC=1, L 1.5 and D1/D2=2.0 Fixed)

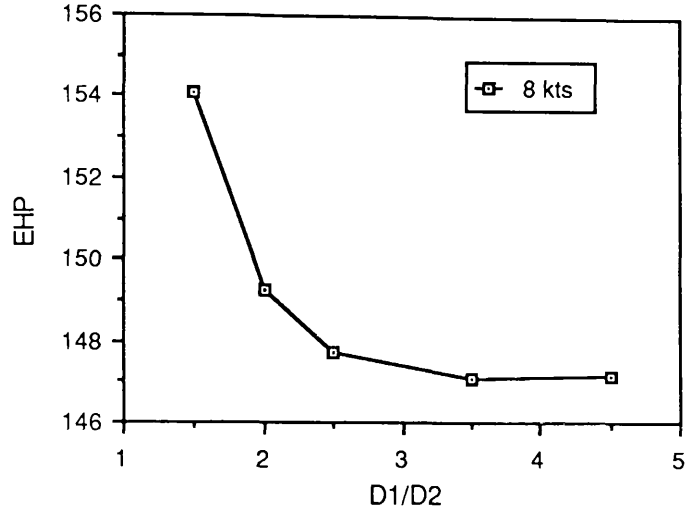

Fig.5.28-a

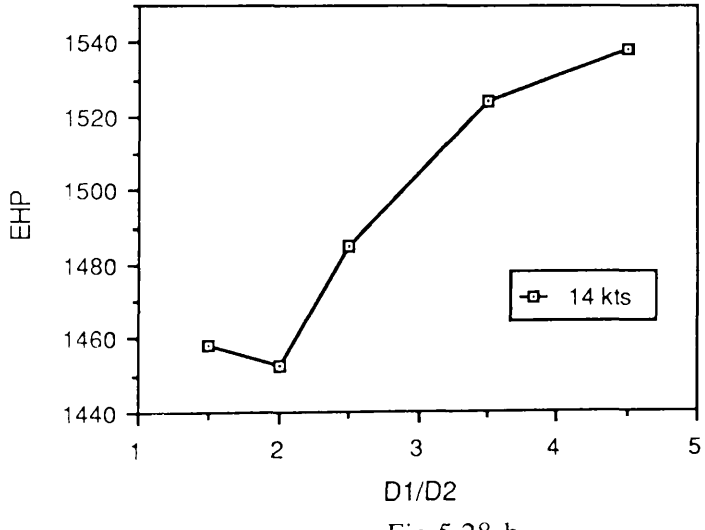

Fig.5.28-b

Fig.5.28 EHP Variation of a 2405 tonne SWATH Demihull with D1/D2
(RC=1.0m, D_S=1.5 and (l1,l2)=(5,7) Fixed)

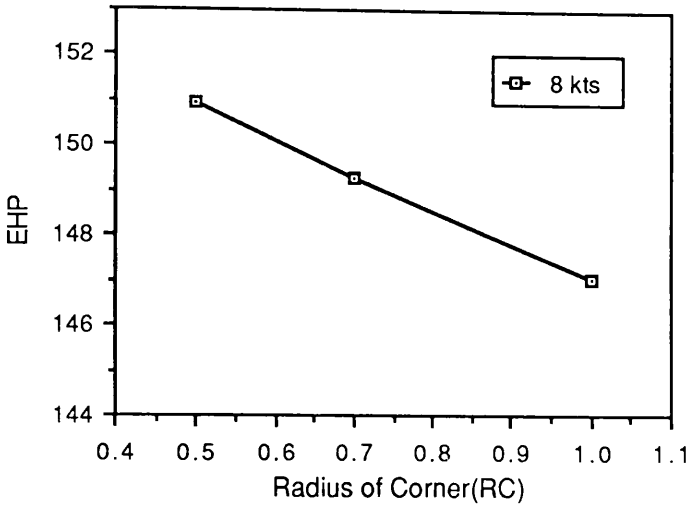

Fig.5.29-a

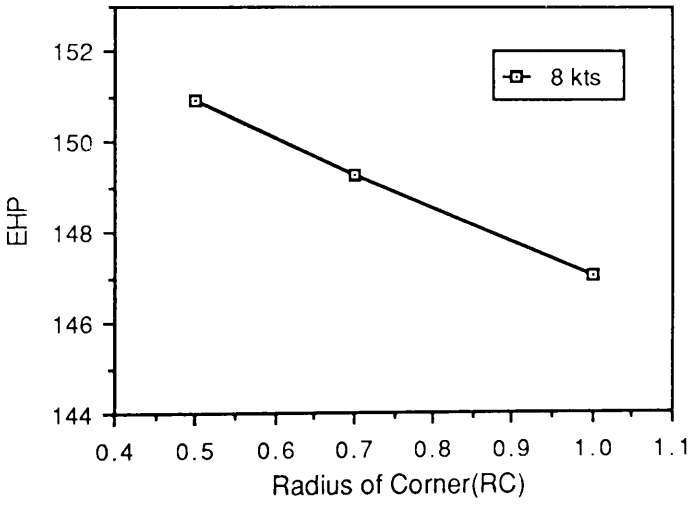

Fig.5.29-b

Fig.5.29 EHP Variation of a 2405 tonne SWATH Demihull with RC (D_S=1.5, (l1,l2)=(5,7) and D1/D2=3.5 Fixed)

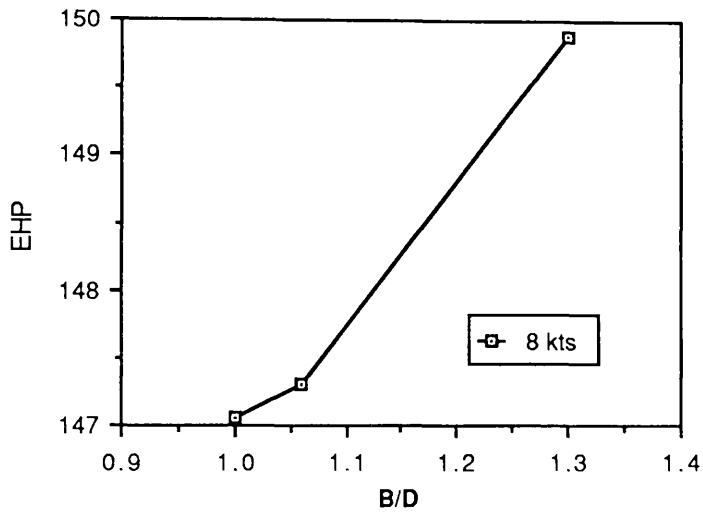

Fig.5.30-a

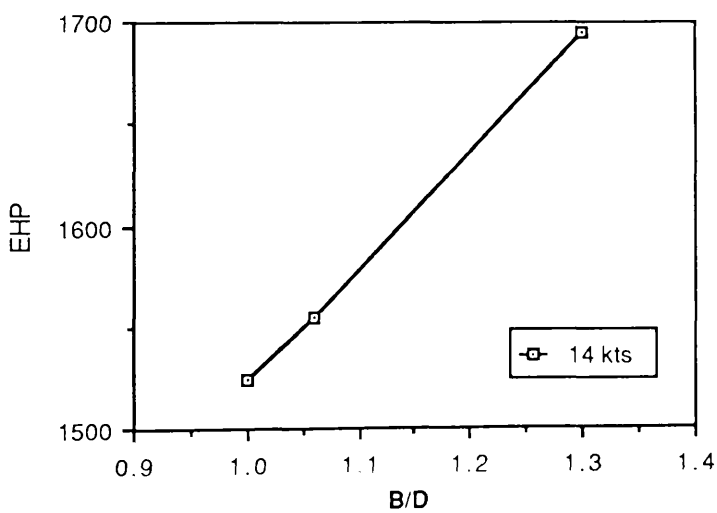

Fig.5.30-b

Fig.5.30 EHP Variation of a 2405 tonne SWATH Demihull with B/D

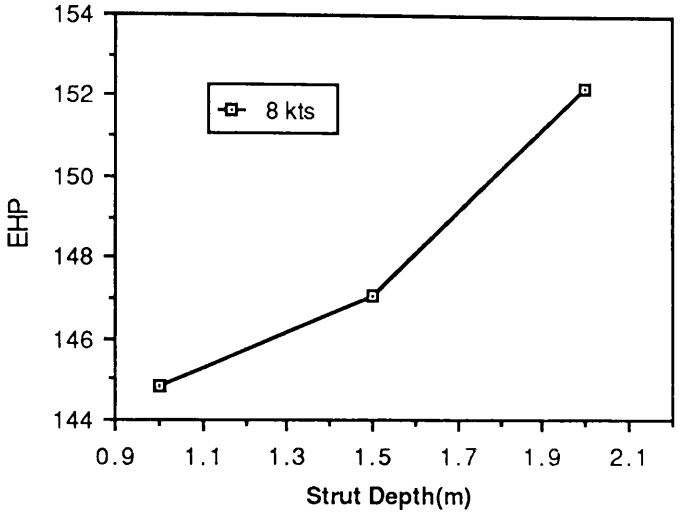

Fig.5.31-a

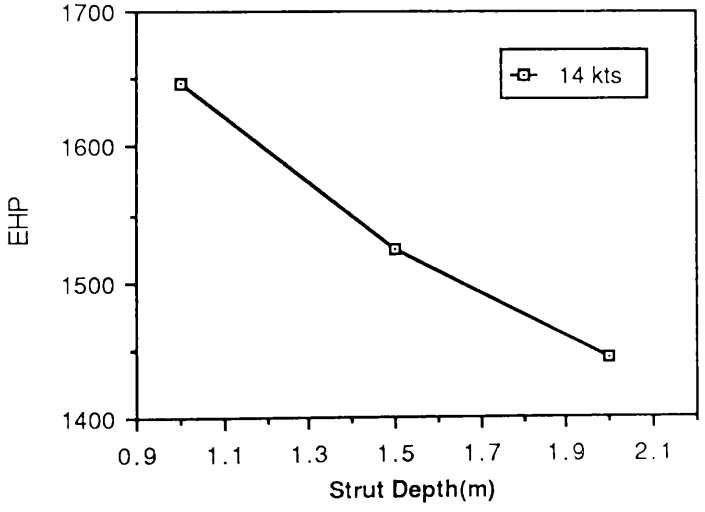

Fig.5.31-b

Fig.5.31 EHP Variation of an Optimum(at 8 kts) 2405 tonne SWATH Demihull

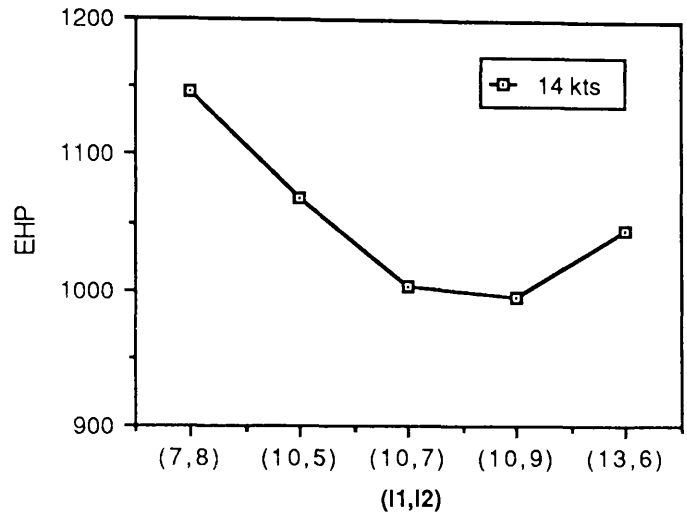

Fig.5.32 EHP Variation of a 2405 tonne SWATH Demihull with (l1,l2)
(RC=1.0m, D1/D2=5.0 and Draft=7.4 Fixed)

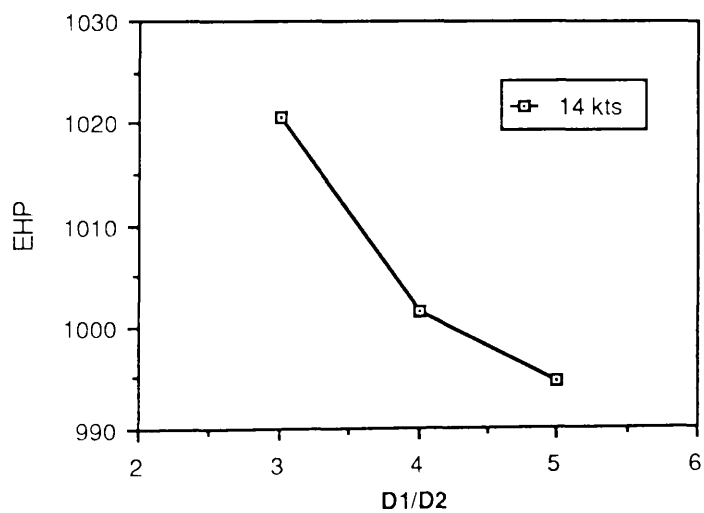

Fig.5.33 EHP Variation of an Optimum(at 14 kts) 2405 tonne SWATH Demihull
with D1/D2 (RC=1.0m and Draft=7.4 Fixed)

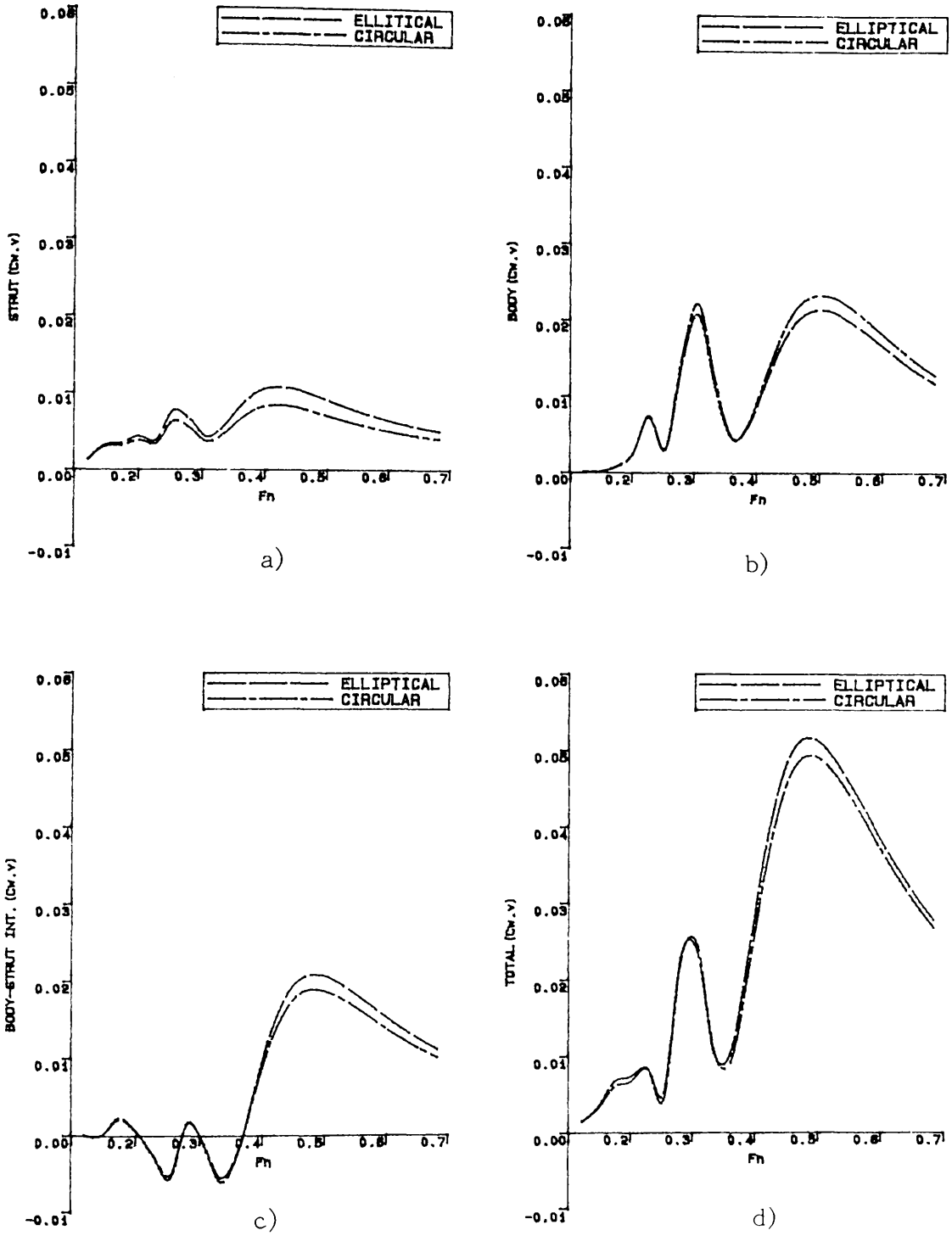

Fig.5.34

Comparison of The Wave Resistance Coefficient of Two Different Cross Section SWATH Ships at the Same SDBC

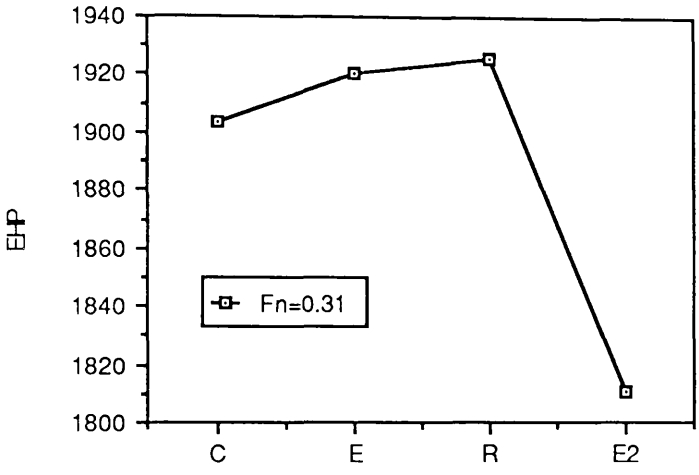

Fig.5.35 EHP(Demihull) Variation of a 2405 tonne SWATH Ship with Different Cross Section Bodies(Circular, Elliptical, Rectangular)

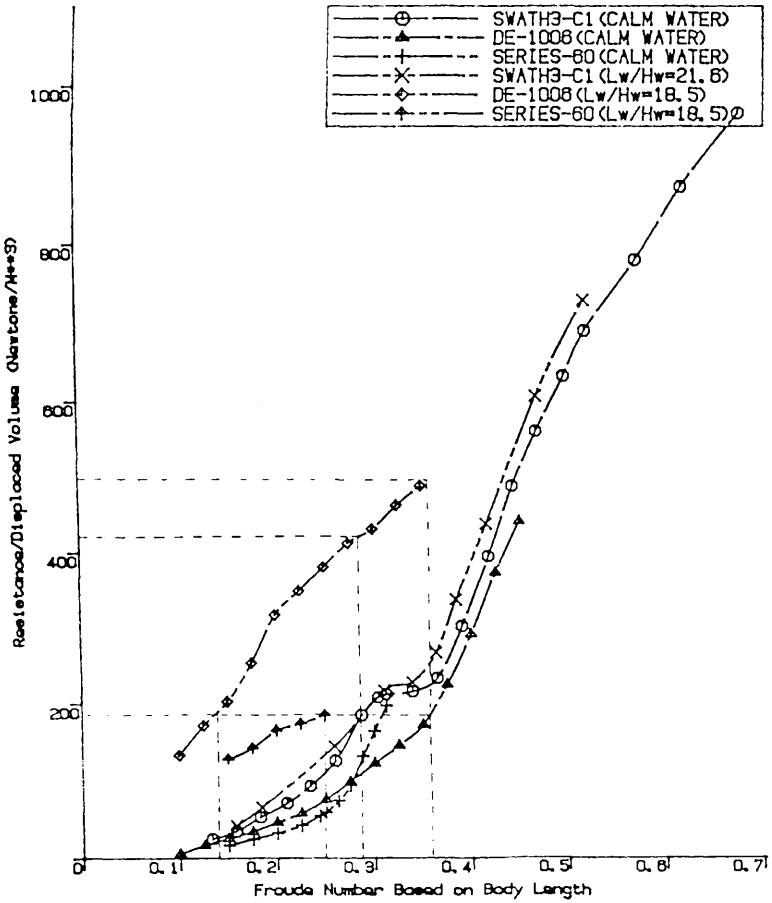

Comparison of Total Resistances(Per Unit Displacement) in Calm Water and in Waves of Three Models, SWATH3-C1, Destroyer DE-1006(Cb=0.49) and Series-60(Cb=0.7)

Fig.5.36

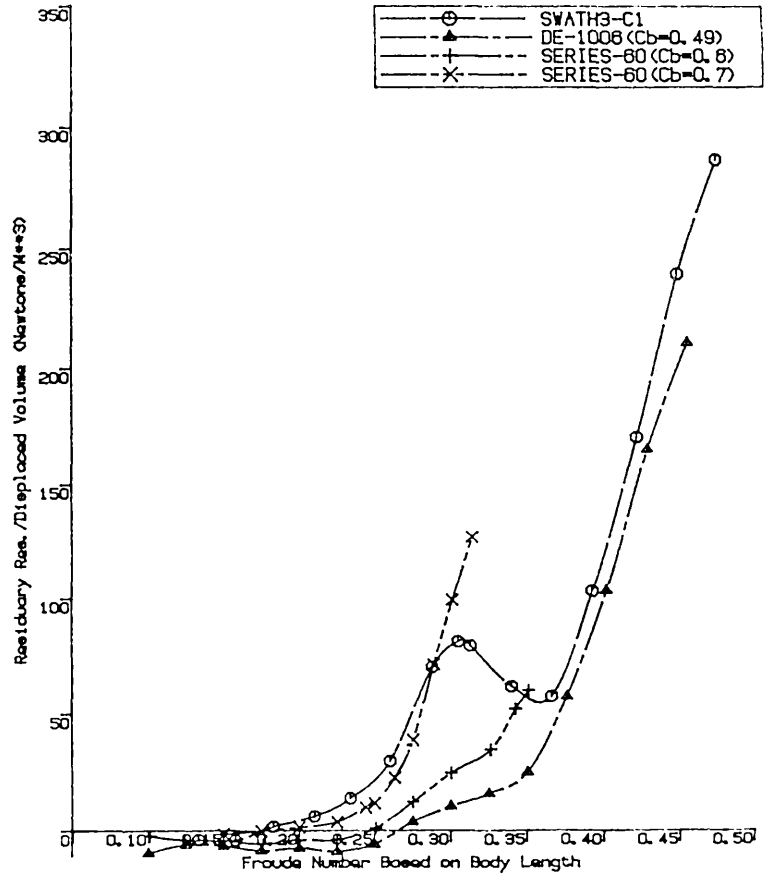

Comparison of Residuary Resistances(Per Unit Displacement) of Four Models, SWATH3-C1, Destroyer DE-1006(Cb=0.49) and Series-60(Cb=0.6 and 0.7)

Fig.5.37

CHAPTER 6 CONCLUDING REMARKS

As mentioned in the Introduction, the objectives of the work presented in this thesis are

i) to develop an analytical tool which can give an improved prediction of SWATH ship resistance,

ii) to compare the computed values of resistance with the experimental results to verify the applicability of the tool and

iii) on the basis of the computational and experimental analysis, to provide recommendations for the design of high performance ships with special reference to finding the feasibility of practical SWATH ship developments such as a rectangular(with rounded corners) hulled SWATH ship.

In general, it can be concluded that these objectives have been satisfactorily fulfilled with the present studies. Detailed conclusions have been drawn at the end of each Chapter and some general and important remarks are made below together with some recommendations for future study.

1) Perhaps the most important thing is that the analytical tool developed gives excellent correlations with various SWATH configurations(9 SWATH models together with 51 individual configurations) including single and tandem struts, circular and non-circular hulls, with and without fins and such parametric changes as two demihull spacing, draft, strut position on the demihull and slenderness ratios of body as well as strut etc. Therefore, those computer programs can be used, with good confidence, for parametric studies and for an optimisation process in selecting hull form with regard to resistance.

2) The calculated wave-making resistance based on the present approach utilising the plane source distribution for the submerged body gives satisfactory agreements with the measured residuary resistance on the variety of SWATH configurations mentioned above. The other published computational methods give lower predicted values than the present method(which is dependent upon the submergence of the main body). It is suggested that this improvement in accuracy of prediction is due to the utilisation of the

plane source distribution technique. In particular, this is marked for non-circular hulled SWATH ships.

3) Although linear wave theory and relatively simple centre plane source distribution technique are used, the agreement between the predictions and the measurements are very good. This order of accuracy can not be expected from a theoretical resistance investigation for conventional monohulls. This seems to be due to the fact that SWATH ships have much thin and slender demihulls which satisfy the assumptions of the theory compared to monohulls. Also, lifting effects seem to be less important for SWATH configurations. Therefore, the introduction of non-linear boundary conditions, or complicated panel source distribution techniques using either constant source strength distribution or higher order source distribution, which have been directed to improve the predictions for monohulls at the cost of a huge amount of computing time, seems to be unnecessary for SWATH ships. Instead, research into the viscous flow including the boundary layer and wake region is most desirable towards reducing the viscous resistance components which compose a great proportion of the total resistance of SWATH ships. In this connection long chain polymers or other friction reducing agents may have more use in SWATH ships than in conventional ships. Also, SWATH ships are so sensitive to sinkage and trim that the resistance prediction at a condition of sinkage and trim is recommended to improve the accuracy of prediction.

4) Based on the difference between the calculated wave-making resistance and measured residuary resistance with 16 SWATH configurations(including single and tandem strut configurations, and circular and rectangular hulled SWATH configurations), two form drag coefficients have been derived. One is for circular hulled SWATH ships and the other is for non-circular hulled SWATH ships. It has been proved that these curves can be used to estimate the form drag for the practical range of SWATH ships.

5) Using the empirical formulae known for foils and streamlined bodies and including the free surface effects, the resistance caused by the controllable fins is

estimated and compared with experimental results of two SWATH models(one is fitted with a pair of fins and the other with two pair of fins). It has been shown that the agreement between the two curves is extremely good.

6) The two computer programs of MSWATH(written for SWATH ships defined by mathematical formulae) and OSWATH(for offset input) have their own advantages and disadvantages. Despite the mathematical modelling difference, the two computer programs give exactly the same results for a same SWATH ship which can be defined by either technique. Therefore, they can be used in a complementary way. A SWATH geometry may be accurately defined by simple mathematical shapes. Hence, MSWATH can be useful for a Concept Exploration Model Study(CEMS) at the very early stage of design process because the surface area can be calculated exactly, the parametric studies can be carried out easily and most importantly, computing time is very short compared to the offset input program OSWATH. Then, if the final design of the SWATH ship cannot be expressed by simple mathematical formulae, OSWATH can be used to obtain the resistance estimate

7) An interference wave system created by two demihulls affects the resistance favourably or unfavourably, depending on speed. Owing to unfavourable interferences at higher speeds the wider the spacing between two demihulls, the better is the resistance. However, up to moderately high speeds, there are some favourable interference effects between two demihulls. A well chosen spacing between the two demihulls of a SWATH results in a considerable resistance reduction(for the present model SWATH1, 2 and 3, up to around 40% the resistance of the twin hull at infinite spacing) around Fn=0.35-0.45. This range is not much changed with geometry changes(such as single and tandem strut SWATH) and draft variations. Therefore, special attention should be paid to the two demihull spacing for SWATH ships whose operating speed is within the range of Fn=0.35-0.45. This means that the demihull spacing need not necessarily be wider to avoid the two demihull interference.

8) As the draft of a SWATH ship increases, the wave-making resistance of its components including several interference effects between them are decreased or increased in magnitude while the patterns of the coefficients remain nearly unchanged.

As a result of these changes in magnitude, it is possible to have an optimum draft for a certain SWATH design. Definitely, over the viscous dominant speed range, the lighter the draft, the smaller the resistance. However, over the wave-making speed range, there are two patterns. SWATH ships having a large hull slenderness ratio(L_b/Di_b) are unlikely to obtain a resistance benefit from ane increase in draft because the contribution of the hulls to the total wave-making resistance is relatively small and any reduction in wave-making resistance cannot counteract the increase of frictional resistance. This is the case with the SWATH1, SWATH2 and SWATH3 models(both SWATH1 and SWATH3 have the hull ratios(L_b/Di_b) of 16.93 and the rectangular hulled SWATH2 has L_b/D_b=23.23 and L_b/B_b=15.1). On the other hand, a SWATH ship having a small slenderness ratio lower than around 12 will have a certain draft at which the total resistance is least. Therefore, at a given displacement, the proper distribution of the displacement on struts and bodies is essential depending on the draft as well as the speed of interest.

9) The hollow and hump in the resistance curve is significantly changed by the strut(s) position on the demihull. In particular, this is much exaggerated with the tandem strut SWATH designs. Therefore, when designing a SWATH with tandem struts, careful attention should be paid to the position of the struts on the demihull depending on speed. A short strut located on the longitudinal centre of the demihull gives rise to favourable interferences over the moderate speed range, while being unfavourable at higher speeds. On the other hand, the result is reversed with an overhanging strut, significantly reducing the unfavourable interference at higher speeds. The interference effect between the fore and aft struts (placed in tandem) changes depending on the distance between them. particularly at slow speeds. If two struts are placed beyond a distance of a strut chord length apart, the two strut interference becomes negligible at high speeds. In general, at higher speeds, it is desirable to place two struts near the ends of the lower demihull

10) In general, a short strut-body combination(with single strut design) gives less resistance than a long strut-body combination beyond moderately high speeds while the result is reversed at slow speeds. By changing the longitudinal thickness distribution of

a strut(contoured strut), the wave-making resistance can be considerably varied depending on the speed of interest, but may give a serious resistance penalty at other speeds. By the same principle, a triple strut configurations can be beneficial at certain speeds (in particular, higher speeds) from the wave-making resistance point of view, compared to single and tandem strut configurations.

11) To summarise 7) to 10) above, interference effects are dependent upon the relative distance between the components of a SWATH design as well as the operating speed. Hence, a SWATH arrangement which will give favourable interference characteristics at all speeds cannot be obtained. However, reductions in wave resistance at certain speeds can be obtained by a proper location of the struts on the hulls and a well chosen spacing between the hulls. Most importantly, at a certain draft, a proper distribution of the displacement on the struts and bodies, keeping the breadth to length ratio of the strut as low as possible, seems to be essential. In general, a short strut-body combination give less resistance than a long strut-body combination at higher speeds, but the result is reversed at slow speeds. Therefore, a single strut SWATH is recommended up to moderately high speeds, but at higher speeds a tandem strut configuration is better from the point of view of resistance. A triple strut configuration can be beneficial at certain speeds(particularly, higher speeds) from the wave-making resistance point of view, as compared to single and tandem strut configuration. However, in general, total resistance and practical point of view, this design seems to be worse.

12) The sinkage and trim of the tandem strut models are independent of the wave length but dependent on the wave height. However, with the single strut SWATH3, they are both nearly independent of the wave height. The sinkage and trim of the single strut SWATH are both much smaller than those of the tandem versions. Both the sinkage and trim follow nearly the same trends as the total resistance variations associated with parametric changes such as spacing and draft. Namely, the wider the spacing between the two demihulls, the smaller the sinkage and trim, and they are both increased with draft. In general, the sinkage and trim are both increased with increase of speed which creates severe bow trim and accordingly green water at higher speeds. In

particular, the resistance of the SWATH2 model with rectangular hulls with rounded corners is substantially increased by the trim at high speeds. Thus, stabilising fins are needed for the SWATH models with regard to resistance increase, sea-keeping and propeller emergence problems. With regard to these points, a 'sledge' bow seems to be promising in terms of reducing the bow trim and hence, a resistance reduction can be expected as well as the omission of fins. The contribution of fin drag to total resistance is substantial, as mentioned below. If controllable fins can be removed from the SWATH concept, this will be a great breakthrough in the further development of SWATH ships. Thus, it is recommended that further research should follow on the 'sledge' concept.

13) The contribution of controllable fins to total resistance is substantial and is mostly caused by induced drag(at non-zero angle of attack) and frictional resistance plus pressure component. The component of wave-making resistance is negligibly small but, at high angles of attack, the amount is considerably increased at higher speeds. Although the magnitude is dependent upon the fin size(chord, maximum thickness and span) and angle of attack to the local flow, in general, the contribution of a pair of fins is around 5-7% the total resistance and 10-14% for two pair of fins.

14) The resistance increase of the SWATH models in waves is very much smaller than those of the monohull ships. There is little increase in the added resistance as speed increases. Further, in the supercritical zone, as wave height increases, the resistance of the tandem strut models systematically decreases by as much as 24 % of the calm water resistance over the speed range Fn=0.31-0.39 with the tendency that the resistance peak shifts to the slower speeds and that the hump and hollow are flattened. This seems to be due to the combination of several complicated hydrodynamic interferences such as trim and sinkage changes in waves relative to those in calm water, increased apparent speed of the models due to the oncoming waves and changed speed of water particles near the models due to the increased surge motion with the increase of wave height etc. However, this negative resistance increase does not occur with the single strut SWATH3 model. Therefore, this reason seems to be caused mostly by the interference effects between the twin struts combined with some motion aspects of the tandem strut SWATH models. From the propulsion point of view, this negative

resistance increase in waves is one of the greatest advantages with the tandem strut SWATH design compared to the single strut as well as monohulls. As a result, the tandem strut SWATH ship can be recommended to apply to naval combatants where operational speed reduction is of prime importance. In order to substantiate the resistance decrease in regular waves, further experiments in random waves will be desirable.

15) It can be seen that the heaving, pitching and surging responses are proportional to the wave height. However, the added resistance for the three models tested is not proportional to the square of the wave height. The added resistance divided by the square of the wave height decreases as the wave height increases. The break in the square law is more significant in lower wave heights compared to in high wave heights.

16) The motion response of the SWATH2 is much less than that of the SWATH1 model. This fact results in less added resistance for SWATH2 compared to SWATH1 at the same wave steepness and same submergence ratio of the main body and demonstrates one of the advantages of rectangular hulls over circular ones provided the resistance penalty in calm water can be controlled.

17) The resistance increase of the single strut SWATH in waves is larger than that of the tandem versions at higher speeds possibly due to the increased trim and sinkage compared to those in the calm water(the trim of the tandem strut in waves is significantly reduced as the wave height increases). The most resistance increase or decrease of the tandem strut versions occurs at around the pitch resonant region while the large resistance increase for the single strut occurs at around the heave resonant possibly due to the much exaggerated heave motion around the resonant frequency. Unlike the tandem strut, the heave response reaches up to three times the wave height at the resonant frequency. The heave and surge motions of the tandem strut are less than those of the single strut excepting around the resonant regions, but the pitch motion of the tandem is larger than that of its counterpart.

18) In general, a circular hulled SWATH ship is superior to a non-circular hulled SWATH ship with regard to resistance. However, at certain speeds(medium range), a well designed SWATH ship having non-circular cross section bodies has a possibility of less resistance than that of a circular hulled SWATH at a certain draft. Therefore, a SWATH ship with rectangular cross section hulls with rounded corners can be recommended for the next generation of SWATH development in terms of less motion responses, less resistance increase in waves, draft reduction and construction cost compared to circular hulled SWATH ships. The trim of the SWATH2 model is less than that of the SWATH1 circular hulled model. In addition, the 'sledge' bow can be easily introduced to rectangular hulled SWATH ships. Therefore, a rectangular cross section hull can be applied to the design of practical SWATH ships up to moderately high speeds without any serious penalty in resistance compared to the circular counterpart. However, at higher speeds, a well streamlined hull is better in terms of the total resistance.

19) By contouring the submerged bodies, a great proportion of the wave-making resistance can be reduced over the medium speed range. For the present 2405 tonne SWATH ship used for the optimisation study, the wave-making resistance of the optimum configuration at 14 knots is reduced by as much as 70% that of an equivalent non-optimised configuration. There is another benefit that the machinery can be placed inside the body making an efficient utilisation of the increased space. It is, however, worthwhile noting that the SWATH ship optimised at 14 knots is subject to a significant resistance increase at higher speeds.

20) The calm water resistance per unit displacement of the SWATH3 model is 8-10% greater than that of Destroyer DE-1006(C_b=0.49) at high speeds and 10-20% at slow speeds. However, in waves(at λ/ζ_w=18.5 investigated), the powering requirement of the SWATH is around 60% less than that of the Destroyer. Speed reduction of as much as 65% occurs for the destroyer in the wave condition, while less than 1% speed reduction is observed with the SWATH3. Although the added resistance is only a part of the total resistance, ships usually operate in wave conditions. With regard to this, the slightly higher calm water resistance of the SWATH ship is trivial compared to the power increase of the equivalent monohull in waves. In conclusion, it

can be said that the powering requirement of a SWATH ship is very much less than that of equivalent displacement of monohulls at sea (not only in rough seas). In addition, it is reported[108] that the propulsion efficiencies of SWATH ships are much higher than those of monohulls. Therefore, there is no reason why SWATH ship cannot be developed further at sea from the propulsion point of view(not only seakeeping point of view). This conclusion is in fact opposed to the several unsupported 'verbal' statements that the powering requirement of a SWATH ship is generally higher than that of an equivalent displacement of monohull.

21) As mentioned earlier, the negative resistance increase in waves of the tandem strut design is one of the most important findings from the experimental study reported in this thesis. Therefore, a theoretical investigation of first and second order wave effects based on the 3-D source distribution technique should be carried out in order to explain the cause fully. There are several reports[102,103] that a free oscillating airfoil(s) in waves attached to the hull creates the propulsive energy by which the ship moves forward. As mentioned above, stabilising fins are essential for the conventional SWATH ships in the light of pitch stability requirement. Therefore, this free oscillating fins can be utilised for the further development of SWATH design to improve the propulsive efficiency by making the utilisation of wave energy. Further, if it is confirmed that a SWATH ship with 'sledge' bow can run at level trim in most operating seas, retractable free oscillating fins can be recommended. In resonant sea conditions, these fins can be effectively used to reduce not only motion responses but also to reduce the resistance increase due to the severe motion. With regard to these points, free oscillating fins as well as 'sledge' bow concept is recommended for future study.

REFERENCES

1. Chapman R.B., ' Hydrodynamic Drag of Semi-submerged Ships ', Trans. of the SNAME, Journal of Basic Engineering, Vol.94, Dec., 1972

2. Koops A. and Nethercote W.C.E, ' SWATH Model Resistance Measurements ', Int. Conference on SWATH Ships and Advanced Multi-hulled Vessels by RINA, London, April, 1985

3. Lin W.C. and Day W.G.Jr., ' The Still Water Resistance and Propulsion Characteristics of Small-Waterplane-Area Twin-Hulled(SWATH) Ships ', AIAA/SNAME Advanced Marine Vehicles Conference, AIAA Paper No.74-325, San Diego, California, Feb., 1974

4. Nethercote W.C.E. and Schmitke R.T., ' A Concept Exploration Model for SWATH Ships ', Trans. RINA, Vol.124, 1982

5. Salvesen N., von Kerczek C.H. et al, ' Hydro-Numeric Design of SWATH Ships ', Trans. of SNAME, Vol.93, 1985

6. Huang D.L., ' A Modified Method for Calculating the Wave Resistance of SWATH Ships', Int. Shipbuilding Progress, Vol.,34, April, 1987

7. Conn J.F.C., ' Ship Wave and Hull Resistance ', Trans. of Royal Phy. Society of Glasgow, Vol.9, No.2, 1972

8. Chapman R.B., ' Spray Drag of Surface Piercing Struts ' AIAA/SNAME Advanced Marine Vehicles Meeting, AIAA Paper No.72-605, Annapolis, Maryland, July, 1972

9. Gersten A., ' Seakeeping Characteristics of the Baseline Design for a SWATH T-AGOS Ship ', DTNSRDC SPD-1007-01, 1982

10. Rivlin T.J., ' An Introduction to the Approximation of Functions ', Dover Publications Inc., 1969

11. Filon L.N.G., ' On a Quadrature Formula for Trigonometric Integrals ', Proc. Roy. Soc. Edinbourgh, Vol.49, 1928

12. Watson G.N., ' A treatise on the Theory of Bessel Functions ', Cambridge, 1922

13. Kuo S., ' Computer Applications of Numerical Methods', Published by Addison-Wesley Publishing Company Inc., 1972

14. Spiegel M.R., ' Mathematical Handbook of Formulas and Tables ' Schaum's Outline Series in Mathematics, McGraw-Hill Book Company, 1968

15. ' Principles of Naval Architecture ', Edited by Comstock J.P., Published by SNAME, 1977

16. Stenson R.J., ' Full-Scale Powering Trials of the Stable Semisubmerged Platform, SSP Kaimalino ', DTNSRDC SPD-650-01, April, 1976

17. Huang D.L., ' Private Letter to the Author', dated on 10th Sep., 1987

18. Pien P.C. and Lee C.M., 'Motion and Resistance of a Low Waterplane Catamaran ', Proc. of 9th Symposium on Naval Hydrodynamics, 1972

19. Byquist T., ' Wave-Making Resistance of a Series of Bodies of Revolution '. The Royal Institute of Technology Sweden, June, 1973

20. Hoerner F.S., ' Fluid-Dynamic Drag' Published by the Author, 1965

21. Gertler M., ' Resistance Experiments on a Systematic Series of Streamlined Bodies of Revolution - for Application to the Design of High-Speed Submarines'. DTNSRDC Report C-297, April, 1950

22. Schoenherr K.E., ' Resistance of Torpedo forms ', DTMB Report, Oct., 1941

23. Chun H.H., ' Analysis of SWATH-386 Model Experiments and Comparison with Computational Results', Report NAOE-87-47, Dept of Naval Architecture and Ocean Engineering, Glasgow University, 1987

24. Report of the High-Speed Marine Vehicle Committee, Proc. of 17th ITTC Conference, Vol.1, Goteborg, Sweden, Sep.1984

25. Peter D.C. and Eames M.C., ' High-Speed Small Craft ', Published by David and Charles, 1974

26. Schlichting H. and Erich Truckenbrodt, ' Aerodynamics of the Airplane ', Translated by Ramm H.J., McGraw-Hill Int. Book Company, 1979

27. Lasky M.P., ' An Investigation of Appendage Drag ', DTNSRDC/SPD Report 458-H-01, March,1972, Reissued 1980

28. Havelock T.H., ' Wave Resistance : the Mutual Action of Two Bodies ', Proc of Royal Society of London A, Vol.,155, 1936

29. Srettensky L.N., ' On the Wave- Making Resistance of a Ship Moving along in a Canal ', Philosophical Magazine, Vol.,22, 1936

30. Lunde J.K., ' On the Linearised Theory of Wave Resistance for Displacement Ships in Steady and Accelerated Motion ', Trans. of SNAME, Vol.,59, 1951

31. Eggers K., ' Resistance Conditions of Two-Body Ships ', BSRA Translation 1860 (Uber Widerstandsverhaitnisse von Zweikorperschiffen, J. Schiffbautech Gesellschaft , 1955)

32. Lackenby H. and Slater C., ' The Case for Multihull Ships with Particular Reference to Resistance Characteristics ', Trans. of SNAME, Vol.,76, 1968

33. Everest J.T., ' Some Research of the Hydrodynamics of Catamarans and Multi-hull Vessels in Calm Water ', Trans. of SNAME, Vol.,84, 1968

34. Lin W.C., ' The Force and Moment on a Twin- Hull Ship in a Steady Potential Flow ', 10th Symposium on Naval Hydrodynamics, M.I.T., Mass., U.S.A, 1974

35. Rich A.J., Spooston J.L. and Millward A., ' A Theoretical Prediction of the Effect of a Wall on the Resistance of a Fast Ship Shape in Water of Uniform Depth ', Int. Shipbuilding Progress, Vol.,32 Dec., 1985

36. Pien P.C., ' Catamaran Hull-Form Design ', Int. Seminar on Wave Resistance, Tokyo, 1976

37. Tuck E.O., 'A Systematic Asymptotic Expansion Procedure for Slender Ships ', Journal of Ship Research, Vol.,8, No.1, 1964

38. Michell J.H., ' The Wave Resistance of a Ship ', Philosopical Magazine, Vol.,45, 1898

39. Hess,J.L and Smith A.M.O., ' Calculation of Non-lifting Potential Flow about Arbitrary Three Dimensional Bodies ', Douglas Report No.E.S.40622, 1962

40. Gadd G.E., ' A Method of Computing the Flow and Surface Wave Pattern around Full Forms ', Trans. of RINA, Vol.,118, 1976

41. Gadd G.E., A Convenient Method for Estimating Wave Resistance, and its Variation with Small Changes of Hull Shape, for a Wide Range of Ship Types , Shipbuilding Marine Technology Monthly, Vol.,28, 1981

42. Proceedings of the Workshop on Ship Wave-Resistance Computations, DTNSRDC, Nov., 1979

43. The Proceedings of the Second DTNSRDC Workshop on Ship Wave-Resistance Computations, DTNSRDC, Nov., 1983

44. Seo S.G., 'The Calculation of Potential Flow around and in the Wake of a Surface Ship', Ph.D Thesis, Dept of Naval Architecture and Shipbuilding, University of Newcastle Tyne, 1985

45. Xia F., ' Numerical Calculations of Ship Flows, with Special Emphasis on the Free Surface Potential Flow ', Ph.D Thesis, Division of Marine Hydrodynamics, Chalmers University of Technology, Goteborg, Sweden, 1986

46. Ni.S.Y., ' Higher Order Panel Methods for Potential Flows with Linear or Non-linear Free Surface Boundary Conditions ', Ph.D Thesis, Division of Marine Hydrodynamics, Chalmers University of Technology, Goteborg, Sweden, 1987

47. Havelock T.H., ' The Collected Papers of Sir Thomas Havelock on Hydrodynamics ', Edited by W.C.S. Wigley, Office of Naval Research, Dept of the Navy, ONR/ACR-103, Washington D.C., 1963

48. Peters A.S., and StokerJ.J., ' Water Waves, The Mathematical Theory with Applications', Published by Interscience Publishers Inc., New York, 1957

49. Ogilvie T.F., ' On Non-linear Wave Resistance Theory ', Int. Seminar on Wave Resistance by the Society of Naval Architects of Japan, Feb. 1976

50. Hogner E., ' Ueber die Theorie der von einen schiff erzengtem Wellen und des Widerstandes', Proc., 1st Int. Congr. Appli. Mech., Delft, 1924

51. Maruo H., ' Calculation of the Wave Resistance of Ships, the Draught of which is Small as the Beam ', The Society of Naval Architects of Japan, Vol.,112, 1962

52. Chung J.H., ' A Study of the Modification of the Slender Ship Theory ', Bulletin of Eng. College of Pusan National University, Report No.14, Republic of Korea, 1975

53. Chun H.H., ' A Study on the 1st and Higher Order Wave Resistance ', MSc Thesis, Pusan National University, Pusan, Republic of Korea, 1985

54. Wehausen J.V., ' The Wave Resistance of Ships ', Advances in Applied Mechanics, Academic Press, Vol. 13, pp. 93-245, 1973

55. Chun H.H., ' A Study on the Wave Making Resistance of Multi-Hulled Vessels SWATH Ships ', Report NAOE-86-67, Dept of Naval Architecture and Ocean Engineering, Glasgow University, 1986

56. Lamb H., Hydrodynamics, Published by Dover Publication, 6th Edition, 1932

57. Kellog O.D., ' Foundation of Potential Theory ', Dover Publications, N.Y., 1929

58. Havelock T.H., ' The Calculation of Wave Resistance ', Proc. Royal Society of London, Vol.,104, 1934

59. Maruo H., ' A Note on the Higher Order Theory of Thin Ships ', Bulletin of the Faculty of Eng., Yokohama National University, Vol.15, Japan, 1966

60. Inui T., ' Wave-Making Resistance of Ships ', Trans. of SNAME, Vol.,70, 1962

61. Chun H.H., 'Computational and Experimental Studies on SWATHs Resistance - Interim Report -', Report NAOE-86-64, Dept of Naval Architecture and Ocean Engineering, Glasgow University, 1986

62. Shor S.W.W, 'Mathematical Methods for Calculating Ship Hull Forms of Decreased Wave-making Resistance ' Dept of the Navy, Report No., ONR 438, Washington, 1963

63. Chun H.H., ' A New Approach to Determine the Wave Resistance of SWATH ships', Report NAOE-87-46, Dept of Naval Architecture and Ocean Engineering, Glasgow University, 1987

64. Chun H.H., 'SWATH1 Model(Tandem Struts) Resistance Measurements in Calm Water ', Report NAOE-87-28, Dept of Naval Architecture and Ocean Engineering, Glasgow University, 1987

65. Chun H.H., 'SWATH1 Model Resistance and Motion in Calm Water as well as in Waves ', Report NAOE-88-02, Dept of Naval Architecture and Ocean Engineering, Glasgow University, Jan., 1988

66 Kusaka Y., Nakamura H., and Kunitake Y., ' Hull Form Design of the Semi Submerged Catamaran Vessel ', 13th Symposium on Naval Hydrodynamics, Tokyo Oct., 1980

67. Ferguson A.M., ' Description of the Ship Model Test Tank and Its Equipment ', Dept Report No 5, May, 1964

68 Tsutsumi T., Ogiwara S., and Jinnaka T., ' On the Principal Particulars of Ship Hull Form and Wave Resistance ', Slected Papers from the Journal of the Society of Naval Architects of Japan, Vol.14, 1976

69. Ferguson A.M., ' Factors Affecting the Components of Ship Resistance ', Ph.D Thesis, Glasgow University, 1976

70. Smith S.N., ' Design and Hydrodynamic Assessment of a Small Semi-Submersible(SWATH-Type) Vessel ', Ph.D Thesis, Dept of Naval Architecture and Ocean Engineering, Glasgow University, 1982

71. Seren D.B., ' Monohulls and multihulls in Transit : Aspects of Physical and Theoretical Modelling in Restricted Water ', Ph.D Thesis, Dept of Naval Architecture and Ocean Engineering, Glasgow University, Oct., 1982

72. Wu J.Y., ' SWATH Vertical Motions with Emphasis on Fixed Fins Control ', Ph.D Thesis, Dept of naval Architecture and Ocean Engineering, Glasgow University, 1985

73. Djatmiko E.B., ' Experimental Investigation into SWATH Ship Motions and Loadings ', M.Sc. Thesis, Dept of Naval Architecture and Ocean Engineering, Glasgow University, Dec.,1987

74. Wilson M.B., Written Discussion to the Paper of ' Hydro-Numeric Design of SWATH Ships ', by Salvesen N. et al, Trans. of SNAME, Vol.93, 1985

75. Narita H., Mabuchi T. et al, ' Design and Full Scale Test Results of Semi-Submerged Catamaran(SSC) Vessels ', 1st Int. Marine Systems Design Conference(IMSDC), London, April, 1982

76. Yeh H.Y.H. and Neal E., ' Powering Characteristics of SWATH-6A in Calm Water and Head Seas Represented by Model 5337-A and Using Propellers 4415-4416 ', DTNSRDC Report SPD-396-20, March, 1977

77. MacGregor J.R., Unpublished Work , Dept Naval Architecture and Ocean Engineering, Glasgow University, July, 1987

78. Report of Performance Committee of ITTC, Proceedings of 15th International Towing Tank Conference(ITTC), Vol.1, Hague, Sep., 1978

79. Sibul O.J., ' Constant Thrust vs. Conatant Velocity Method for Resistance Measurement in Waves ', College of Engineering, University of California, Berkeley, Report No. NA-71-1, June, 1971

80. Bhattacharyya R., Dynamics of Marine Vehicles published by John Wiley and Sons, 1978

81. Sibul O.J., ' Measurements and Calculations of Ship Resistance in Waves ', University of California, Berkeley, Report No. NA-71-2, Dec., 1971

82. Sibul.O.J., ' Measurements and Calculations of Ship Resistance in Waves, Part 2', University of California, Berkeley, Report No. NA-71-3, Dec., 1971

83. Blume P. and Kracht A.M., ' Prediction of the Behaviour and Propulsive Performance of Ships with Bulbous Bow in Waves ', Trans. SNAME, Vol.93, 1985

84. Sibul O.J., ' Ship Resistance in Uniform Waves ', University of California, Berkeley, Report No. NA-64-1, Jan., 1964

85. Drysdale L., ' Solution of Linear Motion Equation for Coupled Heave and Pitch for a SWATH Ship - Including Programming Manual ', Report NAOE-86-53, Dept of Naval Architecture and Ocean Engineering, Dec., 1986

86. Baitis A.E., Mayers W.G. et al ' A Seakeeping Comparison between Three Monohulls, Two SWATHs, and a Column- Stabilized Catamaran Designed for the Same Mission ' DTNSRDC Report SPD-522-01, July, 1975

87. Lee C.M., ' A General Overview of SWATH Hydrodynamics ', The Nineth Annual Energy-Source Technology Conference and Exhibition, New Oreans, Louisiana, Feb., 1986

88. Wu J.Y. and McGregor R.C., ' SWATH Seakeeping in the Presence of Control Fins ', 5th International High Speed Surface Craft Conference, Southampton, England, May, 1986

89. Bebar M.R., Kennell C.G. et al, ' Advanced Marine Vehicles - A Review ', Workshop on Developments in Hull Form Design, Wageningen, Oct., 1985

90. Chun H.H., ' SWATH2 Model Resistance and Motion in Calm Water and in Waves ' , Report NAOE-88-03, Dept of Naval Architecture and Ocean Engineering, Jan., 1988

91. Proceedings of the RINA Conference on ' SWATH Ships and Advanced Multi-Hulled Vessels ', RINA, London, April, 1985

92. Lang T.G. and Sloggett J.E., ' SWATH Developments and Performance Comparisons with Other Craft ', Int. Conference on SWATH Ships and Advanced Multi Hulled Vessels, RINA, London, April, 1987

93. Oshima M., Narita H. and Kunitake Y., ' Experiences with 12 Meter Long Semi Submerged Catamaran(SSC) ' MARINE ACE' and Building of SSC Ferry for 446 Passengers ', AIAA/SNAME Advanced Marine Vehicles Conference, Baltimore, Maryland, 1979

94. Mcpherson J.L., and Voigt B.D., ' An Experimental Comparison of Zero-Speed Seakeeping Characteristics of Single and Double strut SWATHs', United States Naval Academy, Report EW-15-83, Annapolis, Maryland, April, 1983

95. Dand I.W., ' The Effect of Towing Point Heights on Resistance, Sinkage and Trim Measurements for a Model in Steady Motion ', Dept Report No.7, Dept of Naval Architecture and Ocean Engineering, Glasgow University, May, 1967

96. Report of the High-Speed Marine Vehicle Committee, Proc. of 18th ITTC Conference, Vol.1, Kobe, Japan, Oct. 1987

97. Report of the Resistance Comittee, Proc. of 17th ITTC Conference, Vol.1, Goteborg, Sweden, Sep. 1984

98. Grygorowicz M., ' Official Letter to the Author', Dated on 14th, Dec. 1987

99. Chun H.H., ' Documentation for Resistance Program of SWATH ships Defined in Mathematical forms -MSWATH', In preparation as Dept Report

100. Chun H.H., ' SWATH3 Model(Single Strut) Resistance and Motion in Calm Water as well as in Uniform Waves ', Report NAOE-88-04, Dept of Naval Architecture and Ocean Engineering, Glasgow University, Jan., 1988

101. Seren D.B., Miller N.S, Ferguson A.M. and McGregor R.C., ' Some Motion and Resistance Aspects of SWATH -Ship Design ', Int. Conference on SWATH Ships and Advanced Multi-Hulled Vehicles, RINA, April, 1985

102. Isshiki H. and Murakami M., ' Wave Power Utilization into Ship Propulsion ', 5th Int. Sym. and Exihibition on Offshore Mechanics and Arctic Engineering(OMAE), Toyko, 1986

103. Isshiki H. and Naito S., ' An Application of Wave Energy - Thrust Generation by a Hydrofoil in Waves ', 9th Annual Energy - Sources Technology Conference and Exhibition ', New Orelans, Louisiana, Feb., 1986

104. Everest J.T., ' Some Research on the Hydrodynamics of Catamarans and Multi-Hulled Vessels in Calm Water ', Trans. NECIES, 1967-68

105. Cannon T.R., ' Large SWATHS A Discussion of the Diminishing Returns of Increasing SWATH Ship Size', AIAA 8th Advanced Marine Systems Conference, AIAA-2385, San Diego, California, Sep. 1986

106. Cannon T.R., ' Research Colloquium on ' U.S. Navy SWATH Design Practice and Application', Held at Dept of Naval Architecture and Ocean Engineering, Glasgow University, 29th Feb. 1988

107. Chun H.H., ' An Optimum Study of a 2405 tonne SWATH Ship at Three Speeds of 3, 8 and 14 knots ', Unpublished Dept Work, Dept of Naval Architecture and Ocean Engineering, Glasgow University, Feb. 1988

108. Lin A.C.M., Crook L.B. and Murray L.O., ' Prediction of Resistance and Propulsion Characteristics for a SWATH Form Represented by Model 5287', DTNSRDC/SPD–78/396–08, 1978

109. Lang T.G. et al ,'Naval Feasibility of the NUC Semi-Submerged Ship Concept ', Naval Undersea Research and Development Centre, TP-235, 1971

110. Lang T.G. and Higdon D.T, ' Hydrodynamics of the 190 Ton SSP ', AIAA 78-328, 1974

111. Allen R.G. and Holcomb R.S., ' The Application of Small SWATH Ships to Coastal and Offshore patrol Missions ', Symp. on Small Fast warships and Security Vessels, RINA, London, 1982

112. MacGregor J.R., ' Historical Development of the SWATH Ship Concept ', Report NAOE-87-44, Dept of Naval Architecture and Ocean Engineering, Glasgow University, 1987

113. Serter E.H., ' Comparative Studies for New U.S. Frigate Hull ', International Deffence Review, Feb. 1988